United States
Environmental Protection
Agency

Industrial Environmental Research
Laboratory
Research Triangle Park NC 27711

EPA-600/7-79-044d
February 1979

EPA

Symposium on the Transfer and Utilization of Particulate Control Technology:
Volume 4. Fugitive Dusts and Sampling, Analysis and Characterization of Aerosols

Interagency Energy/Environment R&D Program Report

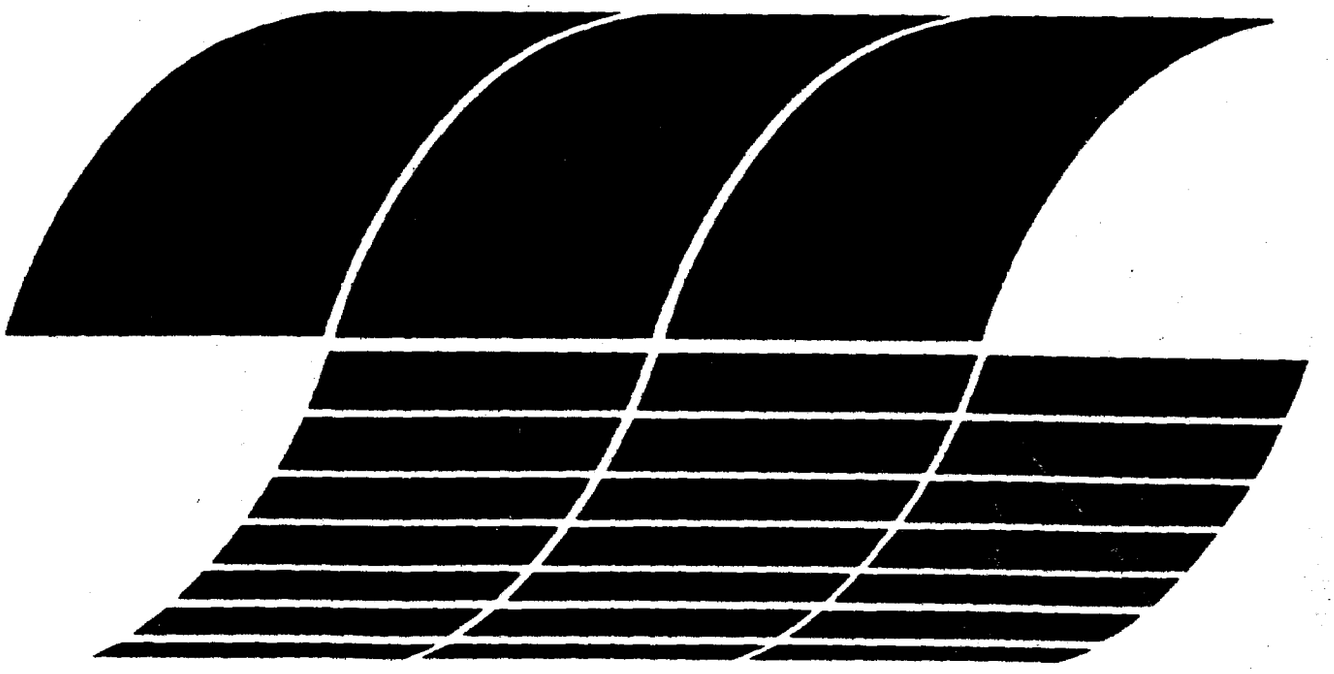

RESEARCH REPORTING SERIES

Research reports of the Office of Research and Development, U.S. Environmental Protection Agency, have been grouped into nine series. These nine broad categories were established to facilitate further development and application of environmental technology. Elimination of traditional grouping was consciously planned to foster technology transfer and a maximum interface in related fields. The nine series are:

1. Environmental Health Effects Research
2. Environmental Protection Technology
3. Ecological Research
4. Environmental Monitoring
5. Socioeconomic Environmental Studies
6. Scientific and Technical Assessment Reports (STAR)
7. Interagency Energy-Environment Research and Development
8. "Special" Reports
9. Miscellaneous Reports

This report has been assigned to the INTERAGENCY ENERGY-ENVIRONMENT RESEARCH AND DEVELOPMENT series. Reports in this series result from the effort funded under the 17-agency Federal Energy/Environment Research and Development Program. These studies relate to EPA's mission to protect the public health and welfare from adverse effects of pollutants associated with energy systems. The goal of the Program is to assure the rapid development of domestic energy supplies in an environmentally-compatible manner by providing the necessary environmental data and control technology. Investigations include analyses of the transport of energy-related pollutants and their health and ecological effects; assessments of, and development of, control technologies for energy systems; and integrated assessments of a wide range of energy-related environmental issues.

EPA REVIEW NOTICE

This report has been reviewed by the participating Federal Agencies, and approved for publication. Approval does not signify that the contents necessarily reflect the views and policies of the Government, nor does mention of trade names or commercial products constitute endorsement or recommendation for use.

This document is available to the public through the National Technical Information Service, Springfield, Virginia 22161.

EPA-600/7-79-044d

February 1979

Symposium on the Transfer and Utilization of Particulate Control Technology: Volume 4. Fugitive Dusts and Sampling, Analysis and Characterization of Aerosols

by

F.P. Venditti, J.A. Armstrong, and Michael Durham

Denver Research Institute
P.O. Box 10127
Denver, Colorado 80208

Grant No. R805725
Program Element No. EHE624

EPA Project Officer: Dennis C. Drehmel

Industrial Environmental Research Laboratory
Office of Energy, Minerals, and Industry
Research Triangle Park, NC 27711

Prepared for

U.S. ENVIRONMENTAL PROTECTION AGENCY
Office of Research and Development
Washington, DC 20460

Environmental Protection Agency
Region V
230 South Dearborn Street
Chicago, Illinois 60604

ABSTRACT

The papers in these four volumes of Proceedings were presented at the Symposium on the Transfer and Utilization of Particulate Control Technology, held in Denver, Colorado during 24 July through 28 July 1978 sponsored by the Particulate Technology Branch of the Industrial Environmental Research Laboratory of the Environmental Protection Agency and hosted by the Denver Research Institute of the University of Denver.

The purpose of the symposium was to bring together researchers, manufacturers, users, government agencies, educators and students to discuss new technology and to provide an effective means for the transfer of this technology out of the laboratories and into the hands of the users.

The three major categories of control technologies, electrostatic precipitators, scrubbers, and fabric filters were the major concern of the symposium. These technologies were discussed from the perspectives of economics; new technical advancements in science and engineering; and applications. Several papers dealt with combinations of devices and technologies, leading to a concept of using a systems approach to particulate control rather than device control.

These proceedings are divided into four volumes, each volume containing a set of related session topics to provide easy access to a unified technology area.

TABLE OF CONTENTS

Volumes 1 through 4

VOLUME I

ELECTROSTATIC PRECIPITATORS

Section A - ESP's for Coal Fired Boilers

	Page
ELECTROSTATIC PRECIPITATOR PERFORMANCE J. P. Gooch	1
SPECIFICATIONS OF A RELIABLE PRECIPITATOR R. L. Williams	19
EXPERIENCE WITH COLD SIDE PRECIPITATORS ON LOW SULFUR COALS S. Maartmann	25
A PERFORMANCE ANALYSIS OF A HOT-SIDE ELECTROSTATIC PRECIPITATOR G. H. Marchant, J. P. Gooch, L. E. Sparks	39
AIR FLOW MODEL STUDIES FOR ELECTROSTATIC PRECIPITATORS H. L. Engelbrecht	57

Section B - Flue Gas Conditioning for ESP'S

CHEMICAL CONDITIONING OF FLY ASH FOR HOT-SIDE PRECIPITATION P. B. Lederman, P. B. Bibbo, J. Bush	79
CONDITIONING OF DUST WITH WATER-SOLUBLE ALKALI COMPOUNDS H. H. Petersen	99
CHEMICAL ENHANCEMENT OF ELECTROSTATIC PRECIPITATOR EFFICIENCY R. P. Bennett, A. E. Kober	113
METHOD AND COST ANALYSIS OF ALTERNATIVE COLLECTORS FOR LOW SULFUR COAL FLY ASH E. W. Breisch	121

Page

BENCH-SCALE EVALUATION OF DRY ALKALIS FOR REMOVING SO_2 FROM BOILER FLUE GASES
N. D. Shah, D. P. Teixeira and L. J. Muzio 131

ANALYSIS OF THERMAL DECOMPOSITION PRODUCTS OF FLUE GAS CONDITIONING AGENTS
H. K. Dillon and E. B. Dismukes 155

FLUE GAS CONDITIONING EFFECTS ON ELECTROSTATIC PRECIPITATORS
R. Patterson, R. Riersgard, R. Parker and L. E. Sparks 169

FLUE GAS CONDITIONING AT ARIZONA PUBLIC SERVICE COMPANY FOUR CORNERS UNIT NO. 4
R. E. Pressey, D. Osborn and E. Cole 179

SODIUM CONDITIONING TEST WITH EPA MOBILE ESP
S. P. Schliesser 205

Section C - Novel Electrostatic Precipitators

NOVEL ELECTRODE CONSTRUCTION FOR PULSE CHARGING
S. Masuda 241

PULSED ENERGIZATION FOR ENHANCED ELECTROSTATIC PRECIPITATION IN HIGH-RESISTIVITY APPLICATIONS
P. L. Feldman and H. I. Milde 253

A NEW PRECHARGER FOR TWO-STAGE ELECTROSTATIC PRECIPITATION OF HIGH RESISTIVITY DUST
D. H. Pontius, P. V. Bush and L. E. Sparks 275

ELECTRON BEAM IONIZATION FOR COAL FLY ASH PRECIPITATORS
R. H. Davis and W. C. Finney 287

WIDE SPACING E.P. IS AVAILABLE IN CLEANING EXHAUST GASES FROM INDUSTRIAL SOURCES
R. Ito and K. Takimoto 297

Section D - Fundamentals--Electrical and Particle Characteristics

Page

DESCRIPTION OF A MATHEMATICAL MODEL OF ELECTROSTATIC PRECIPITATION
J. R. McDonald and L. E. Sparks 307

BACK DISCHARGE PHENOMENA IN ELECTROSTATIC PRECIPITATION
S. Masuda 321

MEASUREMENT OF EFFECTIVE ION MOBILITIES IN A CORONA DISCHARGE IN INDUSTRIAL FLUE GASES
J. R. McDonald, S. M. Banks and L. E. Sparks 335

PILOT SCALE ELECTROSTATIC PRECIPITATORS AND THE ELECTRICAL PERFORMANCE DIAGRAM
K. J. McLean and R. B. Kahane 349

THEORETICAL STUDY OF PARTICLE CHARGING BY UNIPOLAR IONS
D. H. Pontius, W. B. Smith and J. H. Abbott 361

AGING CAUSED INCREASE OF RESISTIVITY OF A BARRIER FILM AROUND GLASSY FLY ASH PARTICLES
W. J. Culbertson 373

ELECTROSTATIC PRECIPITATORS: THE RELATIONSHIP OF ASH RESISTIVITY AND PRECIPITATOR ELECTRICAL OPERATING PARAMETERS
H. W. Spencer, III 381

A TECHNIQUE FOR PREDICTING FLY ASH RESISTIVITY
R. E. Bickelhaupt 395

ELECTRICAL PROPERTIES OF THE DEPOSITED DUST LAYER WHICH ARISE BECAUSE OF ITS PARTICULATE STRUCTURE
K. J. McLean 409

VOLTAGE AND CURRENT RELATIONSHIPS IN HOT SIDE ELECTROSTATIC PRECIPITATORS
D. E. Rugg and W. Patten 421

PRECIPITATOR EFFICIENCY FOR LOG-NORMAL DISTRIBUTIONS
P. Cooperman and G. D. Cooperman 433

Section E - Industrial Applications of ESP's

Page

ELECTROSTATIC PRECIPITATION USING IONIC WIND FOR VERY LOW RESISTIVITY DUSTS FROM HIGH TEMPERATURE FLUE GAS OF PETROLEUM-COKES CALCINING KILN
F. Isahaya 453

THE USE OF ELECTROSTATIC PRECIPITATORS FOR COLLECTION OF PARTICULATE MATTER FROM BARK AND WASTE WOOD FIRED BOILERS IN THE PAPER INDUSTRY
R. L. Bump 467

ROOF-MOUNTED ELECTROSTATIC PRECIPITATOR
S. Ito, S. Noso, M. Sakai and K. Sakai 485

POM EMISSIONS FROM COKE OVEN DOOR LEAKAGE AND THEIR CONTROL BY A WET ELECTROSTATIC PRECIPITATOR
R. E. Barrett, P. R. Webb, C. E. Riley and A. R. Trenholm 497

VOLUME II

FABRIC FILTERS AND CURRENT TRENDS
IN CONTROL EQUIPMENT

Section A - Fabric Filters

	Page
FABRIC FILTER USAGE IN JAPAN K. Iinoya	1
PERFORMANCE OF A PULSE-JET FILTER AT HIGH FILTRATION VELOCITIES D. Leith, M. W. First, M. Ellenbecker and D. D. Gibson	11
ELECTROSTATIC EFFECTS IN FABRIC FILTRATION E. R. Frederick	27
EPA IN-HOUSE FABRIC FILTRATION R&D J. H. Turner	45
ENVIRONMENTAL PROTECTION AGENCY MOBILE FABRIC FILTER PROGRAM - A COMPARISON STUDY OF UTILITY BOILERS FIRING EASTERN AND WESTERN COAL B. Lipscomb	53
EVALUATION OF FELTED GLASS FILTER MEDIA UNDER SIMULATED PULSE JET OPERATING CONDITIONS L. R. Lefkowitz	75
INFLUENCE OF FIBER DIAMETER ON PRESSURE DROP AND FILTRATION EFFICIENCY OF GLASS FIBER MATS J. Goldfield and K. D. Gandhi	89
FUNDAMENTAL EXPERIMENTS OF FABRIC FILTERS K. Iinoya and Y. Mori	99
A DUAL PURPOSE BAGHOUSE FOR PARTICLE CONTROL AND FLUE GAS DESULFURIZATION S. J. Lutz	111
SIMULTANEOUS ACID GAS AND PARTICULATE RECOVERY A. J. Teller	119

Page

TECHNOLOGY OF FIBER GLASS FILTER FABRIC DESIGN
C. E. Knox, J. Murray and V. Schoeck 133

VERIFICATION OF PROJECTED FILTER SYSTEM DESIGN AND OPERATION
R. Dennis and H. A. Klemm 143

PRECIPITATORS? SCRUBBERS? OR BAGHOUSES? FOR SHAWNEE (WHY TVA IS INSTALLING BAGHOUSES)
J. A. Hudson 161

HIGH RATIO FABRIC FILTERS FOR UTILITY BOILERS
B. L. Arnold and B. Melville 183

RETRO-FITTING BAGHOUSES ON COAL-FIRED BOILERS - A CASE STUDY
J. M. Osborne and L. R. Cramer 197

MATCHING A BAGHOUSE TO A FOSSIL FUEL FIRED BOILER
D. W. Rolschau 211

START-UP, OPERATION AND PERFORMANCE TESTING OF FABRIC FILTER SYSTEM-HARRINGTON STATION, UNIT #2
G. Faulkner and K. L. Ladd 219

APPLYING HIGH VELOCITY FABRIC FILTERS TO COAL FIRED INDUSTRIAL BOILERS
J. D. McKenna, G. P. Greiner and K. D. Brandt 233

FABRIC FILTER RESEARCH AND DEVELOPMENT FOR PC BOILERS USING WESTERN COAL
D. A. Furlong, R. L. Ostop and P. Gelfand 247

A PILOT PLANT STUDY OF VARIOUS FILTER MEDIA APPLIED TO A PULVERIZED COAL-FIRED BOILER
J. C. Mycock 263

APPLICATION OF SLIP-STREAMED AIR POLLUTION CONTROL DEVICES ON WASTE-AS-FUEL PROCESSES
J. M. Bruck, C. J. Sawyer, F. D. Hall and T. W. Devitt 287

Section B - Current Trends in Control Equipment

ASSESSMENT OF THE COST AND PERFORMANCE OF PARTICULATE CONTROL DEVICES ON LOW-SULFUR WESTERN COALS
R. A. Chapman, T. F. Edgar and L. E. Sparks 297

ELECTROSTATIC PRECIPITATION IN JAPANESE STEEL INDUSTRIES
S. Masuda 309

INSTALLED COST PROJECTIONS OF AIR POLLUTION CONTROL EQUIPMENT IN THE U. S.
R. W. McIlvaine 319

DUST EMISSION CONTROL FOR STATIONARY SOURCES IN THE FEDERAL REPUBLIC OF GERMANY: STANDARDS OR PERFORMANCE, BEST AVAILABLE CONTROL TECHNOLOGY AND ADVANCED APPLICATIONS
G. Guthner 333

ENGINEERING MANAGEMENT TRENDS IN THE DESIGN OF PRECIPITATORS AND BAGHOUSES
S. Negrea 361

CONTROL OF PARTICULATES FROM COMBUSTION
J. H. Abbott and D. C. Drehmel 383

VOLUME III

SCRUBBERS, ADVANCED TECHNOLOGY, AND HTHP APPLICATIONS

Section A - Scrubbers

	Page
ENTRAINMENT SEPARATORS FOR SLURRY SCRUBBERS S. Calvert, H. F. Barbarika and L. E. Sparks	1
SCRUBBER DEMISTER TECHNOLOGY FOR CONTROL OF SOLIDS EMISSIONS FROM SO_2 ABSORBERS W. Ellison	13
IMPROVED MIST ELIMINATOR PERFORMANCE THROUGH ADVANCED DESIGN CONCEPTS R. P. Tennyson, S. F. Roe, and R. H. Lace	35
FINE PARTICLE COLLECTION IN A MOBILE BED SCRUBBER S. Yung, R. Chmielewski, S. Calvert and D. Harmon	47
CONTROL OF PARTICULATE EMISSIONS WITH U.W. ELECTROSTATIC SPRAY SCRUBBER M. J. Pilat and G. A. Raemhild	61
UNION CARBIDE'S HIGH INTENSITY IONIZER APPLIED TO ENHANCE A VENTURI SCRUBBER SYSTEM M. T. Kearns and C. M. Chang	73
PERFORMANCE TESTS OF THE MONTANA POWER COMPANY COLSTRIP STATION FLUE GAS CLEANING SYSTEM J. D. McCain	85
RESULTS OF THE TEST PROGRAM OF THE WEIR HORIZONTAL SCRUBBER AT FOUR CORNERS STEAM ELECTRIC STATION UNIT NO. FIVE G. Bratzler, G. T. Gutierrez and C. F. Turton	99
MATERIALS PERFORMANCE PROBLEMS ASSOCIATED WITH THE SCRUBBING OF COKE OVEN WASTE HEAT FLUE GAS M. P. Bianchi and L. A. Rosales	113
VENTURI SCRUBBER DESIGN MODEL S. C. Yung, H. Barbarika, S. Calvert and L. E. Sparks	149
EXPERIMENTAL STUDY OF PARTICLE COLLECTION BY A VENTURI SCRUBBER DOWNSTREAM FROM AN ELECTROSTATIC PRECIPITATOR G. H. Ramsey, L. E. Sparks and B. E. Daniels	161

Page

EFFECTS OF SURFACE TENSION ON PARTICLE REMOVAL
G. J. Woffinden, G. R. Markowski and D. S. Ensor 179

CONCLUSIONS FROM EPA SCRUBBER R&D
D. L. Harmon and L. E. Sparks 193

Section B - Advanced Technology

FINE PARTICLE EMISSION CONTROL BY HIGH GRADIENT MAGNETIC SEPARATION
C. H. Gooding and D. C. Drehmel 219

THE USE OF ACOUSTIC AGGLOMERATORS FOR PARTICULATE CONTROL
J. Wegrzyn, D. T. Shaw and G. Rudinger 233

ANALYTICAL AND EXPERIMENTAL STUDIES ON GRANULAR BED FILTRATION
C. Gutfinger, G. I. Tardos and N. Abuaf 243

THE EFFECTS OF ELECTRIC AND ACOUSTIC FIELDS ON THE COLLISION RATES OF SUBMICRON SIZED DOP AEROSOL PARTICLES
P. D. Scholz, L. W. Byrd and P. H. Paul 279

ELECTROSTATIC SEPARATION IN CYCLONES
W. B. Giles 291

EVALUATION OF THE ELECTRIFIED BED PROTOTYPE COLLECTOR ON AN ASPHALT ROOFING PLANT
R. M. Bradway, W. Piispanen, and V. Shortell 303

EVALUATION OF AN APITRON ELECTROSTATICALLY AUGMENTED FABRIC FILTER
J. D. McCain, P. R. Cavenaugh, L. G. Felix and R. L. Merritt 311

CORONA ELECTRODE FAILURE ANALYSIS
R. E. Bickelhaupt and W. V. Piulle 323

HIGH TEMPERATURE AND HIGH VELOCITY POROUS METAL GAS FILTRATION MEDIA
L. J. Ortino and R. M. Bethea 341

DRY DUST COLLECTION OF BLAST FURNACE EXHAUST GAS BY MOVING GRANULAR BED FILTER
H. Kohama, K. Sasaki, S. Watanabe and K. Sato 351

Page

CERAMIC FILTER, SCRUBBER AND ESP
R. A. Clyde 361

Section C - High Temperature High Pressure Applications

FUNDAMENTAL PARTICLE COLLECTION AT HIGH TEMPERATURE AND PRESSURE
R. Parker, S. Calvert and D. Drehmel 367

PARTICULATE CONTROL FOR FLUIDIZED BED COMBUSTION
D. F. Becker and M. G. Klett 379

HIGH TEMPERATURE GLASS ENTRAINMENT OF FLY ASH
W. Fedarko, A. Gatti and L. R. McCreight 395

A.P.T. DRY SCRUBBER FOR PARTICLE COLLECTION AT HIGH TEMPERATURE AND PRESSURE
R. Patterson, S. Calvert, S. Yung and D. Drehmel 405

ELECTROSTATIC PRECIPITATION AT HIGH TEMPERATURE AND PRESSURE: CAPABILITIES, CURIOUSITIES AND QUESTIONS
M. Robinson 415

HIGH TEMPERATURE, HIGH PRESSURE ELECTROSTATIC PRECIPITATION
J. R. Bush, P. L. Feldman and M. Robinson 417

BARRIER FILTRATION FOR HTHP PARTICULATE CONTROL
M. A. Shackleton and D. C. Drehmel 441

AEROSOL FILTRATION BY GRANULAR BEDS
S. L. Goren 459

PERFORMANCE CHARACTERISTICS OF MOVING-BED GRANULAR FILTERS
J. Geffken, J. L. Guillory and K. E. Phillips 471

VOLUME IV

FUGITIVE DUSTS AND SAMPLING, ANALYSIS AND CHARACTERIZATION OF AEROSOLS

Section A - Fugitive Dusts

	Page
FUGITIVE SULFUR IN COAL-FIRED POWERPLANT PLUMES R. F. Pueschel	1
RESEARCH IN WIND-GENERATED FUGITIVE DUST D. A. Gillette and E. M. Patterson	11
DEVELOPING CONTROL STRATEGIES FOR FUGITIVE DUST SOURCES G. Richard and D. Safriet	25
STATE OF CONTROL TECHNOLOGY FOR INDUSTRIAL FUGITIVE PROCESS PARTICULATE EMISSIONS D. C. Drehmel, D. P. Daugherty and C. H. Gooding	47
FUGITIVE DUST EMISSIONS AND CONTROL B. H. Carpenter and G. E. Weant	63
SETTING PRIORITIES FOR THE CONTROL OF PARTICULATE EMISSIONS FROM OPEN SOURCES J. S. Evans, D. W. Cooper, M. Quinn and M. Schneider	85
USE OF ELECTROSTATICALLY CHARGED FOG FOR CONTROL OF FUGITIVE DUST, SMOKE AND FUME S. A. Hoenig	105
COLLECTION AND CONTROL OF MOISTURE LADEN FUGITIVE DUST C. D. Turley	131

Section B - Sampling, Analysis, and Characterization of Aerosols

THE VISIBILITY IMPACT OF SMOKE PLUMES D. S. Ensor	141
MUTAGENICITY OF COAL FLY ASH C. E. Chrisp	153

Page

BIO-ASSESSMENT OF CHRONIC MANGANESE INGESTION IN RATS
G. L. Rehnberg, D. F. Cahill, J. A. Elder, E. Gray and J. W. Laskey 159

THE USE OF SHORT TERM BIOASSAY SYSTEMS IN THE EVALUATION OF ENVIRONMENTAL PARTICULATES
N. E. Garrett, J. A. Campbell, J. L. Huisingh and M. D. Waters 175

A KINETIC AEROSOL MODEL FOR THE FORMATION AND GROWTH OF SECONDARY SULFURIC ACID PARTICLES
P. Middleton and C. S. Kiang 187

PARTICLE GROWTH BY CONDENSATION AND BY COAGULATION--BASIC RESEARCH OF ITS APPLICATION TO DUST COLLECTION
T. Yoshida, Y. Kousaka, K. Okuyama and K. Sumi 195

TRANSIENT CHEMISORPTION OF A SOLID PARTICLE IN A REACTIVE ATMOSPHERE OF RECEDING GAS CONCENTRATION
R. Wang 213

STABILITY OF FINE WATER DROPLET CLOUDS
Y. Kousaka, K. Okuyama, K. Sumi and T. Yoshida 231

PARTICLE SIZE ANALYSIS OF AEROSOLS INCLUDING DROPLET CLOUDS BY SEDIMENTATION METHOD
Y. Kousaka, K. Okuyama and T. Yoshida 249

PARTICLE MASS DISTRIBUTION AND VISIBILITY CONSIDERATIONS FOR LARGE POWER PLANTS
T. L. Montgomery and J. C. Burdick III 261

AN OPTICAL INSTRUMENT FOR DILUTE PARTICLE FIELD MEASUREMENTS
W. D. Bachalo 275

IMPACT OF SULFURIC ACID EMISSIONS ON PLUME OPACITY
J. S. Nader and W. D. Conner 289

PARTICLE CHARGE EFFECTS ON CASCADE IMPACTOR MEASUREMENTS
R. Patterson, P. Riersgard and D. Harmon 307

A HIGH-TEMPERATURE HIGH-PRESSURE, ISOKINETIC-ISOTHERMAL SAMPLING SYSTEM FOR FOSSIL FUEL COMBUSTION APPLICATIONS
J. C. F. Wang, R. R. Boericke and R. A. Fuller 319

Page

A PROTOTYPE OPTICAL SCATTERING INSTRUMENT FOR PARTICULATE SIZING IN STACKS
A. L. Wertheimer, W. H. Hart and M. N. Trainer 337

UTILIZATION OF THE OMEGA-1 LIDAR IN EPA ENFORCEMENT ACTIVITIES
A. W. Dybdahl and M. J. Cunningham 347

THE MONITORING OF PARTICULATES USING A BALLOON-BORNE SAMPLER
J. A. Armstrong and P. A. Russell 357

A STUDY OF PHILADELPHIA PARTICULATES USING MODELING AND MEASUREMENT TECHNIQUES
F. A. Record, R. M. Bradway and W. E. Belanger 377

DECISION-TREE ANALYSIS OF THE RELATIONSHIP BETWEEN TSP CONCENTRATION AND METEOROLOGY
J. Trijonis and Y. Horie 391

DESIGNING A SYSTEMATIC REGIONAL PARTICULATE ANALYSIS
J. A. Throgmorton, K. Axetell and T. G. Pace 403

IMPORTANCE OF PARTICLE SIZE DISTRIBUTION
L. E. Sparks 417

THE MORPHOGENESIS OF COAL FLY ASH
G. L. Fisher 433

THE EFFECT OF TEMPERATURE, PARTICLE SIZE AND TIME EXPOSURE ON COAL-ASH AGGLOMERATION
K. C. Tsao, J. F. Bradley and K. T. Yung 441

TEST PROGRAM TO UPDATE EQUIPMENT SPECIFICATIONS AND DESIGN CRITERIA FOR STOKER FIRED BOILERS
S. C. Schaeffer 457

TRACE ELEMENT EMISSIONS FROM COPPER SMELTERS
R. L. Meek and G. B. Nichols 465

AUTHOR NAME	PAGE
Abbott, James H.	I-361, II-383
Abuaf, Nesim	III-243
Armstrong, James A.	IV-357
Arnold, B. L.	II-183
Axetell, Kenneth W.	IV-403
Bachalo, William D.	IV-275
Banks, Sherman M.	I-335
Barbarika, Harry F.	III-1, III-149
Barrett, Richard E.	I-497
Becker, David F.	III-379
Belanger, William E.	IV-377
Bennett, Robert P.	I-113
Bethea, Robert M.	III-341
Bianchi, M. P.	III-113
Bibbo, P. B.	I-79
Bickelhaupt, Roy E.	I-395, III-323
Boericke, Ralph R.	IV-319
Bradley, Jeffrey F.	IV-441
Bradway, Robert M.	III-303, IV-377
Brandt, Kathryn D.	II-233
Bratzler, Gene E.	III-99
Breisch, Edgar W.	I-121
Bruck, John M.	II-287

AUTHOR NAME	PAGE
Bump, Robert L.	I-467
Burdick, J. Clement	IV-261
Bush, John R.	I-79, III-417
Bush, P. V.	I-275
Byrd, Larry W.	III-279
Cahill, D. F.	IV-159
Calvert, Seymour	III-1, III-47, III-149 III-367 III-405
Campbell, James A.	IV-175
Carpenter, B. H.	IV-63
Cavenaugh, Paul R.	III-311
Chang, C. M.	III-73
Chapman, Richard A.	II-297
Chmielewski, Richard D.	III-47
Chrisp, Clarence E.	IV-153
Clyde, Robert A.	III-361
Cole, Edward A.	I-179
Conner, William D.	IV-289
Cooper, Douglas W.	IV-85
Cooperman, Gene D.	I-433
Cooperman, Phillip	I-433
Cramer, Larry R.	II-197
Culbertson, William J.	I-373
Cunningham, Michael J.	IV-347

AUTHOR NAME	PAGE
Daniels, B. E.	III-161
Daugherty, David P.	IV-47
Davis, Robert H.	I-287
Dennis, Richard	II-143
Devitt, Timothy W.	II-287
Dillon, H. Kenneth	I-155
Dismukes, Edward B.	I-155
Drehmel, Dennis C.	II-383, III-219, III-367 III-405, III-441, IV-47
Dybdahl, Arthur W.	IV-347
Edgar, Thomas F.	II-297
Elder, J. A.	IV-159
Ellenbecker, Michael	II-11
Engelbrecht, Heinz L.	I-57
Ensor, David S.	III-179, IV-141
Evans, John S.	IV-85
Faulkner, George	II-219
Fedarko, William	III-395
Feldman, Paul L.	I-253, III-417
Felix, Larry G.	III-311
Finney, Wright C.	I-287
First, Melvin W.	II-11
Fisher, Gerald L.	IV-433
Frederick, Edward R.	II-27

AUTHOR NAME	PAGE
Fuller, R. A.	IV-319
Furlong, Dale A.	II-247
Gandhi, Kumud	II-89
Garrett, Neil E.	IV-175
Gatti, Arno	III-395
Geffken, John	III-471
Gelfand, Peter	II-247
Gibson, Dwight D.	II-11
Giles, Walter B.	III-291
Gillette, Dale A.	IV-11
Goldfield, Joseph	II-89
Gooch, John P.	I-1, I-39
Gooding, Charles H.	III-219, IV-47
Goren, Simon L.	III-459
Gray, E.	IV-159
Greiner, Gary P.	II-233
Guthner, Gerhard O.	II-333
Guillory, J. L.	III-471
Gutfinger, Chaim	III-243
Gutierrez, Gilbert T.	III-99
Hall, Fred D.	II-287
Harmon, D. L.	III-47, III-193, IV-307
Hart, W. H.	IV-337

AUTHOR NAME	PAGE
Hoenig, Stuart A.	IV-105
Horie, Yuji	IV-391
Hudson, J. A.	II-161
Huisingh, Joellen L.	IV-175
Iinoya, Koichi	II-1, II-99
Isahaya, Fumio	I-453
Ito, Shijo	I-485
Ito, Ryozo	I-297
Kahane, Ronald B.	I-349
Kearns, Michael T.	III-73
Kiang, C. S.	IV-187
Klemm, Hans A.	II-143
Klett, Michael G.	III-379
Knox, Charles	II-133
Kober, Alfred E.	I-113
Kohama, Hiroyuki	III-351
Kousaka, Yasuo	IV-195, IV-231, IV-249
Lace, Robert H.	III-35
Ladd, Kenneth L.	II-219
Laskey, J. W.	IV-159
Lederman, Peter B.	I-79
Lefkowitz, Leonard R.	II-75
Leith, David	II-11

AUTHOR NAME	PAGE
Liscomb, Bill	II-53
Lutz, Stephen J.	II-111
Maartmann, Sten	I-25
Marchant, G. H.	I-39
Markowski, Gregory R.	III-179
Masuda, Senichi	I-241, I-321, II-309
McCain, Joseph D.	III-85, III-311
McCreight, Louis R.	III-395
McDonald, Jack R.	I-307, I-335
McIlvanine, Robert W.	II-319
McKenna, John D.	II-233
McLean, Kenneth J.	I-349, I-409
Meek, Richard L.	IV-465
Melville, B.	II-183
Merritt, Randy L.	III-311
Middleton, Paulette	IV-187
Milde, Helmut I.	I-253
Montgomery, Thomas L.	IV-261
Mori, Yasushige	II-99
Murray, Joel	II-133
Muzio, L. J.	I-131
Mycock, John C.	II-263
Nader, John S.	IV-289

AUTHOR NAME	PAGE
Negrea, Stefan	II-361
Nichols, Grady B.	IV-465
Noso, Shigeyuki	I-485
Okuyama, K.	IV-195, IV-231, IV-249
Ortino, Leonard J.	III-341
Osborn, D. A.	I-179
Osborne, J. Michael	II-197
Ostop, Ronald L.	II-247
Pace, Thompson G.	IV-403
Parker, Richard D.	I-169, III-367
Patten, Whitney	I-421
Patterson, Edward M.	IV-11
Patterson, Ronald G.	I-169, III-405, IV-307
Paul, Phillip H.	III-279
Petersen, Hoegh H.	I-99
Phillips, K. E.	III-471
Piispanen, William	III-303
Pilat, Michael J.	III-61
Piulle, Walter V.	III-323
Pontius, D. H.	I-275, I-361
Pressey, Robert E.	I-179
Pueschel, Rudolf F.	IV-1
Quinn, Margaret	IV-85

AUTHOR NAME	PAGE
Raemhild, Gary A.	III-61
Ramsey, Geddes H.	III-161
Record, Frank A.	IV-377
Rehnberg, Georgia L.	IV-159
Richard, George	IV-25
Riersgard, Phillip	I-169, IV-307
Riley, Clyde E.	I-497
Robinson, Myron	III-415, III-417
Roe, Sheldon F.	III-35
Rolschau, David W.	II-211
Rosales, L. A.	III-113
Rudinger, G.	III-233
Rugg, Don	I-421
Russell, Phillip A.	IV-357
Safriet, Dallas W.	IV-25
Sakai, Kiyoshi	I-485
Sakai, Masakazy	I-485
Sasaki, K.	III-351
Sato, K.	III-351
Sawyer, Charles J.	II-287
Schaeffer, Stratton C.	IV-457
Schliesser, Steven P.	I-205
Schneider, Maria	IV-85

AUTHOR NAME	PAGE
Schoeck, Vincent	II-133
Scholz, Paul D.	III-279
Shackleton, Michael A.	III-441
Shah, N. D.	I-131
Shaw, David T.	III-233
Shortell, Verne	III-303
Smith, Wallace B.	I-361
Sparks, Leslie E.	I-39, I-169, I-275 I-307, I-335 II-297 III-1, III-149, III-162 III-193, IV-417
Spencer, Herbert W.	I-381
Sumi, K.	IV-195, IV-231
Takimoto, Ken	I-297
Tardos, Gabriel I.	III-243
Teixeira, D. P.	I-131
Teller, Aaron J.	II-119
Tennyson, Richard P.	III-35
Throgmorton, James A.	IV-403
Trainer, M. N.	IV-337
Trenholm, Andrew R.	I-497
Trijonis, John C.	IV-391
Turner, James H.	II-45
Tsao, Keh C.	IV-441
Turley, C. David	IV-131

AUTHOR NAME	PAGE
Turton, C. F.	III-99
Wang, James	IV-319
Wang, Roa-Ling	IV-213
Watanabe, S.	III-351
Waters, Michael D.	IV-175
Weant, George E.	IV-63
Webb, Paul R.	I-497
Wegrzyn, J.	III-233
Wertheimer, Alan L.	IV-337
Williams, Roger L.	I-19
Woffinden, George J.	III-179
Yoshida, T.	IV-195, IV-231, IV-249
Yung, Kuang T.	IV-441
Yung, Shui-Chow	III-47, III-149, III-405

FUGITIVE SULFUR IN COAL-FIRED POWER PLANT PLUMES

Rudolf F. Pueschel
Atmospheric Physics and Chemistry Laboratory
National Oceanic and Atmospheric Administration
Boulder, Co. 80303

ABSTRACT

Plume aerosols were collected at distances between 0 and 80 km downwind from the stacks of the Four Corners Power Plant with a 10-stage cascade quartz crystal microbalance and on nuclepore membrane filters. In the diameter range 0.05 μm < D < 12 μm the aerosol mass distribution is multimodal. The accumulation mode at 0.8 μm particle diameter is present at all times and does not vary systematically with plume travel. The condensation mode at 0.1 μm diameter increases with travel distance due to the formation of a secondary sulfate aerosol by a gas-to-particle conversion mechanism of initially 7×10^4 μg m^{-3} of SO_2. The acquisition mode at D > 1.0 μm decreases due to fall-out and dispersion of the primary aerosol of an initial mass loading of about 800 μg m^{-3}. Associated measurements of particle shape and elemental composition by scanning electron microscopy and X-ray energy dispersive analysis show that the primary aerosol is siliceous fly ash that has scavenged 16 μg m^{-3} of particulate sulfur.

INTRODUCTION

Among the pollutants that are formed during coal combustion and that have been identified as having detrimental environmental effects are the various oxidation products of sulfur. The emissions of the Four Corners Power Plant near Farmington, N.M. include 3.2×10^5 kg day^{-1} of SO_2 and 8.0×10^4 kg day^{-1} of particulates at a coal combustion rate of 25.1×10^6 kg day^{-1} resulting in an average energy production of 1590 megawatts (Arizona Public Service[1]).

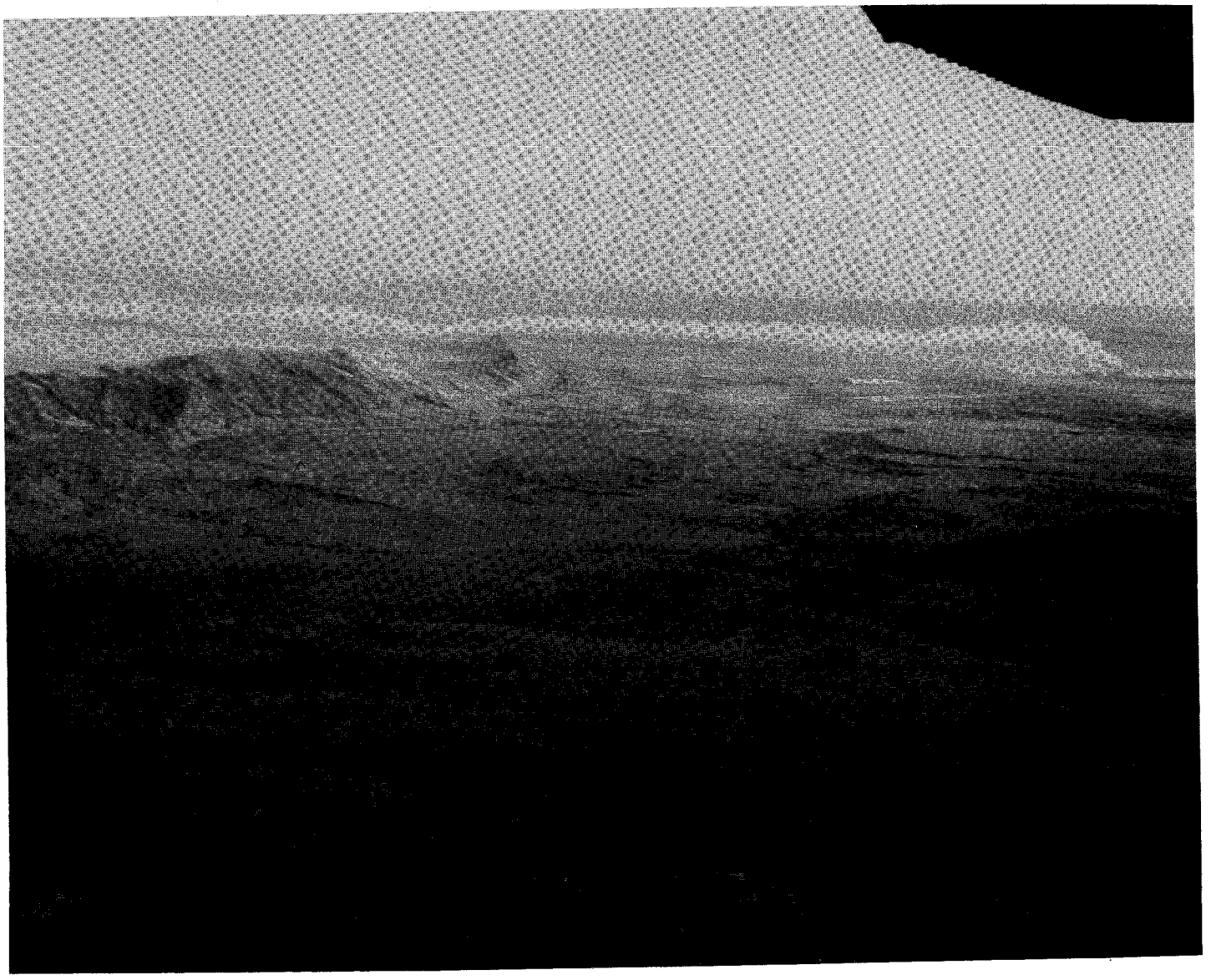

Figure 1: Visual appearance of the Four Corners Power Plant plume within about 12 km from the stacks at the temperature inversion level.

Past research in the plume of the Four Corners Power Plant has demstrated that:

1. The primary aerosol consists predominantly of siliceous fly ash, 2% of the mass of which consists of sulfur or sulfates in particulate form that is deposited on the surface of the fly ash particles (Parungo et al.[2], Pueschel[3]).

2. By far the largest portion of sulfur compounds is emitted as sulfur dioxide, the effects of which extend over hundreds of kilometers and tens of hours due to a slow conversion rate to particulate sulfates. (Pueschel and Van Valin[4]).

These findings are substantiated by the results of *in situ* particle mass analysis with a ten stage quartz crystal microbalance (Chuan[5]). In addition, the aerosol mass measurements permit an estimate of the amount of sulfur that is being emitted in solid form in the stack gases. It turns out that this is a negligibly small amount of the total sulfur that is being emitted. It follows from these results that (a) fly ash is a very poor scavenger for sulfur and (b) control strategy must concentrate on the reduction of emission of gaseous sulfur dioxide if detrimental effects are to be avoided.

EXPERIMENTAL

A Rockwell Aerocommander Model 680E twin-engine aircraft has been equipped with the instruments listed in Table 1. Sampling was conducted in the plume of the Four Corners Power Plant near Farmington, N. M., between 0 and 80 km from the stacks. Fig. 1 shows the plume in a typical situation of drainage flow to the northwest down the San Juan river valley.

Aerosols were collected on Nuclepore^{R} membrane filters at different distances from the stacks. The filters were exposed to controlled airflow for predetermined time intervals and brought back to our Boulder laboratory for electron microscopic and X-ray energy dispersive analysis of the filter deposits. Direct observation of the particles in a scanning electron microscope interfaced with an X-ray energy dispersive spectrometer gave additional information on the elemental composition of the particles as function of particle size, and of the distribution of elements in relation to the particle's dimension (Fig. 2).

During February 1975, in addition to the equipment listed in Table 1, a quartz crystal microbalance was used to measure *in situ* the distribution of aerosol mass as a function of particle size. In the following discussion we relate the results of these aerosol mass measurements to findings on elemental composition of plume aerosols in order to (1) estimate the amount of particulate versus gaseous sulfur that is being emitted by the power plant and (2) postulate a mechanism of aerosol formation by the conversion of gaseous-to-particulate sulfur.

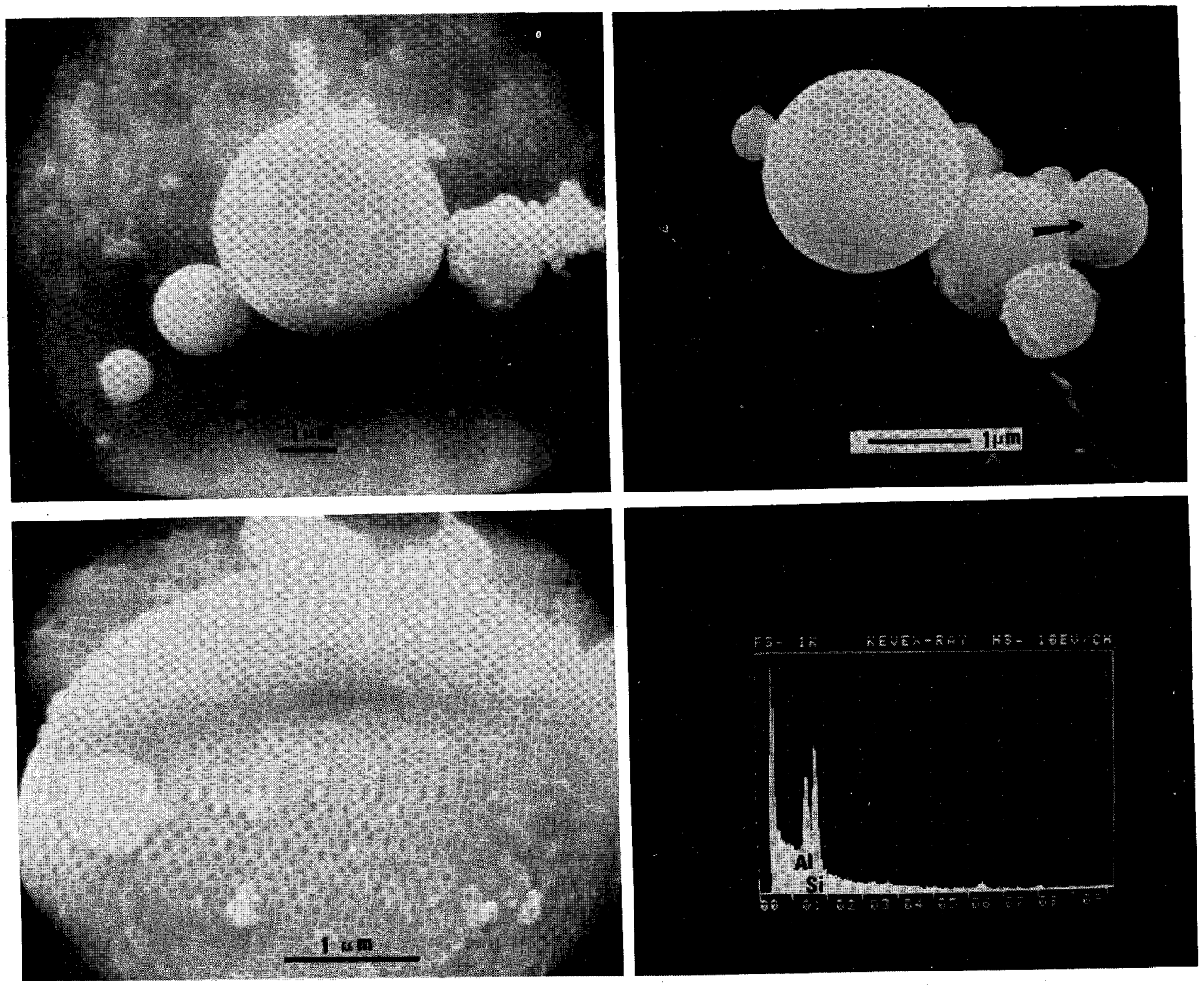

Figure 2. Typical shape and elemental composition of fly ash in the plume of a coal-fired power plant.

RESULTS AND DISCUSSION

Figure 3 shows four aerosol mass distributions as measured with the 10-stage quartz crystal microbalance at distances between 0 and 80 km downwind from the stacks. It follows from Fig. 3 that at 0 miles distance the aerosol mass distribution is multi-modal with a major mode at 0.8 μm and secondary modes at 12 μm, 3.0 μm and 0.1 μm. At 24 to 48 km (15-30 miles) downwind from the stacks, corresponding to 3-6 hours residence time at an average wind speed of 5 miles $hour^{-1}$, the 12 μm mode has disappeared, most likely due to settling. (The terminal velocity of a fly ash particle of 12 μm diameter and with a density of 2 g cm^{-3} is 14 cm sec^{-1}. Therefore, it takes about 0.6 hours to travel the distance of 300 meters, the maximum height of the plume that was observed.)

It further follows from Fig. 3 that during an atmospheric residence time of 3-5 hours, a distinct mode at 0.1 μm diameter has developed, which was virtually absent at 0 miles distance. As we go further downwind in the plume, the mass at the 0.1 μm mode increases while at the same time the mass at the modes $D > 1.0$ μm decreases. The mode of $D \approx 0.8$ μm does not change significantly.

The results in Fig. 3 substantiate the presently accepted notions about the dynamic behavior of atmospheric aerosols (Whitby[6]): The aerosol mass distribution is characterized by several modes which, from small to large sizes, are called the condensation mode, the accumulation mode, and acquisition modes. In the Four Corners Power Plant plume, the acquisition modes typically consist of primary fly ash and disappear with time due to the combined effects of settling and dispersion. Simultaneously, the condensation mode increases with time due to secondary aerosol formation by a gas-to-particle conversion mechanism.

Studies of the fly ash aerosols by scanning electron microscopy and X-ray energy spectrometry have shown that about 60% by number of the fly ash aerosol contain sulfur (Parungo et al.[2]) and that the solid sulfur compound is concentrated on the fly ash particle's surface (Pueschel[3], Parungo et al.[2]) Parungo et al.[2] showed that about 2% by mass of the fly ash aerosol contained S in the form in Na_2SO_4 and $CaSO_4$. In conjunction with the data in Fig. 3 one can calculate that the total mass of sulfur compounds that is emitted by the stacks in solid form amounts to about 16 μg m^{-3}. This is only 0.02 percent of the amount of sulfur that is being emitted at SO_2; thirteen measurements conducted between October 1975 and October 1976 showed average SO_2 concentration in the stack gases of 7.7×10^4 μg m^{-3} (Pueschel and Van Valin[4]), in good agreement with the emission data provided by Arizona Public Service[1]. It has been shown by the same authors that due to a small conversion rate of SO_2 to sulfates of a few percent per hour, a secondary particle formation takes place over distances of several hundred kilometers, or times of tens of hours.

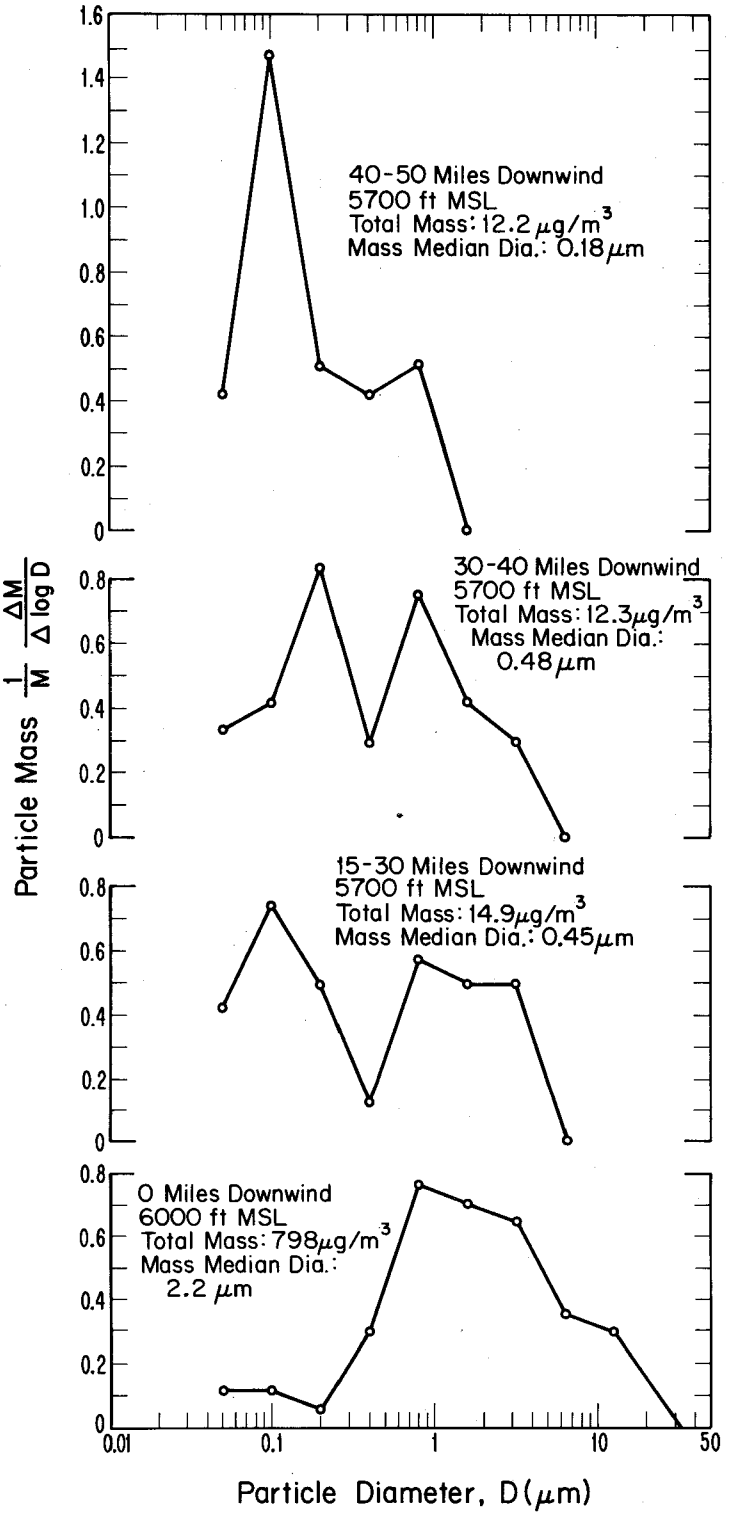

Figure 3. Aerosol mass distributions as function of particle size at various distances downwind from the stacks in the plume of the Four Corners Power Plant.

SUMMARY AND CONCLUSIONS

The coal-fired Four Corners Power Plant near Farmington, N. M. emits sulfur in both particulate and gaseous forms. The particulate emissions result in the concentration of sulfates in the stack gases of only 16 $\mu g\ m^{-3}$. Although of small magnitude, this mass of water soluble sulfate is deposited on the surface of initially water-insoluble fly ash particles. Minute amounts of water soluble materials are required to increase the hygroscopicity, hence, the cloud nucleating capibility, of fly ash particles through this mechanism (Junge and McKlaren[7], Pueschel[3]).

Of still greater environmental consequence are the tens of thousands of micrograms per cubic meter of sulfur dioxide which are found in the stack gases. Slow conversion rates of SO_2 to sulfates and long residence times of small sulfate aerosols result in effects that are spread over hundreds to thousands of square miles.

There is no basis for an argument that postulates the efficiency of fly ash as a scavenger for fugitive sulfur. Emission control technologies must concentrate on SO_2 removal if a build up of sulfate concentration in the atmosphere is to be avoided.

ACKNOWLEDGMENTS

It is a pleasure to thank Dennis Wellman and Dick Proulx for installing and operating the aircraft equipment and Helen Proulx for the micro-physical and micro-chemical aerosol analyses. The aerosol mass measurements were performed by Dr. Ray Chuan, Celesco Instruments under contract No. 05-6-022-51682. The work as a whole was supported by EPA under Interagency Agreement No. D5-E693.

REFERENCES

1. Arizona Public Service. Four Corners Power Generating Plant and Navajo Coal Mine, Environmental Report, 1975.

2. Parungo, F. P., E. Ackerman, H. Proulx, R. Pueschel. Nucleation Properties of Fly Ash in a Coal-Fired Power Plant Plume, Atmos. Env. 12, 929-935, 1978.

3. Pueschel, R. F. Aerosol Formation During Coal Combustion: Condensation of Sulfates and Chlorides on Fly Ash, Geophys. Res. Let. 3, 651-653, 1976.

4. Pueschel, R. F. and C. C. Van Valin. Cloud Nucleus Formation in a Power Plant Plume, Atmos. Env. 12, 307-312, 1978.

Table 1. EQUIPMENT INSTALLED IN AIRCRAFT TO STUDY THE ENVIRONMENTAL IMPACT OF POWER PLANT OPERATIONS.

PARAMETER	METHOD	INSTRUMENT MANUFACTURER/MODEL	TYPICAL OPERATING RANGE	MINIMUM DETECTABLE CONCENTRATION
Cloud Condensation Nuclei	Thermal Diffusion Chamber Photography	NOAA	20-2000 cm^{-3}	20 cm^{-3}
Aitken Nuclei	Expansion Chamber	Environment-one/RICH 100 Gardner/7000 4 G 2	300 to 10^7 cm^{-3}	1 x 10^2 cm^{-3}
Light Scattering Coefficient	Integrating Nephelometer	MRI 1550	0 - 10 x $10^{-4}m^{-1}$	.15 x $10^{-4}m^{-1}$
Temperature	Platinum resistance	Rosemount 102 AN 1 AF	-40°C to +40°C	
Relative Humidity	Thermoelectric dew point	GE 1011	-75°C to 50°C	
Ozone	Chemiluminescence	ML 8410	0 - 5 ppm	5.0 ppb
Nitrogen Oxide	Chemiluminescence	ML 8440	0 - 5 ppm	5.0 ppb
Nitrogen Dioxide	Chemiluminescence	ML 8440	0 - 5 ppm	5.0 ppb
Sulfur Dioxide	UV Pulsed Fluorescence	Teco 43	0 - 5 ppm	2.0 ppb
Aerosol Size	Aerosol Filtration Electron Microscopy	NOAA Sampler RCA TEM		5.0 cm^{-3}
Aerosol Composition	Aerosol Filtration Electron Microscopy X-ray Spectrometry	NOAA Sampler Coates & Welter SEM Kevex 5000		5.0 cm^{-3}
Ice Nuclei	Aerosol filtration	Thermal diffusion chamber, NCAR		.5 cm^{-3}
Aerosol Size Distribution	He-Ne laser light Scattering	Particle Measuring Systems ASASP-X, FSSP	0.08-50 μm	
Potential Gradient	Electric field mill	NOAA	0-10^6 volts/meter	1 volt/meter
Infrared Radiation	Bead thermistor	Barnes, PRT-5	-20 - +75 C	
Data Acquisition	Digital Processing	Particle Measuring Systems DAS 64		
	Magnetic tape recording	Pertec F6X9 formatter Pertec T7640 transport		
	Digital printer	HP 5055A		
	Analog recording	Gulton tmd 840/S-1289		

5. Chuan, R. L. Particulate Mass Measurement by Piezoelectric Crystal, Aerosol Measurements, NBS Special Publication 412, U. S. Dept. of Commerce, 137-148, 1974.

6. Whitby, K.T. Modeling of Atmospheric Aerosol Particle Size Distributions, Progress Report on EPA Research Grant # R800971, 1975.

7. Junge, C. and E. McLaren. Relationship of Cloud Nuclei Spectra to Aerosol Size Distribution and Composition, Jour. Atmos. Sci. 28, 382-390, April 1971.

RESEARCH IN WIND-GENERATED FUGITIVE DUST

Dale A. Gillette and Edward M. Patterson
National Center for Atmospheric Research*
Boulder, Colorado 80307

ABSTRACT

Research on wind generated fugitive dust is summarized. Fast-response instrumentation has allowed us to elucidate transport mechanisms and to arrive at an estimate of a depositional velocity for fine dust. Measurements of vertical fluxes of fugitive dust generated by wind are related to soil conditions. A wind tunnel simulation of of dust generation is described in which wind speed, soil textures, soil coherence, and sand influx were varied.

We have also related measured dust concentrations to the optical effects of the dust. Observations of prevailing visibility have been used to verify simultaneous aerosol size-distribution measurements during dust storm conditions. A number of different size-distribution observations for soil-derived aerosols are compared; commonalities in the distributions are described and differences are related to differing measurement conditions. Mass concentrations for the dust aerosols have been related to visibility reductions.

INTRODUCTION

Fugitive dust generated by wind has been recognized as an important air pollutant and one that may be difficult to deal with. The Council on Environmental Quality lists 33 major cities in 14 states for which air quality standards cannot be met because of soil erosion

*The National Center for Atmospheric Research is sponsored by the National Science Foundation.

particulates from desert, farm fields, unpaved roads, and construction areas (Kimberlin et al., 1976). The effects of atmospheric dust include loss of visibility leading to safety problems on highways (Patterson et al., 1976); health hazards, especially to the respiratory system (Fuchs, 1964); closing of normal business; and reduction of property values and income.

Research at the National Center for Atmospheric Research may be helpful in some of the problems of wind-generated fugitive dust. We will briefly describe our research efforts on the generation of fugitive dust, the size distributions of windborne dust, and the optical properties of windborne dust.

Threshold Velocities for Wind-Generated Fugitive Dust

The wind speed at which generation of dust begins is that for which aerodynamic forces are sufficient to overcome those forces holding individual particles in the soil. A number of theoretical and experimental studies have been made for idealized particle systems, (see, for example, Punjrath and Heldman, 1972; Iverson et al., 1976; Bagnold, 1941; Chepil, 1951; and Greeley et al., 1973). These studies have not considered natural soil surfaces, however, nor man's impact upon soil surfaces and aggregate storage. Gillette et al. (in preparation) measured threshold velocities on dry soils which were in both undisturbed and disturbed condition. The disturbance was a pulverization of the surface by the wheels of a 3/4 ton pickup truck. A table of priority of threshold velocities versus soil types follows.

Table 1. WIND SPEED FOR INITIATION OF DUST PRODUCTION vs UNDISTURBED OR DISTURBED SOIL TYPE

Increasing Wind Speed	1. Disturbed soils having less than 50% clay and less than 20% pebble (< 1 cm diameter) cover.
	2. Tilled bare sandy soils.
	3. Disturbed pebbly soils.
	4. Bare clay soils have been disaggrgated by natural forces.
	5. Disturbed soils having a high salt content or more than 50% clay.
	6. Undisturbed sandy soils having a crust and soils covered with fine gravel.

7. Undisturbed soils having more than 50% clay and surface crusts and salt crusted soils.

8. Soils covered by coarse (> 5 cm pebbles).

The above ordering of threshold velocities suggests that the threshold velocity is determined by the availability of loose erodible sand-sized particles at the surface and that the threshold velocity is increased (erosion decreased) by the effect of aerodynamic partitioning of wind stress by nonerodible elements such as pebbles and larger objects and by the cementation of the soil by clay and salts.

Marshall (1971) studied the effect of pebble-like nonerodible elements in absorption of wind stress. He found that for a configuration in which the silhouette area of the nonerodible roughness element per floor area per element (L_c) was greater than 0.1, most of the wind momentum was absorbed by the elements and little stress was available for movement of fine particles lying between nonerodible elements. Lyles and Allison (1976), studying the threshold velocity of sand between nonerodible dowel rods, found a similar effect for $L_c > 0.1$. Thus, it would seem that even a relatively sparse pebble, brush or boulder cover will give a large amount of protection from fugitive dust production by the wind.

A wind tunnel experiment by Gillette (1978) investigated the effects of wind and sandblasting on consolidated and unconsolidated samples of six different dry soil textures. Surface crusts had the effect of raising threshold velocities to values beyond the wind tunnel range. Sand blasting with spherical glass beads was sufficient to break the surface crust of the samples that had surface textures of fine sand and loamy fine sand; erosion was initiated within a few minutes of exposure. The surface crust samples having finer surface textures were not disintegrated by sandblasting in the wind tunnel exposures (10 min at a friction velocity of about 100 cm s^{-1}). Threshold velocities of the loose soil samples varied, with sandy and powdery soils eroding at lower velocities than soils having some remaining aggregation.

Bisal and Ferguson (1970) investigated the effect of nonerodible aggregates on threshold wind velocity (in this case wind velocity at 30.5 cm above the soil surface). Their empirical relationship was

$$\ln V_T = 6.0438 + 0.02332\ C$$

where V_T is the threshold velocity in cm s^{-1} at 30.5 cm, and C is the percentage of soil mass in a sample in aggregates larger than 1 mm. On the basis of analysis, we believe that the effect observed

by Bisal and Ferguson is a result not of the partitioning of momentum by nonerodible elements but of increased soil cohesion, which requires larger wind forces for the onset of wind erosion.

Since finer textured soils in general tend to have more stable large soil aggregates, we would expect finer soil textures to correlate with higher threshold velocities. Mineralogical effects such as the cracking and breakage of montmorillonitic clays would tend to reduce aggregate size and reduce threshold velocity, however.

The Transport of Dust into the Air

Sand-sized particles are important in wind input of fugitive dust since their availability as loose individual particles largely determines the threshold velocity of erosion and since they carry most of the mass of moving soil near the ground, acting as sandblasters of the surface. However, only a few centimeters above the surface the concentration of sand decreases greatly (Gillette and Goodman, 1974) and the sand is not transported very far compared to dust smaller than 20 μm (Gillette, 1977).

The production of dust smaller than 20 μm and the total soil movement of a number of soil textures under natural conditions are shown in Fig. 1. In the figure, F_a' is the vertical flux of particles smaller than 20 μm, q is the horizontal flux of all particles moving with the wind up to an infinite height, q' is the horizontal flux of all particles moving with the wind up to a height of 76 cm[1] and F_a'/q' is the ratio of vertical flux of fine particles to measured total movement of soil. The soil textures are shown on the figure. Total particle flux for all soil textures asymptotically approaches a friction velocity cubed (u_*^3) law first proposed by Bagnold (sand flux varies as the friction velocity cubed). The fine ($d < 20$ μm) particle flux is more variable. In the plot of F_a'/a' it is shown that for sandy loam soils an increasing part of total soil movement is fine particle movement as the wind speed increases. In general, soils having finer textures produced more fine dust for unit soil movement except fine-textured soils whose mineral components formed small aggregates that were hard enough to resist impact breakage at mean wind speeds up to 25 m s^{-1}. Fine particles are generated by breakage of soil aggregates or by the splashing of loose fine material by saltating sand grains (Gillette and Walker, 1977).

Gillette and Porch (1978) used fast-response instrumentation to resolve fluctuations of the vertical wind speed, horizontal wind

[1]A method of calculating total soil movement for individual soils is given by Gillette, 1978.

speed, and aerosol concentration of a portion of the fine airborne particles during a wind erosion episode in a farm field. Each of the above quantities was reduced by the average value and divided by the standard deviation of that quantity. The three-dimensional probability distribution for these fluctuations so altered is schematically shown in Fig. 2 for emission of dust into the air. Although fluctuations appear in all octants of the probability distribution, the dominating octants for this case when particles are being transported upward are: (1) negative horizontal wind, negative vertical wind, negative concentration fluctuation, and (2) positive horizontal wind, positive vertical wind, positive concentration. Physically, this corresponds to downward moving clean air during slow horizontal wind periods and upward moving dirty air during faster horizontal wind periods.

By using the fast response data, Porch and Gillette (1978) calculated a depositional velocity (V_o) for fine dust generated by wind of

$$V_o = 0.04\ U*$$

where $U*$ is the friction velocity of the wind. Thus the settled dust rate (fugirate) for an area not far from a source of fugitive dust would be

$$\text{fugirate} = C\ V_o$$

where C is the mean concentration of dust measured at the location of interest.

Size Distributions for Fugitive Dust

Soil-derived aerosols are an important component of the total atmospheric aerosol burden; but perhaps for no other aerosol component is there as much variation in reported results of size distribution measurements. Reported size distributions range from those in which the significant particles have radii between 20 and 50 μm on a volume distribution plot (Chepil, 1957; Slinn, 1975) to those in which the optically important particles are smaller than 0.1 μm in radius (Kondratyev, 1973).

We have measured size distributions for these aerosols under a variety of conditions, ranging from cases of heavy aerosol loading in the atmosphere, with a consequent reduction in visibility, to cases of very light loading of aerosols, with very high visibilities. These measurements show certain similarities primarily in a common mode structure, with differences in the relative importance of the modes that can be related to differences in the experimental conditions. We have also compared some of our representative results with other measurements of size distributions that were taken under comparable

conditions and has been able to make some generalizations on the important components of the aerosol size distributions for soil-derived aerosols under varying experimental conditions. In general, the NCAR measurements have been made using a combination of electron microscope analyses of samples collected onto nuclepore filters and gravemetric analysis on Bagnold catcher samples. Measurement procedures have been discussed by Gillette and Goodwin (1974) and Patterson et al. (1976). Simultaneous visibility measurements were used to verify our size distributions obtained by these methods during several incidences of soil erosion. The visibility measurements, reported by Patterson et al. (1976), showed that in these incidences of erosion the actual size distribution of the aerosol did not differ from our measured size distribution in any significant way. In our analysis procedure, the measured size distributions are converted to the form of dN/d(log r) distributions, which are then fitted to multi-model log-normal distributions. A typical measured size distribution (from Patterson and Gillette, 1976b), taken under conditions of reduced visibility, is shown as the solid line in Fig. 3; at the time of the measurement, the observed visibility was approximately 8 km. This size distribution is characterized by the presence of two modes: (1) Mode A, centered between 1 μm and 10 μm on the dV/d log r plot; (2) Mode B, centered between 10 μm and 50 μm in radium.

Mode A is derived from the soil by a process of sandblasting (Gillette and Walker, 1977) and appears to be a characteristic mode that is generally seen in measurements of the size distribution of soil-derived aerosols (Patterson and Gillette, 1977b); Mode B appears to be characteristic of the soil from which the aerosol is derived. Because of the relatively large settling velocity of the Mode B particles, this mode is significant only in the source region for aerosols; in addition, the concentration of these particles shows a rapid decrease with altitude. Under the conditions of relatively heavy dust-aerosol loading (mass concentration approximately 2×10^{3} gm/m^{3}) in which this size distribution was measured, a mode corresponding to the accumulation mode discussed (for example, by Willeke et al., 1974) was not seen, even though the size distribution was based on measurements of particles as small as 0.1 μm in radius.

By comparison, the size distribution shown as the dashed line in Fig. 3 does show a mode, Mode C, that may be identified with the accumulation mode. This size distribution of low concentration was measured under conditions of only slightly reduced visiblity; the visual range calculated from the distribution is approximately 60 km. Mode C does not appear to consist of fugitive dust, so the properties of this dust will be determined by Modes A and B.

Optical Properties of Fugitive Dust

A series of measurements of the optical properties of dust aerosols have been reported in Patterson et al. (1977). The real refractive index is known to be approximately 1.5; the imaginary index of refraction, a measure of the absorption properties of the aerosol, shows more variation with wavelength and with variation in aerosol composition. The imaginary index of refraction for two Denver aerosol samples dominated by dust aerosol is shown in Fig. 4 (Patterson 1978). The lower curve is a typical absorption curve for soil derived aerosols. The upper curve shows increased absorption more typical of urban areas, probably due to the inclusion of carbon in the sample. We have shown (Patterson et al., 1976) that differences in absorption such as those shown in Fig. 4 will have little effect on particle extinction due to particles in the size range of the dust particles (Modes A and B in Fig. 3). Properties calculated for soil aerosols in rural areas, then, will also be applicable to dust generated in urban areas, even if the absorption of the urban dust is higher. In particular, relations between mass and visibility and the relative extinction with wavelength will not be sensitive to such variation in the absorptive properties of the aerosol.

Relation Between Mass Concentration and Visibility

The relation between visibility and mass concentration of aerosols in the atmosphere is of interest because regulatory standards are generally written in terms of mass concentrations while the most notable effect of an aerosol, at least to the average citizen, is in its optical effect, i.e. the reduction in visibility. The visibility is related to the extinction due to aerosols by the Koschmieder relation

$$V = \frac{3.912}{\text{ext}}$$

For a given size distribution, the ratio of mass concentration to total extinction is a constant, so that we would expect that the product of the visual range and the mass concentration will be constant for constant size distributions

$$M\,V = C$$

Based on our observations we have calculated values of the constant C relating mass concentration and visibility for several cases similar to that of our high concentration case in Fig. 3 (Patterson and Gillette, 1977a). We found that the measured values for C were approximately 2×10^{-2} g m^{-c} km. If the mode A only were considered, the value of C decreased to approximately 1×10^{-2} g m^{-3} km, a condition that might be expected when the dust concentrations are relatively

small. These values may be compared to a value of C equal to approximately 6 x 10^{-2} g m^{-3} km measured by Chepil and Woodruff (1957) under drought conditions on the Great Plains and values of 2 x 10^{-3} for urban conditions reported by Charlson (1969) for urban conditions in which the aerosol loading would be expected to be dominated by particles in the size range of Mode C. Details of the study may be found in Patterson and Gillette (1977a). Further calculations shown in Fig. 5 for particles in the size range of our Modes A and B show that the extinction for these particles is not strongly dependent on wavelength (Patterson, 1977). The implication of this study is that measurements of the optical extinction of dust aerosols may be made at convenient laser wavelengths, such as eyesafe wavelengths in the near infrared, with results that will be approximately the same as those visually at 0.55 μm, the wavelength of peak sensitivity of the eye in photopic vision.

REFERENCES

Bagnold, R. A., 1941, The Physics of blown and sand and desert dunes, Methuen, London, 265 pp.

Bisal, F., and Ferguson, W., 1970, Effect of nonerodible aggregates and wheat stubble on initiation of soil drifting: Can. J. Soil Sci., 50, pp 31-34.

Charlson, R. J., 1969, Atmospheric visibility related to aerosol mass concentration: Environ. Sci. Technol. 3, 913-918.

Chepil, W. S., 1951, Properties of soil which influence wind erosion, 4, state of dry aggregate structure: Soil Sci., 72, pp 387-401.

Chepil, W. S., 1957, Sedimentary characteristics of dust storms, 3, Composition of suspended dust: Amer. J. Sci., 255, 206-213.

Chepil, W. S., and N. P. Woodruff, 1957, Sedimentary characteristics of dust storms, 2. Visibility and dust concentration: Amer. J. Sci., 255, 104-114.

Fuchs, N. A., 1964, The mechanics of aerosols, Pergamon Press, Oxford, 402 pp.

Gillette, D. A., and P. A. Goodwin, 1974, Microscale transport of sand-sized aggregates eroded by wind: J. Geophys. Res., 79, 4080-4084, 1974.

Gillette, D., 1977, Fine particulate emissions due to wind erosion: Transactions of the ASAE, 20, 890-897.

Gillette, D. A. and Walker, T. R., 1977, Characteristics of airborne particles produced by wind erosion of sandy soil, high plains of west Texas: Soil Sci., V. 123, No. 2, pp 97-110.

Gillette, D., 1978, A wind tunnel simulation of the erosion of soil: effect of soil texture, sandblasting, wind speed, and soil consolidation on dust production: Atmospheric Environment, in press.

Gillette, D. A. and Porch W., in preparation, The role of vertical and horizontal wind fluctuations in the production and transport of dust by wind erosion: to be submitted to J. Geophys. Res.

Gillette, D. A., J. Adams, A. Endo, D. Smith, in preparation, Threshold wind velocities for natural desert soil surfaces before and after disturbances by offroad vehicles.

Greeley, R., Iverson, J. D., Pollack, J. B., Udovich, N. and White, B., 1973, Wind tunnel studies of Martian aeolian processes: NASA Technical Memorandum 62, 297.

Hays, W., 1972, Designing wind erosion control systems in the midwest region: RT SCS-Agron Tech. Note LI-9, Soil Conserv. Serv., U.S.D.A., Lincoln, Nebraska.

Iversen, J. D., Pollack, J. B., Greeley, R., and White, B. R., 1976, Saltation threshold on Mars; the effect of interparticle force, surface roughness and low atmospheric density: Icarus, V. 29, pp 381-393.

Kimberlin, L. W., Hidlebaugh, A. L. and Grunewald, A. R., The wind erosion problem in the United States: submitted to Transactions of the ASAE.

Kondratyev, K. Ya., 1973: The complete atmospheric energetics experiment: Garp Publ. Ser. 12, 44 pp., World Meteorol. Organ./Int. Counc. of Sci. Unions, Geneva, 1973.

Lumley, J. L. and Panofsky, H. A., 1964, The structure of atmospheric turbulence: Wiley and Sons, New York, 239 pp.

Lyles, L. and Allison, B., 1976, Wind erosion: The protective role of simulated standing stubble: Trans. of the ASAE, V. 19, pp 61-64.

Marshall, J., 1971, Drag measurements in roughness arrays of varying density and distribution: Agr. Meteor., V. 8, pp 269-292.

Patterson, E., Gillette, D., and Grams, G., 1976, On the relation between visibility and the size-number distribution of airborne soil particles: J. Appl. Meteor., V. 15, pp 470-478.

Patterson, E. M., D. A. Gillette, and B. H. Stockton, 1977, Complex index of refraction for Saharan aerosols between 300 and 700 nm: J. Geophys. Res., 82, 3153-3160.

Patterson, E. M., 1977, Atmospheric extinction betwen 0.55 m and 10.6 m due to soil derived aerosols: Appl. Opt., 16, 2414.

Patterson, E. M. and D. A. Gillette, 1977a, Measurement of visibility vs mass concentration for airborne soil particles: Atm. Environ., 11, 193-196.

Patterson, E. M. and D. A. Gillette, 1977b, Commonalities in Measured Size Distributions for aerosols having a soil-derived component: J. Geophys. Res., 82, 2074-2082.

Patterson, E. M., 1978, Optical properties of urban aerosols containing carbonaceous materials: paper presented at the Conference on Carbonaceous aerosols March 20-22 1978, Berkeley, CA sponsored by the National Science Foundation and Lawrence Berkeley Laboratory.

Porch, W. M., and D. A. Gillette, 1978, A comparison of aerosol and momentum mixing in dust storms using fast-response instruments: J. Appl. Met., 16, 1273-1281.

Punjrath, J. S., and Heldman, D. R., 1972, Mechanisms of small particle reentrainment from flat surfaces: J. Aerosol Science, V. 3, pp 429-440.

Slinn, W. G. N., 1975, Atmospheric aerosol particles in surface level air: Atmos. Environ., 9, 763-764.

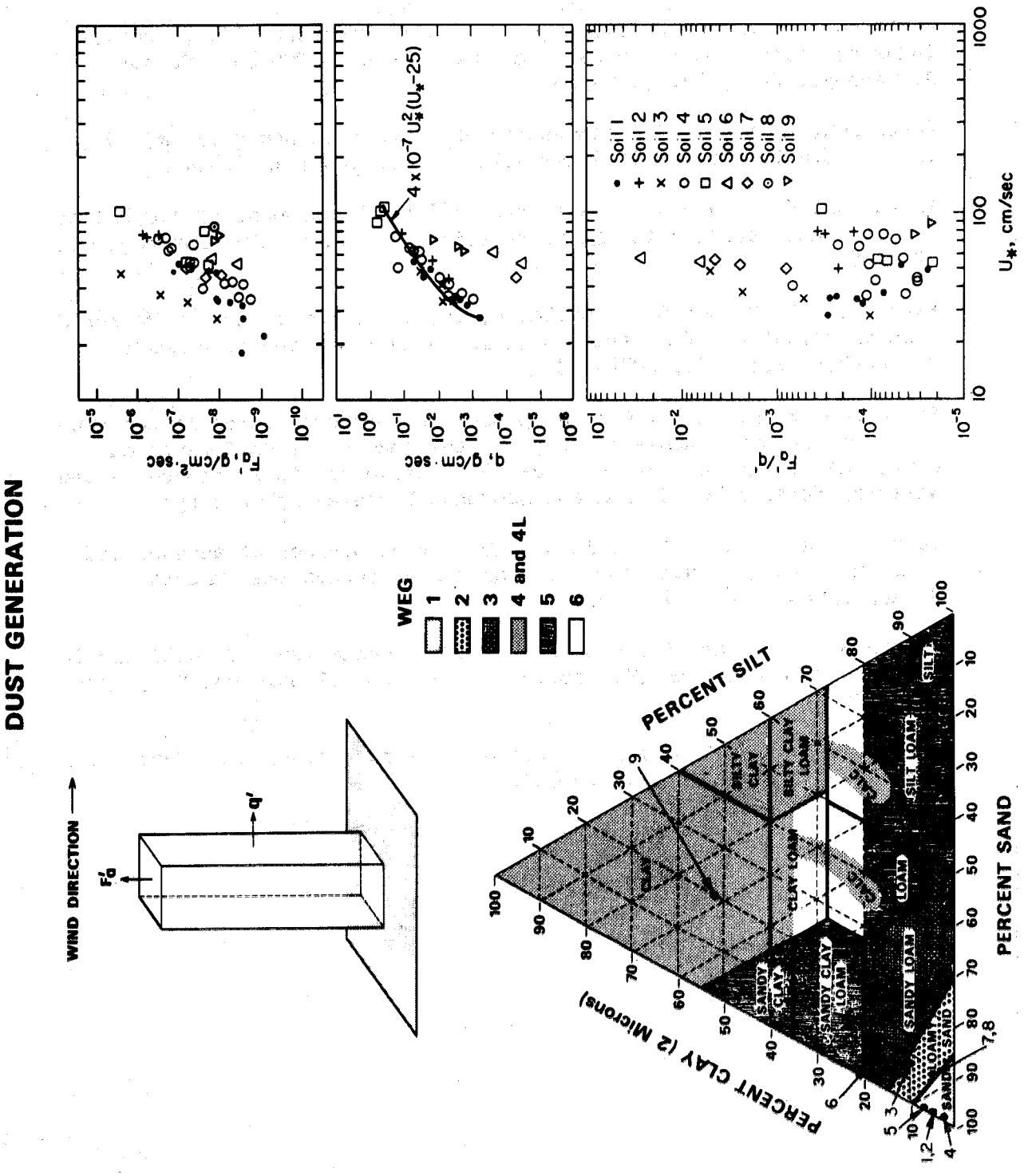

Figure 1. Textures of sampled soils; total soil movement vs wind friction velocity; vertical flux of particles smaller than 0.02 mm vs wind friction velocity; ratio of vertical flux of particles smaller than 0.02 mm to total soil movement per unit area per time versus wind friction velocity. After Gillette, 1977.

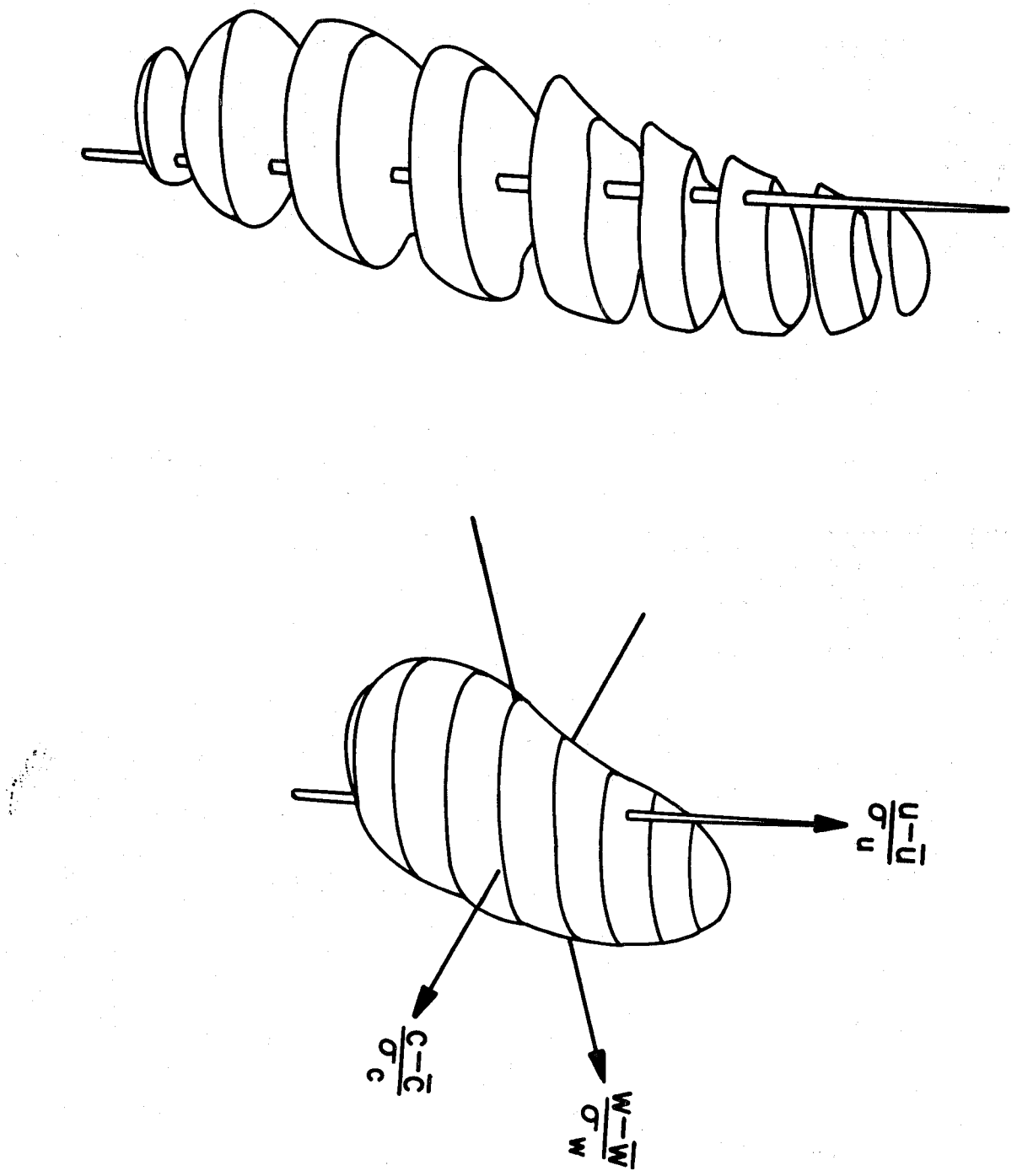

Figure 2. A schematic view of a three-dimensional probability distribution of vertical velocity wind fluctuations, particulate concentration, and horizontal wind speed fluctuations for a case in which dust is being emitted to the air. Each quantity has been reduced by its mean and that reduced quantity divided by its standard deviation. After Gillette and Porch, 1978.

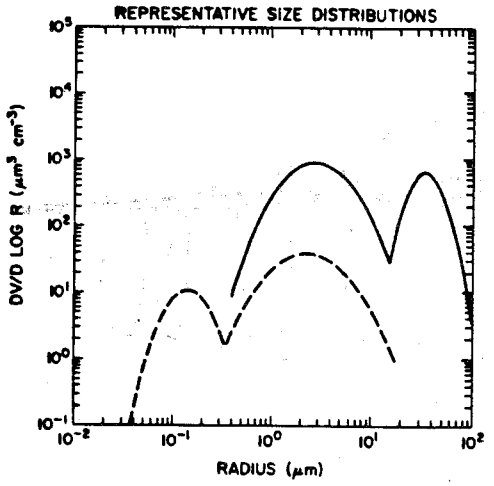

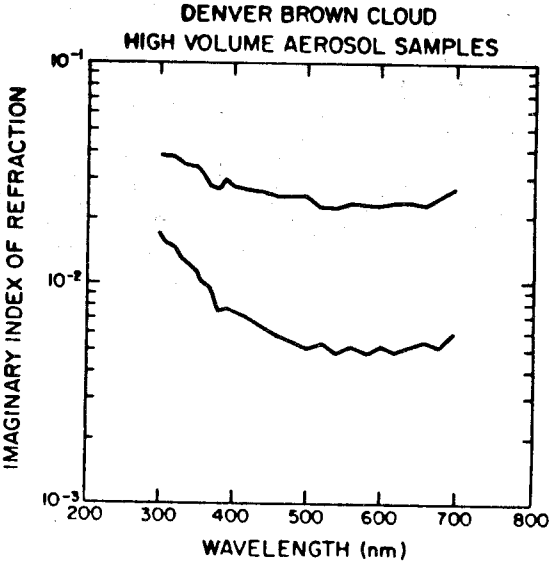

Figure 3. Typical measured aerosol size distributions. The solid line (____) represents a distribution measured under conditions of greatly reduced visibility (V = 8 km), while the dashed line (----) represents a size distribution of much lower total mass concentration measured under conditions of only slight visibility reduction. Mode A, between 1 μm and 10 μm, appears on both distributions. Mode B, between 10 μm and 100 μm radius, is seen only on the low visibility size distribution, and Mode C, between 0.1 μm and 1 μm, is seen only on the high visibility size distribution.

Figure 4. Imaginary index of refraction for two samples of Denver aerosol. The upper curve is the imaginary index for a sample containing a relatively large amount of a dark uniformly absorbing material; the lower curve is for a sample not containing this material.

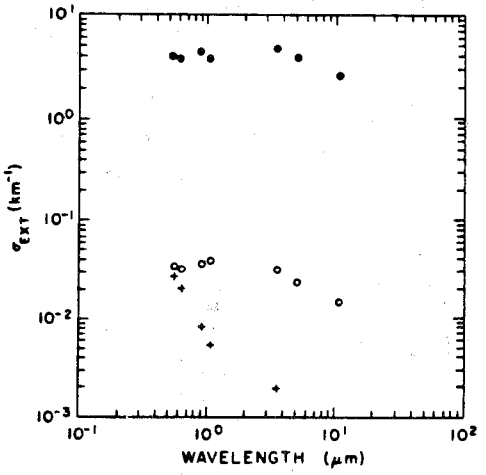

Figure 5. Values of extinction for laser wavelengths calculated for soil aerosols. The solid dots (●●●) show the extinction calculated on the basis of the typical high-concentration size distribution normalized to an extinction of 1 km at 0.55 μm. The relative values of extinction should be valid for visibility reductions below 20 km due to these aerosols. The open circles (ooo) show the extinction calculated for the soil-aerosol mode of the low concentration size distribution typical of high visibility (V > 50 km) conditions. Also shown are values of extinction calculated for the same wavelengths for sulfate aerosols characteristic of those if our Mode C (++++++).

DEVELOPING CONTROL STRATEGIES FOR FUGITIVE DUST SOURCES

George Richard
TRW Environmental Engineering
Redondo Beach, California 90278

Dallas Safriet
EPA Air Quality Planning & Standards
Durham, N. C. 27711

While considerable progress has been achieved in improving air quality in many areas, several states are experiencing problems in attaining the primary National Ambient Air Quality Standards for total suspended particulate matter (TSP). Despite the execution of State Implementation Plans (SIPs) and the associated imposition of numerous emission controls, TSP levels remain high in many regions. In most nonattainment areas, fugitive dust, a major source of TSP, had been neglected in the original air program planning. Evidence now suggests that TSP levels of almost all rural and urban areas are strongly influenced by fugitive dust sources, and states must now revise their SIP plans accordingly. To provide guidance in the development of control strategies for fugitive dust, the EPA office of Air Quality Planning and Standards contracted TRW for a pilot study to develop an attainment plan for TSP in the Phoenix area, and has incorporated the methodology of the Phoenix study into the EPA Guideline Series for general application to other areas troubled by fugitive dust.

The control strategy development procedure is divisible into four distinquishable and sequential elements: 1) evaluation of air quality data to determine the extent and nature of the TSP problem, 2) estimation of the magnitude and spatial distribution of emission sources, 3) development of an air quality simulation process to relate emissions to TSP levels, and 4) formulation and assessment of candidate control strategies for attaining the air quality standards.

AIR QUALITY ANALYSIS

An analysis of air quality data is conducted to define the extent and nature of the air pollution problem. In most areas, there are sufficient number of monitors to reveal the extent of the air pollution problem. Compilation of Hi-Vol data from the monitor network will reveal the geographic and temporal distribution of TSP levels, and the severity

of air quality violations. To gain insights into the origin of the TSP, there are several options. A direct and effective means of determination consists of microscopic and chemical analysis of the Hi-Vol filters to determine the size and type of particulate in the atmosphere. For example, a study conducted by IITRI[1] in the Phoenix area has shown that roughly 70% of the particle mass collected by Hi-Vol samplers was comprised of particles 20 micron or larger in diameter. This finding was consistent for essentially all monitors in the Phoenix area, and occurred for days of both high winds or stable atmospheres. It was clear, therefore, that measured TSP levels were originating primarily from local sources (the transport range of 20 micron particles is limited), and that the particles were derivitive of fugitive dust sources. These facts were further confirmed when analysis of the filter samples revealed the substantial portion of particulate mass was mineral.

Insights into TSP origins may also be gained by studying the apparent relationships between TSP levels and meteorology. For example, it is known that fugitive sources are strongly affected by rainfall drought. Figure 1 illustrates the apparent influence of rainfall on TSP levels in the Phoenix area. The effect or wind on the spatial distribution of TSP levels is also revealing. In the civic center, where fugitive sources result from human activity, wind appears to exert a cleaning effect on TSP, however, in the rural locations, where there are often substantial areas of disturbed soil surfaces, TSP levels generally increase with increasing winds.

Evaluation of air quality data is performed primarily to establish preliminary insights of the TSP problem. The air quality analyses will show if local or specific sources contribute substantially to the problem, and indicate the type of sources needing control. Various additional analyses of the data may be performed to characterize the particulate problem. Examination of TSP trends, statistical correlations between TSP levels, interpretations of pollution roses, monitor site surveys, evaluation of geographic distributions of TSP levels, arê a few examples of the analyses which may be performed.

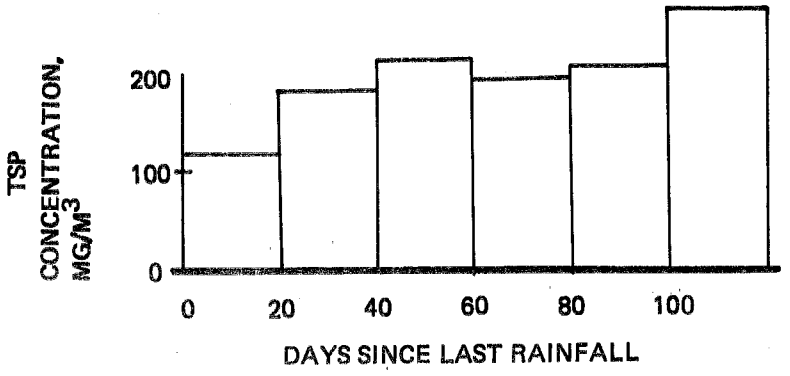

Figure 1. Typical profile for TSP versus number of days since last rainfall, Phoenix area, 1975.

EMISSIONS INVENTORY

With increasing awareness of the significance of fugitive dust sources, methods for quantitative characterization of fugitive sources has improved appreciably in the past few years. Table 1 summarizes current methodology for estimating emission rates of various types of fugitive dust sources.

For potential utility in air quality simulation and impact analysis, estimates of emissions are organized for description in a grid network of the study area. The grid boundaries are defined by considering all sources which might significantly affect air quality in the target control area. When practical, sources should be spatially resolved to a greater level of discrimination immediately around the monitor sites.

In several areas, particularly those of the Southwest region, unpaved roads are responsible for a substantial portion of the TSP levels. The emission rate of particulate matter from unpaved roads depends on the speed of the vehicle, the percentage of fines in the surface soil of the road (silt content), the amount of time the road is wet, and the number of tires on the vehicle. Because of practical considerations or limitations in the data base, calculations are generally conducted for aggregated (rather than individual) road links exhibiting certain traffic volumes and surface silt levels. Typical traffic volumes and average speed on unpaved roads must usually be based on crude data from studies conducted for representative road types. The soil silt content of the road surface should be determined by field tests. Results of field sampling in the Phoenix area indicate that the silt content (percentage

Table 1. EMISSION FACTORS FOR MAJOR FUGITIVE DUST SOURCES[2,3,4]

Source	Emission Rate	Influence Parameters	Units
Unpaved Roads	$.81s\left(\frac{S}{30}\right)\left(\frac{365-W}{365}\right)$	(s) Soil silt content, % (S) Speed of vehicle, mph (S) No. of days of rain/yr.	lb/vehicle mi.
Paved streets	$(15X10^{-7})$ Ls	(L) Street dust loading, lb/curb mile (s) Dust silt content, %	lb/vehicle mi.
Construction	1.2	Average for construction period	tons/acre/month
Agricultural tilling	$\frac{1.4s}{\left(\frac{PE}{50}\right)^2}\left(\frac{S}{5.5}\right)$	(s) Soil silt content, % (PE) Thornthwaite's precipitation evaporation index (S) Implement speed, mph	lbs/acre
Soil suspended by wind	AIKCL'V'	(A) Suspension ratio (I) Soil errodibility,tons/acre/yr (K) Surface roughness ratio (C) Climatic factor (L') Field length factor (V') Vegetative cover factor	tons/acre/yr.

of particles less than 75 μ diameter) of soils on unpaved roads attains an equilibrium value appreciably less than that of the native soil.[2] Fines are readily removed from the road surface by vehicle traffic, leaving on the road surface a higher percentage of coarse particles than are observed in the native soil. The spatial variation of road surface silt levels throughout an area may be estimated by relating predominant soil associations in the study area to the field test results.

Studies in Chicago have demonstrated that emissions from paved streets are also a major cause of high levels of TSP.[5] According to a recent study by MRI,[4] the most important variable affecting emissions from paved streets is street dust loading. Dust loadings on any given street may vary greatly depending on frequency of rainfall or street sweeping. The data base available to characterize street dust loadings is typically very limited. A nationwide EPA survey[6] of representative streets in selected cities has shown that street dust loadings vary from about 350 pounds of solids per curb mile to levels in excess of 1,000 pounds per curb mile. The specific street dust loadings in any given study area must usually be crudely approximated, based on whatever measurements of collected roadway debris are available, knowledge of city street sweeping practices, and the EPA national survey results. Based on a study conducted by the American Public Works Association, dust loadings are increased by a factor of four for uncurbed streets. The emission factors for paved streets are estimated by applying the MRI model (Table 1) to traffic volumes for the various links of the overall transportation link network. Emissions calculated for each link are assigned to grid squares of the study area network (usually by means of software techniques).

The potential significance of entrained street dust in for high TSP levels of some major metropolitan areas is illustrated in Table 2. The 1972 emission figures reflect approximate levels which were used in the

Table 2. SIGNIFICANCE OF STREET DUST EMISSIONS FOR VARIOUS METROPOLITAN AREAS

City	1972 Total Particulate Emissions Inventory, tons/day*	Street Dust Emissions tons/day
Los Angeles	211	858
Sacramento	110	82
Dallas	54	129
Phoenix	35	248

*excludes all fugitive sources.

development of SIP plans several years ago. A relatively low average street dust loading of 700 lb/curb mile is assumed to be representative of each area, and total daily vehicle mileage in the area is based on levels used to development State Implementation plans. Although the emission totals do not translate directly into TSP levels (other factors such as secondary precursors of TSP, particle sizes, and distribution of sources must be considered), it is clear that entrained dust emissions from streets exert a major impact on TSP levels in any metropolitan area.

Another fugitive dust source of potential significance in all metropolitan areas is construction activity. Measurements[3,8] in the vicinity of construction sites have shown that fugitive dust emissions average about 1.2 tons/acre/month during the periods of active construction (including a mix of days with no activity, moderate activity, and heavy early morning equipment and truck traffic). Construction emissions are estimated by determining the acres of soil disturbed from road construction projects and residential/commercial/industrial construction. Data required for these estimates and for locating the emission source is derived from local building and safety departments, and land use studies. Typically, the substantial portion of construction activity is residential and usually concentrated around the perimeter of urbanized areas.

The significance of windblown sources varies greatly by region. In dry areas where large amounts of exposed earth are prevalent, entrainment of soil particles by force of wind may contribute significantly to TSP levels. The magnitude of windblown dust changes seasonally with climate. Table 3 summarizes windblown dust emissions levels estimated to have occurred in Phoenix during 1975, and illustrates clearly the seasonal variation. The combined effect of temperature, precipitation and wind speed produced progressively greater forces of soil wind erosion during each successive quarter of the year. The estimates include erosion occurring under all conditions, including windstorms, and are therefore, overstatements of the levels of windblown emissions contributing to those days on which the NAAQS are potentially violated (under EPA designation air quality violations do not occur when natural causes, such as windstorms, create high TSP levels).

Table 3. WINDBLOWN SOIL EMISSIONS IN PHOENIX AREA, tons/day

Source Category	1st Quarter	2nd Quarter	3rd Quarter	4th Quarter	Annual
Agricultural Fields	4	4	4	4	4
Unpaved Road Surfaces	1	2	3	4	3
Undisturbed Desert	160	244	321	450	294
Tailings Piles	1	1	1	1	1
Disturbed Soil	161	248	323	456	297
Total	328	500	652	915	599

Of the five windblown sources investigated in the Phoenix area, two are of major importance. Emissions from the desert are substantial because of the vast amounts of this source surrounding the urban area. Dust from disturbed soil areas (vacant lots, parking lots, dirt residence yards) are appreciable because of the suspendable nature of these disaggregated surface soils and the large amounts of such surfaces throughout the Phoenix area. Despite extensive agricultural activity surrounding the Phoenix area, windblown dust from agricultural fields are estimated to be relatively insignificant because of the consolidated structure of the irrigated soils and subsequent resistance to suspension by wind.

The physical mechanisms causing entrainment of soils by wind are not fully understood, and empirical data describing the atmospheric-surface exchange of soil particles is relatively limited. Accordingly, methodology now available to estimate soil erosion emissions is somewhat crude. Presently, the most plausible approach for estimating soil erosion emissions involves an application of the wind erosion equation, adapted to include a suspension factor, A, for the portion of eroded soil which is entrained (Table 1). Except for the difficulty in evaluating resonable values for the factor A, the procedure for employing the wind erosion equation is well established and documented.[2,3,9] Area-specific values for the various factors should be developed, based on baseyear meteorology, and geographic and soils data collected for the study area. The value of the suspension ratio, A, depends on the distribution of soil particle sizes and the aggregate structure of the soil. Various field and laboratory studies [3,8,10,11,12] have suggested models to describe the vertical dust flux of different soil structures under varying wind forces. The studies are limited in scope and tentative in nature, and cannot be used to support emissions models more precise than the adapted wind erosion equation. A review of the various tests has been conducted to establish best estimates of suspension ratios (Table 4).

Table 4. SOIL EROSION SUSPENSION FACTOR FOR VARIOUS SOIL SURFACE CATEGORIES

Soil Surface Category	Dust Suspension Factor
Agricultural fields	.025
Unpaved road surfaces	.038
Undisturbed desert	.018
Disturbed native soil (parking lots, residence yards, excavation clearings)	.038

The magnitude and spatial distribution of windblown emissions and anthropogenic emissions can be expected to change in the future. For example, in the Phoenix area, forecasted emissions from wind erosion in 1980 and 1985 are appreciably less than in 1975, due to the assumption that typical historical meteorology will prevail in those future years and the fact that the amount of disturbed soil surfaces will diminish. In contrast, anthropogenic fugitive dust source emissions will increase due to population growth and associated increased source activities. Table 5 illustrates the changes between baseyear and projected emission inventories for sources in the Phoenix area. Included in the inventory are minor sources not addressed in the body of this text.

MODEL SIMULATION OF TOTAL SUSPENDED PARTICULATE LEVELS

The ultimate utility of the emissions inventory in air program planning depends on an understanding of the source-receptor relationship between emissions and ambient TSP levels. In addition to the magnitude of emissions, the factors which determine the effect of source emissions on air quality include the distribution of the emissions, the particle size distribution of the particulate matter, source configuration, and meteorology. Standard air quality models incorporate consideration of most of these factors, and are used routinely to forecast TSP levels for conventional emitters of particulate matter. However, such models treat

Table 5. PARTICULATE EMISSIONS INVENTORY FOR PHOENIX AREA, tons/day

Source Category	1975	1980	1985
Conventional Sources			
Stationary sources	22	27	31
Area sources	1.4	1.8	2.1
Mobile sources	11	13	17
Aircraft	0.4	0.4	0.5
Anthropogenic Fugitive			
Agricultural Tilling	20	19	19
Unpaved roads	1281	1454	1553
Paved roads	248	295	322
Cattle feedlots	6	8	8
Off-road vehicles	71	91	107
Construction	100	254	256
Aggregate piles	0.1	0.1	0.1
Soil Erosion			
Agriculture fields	4.0	1.7	1.7
Unpaved road surfaces	2.5	.6	0.6
Undisturbed desert	294	85	85
Disturbed soil	297	114	58
Tailings piles	1.4	1.9	2.3
Total	2360	2367	2462

pollutants as unreactive gases and fail to consider gravitational settling and deposition of particulate matter. Settling and deposition become increasingly important as the diameter of the particles exceeds 10 microns. Since most of the mass of fugitive dust emissions are comprised of particles in the 20 to 70 micron diameter range (Figure 2), application of conventional Gaussian plume models is inadequate for air quality evaluation when fugitive dust sources are predominant.

In the Phoenix study,[13] TRW developed a modeling procedure that uses a standard diffusion model (the Climatological Dispersion Model, or CDM) to evaluate that portion of the emissions comprised of particles smaller than 20 microns and uses a proportional (rollback) analysis to represent the contribution of the larger particles. The gridded emissions inventory was prepared for four particle diameter ranges representing approximate cutoff points in dispersive behavior: 0-10 microns, 11-20 microns,

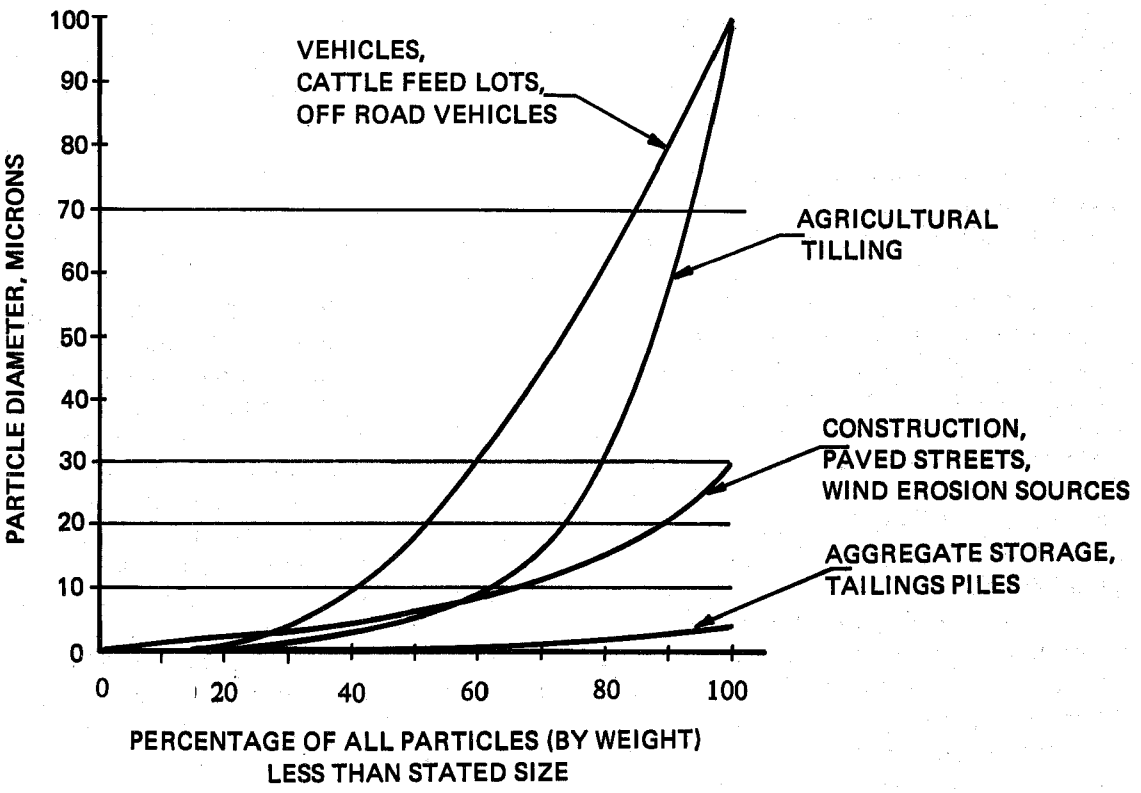

Figure 2. Size distribution of particulate emissions from various fugitive dust sources.

21-70 microns, and greater than 70 microns. The CDM is applied to the first two ranges, however, the effect of gravitational settling is approximated with the assignment of a decay constant for the emissions in the 11-20 micron size range. The modeling of TSP levels in the 21-70 micron range was accomplished by a simple rollback scheme which assumed the concentration within any given grid square is directly proportional to the emissions within that grid. The assumption is plausible, considering the limited transport range of the larger particles. Particles greater than 70 microns in size are ignored in the analysis. The range of travel of these particles is only a few meters, generally not enough to impact the air quality monitors.

The relative contribution of TSP computed by the CDM, rollback and background portions of the model are determined by analysis of particle size distribution of matter on the Hi-Vol filters from each of the monitoring sites. In the Phoenix study, analysis of Hi-Vol filters revealed a consistent result throughout the Phoenix area: 70% of the particulate matter weight is comprised by particles greater than 20 micron in diameter and 30% of the particulate matter collected was smaller than 20 microns. These fractions were applied to the various measured TSP levels on the baseyear to establish the basis for calibrating the CDM and the rollback terms of the model. The model was then executed for the baseyear emissions and meteorology, and calibration was achieved by fitting the TSP forecasts to the measured TSP levels.

The calibrated model is used to evaluate contributions of each of the source categories to total TSP levels, and to evaluate the impact of changes in the magnitude and distribution of emission sources on TSP levels. Table 6 illustrates modeling results for the Phoenix Study. The results show that in 1975 four particulate sources dominated TSP levels: unpaved roads, entrained street dust, construction activities and wind erosion. By 1985, wind erosion will not be a major source because of 1) the likelihood that typical meteorology will prevail, and 2) a diminishing of open soil surfaces. As a result of changes in emission source magnitude and distribution, TSP levels in 1985 will decrease significantly at 11 of the 13 monitoring sites. The expected air quality improvements are due to the forecasted regional development. This development will reduce the proportion of open surfaces and diminish the magnitudes of several local sources currently affecting samplers. However, expected development will not achieve the primary air quality standard (75 $\mu g/m^3$) at most sites; control measures must be applied if the standards are to be met. The air quality model can be used to estimate the impact of various candidate control strategies, and to develop an overall attainment strategy for a given area.

Table 6. IMPROVEMENT IN TSP LEVELS DUE TO ANTICIPATED DEVELOPMENT IN THE PHOENIX AREA

Monitor Site	Observed (Total)	Percentage Reduction in TSP	Unpaved Roads	Paved Roads	Construction	Percentage of TSP contributed by 3 major sources and background
C. Phoenix	112(87)	22.3	25(8)	31(37)	4(5)	80(92)
S. Phoenix	144(101)	29.8	75(32)	20(24)	2(9)	88(94)
Arizona St.	169(132)	21.9	35(12)	59(68)	7(9)	78(90)
Glendale	101(65)	35.6	30(9)	17(20)	7(2)	83(94)
N. Phoenix	121(83)	30.4	26(8)	28(32)	7(7)	75(93)
N. Scott/Paradise	149(101)	32.2	24(32)	8(9)	14(25)	51(95)
Scottsdale	115(93)	19.1	27(10)	33(42)	6(5)	83(94)
Mesa	117(95)	18.8	32(13)	13(35)	8(4)	90(97)
Downtown	200(155)	22.5	42(15)	70(80)	8(10)	75(89)
St. Johns	145(157)	-8.3	93(116)	2(0)	2	66(96)
Sun City	88(74)	15.9	15(6)	12(17)	3(16)	68(93)
Paradise Valley	184(93)	49.4	42(14)	14(17)	17(25)	56(93)
Chandler	119(160)	-34.5	64(91)	10(12)	7(23)	93(97)

Note: Figures in parenthesis represent 1985 forecast levels; other figures are 1975 levels.

CONTROL STRATEGY FORMULATION

In areas where fugitive dust is the cause of high levels of TSP, the major sources are typically unpaved roads, construction activities, entrained street dust, and suspended soil eroded by wind off vacant lots and disturbed soil surfaces. While the impact of these sources is generally localized in nature, the sources are typically found throughout a given area and therefore may create widespread problems of high TSP concentrations. Other sources of fugitive dust (e.g., tailing piles) are generally less widespread and create more of a truly localized limited impact for a specific area. A review of the emissions and air quality modeling for the specific area will determine the sources most responsible for high TSP levels and will establish priorities for investigation of alternative control measures.

Control of Dust from Unpaved Roads

Control methods to reduce dust emissions from unpaved roads consist of: 1) paving, 2) chemical stabilizers, 3) watering, 4) graveling, and 5) traffic related controls. Characterization of these controls (Table 7) shows that road paving with a chip seal is the most effective and cost effective control measure in the long term. In addition, road paving is compatible with planning objectives of local agencies, and provides cost benefits to many sectors of the community. The effectiveness of chemical stabilizers as an unpaved dust control has improved in recent years[14] but the high annualized cost of this measure for only partial reduction of road emissions is a major drawback to its use. Water and graveling controls are generally affected with the same shortcoming as road dust palliatives.

Table 7. EFFECTIVENESS OF ALTERNATIVE ROAD TREATMENTS IN REDUCING DUST EMISSIONS FROM AN UNPAVED ROAD IN PHOENIX[21]

Road Type	Emission Rate Lb/Vehicle Mi.	Annual Efficiency	Cost Effectiveness $/Ton of Dust
Dirt surface	22	---	---
Gravel	11	50%	11.0
Oil surface (dust control oil)	5	75%	19.5
Oiled surface (low cost application)	11	50%	13.5
Chip seal	0	100%	10.8
Asphalt	0	100%	19.6

Traffic controls also offer potential for dust emissions reductions from unpaved roads. Dust emissions increase exponentially with vehicle speed up to 30 mph,[15,16] and linearly thereafter. The reduction in emissions achieved by limiting vehicle speed from 35 mph to 20 mph would be 62 percent.

Control of Emissions from Paved Streets

Dust entrained from paved streets may be best controlled by either eliminating sources of street dust, or by more frequent and efficient removal of street dust loadings. Dust sources, consisting primarily of exposed soil areas near the streets, are significantly reduced when unpaved road shoulders are upgraded with curb and sidewalks. Further elimination of sources is attained by providing soil cover (e.g., vegetation) or stabilization of adjacent soil areas. For the Phoenix area, it has been estimated that scheduled road improvements will reduce the average dust emission rate from 11.1 gm/vehicle mile to 5.2 gm/vehicle mile. Since the major portion of vehicle miles traveled in any area are concentrated within the cities, the urban street improvements will have far greater impact on TSP levels than would similar improvements implemented in county road networks. Accordingly, intensification of the street improvement plans should be considered as a potential control for street dust emissions.

Typical city construction costs for street curbs are currently about $5 per curb foot. The cost of sidewalk construction is $6 per running foot of a standard 5 foot wide sidewalk.[18]

Intensified street cleaning offers a potentially effective means of reducing street dust emissions but remains unproven based on the limited studies performed to date. The effectiveness of street cleaning in reducing street dust emissions depends on the dust removal efficiency of the street cleaning device and the frequency of cleaning. Controlled

experiments [6,7] have demonstrated a dramatic difference in the performance of the vacuum sweeper and the broom sweeper. The broom sweeper is ineffective in removing those particles most likely to become airborne (<100 microns) by passing vehicles. By contrast, the vacuum sweeper will collect roughly twice the small size material of the broom sweeper (Table 8).

Because street dust loadings increase rapidly after cleaning,[6] the effect of street cleaning frequency on loading intensity is appreciable. Figure 3 shows the typical dust loading accummulation rates after a complete cleaning.

The sweeper efficiency data and dust loading rates may be utilized to construct estimates of average street dust loadings associated with different street cleaning programs. Figure 4 summarizes such estimates for various sweeping schedules using either a broom sweeper or a vacuum sweeper, and illustrates the importance of frequent street cleaning in maintaining low average street dust loadings. Infrequent sweeping (weekly or less after) has little effect on average loading levels, and would be expected to result in minimal short term emission reductions. This is confirmed by recent field studies[17] which show improvements in ambient TSP levels on the day following street cleaning, but a rapid return to normal TSP levels the following day.

Caution must be exercised in applying the evaluation procedures underlying the results shown in Figure 4. The available data base for street dust loadings and sweeper efficiencies is very limited, and analytical estimation procedures are highly suspect at this time. Ultimately, street cleaning controls for emissions from paved streets must be based on field test results which verify that a target dust loading level is attainable with a given quality and frequency of street sweeping.

Table 8. COMPARISON OF COLLECTION EFFICIENCY OF BROOM-SWEEPING AND VACUUM SWEEPING[6]

Machine Type	Relative Effort	Collection Efficiency, %		
		Dust Loading: 20 g/ft^2 Particle Size: 177-300μ	100 g/ft^2 74-177μ	600 g/ft^2 74-177μ
Motorized	2.17	92.5	58.0	46.0
Vacuumized	2.88	95.0	94.5	89.5
Motorized	4.32	94.5	--	62.6
Vacuumized	5.83	98.5	--	91.4

Relative Effort = effort (time spent by sweeper covering a given area) relative to the minimum level of effort attainable by the sweeping equipment. For the tests above, unit relative equipment effort corresponds to a forward speed of 1200 ft/min. Therefore, relative effort = 1200/forward speed (ft/min.).

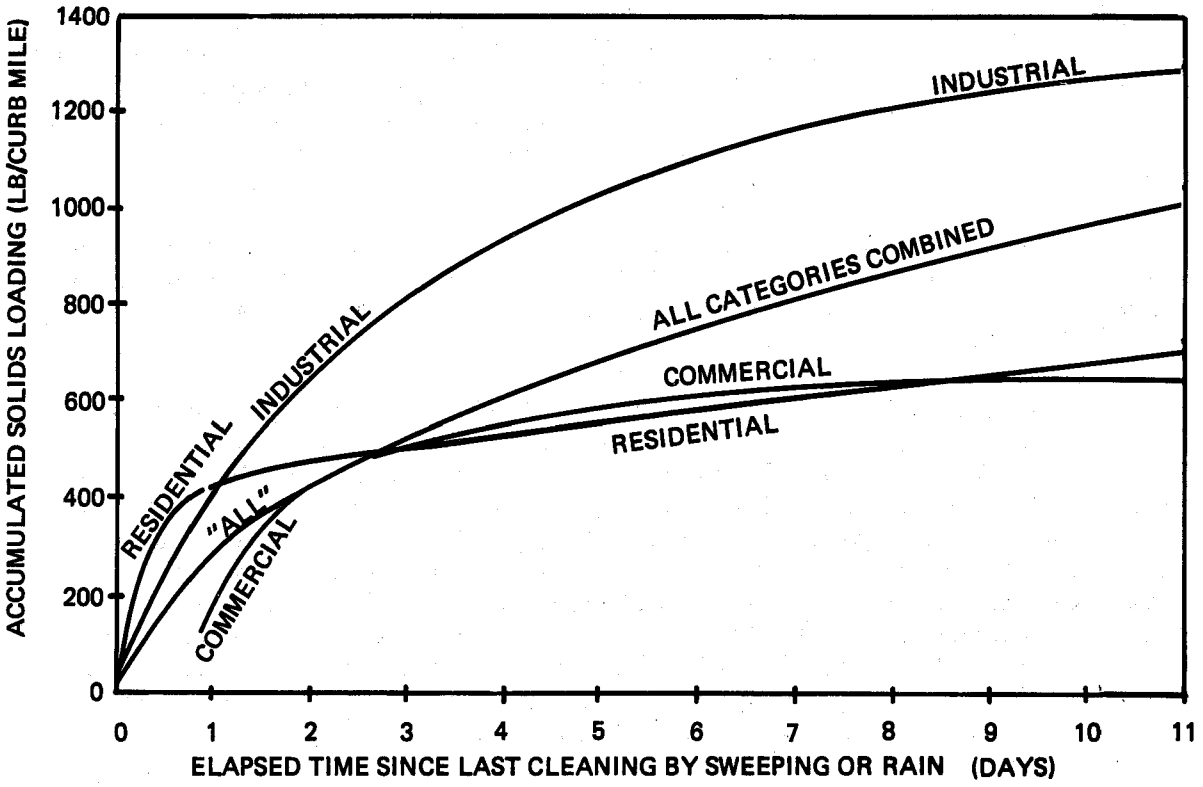

Figure 3. Street dust loading versus time since last sweeping.[6]

The cost of street sweeping varies widely from city to city. Because the full scale street vacuum sweeper has been marketed for a limited time in the United States (beginning in 1971), nearly all cost data available pertain to the conventional broom sweeper. The American City Survey[16,19] showed sweeping costs varying from $2.18 to $8.42 per curb mile sweep. This cost range is due to differences in maintenance practices, operators pay, and accounting reporting practices. Few cities have experimented with vacuum sweepers, but there is indication from these trials that it may provide satisfactory performance at overall costs roughly equivalent to that of the broom sweeper.[20]

Control of Dust Emissions from Construction Activities

Wetting the surfaces of unpaved access trails for construction vehicles and trucks is an effective control for dust emissions provided the surface is maintained wet. In arid regions this generally requires an appreciable amount of water. A study[8] on the effect of watering on construction sites indicates that extensive wetting of the soil may reduce emissions by an average of 30%. Another study[15] has shown emissions from unpaved roads are reduced by 30% when the surface is maintained moist. The cost of implementing this control is about $6/acre/day.[21]

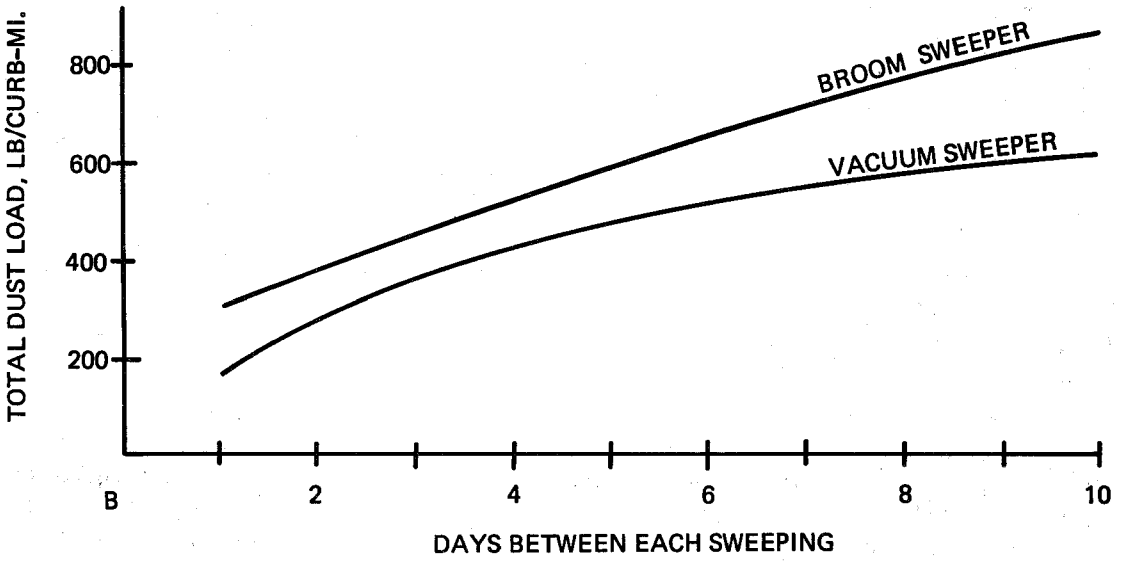

Figure 4. Effect of sweeping frequency on average street dust loading (an approximation synthesized from sweeper efficiency data and typical street dust loading data).

A negative tradeoff associated with watering controls at construction sites concerns the carry-out of mud onto adjacent streets. The street dust resulting from the mud carry-out is susceptible to suspension from passing vehicles. Street sweepers may be employed daily to clean the affected public roads where dust has accummulated. Good housekeeping measures (cleaning construction vehicles before leaving site) may be employed as a cost effective alternative to street sweeping. It is not possible to specify an effectiveness for these actions, but a recent study[17] in Kansas City has provided supporting evidence that cleanup of mud carry-out from construction sites significantly reduces TSP levels in the immediate vicinity. Minimum cleanup cost would be about $5/day/site, or significantly higher depending on accessibility and availability of street cleaning equipment.

Selection of Control Strategy

A primary consideration in the construction of a control strategy is the resonableness of the composite control measures. Resonable control measures are defined as those which are technically and economically feasible to implement, and which attain significant benefits in air quality. General factors affecting the resonableness of a control

measure include: 1) the compatibility of the controls with the overall goals and plans for the area, 2) the timeable for implementation, 2) the degree of control required, and 4) the financing mechanisms available for implementation. Considering these factors and the various candidate controls, specific reasonable measures are formulated into a trial strategy. For each selected measure, the reduction in emissions of fugitive dust is estimated and air quality impacts are estimated using the air quality simulation model discussed earlier. This evaluation is carried out in an iterative fashion with successive strategy trials until area-wide attainment is forecast.

It is important to distinguish between the controls needed to attain the standard throughout the region and that needed to attain the standard only at the monitoring sites. Because of the very localized impact of fugitive dust sources, it is possible to achieve localized attainment by application of controls in limited areas. This approach should not be used to circumvent widespread TSP problems. The strategy should be applied on a broad scale to improve air quality throughout the area, and the grid network air quality analysis should be examined to predict various locations where additional controls may be necessary.

In general, most of the measures for control of fugitive dust are reasonable with a few exceptions, the major one being the widespread application of chemical stabilizers to agricultural lands. Selection, therefore, involves a determination of the most cost effective measures which will provide the air quality improvements needed for standards attainment. The major obstacle confronting implementation of a fugitive dust control strategy concerns the socioeconomic acceptability of the proposed actions. Appropriations for the measures require financial support of the citizenry, whether by taxes, bonds, or assessment districts. Such support may be facilitated by phasing in the controls with implementation of a demonstration project as the first phase to validate the benefits of the proposed strategy. Because the impact of fugitive dust sources is typically very localized, a limited control demonstration project is particularly appropriate to validate the achievement goals of the controls.

The proposed emissions control strategy for the Phoenix area consists of three major control measures. The main control element consists of an intensive road surfacing program (costing $2.5 million per year) in the county for the next 20 years. Road surfacing is to be conducted by applying a chip seal to the section line roads. Priorities for the paving program would be assigned in the order of those section roads receiving greatest traffic volume, and the local department of transportation would administer the program. A control is also proposed for existing or future unpaved roads. A speed restriction for unpaved roads is especially cost effective, and is considered reasonable when phased in concurrently with the road surfacing measure.

A second control measure of the Phoenix strategy includes an intensive street cleaning program in designated areas where reduction of

entrained street dust emissions is necessary to attain the air quality standards. It is proposed major streets be swept more frequently, alternating from vacuum sweeping to broom sweeping to attain a target overall reduction of 60% in street dust loadings. Because of the limited data base available to characterize street dust loadings and sweeping efficiencies, it is not possible to specify with certainty a street sweeping program to accomplish the targeted emission reductions. A field measurement program is proposed to establish baseline loadings for various streets and to determine by test the actual sweeping programs needed to obtain the required dust levels. Based on the crude estimation procedures for street dust loadings discussed earlier, it appears than an adjustment from existing sweeping frequencies (once per week for most major streets) to 3 times per week may produce the targeted emission reductions.

The final element comprising the Phoenix control strategy entails enforcement of more rigorous regulations for construction activities. The measures are relatively cost effective in terms of total emissions reductions, and produce significant benefits in air quality for those areas affected by construction emissions.

The measures comprising the proposed Phoenix control strategy represent the most cost effective options, are compatible with the long term planning goals for the region, and are effective as substantial dust controls. However, it is expected that substantial social resistance may develop against this strategy. Consequently, a special feature of the overall strategy is a demonstration project to develop social acceptance as a prerequisite to full scale strategy implementation.

Impact of Selected Control Strategy

The estimated effect of the proposed Phoenix strategy on emissions levels is considerable. The predicted change in total emission levels in 1985 due to the control strategy amounts to a reduction of 26% from the 1985 baseline level, and 23% from the 1975 baseyear level. Equally important as the overall emissions level reductions are the distribution of these reductions. Figure 5 shows the level and spatial distribution of emissions before and after strategy application. With strategy, emissions are reduced substantially in the area near the monitor sites (i.e., in and bordering the metropolitan Phoenix region). Entrainment of street dust is prevented by control programs within specified cities, roads are paved by priority of vehicle count in areas closely surrounding the metropolitan area, and construction controls are applied throughout the cities and particularly insuburb areas. When the controlled emissions levels are translated into TSP levels using the adapted air quality model, substantial air quality improvements are predicted at each monitoring site. Considering the relatively high background TSP contribution, which is unaffected by the strategy, the improvement leverage provided by the emissions reductions is appreciable. The prescribed controls are expected to decrease TSP levels at the various monitors by

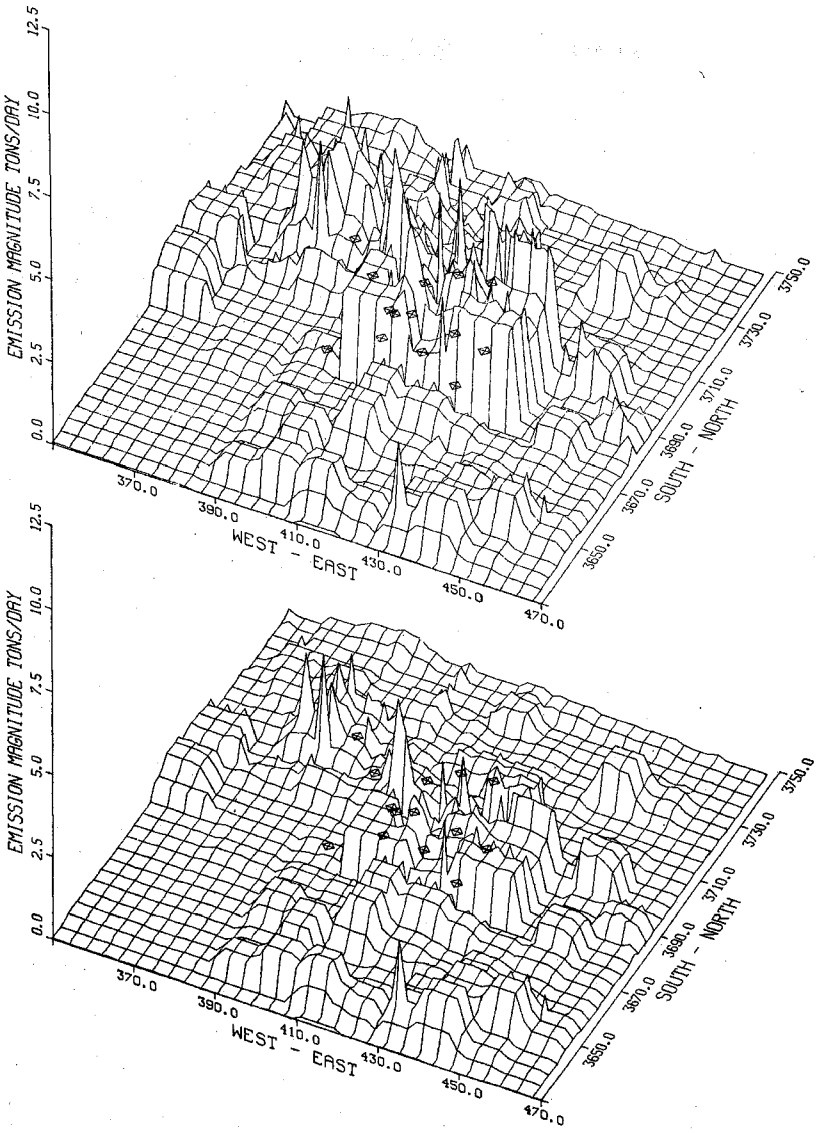

Figure 5. Effect of control strategy on total particulate emissions in Phoenix area, 1985.

11 to 57% of the projected 1985 levels. Between the improvements achieved by normal regional development and the strategy together, base-year TSP levels at the various monitors are reduced 31 to 76% by 1985. Moreover, air quality at all 13 monitor sites is forecasted to attain (or be very close to attaining) the primary standard for TSP (75 $\mu g/m^3$). Table 9 summarizes the forecasted impact of the control strategy on TSP levels in future years.

CONCLUSIONS

There is considerable basis for optimism when constructing air program plans for attainment of the federal ambient TSP standard. In Phoenix, an area experiencing widespread nonattainment caused by appreciable levels of fugitive dust emissions, it is estimated that the

Table 9. IMPACT OF CONTROL OF MAJOR SOURCE CATEGORIES ON TSP LEVELS IN THE PHOENIX AREA

Monitor Site	Baseline 1975/1985	Strategy 1985	1985 Baseline TSP Due to Strategy	1975 TSP Due To Strategy & Projected Development
1. Central Phoenix	112/87	77	11.4%	31.2%
2. S. Phoenix	144/101	73	27.7%	49.3%
3. Arizona State	169/132	73	44.6%	56.8%
4. Glendale	101/65	56	13.8%	44.6%
5. N. Phoenix	121/83	73	12.1%	39.6%
6. N.Scottsdale/ Paradise	149/101	78	22.8%	47.6%
7. Scottsdale	115/93	73	21.5%	36.5%
8. Mesa	117/95	74	22.1%	36.7%
9. Downtown Phoenix	200/155	85	45.1%	57.5%
10. Sun City	88/74	64	32.4%	76.1%
11. Paradise Valley	184/93	73	21.5%	60.3%
12. Chandler	119/160	68	57.5%	42.8%
13. St. John	145/157	85	45.8%	41.4%

Note: The area-wide background TSP level was determined to be 30 $\mu g/m^3$.

execution of technically and economically feasible emission control measures can achieve the emissions reductions required for attainment. The annual cost of attainment in Phoenix is estimated to be $3 per capita, or $4.4 million per year. Compared to the cost of current SIP-imposed controls for conventional sources, the cost effectiveness of lowering TSP originating from fugitive dust is an order of magnitude less.

In most areas experiencing fugitive dust problems, attainment of the TSP standard will be aided considerably by the planned regional development. Such development will reduce the proportion of open surfaces, change the distribution of sources substantially, and diminish the magnitude of several local sources currently affecting air monitoring samplers.

The data base used in the control strategy development process will be enhanced greatly if field sampling is conducted to determine the percentage of fines in the surface soil on unpaved roads, and the amount of dust loading on paved streets. The nature and origin of the TSP problem will be better understood if microscopy and chemical analyses are utilized to evaluate the atmospheric loadings of TSP.

A special feature of the major fugitive dust control measures is their compatibility with overall planning objectives for the area. The dust controls for unpaved roads and paved city streets are merely intensified extensions of current local programs. This consistency permits the

measures to be instituted as on-line operations of the various local agencies as opposed to the more conventional procedure employing direct regulatory actions.

The major obstacle confronting implementation of a fugitive dust control strategy concerns the socioeconomic acceptability of the proposed actions. Appropriations for some of the measures require public support through taxes, bonds, or assessment districts. Further resistance to a control plan may arise due to technical uncertainties associated with the effectiveness of the proposed controls. These obstacles may be resolved by instituting a control demonstration project to verify or adjust the specified controls needed for attainment. A demonstration project is also useful in enlisting and promoting coordination between agencies which will ultimately be involved in the execution of the total strategy controls.

Caution should be employed when applying the evaluation procedures underlying the control strategy development for the Phoenix area. Due to limitations in the data base, considerable uncertainties enter into all phases of the strategy development. Probably the most unreliable part of the analysis concerns the quantification and control aspects for emissions from paved streets. Recent and ongoing studies are proving inconclusive with regard to the effectiveness of improved street cleaning, and additional investigation is needed to carefully assess the relationship of street dust emissions with the various known influence parameters. Additional data is also needed to characterize the efficiency of current sweeper technology under various operational modes. Until such information is available, simplistic analytic procedures may be useful in developing preliminary assessments of candidate controls, however, prior to full scale implementation, pilot studies should be instituted to verify the effectiveness of the proposed measures.

REFERENCES

1. Snow, R. H., Draftz, R. G., and J. Graf of IITRI. Field Air Sampling Study - Phoenix, Arizona. Environmental Protection Agency, Contract No. 68-01-3163, April 1976.

2. Richard, G., Tan, R., and J. Avery of TRW Environmental Engineering Division. An Implementation Plan for Suspended Particulate Matter in the Phoenix Area, Volume II, Emission Inventory Environmental Protection Agency, Report No. EPA-450/3-77-0216, December 1977.

3. Cowherd, C., Axetell, K., Guenther, C. M., and G. A. Jutze of Midwest Research Institute. Development of Emission Factors for Fugitive Dust Sources. Environmental Protection Agency, Report No. EPA-450/3-74-037.

4. Cowherd, C., Guenther, C. M., Nelson, D., and N. Stich of Midwest Research Institute. Quantification of Dust Entrainment from Paved Roadways. Environmental Protection Agency, EPA Contract No. 68-02-1403 (Task 7), March 1976.

5. Harrison, P., Draftz, R. and W. H. Murphy. Identification and Impact of Chicago's Ambient Suspended Dust. Paper submitted to Atmospheric Environment, 1974.

6. Sartor, J., and Gail Boyd. Water Pollution Aspects of Street Surface Contaminants. Environmental Protection Agency, Report No. EPA-R2-72-081, November 1972.

7. American Public Works Association. Water Pollution Aspects of Urban Runoff, 1969.

8. Jutze, G., and K. Axetell of PEDCo Environmental Specialists, Inc. Investigation of Fugitive Dust, Volume I - Sources, Emissions, and Control. Environmental Protection Agency, Report No. EPA-450/3-74-036-a, June 1974.

9. Woodruff, N. P., and F. H. Siddoway of Soil and Water Conservation Research Division, U.S., Department of Agriculture. A wind Erosion Equation. Kansas Department of Agronomy Contribution Nw. 897, March 1965.

10. Gillette, D., and I. Bliford of National Center for Atmospheric Research. The influence of Wind Velocity Research. The influence of Wind Velocity on the Size Distributions of Aerosols Generated by the Wind Erosion of Soils. Journal of Geophysical Research, September 20, 1974.

11. J. H. Shinn of Lawrence Livermore Laboratory. Observations of Dust Flux in the Surface Boundary Layer for Steady and Nonsteady Cases. In: Proceedings of a Symposium on Atmosphere-Surface Exchange of Particulate and Gaseous Pollutants. Technical Information Center, Energy Research and Development Administration, January 1976.

12. D. Gillette of National Center for Atmospheric Research. Production of Fine Dust by Wind Erosion of Soil: Effect on Wind and Soil Texture. In proceedings of a symposium on Atmosphere-Surface Exchange of Particulate and Gaseous Pollutants. Technical Information Center, Energy Research and Development Administration, January 1976.

13. Richard, G., Avery, J., and L. Baboolal of TRW Environmental Engineering Division. An Implementation Plan for Suspended Particulate Matter in the Phoenix Area, Volume III. Model Simulation of Total Suspended Particulate Levels. Environmental Protection Agency, Report No. EPA-450/3-77-021c, August 1977.

14. Sultan, H. A. of Arizona Transportation and Traffic Institute. Soil Erosion and Dust Control of Arizona Highways, Part IV, Final Report Field Testing Program. Arizona Department of Transportation, Report No. ADOT-RS-13(141)IV, November 1975.

15. Roberts, J. W., Rossano, A. T., Bosserman, P. T. Hafer, C. G., and H. A. Watters. The Measurement, Cost and Control of Traffic Dust and Gravel Roads in Seattle's Duwamish Valley. In: Annual meeting of the Pacific Northwest International Section of Air Pollution Control Association, Paper No. AP-72-5, November 1972.

16. J. B. Scott, the American City 1970 Survey of Street Sweeping Equipment. The American City and the Municipal Index, December 1970.

17. Axetell, K., and J. Zell of PEDCo Environmental, Inc. Control of Reentrained Dust from Paved Streets. Environmental Protection Agency. Report No. EPA-907/9-77-007, August 1977.

18. Communication with City Department of Transportation, Phoenix, June 1976.

19. Laird, C. W., and J. Scott. How Street Sweepers Perform Today - in 152 Selected Cities Across the Nation. The American City and the Municipal Index, December 1970.

20. R. D. Jackson of City of Columbus, Ohio, Department of Public Service. Street Cleaning, the Best Way. In: the Governmental Refuse Collection and Disposal Association Seminar and Equipment Show, Santa Cruz, California, November 1973.

21. G. Richard of TRW Environmental Engineering Division. An Implementaion Plan for Suspended Particulate Matter in the Phoenix Area, Volume IV - Control Strategy Formulation. Environmental Protection Agency, Report No. EPA-450/3-77-021d, June 1977.

STATE OF CONTROL TECHNOLOGY FOR

INDUSTRIAL FUGITIVE PROCESS PARTICULATE EMISSIONS

D. C. Drehmel
Industrial Environmental Research Laboratory
U.S. Environmental Protection Agency
Research Triangle Park, N.C. 27711

David P. Daugherty
Charles H. Gooding
Energy and Environmental Research Division
Research Triangle Institute
Research Triangle Park, N.C. 27709

ABSTRACT

The results of a literature survey of size distribution data for fugitive particulate emissions from the metallurgical industry are summarized. In most cases, fugitive emissions consisted of particulates less than 15 μm in diameter.

The status of fugitive particulate control techniques and some implications of a standard based on "inhaleable" particulate (less than 15 μm) are discussed.

I. OVERVIEW OF FUGITIVE CONTROL TECHNOLOGY

Perhaps the state of industrial fugitive process particulate (IFPP) controls can best be characterized by the terms "emerging" and "site-specific." Only within the last two to three years have IFPP emissions been studied and means for their measurement and control considered. The sources of IFPP emissions are numerous and quite varied, not only from industry to industry, but also between different sources within the same plant. Accordingly, the control equipment requires design and development almost on a case-by-case basis. For example, the hooding required to collect fugitive emissions from pushing coke is entirely

different from that used in collecting offgases from blowing a copper converter. In the future, it is unlikely that any single method of fugitive control will predominate, and we can expect the process systems will continue to require individual control strategies. The central points here are: (1) control technology for fugitive emissions is new and changing; and (2) the industrial applications are highly individual and are much more difficult to generalize than stack emissions.

By definition, fugitive emissions are difficult to collect and control. They are diffuse and typically come from many small sources as opposed to a single large emitter. For example, in a primary lead smelter, 25 different groups of emission sources have been identified[1], with each group containing several emission sources within the plant. Fugitive emissions can also be diffuse in the sense that there are low level emissions from a large area, as in the case of wind erosion from storage piles or dust from in-plant vehicular traffic. Many of the fugitive emissions are intermittent as well: unloading railcars, slag dumping, process upsets, etc.

Because of the intermittent and diffuse nature of fugitive emissions, their measurement is difficult. Briefly, sampling can be via (1) quasi-stack sampling where a collection hood near the source is sampled; (2) roof monitor sampling in which a large enclosed area such as a building is sampled; or (3) upwind-downwind sampling where fugitive emissions are back-calculated from particulate measurements around the source perimeter. Accuracy of such methods varies from 50 to 500 percent.[2]

Because of the relatively recent interest in fugitive process emissions and the measurement difficulties, data on the size and rate of IFPP emissions are spotty; often several fugitive sources are grouped together for measurement purposes. Field data on control device efficiencies are even more scarce. In the sections on control equipment and particulate characteristics which follow, engineering judgment and the results of a recent literature survey were used to provide information relevant to a standard based on particulate matter less than 15 μm.

II. FUGITIVE EMISSION CHARACTERISTICS

Particle size distributions for various fugitive emissions are shown in two figures--Figure 1 for the iron and steel industry and Figure 2 for the nonferrous metallurgical industry. The accompanying legends give the source of the emissions together with the literature references. Characteristics for some of the fugitive emissions have been estimated from ducted sources. Note that for the majority of the nonferrous sources, most of the fugitive emission mass is below 15 μm while for iron and steel sources the size range is broader.

Table 1 gives emission rate data for fugitive process emissions from integrated iron and steel plants. Uncontrolled fugitive emission

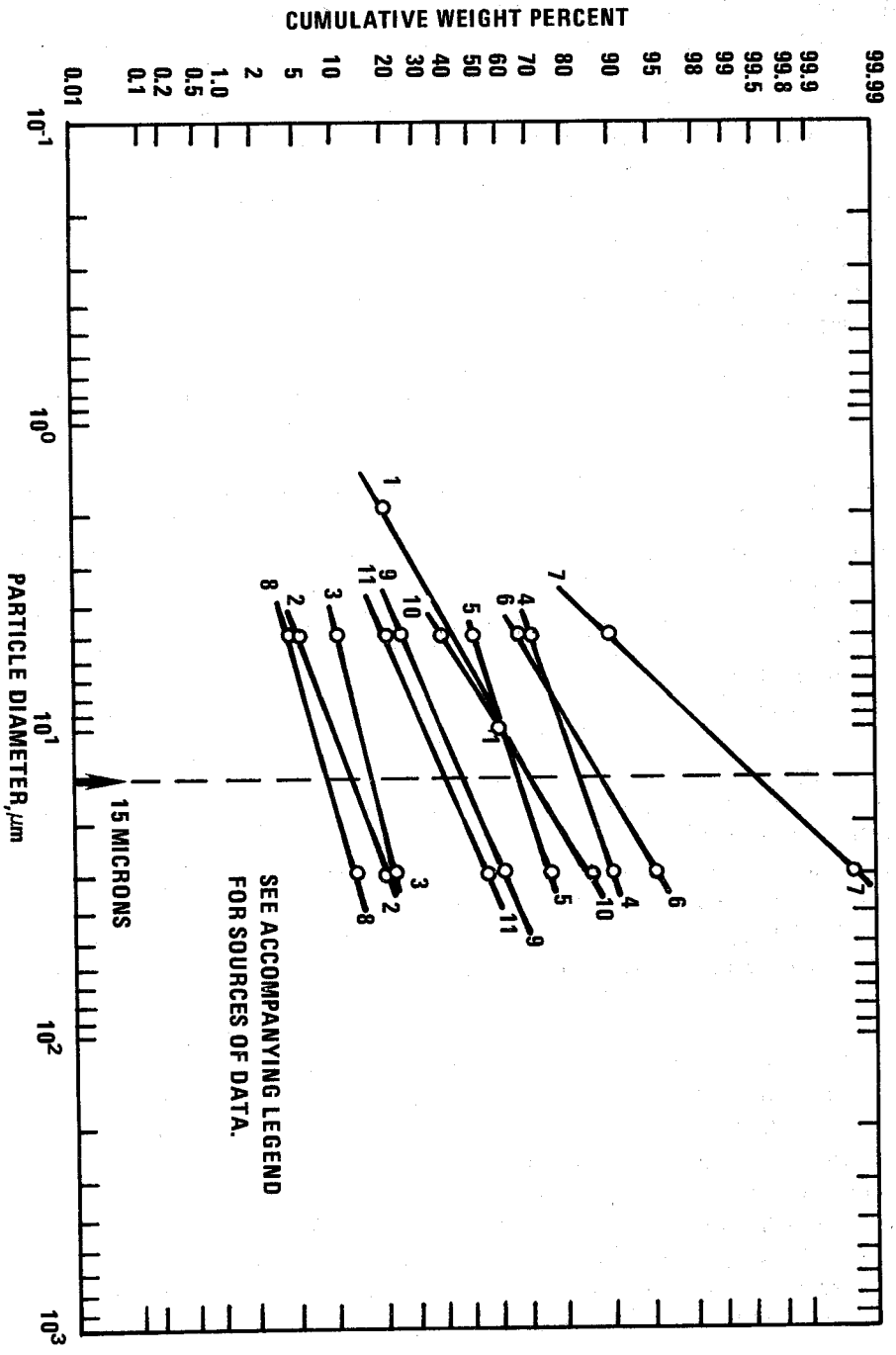

Figure 1. Particle Size Distribution Data for Iron and Steel Industry.

LEGEND FOR FIGURE 1

PARTICLE SIZE DISTRIBUTION FOR IRON AND STEEL INDUSTRY

Curve	Fugitive Particulate Source	Reference
1	Coke Pushing	1
2	Sintering Machine	3
3	Hot Metal Transfer	3
4	Electric Arc Furnace	3
5	Basic Oxygen Furnace	3
6	Open Hearth Furnace	3
7	Scarfing	3
8	Raw Material Handling and Storage Pile Activity	3
9	Vehicular Traffic (Unpaved Roads)	3
10	Vehicular Traffic (Paved Roads)	3
11	Conveyor Transfer Stations	3

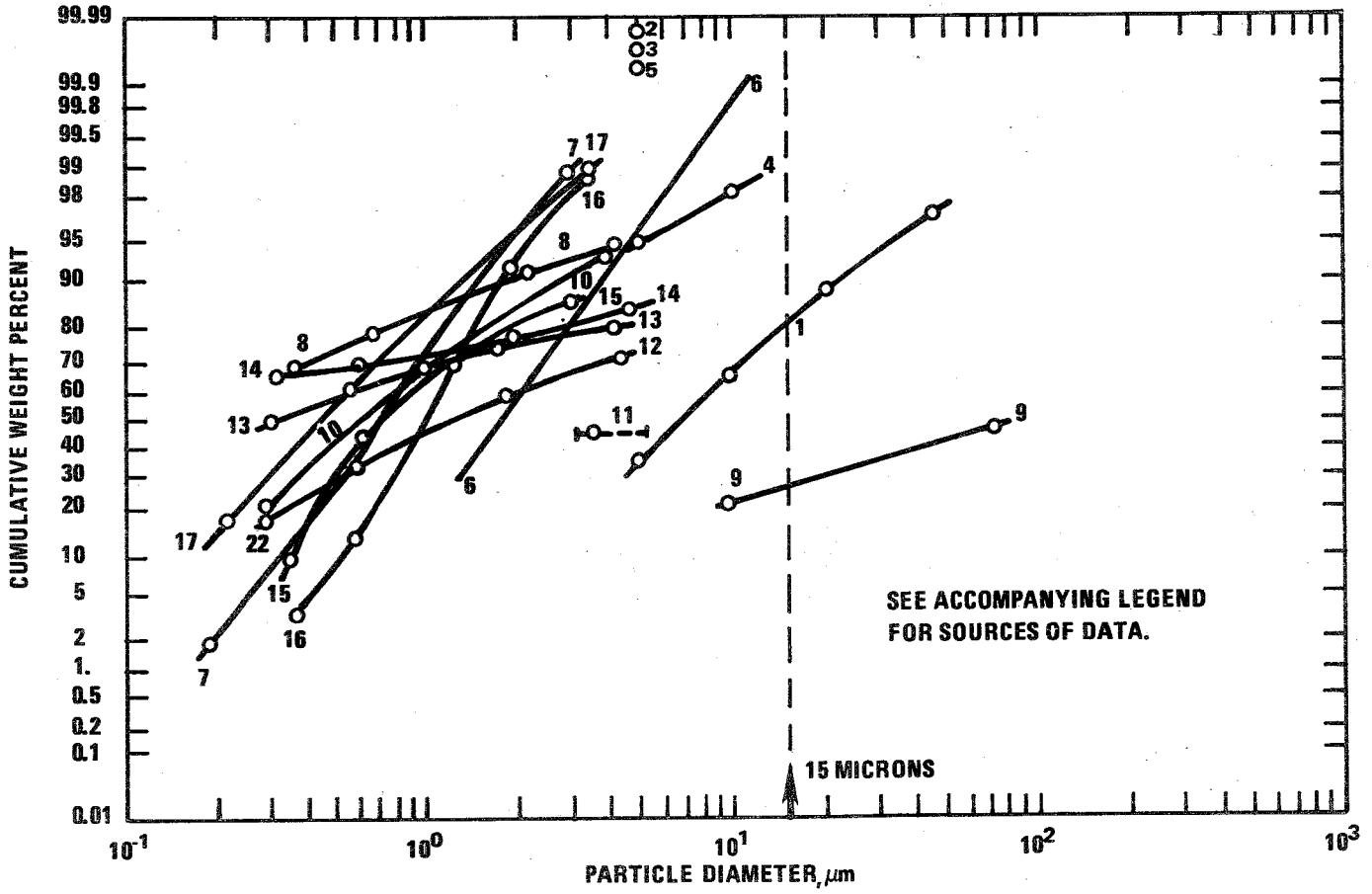

Figure 2. Particle Size Distribution Data for Nonferrous Metals Industry.

LEGEND FOR FIGURE 2.

PARTICLE SIZE DISTRIBUTION DATA FOR NONFERROUS METALS INDUSTRY

Curve	Fugitive Particulate Source	Reference
1	Metal Melting, Secondary Aluminum Smelting	4
2	Metal Melting, Secondary Brass Smelting	4
3	Metal Melting, Secondary Bronze Smelting	4
4	Metal Melting, Secondary Lead Smelting	4
5	Metal Melting, Secondary Zinc Smelting	4
6	Blast Furnace Stack Gases, Secondary Lead Smelting	4
7	Sintering Machine ESP Inlet, Primary Zinc Production	5
8	Fugitives, Sintering Building, Primary Lead Production	6
9	Pouring and Casting, Primary Copper Smelting	1
10	Reverberatory Furnace, Primary Copper Smelting	7
11	Limestone Storage and Material Handling	1
12	Fugitives, Blast Furnace Tapping Area, Primary Lead Smelting	6
13	Fugitives, Ore Storage Bins, Primary Lead Smelting	6
14	Fugitives, Blast Furnace Charging Area, Primary Lead Smelting	6
15	Sintering Baghouse Inlet, Primary Lead Smelting	5
16	Converter EPS Inlet, Primary Copper Smelting	5
17	Roaster ESP Inlet, Primary Zinc Production	5

rates are highest for electric arc furnaces and sintering machines. With the application of control, the greatest inhaleable* fugitive emissions are from coke ovens and electric arc furnaces. For comparison, stack emissions with control are also shown for inhaleable particles. Although sintering machine stack emissions are greater than any fugitive source, the total emissions from fugitive process sources are greater than the total emissions from stack sources. Table 2 gives data for fugitive open source emissions from integrated iron and steel plants. Considering both process and open source fugitive emissions, the largest six account for 95 percent of the overall emissions. These first six include coke ovens, three process sources, and two open sources. Coke oven emissions are primarily in the inhaleable size range. Process emissions from the two most important sources are mainly under 15 μm and primarily less than 5 μm and can be described as fine particles. Open source emissions are generally greater than 15 μm except for vehicular traffic on paved roads.

Tables 3 and 4 give data on fugitive process emissions from lead and copper smelting. (Note: Emission rates from vehicular traffic in lead and copper smelters were not available. Extrapolating from iron and steel data, it may be a sizeable source.) The highest uncontrolled rates for fugitive emissions in lead smelters come from sintering and concentrate storage and transfer. The highest uncontrolled rates for fugitive emissions in copper smelters come from unloading of concentrate, roaster charging, and converter charging and tapping. For these sources and most smelter operations, the emissions are primarily less than 15 μm.

III. EQUIPMENT FOR CONTROL OF FUGITIVE EMISSIONS

Some degree of fugitive particulate control can be obtained with little or no equipment investment via good housekeeping and plant maintenance practices. Prompt repair of hood damage, maintenance of seals on coke oven doors, the proper handling and disposal of dusts from fabric filters, quick cleanup and disposal of particulate spills, and any of the numerous other elements of good manufacturing practice all serve to reduce the amount of fugitive particulate emissions. This type of control depends on work practices; equipment costs (if any) for these control measures would be independent of whether the standard was based on total suspended particulate or the minus 15 μm fraction.

For open source fugitive particulate emissions such as agricultural tilling, construction activity, and traffic on unpaved roads,

---

*For this report, particles whose diameters are less than 15 μm are called inhaleable particulate matter (IPM). "Inhaleable," in this sense, is not the same as "respirable" as used in OSHA sampling. The samplers used in determining "respirable" dust for OSHA have a 50 percent cut point for a unit density sphere at 3.5 μm and pass zero percent of 10 μm particles.[8]

TABLE 1. FUGITIVE PROCESS EMISSIONS FROM INTEGRATED IRON AND STEEL PLANTS

Process	Estimated uncontrolled fugitive emission rates, process basis		Percent of mass less than 15 μm	Estimated controlled emissions in 1976 – nationwide mass in Mg/yr less than 15 μm	
	kg/Mg	(lb/ton)		Fugitive	Stacks
Coke Ovens					
Charging	0.50	(1.0)	50	33,100	Not applicable
Pushing	0.35	(0.7)	60	22,000	Not applicable
Quenching	0.30	(0.6)	60	3,300	Not applicable
Sintering Machine	2.20	(4.4)	10	8,800	57,300
Hot Metal Transfer	0.10	(0.2)	15	1,300	Not applicable
Electric Arc Furnace					
Alloy steel	0.75	(1.5)	85	4,200	14,300
Carbon steel	1.85	(3.7)	85	29,800	
Basic Oxygen Furnace	0.25	(0.5)	65	14,300	13,200
Open Hearth Furnace	0.08	(0.17)	90	2,000	4,400
Scarfing					
Machine	0.002	(0.005)	100	33	110
Hand	0.55	(0.11)	100	770	

Source: References 3, 9, 10, and 11.

TABLE 2. FUGITIVE OPEN SOURCE EMISSIONS FROM IRON AND STEEL PLANTS (NATIONWIDE TOTALS IN 1976)

Source	Estimated emissions less than 30 μm, Mg/yr	Estimated emissions less than 15 μm, (by interpolation) Mg/yr	Estimated emissions less than 5 μm, Mg/yr
Unloading Raw Materials	1,500	1,000	240
Conveyor Transfer Stations	2,800	2,100	1,100
Storage Pile Activities	20,900	14,300	6,300
Vehicular Traffic	35,300	26,500	14,300
Wind Erosion of Exposed Areas	2,000	1,300	600

Source: Reference 3.

TABLE 3. FUGITIVE PROCESS EMISSIONS FROM PRIMARY LEAD SMELTERS

Process	Estimated uncontrolled fugitive emission rates kg/Mg	(lb/ton)	Estimated percent of mass less than 15 μm
Railroad Car and Truck Unloading	0.34	(0.67)	50
Materials Storage and Transfer			
Limestone	0.10	(0.21)	80
Silica	0.01	(0.02)	80
Concentrate	2.9	(5.8)	80
Iron ore	0.37	(0.74)	80
Coke	0.08	(0.15)	80
Mixing and Pelletizing	1.1	(2.2)	
Sintering	10.6	(21.1)	95
Blast Furnace	0.08	(0.15)	90
Slag Pouring and Disposal	1.7	(3.4)	70
Zinc Fuming Furnace	2.3	(4.6)	100
Dross Kettle	0.24	(0.48)	100
Reverberatory Furnace Leakage	1.5	(3.0)	100
Lead Casting	0.94	(1.87)	95

Sources: Reference 1 (Uncontrolled emission rates from PEDCo Environmental, Inc.).
Size data from several sources noted in Figure 2 legend.

TABLE 4. FUGITIVE PROCESS EMISSIONS FROM PRIMARY COPPER SMELTERS

Process	Estimated uncontrolled fugitive emission rates kg/Mg	(lb/ton)	Estimated percent of mass less than 15 μm
Unloading of Concentrate	16.8	(33.7)	50
Materials Storage and Transfer			
Ore concentrate	0.55	(1.1)	80
Limestone flux	0.25	(0.5)	80
Roaster Charging and Leakage and Calcine Transfer	11.5	(23.0)	No data; see note
Reverberatory Furnace: Charging, Leakage, and Tapping	4.2	(8.5)	95
Converter: Charging, Leakage, and Tapping	6.0	(12.0)	95
Blister Copper: Furnace Charging and Tapping	2.2	(4.4)	20

Note: No reliable fugitive size data available. Might expect fugitives to be similar in size to fugitives from ore concentrate materials handling; i.e., 80 percent less than 15 μm.

Sources: Reference 1 (Uncontrolled emission rates from PEDCo Environmental, Inc.).
Size data from several sources noted in Figure 2 legend.

water suppression is the major means of fugitive particulate control. Wetting with sprays can also be used to reduce fugitive process particulates from storage bins, conveyors, or raw materials storage. Additives of various sorts may be used to form a "crust" on the particulate and improve control efficiency.[12]

Water sprays are not nearly so effective in removing particulates that have already been suspended, especially for the sizes less than 10 μm. Some recent work has been directed at removing small sized, suspended fugitive particulates with charged water sprays.[13] It was found that most particulates carry a negative electrostatic charge, and by inducing a positive charge on water droplets, good removal of respirable size particulates is achieved. IERL-RTP is currently directing an evaluation of this device for fugitive control in lead and copper smelters.[14]

A serious disadvantage of water spray suppression is that it can only be used (1) when the process and product can tolerate the additional water and (2) when capture of the particles is not required. Water sprays help agglomerate suspended particulates so they settle out of the air faster, but they do not, by themselves, collect the settled material. This is not a disadvantage for bins, car unloading, or conveyor transfer points where the settled material returns to the process. However, in many other applications, the settled particulate would dry out and be resuspended.

To remove fugitive particulates from a gas stream, conventional control devices are used: predominantly bag filters, also electrostatic precipitators, scrubbers, and in some cases cyclones. With the exception of cyclones, efficiencies for particulate less than 15 μm are relatively good for these control devices. However, for fugitive emissions, the control problem is not usually the removal of particulates from the gas; it is instead the gathering and collection of the gas streams. Emissions from the many diffuse sources of fugitive particulates must be gathered and transferred to the control device via a ventilation system before the particulates can be removed.

Ventilation systems for fugitives are typically either secondary hooding at the local source of emissions or total building enclosure and evacuation. Both methods have their drawbacks and, for large airflows, have high energy and capital requirements. The ventilation system for collecting fugitives requires individual consideration for each fugitive source. Personnel and equipment access must be considered, the areas to be vented must be selected, and ductwork layout can be difficult in retrofitting existing plants. While the problems in ventilation control of fugitive particulates are considerable, their severity is not sensitive to particulate size, and an IPM standard will not significantly increase the difficulty of ventilation design.

IV. CONTROL FLEXIBILITY AND FACTORS AFFECTING COMPLIANCE WITH AN IPM STANDARD

Equipment Flexibility

The critical factor in reducing the overall emission rate of process fugitive particulates is not how efficiently the control device removes particulates from the ducted gases. Instead, the overall effectiveness is determined by how well the ducting and hoods gather fugitive particulates and how many of the various fugitive sources are controlled. There is little room to "fine-tune" overall removal by varying the design of the central control device--any flexibility in system performance would come from varying the fraction of the numerous fugitive sources that are hooded and routed to the central control device. We do not now have the technology to be able to accurately predict the relative reduction attributed to various fugitive sources, so attempting to meet standards by partial control would be a risky, trial-and-error process.

Level of Standard

Since the primary problem with current fugitive emission control methods is one of containment of the gases rather than removal of the particles from the gas stream, and since most of the particulate is under 15 μm, the importance of an ambient standard based on a 15 μm upper size limit as opposed to total suspended particulate does not seem to be critical if the level is the same for both standards. Control techniques to prevent total suspended particulate (TSP) will be the same as control to prevent inhaleable particulate matter (IPM) if the emissions to be controlled are primarily in the inhaleable size range. This is true for nonferrous metal industry fugitive emissions and for two-thirds of the iron and steel industry fugitive emissions. Controls applied to larger particulate sources (such as sintering and open sources) would have to be better to meet TSP requirements than they would to meet IPM requirements of the same level. If an IPM level much lower than the TSP level were required, greater control would be needed and costs would increase greatly because no control for fugitive emissions is highly efficient. Control equipment installed to meet a high standard could not be inexpensively modified to provide control to a lower level of particulate.

Sampling Location

The ultimate fate of fugitive particulate emissions from an industrial process is not well known. We would expect that the fugitive emissions measured at the plant boundary have fewer large particles because these would settle out inside the plant boundaries. It depends, in general, on the height of the emission point, on the location of surrounding structures, on meteorological conditions at the site

(particularly wind patterns), on the topography of the area, and on the size distribution of the emissions. For example, mathematical modeling[15] has shown that the average drift distance of 15 μm particles emitted 3 meters above the level of surrounding structures can vary from 300 to 800 meters depending on topography alone. (Almost a 300 percent variation.) The corresponding drift distance of 5 μm particles varies from 2 to 6 kilometers. This means, of course, that the achievement of any ambient suspended particulate standard depends not only on the above factors but also on the point and method of compliance testing. A change in the sampling method or point or in the size basis of ambient standards could easily reverse the compliance status of any particular site for either a total or a minus 15 μm standard.

REFERENCES

1. PEDCo Environmental, Inc. Technical Guidance for Control of Industrial Process Fugitive Particulate Emissions. EPA-450/3-77-010 (NTIS PB 272 288/AS), U.S. Environmental Protection Agency, Research Triangle Park, NC, 1977.

2. Kolnsberg, Henry J. "A Guideline for the Measurement of Air-Borne Fugitive Emissions from Industrial Sources," in: Symposium on Fugitive Emissions Measurement and Control (May 1976, Hartford, CT). EPA-600/2-76-246 (NTIS PB 261 955/AS), U.S. Environmental Protection Agency, Research Triangle Park, NC, 1976. pp. 33-50.

3. Bohn, R., T. Cuscino and C. Cowherd, Fugitive Emissions from Integrated Iron and Steel Plants, EPA-600/2-78-050 (NTIS PB 281 322/AS), March 1978.

4. Jones, H. R. Pollution Control in the Nonferrous Metals Industry, 1972, Noyes Data Corp., Park Ridge, NJ.

5. Harris, D. B. and D. C. Drehmel. "Fractional Efficiency of Metal Fume Control as Determined by Brink Impactor," presented at 66th Annual Meeting of the Air Pollution Control Association, Chicago, Illinois. June 24-28, 1973.

6. Constant, P., M. Marcus, and W. Maxwell. Sampling Fugitive Lead Emissions from Two Primary Lead Smelters. EPA-450/3-77-031, U.S. Environmental Protection Agency, Research Triangle Park, NC, 1977. p. 407.

7. Thompson, G. S., Jr. and G. B. Nichols. "Experience with Electrostatic Precipitators as Applied to the Primary Copper Smelting Reverberatory Furnace" in Proceedings: Particulate Collection Problems Using ESP's in the Metallurgical Industry. EPA-600/2-77-208 (NTIS PB 274 017/AS), U.S. Environmental Protection Agency, Research Triangle Park, NC, 1977. pp. 234-251.

8. "Interim Guide for Respirable Mass Sampling," AIHA Aerosol Technology Committee, AHIA J, 31:2, 1970, p. 133.

9. Zoller, J., G. Wood, and T. Janszen, "Current Status of Process Fugitive Particulate Emission Estimating Techniques," Second Symposium on Fugitive Emissions: Measurement and Control, EPA-600/7-77-148 (NTIS PB 276 973/AS), December 1977.

10. Jacko, R., "Coke Oven Emission Measurements During Pushing," in Symposium on Fugitive Emissions Measurement and Control (May 1976, Hartford, CT), EPA-600/2-76-246 (NTIS PB 261 955/AS), September 1976.

11. Kenson, R. E., N. E. Bowne, and W. A. Cote. "The Cost Effectiveness of Coke Oven Control Technology" in Symposium on Fugitive Emissions Measurement and Control (May 1976, Hartford, CT), EPA-600/2-76-246 (NTIS PB 261 955/AS), U.S. Environmental Protection Agency, Research Triangle Park, NC, 1976, pp. 247-266.

12. Dean, K. C., R. Havens, and M. W. Glantz. "Methods and Costs for Stabilizing Fine-Mineral Wastes." U.S. Department of the Interior, Bureau of Mines, R.I. 7894, 1974.

13. Hoenig, Stuart A. Use of Electrostatically Charged Fog for Control of Fugitive Dust Emissions. EPA-600/7-77-131 (NTIS PB 276 645/AS), U.S. Environmental Protection Agency, Research Triangle Park, NC, 1977, p. 59.

14. Research Triangle Institute. Assessment of the Use of Fugitive Dust Control Devices. EPA Contract No. 68-02-2612, Task 48. Task Officer D. C. Drehmel, Research Triangle Park, NC.

15. Cowherd, Chatten. The Impact of Fugitive Emissions of Fine Particles," in Symposium on Fugitive Emissions Measurement and Control (May 1976, Hartford, CT). EPA-600/2-76-246 (NTIS PB 261 955/AS), U.S. Environmental Protection Agency, Research Triangle Park, NC, 1976, pp. 143-158.

FUGITIVE DUST EMISSIONS AND CONTROL

George E. Weant, III*
B. H. Carpenter
Research Triangle Institute
Research Triangle Park, North Carolina 27709

ABSTRACT

Many Air Quality Control Regions (AQCR's) do not meet ambient air quality standards for particulates. In a majority of these AQCR's (92 percent), the emissions from fugitive dust sources are higher than those from nonfugitive sources. In most cases, unpaved roads are the largest source of fugitive dust, while agricultural tilling and construction also contribute substantial amounts. The reentrainment of particles from paved roads can also provide large quantities in urban areas.

Present control techniques for fugitive dust are inadequate. Estimates of the relative effectiveness of control techniques are presented in this paper. If the emissions were controlled to the levels reported in the literature, 87 percent of the AQCR's would still show fugitive sources as greater contributors than other sources.

INTRODUCTION

Many Air Quality Control Regions (AQCR's) do not meet the primary and/or secondary standards for total suspended particulates (TSP). This study provides an estimate of the impact of fugitive dust emissions (i.e., nonducted emissions) on the TSP in these AQCR's. In making this estimate, the relationships between fugitive dust emissions and emissions from other sources were examined in each AQCR. The relationship of emissions to ambient concentrations is not explored except in a general fashion by examining published information on this relationship.

---

*Presently with the Phillips Petroleum Company.

Existing control technologies for fugitive dust sources are examined for effectiveness when applied to various sources. Available data on fractional efficiency of control are presented.

FUGITIVE EMISSIONS ASSESSMENT

Area Sources

The 150 AQCR's that do not meet the total suspended particulate standards were identified from a published report.[1] Emission source categories in each were then examined for relative importance. The categories examined were those over which man has some control, and included fugitive and point sources. Classified as area sources under the National Emissions Data System (NEDS), fugitive emissions sources include dirt roads, landings and take offs from dirt airstrips, agricultural tilling, construction, open burning, slash fires, and coal refuse fires. For the first four sources, emissions data were taken from an updated NEDS card file that used countywide emission factors and activity levels. These data are thought to be more accurate than the data derived from nationwide emissions factors because they are corrected by local silt content, precipitation/evaporation indexes, and dry days per year. Of course, other area sources such as paved roads should also be considered. However, data on these types of emissions could not be obtained on a nationwide basis.

The data for coal refuse piles were generated using an emission factor of 10 kg/m^3 (17 lb/yd^3) and assuming that 5 percent of the pile burns each year.[2] The data for the dirt road emissions were calculated by multiplying the number of vehicle miles traveled by a local emission factor. The vehicle miles traveled were based on a nationwide population extrapolation of data from Kansas where an accurate accounting has been made. A check of these data with results from St. Louis indicated that rural data were within approximately 50 percent while urban data could be as much as two orders of magnitude high.[3] In view of this, the computed values for dirt roads were arbitrarily reduced by one order of magnitude.

This analysis provides annual area emissions levels for the seven source categories. The results for the individual AQCR's are not presented here but can be found in the project report for the study.[4]

INDUSTRIAL SOURCES

Some industrial sources have the potential to contribute significant fugitive dust emissions. A list of these sources is given in the project report.[4]

In a recent paper describing the impact of fugitive emissions on TSP, it was stated that in a large industrial city where the TSP loading was influenced by fugitive emissions, the TSP on an annual basis averaged 25 $\mu g/m^3$ higher than industrial areas not influenced by fugitive emission sources.[8] This paper also stated that the results from 20 sites in five heavily industrialized cities indicated that fugitive emissions increased TSP by 10 $\mu g/m^3$.

In discussions with various EPA personnel, it was brought out that fugitive dust emissions from dirt roads have a relatively minor effect on TSP. This statement was based on the assumption that the particle size of the dust from dirt roads is such that most particles fall out of the air within short distances from the dirt roads and that most dirt roads are located in rural areas away from the sampling stations. However, the study performed in Seattle showed that 27 percent of the dust from vehicles traveling over dirt roads at 32 km/h (20 mph) was suspendable (less than 10 μm in size), while 41 percent was suspendable at 48 km/h (30 mph).[5]

Further evidence of the substantial impact of fugitive dust emissions comes from Massachusetts. An item appearing in a weekly publication reported that the air of southeastern Massachusetts had been declared a hazard to public health and that 80 percent of the particulates came from windblown sand and road dirt.[9] A followup discussion with Massachusetts officials indicated that the episodes occurred during the winter months and were the result of the reentrainment of sand that was used for vehicle skid control.[10]

A study of air quality maintenance areas in North Carolina found that the emissions inventories for particulate matter in several counties did not provide enough emissions to account for the ambient air quality measurements obtain in urban areas.[6] The study concluded that paved roads contributed the substantial amount of emissions necessary to make up the difference in TSP observations in urban sections. To account for this difference, the emission factor that was based on the Seattle study[5] was raised by a factor of 2.3 for Mecklenburg County where vacuum street cleaning is used and by 3.5 for Forsyth and Guilford Counties where no vacuum street cleaning is used. As a result, an acceptable calibration of the Air Quality Display Model (AQDM) was achieved.

The data on both emission quantities and impact of emissions on TSP imply a strong relationship between fugitive dust emissions and nonattainment in many AQCR's. It must be emphasized that the precision and reliability of the data base used for this analysis are unknown, basically because of the inconsistencies in sampling, testing, and recording methodologies used throughout the network. However, NEDS is the only data base available for a study of this type. Therefore, the approach has been to rely on a comparison of relative magnitudes and not on an exact quantification of each piece of data.

FUGITIVE DUST CONTROL TECHNIQUES

Currently control of fugitive dusts from area sources is predominantly by prevention rather than capture and separation. Measures are adopted to prevent the dust from becoming airborne. There are four preventive technologies: wetting, physical stabilization, chemical stabilization, and vegetative stabilization. Industrial operations such as mining and beneficiation, included in this study, tend to make moderate use of capture technologies.

Control technologies were examined to estimate their relative effectiveness and to comment on their limitations. Their applications were considered with respect to eight source categories: agriculture, transportation, materials handling, stockpiles and waste heaps, mining operations, beneficiation, construction, and miscellaneous sources (e.g. open burning, incineration, cooling-tower drift).

Wetting

Wet suppression of dust using either water or water plus a wetting agent can be employed for temporary control of fugitive dust from some agricultural activity, cattle feedlots, unpaved roads, transport of raw materials or products, materials handling and beneficiation, stockpiles, waste heaps, and mining and construction activities. The temporary nature of wet suppression restricts its usefulness. In cases when there is continual activity at the source, the suppressive must be repeatedly applied to be useful. This is due to the continual exposure of dry surfaces to climatic elements and is applicable to agricultural activity, unpaved roads, and stockpiles.

Water has proven to be a poor suppressive due to its high surface tension. The high surface tension interferes with the wetting, spreading, and penetrating necessary for effective suppression.

Surface tension can be reduced by the addition of wetting agents. These agents increase the effectiveness of wet suppression by:[14]

1. allowing particles to penetrate the water droplet, and thus exposing a larger water surface;

2. agglomerating particles in the droplet;

3. increasing the number of droplets per unit volume, the surface area, and the contact potential through increased efficiency of atomization; and

4. causing the liquid to wet faster and deeper and spread farther.

In addition to being a temporary control measure, wet dust suppression cannot be used where either the product or the next stage of processing will not tolerate a wet product. Examples of these instances include grain processing and certain beneficiation processes that require dry classification. Drying steps can be taken but present additional environmental problems as well as added costs.

The wet suppression of dust is usually accomplished by spraying the water either with or without a surfactant onto the surface of the exposed material. For many mining and construction roads and other surfaces, this is usually done by a special truck equipped with a tank for the liquid and a series of spray nozzles in the front and back. For the transport of products and raw materials, the carrier vehicle is usually passed under a series of spray bars where the liquid is dispersed onto the surface of the material. For materials handling and beneficiation sources, nozzles located at transfer points and at equipment intakes spray the liquid on the material. For stockpiles, nozzles spray the liquid onto either the pile or the material as it is being transferred. For feedlots, a spray system is also appropriate.

The application of wet dust suppression to many fugitive dust sources is not feasible. These sources include some agricultural activity, unpaved roads, and waste heaps. Reasons for the infeasibility include the potential shortages of water, magnitude of source, lack of suitable equipment for transporting and dispersing water, and the temporary nature of the control method.

In recent years, a new wet dust suppression system has been introduced. The use of foam systems has become an important dust suppression method. Foam systems have been successfully applied to both hard rock drilling operations and transfer points of conveyors.[11,12] These systems have advantages over untreated water in that they increase the wettability, thus requiring a smaller supply of wetting fluid; and in the case of drilling operations, they prevent overinjection of water into the hole which in turn can cause collaring of the bit and decreased penetration rates.

Data on the control efficiency of wet dust suppression is minimal. One reference cites as much as 80 percent control for cattle feedlots, but this is very much dependent on soil conditions, local climatic conditions, number of cattle, activity level, and many other things.[14] This same reference reported efficiencies of 30 to 67 percent for highly disturbed to nondisturbed storage piles, and efficiencies of 0 to 70 percent for construction site watering.[13]

Observations of several North Carolina granite quarries have shown substantially reduced emissions from processing plants, haulage roads, and drilling rigs using wet dust suppression with surfactants.[14]

Control efficiencies from drilling storage piles and construction sites will depend on many factors, including type of material and percentage of fines, local climatic conditions, type of equipment being used, moisture, and activity rate.

A recent study has examined the use of water sprays and foam on materials handling processes.[12] At a coal chain feeder-to-conveyor transfer point with a 3-ft material drop, water controlled 70 percent of the emissions while the foam spray controlled 91 percent. These numbers represent control with a spray under the belt as well as at the transfer point. Under-the-belt sprays were shown by this report to be effective in controlling dust at conveyor transfer points when used in conjunction with transfer point sprays.

Physical Stabilization

Physical stabilization methods can be used for controlling fugitive dust from inactive waste heaps, unpaved roads, and other sites. Physical stabilization requires the covering of the exposed surface with a material that prevents the wind from disturbing the surface particles.

Common physical stabilizer materials for inactive waste heaps and steep slopes include rock, soil, crushed or granulated slag, bark, wood chips, and straw that are harrowed into the top few inches of the material.[16] For dirt roads, paving is a common practice. However, paving is expensive and, in most cases, must be preceded by roadbed buildup and improvement to prevent overdriving by vehicle operators. Other methods of physical stabilization of these sources include covering with elastomeric films, asphalt, wax, tar, oil, pitch, and other cover materials.

Very little information is available on the effectiveness of physical control methods. One reference cites an 85-percent control efficiency with paving and right-of-way improvement on dirt roads.[13] This control efficiency is dependent on how much dirt is brought onto the road and later reentrained by passing vehicles.

Chemical Stabilization

Chemical stabilization requires the use of binding materials that, upon drying, bind with surface particles to form a protective crust. It acts in much the same way as physical controls by isolating the surface from climatic factors and is often used in combination with vegetative stabilization. Applications of chemical stabilization are found on agricultural fields, unpaved roads, waste heaps, and excavation heaps.

Evaluations of the suitability of various chemical stabilizing materials have been reported in the literature. In one study evaluating the cost and effectiveness of 34 stabilizers,[15] the evaluation criteria

were cost, prevention of wind erosion, effect on plant germination and growth of tomatoes and beans, and ease of application. Those stabilizers that proved effective for reducing wind erosion from the piles for 180 days are ranked in Table 2.

TABLE 2. MATERIALS THAT REDUCED SOIL LOSS FOR 180 DAYS RANKED BY 1971 COST

Product	Manufacturer	Nonerosion Rate (per acre)	1971 Cost ($)	Ranked Effectiveness
Elvanol 50-42 Technical Protein Colloid	E. I. du Pont	13 lb	8.20	6
5-V	Swift & Co.	108 lb	34.60	5
Geon 652	Goodrich Chemical	17 gal	51.20	8
Aquatain	Larutan Corp.	68 gal	172.50	7
ORTHO Soil Mulch	Chevron Chemical	681 gal	242.20	1
Anionic Asphalt Emulsion	Phillips Petro.	1226 gal	436.70	3
AGRI-MULCH	Douglas Oil	954 gal	445.70	4
Soil Erosion Control Resin Adhesive Z-3876	Swift & Co.	571 gal	1159.90	2

A later report presented the results of the Bureau of Mines tests on 70 different chemicals.[16] Water and wind erosion tests were performed in the laboratory on applications of these chemicals to various types of mill tailings. The more effective chemicals of those tested are listed below in order of their relative effectiveness based upon the cost required to stabilize 1 yd^2.[12] Long-term effectiveness to wind erosion was not measured.

1. COHEREX - good wind resistance at coverage of 240 gal/acre at cost of $65/acre, good water-jet resistance at cost of $650/acre.

2. Calcium, sodium, ammonium lignosulfonates - effective stabilizers at coverage of 2400 lb/acre at cost of $130 to $170/acre.

3. Compound SP-400, Soil Gard, and DCA-70 - wind and water resistant surfaces at coverage of 55, 90, and 50 gal/acre, respectively. Cost of about $130/acre.

4. Cement and milk of lime - effective stabilization at costs of about $190/acre.

5. Paracol TC 1842 - effective stabilizer at cost of about $250/acre.

6. Pamak WTP - effective at cost of $250/acre.

7. Petroset SB-1 - effective at cost of $250/acre.

8. Potassium silicate (SiO_2 to K_2O ratio of 2.5) - effective at $450 to $950/acre.

9. PB-4601 - effective at $500/acre.

10. Cationic neoprene emulsion and Rezosol - effective at $500/acre.

11. Dresinol TC 1843 - effective at $500/acre.

12. Sodium silicates (SiO_2 to Na_2O ratios of 2.4 to 2.9 to 1) - effective at about $200/acre, with calcium chloride additive, amount of sodium silicate was reduced.

One reference has estimated control efficiencies of chemical stabilization on a number of sources.[13] Examples of these estimates are as follows:

Source	Efficiency (%)
Unpaved roads	50
Construction - completed cuts and fills	80
Agricultural fields	40
Tailings piles	80
Continuous spray of aggregate as it is piled	90
Cattle feedlots	40

The effectiveness of chemical stabilization of unpaved roads would seem to be extremely variable based on the amount of traffic. Heavy traffic would tend to break up the surface crust, pulverize particles, and eject them into the atmosphere in much the same manner as if the road were untreated. Likewise, with cattle feedlots, the effectiveness would seem to be heavily dependent on the activity in the feedlot. It would seem that the effectiveness of continuous spraying of aggregate as it is piled could be highly variable depending on such things as the quantity of fines in the mix, type of stone, etc. In addition, the activity level of the storage pile is also important.

Vegetative Stabilization

Vegetation can be effectively used to stabilize a variety of exposed surfaces. In many cases, modifications must be made to the

surface or the surrounding terrain before effective stabilization can occur (e.g., fertilization, pH modification, and slope reduction).

Vegetative stablization for the control of fugitive dust is restricted to inactive areas where the vegetation will not be mechnically disturbed once it is started. These sources can include refuse piles (coal and mineral) and road shoulders.

Coal Refuse Piles--

Coal mining and preparation usually produce both fine and coarse waste materials. These materials consist of low grade coal, ash, carbonaceous and pyritic shale, slate, clay, and sandstone.[17]

The principal problems encountered in the vegetative stabilization of coal refuse piles occur as a result of the acidic nature of the wastes and from the slopes of the piles' sides. Thus, chemical or physical treatment of the piles' components must be accomplished prior to effective stabilization. Chemical treatment usually involves the addition of a soil neutralizing material such as agricultural limestone. Other materials such as fly ash, mines phosphate rock, and treated municipal sewage sludge have also been used.[17] Even with a neutralization pretreatment, it is recommended that acid-tolerant vegetative species be used for stabilization because the sulfide materials in the waste can oxidize the acid sulfates and thus lower the pH of the soils.

Physical treatment of the piles usually involves such things as the burying of high pyritic materials, covering the piles with a layer of topsoil, or grading to reduce slopes of the piles.[17] A good premining restoration plan can be effective for efficient physical treatment methods.

Many species of plants have been used for the stabilization of coal mine refuse piles: grasses, legumes, trees, shrubs, and vines. For a detailed discussion of these plants and their uses, refer to Reference 17.

Mineral Refuse Piles--

Mineral mining and beneficiation produce wastes in the form of overburden, gangue, and tailings. Overburden and gangue do not usually present problems to vegetative stabilization. However, tailings can present varied and extreme problems due to a deficiency of nutrients, saline or toxic properties, and variable pH.[17]

Most tailings stabilization is accomplished by first covering the waste with a layer of topsoil and then by establishing a vegetative cover. Without the topsoil cover, vegetation usually requires the assistance of other wind erosion preventatives such as mulches, chemical coatings, rapidly established plant covers, and watering.[17] However, even with these aids, stabilization of many mineral wastes has

not been effective. Most species are very site-specific, and small changes in topography, climate, and tailings composition affect their growth success.

Copper Tailings--

The establishment of vegetation on copper tailings is very site-specific. Even with piles in the same general geographic area, it is often difficult to establish the same type of vegetation.

In the western United States, copper tailings have been stabilized with vegetation. In most cases, maintenance in the form of liming, fertilizing, and irrigating after planting is required. However, at Magma, Utah, a form of permanent vegetative stabilization seems to have been established with natural vegetation invading the pile.[17]

Uranium Tailings--

Uranium tailings in Colorado have been stabilized using sweet brome, sweetclover, cereal rye, barley, alfalfa, and various wheat grasses.[17] There has been very little invasion by natural species, and continual maintenance is required.

Iron Tailings--

The vegetative stabilization of iron tailings in Pennsylvania and Minnesota has been relatively successful. Initial stabilization with grasses and legumes followed by the planting of woody plants seems to have been successful.[17] Invasion by native vegetation heightens the prospect of a permanent, maintenance-free stabilization site.

Other Metallic Tailings--

In most cases, plants tolerant to specific conditions must be applied to metallic tailings piles. Some success has been demonstrated with varieties of grasses on gold mining slimes and sands; some species of grasses have been found to be tolerant to lead and zinc; but little long-term success has been demonstrated with rye on molybdenum tailings.[17]

Control Efficiency--

The control efficiency of vegetative stabilization should vary considerably with differences in the amount and type of cover established on the tailings piles. One report estimates a control efficiency of from 50 to 80 percent.[13] This estimate was made using the wind erosion equation and is not based on a measured efficiency. This same report estimates a 93-percent reduction in windblown emissions with a combined chemical/vegetative stabilization program.

It would seem reasonable to assume that these control efficiencies could be achieved. In fact, efficiencies of 100 percent should be approached with complete vegetative covering on some sources.

OTHER CONTROL METHODS

Numerous other control methods are available for various sources of fugitive emissions. Some of the most important include speed reduction on unpaved roads, street cleaning of paved roads, reduction of fall distances for materials handling, and enclosure, hooding, and ducting.

Speed Reduction

Reducing the speed of vehicles traveling over unpaved roads has been shown to reduce the dust emissions from such travel. A reduction in vehicle speed reduces both the pulverization of road material and the turbulent wake of the vehicle. A well-quoted source has shown the following results from vehicle travel at various speeds on dirt roads. (Table 3).[11]

TABLE 3. EFFECT OF SPEED REDUCTION ON EMISSIONS

Average Vehicle Speed (mph)	Dust Emissions (lb/vehicle mile)	Emissions Compared to Those at 40 mph (%)
40	2.50	100.0
35	1.47	58.8
25	0.70	28.0
15	0.48	19.2

In another report, the results of a study in Seattle's Duwamish Valley have shown comparatively higher emissions.[5] In addition, this study showed significant reductions in the quantities of suspendable particulates with speed reduction. The results are shown in Table 4.

TABLE 4. EFFECT OF SPEED REDUCTION ON EMISSIONS IN SEATTLE'S DUWAMISH VALLEY

Vehicle Speed (mph)	Total Emissions (lb/vehicle mile)	Suspendable Emissions (lb/vehicle mile)	Total Emissions Compared to Those at 30 mph (%)	Suspendable Emissions Compared To Those at 30 mph (%)
30	22.2	9	100.0	100.0
20	7.0	2	31.5	22.2
10	3.5	0.5	15.8	0.1

Street Cleaning

With the recent interest on reentrained dust from paved roads as a source of air pollution, attention has been focused on street cleaners as dust control devices. Essentially three types of cleaners are now in use: broom sweepers, flushers, and vacuum and regenerative air sweepers. Their effectiveness has not been overwhelmingly demonstrated. Streetside samples have shown concentration reductions but regional samplers have shown no reductions.

Broom sweeping has been shown to reduce the average concentration of dust in one study but has been shown to be ineffective in two others.[18] It has been estimated that this type of sweeper picks up 20 percent of the material below 140 μm.[19] Also, while recovering this paltry amount of material, the sweeper can actually generate air pollution by stirring up the dust and by moving the material from the curbs into the middle of the road where it can be reentrained by passing vehicles.

Flushing showed significant particulate reduction in two studies and no effect in two other studies. In a fifth study, flushing showed no reduction in the average monthly concentration but did show reduction on days when flushing took place.[18]

Vacuum and regenerative air sweepers have been shown to be ineffective.[18]

Two studies on mud carryover control showed substantial reductions in particulate concentrations.[18] These studies involved manual cleaning at a construction site egress and strip paving and oiling of unpaved parking lots, roads, and shoulders on an areawide basis.

Reduction of Fall Distances

During the transfer of dusty materials from a conveyor or stacker to another location such as another conveyor or a stockpile, the

separation of the fine materials from the large materials can be caused by wind and/or the falling action of the material. A simple method to reduce dusting from these operations is to reduce the fall distances by using hinged-boom conveyors, rock ladders, telescoping chutes, lowering wells, or other devices.[14] The hinged-boom conveyor can raise or lower the conveyor belt and thus reduce the fall distance at the transfer point. Rock ladders allow the material to fall small distances in a step-like fashion. By reversing the direction of travel on successive steps, the momentum that the material receives from the previous fall and the dusting are reduced.

Telescoping chutes carry the material from the discharge point to the receiving point. Thus, the material is not exposed. Lowering wells, or perforated pipes, allow material to flow out of the pipe above the pile surface. The dusting from the impact of the falling material is retained inside the pipe, and the material is protected from wind action.

Enclosure

Simple enclosure of a fugitive dust source is an effective control method in some cases. It has been applied to a number of sources including storage of products, loading and unloading operations, product bagging operations, and classification operations. In process operations, periodic cleaning is necessary and may preclude application.

The enclosure of sources without providing adequate exhaust is not applicable to sources where abrasive materials are handled. This is especially true in hard rock processing plants where a high quartz content of the rock abrades the equipment. Enclosure is also not applicable to sources whose dust would present the danger of explosion such as in many grain handling operations.

Exhaust Systems

Many process sources of fugitive dust emissions can be controlled by the use of exhaust systems in combination with full or partial enclosure or full- or partial-coverage hoods and the associated ducting. Examples of sources amenable to this type of control include materials handling (i.e., conveyors, elevators, feeders, loading and unloading, product bagging, and stockpiling), solids beneficiation (i.e., crushing, screening, and other classifying), mining operations (i.e., drilling), and others (i.e., furnaces and dryers).

Complete enclosure of conveyors, elevators, or feeders has been practiced. Another alternative is to enclose the transfer points. Hoods as well as enclosures can be used on many loading and bagging operations.

For solid beneficiation processes, both enclosures and hoods are used. For drilling operations, enclosure of the drill hole and ducting to a baghouse mounted on the drill rig is used.[14]

Effectiveness of control is highly variable and dependent on many variables. Efficiencies of 90 percent and greater are considered appropriate. For example, 90 percent efficiency is attainable on the enclosure of BOF furnaces.[20]

No attempt has been made to provide detailed descriptions of ventilation practices. However, several excellent references are available on this subject (see References 21 and 22).

EFFECTIVENESS OF CONTROLS

Based on the foregoing discussions and comparisons, the relative effectiveness of the five types of control technologies as applied in the eight source categories is summarized in Table 5. The comparative effectiveness is indicated by VP (very poor, less than 20 percent efficiency); P (poor, about 30 percent efficiency); F (fair, about 50 percent efficiency); G (good, perhaps up to 85 percent efficiency). These efficiencies may be substantially less than indicated, depending upon the circumstances of application. Additional symbols used are: NR (not rated, usually because no application could be cited); VAR (variable); UPR (unpaved roads); PR (paved roads). More extensive tables showing ratings by individual source within each category are given in the project report.[4]

TABLE 5. RELATIVE EFFECTIVENESS OF FUGITIVE DUST CONTROL TECHNOLOGIES, BY SOURCE

Control Technology	Source Category: Agriculture	Transportation UPR	Transportation PR	Materials Handling	Stockpiles, Waste Heaps	Mining Operations	Beneficiation	Construction	Miscellaneous open burning	Miscellaneous incineration	Miscellaneous cooling tower drift
Physical stabilization	NR	G	F	NR	F,G	NR	NR	F,G	-	-	-
Wetting, wet application	F	VP	P	FG	P,F	VP	P,F	VP,P	-	-	-
Chemical stabilization	P	P	F	NR	P	NR	NR	NR	-	-	-
Vegetative stabilization	VP		G	NR	FG	NR	NR	F,G	-	-	-

TABLE 5. (Continued)

Control Technology	Source Category: Agriculture	Transportation: UPR	Transportation: PR	Materials Handling	Stockpiles, Waste Heaps	Mining Operations	Beneficiation	Construction	Miscellaneous: open burning	Miscellaneous: incineration	Miscellaneous: cooling tower drift
Special											
control device											FG
speed reduction		Var									
enclosure				F							
exhausting				F,G		G	F,G				
reduction of fall				F-P							
wind screen					VP						

F = fair ~ 50% G = good ~ 85% P = poor ~ 20% VP = very poor < 20%

UPR = unpaved roads NR = not rated Var = variable
PR = paved roads

Conclusions

While fair control of some agriculture emissions may be obtained by wetting, this source lacks good controls. Physical stabilization remains practically untried, chemical stabilization is rated poor, and vegetative stabilization very poor.

Physical stabilization of dirt roads (that is, paving) is the only good control. Paved roads benefit from vegetative stabilization of shoulders. Materials handling operations can attain fair to good control by wetting when the techniques can be used. Other technologies remain unexploited at this time.

Stockpiles benefit from physical and vegetative stabilization.

Mining operations benefit from exhausting techniques, while wetting is very poor and the stabilization technologies have not been rated, and may not work well.

Exhausting has been fair to good for control of beneficiation emissions, while wetting has been poor to fair, and stabilization unrated.

Physical and vegetative stabilization is fair to good in construction operations, while wetting is poor, and chemical stabilization is not rated.

None of these technologies are effective in open burning or on industrial cooling towers. Incinerators, if properly designed, can be effective as control devices.

EFFECT OF FUGITIVE EMISSION REDUCTION ON AQCR'S

To examine the effects of fugitive dust emissions reduction on total AQCR emissions, emissions from unpaved roads, agricultural tilling, and construction were reduced by appropriate measures reported in the literature. The reductions used were 50 percent for unpaved roads and 40 percent for agricultural tilling (chemical stabilization effectiveness), and 30 percent for construction (wetting).

The results of the emissions reduction are shown in the following summary:

	Before Emissions Reduction	After Emissions Reduction
Total number of AQCR's not meeting TSP Standards	150	150
Point > Area	9	17
Area > Point	139	131
Area 5x > Point	97	68
Area 10x > Point	58	38
Data Missing	2	2

CONCLUSIONS

1. Fugitive dust sources are significant emitters of particulates in a majority of the AQCR's. Of the 150 AQCR's that do not meet the TSP standards, fugitive dust emissions exceed point source emissions in 139 AQCR's, or 92 percent. In fact, fugitive emissions are 10 times greater than point source emissions in 58, or 39 percent, of the AQCR's.

2. In most cases, unpaved roads provide the largest source of particulate emissions in the AQCR's. Agricultural tilling and construction sources are also very important and in some cases are the largest emitters.

3. The reentrainment of particles from paved roads is a source of large quantities of particulates in many AQCR's.

4. Industrial sources of fugitive emissions are plentiful and can have a substantial impact on surrounding areas.

5. Fugitive dust sources can contribute significantly to the TSP burden of an entire AQCR as well as have an impact in a localized area.

6. The relationship between pollutant exposure and human health has been demonstrated. Increased hospitalization rates have been observed with increased particulate pollutant exposure.

7. More attention should be given to the control of fugitive dust emissions because of their contribution to ambient dust loadings.

8. Control effectiveness for fugitive sources is highly variable and depends on such things as type of control, characteristics of the source, local climatic conditions, and source activity.

9. Present control technology for unpaved roads, agricultural tilling, and construction activity is inadequate. Reducing the emissions from these activities by the amounts reported in the literature has only a small influence on fugitive emissions in most AQCR's.

REFERENCES

1. Office of Air and Waste Management, State Air Pollution Implementation Plan Progress Report, Jaunary 1 to June 30, 1976," Office of Air Quality Planning and Standards, U.S. EPA, EPA-450/2-76-026, October 1976.

2. Personal communication, Mr. Chuck Mann, NADB, EPA, Durham, May 9, 1977.

3. Ibid., March 30, 1977.

4. Carpenter, B. H., and G. E. Weant, III, "Particulate Control for Fugitive Dust," EPA 600/7-78-071, April 1978.

5. Roberts, J. W., H. A. Watters, C. A. Mangold, and A. T. Rossano, "Cost and Benefits of Road Dust Control in Seattle's Industrial Valley," J. APCA, 25(9), September 1975, pp. 948-952.

6. Haws, R. C. and H. L. Hamilton, Jr., "North Carolina Air Quality Maintenance Area Analysis, Vol. III: TSP Dispersion Modeling and Analysis for Charlotte, Winston-Salem, and Greensboro AQMA's for 1973, 1975, 1980, 1985," RTI Final Report, EPA Contract 68-02-1385, Task 15, April 1976.

7. Pierson, W. R. and W. W. Brachaczek, "Note on In-Traffic Measurement of Airborne Tire-Wear Particulate Debris," J. APCA, 25(4), April 1975.

8. McCutchen, G., "Regulatory Aspects of Fugitive Emissions," paper in Symposium on Fugitive Emissions Measurement and Control, May 1976, Hartford, CT, EPA 600/2-76-246, September 1976.

9. Air/Water Pollution Report, Business Publishers, Inc., Silver Spring, MD, May 2, 1977, p. 177.

10. Personal communication, Mr. Steve Dennis, Massachusetts Department of Environmental Quality Engineering, Boston, May 27, 1977.

11. Metzger, C. L., "Dust Duppression and Drilling with Foaming Agents," in Pit and Quarry Magazine, March 1976, pp. 132-133 and 138.

12. Seibel, R. J., "Dust Control at a Transfer Point Using Foam and Water Sprays," U.S. Department of the Interior, Bureau of Mines, TPR 97, May 1976.

13. Jutze, G. and K. Axetell, "Investigation of Fugitive Dust, Vol. 1: Sources, Emissions, and Control," EPA 450/3-74-036a, June 1974.

14. Weant, G. E., III, "Characterization of Particulate Emissions for the Stone-Processing Industry," RTI Final Report, Contract No. 68-02-02607, Task 10, U.S. EPA, Industrial Studies Branch, May 1975.

15. Armbrust, D. V. and J. D. Dickerson, "Temporary Wind Erosion Control: Cost and Effectiveness of 34 Commercial Materials," J. of Soil and Water Conservation, July 1971, pp. 154-157.

16. Dean, K. C., R. Havens, and M. W. Glantz, "Methods and Costs for Stabilizing Fine-Mineral Wastes," U.S. Department of the Interior, Bureau of Mines, RI 7894, 1974.

17. Donovan, R. P., R. M. Felder, and H. H. Rogers, Vegetative Stabilization of Mineral Waste Heaps," EPA 600/2-76-087, April 1976.

18. Axetell, K. and J. Zell, "Control of Re-entrainment Dust from Paved Streets," EPA 907/9-77-007, August 1977.

19. Sartor, J. D., B. Boyd, and W. H. VanHorn, "How Effective is Your Street Sweeping," APWA Reporter, 39(4), 1972, p. 18.

20. Nichols, A. G., "Fugitive Emission Control in the Steel Industry," Iron and Steel Engineer, July 1976, pp. 25-30.

21. Committee on Industrial Ventilation, Industrial Ventilation, A Manual of Recommended Practice, 14th ed., 2nd Printing, American Conference of Governmental Industrial Hygienists, Lansing, Michigan, 1977.

22. Environmental Control Division, Control of Internal Foundry Environment, Vol. 1, American Foundrymen's Society, Des Plaines, IL.

SETTING PRIORITIES FOR THE CONTROL OF PARTICULATE EMISSIONS FROM OPEN SOURCES

John S. Evans, Douglas W. Cooper,
Margaret Quinn, and Maria Schneider
Department of Environmental Health Sciences
Harvard School of Public Health
Boston, MA

ABSTRACT

Open sources of particulate emissions include agriculture, roads, forest fires, construction sites, and mineral extraction, etc. Control technology research, development, and application need the setting of priorities to be optimally effective. One criterion for optimization is cost-effectiveness, which can be determined by maximizing the weighted sum of emission reductions, within budgetary and technological constraints. Annual open source emission rates for the United States are reviewed and revised as a guide to the most significant sources. Control cost information is developed and used to formulate a cost-effective strategy for controlling the greatest source, unpaved roads.

INTRODUCTION

The results of air sampling indicate that the National Ambient Air Quality Standards for total suspended particulates (TSP) are not being met for a majority of the Air Quality Control Regions. In 1976 the national average TSP concentration increased from 1975, an increase attributed to higher-than-average contributions from nonindustrial sources of particulate emissions[1]. We are conducting a study for EPA on setting priorities for the control of dust from open sources, sources too large in extent to be controlled by enclosures and ducting. That program has as its goals the identification of the major open sources of particulate emissions and the consideration of alternative analyses for setting priorities for their control, such as ranking on the basis of cost of control or the hazard to the population, etc. In this paper, major open sources of particulate emissions are analyzed

to attempt to rank them in order of emission rate (tons/year) for the U.S. as a whole and for each state; cost and effectiveness of control are analyzed for the suppression of road dust from unpaved roads, one of the largest sources (in tons/year) of suspended dust; and it is shown how the results of many such cost-effectiveness analyses could be combined to determine an optimally cost-effective strategy.

EMISSION FACTORS

The emission factors used to prepare our emission rate estimates are listed in Table 1. Each factor is the estimate of the amount per unit of source extent of emissions of suspendable dust, particles smaller than 30 μm with assumed densities of 2.5 g/cm^3, thus particles with aerodynamic diameters less than 48 μm. These emission factors are discussed very briefly next.

Agricultural Tilling

The amount of dust produced per acre during agricultural tilling depends upon many factors, including soil type, soil moisture, vehicle speed, etc. Emission factor values for the counties in the U.S. were provided by the Environmental Protection Agency[2] based upon the work of Cowherd, Southerland and Mann.[3] We selected the median county value to characterize each state, and these values are listed in the second column of Table 1.

Agricultural Erosion

The dust produced by wind erosion of agricultural soil depends upon soil type and moisture, wind velocity, vegetative cover, and field and surface geometry. The emission factor used in the third column of Table 1 was determined by using the formula:[4]

$$E_s = 0.025\ I\ K\ C\ L'\ V' \qquad (1)$$

where

E_s = suspended particulate erosion from fields, tons/acre-year;
I = soil erodibility, tons/acre-year;
K = surface roughness factor, dimensionless;
C = climatic factor, dimensionless;
L' = unsheltered field width factor, dimensionless;
V' = vegetative cover factor, dimensionless.

This equation was derived from a formula for wind erosion by using field measurements to estimate that 2.5% of the soil which erodes becomes airborne as suspendable particulate material.[4] I, the erodibility, depends upon soil type; it is the erosion for a flat, very large but bare field in a dry and windy climate. K, C, L', and V' are correction factors. C can be determined from:[5]

$$C = 0.345\ \bar{v}_{30}/(PE)^2 \qquad (2)$$

where $\bar{v}_{30}$ = mean wind velocity at 30 feet above ground, mi/hr;
PE = Thornwaite's precipitation-evaporation index.

To determine $\bar{v}_{30}$, we started initially with 237 values for $\bar{v}_{15}$ for the fifty states.[6] These 237 ranged from 4 to 80 miles per hour, but five of them seemed clearly erroneous or atypical; after dropping these five values, we had a new range, 4-15 mph, which illustrates the degree to which these 5 values (35, 56, 65, 73, 80 mph) were outliers. This left no value for Maryland, so the mean of the values for the bordering states was used (8.5 mph). The mean wind velocity for each state was calculated and then corrected for a height of 30 feet by using the formula:[7]

$$v_2/v_1 = (z_2/z_1)^a \qquad (3)$$

with a = 0.5 (appropriate for z = 2 to 10 m under neutral conditions); thus, $(30/15)^{.5} = 1.414$ was used as correction to $\bar{v}_{15}$ to obtain $\bar{v}_{30}$. To check our values for the C factor against those widely used, we determined approximate state-by-state area-averaged values of C from a map of C values covering 37 states.[5] The C factors we calculated ranged from .012 to 1.38; the coefficient of determination for the 37 state area-averaged values versus the corresponding 37 of 50 calculated from equation 2 was $r^2 = 0.86$; the slope was 1.24; one can conclude that the two methods agree rather well, the area-averaged values being generally about one-fourth higher.

Cowherd et al.[4] presented tables which give typical values of K, L, and V for various crops. From the data giving crops and acreage by state,[10] we derived area-weighted averages of K, L, and V for use in determining the surface roughness and the L and V factors to be used in the wind erosion equation.[11]

Although one can estimate the factor for unsheltered field length, L', the correction factor is difficult to compute and is generally quite close to one (see example in the paper by Woodruff and Siddoway[11]). The correction factor was not incorporated into our estimates. We did, however, correct for vegetation, using the vegetative cover factor[11] appropriate to the soil erodibility and vegetation characterizing each state, because vegetation factors can be a factor of two or even greater.

Predominant soil type used to determine I, the erodibility index, was determined from a soil map in The National Atlas of the United States.[12] For most states, the analysis was straightforward: the soil type covering 50% or more of the area was used for the entire state. For several states there was not one soil type covering more than half the area, so the areas of two or more soil types were estimated and used to form a weighted average erodibility index. In the following states, the soil that predominated in the farming areas was used instead: California, Florida, Hawaii, Nevada, New Mexico, New York, Washington State, Wyoming. (The erodibility indices used for each state will be made available upon request.)

Construction

Dust emissions at construction sites are generated by such operations as land clearing, blasting, ground excavation, cut and fill operations, and construction. Dust activity also varies according to level of activity and weather conditions.[9] The median values of construction emission factors were again selected by state from county-by-county data supplied by the Environmental Protection Agency.[4] These factors are based upon the approximate emission factor for construction of 1 ton/acre-month[3] adjusted by the following assumed durations of construction:[3] six months for residential building, eleven months for non-residential building, and eighteen months for non-building construction activities. The resulting emission factors are in column four of Table 1.

Forest Fires: Wildfires

Our review of the literature indicated that the best estimates of emissions from forest fires, both wild and prescribed, are those of Ward et al.[14] The emission factors in column five of Table 1 are obtained by using their estimate that 150 lb/ton of wood burned is emitted as suspendable particulates, along with the typical values presented by Yamate et al. for the tons of wood per acre for forested regions in the respective states, to give tons of particulate emitted per acre burned, by state.[8,9]

Forest Fires: Prescribed Burning

Using 50 lb/ton as the emission from prescribed burning[14] and tons/acre data from Yamate et al. the values in the sixth column of Table 1 were obtained.[8,9]

Mineral Industries: Bituminous Coal

Surface mining of coal produces particulate emissions as the "overburden" material is removed to get at the coal. In the East and Central U.S. the ratio of overburden thickness to coal thickness is 10:1 to 20:1 and in the West the ratio is closer to 1:3.[15] Oschner and Blackwood[16] cited emission factor values of 0.17 lb/ton of overburden removed, based on research done by Monsanto Research Corporation, and cited other estimates from 0.048 to 0.1 lb/ton of overburden. A 10:1 overburden-to-coal ratio and 0.17 lb/ton of overburden gives an emission factor of 1.7 lb/ton of coal from Eastern and Central surface mining operations. In these same regions, the amount of coal per acre is about 2600 tons[15], and the time during which the land is disturbed (from initial removal to return and replanting) is several months[15] (Using the emission factor estimate for construction of 1.2 tons/acre-month of activity gives a value of 3.7 lb/ton of coal produced, not very different from the 1.7 lb/ton factor.). To estimate the emissions from bituminous coal surface mining, we have used 1.7 lb/ton of coal for the East and Central states and about 1/30 of this value (0.06 lb/ton) for Western coal production. These values are very approximate, however, as they do not take into account important details such as climatic factor and soil type. Column seven in Table 1 gives emission factors by state for bituminous coal.

Mineral Industries: Other Surface Mining

Noting the values for coal given above, we used a rough estimate of 2 lb/ton (0.1%) of material which is surface mined, but this we believe correct, as an average for all such mining, only to within an order of magnitude. This estimate is indicated in column eight of Table 1.

Roads: Paved

Column nine in Table 1 indicates an emission factor of 0.013 lb/vehicle-mile as an emission factor for paved roads.[18] This factor depends on land use and indicates a mean value (residential, industrial, commercial).

Roads: Unpaved

Unpaved road emissions depend upon surface texture and material, surface moisture, vehicle speed and type. Cowherd et al.[3] developed an emission factor for roads which depends upon road surface, silt content, average vehicle speed, and the number of dry days per year; from county levels they determined, the median values for each state were selected for use as characteristic of the individual states;

these medians are shown in Table 1 under the last column.

SOURCE EXTENTS

The measures of source extent used to prepare our emission rate estimates are listed in Table 2 and discussed below.

Agricultural Tilling and Wind Erosion

The second column in Table 2 gives the number of acres of harvested cropland by state. This is the measure of source extent for wind erosion from such land; multiplied by three (for an average of three tillings per year), the numbers become the measure of source extent for agricultural tilling emissions.

Construction

Conversion factors developed by Midwest Research Institute were used by us to calculate total acreage of active construction, based upon construction expenditures for each Standard Industrial Code (SIC) classification for each state: [3,19]

SIC code	Description	Factor (acres/10^6)
1521	General contractors-single family houses	5
1522	General contractors-residential buildings other than single family	5
1531	Operative builders	5
1541	Industrial buildings and warehouses	5
1542	Non-residential buildings, N.E.C.	5
1611	Highway and street construction	25
1622	Bridge, tunnel and elevated highway construction	25
1623	Water, sewer and utility lines	5
1629	Heavy construction, N.E.C.	150

Column three in Table 2 gives the calculated acreage of active construction in each state.

Forest Fires: Wildfires and Prescribed Burning

Forest acreage, the source extent for forest fires, was obtained from work by Ward et al.[14] Acreage values were derived by them from averaging ten years of data, 1963-1972, from Wildfire Statistics,[20] published by the Forest Service, U.S. Dept. of Agriculture for those years. (Most, but not all, of forest acreage in the U.S. is included in these values.)

Mineral Industries: Bituminous Coal

Annual tonnage of coal produced, the measure of source extent, was obtained by compiling state coal production figures found in the most recent Minerals Yearbook (1974).[21] These production figures are found in column six of Table 2.

Mineral Industries: Other Surface Mining

State values for material handled at surface mines, available from the latest Minerals Yearbook,[21] provided us with our measure of source extent, total annual tonnage produced.

Roads: Paved and Unpaved

The miles of paved and unpaved roads by state were obtained from statistics issued by the Federal Highway Administration.[22] Information from the State of Mississippi indicated that sand, gravel, slag and dirt surfaced roads receive about ten percent of the per mile use of asphalt and concrete surfaces. Therefore, we apportioned the annual vehicle miles traveled according to the formulas:

$$aP + bU = V \tag{4}$$

$$b/a = 0.1 \tag{5}$$

where

P = paved mileage in state;
U = unpaved mileage in state;
V = total vehicle miles traveled in state yearly;
a = use factor for paved roads;
b = use factor for unpaved roads.

These two equations allowed the calculation of a and b and thus the calculation of the amount of miles traveled annually on unpaved roads, bU, and on paved roads, aP, shown in Table 2.

EMISSION RATES

Our estimates of emission rates for each of the sources was obtained by multiplying its emission factor with its source extent. The resulting emission rate is indicated for each source for each state in Table 3. The national total emission rates by source category are:

Source type	Particulate Emissions (10^6 tons/yr)
Agricultural tilling	3.3
Wind erosion of harvested cropland	23.3
Construction	27.4
Wildfires	3.4
Prescribed burning	0.4
Surface mining	3.2
Unpaved roads	325.6
Paved roads	8.4
Total	395.0

As a point of comparison, total point source emissions in the U.S. are on the order of 20 million tons/year.

ECONOMICS OF OPEN SOURCE CONTROL

Estimation of the magnitude of emissions is a very preliminary step in the evaluation of the significance and feasibility of control of open sources. Particles are thought to impair health, increase rates of weathering and corrosion of materials, contribute to the damage of vegetation, and decrease visibility. The decision to control fugitive dust, and the selection of a strategy of control, affect society in two ways: the amount, type, and location of damage done by particles is altered, and resources are diverted from other uses to control open sources of emissions.

Here is outlined a method which allows one to minimize the national costs (diversion of resources) associated with any level of emission reduction.* We leave to others an examination of the physical and economic benefits of these emission reductions.

Stated briefly, for each source class (i.e., agricultural tilling, unpaved roads, ...), one proceeds through a six step sequence, leading to the evaluation of cost-effectiveness:

1. determine the feasible control methods;
2. evaluate the components of control cost and efficiency;
3. calculate the total annual cost of control per unit of source extent;
4. standardize the total annual costs, dividing by control efficiency;
5. select the dominant control method;
6. calculate the cost efficiency of the dominant method in each state.

Finally, when this analysis is completed for each source class, one can rank the results, and prepare a tabulation of the maximum mass of dust emissions which can be prevented each year for any level of control expenditure.

In highly summarized fashion, we present below our preliminary cost-effectiveness analysis of the largest of the open sources of emissions, unpaved roads.

COST EFFECTIVENESS: EMISSIONS CONTROL FOR UNPAVED ROADS

Widely-used methods of dust control include paving, oiling, watering, and the application of calcium chloride. Speed reduction is often suggested as an emission control method, since emission factors increase at least proportionately with vehicle speed. Although many methods of chemical stabilization have been tested (and appear to be more effective than oiling), not enough economic data is available to permit evaluation of their cost efficiency.

Table 4 presents data on the standardized total annual costs of these methods of control. The wide ranges in these cost estimates reflect two influences: regional variation in the costs, lifetimes and efficiency of control; and imprecision and uncertainty in the estimates

*Alternatively stated, we wish to maximize the reduction in emissions for any level of control expenditure. Note that our problem is analogous to traditional cost-effectiveness or capital budgeting problems.

Table 4. COST EFFICIENCY OF ALTERNATE METHODS OF DUST CONTROL: UNPAVED ROADS

	Annual cost* $/mi-gr-%		
	Low	High	Midrange
Asphalt Paving	-34	199	83
Speed Reduction-30	6	676	341
Calcium Chloride	353	788	571
Speed Reduction-20	12	1,353	683
Watering	1,061	1,847	1,454
Oiling	-22	40,532	20,255

*Cost in 1977 dollars per year per mile of road treated per emission reduction percentage. (Discount rate = 10%)

of these parameters. In the face of uncertainty, an initial selection of the dominant control technology may be made by examining the midranges of the cost estimates. Using this measure, paving appears to dominate, with a standardized total annual unit cost of $83/mile-year-% control, or $7055/mile-year at 85% control efficiency.

To complete the analysis, one must calculate the uncontrolled emission rate from a mile of unpaved road in each state. The cost effectiveness of the dominant control method in each state may then be determined.

$$\text{cost effectiveness} = \frac{\text{uncontrolled emissions (lbs/mile-yr)}}{\text{total annual unit control cost (\$/mile-yr-\%)} \times \text{control efficiency (\%)}} \quad (6)$$

Table 5 gives these data for urban and rural unpaved roads in each state. Clearly, control of municipal roads is more cost effective than control of rural roads. Note that these costs are in the range of $0.01 to $0.02 per pound avoided for municipal roads and $0.03 to $0.12 per pound avoided for rural roads. For comparison, estimates of the costs of control of point sources of particles vary from approximately $0.01 to $0.18 per pound.[23]

Table 5 indicates how much dust can be controlled in each $0.02 per pound price interval. Figure 1 demonstrates how these state-by-state estimates of cost efficiency can be combined for the 50 states to form a piecewise linear function relating annual control expenditure to emission abatement.

These results should not be used as the basis for policy recommendations without first answering several questions:

1. How wrong could these numbers be?
   - Are control costs correct?
   - Are control efficiencies and treatment lifetimes reasonable?
   - What about the relative traffic densities on paved and unpaved roads?

2. Is paving clearly the dominant control technology?
   - Can it be applied everywhere?
   - If so, at the calculated unit cost?

3. Finally, and perhaps most important: Is a pound of emissions from an unpaved road as significant as a pound of emissions from coal combustion, the steel industry, etc.?

CONCLUSIONS AND RECOMMENDATIONS

In summary, open sources are significant emissions sources, approximately 395 million tons per year in the U.S. It appears that roads, agriculture, and construction are the major sources nationally.

Much remains to be done. Emission rate estimates for open sources require more research concerning road dust entrainment and the amount of dust typically on roads of different types and uses, as well as research into the emission factors for construction, surface mining, and for wind erosion of range and desert land. Control methods, their efficiencies, and their costs all warrant further investigation, although much progress has been made in the study of vegetative and chemical stabilization of wastes.[13,17]

For particles not significantly more toxic than soil, cost effectiveness of mass emissions reduction may be a reasonable method of initial control prioritization. The significant regional variations in cost-effectiveness of control should be considered in formulation of control strategies.

It seems that dust from unpaved roads can be controlled at costs similar to those for the control of industrial point sources. However, once dominant, and near dominant, control techniques have been identified for each source class, careful engineering and economic studies may be required to resolve the uncertainties which now shroud estimates of control costs, lifetimes, and efficiencies.

Finally, toxicity, respirability, and transport of dust from open sources must be adequately characterized before sensible policy decisions can be made.

ACKNOWLEDGMENTS

We extend our thanks to Dr. Dennis C. Drehmel of the U.S. EPA for his economic and moral support of this work, the countless Federal and state officials who have graciously responded to our requests for data, Richard Antonelli for his unending assistance in compiling and analyzing data, and Laurie Cassel for her flawless preparation of the manuscript.

REFERENCES

1. U.S. Environmental Protection Agency. National Air Quality and Emissions Trends Report, 1976. EPA/450/1-77/002. U.S. Environmental Protection Agency. Monitoring and Data Analysis Division. Research Triangle Park, NC. December 1977.

2. Mann, C.O. Private correspondence. March 1978.

3. Cowherd, C., J.H. Southerland, and C.O. Mann. Methodology for a National Emissions Inventory of Fugitive Dust Sources. Presented at the 68th Annual Meeting of the Air Pollution Control Association. Boston, MA. June 15-20, 1975.

4. Cowherd, C., K. Axetell, C.M. Guenther, and G.A. Jutze. Development of Emissions Factors for Fugitive Dust Sources. EPA-450/3-74-037. U.S. Environmental Protection Agency. Office of Air and Waste Management. Research Triangle Park, NC. June 1974.

5. Amick, R., K. Axetell, and D.M. Wells. Fugitive Dust Emission Inventory Techniques. Presented at the 67th Annual Meeting of the Air Pollution Control Association. Denver, CO. June 9-13, 1974.

6. Conway, H.M. and L. Liston (eds.). The Weather Handbook. Conway Research, Inc. Atlanta, GA. 1974.

7. Stern, A.C., H.C. Wahlers, R.W. Boubel, and W.P. Lowry. Fundamentals of Air Pollution. Academic Press. New York, NY. 1973.

8. Yamate, G., J. Stockham, W. Vatavuk, and C. Mann. An Inventory of Emissions from Forest Wildfires, Forest Managed Burns, and Agricultural Burns. Presented at the 68th Annual Meeting of the Air Pollution Control Association. Boston, MA. June 15-20, 1975.

9. Yamate, G., J. Stockham, D. Becker, T. Waterman, P. Llewellen, and V.M. Vatavuk. Development of Emission Factors for Estimating Atmospheric Emissions from Forest Fires. Presented at the 68th Annual Meeting of the Air Pollution Control Association. Boston, MA. June 15-20, 1975.

10. U.S. Department of Commerce. Census of Agriculture:1974. U.S. Department of Commerce. Bureau of the Census. Washington, D.C. 1975.

11. Woodruff, N.P. and F.H. Siddoway. A Wind Erosion Equation. Soil Science Society of America Proceedings. 29(5): 602-608, 1965.

12. U.S. Department of the Interior. The National Atlas of the United States. U.S. Department of the Interior. Soil Conservation Service. Washington, D.C. 1970.

13. Dean, K.C., R. Havens, and M.W. Glantz. Methods and Costs of Stabilizing Fine-Sized Mineral Wastes. U.S. Department of the Interior. Bureau of Mines. Washington, D.C. 1974.

14. Ward, D.E., C.K. McMahon, and E.W. Johansen. An Update on Particulate Emissions from Forest Fires. Presented at the 69th Annual Meeting of the Air Pollution Control Association. Portland, OR. June 27-July 1, 1976.

15. Maneval, D.R. Personal communication. July 1978.

16. Ochsner, J.C. and T.R. Blackwood. Fugitive Emissions from Chemical Fertilizer Mining. Presented at the 2nd Symposium on Fugitive Emissions: Measurement and Control. Houston, TX. May 23-25, 1977.

17. Donovan, R.P., R.M. Felder, and H.H. Rogers. Vegetative Stabilization of Mineral Waste Heaps. EPA-600/2-76-087. U.S. Environmental Protection Agency. Industrial Environmental Research Laboratory. Research Triangle Park, NC. 1976.

18. Cowherd, C. and C.O. Mann. Quantification of Dust Entrainment from Paved Roads. Presented at the 69th Annual Meeting of the Air Pollution Control Association. Portland, OR. June 27-July 1, 1976.

19. U.S. Department of Commerce. Census of Construction Industries: 1972. U.S. Department of Commerce. Bureau of the Census, Washington, D.C. 1973.

20. U.S. Department of Agriculture. Wildfire Statistics. Annual Reports 1963-1972. U.S. Department of Agriculture. Forest Service. Washington, D.C.

21. U.S. Department of Interior. Minerals Yearbook: 1974. Vol I. Metals, Minerals, and Fuels. U.S. Department of Interior. Bureau of Mines. Washington, D.C. 1976.

22. U.S. Department of Transportation. Highway Statistics: 1974. U.S. Department of Transportation. Federal Highway Administration. Washington, D.C. 1976.

23. U.S. Environmental Protection Agency. The Economics of Clean Air. Annual Report of the Administrator of the EPA to the Congress. Washington, D.C. 1972.

Table 1. OPEN SOURCE EMISSION FACTORS BY STATE

State	Agriculture		Construction	Forest Fires		Mineral Extraction		Roads	
	Tilling	Wind Erosion		Wild	Prescribed	Coal	Other	Paved	Unpaved
	lb/acre	ton/acre	ton/acre	lb/acre		lb/ton		lb/veh-mi	
AL	3.79	.006	16.50	1350	150	1.7	2	0.013	7.39
AK	11.90		17.70	1650	Negl.	1.7	2	0.013	9.69
AZ	214.00	.721	16.10	1500	400	.06			12.11
AR	4.40	.036	16.20	1350	150	1.7			7.94
CA	30.30	.537	17.50	2700	3500				13.20
CO	53.00	.045	15.70	4500	400	.06			8.17
CT	5.63	.026	16.70	1050	0				6.39
DE	2.66	.030	14.30	300	100				5.99
FL	4.34	.044	15.70	900	200				5.33
GA	4.06	.028	17.20	1350	150				5.58
HI	30.20		14.80						5.97
ID	39.20	.022	17.90	9000	3250				8.17
IL	14.00	.124	17.10	1650		1.7			7.10
IN	9.33	.090	17.20	1650	0	1.7			6.96
IA	12.30	.015	16.80	900	0	1.7			7.39
KS	24.10	.045	17.10	450	0	1.7			8.95
KY	8.14	.034	17.00	1650	Negl.	1.7			6.68
LA	7.93	.034	17.40	1350	150				7.39
ME	5.47	.021	16.60	1350	0				7.25
MD	2.90	.037	13.90	1050	0	1.7			5.99
MA	4.84	.020	13.50	1650	0				6.39
MI	6.72	.100	16.70	1650	150				6.68
MN	11.10	.016	16.80	1650	No data				7.24
MS	5.38	.016	16.20	1350	150				6.85
MO	10.50	.107	16.50	750	No data	1.7			7.39
MT	47.60	.014	15.80	7350	2250	.06			9.59
NE	37.50	.049	16.90	450	0				8.70
NV	245.0	2.226	13.90	1200	No data				10.43
NH	6.39	.005	15.90	1200	0				9.59
NJ	6.03	.052	17.00	1500	150				8.79
NM	103.0	.053	16.00	1500	400	.06			10.26
NY	9.69	.512	16.80	1650	0				6.71
NC	3.08	.037	16.80	1350	150				6.52
ND	30.40	.020	16.10	450	100				9.99
OH	9.14	.081	17.00	1650	0	1.7			6.47
OK	19.40	.023	17.20	450	No data	1.7			8.95
OR	24.50	.026	16.90	9000	1650				9.70
PA	11.10	.020	17.40	1650	0	1.7			8.59
RI	8.03	.041	11.20	1050	0				7.99
SC	3.80	.036	14.90	1350	150				3.87
SD	28.30	.030	16.50	600	No data				9.11
TN	5.83	.019	16.20	1350	No data	1.7			6.44
TX	40.60	.064	17.60	900	150				10.30
UT	144.0	.618	17.00	1200	Negl.	.06			10.21
VT	6.63	.057	14.60	1200	0				6.87
VA	4.32	.019	16.40	750	250	1.7			5.99
WA	5.90	.009	17.20	9150	1700	.06			8.77
WV	11.10	.010	17.40	1800	0	1.7			8.95
WI	10.50	.115	15.70	1650	No data				7.39
WY	67.00	.048	16.80	900	0	.06			8.29

Table 2. OPEN SOURCE EXTENTS BY STATE

State	Agriculture		Construction	Forest Fires		Mineral Extraction		Roads	
	Tilling	Wind Erosion		Wild	Prescribed	Coal	Other	Paved	Unpaved
	10^6 Acres of Harvested Cropland		Acres	Acres		10^3 tons/yr		10^9 veh-mi	
AL	2.794		16,559	151,150	208,505	19,824	39,300	22.90	1.02
AK	.017		3,355	783,994	0	700	127,000	1.68	.41
AZ	1.097		8,615	38,051	25,956	6,448	187,000	14.08	1.61
AR	6.639		8,676	139,970	54,736	455	38,000	11.16	2.35
CA	8.307		277,394	162,070	12,104		171,000	123.42	4.17
CO	5.957		7,459	11,106	2,594	6,896	33,800	13.69	2.47
CT	.159		19,914	1,982	0		15,100	17.91	.10
DE	.452		721	307	950		2,410	3.45	.02
FL	2.304		48,787	703,490	718,877		235,000	59.39	2.63
GA	4.161		26,438	61,123	724,616		54,600	32.57	2.51
HI	.151		4,203				9,010	3.89	.03
ID	4.531		1,363	120,892	27,906		17,800	4.65	1.01
IL	21.518		79,921	13,881	0	58,215	104,000	56.97	2.24
IN	11.234		44,921	10,812	0	23,726	58,400	35.14	1.85
IA	23.085		15,042	4,200	0	590	49,400	16.01	3.06
KS	19.871		14,333	292,279	0	718	28,500	12.00	3.20
KY	3.701		15,866	75,750	0	137,197	36,600	22.50	1.31
LA	3.628		50,054	108,107	220,791		24,500	18.52	1.02
ME	.450		5,253	3,696	0		5,390	6.52	.20
MD	1.439		9,170	2,699	0	2,337	30,500	23.66	.23
MA	.188		93,299	10,184	0		25,700	28.02	.21
MI	6.318		44,488	9,314	3,831		139,000	53.10	2.64
MN	17.896		26,906	37,347	No data		216,000	21.40	3.19
MS	4.793		8,509	116,479	168,890		18,200	12.49	1.24
MO	11.765		20,973	319,530	No data	4,623	56,100	26.92	2.79
MT	8.427		1,967	27,102	47,000	14,106	33,900	4.21	1.61
NE	16.309		11,635	88,911	0		16,900	8.50	2.44
NV	.551		1,575	24,643	No data		36,800	3.26	.94
NH	.118		4,363	760	0		6,750	4.82	.26
NJ	.541		49,670	31,325	20,000		44,900	46.80	.44
NM	.976		3,836	26,483	7,136	9,392	42,500	7.36	2.07
NY	4.156		87,001	7,331	0		75,600	63.72	1.54
NC	4.075		38,071	111,209	117,175		57,100	33.82	1.18
ND	19.207		4,946	2,096	1,998		5,110	2.61	1.76
OH	9.680		80,283	6,247	0	45,409	95,900	61.90	1.18
OK	3.990		19,329	514,772	No data	2,356	32,000	18.84	2.65
OR	3.213		12,547	43,658	26,125		45,000	12.74	2.50
PA	3.885		120,113	15,609	0	80,462	90,700	65.26	2.35
RI	.021		7,289	1,311	0		3,210	5.45	.10
SC	2.251		11,885	64,645	388,708		24,300	19.32	.70
SD	14.855		2,358	15,891	No data		12,400	3.70	1.40
TN	3.746		20,579	41,003	No data	7,541	56,000	29.40	1.36
TX	19.014		213,620	42,482	83,255		116,000	73.13	5.56
UT	1.089		11,958	16,707	0	5,858	55,800	6.39	1.06
VT	.575		1,197	366	0		5,280	2.68	.34
VA	2.447		12,946	14,910	30,964	34,326	58,700	32.85	.78
WA	4.946		25,997	35,917	66,777	W(3915)	38,100	21.05	1.53
WV	.511		12,331	82,475	0	102,462	14,600	9.24	8.76
WI	9.340		13,895	8,322	No data		53,900	27.07	.90
WY	1.681		3,509	18,538	0	30,703	17,900	2.87	.59

Table 3. OPEN SOURCE EMISSION RATES BY STATE

State	Agriculture		Construction	Forest Fires		Mineral Extraction		Roads	
	Tilling	Wind Erosion		Wild	Prescribed	Coal	Other	Paved	Unpaved
	10^3 tons/yr	10^6 tons/yr	10^5 tons/yr	10^3 tons/yr		10^3 tons/yr		10^6 tons/yr	
AL	5.29	.0168	2.73	102.0	15.64	16.85	39.3	0.149	3.76
AK	.10		.59	646.8	Negl.	.60	127.0	0.011	1.99
AZ	117.	.7909	1.39	28.54	5.19	.19	187.0	0.092	9.74
AR	14.60	.2390	1.41	94.48	4.11	.37	38.0	0.073	9.34
CA	126.	4.4608	48.54	218.8	21.18		171.0	0.803	27.53
CO	158.	.2681	1.17	24.99	.52	.21	33.8	0.089	10.08
CT	.45	.0041	3.33	1.04	0		15.1	0.117	.32
DE	.60	.0136	.10	.05	.04		2.4	0.023	.07
FL	4.99	.1014	7.66	316.6	71.89		235.0	0.386	7.01
GA	8.45	.1165	4.55	41.26	54.35		54.6	0.212	7.01
HI	2.28		.62				9.0	0.026	.08
ID	88.80	.0997	.24	544.0	45.35		17.8	0.030	4.12
IL	151.	2.6682	14.15	11.45	0	49.48	104.0	0.370	7.96
IN	52.4	1.0110	7.73	8.92	0	20.17	58.1	0.229	6.45
IA	142.	.3463	2.53	1.89	0	0.50	49.4	0.104	11.31
KS	239.	.8942	2.45	65.76	0	0.61	28.5	0.078	14.33
KY	15.1	.1258	2.70	62.49	0	116.62	36.6	0.146	4.38
LA	14.4	.1234	8.7	72.97	16.56		24.5	0.121	3.79
ME	1.23	.0094	.87	2.50	0		5.4	0.043	.71
MD	2.09	.0532	1.28	1.42	0	1.99	30.5	0.154	.71
MA	.46	.0038	12.60	8.40	0		25.7	0.182	.68
MI	21.2	.6318	7.43	7.68	.29		139.0	0.345	8.83
MN	99.3	.2863	4.52	30.81	No data		216.0	0.139	11.56
MS	12.9	.0767	1.38	78.62	12.67		18.2	0.081	4.26
MO	61.7	1.2588	3.46	119.8	No data	3.93	56.1	0.175	10.33
MT	200.	.1180	.31	99.6	52.88	0.42	33.9	0.028	7.73
NE	306.	.7991	1.97	20.0	0		16.9	0.056	10.61
NV	68.	1.2265	.22	14.79	No data		36.8	0.021	4.89
NH	.38	.0006	.69	.46	0		6.8	0.032	1.25
NJ	1.63	.0281	8.44	23.49	1.50		44.9	0.304	1.95
NM	50.3	.0517	.61	19.86	1.43	.28	42.5	0.048	10.64
NY	20.1	2.1279	14.62	6.05	0		75.6	0.414	5.16
NC	6.28	.1508	6.40	75.07	8.79		57.1	0.220	3.86
ND	292.	.3841	.80	.47	.10		5.1	0.017	8.80
OH	44.2	.7841	13.65	5.15	0	38.60	95.9	0.403	3.82
OK	38.7	.0918	3.32	115.8	No data	2.00	32.0	0.123	11.86
OR	39.4	.0835	2.12	196.5	21.55		45.0	0.083	12.11
PA	21.6	.0777	20.90	12.88	0	68.39	90.7	0.424	10.10
RI	.08	.0009	.82	.69	0		3.2	0.036	.39
SC	4.28	.0810	1.77	43.64	29.15		24.3	0.126	1.35
SD	210.	.4456	.39	4.77	No data		12.4	0.024	6.37
TN	10.9	.0712	3.33	27.68	No data	6.41	56.0	0.191	4.38
TX	386.	1.2169	37.60	19.12	6.24		116.0	0.476	28.64
UT	78.4	.6730	2.03	10.02	Negl.	.18	55.8	0.042	5.41
VT	1.91	.0328	.17	.22	0		5.3	0.018	1.18
VA	5.29	.0465	2.12	5.59	3.87	29.18	58.7	0.214	2.34
WA	14.6	.0445	4.47	164.3	56.76	.12	38.1	0.137	6.71
WV	2.84	.0051	2.15	74.23	0	87.09	14.6	0.060	3.92
WI	49.0	1.0741	2.18	6.87	No data		53.9	0.176	3.31
WY	56.3	.0807	.59	8.34	0	.62	17.9	0.019	2.44

Table 5. ESTIMATED COSTS OF CONTROL FOR UNPAVED ROAD DUST FOR URBAN AND RURAL ROADS, BY STATES

Estimated Cost of Control $/lb	Rural Unpaved Roads	Municipal Unpaved Roads	Amount of Unpaved Road Dust Controllable 10^9 lb/yr	Total Cost of Control $\$10^9$/yr
0.000-0.005	DE.	CA, MD, NJ.	13.0	0.047
0.005-0.010	RI.	AK, AZ, DE, MI, NV, PA, CO, FL, IL, IN, KY, MA, NM, OH, OR, RI, TN, TX, UT, VA, WA, WV.	35.8	0.289
0.010-0.015	AZ, CA, NJ.	CT, GA, MO, MT, NE, OK, WI, KS, LA, MN, NY, NC, WY.	72.6	0.904
0.015-0.020	AK, CT, HI, NH, PA.	AL, IA, ME, MS, AK, ID, NH, ND, SD, VT.	23.3	0.409
0.020-0.025	AR, LA, MD, NM, NY, TX, WV.	SC.	89.0	2.00
0.025-0.030	CO, FL, IN, IA, MA, MI, NC, OK, OR, UT, VT, VA.		122.	3.36
0.030-0.035	GA, IL, KS, KY, ME, MN, MO, NE, OH, TN, WA.		122.	3.97
0.035-0.040	AL, MS, MT, NV, WY.		36.5	1.37
0.040-0.045	ID, SD.		17.2	0.731
0.045-0.050	ND, WI.		19.1	0.907
0.050-0.055			0.0	0.0
0.055-0.060			0.0	0.0
0.060-0.065	SC.		2.06	0.129

Figure 1. Unpaved road dust emission reduction versus control cost

USE OF ELECTROSTATICALLY CHARGED FOG FOR CONTROL OF FUGITIVE DUST, SMOKE AND FUME

Stuart A. Hoenig
University of Arizona
Department of Electrical Engineering
Tucson, Arizona 85721

ABSTRACT

We have demonstrated that most respirable industrial pollutants acquire an electrostatic charge as they are dispersed into the air. If this charged, airborne, material is exposed to an oppositely charged water fog there is enhanced contact between the particulates and the fog droplets. After contact is made the wetted particulates agglomerate rapidly and fall out of the atmosphere. This technique has been tested on a wide variety of industrial pollutants ranging from silica flour to sulfur dioxide and fly ash. In general, there has been significant suppression with a minimum of water fog. The system is therefore suited to control of moving or fugitive dust sources where the usual duct and baghouse systems are too costly or ineffective.

INTRODUCTION

Beginning in 1973 a number of studies were done at the University of Arizona to determine if electrostatic charging was a factor in the levitation of dust on Mars. No Mars dust samples were available and tests were run on a variety of industrial and naturally occurring particulate materials. The results indicated that in the great majority of cases the respirable materials (below eight micrometers in diameter) were charged and that the finer (one micrometer) particles were almost always charged negatively.

These results suggested that it might be possible to suppress industrial pollutants by exposing them to an oppositely charged water fog. The electrostatic effect would encourage fog-dust contact and the wetted

particulates would be expected to agglomerate and fall out. There were several potential advantages to a system of this type.

1. The quantity of water involved would be very low thereby conserving water resources in the arid Southwest. Limited water use would permit the application of fog on water sensitive materials, i. e.; flour, cement, etc.

2. A system of this type would be suitable for control of moving dust sources, i.e.; trucks, sweepers, front loaders, where conventional methods could not possibly be used.

3. Charged water fog might be used for preagglomeration of dusts before final collection by other means. One example might be cyclones. They are not effective on dust below ten micrometers. If the respirable dust was agglomerated before it entered the cyclone, it might well be removed by the centrifugal action.

4. Many aerosols, i.e.; SO_3, NO_x, NH_3 are water soluble and would be expected to interact with charged water fog. The droplets would absorb on ambient dust particles (that are in the process of agglomerating) thereby removing both the dust and the aerosol at the same time. Another mechanism might involve direct fog induced agglomeration of the smoke or aerosol. Once again the large drops would be expected to fall out quite rapidly.

EXPERIMENTAL STUDIES

The first investigation was aimed at a determination of the charge versus size spectrum for typical industrial dusts, after grinding and dispersion into the air. The test materials, obtained from a variety of sources, were ground and dispersed by means of the arrastra mill shown in Figure 1.

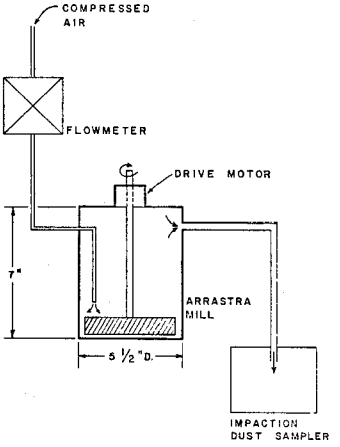

DUST GENERATOR AND SAMPLING SYSTEM (1)

The powdered material was blown into a small dust tunnel, Figure 2, samled and analyzed by a modified Anderson-2000 Company Impaction Sampler* (shown in Figure 3). Typical results for silica sand are shown in Figure

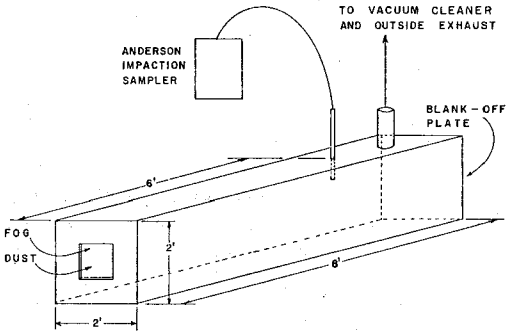

EXPERIMENTAL DUST TUNNEL ②

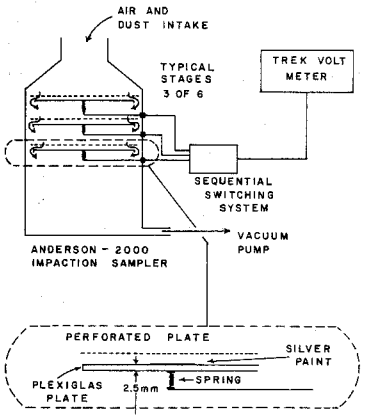

③

4. Data on some fifty other materials has been reported in our EPA reports[1]. In this connection it is important to note that all of the charge versus size data is in relative rather than absolute units. We recognized that it would be advantageous to have the charge data in absolute rather than relative units. However, tests indicated that the process would be difficult, time consuming and subject to severe error. In any case the important fact was that the dust was charged and that

*The sampler flow rate was 28.2 1/min.; a sample run required some nine minutes.

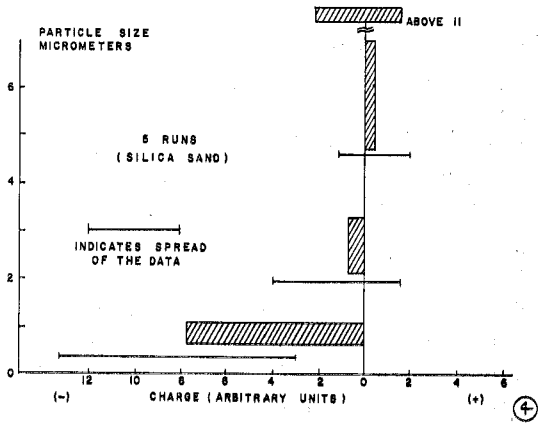

the respiratory material was predominately negative in sign. Constraints of time and funding precluded any further effort to measure absolute charge for the industrial materials of interest.

There have been a number of studies on the question of how and why dust charging occurs, i.e.; Loeb[2], Harper[3], Gallo and Lama[4]. There is no general agreement but we prefer the theory of Gallo and Lama that predicts a negative charge on the smaller dust particles. In this connection it is important to note the effect of impurities as discussed by Loeb. His book indicates that when pure quartz is ground there are as many positive as negative particles, at every size level. When the quartz was contaminated with a metal (platinum) a predominance of negative charge was observed. In this connection it is important to note that small dust particles are frequently contaminated with absorbed metals from vapors generated during combustion or melting[5]. An effect of this type may be responsible for the results of Figure 4.

In any case, the above data suggests that under normal conditions respirable dust <u>will not</u> agglomerate and fall out, because the uniformity of charge will reduce the number of particle collisions. Since most particles are negative and the earth's surface normally carries a negative charge[6], it appears that electrostatic levitation would further reduce the rate at which such particles fall out of the atmosphere.

Many attempts have been made to encourage dust agglomeration by wetting down the dust; however, the difficulties of generating a micron sized fog and inducing the fog to make contact with the dust particles have almost precluded the use of fogging to control open air dust problems. (Some closed dust control systems use electrostatic techniques to charge the dust. The charged particles are then sprayed with oppositely charged water which is effective in making contact with the dust. This method requires a closed vessel and the dust must be properly charged by

induction or ion diffusion. The resultant system is complex and only suited for dust that has been captured by hoods and collectors.)

Generation of Charged Fog

We have made use of a modified commercial* electrostatic paint spray gun plus a University of Arizona designed apparatus** for generation of highly dispersed, micron sized, fog that carries a positive or negative charge, as desired. No clogging or deposits have been observed after many hours of operation with untreated tap water.

Dust Tunnel Studies

The interaction between industrial dusts and charged fog was investigated in the dust tunnel shown in Figure 2. The charged fog and the dust were blown in at one end of the tunnel, and an industrial vacuum cleaner was used to extract the remaining dust at the other end. The Anderson Sampler was connected some two feet from the downstream end of the tunnel.

Typical results with this system, using foundry dust, are shown in Figure 5; without the fog, the dust level was quite high. There was some

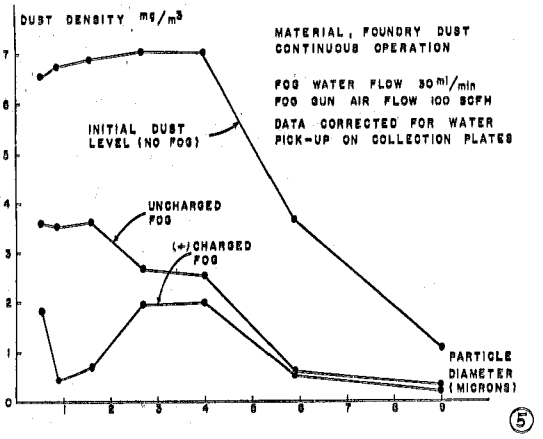

⑤

decrease in the dust level with uncharged fog, but with positively charged fog the decrease was dramatic. (The choice of positively charged fog was made on the basis of tests that indicated the respirable material was (-) in sign.

---

*Provided by the Ransburg Corporation of Indianapolis, Indiana.

**A commercial version of this system is marketed by the Ransburg Corporation.

Similar data demonstrating the ability of charged water fog to suppress a wide variety of industrial dusts has been presented in various EPA reports[1].

In all of the above cases there was a significant difference between the effects of positive versus negatively charged water fog. This would be expected from the earlier discussion of dust charging. However, we have noted some cases in which the charging of the fog does not have a significant effect on the suppression of respirable dust. We suspect that these samples contain materials that charge both positively and negatively (a mixture of red lead and sulfur would display this characteristic). Little coagulation occurs when the materials are very dry; if charged fog is used, one of the components is wetted and agglomeration of both species occurs. This is a speculation at present and the phenomena will be the subject of further investigation.

Effects of Reduced Water Flow and Chemical Additives

Another aspect of the study was aimed at evaluating the effects of reduced water flow on dust control. Typical results are shown in Figure 6, where we have plotted the percent reduction of respirable foundry dust

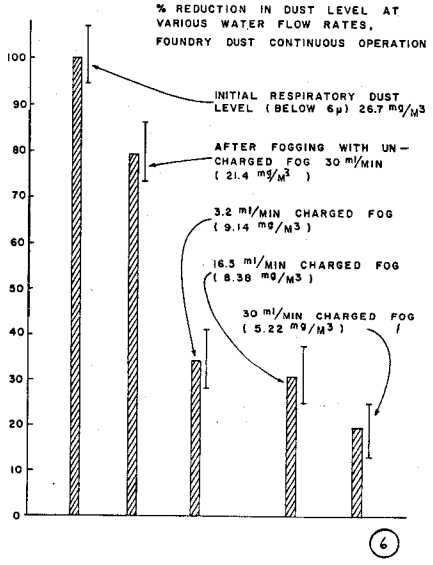

6

with uncharged (30 ml/min) and with charged water at flow rates of 30, 16 and 3.2 ml per min. The largest reduction was observed with charged fog at 30 ml/min, but the significant reduction was observed even at 3.2 ml/min. This suggests that only a limited amount of fog will be required for effective dust control. A calculation of the effect of these fog levels on the humidity in a typical foundry is given at the end of the paper.

There have been suggestions that various dust control chemicals, detergents, etc., be added to the water in order to improve the dust con-

trol system or make the agglomerates more stable. In general* we have resisted this idea on the basis that no dust control chemicals have FDA approval for human exposure. Anyone working in the area where the charged fog was used could certainly be exposed to the vapors and the effects of dust control chemicals have simply not been evaluated in this mode. We have done studies with various mixtures of glycerine(glycerol) and water in cases where the fogging technique might be used at low temperatures.

Studies of Coal Tar Volatiles and Benzene Solubles

The increased burning of coal raises the hazard of greater public exposure to fly ash, coal particulates and the volatiles generated when coal is heated.

To investigate coal tar volatiles, a metal pipe some 100 mm in diameter was cut off and sealed with screw caps to form a closed tube some 300 mm long. The tube was filled with coarsely ground coal,** provided with a 10 mm tube to permit vapors to escape and heated to 700°C in a small oven. The vapors were blown into an outside dust tunnel and exposed to charged fog. Two experiments were done. One was to observe volatile particulates that were usually collected on filters. The other experiment was aimed at observing benzene solubles. The data on volatile particulates is shown in Figure 7. The (+) charged fog was most effective

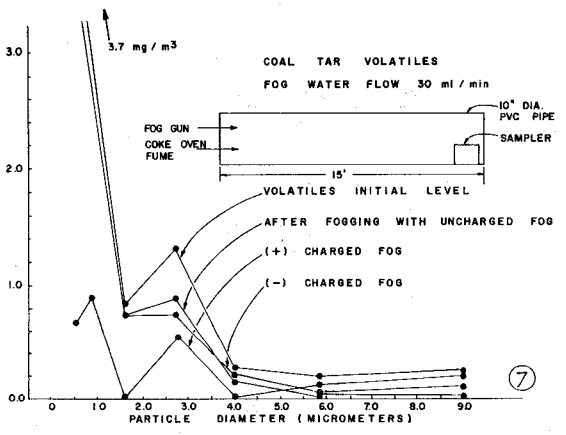

*Certain types of power plant fly ash appear to be hydrophobic and with this dust we have seen improved results when a commercial dust control chemical was added to the fogging water. This data will be discussed below. We suggest that the method is of potential value when fogging is to be done in a closed environment, i.e.; a stack or duct.

**Pittsburg Seam #8 Coking Coal (Ohio).

in reducing this pollutant.

Measurement of benzene soluble vapors involved drawing the fumes through a bubbler containing a benzene solution for absorption; the benzene was then analyzed by a gas chromatograph (GC). A typical test involved first making a GC run with benzene alone, then a run was made with benzene after absorption of coal tar volatiles, and a last run was made with benzene and coal tar volatiles where the volatiles were fogged with (+) fog before reaching the benzene absorbent.

Typical results are shown in Figure 8. In the presence of charged

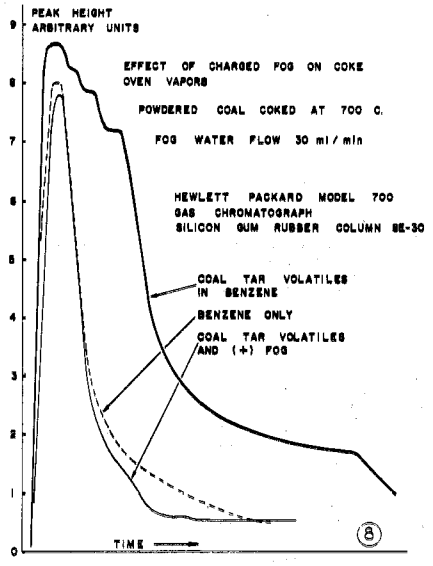

fog there was a marked reduction in pickup of benzene solubles by the bubbler, suggesting that this material had been induced to agglomerate and fall out in the tunnel before reaching the collecting device. We suggest that there may well be applications for charged fog in the control of coal dust and coal tar volatiles.

Application of Charged Fog to Control of Cotton Dust

The cotton industry has been cited in several areas for excessive dust and we have investigated the application of the charged fog system for control of cotton dust and brack. Typical results for cotton brack are shown in Figure 9; there was a significant reduction with the charged fog. Other field test data taken at the University of Arizona Cotton Research Facility (courtesy of Professor H. Muramito) are shown in Figure 10; once again good results were achieved.

Results from a test in an operating cotton gin (Company C) are shown in Figure 11; here a spinning cup fog generator (to be discussed below) was used because no compressed air was available. Once again the results were quite satisfactory. We are working with the local cotton gin owners and the USDA Cotton Laboratory to develop the applications of this tech-

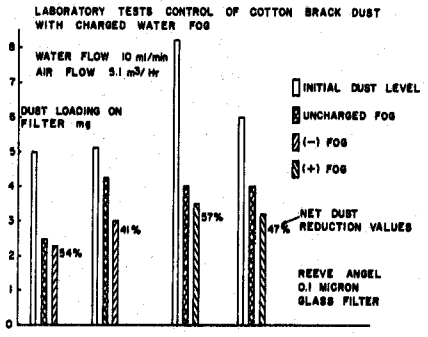
LABORATORY TESTS CONTROL OF COTTON BRACK DUST
WITH CHARGED WATER FOG
WATER FLOW 10 ml/min
AIR FLOW 5.1 m³/Hr
DUST LOADING ON FILTER mg
INITIAL DUST LEVEL
UNCHARGED FOG
(-) FOG
(+) FOG
54%
41%
57%
47%
NET DUST REDUCTION VALUES
REEVE ANGEL 0.1 MICRON GLASS FILTER

(9)

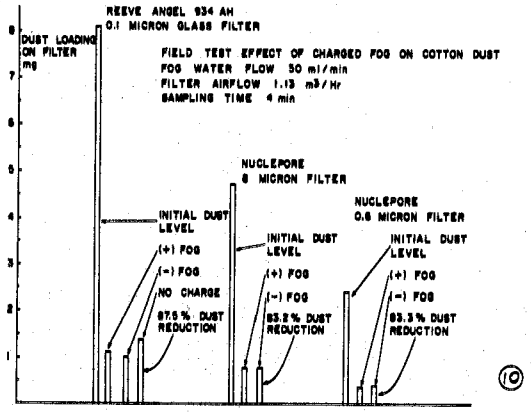
REEVE ANGEL 934 AH
0.1 MICRON GLASS FILTER
DUST LOADING ON FILTER mg
FIELD TEST EFFECT OF CHARGED FOG ON COTTON DUST
FOG WATER FLOW 50 ml/min
FILTER AIRFLOW 1.13 m³/Hr
SAMPLING TIME 4 min
NUCLEPORE 8 MICRON FILTER
NUCLEPORE 0.8 MICRON FILTER
INITIAL DUST LEVEL
(+) FOG
(-) FOG
NO CHARGE
97.5 % DUST REDUCTION
83.2 % DUST REDUCTION
83.3 % DUST REDUCTION

(10)

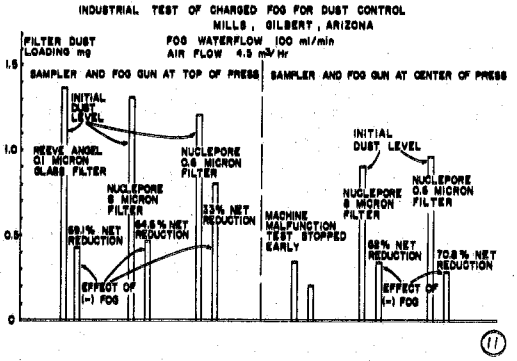
INDUSTRIAL TEST OF CHARGED FOG FOR DUST CONTROL
MILLS, GILBERT, ARIZONA
FILTER DUST LOADING mg
FOG WATERFLOW 100 ml/min
AIR FLOW 4.5 m³/Hr
SAMPLER AND FOG GUN AT TOP OF PRESS
SAMPLER AND FOG GUN AT CENTER OF PRESS
INITIAL DUST LEVEL
REEVE ANGEL 0.1 MICRON GLASS FILTER
NUCLEPORE 8 MICRON FILTER
NUCLEPORE 0.8 MICRON FILTER
69.1% NET REDUCTION
64.6% NET REDUCTION
33% NET REDUCTION
EFFECT OF (-) FOG
MACHINE MALFUNCTION TEST STOPPED EARLY
68% NET REDUCTION
70.8% NET REDUCTION

(11)

nique to the reduction of dust pollution.

Improving the Operation of Dry Cyclones Used for Collection of Industrial Dust

Dry cyclones are relatively simple devices that operate at low pressure drop, without moving parts and with minimum maintenance. As such they are widely used for control of dust and fibrous particulates. The major problem with these devices is their inability to collect respirable material and for this reason we began investigation of the use of charged fog in conjunction with a cyclone collecting cotton gin trash.

In one series of experiments charged fog was injected into the air/dust mixture going to the cyclone. Some reduction in respirable dust output was observed but we felt it would be more effective to inject the fog directly into the "clean air" before it escaped from the cyclone. This would induce agglomeration of the fine particulates which would then be thrown to the side of the cyclone by centrifugal force. This system is under test at the moment and appears to be quite promising.

Control of Fume and Smoke From Welding

Welding generates significant quantities of fume and smoke especially when flux coated rod is used. Welding often requires close operator control and as a result the metal fumes go past the welder before they can be captured by hoods and exhaust systems. We hoped that the charged fog would be effective in suppressing the fume at the actual source.

The set up for the first experiment is shown in Figure 12. The

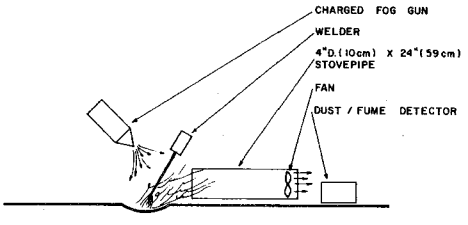

WELDING SMOKE / FUME CONTROL AND TEST SYSTEM

(12)

continuous wire welder (Miller Electric Company, Model 35S) was loaned to the University by T. M. Caid and Sons of Tucson, Arizona. This welder

was a bare wire, CO_2 shielded, system and operated without flux. For this reason there was no flux smoke and the fume was primarily finely divided metal particles. To see the effects, if any, of added flux we placed the flux (Linde Company type AWS-A5.17-69) in the welding area by hand and sampled the emissions with glass fiber filters. The analytical data, provided by the University Analytical Laboratory, indicated little difference between the flux and no-flux results except for somewhat higher levels of Ca, Sr, K and Mg when flux was used. We do not consider these differences significant in terms of pollution emitted during welding.

The first experimental results in terms of the reduction in metal fume with charged fog are shown in Figure 13.

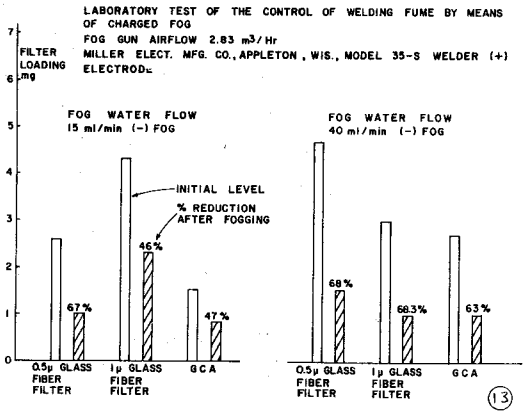

In general there was about a fifty percent reduction in captured particulates but the data was subject to wide variations. At first we suspected that these variations were the result of changes in operator control since our technician is not a trained welder. We arranged for a certified welder to run another test that indicated the same variations observed earlier. It appears that hand held welding is a highly variable process and that quantifying the fog control system will be a difficult process.

In this connection we were concerned about the effects, if any, of the fog on the welder or the work. Our technician and the certified welder observed no changes that might have been due to charged fog and to all appearances the fog evaporated before reaching the actual welding site.

Control of Dust From Hand Grinders, Chippers and Sanders

These tools are a source of dust and since they are often used in confined areas, where hoods would interfere with the work, they have a potential factor in workman injury. Some companies have marketed collectors and vacuum manifolds to go on the grinder but in general these units have not been popular because they change the balance of the tool and

interfere with the workman's view.

We have developed* a system for adding small quantities of water fog to the contact area between the tool and the work. This effectively reduces the respirable dust level while at the same time acting as a cooling agent. Typical results with a hand grinder are shown in Figure 14.

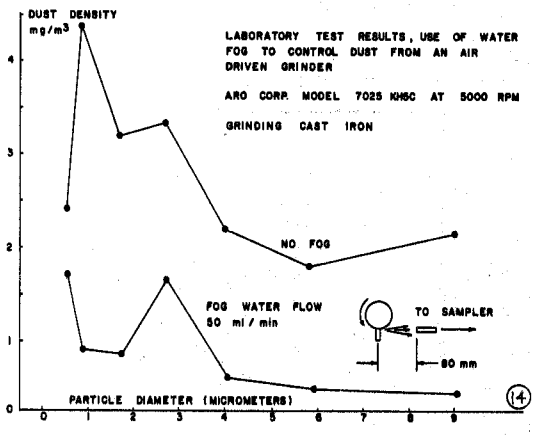

Arrangements are being made with a manufacturer** of hand tools to bring this device into the commercial market. Further development of systems to reduce dust during wire brushing, swing grinding and electric arc washing are under consideration.

Investigations at Elevated Temperatures (The Control of Fly Ash and Sulfur Oxide Gases)

One of the questions raised about the charged fog dust control system is the application in high temperature environments where some of the fog might be lost to evaporation. In earlier discussions we suggested that most of the fog would be captured by dust and therefore be available for agglomeration, even at high temperatures. At that time there was only a limited amount of data to support this idea. Further data has been obtained with the system shown in Figure 15 where temperatures up to 370°C can be generated***. The first results are shown in Figure

*This device is the subject of a patent disclosure to the Ransburg Corporation of Indianapolis, Indiana.

**The ARO Corporation of Bryan, Ohio.

***The respirable dust level was measured with a GCA Corporation (Bedford, Massachusetts) RDM-101 Beta Ray Monitor. The SO_2 level was measured with a CEA Instruments (Westwood, New Jersey) U2-DS SO_2 Monitor.

16 for a typical copper smelter fly ash. It is clear that the fog is effective in suppressing the respirable dust and that the presence of

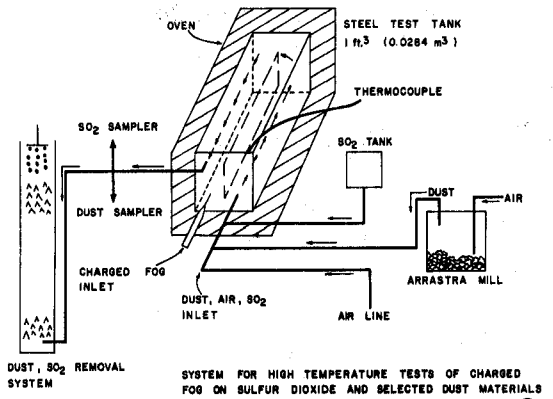

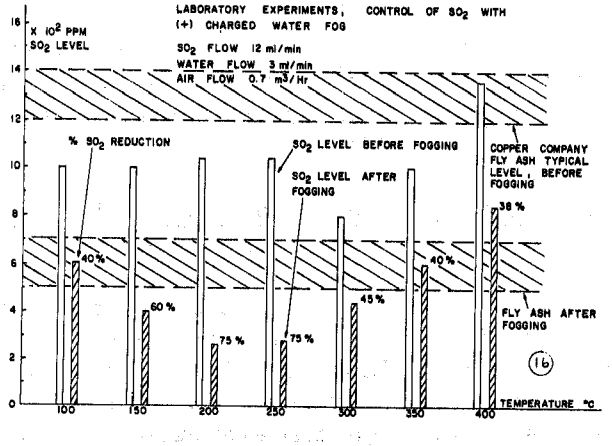

significant levels of SO_2 does not affect the process.

In another series of tests, with the system of Figure 15, we held the initial level of dust (copper company fly ash) and SO_2 constant and observed the effect of charged fog on the reduction of SO_2 and fly ash. Typical results, over a range of temperatures are shown in Figure 17. It is clear that the charged fog is effective in reducing the SO_2 and the dust level. The effect of charged fog, on the dust, does not vary appreciably with temperature but the SO_2 effect is a maximum at about 250°C. This was observed consistently and we suggest that below 250°C most of the SO_2 has not converted to SO_3 and is relatively insoluble in the fog. At 250°C the conversion is almost complete and the effect is large while at higher temperatures the SO_3 becomes less soluble in the

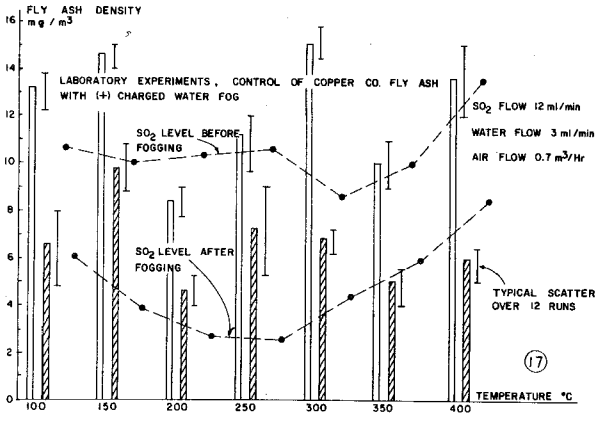

fog and the effect falls off. At present we have no apparatus for measurement of SO_3 versus SO_2 so this is mere speculation. We hope to continue these tests and develop apparatus that will allow continuous monitoring of the SO_2 and SO_3 concentrations.

One question of interest here is the actual "fate" of the SO_2 or SO_3 after fogging. In earlier reports we suggested that the SO_2/SO_3-water mixture is absorbed by the dust and assists in the process of dust agglomeration. If this is true, it provides a method for suppressing both dust and SO_2 at the same time. Further tests of this hypothesis will involve the larger test system to be discussed below.

The success with highly metallic copper company dust suggested that the system be tried with a nonmetallic fly ash material from a power plant burning low sulfur western coal. This fly ash has proved difficult to collect by conventional techniques and we hoped that the fog might be a low cost way of agglomerating the dust ahead of the other collection systems. The apparatus of Figure 15 was used. There was some reduction but not to the degree observed with the copper company fly ash. We suspected that this was due to the hydrophobic nature of the dust and added Johnson March Company Compound MR at the recommended 1% level by volume. The results with this mixture are shown in Figure 18; there was some significant improvement which we hope to verify in further tests.

LARGER SCALE EXPERIMENTS AND INDUSTRIAL TESTING

The laboratory tests, while encouraging, are no substitute for pilot plant studies or full scale industrial demonstrations. We have been active in these areas but there seems to be two major difficulties in these large scale applications of charged fog.

1. Industrial conditions usually involve large open areas where the flow of dust is generated by many sources. The irregular nature

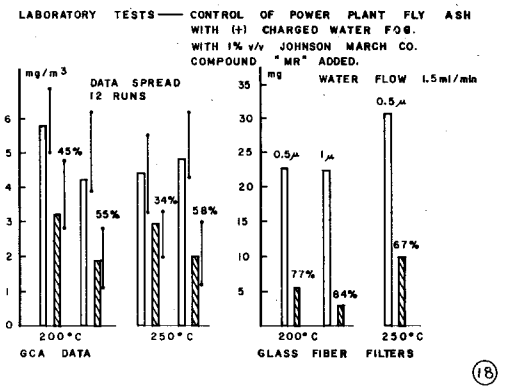

of the operations makes it difficult to establish a steady state background level so that the charged fog data is subject to wide variations. In some cases we have found it simpler to use spotlights to demonstrate the dust reduction when charged fog is used. In many cases management personnel seem suspicious of instrumental readings and prefer to rely on visual observations.

Part of this problem is due to the surprisingly primitive state of the dust measurement instruments in rather large corporations. In many cases the job of Dust Measurement and Control is simply added to the laboratory tasks without providing for the necessary funding or training to perform the job. This problem and the limited availability of good dust measurement instruments has put us in the position of having to "teach" the users how to set up the dust control equipment and how to measure the effects of the charged fog. The lack of appropriate instruments has encouraged the development of some low cost dust evaluation devices, to be discussed below.

2. We have found that many industrial organizations harbor an almost pathological fear of government agencies particularly EPA and OSHA. In some cases this has extended to the point of denial that the charged fog equipment has been purchased or put into operation to say nothing of revealing the results. We have done our best to alleviate the problem by presenting industrial data without corporate identification but a residual attitude of "paranoia" seems to persist. We suggest that the best solution is closer cooperation between regulatory agencies and the industries that they regulate.

Control of Dust Boil-Up During Rapping of ESP Collection Plates

One problem with electrostatic precipitators (ESP) involves the boil-up of dust as the collection plates are rapped. This boil-up re-

sults in reentrainment and, when it occurs in the last stages of the ESP, the dust can escape from the unit to become an environmental problem. One application of charged fog would involve fogging into the collecton bin to reduce this boil-up effect. We examined the ESP at a nearby facility (Arizona Portland Cement) but the system did not lend itself to a practical first test of the fogging system and we chose to build a unit that would simulate the boil-up problem.

The system is shown schematically in Figure 19; typical results with

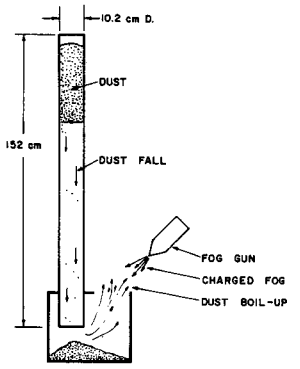

APPLICATION OF CHARGED FOG TO THE CONTROL OF DUST BOIL-UP

(19)

the fogging system "off" and "on" are shown in Figures 20 and 21. It is

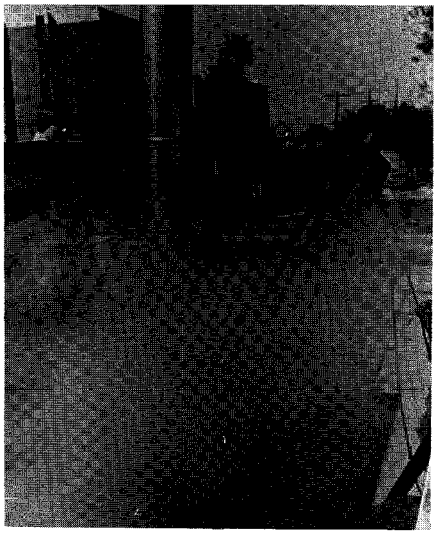

clear that the charged fog has significantly reduced the dust level but the pulsatile nature of the emission made it difficult to obtain quantitative data. We are building an optical system that will allow the rapid measurement of dust levels even under rapidly changing conditions. When this unit is available we should be able to demonstrate the effect of

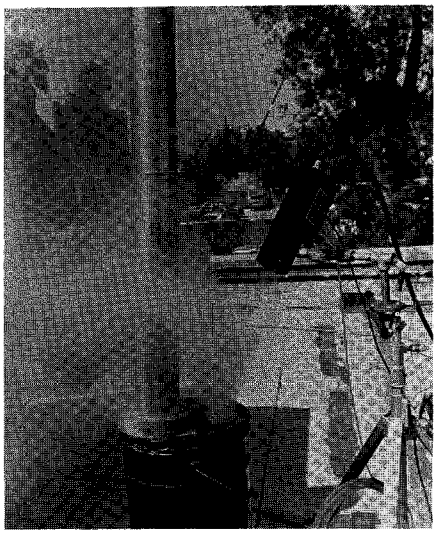

charged fog in reducing the pulses of dust under simulated "rapping" conditions.

Testing of Larger Fog Guns (Fogger II)

Part of the work on this program has included the development of larger fog guns that would "throw" the fog some distance (8 to 10 meters). One system for this purpose involved a dust generator made from a five gallon paint can filled with fly ash and "blown" by an air hose to provide a large scale source of dust. The system "in operation" is shown in Figure 22 with the fog "off". In Figure 23 we show the same system

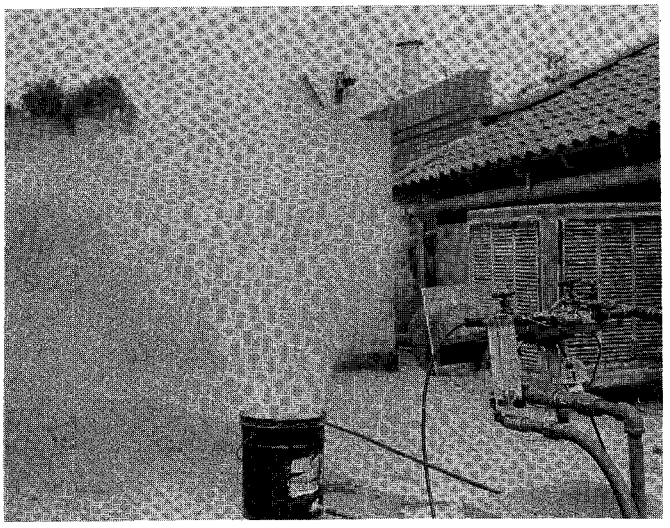

(22)

with the fog "on". There was a significant reduction and in this case we were able to obtain quantitative data with the GCA-RDM 101. These results are shown in Figure 24. We hope to test this system at a local cement plant and grain storage facility in the very near future.

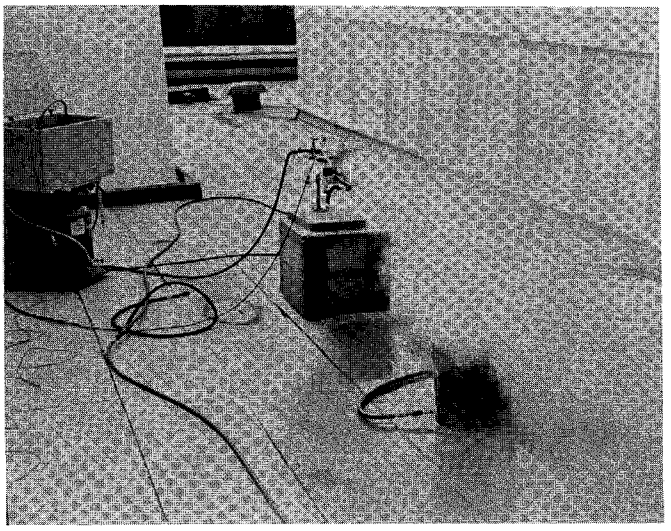

(23)

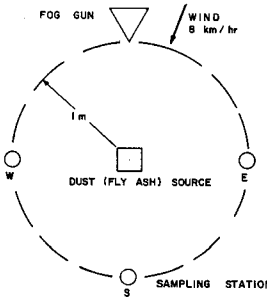

STATION	E	W	S
DUST LOADING AVERAGE OF 4 RUNS	2.23 mg/m³	2.0 mg/m³	3.48 mg/m³
DUST LOADING WITH (+) FOG .3 GAL./min	0.2	0.0	1.1
NET REDUCTION	91 %	100 %	68.4 %

OUTDOOR TEST OF CHARGED FOG FOR DUST REDUCTION

(24)

Development of a Stack Simulation System

Another test system under development at the University is a "stack simulator" funded by the Anaconda Company of Butte, Montana. This system is shown schematically in Figure 25 and will allow us to mix appropriate quantities of high temperature air, SO_2 and fly ash. The mixture will be exposed to charged fog and we hope to demonstrate that the control system can be used on a larger scale. This system will be made available to the local Copper Industry for testing of stack instrumentation and dust tracking techniques.

Industrial Testing

Cement Plant "A"-

A sample was taken from the belt conveyor in the quarry surge build-

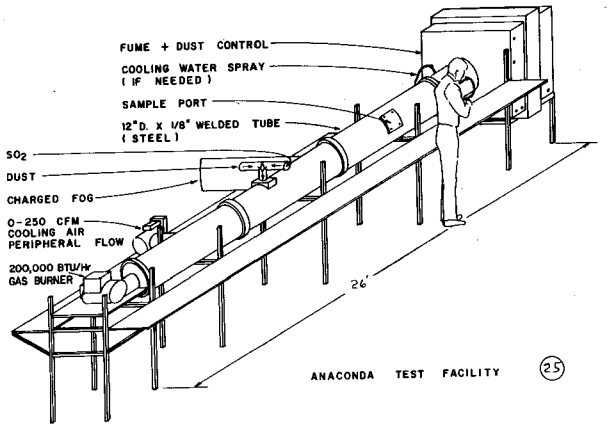

ing. The dust was tested in the system shown in Figure 3, and found to be negatively charged suggesting that positively charged fog should be used. The in-plant fog tests made use of two modified Ransburg REA guns, mounted as shown in Figures 26 and 27. The curtains shown in Figure 27

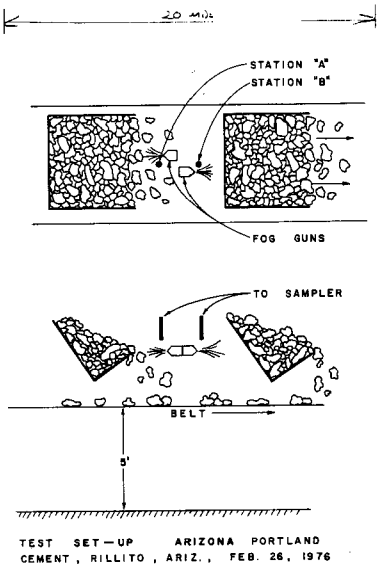

TEST SET-UP ARIZONA PORTLAND CEMENT, RILLITO, ARIZ., FEB. 26, 1976

were used to prevent dust from blowing in or out of the test area. In the case of Figure 26, we were interested in the dust suppression right at the hoppers. In Figure 27, the reduction in dust in the working area was of importance. The results are shown in Figures 28 and 29. In both cases there was significant reduction in the dust level.

Steel Casting Company "A"-

The test area for this study was a standard railroad boxcar used for shipping silica sand. Under normal conditions, the dust level during unloading was quite high. The control system involved four Ransburg REA

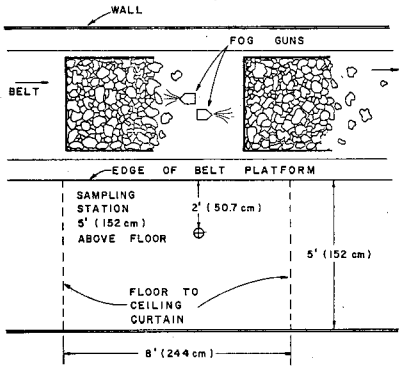

PLAN VIEW SURGE BUILDING
ARIZONA PORTLAND CEMENT CO.
RILLITO PLANT
MARCH 15, 1976

(27)

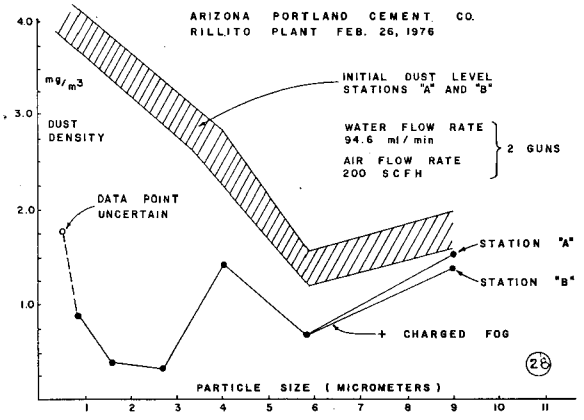

(28)

guns fastened to the inside roof of the boxcar as shown in Figure 30. The dust levels during unloading were monitored by MSA Gravimetric Dust Samplers for a two hour working period. The total dust level and the fraction of free silica were measured with and without charged fog. The results are shown in Figure 31. It is apparent that both the total dust concentration and the respirable silica level were significantly reduced. It is interesting to note that the free silica was reduced by a factor of 1.09/0.19 = 57.4, suggesting that the positively charged fog was most effective on the negatively charged (Figure 4) silica dust. This very significant effect is a measure of the effectiveness of the charged fog technique. Further experiments in this facility are planned.

Gates Learjet Corporation, Tucson-

The operation here involved a belt sander used for a variety of wood

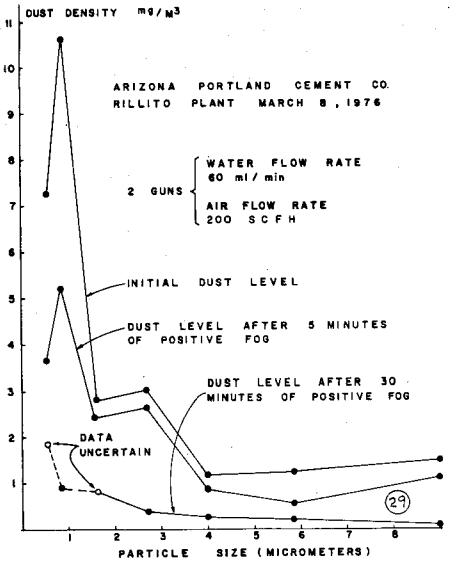

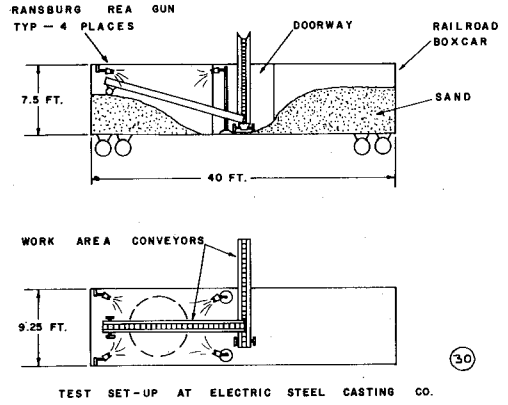

and plastic materials. The plant layout precluded the use of a hood and the application of a Fogger I unit seemed most appropriate. The irregular nature of the sander operation and the movement of the workmen, lift trucks, etc., in the area precluded numerical measurements of the dust level. It was decided to look for "visual results" with charged fog. Typical before and after photographs are shown in the attached Figures 32 and 33; it was very apparent that the charged fog reduced visible dust generated by the sander and Company management has made arrangements for plant modifications to accommodate one or more fog guns.

SPECIALIZED INSTRUMENTS FOR DUST EVALUATION

Commercial instruments for dust evaluation fall into two classes; the filter systems that are low in cost but do not provide an on-line reading of the dust level and the optical or beta ray absorption systems

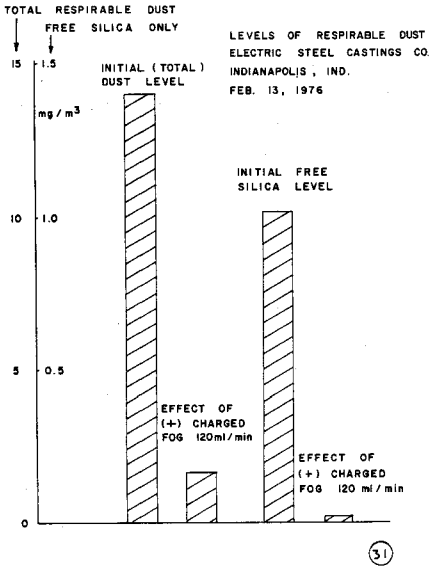

(31)

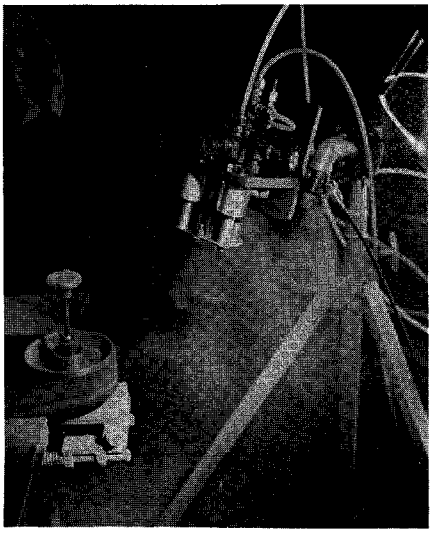

(32)

that provide on-line readings at the expense of high cost and significant complexity. Another problem with the beta ray systems, typified by the GCA Corporation RDM-101, is the fact that the dust build-up on the collection plate changes with the moisture level in the dust. If the dust is dry it forms a low mound while if moisture has been added, by charged fog, the total quantity of dust may be much less but the collected dust forms a sharply rising peak that yields a larger beta ray absorption even though the actual quantity of dust is less. This has led to some confusion among earlier users of the fog guns; one industrial dust control engineer indicated that the fog "made the problem worse". Subsequent tests with filters indicated that a substantial reduction in dust level was taking place but that this would not be revealed by the RDM-101 data.

In any case the high cost ($4,000.00) of the GCA unit and the even higher ($8,000.00) cost of the Leitz optical dust monitor make them un-

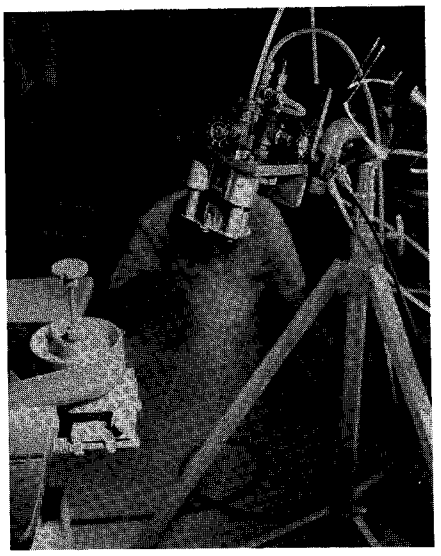

(33)

suitable for wide in-plant use. We have chosen to develop a low cost ($40.00) commercial smoke tester (RAC Incorporated, Gibsonia, Pennsylvania) as a device to draw a known quantity of dust through a filter/cyclone combination to make sure the readings refer only to respirable dust. The filters are evaluated for dust loading by a battery driven optical system using a light source and a photocell. Typical readings for a variety of dusts are shown in Figure 34. Naturally there is some

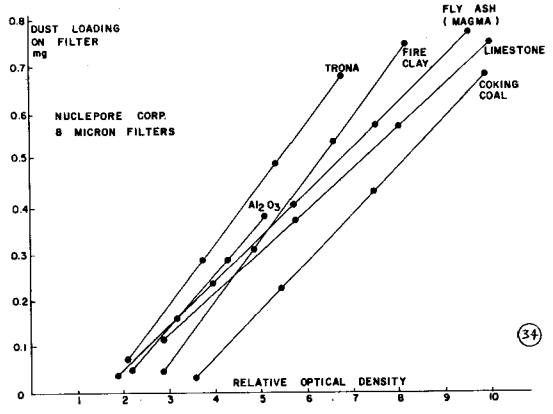

(34)

variation between the very light dusts (aluminum oxide) and the dark coal dust but in general the curves have very similar slopes. We suggest that for evaluating the effect of the charged fog it would only be necessary to take a filter reading with and without the charged fog. If more accurate data is needed calibration curves for specific dusts can be easily generated. One advantage of this optical system is that it is insensitive to the presence of water vapor; the filters do not have to be dried before measurement.

We have been discussing the manufacture and sale of devices of this type with the Mine Safety Appliance Company of Pittsburgh, Pennsylvania and hope to see systems of this type on the market by 1979. The fact that the devices will be low in cost should encourage their wide use.

DEVELOPMENT OF CHARGED FOG SYSTEMS FOR MOVING VEHICLES

Moving vehicles are a significant source of dust pollution and we have been interested in fogging systems that might be used on this type of equipment. We felt that the fog generating system had to operate without a supply of compressed air or a high pressure pump. Under these circumstances the only possible fog generation and propulsion system was a spinning cup with a row of fan blades on the periphery. The rotating cup generated the fog while the fan blades provided a flow of sheath air to carry the fog to the target.

Charging of the fog could be accomplished by holding the cup at a high voltage but this would require the use of an insulating shaft and a break in the liquid line to prevent electrical leakage. It seems simpler to have a high voltage ring just in front of the spinning cup and allow the water fog to be charged by the resulting corona. A system of this type has been designed and discussion with potential manufacturers are under way. The first application will be a fork lift truck.

ACKNOWLEDGMENTS

Many organizations and individuals contributed to this work; University of Arizona laboratory personnel included Mr. Werner H. Alchenberger, Mr. Brock A. Bazzell, Mr. Joseph B. Bidwell, Mrs. Jeanine M. Climer, Mr. Glen C. Cole, Mr. and Mrs. Douglas K. Darlington, Mr. John L. Griffith, Dr. Charles F. Russ, Mr. Christian W. Savitz, Mr. Steven W. Schroeder, Dr. Godfrey T. Sill, Mr. Carl R. Tornquist and Mr. A. Philip Verbout. Federal agencies, corporations and industrial organizations included the American Foundrymen's Society, the Ransburg Corporation, the ARO Corporation, the National Aeronautics and Space Administration, the Environmental Protection Agency and the National Institute of Occupational Safety and Health.

REFERENCES

1. Hoenig, S. A., et al. Use of Electrostatically Charged Fog For Control of Fugitive Dust Emissions. Environmental Protection Agency, Research Triangle Park, N.C. Publication Number EPA-600/7-77-131. November 1977. 85 p. Plus quarterly reports.

2. Loeb, L. B. Static Electrification. Springer, Berlin, 1958. 240 p.

3. Harper, W. R. Contact and Frictional Electrification. Oxford University Press, New York, 1967. 369 p.

4. Gallo, C. F., W. L. Lama. Classical Electrostatic Description of the Work Function and Ionization Energy of Insulators. IEEE Transactions on Industry Applications. Vol. 1A-12, 1:7, 1976.

5. Natusch, D. F. S., et al. Toxic Trace Elements: Preferential Concentration in Respirable Particles. Science. 183:202-204, 1974.

6. Israel, H. Atmospheric Electricity. Vol 1, U. S. Department of Commerce NTIS, Springfield, Virginia. 11:75, 1973.

COLLECTION AND CONTROL

OF MOISTURE LADEN FUGITIVE DUST

C. David Turley
International Minerals
& Chemical Corporation
Post Office Box 867
Bartow, Florida 33830

INTRODUCTION

International Minerals and Chemical Corporation, Minerals Division, Florida Operations, has undertaken an extensive program to control dust at several of its facilities. It entails the modification of existing dust collection systems and installation of new systems where necessary. The program is approximately 75% complete at this time.

IMC mines approximately 12 million tons of phosphate rock per year. The rock is removed from the ground as a mixture of rock, sand, and clays. It is then separated and refined at recovery plants by various aqueous processes. Two-thirds of this rock is dried in preparation for further processing, grinding and transporting. It is dried to 2-3% (wt.) moisture and remains at a temperature of 150-250°F. Once dried, the rock may be stored or loaded twice and pass as many as twelve conveyor transfer points. Each of these handling operations generate dust.

In the past, several dust control systems were installed. Their design was based on conventional duct velocities of 3000-4000 fpm. The smaller ducting in these systems quickly clogged caused by formation of mud from the collected dust and the condensation of moisture which evolves from the rock because of its elevated temperature. A point was soon reached where cleaning these systems was impractical.

The work of this program is done to comply with the State of Florida, Department of Environmental Regulation requirements which allow no "Fugitive Particulate" emission. Fugitive Particulate is

defined as any emission which does not pass through a duct or stack. The installation of these controls will also achieve compliance with MESA, now MSHA, personnel exposure limitations.

PROGRAM APPROACH

The dust control program has been implemented under several design guidelines. These guidelines were subject to the following constraints:

1. The dust control requirements were defined in terms of dust generating activity.

   (a) Material Transfer and Storage. Conveyor rates range from 25 to 2000 TPH.

   (b) Unground Rock Loading. Instantaneous rates range from 15 to 65 TPM.

   (c) Ground Rock Loading. Rates range from 40 to 90 TPH.

2. All existing dust collection devices were to be used by modification of their ducting systems.

3. The dust control systems were to be added to existing physical facilities with the exception of three new unground loading stations.

4. The dust control systems had to operate continuously in spite of intermittent generation of dust by operations such as loading.

The guidelines outlined for the program were as follows:

1. Collection devices were to be wet scrubbers for compatibility with the condensing moisture which would be collected into the systems.

2. Collection systems were to be dedicated to only one or two dusty activities. Exceptions were made for existing large capacity units.

3. Venting of dust into systems was to be through large vertical risers with low velocity, less than 1000 fpm. These were to approximate convective-type vents

4. Direct connection, no miters, were to be made by ducting to the risers or vents. The ducts were to be sloped to allow positioning of a duct spray at the point of connection.

5. Access covers were to be provided at each duct to riser connection for routine inspection of the spray by the operator. All additional duct runs were to be accessible for straight through cleaning if necessary.

6. Recirculating water systems were to be used to minimize overall fresh water consumption.

7. The collection device selection was targeted at a performance of 10% equivalent opacity or less.

8. The systems were to be simple to operate.

9. The systems were to be as standardized as possible.

GUIDELINE IMPLEMENTATION

The intial emphasis of the program was upgrading the existing systems and installation of trial systems in each of the identified areas, transfer and storage, unground loading and ground loading. These trials were for verification of the initial guidelines and refinement where necessary.

Wet Scrubbers

Impingement-type scrubbers with fan sprays were initially selected. These scrubbers were appealing because they eliminated the potential operating problem of mud build-up on the fan. These scrubbers are performing well with the exception of one which exceeds the opacity target. Proper particle size data was lacking in its original specification. The fan sprays serve as fresh water make-up for the recirculating water system to reduce the potential of that nozzle clogging.

Dedicated Systems

The new dust control systems have capacities of 3000-5000 cfm. They are located lower than the dust vents to allow water return from duct sprays which also makes them more accessible for service. The use of small systems minimizes flow balancing requirements for the ducting systems. In most cases flow regulation by blast gate was not necessary.

Two examples of these systems are shown in Figures 1 & 2. The first system collects dust ground rock rail car loading. Ground product is conveyed via air slide to a surge hopper. The rock loads by a retractable chute into a single door in each car compartment. Dust is vented from the adjacent door to the one being loaded by a retractable hood. The system in Figure 2 vents two conveyor transfer hoods. This system operates when one or both conveyors are in use. The hoods are double flapped to establish air flow to the unit along the normal conveyor skirts.

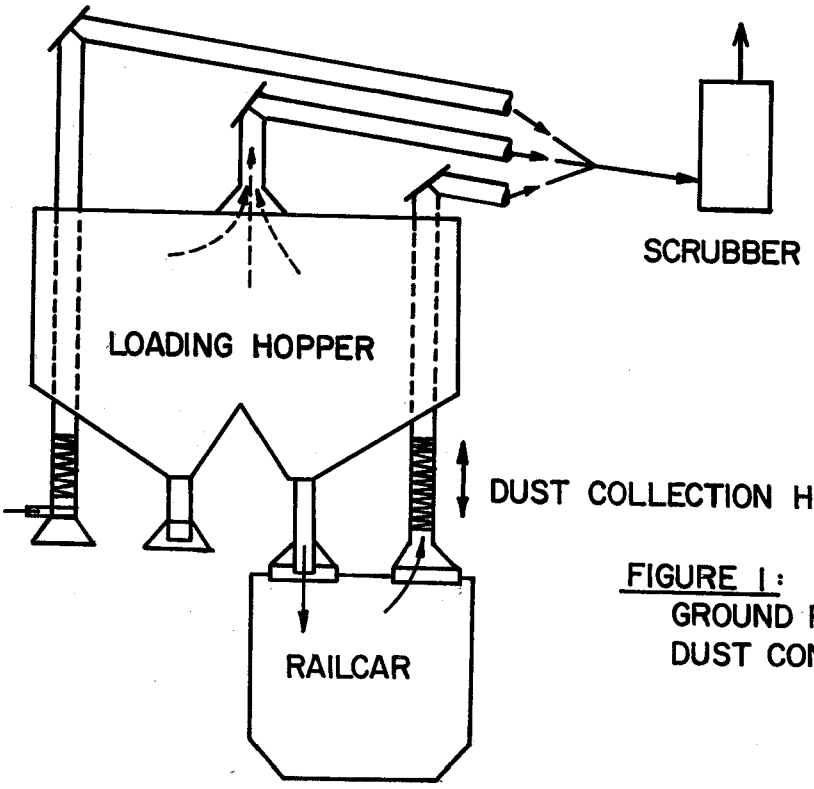

FIGURE 1:
GROUND ROCK LOADING
DUST CONTROL SYSTEM

FIGURE 2:
CONVEYOR TRANSFER
DUST CONTROL SYSTEM

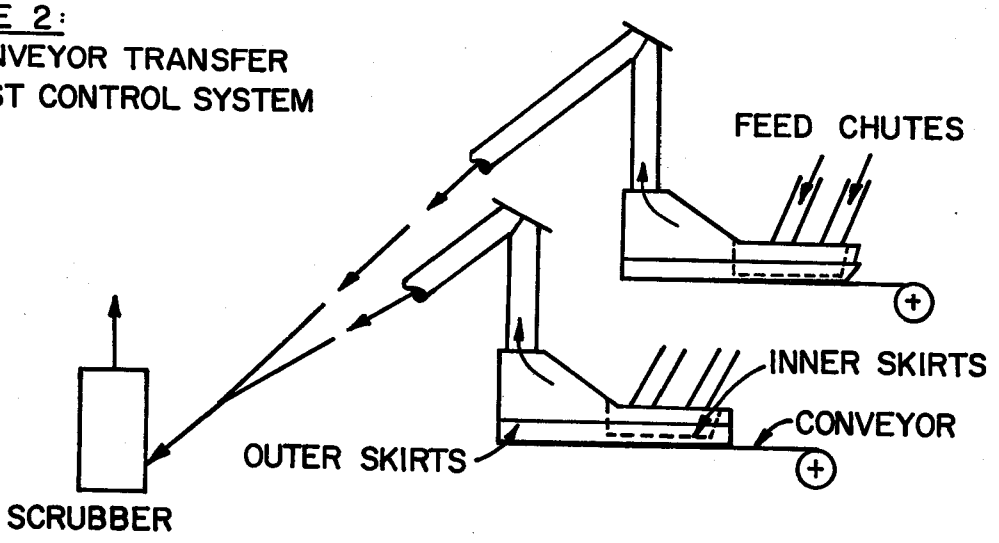

Vertical Vents

Each dust enclosure is vented vertically. These vents or risers were sized for velocities of 500-1000 fpm. This promotes fall-out of large particles, prevents entrainment of material and minimizes build-up on duct walls. Essentially the idea was to make these ducts vented convective risers with such a diameter that any build-up would fall before it could bridge. In loading situations where a retractable hood was necessary, the vertical duct was a lightweight flexible hose made on a weak spring. The flexible hose acts as an accordion as it raises. Under -½ to -1 in. static pressure, the hose remains vertical and performs well. At lower static pressures, it tends to close on itself. Examples of vertical vents are shown in Figure 3.

Duct Sprays

Water sprays are located at the connection of the dust riser and the system duct work. These sprays are generally supplied by recirculating water at rates of 10 to 15 gpm. The nozzles are spiral-type which produce full cone spray patterns. The spray pattern must directly hit the duct walls. Sprays are positioned at the center or bottom of the duct and with sufficient depth, maximum six inches, to prevent drip down the vertical vent with no air flow.

The sprays do not eliminate build-up in the ducts. They do, however, make it occur in a specific location, the wet-dry zone around the spray. As this build-up occurs, air flow can be restricted. No duct has been observed to completely close off. The build-up rate depends on amount of dust generated by an activity. Some ducts need daily cleaning while others have not been cleaned since installation. Spray operation is checked daily. Cleaning consists of simply pushing build-up material further into the duct so that the spray will remove it into the water system.

The ducts which connect to the vertical vents require a minimum slope of 1 in/ft with 3 to 4 in/ft slopes being more satisfactory. The best situation occurs with the spray and duct going vertically downward as in the example in Figure 3. In the modification of existing systems, it became necessary to make provision for flow adjustment. In these cases, the blast gates were tilted toward the duct sprays at angles of 45^{o} to 60^{o} with the duct. The gates were positioned in this manner to create small precleaning verturi sections in the duct. See Figure 3.

Accessibility

Two levels of accessibility were provided in the ducting systems. While operating, direct access to the sprays is provided for the operator for routine inspection and cleaning if necessary. There are generally lipped covers which fit over the vertical vents which have been cut at an angle, shown in Figure 4. In one case, the vent was cut at

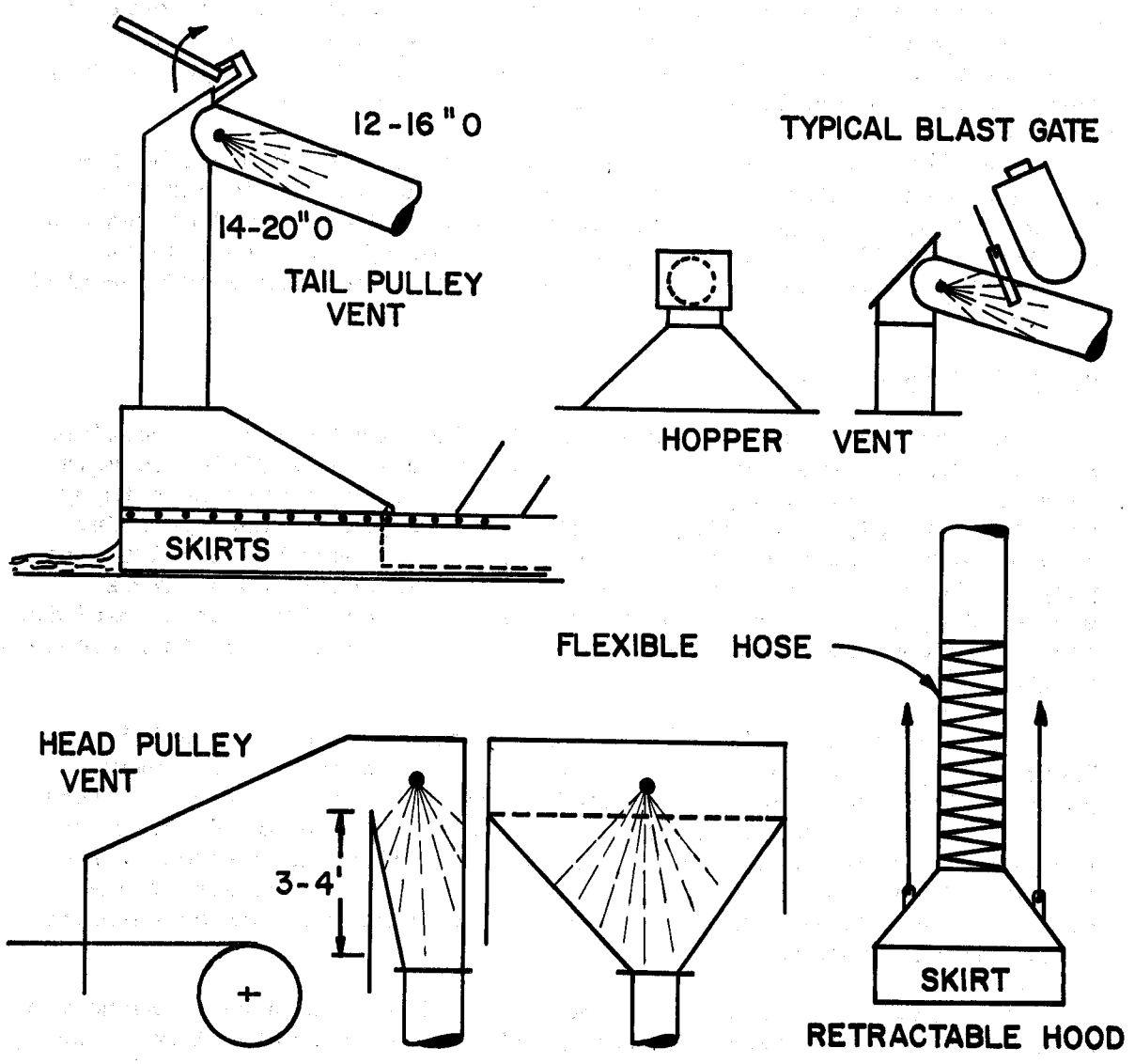

FIGURE 3:

TYPICAL DUST ENCLOSURE VENTS OR RISERS

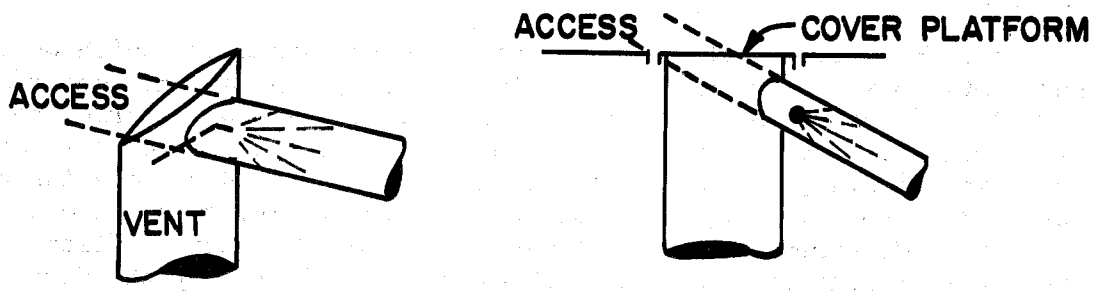

FIGURE 4:

DUCT CLEANING ACCESS

the platform level above the vented area. Its cover was then part of the upper platform. The access covers are positioned such that the duct may be directly rodded from the end if necessary. In some cases, these covers are not hinged or attached except by chain.

The second level of access are bolted covers which would be removed when the system is not operating. At each change in direction of the ducts, a flange and cover is provided so that each duct run can be directly rodded. These flanges are located by platforms, doors, etc. so that they can be reached if necessary. An example is presented in Figure 5.

Water Recirculation

The water recirculation systems minimize fresh water consumption. Each system requires nominally 10-20 gpm fresh water addition to maintain approximately 1% solids in the system. It is particularly important that the piping completely drain when the pump is not operating because of the recirculating solids. The piping must be sloped to the pump as the ducts are to the scrubbers. Nozzle supply connections should be at a right angle to the main supply line direction to minimize heavy particle flow through the nozzles. An example system is presented in Figure 6.

Level control in the system sumps is achieved using an SSPH* Fluidic Valve.[1] This is a flow directing device which has no moving parts. Flow direction is determined by air port on the valve. A tube or line connected to this port is positioned at the desired level in the sump. Recirculating water is either bled from the systems or returned to a duct or the sump as the sump level either covers or uncovers the end of the air port line. The valve may be placed anywhere in the piping system.

Pumps used for the systems are rubber lined. Each has a mechanical seal which is protected by a flow switch in the seal water line. The sumps contain low level sensors to guarantee that they have sufficient water to operate.

Opacity Target

The objective of the program was to select scrubbers which would have emissions less than 10% equivalent opacity. An attempt was made to model[2,3] the overall opacity of the available scrubbers prior to final selection of the units to be installed. It proved to be a good exercise; however, the actual performance probably had no relation to the prediction. The apparent fallacy in this prediction was the inability to determine the correct particle size. The actual distribution that is delivered to the scrubber will be altered by the duct spray and must be considered in the specifications for a scrubber.

*Trademark, Moore Products, Co., Spring House, Penn.

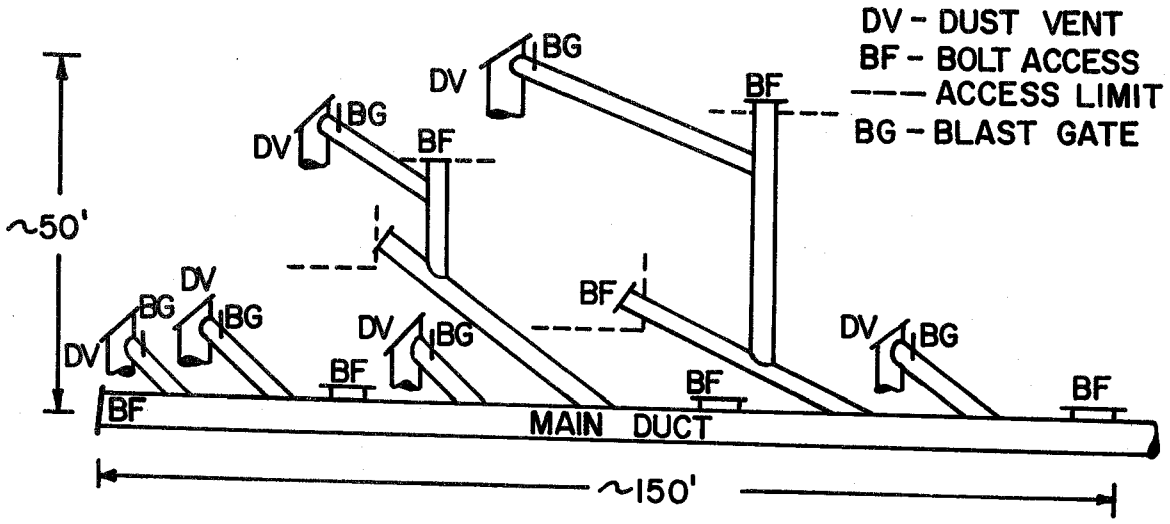

FIGURE 5:

DUCT SYSTEM USED FOR LARGE CAPACITY EXISTING SCRUBBER

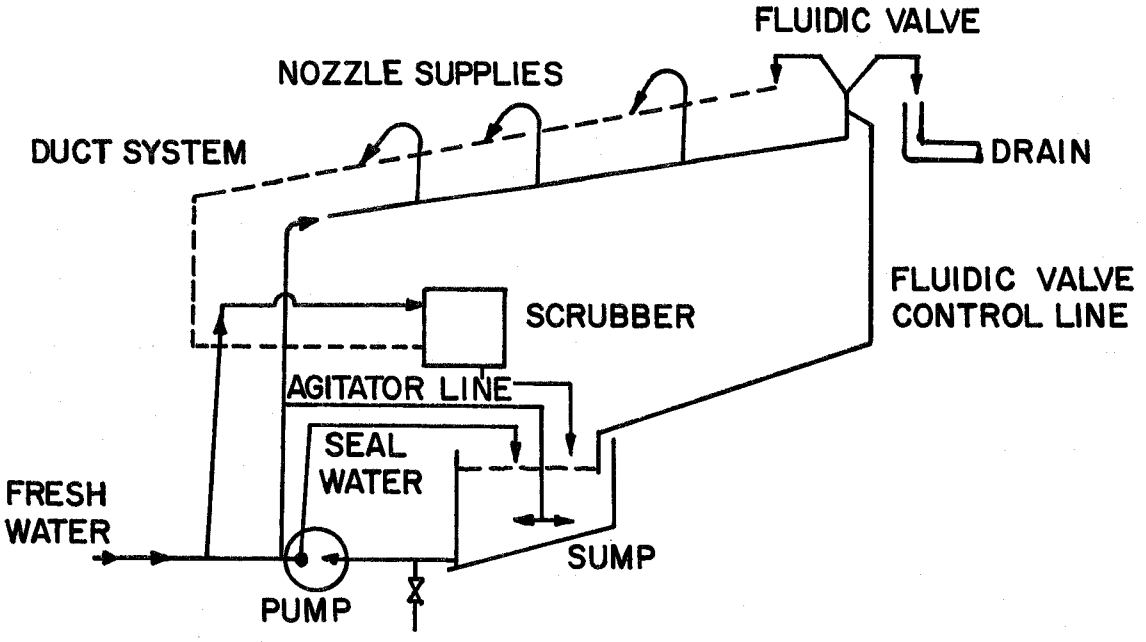

FIGURE 6:

TYPICAL WATER RECIRCULATION SYSTEM

Simplicity

Each dust control system design was approached with the idea that any additional effort required of the operator be made as simple as possible. It was the intention that the benefit to the operator by the elimination of dust from his area would be worth the extra effort required of him. The controls are generally pump and fan switches on a panel. For later systems, a switch is being added for clean water supply.

Standardization

The idea of standardization has implementation on two levels. The first is the use of duplicate equipment as is possible with the choice of pumps, nozzles, valves and instrumentation. The second level applies to similar equipment such as scrubbers with different flow rates and, therefore, different physical size. This has importance to the familiarity and understanding of operation of the mechanic who must service several systems.

CONCLUSIONS

The dust control design features presented by this paper have been developed to combat specific collection problems created by moisture laden fugitive dust. They have proven successful as applied. They create specific areas of build-up, the wet-dry zones at the duct sprays which must be accessible to the operators for cleaning. Inherent in these types of installations must be the provision for routine inspection by operating personnel.

The primary choice in the design of new installations for this type of dust control should be for the use of small, dedicated wet scrubbers. Larger venting systems can be operated by the use of sprayed blast gates into low velocity ducts. Water sprays must be applied to the complete ducting system. The sprays must be applied so that they are accessible to operators. Failure to spray all ducts may create wet-dry zones at duct junctions and cause clogging where it is not readily accessible. If wet collectors cannot be used, bag collectors can be used as a last resort by equiping them with thermostatically controlled auxiliary fan and heater system to maintain bag temperature when not venting dust source.

The ultimate conclusion of this type of approach is the elimination of ducting by making the collection device an integral part of the enclosure. One example of this could be the use of a Lone Star Steel Hydrosonic Cleaner.[4] This means of collection has been applied in commercially available scrubber units. The collection equipment of one version of this cleaner is a steam ejector, producing draft, with a ring of water sprays around the ejector. This equipment could be applied in the duct enclosure as the duct sprays of this paper have

been. The enclosure would then require the passages needed for collection of droplets and venting of clean gases. This use of this type of equipment would be appealing in facilities with a readily available steam supply. Reference 5 presents several small scrubbers which have been developed for use mainly in coal mining operations. These types of unit also have the potential for incorporation into the dust enclosure as was discussed for the previous example.

REFERENCES

Adams, Robert D. Applications of Fluidic Valves. ASME Annual Winter Meeting. Chicago, Ill. November 1965.

Larssen, Steinar, D. S. Ensor, and M. J. Pilat. Relationship of Plume Opacity to the Properties of Particulates Emitted from Karft Recovery Furnaces. TAPPI, Vol. 55, No. 1: pp. 88-92. January 1972.

Connor, W. D. Measurement of Opacity and Mass Concentration of Particulate Emission by Transmissometry. Prepared for E.P.A. by National Environmental Research Center. NTIS Publication No. PB241-251. Research Triangle Park, N. C. November 1974. 32 p.

Ewan, Thomas K. and Jay S. Master. Fine Particle Scrubbing with Lone Star Steel Hydro-sonic Cleaners, "The Coalescer". Lone Star Steel Company, Lone Star, Texas (presented Second E.P.A. Fine Particle Scrubber Symposium) EPA-600/2-77-193. September 1977. pp. 319-337.

Divers, E.F. and J.J. Janosik. Comparison of Five Types of Low-Energy Scrubbers for Dust Control. U. S. Department of the Interior, Bureau of Mines. TN23.U7, no. 8289, 622.06173. 1978.

THE VISIBILITY IMPACT OF SMOKE PLUMES

David S. Ensor
Meteorology Research, Inc.
464 West Woodbury Road
Altadena, California 91001

ABSTRACT

The appearance of smoke and haze is an obvious manifestation of air pollution. The opacity of plumes near the top of the stack has long been used to regulate emissions. In recent years, the visibility downwind from sources is of increased concern and possible regulation.

This paper is a review of the basic physical aspects of opacity and visibility. In addition, plume visibility data will be discussed.

INTRODUCTION

Background

Visible haze and smoke which may also obscure scenic vistas are an obvious adverse effect of air pollution. The appearance or opacity of smoke has long been used to regulate the emissions from stationary sources. Also the ability to see and identify objects has been important in navigation from the standpoint of safety. Last year, Congress approved Section 169A of the 1977 Clean Air Act Amendment which provides a mandate for the protection of visibility in and near Class I areas. The Environmental Protection Agency (EPA) must provide a report to Congress by February 1979 on implementation of the Act. Regulations and methods to prevent future and to remedy existing visibility reduction must be promulgated by EPA by August 1979. This

regulatory action has stimulated interest in visibility impact of stationary sources and techniques to measure visibility.

Definition

The word "visibility" has two definitions. The general usage, and the meaning in architecture and illumination engineering is the ability to see an object against its background. The meteorological usage as defined by Huschke[1] is "the greatest distance in a given direction at which it is just possible to see and identify a prominent dark object against the sky at the horizon, and at night a known preferably unfocused moderately intense light sources." The use of the word "visibility" to describe a distance has been disturbing to some atmospheric scientists, Middleton[2] suggested the term "visual range" to indicate the distance at which a dark object against the horizon can be seen.

Objectives

The objectives of this paper are to discuss the general concepts of visibility and the application to plumes. It is intended to be a general overview of the problem.

FUNDAMENTALS

Time and Magnitude Scale

The nature of plume related visual effects depends on the location of the point of interest relative to the emission source. The three magnitudes of scale are compared in Table 1. At the top of the stack the opacity will depend on the particle size distribution, concentration and concentration of the primary aerosol emissions. In some sources such as oil-fired power plants sulfuric acid vapor may condense and form a visible plume. Condensing water vapor will also affect the opacity at the top of the stack. The condensation effects and mixing near the stack will depend on the local micrometeorology. Downwind from the plant, as the plume reaches thermal equilibrium, the plume opacity will steadily decrease from dilution. Coagulation of submicron particles into the 0.1 to 1.0 particle diameter size region may increase the particle light scattering in the plume. As the plume is carried downwind gaseous pollutants such as SO_2 will undergo chemical reactions and form particulate matter. In the Macroscale, the secondary aerosol may be the most significant source of visibility reduction.

Table 1. SCALE OF PLUME VISIBILITY PHENOMENA

		Time and Distance Scale		
		Microscale Sec-Min-m Stack Exit	Mesoscale Min-Hrs-m-km Developed Plume	Macroscale Hrs-Days-km Dispersed Plume
Plume Shape and Size		Buoyancy Stack velocity Micometeorology	Local Winds Local Stability	Air Mass Characteristics
Extinction Coefficient	Source	Fuel type and composition. Nature and operation of source control device. Water and acid condensation	Aerosol coagulation. Gas to particle conversion	Other sources. Gas to particle Conversion
	Sinks	Local rain out Large particle fallout	Deposition Sedimentation	Removed by precipitation
Visibility Impact		Plume opacity	Visibility of and through a plume	Atmospheric Visibility

Properties of the Eye

The discussion of visual effects should begin with the properties of vision. The eye is sensitive to a narrow range of wavelengths of electromagnetic radiation from 0.4 to 0.7 microns. For photopic (or light adapted vision) the maximum sensitivity of the eye is in the green at 0.555 microns. Instrumentation used to measure visible light should have a wavelength response similar to the eye.

The ability to see an object in the absence of color effects depends on the contrast of the object to its background as defined in the following equation:

$$C = \frac{B_o - B}{B} \tag{1}$$

where B_o is the brightness of the object (candles/m^2) and B is the brightness of the background (candles/m^2). The contrast of a black object against a bright background is -1. While the contrast of a bright object against a black background can be 10 or more, when the contrast is zero the object will be invisible. The contrast at which the object will just be visible depends on the background illumination whether the eye is in a state of light or dark adapted vision, the size of the object and if the object needs to be detected or identified. The results of extensive studies have been reported by Blackwell.[3]

Transfer Equation

The propagation of light through a scattering media such as smoke and the atmosphere is described by the transfer equation. The transfer equation formulated by Chandrasekhar[4] is given by

$$\frac{dI}{b_{ext}\, dx} = I - S \tag{2}$$

where I is an intensity, S is a source term, x is distance and b_{ext} is the extinction coefficient. In the atmosphere, solution of the transfer equation can become very complex because of the scattered light-source term S. Particles and gas molecules have directional dependent scattering. Thus, a volume of gas containing particles may act as a light source by light scattering into the direction of view. The radiation field in the atmosphere is from sky light (light scattered from other parts of the atmosphere by gas molecules and haze) and sunlight. The description of the source term is complex as shown by Jarman

and de Turville[5] and Harlow and Zeek[6]. When the scattered light source term can be neglected, the transfer equation reduces to Beer's law

$$I/I_o = \exp [- b_{ext} L] \tag{3}$$

where L is the path length.

Another simplification of the transfer equation is the Koschmieder formula describing the distance that a black object can be seen against the horizon sky. The source term is called air light or light scattered into the field of vision by the atmosphere. The air light increases the apparent brightness of the dark object. When the apparent brightness of the object is within 2% of the background sky, the object is invisible. One of the assumptions of the derivation is a flat earth with the result that the brightness of the sky at the object and at the observer are identical. The derivation as given by Middleton[2] for a contrast threshold of 0.02 is

$$L_v = \frac{-\ell n C}{b_{ext}} = \frac{3.9}{b_{ext}} \tag{4}$$

This equation has been extensively studied, Horvath[7] reported that the major source of error in the practical application of the equation was the use of nonblack targets. Often L_v is called the "meteorological range" to indicate the use of a 0.02 contrast threshold.

Calculation of Plume Light Scattering

The equations describing aerosol light scattering are described in several standard texts such as Van de Hulst[8]. Ensor and Pilat[9] reported methods for estimating light transmittance and plume opacity for aerosols with a lognormal size distribution. Harlow and Zeek[6] described Ringelmann number estimations incorporating the effects of sun angle and directional light scattering. The prediction of opacity is very sensitive to the errors in the particle size distribution as reported by Campbell et al.[10] Also the condensation of volatile material such as sulfuric acid resulting in a difference between instack and top of the stack opacity as observed by Conner[11] is not well understood.

There are limited studies of the visual effects of plumes downwind of the stack. Jarman and de Turville[5] calculated the disappearance of a plume by dilution for an observer looking directly up through the plume at the sky. Ensor et al.[12] reported equations to predict

transmittance of a plume and average extinction coefficient for a path length across the plume. In this analysis the formation of secondary aerosol from gas to particle conversion was neglected.

There is limited data for the micro and meso scale plume cases. On the macro scale, gas to particle reactions are very significant. Much of the current research work on regional transport and conversion of sulfur compared was summarized at the Dubrovnik conference[13]. A striking example of the effects of gas to particle conversion was reported by Trijonis[14] that 2/3 of the visibility reducing aerosol in the southwest resulted from SO_2 emitted by smelters.

MEASUREMENT

The major techniques used to measure the visual effects are shown in Table 2; and the advantages and disadvantages of each method described in Table 3.

Observers

The observations of plume opacity and visibility, although different quantities, have some similarities. The similarities are the long history of use and the acceptable results which can be achieved with trained observers.

Plume Opacity -

Plume opacity is estimated by observers under very specific viewing conditions, as described in the Federal Register[15]. Most important is the position of the sun to the back of the observer. Observers are trained to determine plume opacity with a small smoke generator with a reference transmissometer in the stack. The observation and measurement of plume opacity was extensively studied by Conner and Hodkinson[16].

Visibility Observations -

The observation of visibility is conducted at most airports with meteorological stations. The observation consists of noting of known objects at known distances are visible. The observation is dependent on the quality (large black objects against the horizon sky) and number of targets. The main objective of obtaining the data is to allow judgments on the potential safety hazard involved in using the airport.

Table 2. SELECTED MEASUREMENT TECHNIQUES FOR AEROSOL LIGHT EXTINCTION COEFFICIENT

Scale	Micro	Meso	Macro
Range of Extinction Coefficient, m^{-1}	10^{-1} - 10^{-4}	10^{-2} - 10^{-4}	10^{-2} - $2x10^{-5}$
Observer	Plume opacity	Qualitative	Weather observation for visibility
Transmissometer	In-Stack opacity		Fog navigation hazard Developmental for other conditions
Integrating nephelometer	Research use	Plume mapping in Aircraft	Widespread use
Photography	Research use		Research use
Photometry	Research use		Research use
Lidar	Research use		Atmospheric probing Fog measurement

Table 3. EVALUATION OF SELECTED MEASUREMENT TECHNIQUES

Method	Advantages	Disadvantages
Observer	• Traditional	• Subjective
Transmissometer	• Standard for stacks & fog • Integrated over path	• Limited dynamic range • difficult under clean conditions • Scattered light errors
Integrating nephelometer	• Wide dynamic range • Sensitive for very clean conditions • Calibrated with reference gas • Portable and inexpensive	• Point measurement • Angular truncation errors
Photography	• Simple • Record of view • Equipment is fairly inexpensive	• Requires skill to use • Negative, must be calibrated • Labor intensive
Photometry	• Simple	• Light scattering errors • Requires skill to use • Labor intensive
Lidar	• Single ended	• Expensive • Requires very skilled operators • Often only qualitative

Transmissometers

Transmissometers consist of a collimated light source directed toward a photoelectric detector. The instrument has widespread use on smoke stacks required for some new source as specified in the Federal Register[16]. Transmissometers have also been in use at airports to measure visibility in fog as described by Douglas and Young[17]. The baseline or distance between detector and projector for the airport transmissometer is 250 feet. For low concentrations which would be required for measurements of interest from an air quality standpoint much longer baselines are required. Some of the engineering problems for long baseline instruments have been discussed by Kreiss et al.[18]. It is difficult to obtain the 100% transmittance point. Atmospheric turbulence and refraction will often distort the beam.

Integrating Nephelometer

The integrating nephelometer measures the extinction coefficient from scattered light. It was first reported by Beuttell and Brewer[19] and been refined over the years by Charlson et al.[20]. The chamber is illuminated by a light with an opal glass filter. At a right angle a photo detector measures the light scattered from the aerosol in the cone of view. The measured scattered light is proportional to the scattering coefficient. The light loss at the extremes of the integration (angular truncation) generally is not significant as calculated by Ensor and Waggoner[21]. The major advantages of the instrument are its portability, wide dynamic range and sensitivity. The use of the integrating nephelometer in an instrumented aircraft was reported by Blumenthal et al.[22].

Photography

The use of photography to measure visibility in remote areas has been reported by Roberts et al.[23] and Puechel et al.[24]. It has also been used to measure plume opacity as described by Conner and Hodkinson[16]. The negative must be calibrated to obtain a relationship of negative density as a function of brightness. For visibility determination the brightness of a dark target and the horizon sky near the target is measured. The visibility is determined by application of Koschmieder's formula. The use of photography for plume opacity measurement requires that a light and dark background be located behind the plume. Four measurements are performed:

- brightness of light background, B_i
- brightness of dark background, B_d
- brightness of plume against light background, $B_{p\ell}$
- brightness of plume against dark background, B_{pd}

The transmittance is given by

$$T = \frac{B_{p\ell} - B_{pd}}{B_i - B_d} \tag{5}$$

The ratio of the differences of brightness is used to cancel the plume air light.

Photometry

The photometer or telescope with a light meter has been used for plume opacity measurement by Conner and Hodkinson[16] and Cwalenski et al.[25] for visibility measurements. The same approach for plume opacity measurements as used for the photographic techniques is used with the photometer. The visibility is determined by measuring the brightness of distance objects and the background horizon sky. Generally the acceptance angle of the photometer should be small (1/4°) to reduce the detection of scattered light.

Lidar

LIDAR is a pulsed laser projector with a receiving telescope positioned to detect the back scattered light from the pulse. Complex computer processing is used to invert the signal to obtain the transmittance through the plume. The pulse of light after traversing the plume scatters light from the atmosphere. This back scattered light is attenuated by the plume back to the detector. Thus plume transmittance can be measured with a single ended instrument. The state of the art equipment is described by Herget and Conner[28]. Other atmospheric applications include fog measurement and atmospheric probing of haze layers.

SUMMARY

The major aspects of plume visibility have been reviewed. The light transmittance through the plume is the significant extensive property while the extinction coefficient is the important intensive property

of the plume. Many aspects of the impact of plumes are still not well defined. This includes the visibility measurement and prediction of visibility.

REFERENCES

1. Huschke, R. E., 1959. Glossary of Meteorology American Meteorological Society, Boston, MA.
2. Middleton, W. E. K., 1968. Vision through the Atmosphere, University of Toronto Press.
3. Blackwell, H. R., 1946. Contrast Threshold of the Human Eye, JOSA 36 624-643.
4. Chandrasekhar, S., 1960. Radiative Transfer, Dover, New York, p. 9.
5. Jarman, R. T. and C. M. de Turville, 1969. The Visibility and Length of Chimney Plumes, Atmos. Envir. 3 257-280.
6. Harlow, J.S. and S. J. Zeek, 1973. Predicting Ringelmann Number and Optical Characteristics of Plumes, JAPCA 23 676-684.
7. Horvath, H., 1971. On the Applicability of the Koschmieder Visibility Formula, Atmos. Envir. 5 177-184.
8. Van de Hulst, H. C., 1957. Light Scattering by Small Particles, Chapman Hall, London.
9. Ensor, D., and M. J. Pilat, 1971. Calculation of Smoke Plume from Particulate Air Pollutant Properties, JAPCA 21, 496-501.
10. Campbell, K. S., R. W. Scheck, S. D. Severson, F. A. Horney, D.S. Ensor and G. R. Markowski, 1978. Economic Evaluation of Fabric Filtration versus Electrostatic Precipitation for Ultra High Particulate Collection Efficiency, EPRI FP-775, June.
11. Conner, W. D., 1976. A Comparison between in-stack and plume opacity measurements at oil-fired power plants. (Presented at the Fourth National Conference on Energy and the Environment, October 4-7, Cincinnati, Ohio).
12. Ensor, D. S., L. E. Sparks, and M. J. Pilat, 1973. Downwind Transmittance of Smoke Plumes, Atmos. Envir. 7 1267-1277.
13. Husar, R. B., J. P. Lodge, and D. J. Moore (Eds), 1978. Sulfur in the Atmosphere. Proceedings of the International Symposium held in Dubrovnik, Yugoslavia, 7-14 Sept., 1977. Atmos. Envir. 12 p. 1-796.

14. Trijonis, J., 1978, Visibility in the Southwest - An Exploration of the historical data base, #78-4317, presented at the 71st Annual Meeting of APCA Houston, Texas, June 25-30.

15. Federal Register Standards of Performance for New Stationary Sources 36 24894, Dec. 23, 1971.

16. Conner, W. D. and J. R. Hodkinson, 1967. Optical properties and visual effects of smoke-stack plumes. PHS Publ. No. 999-AP-30.

17. Douglas, C. A. and L. L. Young, 1945. Development of a Transmissometer for determining visual range, Report No. 47, Feb.

18. Kreiss, W. T., J. M. Lansinger and W. G. Tank and M. L. Pitchford, 1977. Field testing of a long-path laser transmis someter designed for atmospheric visibility measurements. Proceedings of SPIE Advances in Laser Technology for the Atmospheric Sciences, 125, August 25-26, San Diego, California.

19. Beuttell, R. G. and Brewer, A. W., 1949. Instruments for the measurement of the visual range, J. Sci. Instrum 26, 357-359.

20. Charlson, R.J., N. C. Ahlquist, H. Selvidge and P. B. MacCready, 1969. Monitoring of Atmospheric Aerosol Parameters with the Integrating Nephelometer, APCAJ 19, 937-942.

21. Ensor, D. S. and A. P. Waggoner, 1970. Angular truncation error in the integrating nephelometer, Atmos. Envir. 4, 481-487.

22. Blumenthal, D. L., J. A. Ogren and J. A. Anderson, 1978. Air Borne Sampling System for Plume Monitoring Atmos. Envir. 12, 613-620.

23. Roberts, F. M., J. L. Gordon, D. L. Hoose, R. E. Kary, and J. R. Weiss, 1975. Visibility Measurements in the Painted Desert. Presented at the 68th Meeting at APCA, Boston, Mass., June 15-20.

24. Pueschal, R. F., P. A. Allee, D. L. Wellmore, W. F. Roberts, W. W. Wagner, T. C. Thoem, 1978. Variabilities in Visibility in East Central Utah, #78-43.4, presented at the 71st Annual Meeting of APCA, Houston, Texas, June 25-30.

25. Cwalenski, R., J. M. Lansinger and W. G. Tank, 1975. Field Testing and Evaluation of Methods for Measuring Visibility, EPA-650/2-75-039.

26. Herget, W. F. and W. D. Conner, 1977. Instrumental Sensing of Stationary Source Emissions, Envir. Sci. Tech 10, p. 962-967.

MUTAGENICITY OF COAL FLY ASH*

Clarence E. Chrisp
Radiobiology Laboratory
University of California
Davis, California 95616

ABSTRACT

Coal fly ash was collected from both the electrostatic precipitator hopper and the stack of a large coal burning power plant. Four size-classified fractions were collected from the stack, and one size-classified fraction of hopper fly ash comparable to the smallest sized fraction collected from the stack was prepared. Mutagenicity of these fly ash filtrates was tested with the Ames Salmonella system. Fly ash samples were incubated with horse serum or buffered saline and filtered before testing. Of the five strains tested, mutagenic activity was seen with the frameshift strains TA-98 and TA-1538. Samples of respirable-sized fly ash from the hopper were non-mutagenic; however, the same sized fractions collected from the stack were quite mutagenic. Mutagenicity of various sized fractions of fly ash collected from the stack displayed a particle size dependence.

INTRODUCTION

In our initial studies of the potential health impact of energy technologies, we have performed physical, chemical and mutagenic studies with coal fly ash. The physical and chemical properties have previously

---

*This research was supported by the U.S. Department of Energy

been published.[1,2,3,4] Although the vast majority (85-99%) of the fly ash produced in coal combustion for electric power generation is retained in the power plant, we[5] have estimated that 2.4 million metric tons of fly ash were emitted to the atmosphere from U.S. coal-fired electric plants in 1974. Because the principal particulate emission control technology, electrostatic precipitators (ESP) or wet scrubbers, have low collection efficiency for smaller particles,[6] much of the released fly ash is in the "respirable" size range (aerodynamic diameters <10 μm).[7] This fine particle fraction presents the greatest potential health hazard, since small particles have the longest atmospheric residence time, and thus the greatest potential for ultimate human inhalation[8] and are generally most efficiently deposited in deep lung and least efficiently removed by mucocillary transport. The presence of carcinogenic substances as a result of fossil fuel combustion has been suspected since scrotal cancers were first observed in chimney sweeps in 1775 by Percival Pott.[9] Subsequently, organic compounds from coal tar products proved to be carcinogenic in experimental animals.[10] Many trace elements which we have shown to be important surface-related components of fly ash[2] have been shown to be mutagenic[11] or carcinogenic.[12]

A high positive correlation between carcinogenicity of substances for animals or man and mutagenicity in a bacterial test system has been shown by McCann and Ames.[13] It was decided to use this simple and economical test for detection of putative carcinogens on the surface of fly ash.

MATERIALS AND METHODS

Size fractionated fly ash samples were collected from the stack (downstream of the electrostatic precipitator) of a power plant burning high ash, low sulfur, western coal.[14] The material was fractionated in situ utilizing a specially designed classification system operating at 100°C. The four fractions had volume median diameters 20, 6.3, 3.2, and 2.2 μm respectively, with geometric standard deviations of approximately 1.8. Elemental analyses of the four fractions were performed by atomic absorption spectroscopy (AAS) at the Radiobiology Laboratory and by instrumental neutron activation analysis (INAA) at Lawrence Livermore Laboratory.[4] Preliminary qualitative analyses of the organic compounds on the respirable fly ash fraction were performed utilizing high-resolution glass capillary columns. These results have been reported elsewhere.[15] In addition to the stack collected fractions, unclassified fly ash was collected directly from the hopper. A size-classified fraction of hopper fly ash comparable to the smallest sized stack fly ash was prepared using a commercial classification system which separated reaerosolized particulate matter on the basis of aerodynamic behavior.

Mutagenicity studies were performed with the five Ames tester strains of Salmonella typhimurium kindly supplied by B. N. Ames.[16] Tests were performed with and without the addition of rat liver homogenates (S-9) which were derived from rats previously treated with polychlorinated

biphenyl (Arochlor^{R}). Tests were performed using the spot test as well as the soft top agar pour plates. Extraction of the fly ash was performed with cyclohexane, phosphate-buffered saline (PBS), and pooled horse serum on the finest stack fraction. Evidence for both polar and nonpolar, direct-acting, frameshift mutagens, as well as the possible presence of inorganic mutagens has been previously reported.[5]

RESULTS

Serum proved to be the most effective extractant. TA-1538 proved to be more sensitive than TA-98, so this strain was used in subsequent studies.

A comparison of mutagenicity of various sized fractions of stack fly ash is shown in Figure 1. In general, the smaller the particle size,

Figure 1. Effect of Particle Size Upon Mutagenicity of Fly Ash

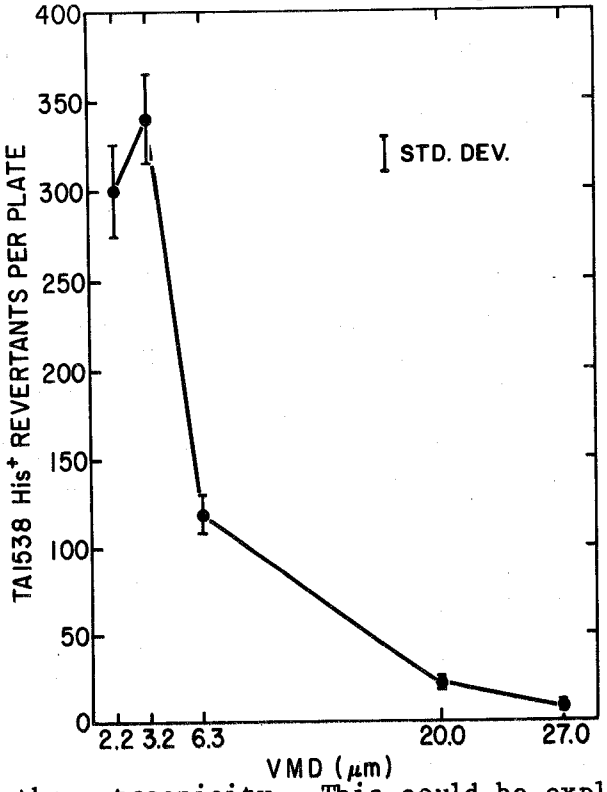

the greater the mutagenicity. This could be explained by a greater specific surface area with decreasing size. An exception was fraction 3 (VMD = 3.2), which had a slightly larger VMD than fraction 4 and increased mutagenicity. Subsequent repeated tests showed this to be a significant difference ($P < 0.01$). This is not readily understood, but may be explained by the surface chemistry. For example, we noted that Se, which has been shown to be an antimutagen, was at lower concentrations in fraction 3 than in fraction 4. It is possible that a greater

concentration of Se or even organic anticarcinogens known to be associated with coal combustion products[10] may be responsible for the lower activity. Work is under way to test this hypothesis.

Mutagenicity of unfractionated hopper fly ash, and respirable hopper and stack fly ash are compared in Table 1. No mutagenicity could be

Table 1. MUTAGENICITY OF HOPPER FLY ASH AND STACK FLY ASH

Fly Ash Type	TA-1538 Revertants/Plate
Hopper (unfractionated)	8 ± 8*
Hopper (VMD = 2.2 μm)	9 ± 3
Stack (VMD = 2.2 μm)	300 ± 59

*Average of five replicate plates ± standard deviation

detected in serum filtrates of either hopper fly ash. We believe the lack of mutagenicity in hopper ash compared to mutagenicity of fine particles in stack fly ash can be largely explained by the condensation of gaseous organic hydrocarbons on the surface of stack fly ash with cooling. This hypothesis is supported by work by Natusch on the properties of known organic hydrocarbons.[17] The time of flight of particles between the electrostatic precipitators and the point of collection in the stack may also be important.

The implications of our work for control technology are as follows: (1) The respirable fractions which are least efficiently collected using present technology may be the most important as far as long-term hazard is concerned; (2) Respirable hopper fly ash may not be a problem in terms of long-term hazards.

However, several words of caution are in order. The correlation of mutagenicity in this bacterial test system with carcinogenicity in man or animals, while good, is not 100%, so possible carcinogenic hazard needs to be confirmed by long-term studies in animals. In addition, other types of coal, combustion conditions, and control technologies may well influence the mutagenicity of respirable airborne particulates.

REFERENCES

1. Fisher, G. L., D. P. Y. Chang, and M. Brummer. Fly Ash Collected from Electrostatic Precipitators: Microcrystalline Structures and the Mystery of the Spheres. Science. 192:553-555, 1976.

2. Fisher, G. L. and C. E. Chrisp. Physical and Biological Studies of Coal Fly Ash. Symposium on Application of Short Term Bioassays in the Fractionation and Analysis of Complex Environmental Mixtures. In press, 1978.

3. Fisher, G. L., B. A. Prentice, D. Silberman, J. M. Ondov, A. H. Biermann, R. C. Ragaini, and A. R. McFarland. Physical and Morphological Studies of Size-Classified Coal Fly Ash. Environ Sci Tech. 12:447-452, 1978.

4. Ondov, J. M., R. C. Ragaini, R. E. Heft, G. L. Fisher, D. Silberman, and B. A. Prentice. Interlaboratory Comparison of Neutron Activation and Atomic Absorption Analyses of Size-Classified Stack Fly Ash. Proc. NBS 8th Materials Research Symposium, Gaithersburg, 1977. p 565-572.

5. Chrisp, C. E., G. L. Fisher, and J. E. Lammert. Mutagenicity of Filtrates from Respirable Coal Fly Ash. Science. 199:73-75, 1978.

6. Davison, R. L., D. F. S. Natusch, J. R. Wallace, and C. A. Evans, Jr. Trace Elements in Fly Ash. Environ Sci Tech. 8:1107-1113, 1974.

7. Hatch, T. F., P. Gross. Pulmonary Deposition and Retention of Inhaled Aerosols. New York, Academic Press, 1964.

8. Yeh, H. C., R. F. Phalen, and O. G. Raabe. Factors Influencing the Deposition of Inhaled Particles. Environ Health Perspect. 15:147-156, 1976.

9. Pott, P. The Chirurgical Works of Percival Pott, Vol. II. Philadelphia, James Webster, 1819. p. 291.

10. Kubota, H., W. H. Griest, M. R. Guerin. Determination of Carcinogens in Tobacco Smoke and Coal-Derived Samples - Trace Polynuclear Aromatic Hydrocarbons. In: Trace Substances in Environmental Health IX, Hemphill, D. D. (ed.), Columbia, University of Missouri, 1975. p. 281-289.

11. Flessel, C. P. Metals as Mutagens. Adv Exp Biol Med. 91:117-128, 1978.

12. Furst, A. An Overview of Metal Carcinogenesis. Adv Exp Biol Med. 91:1-12, 1978.

13. McCann, J., E. Choi, E. Yamasaki, and B. N. Ames. Detection of Carcinogens as Mutagens in the Salmonella Microsome Test. Assay of 300 Chemicals. Proc. of Nat Acad Sci. 72:5135-5139, 1975.

14. McFarland, A. R., R. W. Bertch, G. L. Fisher, and B. A. Prentice. A Fractionator for Size-Classification of Aerosolized Solid Particulate Matter. Environ Sci Tech. 11:781-784, 1977.

15. Jennings, W. G., L. Sucre, G. L. Fisher, O. G. Raabe. Analysis of the Organic Constituents of Coal, Fly Ash, Coke and Coal Tar. In: Radiobiology Laboratory Annual Report, University of California, Davis, 1977. p. 24-33.

16. Ames, B. N., J. McCann, and E. Yamasaki. Methods for Detecting Carcinogens and Mutagens with the Salmonella Mammalian Microsome Mutagenicity Test. Mutat Res. 31:347-363, 1975.

17. Natusch, D. F. S. Potentially Carcinogenic Species Emitted from Fossil Fuel Power Plants. Environ Health Perspectives. 22:78, 1978.

BIO-ASSESSMENT OF CHRONIC MANGANESE INGESTION IN RATS

G.L. Rehnberg, D.F. Cahill, J.A. Elder,
E. Gray and J.W. Laskey
Experimental Biology Division
Health Effects Research Laboratory
United States Environmental Protection Agency
Research Triangle Park, North Carolina 27711

Methylcyclopentadienyl manganese tricarbonyl (MMT) is used in distillate fuel for power generating turbine engines to reduce smoke and particulates. With the introduction of catalytic converters to control automotive exhaust, use of MMT as an antiknock gasoline additive has increased significantly. A major combustion product of MMT is Mn_3O_4 and presently, there is very little information on the biological consequences of prolonged exposure to this manganese compound.

In general, the adult population appears to be protected from manganese accumulation by three barriers: the intestinal barrier, the blood-brain barrier and the testicular barrier. However, the fetus, the newborn and the infant are probably not protected by these barriers. The iron deficient or anemic population has increased GI absorption of Mn. Thompson et al.[1] found that variations in iron stores in the rat resulted in marked alterations in manganese absorption, however, no significant differences were observed between the iron deficient and iron-loaded rats in the retention of a ^{54}Mn dose over a period of 11 days. Less than 0.6% of the test dose was retained by iron-loaded and iron-deficient animals. Unlike iron, the body retention of an oral dose of manganese was not increased by iron deficiency, implying a compensation for the enhanced absorption by an increased excretion (of radiomanganese) in the feces.

This series of studies was undertaken to determine biological effects of ingested manganese. Neonatal or pre-weanling rats and adult rats were dosed orally with manganese as the oxide or chloride in varying amounts to determine the effects of age of the animal, chemical form and quantity of Mn ingested on absorption, retention and distribution of this element and the effect of manganese on growth, survival and blood variables.

In addition, a long-term manganese feeding study was undertaken to determine the biological characteristics and effects of chronic Mn_3O_4 exposure. Four dietary levels of manganese were fed to Long Evans rats from conception of the F_1 generation through the early growth (24 days) of the second generation. A low iron diet (20 ppm Fe) supplemented with the same four levels of manganese was fed to another group of Long Evans rats for the same time period to determine the effects of low iron diet on manganese accumulation.

24 and 48 Hour Retention of $MnCl_2$ and Mn_3O_4

A study comparing ingested water soluble $MnCl_2$ to insoluble Mn_3O_4 demonstrated that chemical form, quantity ingested, and age of the animal are important factors in the absorption, retention and distribution of manganese.

Neonatal rats (6-12 days old) were intubated with 25 or 500 µg Mn as either $^{54}MnCl_2$ or $^{54}Mn_3O_4$. Twenty-four hours post-intubation, the stomach and gastrointestinal tract were removed and the retention of ^{54}Mn was determined by gamma scintillation spectrometry. Twenty-five µg of Mn as $^{54}Mn_3O_4$ was also given to 63 and 104 day old animals and the 24-hour retention of ^{54}Mn was determined. Pre-weanling rats had similar 24-hour whole body retention of manganese as the chloride and as the oxide when given a relatively low dose of 25 µg (Table 1). However, when the dose was increased to 500 µg Mn, the 24-hour retention of the chloride ranged from 14 to 20 times greater than for the oxide. Percent retention of Mn_3O_4 decreases significantly with increasing dose and $MnCl_2$ retention was relatively insensitive to dose. The 24-hour retention of manganese as the oxide seemed to reach a maximum

of 5-7 μg Mn/day at the peak point for uptake at 8-12 days of age. Manganese chloride was in solution when administered and the Mn^{++} ion was readily available for absorption through the intestine, whereas the insoluble Mn_3O_4 was not as easily absorbed. The 24-hour retention of 25 μg Mn as the oxide was approximately 19% in the neonate but dropped to approximately 2% in the adult animal. The intestine of the newborn or neonatal rat takes up macromolecules by pinocytosis[2]. However, after infancy (about 18 days of age) pinocytotic activity decreases significantly, and the decrease in absorption and retention of manganese could be due to the maturation of intestinal absorptive cells[3] as well as the onset of biliary excretion of Mn at 17 days of age.[4]

Retention of manganese ingested as the chloride was lower at 48 hours than manganese ingested as the oxide which may be due to difference in solubilities of the $MnCl_2$ and Mn_3O_4. Absorption of ingested $MnCl_2$ probably reaches a peak [as high as 70% absorption is reported[5]] early after ingestion. When the retention measurement is made at 24 hours, the absorption has already reached a peak and is on a downward trend which continues to decrease to 15% at 48 hours. The absorption of Mn_3O_4 is a much slower, more continuous process; the absorption at 48 hours is still near its peak due partially to a slower movement of Mn_3O_4 through the gut with absorption along the full length. Mn_3O_4 is initially absorbed by pinocytosis, broken down in the cells of the intestinal mucosa and then enters portal circulation. Here the manganese either remains free or is rapidly bound before entering the liver, where it is almost quantatively removed from the blood. From the liver, manganese is either released into the bile and excreted in the feces or enters the systemic circulation and is bound to transferrin. Prior to 15-18 days of age excretion of manganese via the bile and mucosal cell sluffage has not begun, causing manganese to enter systemic circulation. In the absence of blood-brain and blood-testicular barriers in young animals, a significant amount of manganese reaches the brain and testes, target organs in manganese poisoning.

Survival and Growth of Pre-Weanling Rats Dosed with $MnCl_2$ and Mn_3O_4

Neonatal rats were dosed with 10, 20, 30, 40 or 50 µg Mn as the chloride/gm body wt/day from day 1 through 21 after birth. Controls and animals receiving 10 µg Mn (as $MnCl_2$)/gm body wt/day showed no weight loss or fatalities (Figure 1). Twenty µg Mn (as $MnCl_2$) produced growth retardation by postnatal day four. Animal deaths occurred by day 9 in the 20 µg Mn dose group. The percent fatalities increased with increasing dose of $MnCl_2$. In the 50 µg Mn group, all animals were dead by day 17 of treatment.

Another group of neonatal rats were intubated daily with manganese oxide from birth through 21 days of age. This portion of the study consisted of four treatment groups including a control, 21, 71 and 214 µg Mn/g body wt/day. Animals were sacrificed at 3-day intervals and liver, kidney, brain and testes were removed, weighed and analyzed for manganese and iron content.

The lowest dose group (21 µg Mn/g body wt/day) had weight gains over the 21 day period that were normal. Animals receiving 71 µg Mn/g body wt/day had significantly lower weight gains than the control animals, but not significantly different from the dose group receiving 3 times as much Mn_3O_4 (Figure 2). As mentioned above, it may be that the neonates absorb a maximum of 5-7 µg Mn as Mn_3O_4/day, which is not exceeded even when the amount ingested is exceedingly high.

Weight gain of pre-weanling rats intubated daily with 20 µg Mn as the chloride or as the oxide from birth through day 21 after birth was compared. All animals on Mn_3O_4 survived and gained weight about the same as controls. Animals on $MnCl_2$ had a 6% fatality rate and their weight gain over the 21 day period was significantly lower than that of the controls and the slower weight gain was obvious by day 4 after birth.

Manganese concentrations in the livers of animals dosed orally with Mn_3O_4 for 21 days after birth reached a peak about day 12 of treatment and dropped significantly on day 15. Liver Mn concentrations in the highest dose group (214 µg Mn/gm body wt/day) reached a second peak from

day 15 to 18 and then began to decline (Figure 3). Variable concentrations of manganese observed in the liver of pre-weanling rats is possibly the result of a developing homeostatic mechanism. Excretion of manganese in the bile of pre-weanling rats usually begins about day 17 after birth. However, by giving large doses of Mn, excretion in the bile will begin prematurely, thereby resulting in a depletion of Mn from the tissues. Physiology of the neonatal or postnatal rat gastrointestinal tract changes significantly between birth and day 16-17 after birth; pH of the stomach also decreases; and cell sluffage from the intestinal wall begins prior to day 21 after birth. These changes make the gut more efficient in excluding Mn_3O_4.

Effects of Chronic Manganese Oxide Ingestion

In order to assess the biological characteristics and effects of chronic Mn_3O_4 exposure, three dietary levels of manganese (control, 350, 1050 and 3500 mg Mn/kg) were fed to Long Evans rats. Exposure was continuous from conception of the F_1 generation through the early growth of the F_2 generation. A low iron diet (20 ppm Fe) supplemented with the same 3 levels of manganese (control, 350, 1050, 3500 mg Mn/kg) was fed to rats for the same time period to determine effects of iron deficiency on manganese accumulation. The composition of essential elements in the diet was controlled by using a defined synthetic diet. The general health of the animals was monitored by routine observations and weighing.

Bio-Evaluations were made as follows:

1. Body weights were obtained periodically to measure the effect of Mn_3O_4 exposure on normal growth. Growth retardation is a general indicator of toxicity.
2. Concentrations of Mn and Fe in selected tissues were determined in animals at specific ages during exposure.
3. Blood variables were measured at intervals primarily to detect the development of microcytic anemia.
4. Certain behavioral indices were measured at selected ages.
5. Reproductive parameters namely hormone levels (FSH, LH and testosterone), sperm production, fertility and teratogenesis were evaluated.

Body Weights

Body weights of animals at all dose levels were measured periodically throughout the study, to evaluate the effect of Mn_3O_4 exposure on normal growth. The addition of Mn_3O_4 (up to 3500 ppm Mn) to a normal iron diet had no effect on growth whereas, animals maintained on an iron deficient diet supplemented with lower levels of Mn_3O_4 (350 or 1050 ppm) had dose related decrements in body weight through 100 days of age. The animals on an iron-deficient diet receiving 3500 ppm Mn_3O_4 had 100% mortality by 40 days of age. However, by 224 days of age, there was no dose-related effects in any group (Figure 4).

Tissue Concentrations

Manganese and iron levels were determined in liver, kidney, brain and testes of animals (24, 40, 60, 100 and 224 days of age) during chronic exposure of Mn_3O_4. The highest Mn tissue levels were found in 24 day old animals. Of the tissues analyzed, Mn levels were highest in the liver at all ages. By 60 days of age tissue levels of all manganese dosed animals had dropped to levels only slightly greater than in the controls (Figure 3). The effect of dietary manganese on tissue Mn levels appears to be a combination of absorption and excretion efficiencies. Susceptibility to excess manganese seemed to be dependent on several maturational factors including the inability of the postnatal or neonatal animal to eliminate manganese via the bile and the intestinal mucosa, a high capacity for absorption (pinocytosis), and the absence of the testicular and blood-brain barriers. Iron levels in the liver of animals exposed chronically to Mn_3O_4 in their diet show a dramatic decrease at 24 days with slight or no decreases in the other organs (Figure 5). Iron levels in these same tissues at 224 days are normal or near normal with the liver exhibiting a 35% decrease (Figure 6).

Liver iron levels decreased in relation to increased Mn levels in the tissue. At 24 days of age the increase of Mn and the decrease of iron in tissue relative to dose was quite evident. However by 224 days of age Mn levels in the tissue were only slightly increased and iron levels slightly decreased (Table 2).

Table 2

Iron concentrations (µg/gm) in the liver of rats exposed to 3500 ppm Mn (as Mn_3O_4) in their diet

	24 days			224 days		
	Control	Treated	Decrease	Control	Treated	Decrease
Liver	182	36	400%	182	118	35%
Kidney	38	36	----	118	104	12%
Brain	23	19	17%	24	21	12%
Testes	19	14	26%	37	38	---

Manganese concentrations (µg/gm) in the liver of rats exposed to 3500 ppm Mn (as Mn_3O_4) in their diet

	24 days			224 days		
	Control	Treated	Increase	Control	Treated	Increase
Liver	2.1	16.7	680%	2.6	3.5	35%
Kidney	.6	2.4	280%	.9	1.2	24%
Brain	.5	2.8	470%	.4	.4	14%
Testes	.5	1.3	140%	.4	.5	25%

No effect was seen on hematocrit, hemoglobin, mean cell volume and red blood cell values determined on animals exposed chronically to various levels of Mn_3O_4 in a normal iron (240 ppm Fe) diet. However, when experimentally-produced-iron-deficient animals (maintained on a 20 ppm Fe diet) were exposed to the same Mn_3O_4 levels, dose-dependent depressions in these same red cell variables were significantly depressed up to 100 days of age, but returned to normal by 224 days of age (Figure 7).

At 45 and 95 days of age the exploratory activity levels of individual male and female rats were observed for 90 minutes in residential mazes. For comparative purposes, male and female rats were also tested for activity in an open-field at 110 days of age and for their reaction to handling at 120 days of age. Attempts to escape, vocalization, struggling, biting and freezing during handling were scored. Results of these behavioral tests indicated that Mn lowered the residential maze activity in a dose-related manner in post pubertal animals. The Mn_3O_4 treated rats at the higher doses were approximately 20% less active than the controls. It is concluded that Mn has a subtle behavioral effect, reducing activity in post pubertal male and female rats. Physiological data, also collected in this study, suggest that this effect may be mediated through the animal's reproductive physiology. Testosterone, for example, was depressed in post pubertal (100 day old) males in a dose-related manner which correlates with the depression in locomotor activity.

The studies presented here are the result of an interdisciplinary approach to the evaluation of a potential environmental hazard. Subtle alterations were seen in the behavioral and reproductive parameters monitored. In addition, maximum tissue concentrations were reached and the longest whole body and organ retention times were seen in animals receiving exposure prior to weaning (0 to 21 days).

These studies indicate that ingestion of large amounts (mg/kg/day of the oxide chronic) of manganese is relatively inocous unless ingested in ionic form, or by iron deficient or very young animals.

(1) Thompson, A.B.R., Olatunbosun, D., Valberg, L.S., Interrelation of Intestinal Transport System for Manganese and Iron, J. Lab. Clin. Med. Vol. 78, No. 4, Oct. 1971.

(2) LeFeure, M.E., Joel, D.D., Intestinal Absorption of Particulate Matter, Life Sciences, Vol. 21, No. 10, 1977.

(3) Clark, Sam L., The Ingestion of Proteins and Colloidal Materials by Columnar Absorptive Cells of the Small Intestine in Suckling Rate and Mice, Biophysic. and Biochem. Cytol., 1959, Vol. 5, No. 1.

(4) Cotzias, George C., Miller, Samuel T., Papavasiliou, Paul S., Tang, Lily C., Med. Clinc. of North Amer., Vol. 60, No. 4, July 1976.

(5) Mena, Ismael, The Role of Manganese in Human Disease, Annals of Clin. and Lab. Sci., Vol. 4, No. 6, 1974.

TABLE 1

WHOLE BODY 24 HOUR RETENTION OF MANGANESE INGESTED AS $MnCl_2$ AND Mn_3O_4

	25 μgm	
	$MnCl_2$	Mn_3O_4
YOUNG (6-12 DAYS)	18%	19%
OLDER (63-104 DAYS)	2%[a]	2%
	500 μg	
	$MnCl_2$	Mn_3O_4
YOUNG (6-12 DAYS)	14%	1%

[a] Literature value

Figure 1

SURVIVAL OF RATS DOSED ORALLY WITH $MnCl_2$ FROM BIRTH TO WEANING RATS WERE INTUBATED DAILY WITH 10,20 30, 40 or 50 μg Mn/gram BODY WEIGHT IN 5% SUCROSE

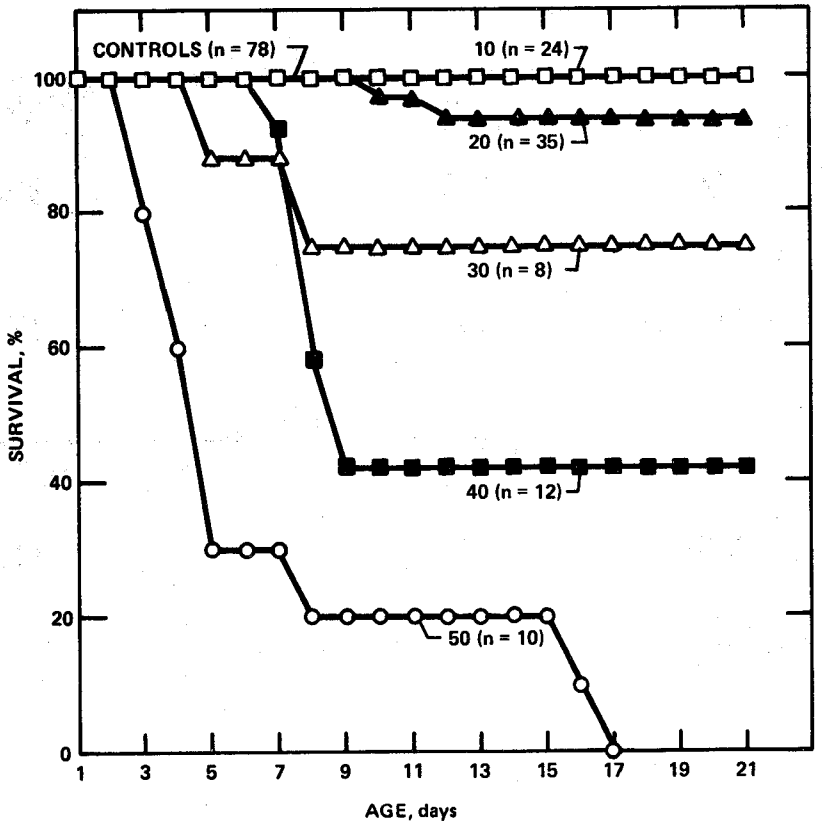

Figure 2

GROWTH OF PRE WEANLING RATS DOSED ORALLY WITH Mn_3O_4 FROM DAY 1 TO DAY 21 AFTER BIRTH

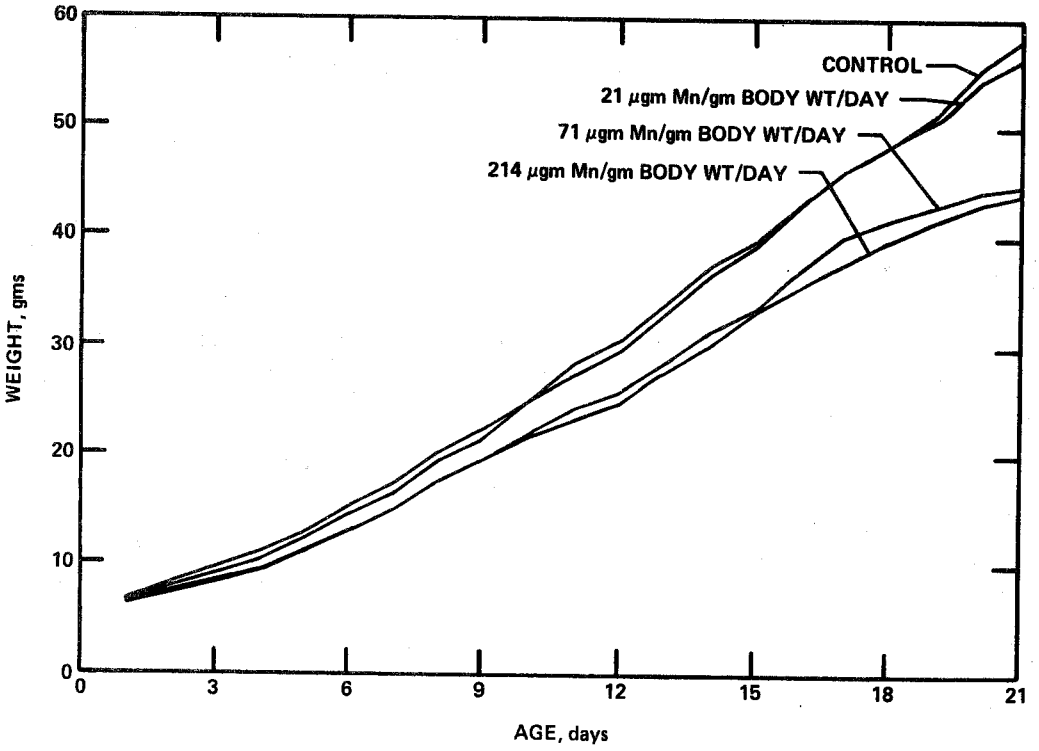

Figure 3

LIVER CONCENTRATIONS OF MANGANESE IN RATS DOSED WITH Mn_3O_4

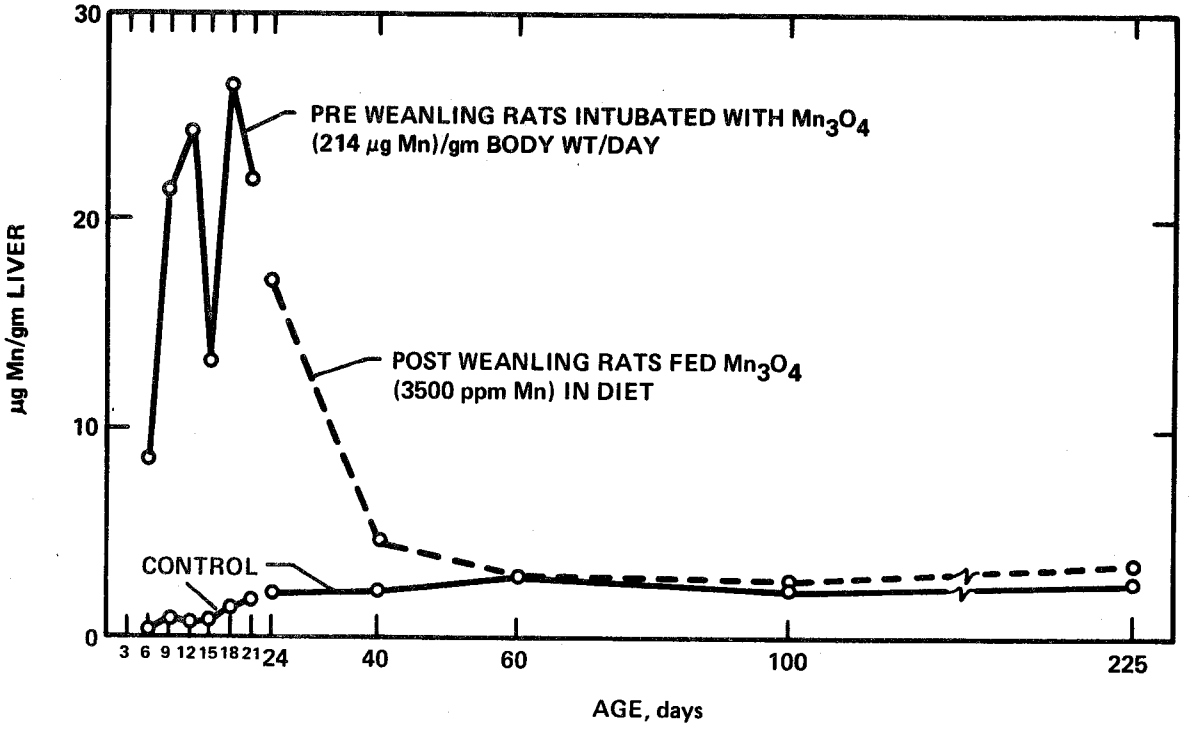

Figure 4

BODY WEIGHTS OF ANIMALS FED Mn_3O_4 IN A NORMAL IRON (240 ppm), OR AN IRON DEFICIENT (20 ppm) DIET. WEIGHTS ARE EXPRESSED AS A PERCENTAGE OF CONTROL ANIMAL WEIGHTS.

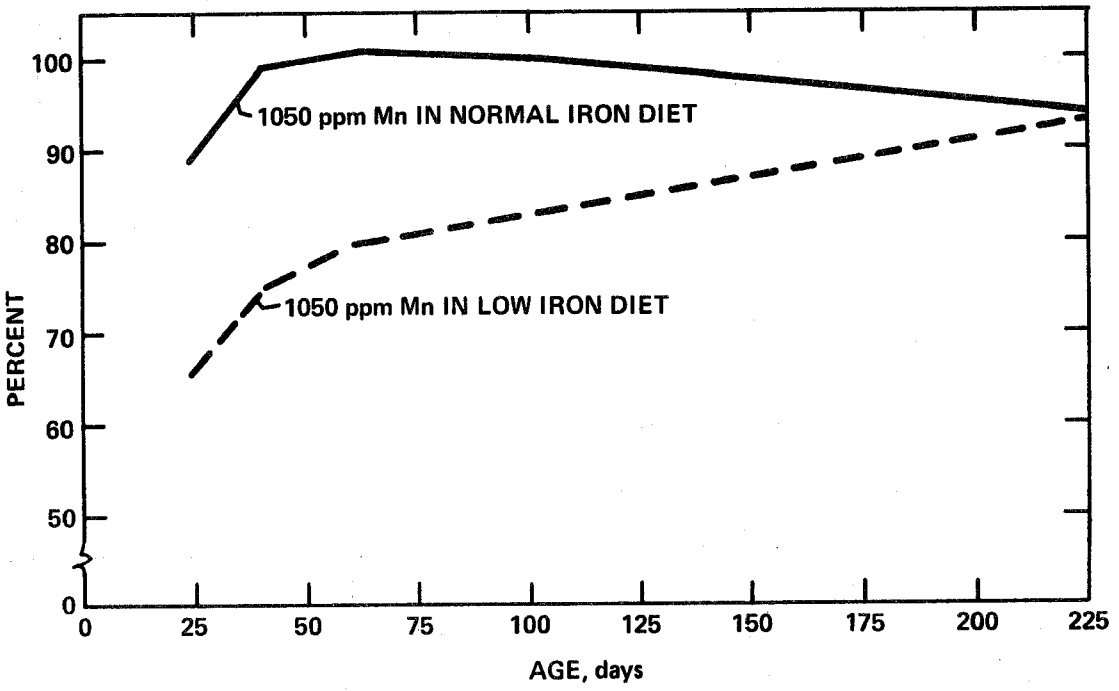

Figure 5

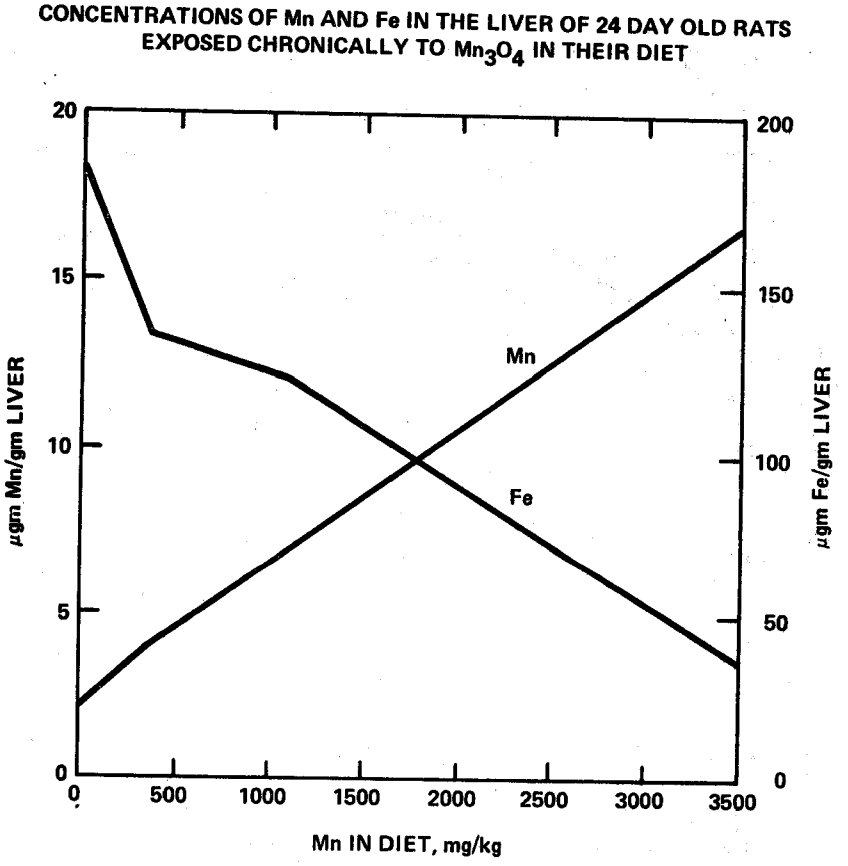
CONCENTRATIONS OF Mn AND Fe IN THE LIVER OF 24 DAY OLD RATS
EXPOSED CHRONICALLY TO Mn_3O_4 IN THEIR DIET
20
15
10
5
0
200
150
100
50
0
Mn
Fe
μgm Mn/gm LIVER
μgm Fe/gm LIVER
0
500
1000
1500
2000
2500
3000
3500
Mn IN DIET, mg/kg

Figure 6

CONCENTRATIONS OF Mn AND Fe IN THE LIVER OF 224 DAY OLD RATS EXPOSED CHRONICALLY TO Mn_3O_4 IN THEIR DIET

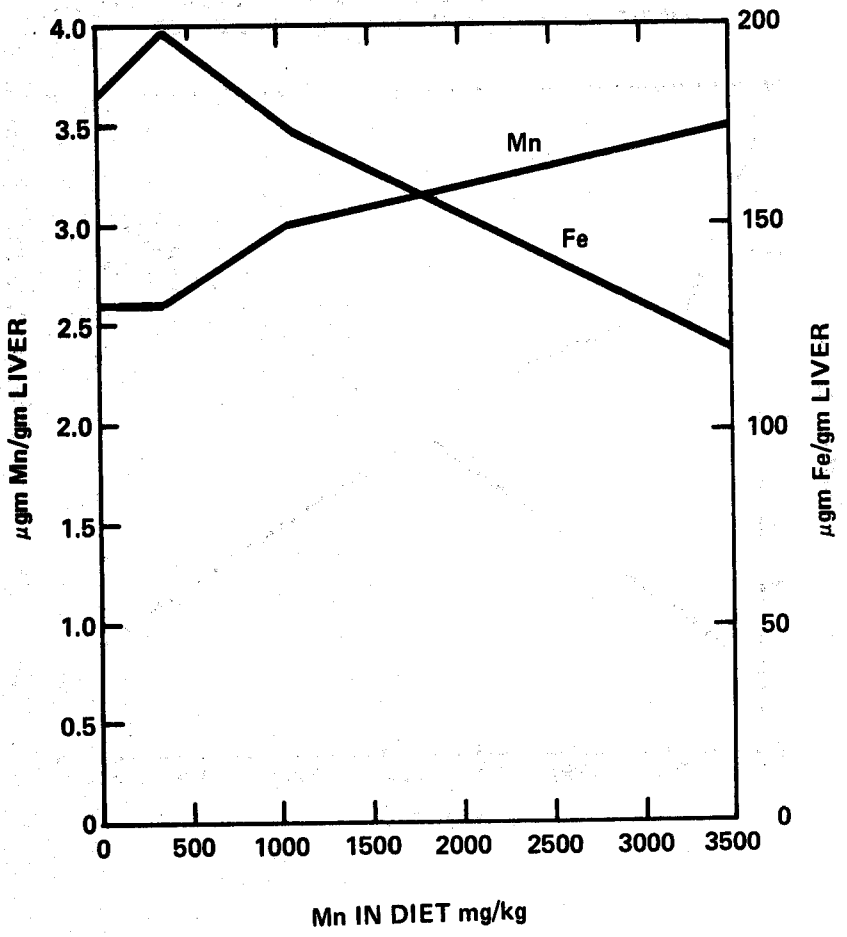

Figure 7

RED BLOOD CELLS OF ANIMALS EXPOSED CHRONICALLY TO Mn_3O_4 IN A NORMAL IRON DIET (240 ppm Fe) VS. A LOW IRON DIET (20 ppm Fe)

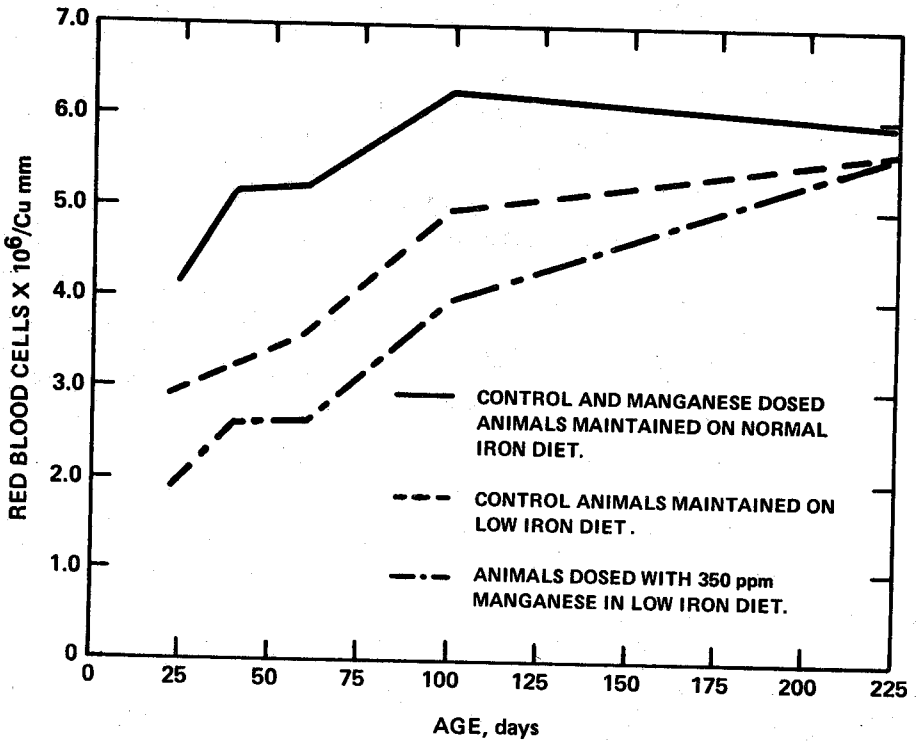

THE USE OF SHORT TERM BIOASSAY SYSTEMS IN THE EVALUATION OF ENVIRONMENTAL PARTICULATES

Neil E. Garrett and James A. Campbell
Cytotoxicity and Biochemistry Section
Environmental Sciences Group
Northrop Services, Inc.
Research Triangle Park, N.C. 27709

and

Joellen L. Huisingh and Michael D. Waters
Biochemistry Branch
Environmental Toxicology Division
Health Effects Research Laboratory
Environmental Protection Agency
Research Triangle Park, N.C. 27711

ABSTRACT

The cytotoxic effects of a variety of model and industrial particulates of respirable size were investigated using the rabbit alveolar macrophage (RAM) and the Chinese hamster ovary (CHO) cell; human lung fibroblasts (WI-38) were also used in some experiments. The RAM and CHO *in vitro* bioassay procedures were found to be particularly sensitive to toxic particulate materials. In the RAM system, the most sensitive parameter investigated was cellular adenosine triphosphate (ATP); total protein content and viability by dye exclusion were also useful indicators of toxicity of some samples. The CHO cell was determined to be phagocytically active in culture and it may provide a potential surrogate for the RAM system. Both the RAM and CHO bioassay systems are amenable to studies of biochemical changes resulting from exposure to particulates.

INTRODUCTION

The toxic, mutagenic, carcinogenic, and teratogenic potential of particulates found in the environment are largely unknown. Particulates may influence the toxicity and genotoxicity of other compounds in an

additive or perhaps synergistic fashion[1]. For any given particulate, a combination of physical and chemical characteristics will determine the ultimate biological effects. The relationship between the physical characteristics of particulate materials and known carcinogenicity is documented in studies of fibrous glass, asbestos, and aluminum oxide particles[2,3]. That chemical components contribute to the carcinogenic response is suggested by the work of Chrisp et al. who showed that extracts of well-characterized respirable fly ash are mutagenic in Salmonella typhimurium[4].

Several cytotoxicity assays have recently been employed to evaluate particulate emissions from industrial and energy related sources in pilot studies for the EPA Environmental Assessment Program[5]. These assays were used to rank the potential hazard of emissions for control technology research. The three cellular toxicity assays that were employed and reported here include primary cultures of RAM cells and continuous cultures of WI-38 and CHO cells. The RAM acts in pulmonary defense by engulfing and removing particulate materials deposited in the lower airways and deep lung. WI-38 cells are perhaps the best characterized diploid human cell available for toxicity bioassays. The CHO cell system is also well-characterized and exhibits the useful property of forming discrete colonies from single cells[6].

EXPERIMENTS WITH MODEL PARTICULATES

Polystyrene latex particles are widely used in studies of phagocytic activity. In our studies, phagocytosis was measured after adding 1.1 μm latex spheres to cells cultured in Lab-Tek four-chamber microslides. After air-drying and staining, the slides were placed in xylene for 1 hour to dissolve extracellular latex spheres[7,8]. Each cell that contained at least one particle was considered phagocytically active. The time course of phagocytosis of 1.1 μm spheres by RAM, WI-38, and CHO cells is shown in Figure 1. Although the detailed shape of the phagocytosis curve is not defined in this figure, the general trend is that the RAM, as well as the CHO and WI-38, rapidly engulf latex spheres. RAM, WI-38, and CHO cells were found to be capable of ingesting latex spheres as large as 5.7 μm.

Silica (silicon dioxide) is a model particulate that has proven useful in studies of cytotoxicity[9]. Fly ash particles obtained from combustion of coal contain high quantities of silicon complexes with the particle surface being predominantly aluminosilicate glass[10]. Most crystalline forms of silica are hemolytic and cytotoxic, and stimulate a fibrogenic reaction in the lung[11].

In our studies, the toxicity of silica was evaluated using a CHO clonal assay. Two hundred cells were plated per 25 square centimeter tissue culture flask. Culture media contained 10% fetal calf serum (FCS). After a 24-hour incubation to allow for cell attachment, the flasks were exposed to particulate samples. Discrete colonies of cells developed after 6 to 7 days. The colonies were fixed, stained, and

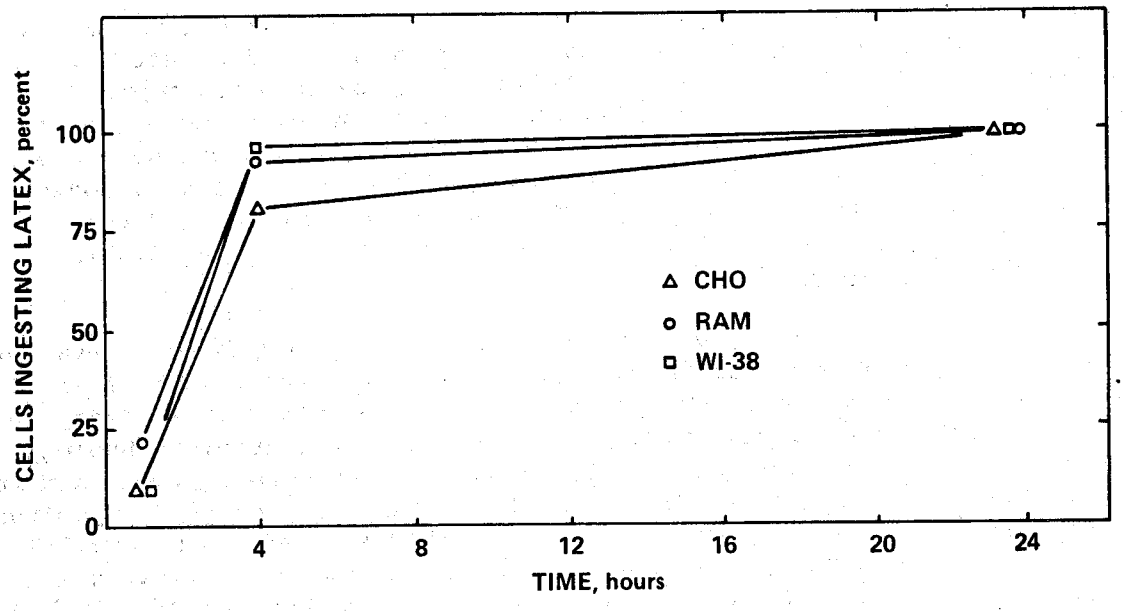

Figure 1. Phagocytosis of latex spheres by CHO, RAM, and WI-38 cells. Approximately 25 spheres were added per cell and a minimum of 200 cells of each type were scored.

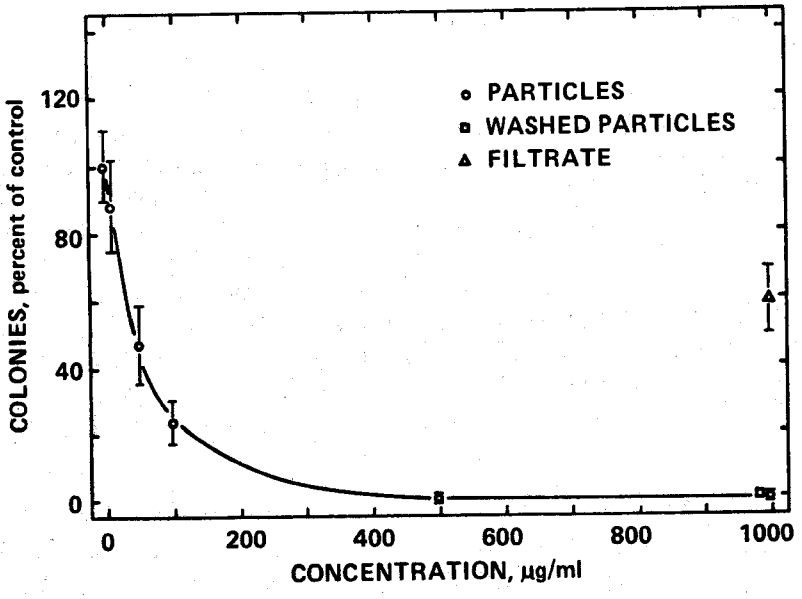

Figure 2. Effect of silica on CHO colony survival. Data are presented as mean ± standard deviation. Washed particles and filtrate were assayed at 1000 µg/ml.

enumerated with a stereo microscope. Data for silica toxicity are shown in Figure 2. No colonies developed if cells were incubated with either silica particles or washed particles at 1000 µg/ml. If the supernatant medium derived by extracting silica particles (1000 µg/ml) was employed, clonal growth was reduced to about 60% of the control indicating that most of the toxicity was associated with the particles.

It has been suggested that in aqueous solution silicic acid forms the surface component of silica and acts in hydrogen-bonding reactions with cellular membrane phospholipids[11]. The cytotoxicity of silicic acid was measured using both the CHO clonal assay and primary cultures of RAM. In the RAM system, 2 x 10^6 cells were added with the particulate (total volume 2 ml) to wells of cluster dishes. Culture media contained 10% FCS. After gentle mixing the dishes were incubated on a rocker platform for a 20-hour period at 37° C in a humidified atmosphere containing 5 percent carbon dioxide in air. At the end of incubation, cells were collected by trypsinization and aliquots of the cell suspension were used for assay of cell ATP by luminescence assay[12], viability by trypan blue exclusion, and cell number by optical enumeration with a hemocytometer. In some experiments cells were washed by low-speed centrifugation and total protein was determined using the Lowry method. Data obtained on cytotoxicity of silicic acid are shown in Figure 3. In the RAM assay, viability, viability index[13], and ATP were depressed to an extent similar to clonal growth for CHO cells. Silicic acid was highly toxic at concentrations of 500 µg/ml and 1000 µg/ml, and also caused significant decreases in total numbers of cells by lysis.

The oxide of titanium, a metal resembling silicon, was also tested using the CHO system. Electron microprobe analysis has shown that titanium forms a minor component of the surface of fly ash particles[10]. Particles of titanium dioxide have been used frequently as "inert particles" in deposition and clearance studies in intact animals. In preliminary experiments, titanium dioxide was found to be nontoxic at 500 µg/ml concentration.

EXPERIMENTS WITH MODEL FLY ASH PARTICLES

Fly ash particles coated with selected metallic oxides form a model system which was utilized in comparative cytotoxicity experiments using RAM, CHO, and WI-38 cells. Fly ash collected from an electrostatic precipitator was size-fractionated, coprecipitated with lead, nickel, or cadmium, and treated to oxidize the metals[14]. The approximate metal content of the particles determined by atomic absorption spectrometry was 2.63 to 2.91 percent for nickel, 3.15 to 3.85 percent for lead, and 11.9 to 12.3 percent for cadmium[15,16]. Nickel and lead bind tightly and do not appreciably dissociate from the fly ash in tissue culture medium at physiological pH. These particles have been used in cytotoxicity studies by Aranyi et al[16].

The corresponding uncoated control fly ash (< 2 µm) was found to be relatively nontoxic in experiments conducted using the RAM assay. After

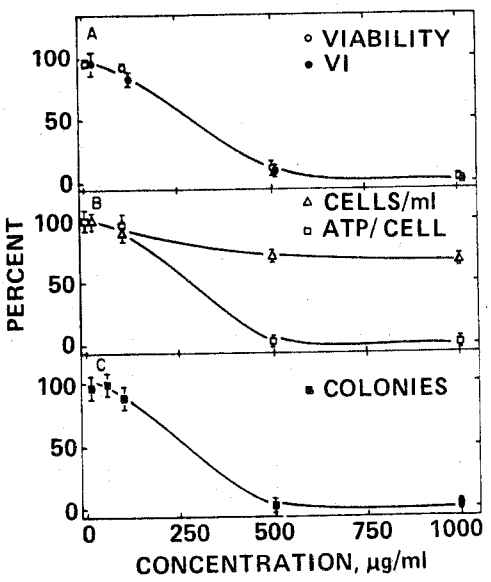

Figure 3. Cytotoxicity of silicic acid in the RAM (A, B) and CHO (C) cell systems. Data are presented as the mean ± standard deviation [n = 4 for the RAM assay (no FCS); n = 5 for the CHO assay].

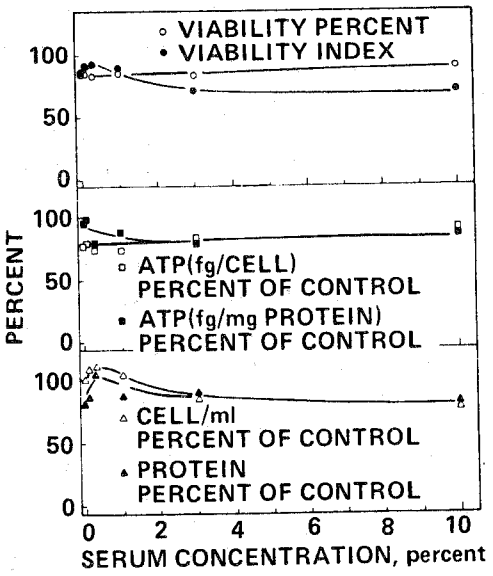

Figure 4. Influence of serum concentration on the RAM bioassay of fly ash (< 2 µm). Cells were exposed for 20 hours to 1000 µg/ml fly ash. Data points are mean values of three replicates.

a 20-hour exposure, macrophage viability, viability index, cell number, ATP, and protein in treated cultures were not significantly different from control values. To determine if the overall sensitivity of the system could be increased, the effect of reducing the concentration of serum in the culture medium was investigated (Figure 4). No appreciable effect was apparent in an experiment with cells exposed to 1000 µg/ml of uncoated fly ash. In the RAM system, this relatively nontoxic particle could not be made appreciably toxic if the serum content of the media was reduced to zero.

In order to examine further the toxicity of uncoated fly ash, experiments were conducted using the CHO clonal assay. Results of experiments performed with uncoated and nickel-coated particles are shown in Figure 5. The uncoated fly ash was also relatively nontoxic in this system at concentrations $\leq$ 500 µg/ml. A depression in clonal growth was observed at a concentration of 1000 µg/ml for the two smaller particle sizes. The 5 to 8 µm uncoated fly ash was nontoxic, possibly as a result of decreased phagocytosis of this particle. It is clear from Figure 5 that all sizes of the nickel-coated particles give a toxic response.

Nickel oxide-coated fly ash was also found to be toxic in the RAM system. Data in Figure 6 illustrate the relative sensitivity of the endpoints: viability, viability index, cell number, total protein, and ATP (expressed on a per cell and per total protein basis). Cellular ATP was the most sensitive endpoint studied.

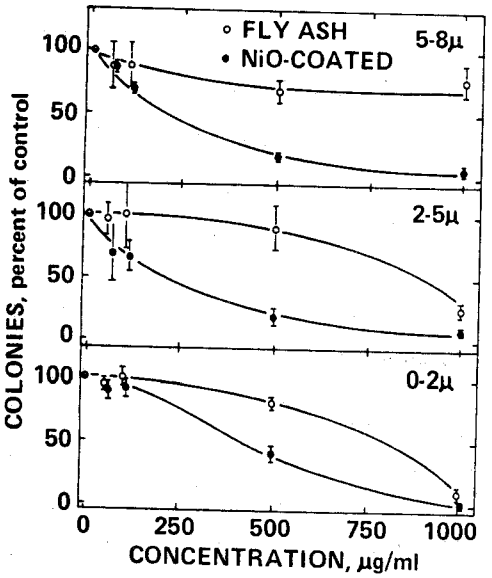

Figure 5. Effect of uncoated and nickel oxide-coated fly ash on CHO clonal growth after a 6-day exposure. Data are presented as mean ± standard deviation (n = 5).

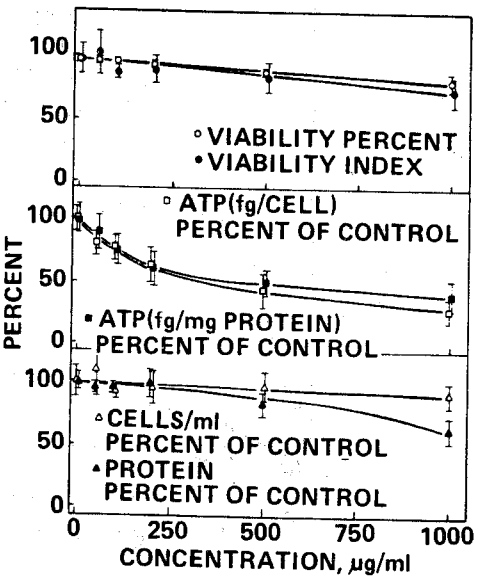

Figure 6. Response of RAM cells to nickel oxide-coated fly ash (< 2 μm) after a 20-hour exposure. Data are presented as mean ± standard deviation from three experiments (n = 9).

Lead oxide-coated particles were significantly more toxic than nickel-coated particles. The lead oxide-coated particles were used to further examine the influence of serum on the various endpoints studied in the RAM assay. It may be seen in Figure 7 that cellular ATP, viability, and viability index decreased as the serum content of the culture media was reduced. Again, ATP was the most sensitive index of toxicity of lead oxide-coated fly ash. However, cell viability and viability index were sharply reduced at serum concentrations less than one percent. Protein and cell number as a percent of control were not appreciably affected. Data plotted in Figure 8 give the absolute values of ATP and protein per cell for RAM cultures treated with lead oxide-coated and uncoated fly ash (both < 2 μm). Protein per cell is reduced as the serum content is lowered below 3 percent in the control or cultures exposed to either coated or uncoated particles. Protein per cell is substantially lower in cultures treated with the lead oxide-coated particles. ATP per cell does not vary significantly with serum concentrations in controls or cultures treated with uncoated particles. The scale for ATP is 100 times larger for controls and cultures treated with uncoated particles. It is clear from Figure 8 that ATP per cell is dramatically reduced in cultures treated with lead oxide-coated particles. At 1 percent serum, the ATP/cell is about 100 times less in metal-treated cultures and varies over a range of about 20 to 200 times less than that for uncoated fly ash or the control. These experiments illustrate the sensitivity of the ATP luminescence assay and its usefulness in studies with model particulates.

Experiments with cadmium oxide-coated fly ash proved particularly

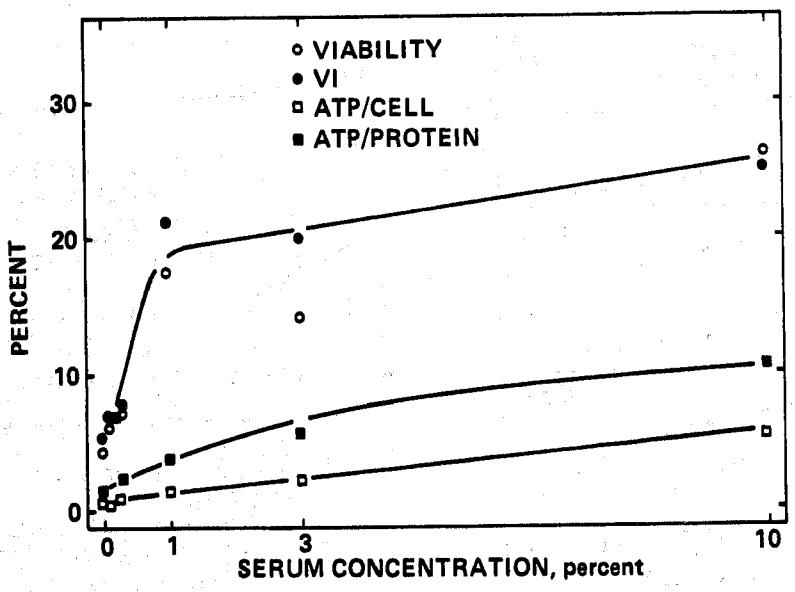

Figure 7. Influence of serum concentration on the response of RAM cells to lead oxide-coated fly ash (< 2 µm). Cells were exposed for 20 hours at a concentration of 1000 µg/ml. ATP data are expressed as percent of control values. Data points are mean values of three replicates.

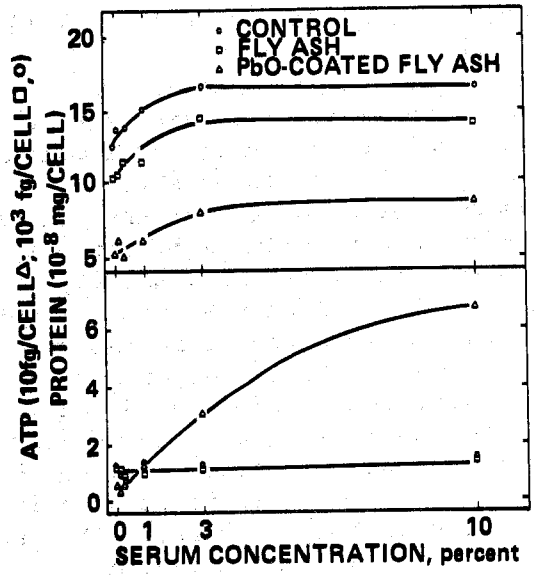

Figure 8. Influence of serum concentration on the response of RAM cells to 1000 µg/ml lead oxide-coated and uncoated fly ash (< 2 µm) after a 20-hour exposure. Data points are mean values of three replicates for treated cells and of six replicates for the control (protein, top panel; ATP, bottom).

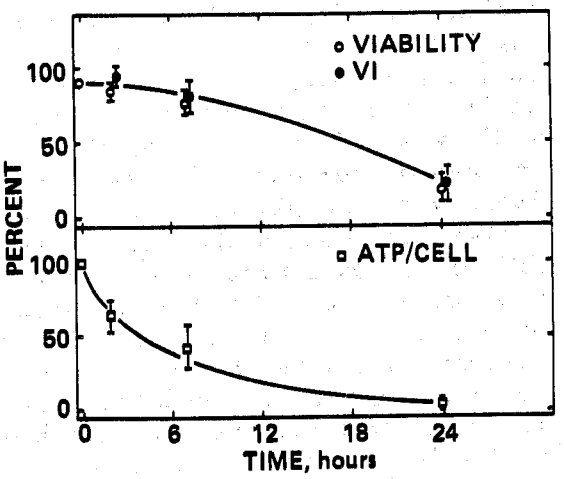

Figure 9. Effect of 60 µg/ml cadmium oxide-coated fly ash (< 2 µm) on RAM cells after a 20-hour exposure. Data are presented as the mean ± standard deviation (n = 6).

interesting since cadmium was found to dissociate from the particles in the biological medium. The time course for toxicity of the cadmium-coated particles to RAM cultures was investigated and is shown in Figure 9. The particles were washed briefly by centrifugation before incubation with the cells. ATP as a percent of control decreased more rapidly with increasing exposure times than did the viability or viability index.

The release of cadmium from the particle provided the opportunity to determine if the dissociation of the metal oxide from the fly ash would show the same toxicity as a comparable quantity of soluble metal. In this experiment, the readily dissociable cadmium was removed by a 2-hour preincubation step. Macrophages were incubated with the cadmium-coated fly ash under the usual conditions and the effect on macrophage viability, viability index, ATP, cell number, and total protein was determined (Figure 10). Viability and viability index decreased with ATP and total protein but cell numbers were unaltered as has been reported previously with soluble cadmium chloride[13]. The cadmium oxide-coated fly ash was considerably more toxic than would have been predicted on the basis of the amount of soluble cadmium released to the medium. This finding may be important with regard to the potential toxicity of dissociable metals which adsorb to the surfaces of particles released from high temperature combustion processes[17,18].

The cadmium oxide-coated fly ash was utilized in several additional studies of comparative cytotoxicity. The CHO and the WI-38 cell lines were compared to the RAM in terms of biochemical response to cadmium oxide-coated fly ash at 30 µg/ml. Results shown in Figure 11 indicate that the CHO cell responded similarly to the RAM. In particular, examination of the viability index and ATP/mg protein shows that the CHO and RAM respond similarly and the WI-38 is less sensitive. Thus, it appears that the CHO and RAM systems exhibit similar responses involving biochemical endpoints.

EXPERIMENTS WITH PARTICULATES FROM ENERGY-RELATED TECHNOLOGIES

In conjunction with the IERL-RTP Level 1 pilot studies, we examined particulate materials obtained from coal gasification and fluidized bed combustion processes. Samples from coal gasification processes included ash, coal feed, and dust collected from a cyclone. No detectable RAM toxicity was observed for these samples at test concentrations of 1000 µg/ml ($p \geq .05$). The cyclone dust was also evaluated in the CHO clonal assay and no cytotoxicity was detected. Samples evaluated in pilot studies for the fluidized bed combustion process included the coal feed, dolomite sorbent feed, the sorbent bed discard, fly ash from the second cyclone discard, and a coarse (> 10 µm, Sample #7) and fine (< 3 µm, Sample #6) particulate from atmospheric stack gas. The results obtained in the RAM assay are shown in Figure 12. The fine particulate was the most toxic sample. Data from the CHO clonal assay of the fine particulates were consistent with ATP assay in the macrophage (Figure 13). In addition, the filtrate from the washed fine particulate was slightly

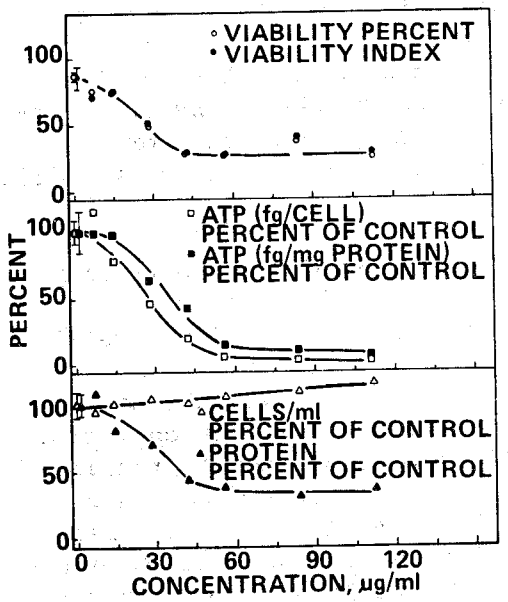

Figure 10. Response of RAM cells to cadmium oxide-coated fly ash after a 20-hour exposure. Data points are mean values of three replicates for treated cells and of six replicates for the control.

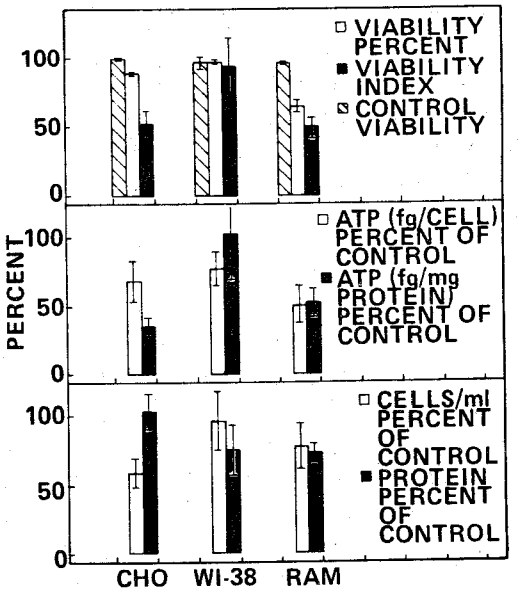

Figure 11. Effect of 30 µg/ml cadmium oxide-coated fly ash (< 2 µm) on CHO, WI-38, and RAM cells. Data are presented as mean ± standard deviation (n = 4).

toxic in the clonal assay.

SUMMARY

The RAM and CHO in vitro bioassay procedures were shown to be sensitive to toxic particulate materials. In the RAM system, the most sensitive parameter investigated was cellular adenosine triphosphate. However, total protein content and viability by dye exclusion are useful indicators of toxicity of some samples. The CHO cell was determined to be phagocytically active in culture such that it may be considered a potential surrogate for the RAM system. The CHO system demonstrates the important property of clonal growth which forms the basis of a highly sensitive and widely used assay for cytotoxicity. Both assay systems are amenable to studies of biochemical changes resulting from exposure to particulate materials. In vitro studies of cytotoxicity at the cellular level are the first stage of the biological evaluation of airborne particulate materials and can be used to rank cytotoxicity of particulates and to establish priorities for further confirmatory bioassays. Determination of initial toxicity or cell survival establishes the range of concentrations needed in mutagenesis and cellular morphological transformation assays. Cytotoxicity assays can also be useful in the fractionation and identification of hazardous agents in complex mixtures. Since energy conversion processes and technologies are still in the experimental stages, the cellular toxicity of particulates should be evaluated as these technologies advance. As the assays are refined, the

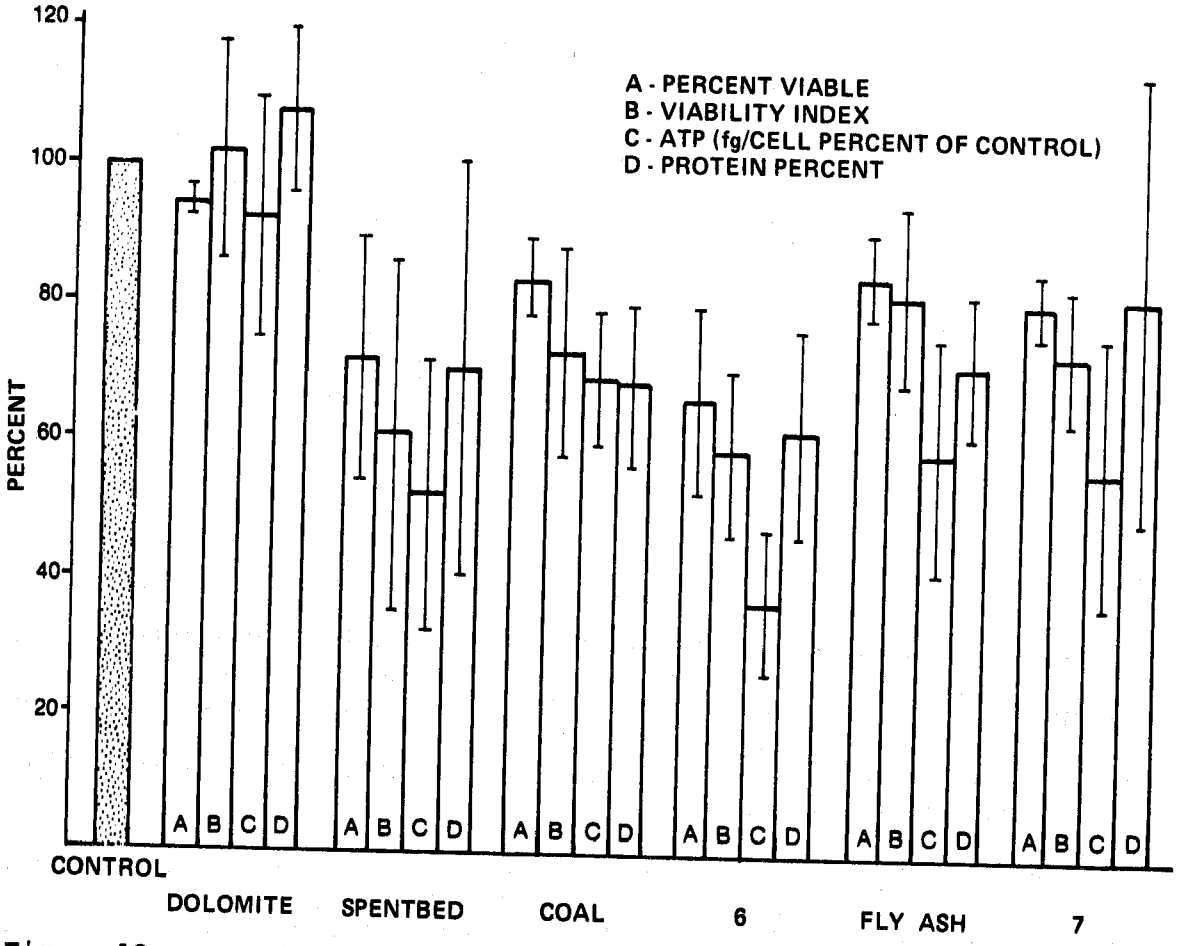

Figure 12. RAM bioassay of fluidized bed combustion samples. Cells were exposed for 20 hours to 1000 µg/ml of particulate. Data are mean values ± standard deviation (n = 6).

cellular toxicity data may be used as input with other fundamental research into the design and improvement of control and collection devices.

REFERENCES

1. Warshawsky, D., R.W. Niemeier, and E. Bingham. Influence of Particulates on Metabolism of Benzo(a)pyrene in the Isolated Perfused Lung. In: Carcinogenesis A Comprehensive Survey Volume 3, Freudenthal and Jones (ed.). Raven Press. 1973. p. 347-360.

2. Stanton, M.F. Some Etiological Considerations of Fiber Carcinogenesis. In: Proceedings of the Conference on the Biological Effects of Asbestos. 1972. p. 289-294.

3. Stanton, M.F. and C. Wrench. Mechanism of Mesothelioma Induction with Asbestos and Fibrous Glass. Journal National Cancer Institute. 48:797-821, 1972.

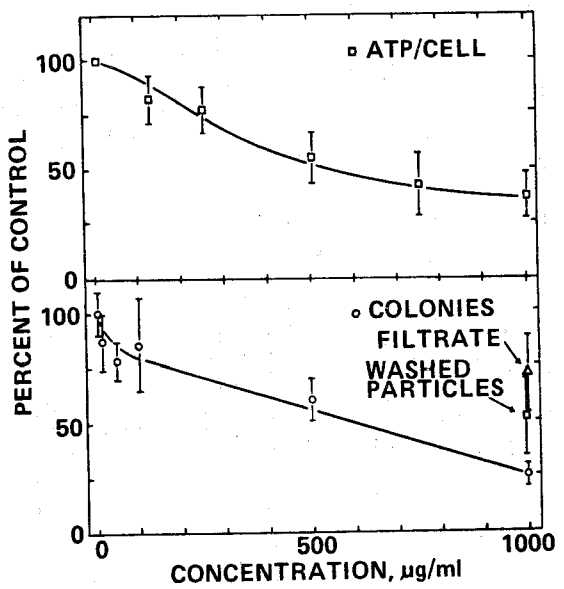

Figure 13. Response of RAM (top panel) and CHO (bottom panel) cells to a fine particulate (< 3 µm) from atmospheric stack gas. Data are mean values ± standard deviation (n = 6 for RAM assays; n = 5 for CHO assays).

4. Chrisp, C.E., G.L. Fisher, and J.E. Lammert. Mutagenicity of Filtrates from Respirable Coal Fly Ash. Science. 199:73-75, 1978.

5. Duke, K.M., M.E. Davis, and A.J. Dennis. IERL-RTP Procedures Manual; Level 1 Environmental Assessment Biological Tests for Pilot Studies. Environmental Protection Agency, Research Triangle Park, N.C. Publication Number EPA 600/7-77-043. April 1977. 106p.

6. Hsie, A.W., et al. Quantitative Mammalian Cell Genetic Toxicology: Study of the Cytotoxicity and Mutagenicity of 70 Individual Environmental Agents Related to Energy Technologies and 3 Subfractions of a Crude Synthetic Oil in the CHO/HGPRT System. In: Proceedings of the Symposium on Short-Term Bioassays in the Fractionation and Analysis of Complex Environmental Mixtures, Williamsburg, Va. 1978.

7. Waters, M.D., et al. Toxicity of Platinum (IV) Salts for Cells of Pulmonary Origin. Environmental Health Perspectives. 12:45-56, 1975.

8. Gardner, D.E., et al. Technique for Differentiating Particles that are Cell-Associated or Injested by Macrophages. Applied Microbiology. 25:471-475, 1973.

9. Nash, T., A.C. Allison, and J.S. Harington. Physico-Chemical Properties of Silica in Relation to Its Toxicity. Nature. 210:259, 1966.

10. Fisher, G.L., D.P.Y. Chang, and M. Brummer. Fly Ash Collected from Electrostatic Precipitators: Microcrystalline Structures and the Mystery of the Spheres. Science. 192:553-555, 1976.

11. Allison, A.C. Pathogenic Effects of Inhaled Particles and Antigens. Annals of the New York Academy of Science. 221:299-308, 1974.

12. Waters, M.D., et al. Adenosine Triphosphate Concentration and Phagocytic Activity in Rabbit Alveolar Macrophages Exposed to Divalent Cations. Journal of the Reticuloendothelial Society. 18:296 Abst., 1975.

13. Waters, M.D., et al. Metal Toxicity for Rabbit Alveolar Macrophages In Vitro. Environmental Research. 9:32-47, 1975.

14. Yamate G. and H. Ashley. Preparation and Characterization of Finely Divided Particulate Environmental Contaminants for Biological Experiments. IIT Research Institute, Chicago, Illinois. IITRI Report No. C6321-5. September 1975.

15. Aranyi, C. SEM EXamination of the In Vivo Effects of Air Pollutants on Pulmonary Systems. IIT Research Institute, Chicago, Ill. Report Number 6070-11. 1976.

16. Aranyi, C., et al. Cytotoxicity to Alveolar Macrophages of Metal Oxides Adsorbed on Fly Ash. In: Pulmonary Macrophage and Epithelial Cells, Sanders, C.L. et al. (ed.). National Technical Information Service. 1977. p. 58-65.

17. Lee, R.E., Jr., and D.J. von Lehmden. Trace Metal Pollution in the Environment. Journal of Air Pollution Control Association. 23: 853-857, 1973.

18. Natusch, D.F.S., J.R. Wallace, and C.N. Evans, Jr. Toxic Trace Elements: Preferential Concentration in Respirable Particles. Science. 183:202-204, 1973.

A KINETIC AEROSOL MODEL FOR THE FORMATION AND GROWTH OF SECONDARY SULFURIC ACID PARTICLES

Paulette Middleton*
Atmospheric Sciences Research Center
State University of New York at Albany
Albany, New York 12222

and

C. S. Kiang+

National Center for Atmospheric Research
Boulder, Colorado 80307

ABSTRACT

A numerical kinetic aerosol model is utilized to study conditions under which secondary sulfuric acid particles formation followed to condensation and coagulation growth can substantially increase the concentration of submicron size aerosols which can contribute significantly to visibility degradation, adverse health effects, injuries to agricultural products and inadvertent weather modification.

This model incorporates the mechanisms of photochemical reactions, heteromolecular nucleation, heteromolecular condensation and thermal coagulation. Sensitivity of the model calculations to uncertainties in the microphysical and chemical input parameters is

*Currently a visitor at the National Center for Atmospheric Research.

+Present address: School of Geophysical Sciences, Georgia Institute of Technology, Atlanta, Georgia.

analyzed. Possible errors arising from the numerical approximations used in the calculations are investigated. The difficulties of model validation by comparison with laboratory and field experiments are also discussed.

Secondary aerosol formation and growth in the presence of preexisting particles is studied under different atmospheric conditions by varying relative humidity, temperature, initial particle size distribution and rate of production of gaseous sulfuric acid molecules. Our model calculations show that the rate limiting factor for the formation and growth of secondary acid aerosols into the submicron size range is the amount of sulfuric acid gaseous molecules available in the atmosphere.

This model can be used as a basic framework for designing a proper air pollution control strategy.

INTRODUCTION

Atmospheric particulate sources can be classified as either primary or secondary. Primary sources are those which emit particulates directly into the atmosphere. Secondary sources are those which lead to the formation of aerosols in the atmosphere through gas-to-particle conversion processes. With the persistent increase in production of aerosols from man-made sources, there has been increasing concern about the possible consequence of pollution on a global scale. In 1970, Hidy and Brock[1] provided a rough global budget for the major natural and anthropogenic sources of the primary and secondary aerosols. From their report it is found that the only sigificant contribution from the man-made source compared to the natural source is the secondary sulfate particles. On the regional scale, substantial increase of the concentration of submicron size secondary sulfate aerosols can contribute significantly to visibility degradation, adverse health effects, injuries to agricultural products and inadvertent weather modification[2].

In order to gain an understanding of the nature and behavior of these suspended sulfate particles and possible related control strategies, one must consider the effects of input, transport, mixing, and removal as well as microphysical and chemical transformations. In this paper we concentrate our efforts on a theoretical study of the chemical and microphysical processes involved in secondary aerosol formation and growth. It is our intention that these theoretical studies can be utilized for designing a proper air pollution control strategy.

A numerical kinetic model is used to identify the most important microphysical and chemical parameters for secondary aerosol formation and growth which can significantly increase the number of

particles in the submicron particle size range under various static atmospheric conditions. The model, developed by Kiang and Middleton in 1977[3], incorporates the mechanisms of photochemical reactions, heteromolecular nucleation, heteromolecular condensation, and thermal coagulation. It is found that the formation and growth of secondary sulfuric acid aerosols depends on the initial particle size distribution, the relative humidity, the production rate of sulfuric acid gaseous molecules, and the temperature.

MODEL DESCRIPTION

The time evolution of the number concentration n(m, t), having mass m in the range m to m + dm at time t, can be expressed as:

$$\frac{\partial n(m,\, t)}{\partial t} = \frac{1}{2} \int_0^m dm'\, K(m-m',\, m')\, n(m-m',\, t)\, n(m',\, t)$$

$$- n(m,\, t) \int_0^\infty dm'\, K(m,\, m')\, n(m'\, t)$$

$$- \frac{\partial}{\partial m} \psi \quad (m)\, n(m,\, t) \quad + J_n \qquad (1)$$

The first two terms in the equation (1) describe the time evolution of the aerosol size distribution due to coagulation. For the coagulation coefficient K(m, m'), we assume that particle collisions are two body and Brownian diffusion is the dominant collision mechanism. We utilize the K(m, m') derived by Fuchs[4]. The third term in the equation (1) represents condensation. For H_2SO_4 - H_2O binary system, we use the heteromolecular condensation theory developed by Hamill[5]. The last term J_n represents the nucleation rates. The rate at which sulfuric acid gaseous molecules and water vapor molecules cluster to form new particle is described by the expression for heteromolecular nucleation derived by Kiang and Stauffer[6].

For the sulfuric acid gaseous molecules, we assume the source term is generated by photochemical reaction and the sink terms are controlled by gas-to-particle conversion:

$$\frac{\partial S_{H_2SO_4}}{\partial t} = R - \int_0^\infty \psi\, (m)\, n(m,\, t)\, dm - m_{H_2SO_4}\, N^*_{H_2SO_4}\, J_n \qquad (2)$$

where $S_{H_2SO_4}$ is the mass concentration of gaseous sulfuric acid

molecules, R is the mass rate of production of sulfuric acid vapor due to photochemical reactions, $N^*_{H_2SO_4}$ is the critical number of sulfuric acid vapor molecules required for nucleation and $m_{H_2SO_4}$ is the mass of a sulfuric acid molecule. For the lower troposphere under non-smog conditions it has been shown by Davis and Klauber[7] that the reaction of SO_2 and OH is the most promising reaction to form H_2SO_4 gaseous molecules. Here we have used the SO_2 and OH reaction for the rate of production of H_2SO_4 (R).

For detailed discussion of the model, sensitivities of model calculations to uncertainties in input microphysical and chemical data, numerical errors and model validation the reader is referred to the recent article written by Middleton and Kiang[8].

RESULTS AND DISCUSSION

The formation and growth of secondary sulfuric acid aerosols under various atmospheric conditions are investigated by varying the relative humidity (RH), initial size distribution (ISD), temperature (T) and production rate of H_2SO_4 (R) (see Table 1).

The initial size distributions used are illustrated in Fig. 1. Urban I curve represents an urban atmosphere[9] and Urban II represents the aerosol size distribution of a relatively clean environment. Urban III is identical to Urban I except in the 0.001 to 0.01 micron (in diameter) size range, where more small particles are present.

Table 1

Various Atmospheric Conditions Used for Model Calculations

Case	RH	ISD	T	R(molecules* cm^{-3} sec^{-1})
a	25%	Urban I	25°C	9.4×10^6
b	50%	Urban I	25°C	9.4×10^6
c	75%	Urban I	25°C	9.4×10^6
d	50%	Urban II	25°C	9.4×10^6
e	50%	Urban III	25°C	9.4×10^6
f	50%	Urban I	10°C	9.4×10^6
g	50%	Urban I	25°C	9.4×10^7

*$R = k_1 SO_2$ OH air with $0.02 < SO_2 < 0.2$ PPMV, $10^6 < OH < 10^7$ $\frac{\text{molecules}}{cm^3}$ $k_1 \simeq 3.2 \times 10^{-31}$ cm^6/sec.

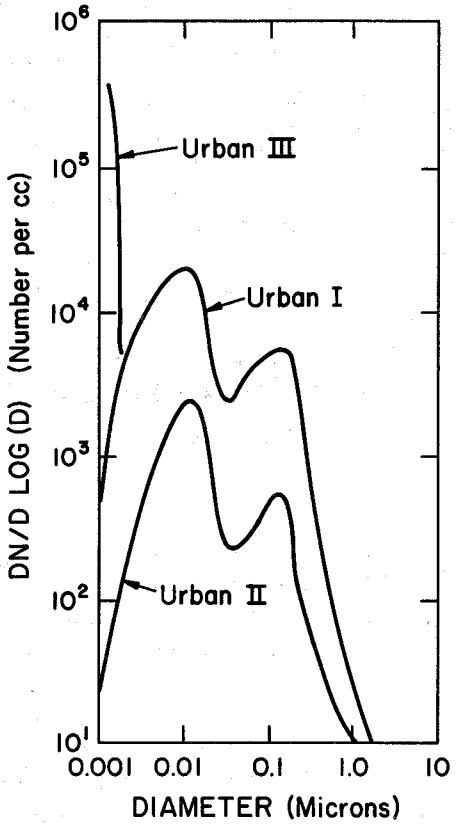

Figure 1. Initial size distribution.

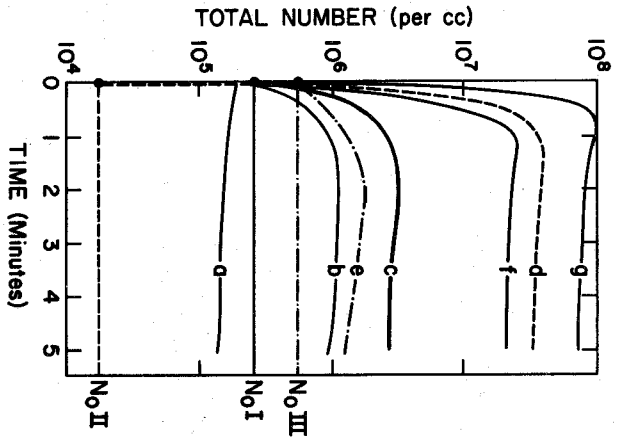

Figure 2. Total number concentration as a function of time.

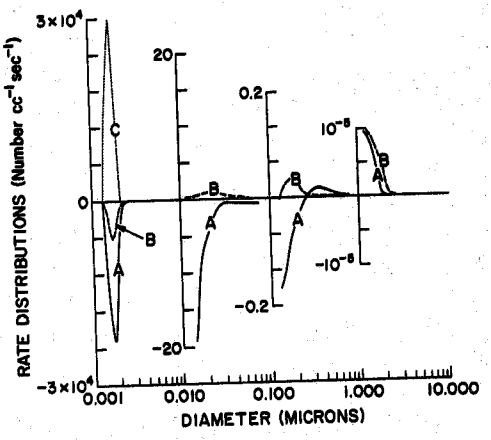

Figure 3a. Rate distribution for case b after five minutes.

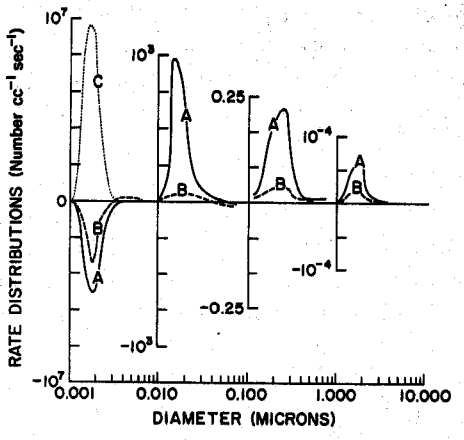

Fig. 3b. Rate distribution for case g after five minutes.

From (Fig. 2, cases a-g are defined in Table 1. N_oI is the initial total particle number concentration for Urban I) the analysis of total particle number concentration, it can be concluded that secondary aerosol formation is favored by conditions of high relative humidity, lower temperature, lower concentration of pre-existing particles, and higher rates of sulfuric acid vapor production. The rate limiting factor is the amount of sulfuric acid present in the atmosphere.

The microphysical processes for determining the growth of aerosol particles are condensation and coagulation. In order to assess the relative importance of these two mechanisms for the growth process, we analyze the rates of condensation and coagulation as a function of particle size.

The interaction between the various mechanisms over the entire particle size range after five minutes is illustrated in Fig. 3a and Fig. 3b (A = coagulation rate, B = condensation rate, C = nucleation rate). Cases b and g represent the same atmospheric conditions except that the rate of production of sulfuric acid vapors varies. From Fig. 3 it is observed that the nucleation rate is higher for more sulfuric acid vapors (case g). By comparing case b and g it is shown that coagulation of submicron particles becomes an important growth mechanism for increasing the number of particles in the size range > 0.1 to 1.0 μ when there is a great amount of new secondary aerosols being formed (case g). For case b, fewer new particles are formed and condensation becomes the more important growth process.

From our model calculations we conclude that the formation rate of secondary sulfuric acid aerosol is more favorable under following conditions (1) high production rate of sulfuric acid vapor, (2) high relative humidity, (3) smaller total surface area of suspended aerosols and (4) lower temperature environment.

ACKNOWLEDGEMENT

The National Center for Atmospheric Research is sponsored by the National Science Foundation. Paulette Middleton is grateful for the hospitality of the Aerosol Project, National Center for Atmospheric Research.

REFERENCES

1. Hidy, G. M. and J. R. Brock, 1970, As assessment of the global sources of tropospheric aerosols. In Proceedings of 2nd Clean Air Congress, IUAPPA, Washington, D.C., 1088-1097.

2. Sulfur and Biological Systems, Summary Report of a Workshop at Missouri Botanical Gardens, May 1975, Publication Number EPRI EA-419-SY, SOA 75-301, 1977.

3. Kiang, C. S. and P. Middleton, 1977, Formation of secondary sulfuric acid aerosols in urban atmosphere, Geophys. Res. Lett., 4: 17-20.

4. Fuchs, N. A., The Mechanics of aerosols, New York, Pergamon Press, 1964.

5. Hamill, P., The time dependent growth of H_2O-H_2SO_4 aerosols by heteromolecular condensation, J. Aerosol Sci., 6: 475-484, 1975.

6. Kiang, C. S. and D. Stauffer, Chemical nucleation theory for various humidities and pollutants, Faraday Symp., 7: 26-33, 1973.

7. Davis, D. D. and G. Klauber, Atmospheric gas phase oxidation mechanisms for the molecult SO_2, Int. J. Chem. Kinetics Symp., 1: 543-556, 1975.

8. Middleton, P. and C. S. Kiang, A kinetic model for the formation and growth of secondary sulfuric acid particles, J. Aerosol Science, to be published, August, 1978.

9. Whitby, K. T., R. B. Husar, and B. Y. H. Liu, The aerosol size distribution of Los Angeles smog, in Aerosols and Atmospheric Chemistry, Hidy, G. M. (ed.), New York, Academic Press, pp 237, 1972.

PARTICLE GROWTH BY CONDENSATION AND BY COAGULATION
——BASIC RESEARCH OF ITS APPLICATION TO DUST COLLECTION——

T. Yoshida, Y. Kousaka, K. Okuyama and K. Sumi
Chemical Engineering Department
University of Osaka Prefecture
Sakai, Japan 591

ABSTRACT

Three industrially applicable methods of the dust particle enlargement technique by condensation are proposed: (1) mixing method, where an exhaust gas is conditioned to obtain two kinds of saturated gases having different temperatures and they are mixed together at a certain ratio to produce supersaturation; (2) steam injection method where steam is injected into an exhaust gas; (3) adiabatic expansion method which essentially appears in venturi scrubber. The mechanisms of particle growth in these methods were analyzed and the size increase to be expected was evaluated. Feasibility of the application of particle growth by turbulent coagulation to dust collection is also discussed for the comparison with the condensation methods. In general, the exhaust gas having high number concentrations of dust particles is advantageous to coagulation, while low number concentrations is advantageous to condensation.

INTRODUCTION

Fundamental analysis and experiment for growth of aerosol particles by condensation[1] and by coagulation[2] were made in our previous papers where it was suggested that the particle growth by condensation and by coagulation could be the promising preconditioning techniques for the collection of submicron dust particles. Industrial application of the results was developed in this paper.

Condensation of water vapor on aerosol particles, not consisting of soluble substances, will essentially occur wherever a certain degree of

supersaturation is produced around the particles. The principle of such a process is very similar to that of fog formation in the atmosphere. Three industrially applicable methods to establish supersaturation are proposed, according to various industrial exhaust gas conditions and various operating conditions. These methods are also verified by experiment.

Coagulation, as another particle enlargement technique, will be effective where the particle number concentration of aerosols is high enough and turbulence is strong enough to enhance the chance of particle collision. The conditions of industrial exhaust gases and the operating conditions to promote coagulation will be discussed.

FUNDAMENTAL ANALYSES

Particle Growth by Condensation

In this section the fundamental analyses of particle growth by condensation are briefly introduced.

The point "i" on the psychrometric chart of Figure 1 indicates a state of supersaturation of air. The value of ΔH shown in the figure represents the quantity of condensable water vapor per unit mass of dry air[1], which is very important to evaluate the particle growth by condensation. In order to attain point "i", the following three methods are considered to be industrially effective.

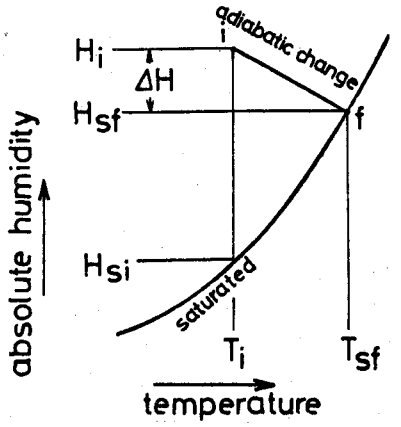

Figure 1 Change in humidity and temperature due to condensation

Mixing Method-

In this method an exhaust gas is conditioned to obtain two kinds of saturated gases having different temperatures and they are mixed together at a certain ratio, R_h, to produce supersaturation. The value of ΔH can be obtained by solving the following enthalpy and material balance equations on dry air basis.

$$R_h i_{sh} + (1-R_h) i_{sl} = i_{sf} + \Delta H i'_{wf} \quad (1)$$

$$R_h H_{sh} + (1-R_h) H_{sl} = H_{sf} + \Delta H \quad (2)$$

Steam Injection Method-

Steam is injected into an exhaust gas in this method. The value of ΔH can be obtained similarly to the mixing methods: as

$$i_g + Q_{st}\{xi''_{st} + (1-x)i'_{st}\} = i_{sf} + Q_{st}(1-x)i'_{wf} + \Delta H'_{wf} \quad (3)$$

$$H_g + Q_{st}x = H_{sf} + \Delta H \quad (4)$$

Adiabatic Expansion Method-

Adiabatic expansion usually appears in the throat of venturi scrubber. The following procedure is necessary to evaluate the value of ΔH for this method.

To simplify the analysis, an ideal gas is assumed and heat generated by friction is neglected. The pressure and the temperature at the venturi throat can be obtained from the following equations when adaibatic change is assumed.

$$p_0 v_0 \frac{\kappa-1}{\kappa}\left\{1 - \left(\frac{p_T}{p_0}\right)^{\frac{\kappa-1}{\kappa}}\right\} = \frac{u_T^2}{2g_c}\left\{1-m^2\left(\frac{p_T}{p_0}\right)^{\frac{2}{\kappa}}\right\} \quad (5)$$

$$\frac{T_0}{T_T} = \left(\frac{p_0}{p_T}\right)^{\frac{\kappa-1}{\kappa}} \quad (6)$$

Because of the pressure drop at the venturi throat, the saturated line in psychrometric chart moves upward as shown in Figure 2 in this case. Then the value, ΔH, can be evaluated from the following equations assuming the change from i to f in the figure to be adaibatic.

$$\Delta H = \frac{0.24 + 0.45H_0}{L_s(T_{sf})}(T_{sf} - T_T) \quad (7)$$

$$\Delta H = H_0 - 0.621\frac{p_s(T_{sf})}{p_T - p_s(T_{sf})} \quad (8)$$

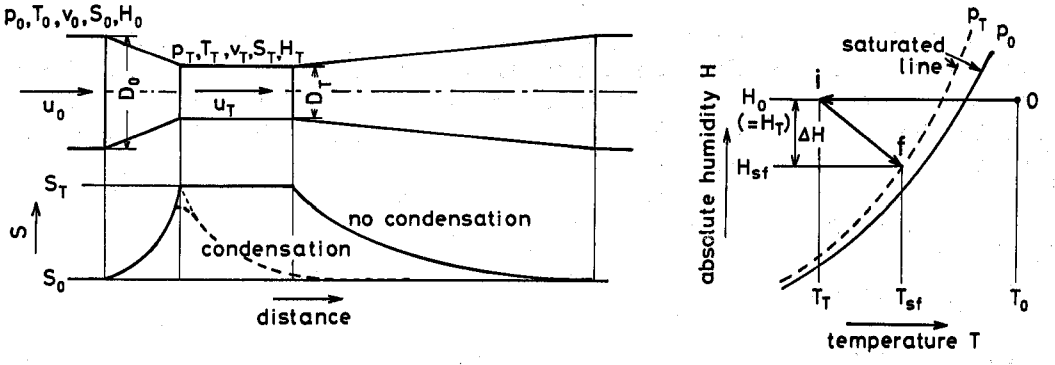

Figure 2 Change in the properties of air in the venturi scrubber

It is easily understood from the figure that the inlet gas conditions to venturi are desirable to be saturated in order to obtain the higher value of ΔH. Another expression instead of ΔH has been given by Amelin, assuming Clausius-Clapeyron's equation for saturation vapor pressure, as[3]:

$$S_T = \left(\frac{p_T}{p_0}\right) \exp\left\{E_C\left(\frac{1}{T_T} - \frac{1}{T_0}\right)\right\} \qquad (9)$$

Evaluation of Particle Growth by Condensation-

Some of the calculated value of ΔH obtained from the above analysis are shown in Figures 3, 4 and 5.

When all of the vapor corresponding to the amount of ΔH are assumed to condense upon particles suspending in the supersaturated atmosphere, the increase in size of particles undergoing condensation can be evaluated by the following equation.

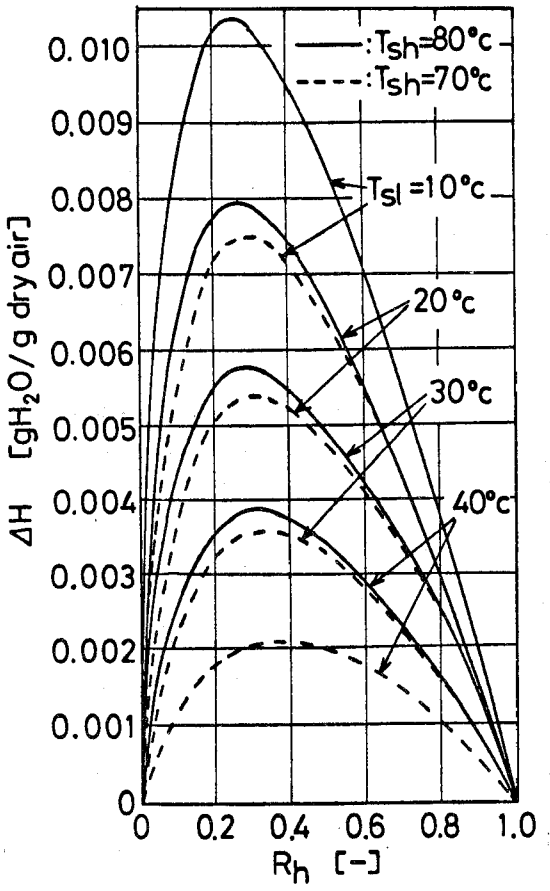

Figure 3 Condensable water vapor ΔH at various mixing conditions
——mixing method——

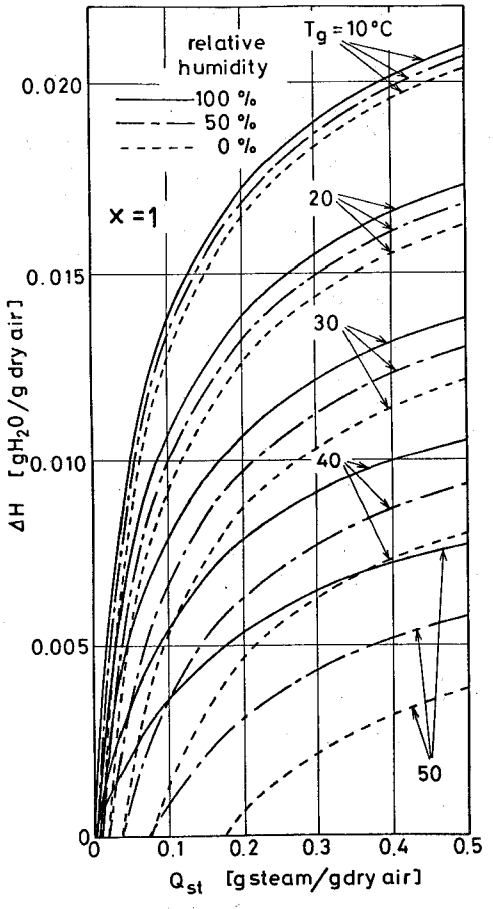

Figure 4 Condensable water vapor ΔH against quantity of steam injection Q_{st} ——steam injection method——

$$D_{vf} \fallingdotseq (6\Delta H/\pi n_w)^{1/3}$$

when $D_{vf}^3 \gg D_{vi}^3$ and $\rho_s \fallingdotseq 1$ (10)

n_w represents the particle number concentration of aerosol on dry air mass basis. D_{vi} and D_{vf} represent the volume mean diameters of the particles before and after growth respectively.

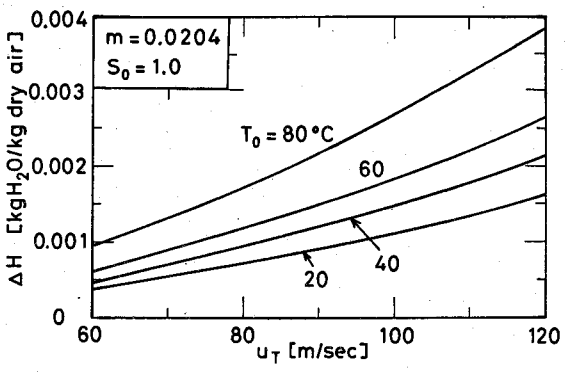

Figure 5 Condensable water vapor ΔH against the velocity at throat u_T ——adaibatic expansion method——

The growing rate of particles undergoing condensation was found to be very rapid in the previous paper[1], so the above analysis in equilibrium state only will be essential in developing this technique to industrial application.

Particle Growth by Turbulent Coagulation

The rate of particle growth is the controlling factor in coagulation, while it is not so important in condensation because of its extremely high growth rate.

The basic equation for the time-dependent change in particle size distribution of polydisperse aerosols undergoing Brownian and turbulent coagulations can be written as:

$$\frac{\partial n(r,t)}{\partial t} = \int_{\rho=0}^{\rho=r/\sqrt[3]{2}} \{K_B(\sqrt[3]{r^3-\rho^3},\ \rho)+K_T(\sqrt[3]{r^3-\rho^3},\rho)\}n(\sqrt[3]{r^3-\rho^3},t)n(\rho,t)$$

$$\times \left(\frac{r}{\sqrt[3]{r^3-\rho^3}}\right)^2 d\rho - \int_{\rho=0}^{\rho=\infty} \{K_B(r,\rho)+K_T(r,\rho)\}n(r,t)n(\rho,t)\,d\rho \quad (11)$$

$K_B(r,\rho)$ is the Brownian coagulation function and is given by

$$K_B(r,\rho) = K_0(r+\rho)\{C_m(r)/r+C_m(\rho)/\rho\},\ K_0=2\kappa T/3\mu \quad (12)$$

$K_T(r,\rho)$ is the turbulent coagulation function and the following relation derived by Saffman and Turner was found to be valid in our previous paper[2]

$$K_T(r,\rho) = 1.30(r+\rho)^3(\varepsilon_0/\nu)^{1/2} \quad (13)$$

The calculation results of the change in particle number concentration and particle size are shown in Figures 6 and 7 respectively, when

$K_D = 1 + K_T/K_B >> 1$ and no turbulent deposition are assumed. The change in the mode diameter of particles is found to be not significant in turbulent coagulation, while the number concentration decreases rapidly. It is interesting to compare this result with that obtained with condensation where the volume mean diameter changes significanltly without any change in particle number concentration.

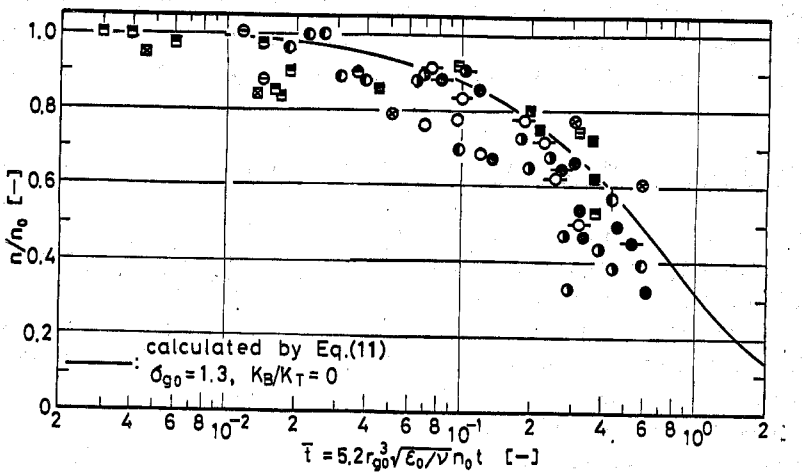

Figure 6 Time-dependent changes in number concentration of particles undergoing turbulent coagulation

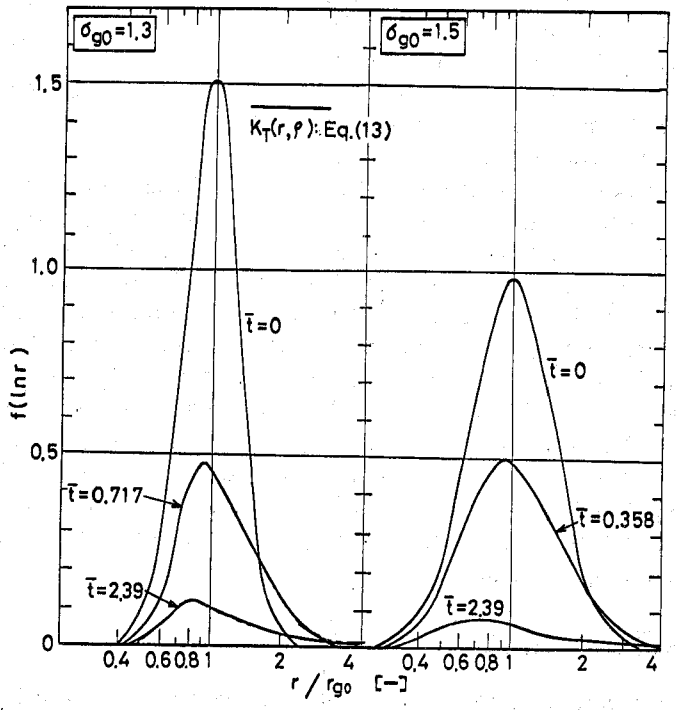

Figure 7 Time-dependent changes in size distribution of particles undergoing turbulent coagulation

APPLICATION OF THE FUNDAMENTAL ANALYSES

Condensation—Mixing and Steam Injection Methods—

Some of the representative industrial processes to produce ΔH are discussed for some typical gas conditions in this section. The property of exhaust gas was regarded the same as that of air in the following discussions.

High Temperature and High Humidity Exhaust Gas-

This is probably the most advantageous case to apply the method of particle growth by condensation when cooling water is available. The flow sheet of this process is shown in Figure 8. The gas is directly contacted with recirculating water shown as (a) in the figure and then the gas is divided into two parts. One part is dehumidified by contacting with cooling water, and is mixed with the other to produce ΔH or to enlarge the particles in the gas at the mixing chamber. This process is named "A". The value of ΔH depends on the temperature T_g and humidity H_g of exhaust gas, and on the temperature of cooling water which is available. The correlation among them was calculated by Eqs.(1) and (2), and was illustrated on the right upper side of the psychrometric chart of Figures 9 and 10. The mixing ratio R_h was chosen in any cases as the optimal calculated values shown in Figure 3. If one may require the value of ΔH=0.006 and if the cooling water temperature of 20°C is available, then the exhaust gas conditions must exist at least on the line of 20°C of cooling water in Figure 10, for instance T_g=1000°C and H_g=0.07 g H_2O/g dry air, T_g=100°C and H_g=0.32 g H_2O/g dry air and so forth. The temperature of saturated air or the equilibrium temperature after adiabatic humidification, in this case, comes to T_e=72.5°C. It is a matter of course that the larger values than ΔH=0.006 can be obtained if the gas conditions exist in the upper side of the line of 20°C of cooling water in Figure 10.

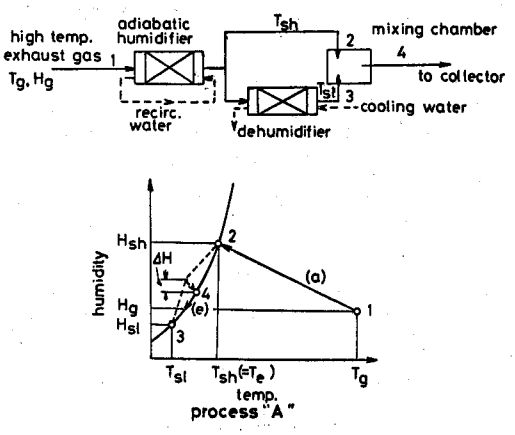

Figure 8 Illustration of process "A"

Low Temperature Exhaust Gas-

In this case steam injection method is effective, but this method has the fault that it requires saturated steam as a heat and water vapor source. This process is very simple as shown in Figure 11 and is named "B". The value of ΔH depends on the steam quantity Q_{st} and on exhaust gas

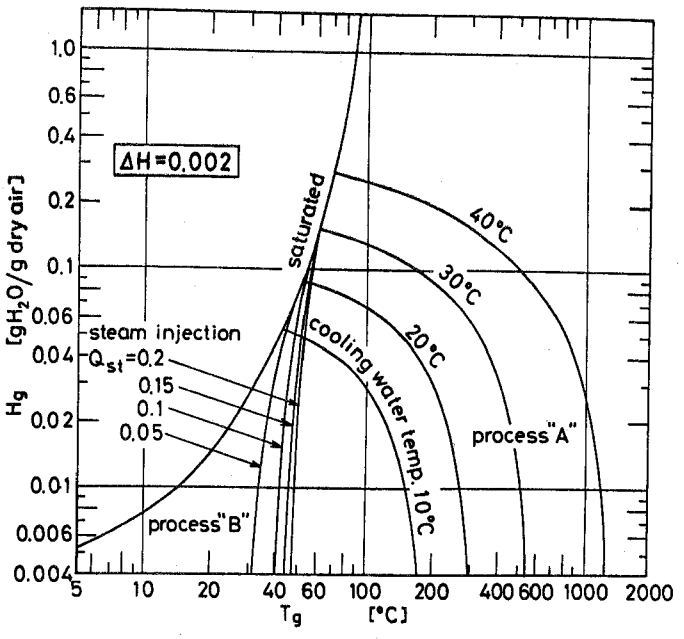

Figure 9 Application of processes "A" and "B" to various exhaust gas conditions (ΔH=0.002)

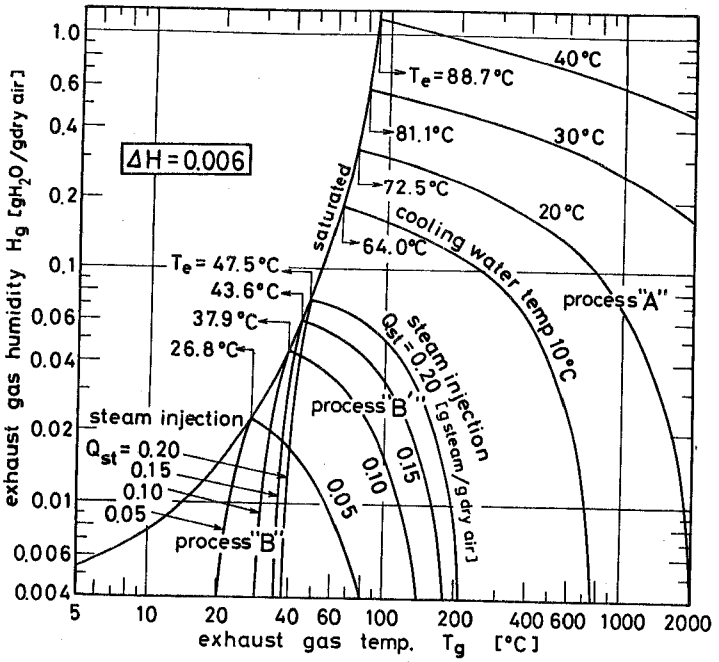

Figure 10 Application of processes "A", "B" and "B'" to various exhaust gas conditions (ΔH=0.006)

conditions such as T_g and H_g. The correlation among them was calculated by Eqs.(3) and (4) and was illustrated on the left side of the psychrometric chart of Figures 9 and 10. As the property of steam, 100°C, 1 ata and unity in dryness fraction were assumed in the calculations. If the same value of ΔH as the above example is required and if the steam quantity of Q_{st}=0.1 g steam per g dry air is available, then the exhaust gas conditions must exist at least on the line of Q_{st}=0.1 in Figure 10. The larger values than ΔH=0.006 can be obtained if the gas conditions exist in the left side of this line. The temperature rise in air was also illustrated in the figure as T_e, in this example T_e=37.9°C. If the saturated air after steam injection has high temperature, the process "A" may be applied successively after steam injection. This is one of the advantages of this process. The FF/C scrubber developed by Calvert[4] will be one of those to which steam injection methods is applied.

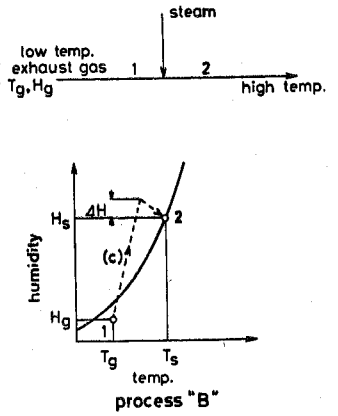

Figure 11 Illustration of process "B"

Gas Having Intermediate Conditions-

When exhaust gas has temperature below about 200°C and low humidity, steam injection can be applied after application of adiabatic humidification. This process is shown in Figure 12, and is named process "B'" because of similarity to process "B". The calculated results in this case were illustrated on the humidity chart of Figure 10.

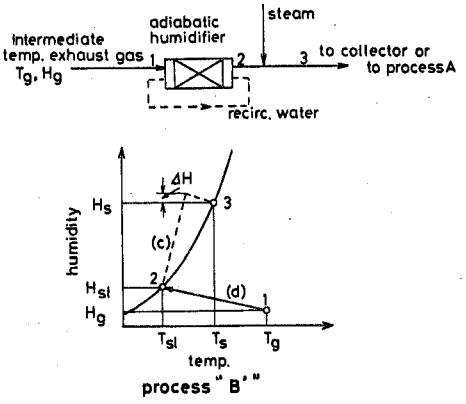

Figure 12 Illustration of process "B'"

When both hot water and cooling water are available, the following process may be applicable. One part of exhaust gas is humidified by hot water to obtain high temperature saturated air, and the remainder is cooled down by contacting with cooling water to obtain low temperature saturated air. Then they are mixed to produce ΔH. The process is shown in Figure 13, and is named process "A'". The calculated results can not be shown in this case in Figures 9 and 10 because the additional parameter of

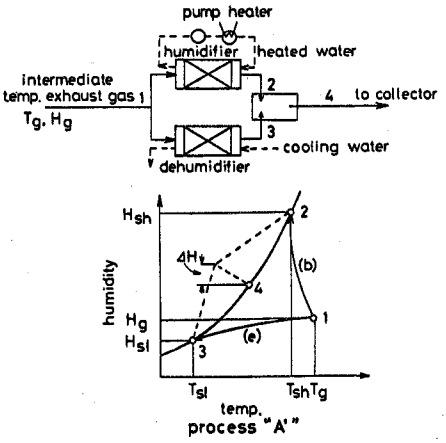

Figure 13 Illustration of process "A'"

heated water temperature is necessary. The value of ΔH, however, is obtainable for every given conditions since the temperature of points "2" and "3" in Figure 13 can be evaluated from given gas conditions.

Utilization of the Above Results-

The steps of procedure to utilize the above reuslts for industrial purpose are as follows. The appropriate process is first selected according to the given temperature and humidity of exhaust gas referring to Figures 9 and 10. The value of ΔH is next evaluated from calculation by setting up the quantity of steam, or the temperature of cooling water which is obtainable. Then the volume mean diameter of grown particles, D_{vf}, can be evaluated from Eq.(10), using the value of ΔH and knowing the particle number concentration of the gas, n_w. A dust collector after the preconditioning gas should be designed using the value D_{vf} thus obtained. If the value D_{vf}, on the other hand, is first given from the point of performance of a collector installed, the value ΔH should be first determined from Eq.(10) knowing the value n_w. Consequently the steam quantity Q_{st} or cooling water temperature will be determined from the figures or calculation using the known value of ΔH and knowing the gas conditions.

Example——T_g=30°C, H_g=0.01 g H_2O/g dry air and $n_w=10^8$ particles/g dry air (roughly corresponds to 10^5 particles/cm^3 gas) are given. It is required to enlarge submicron particles in the gas to 5 microns in D_{vf}.

In this case the value of ΔH which is required is found to be 0.006 g H_2O/g dry air from Eq.(10). The appropriate process in this case is found to be process "B" because of low temperature gas. The required steam quantity Q_{st}(100°C, 1 ata, x=1) is then found to be 0.1 g steam/g dry air from the point of T_g=30°C and H_g=0.01 in Figure 10.

Condensation—Adiabatic Expansion Method——

Figure 14 shows the effect of the degree of saturation, S_0, of venturi inlet gas on supersaturation produced in the throat. In applying this method to industrial venturi scrubbers, it is suggested from the figure that the venturi inlet gas should be humidified to an almost saturated state using a humidifier suitable to the gas conditions. Such a process will be very simple.

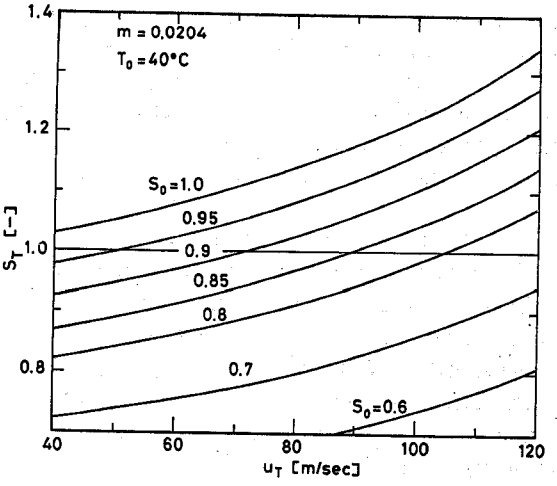

Figure 14 Values of supersaturation produced in the throat of venturi

Coagulation

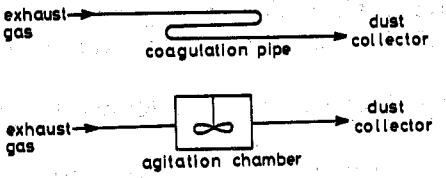

Figure 15 Dust collection systems being applied turbulent coagulation

It is suggested in the previous chapter that the turbulent coagulation is not so much effective to particle growth. This is true when the particle number concentration is less than 10^7 particles/cm^3. If an aerosol has the particle number concentrations more than 10^8 particles/cm^3, which is often observed at the stage of aerosol generation, the concentration of such an aerosol is decreased very rapidly due to coagulation. However most of aerosols we can actually observe are those in almost stable state where coagulation rate has already become slow. As far as such an aerosol is concerned, the coagulation seems to be unfavorable in its application to industrial dust collection.

The essential factors to enhance coagulation are to increase the particle number concentration preventing fresh air leakage to aerosol line, to take a long residence time and to give the violent turbulence to aerosols. These will be obvious from the abscissa of Figure 6. The possible dust collection systems being applied turbulent coagulation will be those shown in Figure 15.

EXPERIMENTAL

Condensation——Mixing and Steam Injection Methods——

Two kinds of experiments are shown in this section in order to examine the applicability of the mixing methods and the steam injection methods to industrial dust collection. The first experiment is to see the increase in particle size using the processes described above, and the second one is to see the increase in the collection efficiency of a scrubber when the preconditioning process is applied. These kinds of the experiments are very difficult because of the difficulty in accurate measurement of the size of droplets suspended in hot gas.

On the first experiment, the experimental results on the process "A'" were reported in the previous paper[1], and so the results on the other processes will be shown in this section. Figure 16(a) shows the schematic diagram of the experimental method. This apparatus can be operated under processes "A", "B" and "B'" by opening and closing valves. The mixture of air with the combustion gas from gas burner was supplied as a high temperature gas from the bottom of the adaibatic humidifier. The temperature of the gas was several hundreds centigrade degree for the process "A", about 200°C for the process "B'" and less than several tens centigrade degree for the process "B". Tobacco smoke(D_{vi}=0.85 micron) and dust particles contained in combustion gas($D_{vi}\leq$0.1 micron) were used as submicron dust particles. Total gas flow rate was 180 l/min. In the

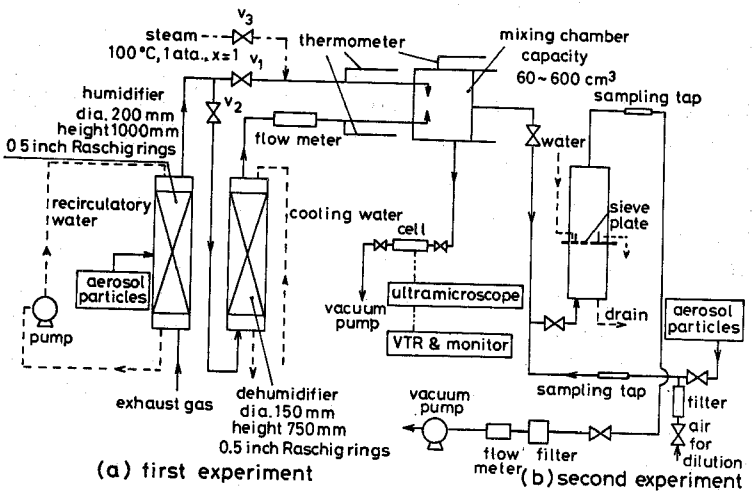

Figure 16 Schematic diagram of experimental apparatus

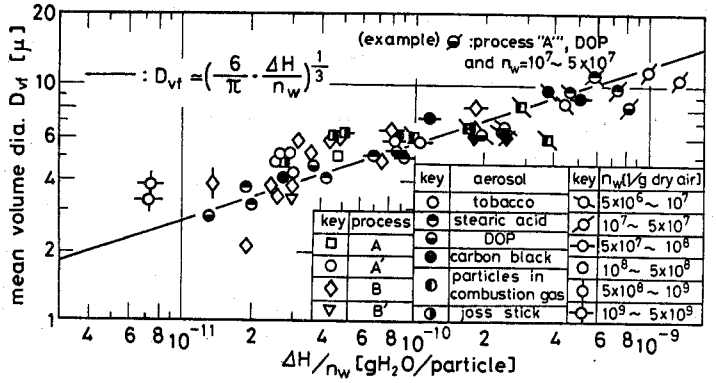

Figure 17 Relation between grown particle diameter D_{vf} and condensable water vapor per single particle

experiment of the process "A", the valves of v_1 and v_2 are adequately opened to obtain a certain mixing ratio R_h keeping v_3 close. In the experiments of processes "B" and "B'", the valve of v_2 is closed and v_3 is moderately opened to inject a certain amount of steam into the gas. The steam condition was 100°C in temperature, 1 atm. abs. in pressure and 1.0 in dryness fraction, and the quantity of steam injection was ranged from 0.05 to 0.5 g steam/g dry air. The technique of size measurement of grown particles was the same as that appeared in the previous papers[1,5]. Experimental results obtained were plotted in the same graph as those of the previous paper[1], which was shown in Figure 17. The results obtained in the previous work were also collectively plotted in the figure. It will be found that the size of grown particles in all processes "A", "A'", "B" and "B'" can be evaluated by Eq.(10).

In the second experiment, a sieve plate scrubber was used, and the schematic diagram is shown in Figure 16(b). The dimension and shape of the scrubber is shown in Figure 18. The test aerosol used was a fog cloud

of aqueous ammonium chloride solution. At upstream and downstream of the scrubber, the aerosol was sampled under isokinetic sampling conditions. The measurement methods of the particle number concentration and the particle size distribution were the same as those used in the first experiment. Figure 19(a) shows the experimental collection efficiency of sieve plate scrubber against superficial velocity u_G, and Figure 19(b) shows the comparison in the particle size distribution before and after the sieve plate scrubber. Aerosol particles without particle growth, namely the supplied aerosol particles themselves, are found to be very difficult to capture as shown in Figure 19(a). When the same particles were grown by condensation after dilution, the collection efficiency of such particles is found to increase by 80 ~ 90%. In this experiment, the particles were grown by the process "A'" and "A". The mechanism of particle collection by a sieve plate scrubber, which has not been clearly analyzed yet, is considered to be that caused by inertia, because the collection efficiency of particles increased with the particle size. Under these experimental conditions, the pressure drop was less than 100 mmH_2O. The improvement in particle collection efficiency due to condensation growth were also seen in other experimental conditions.

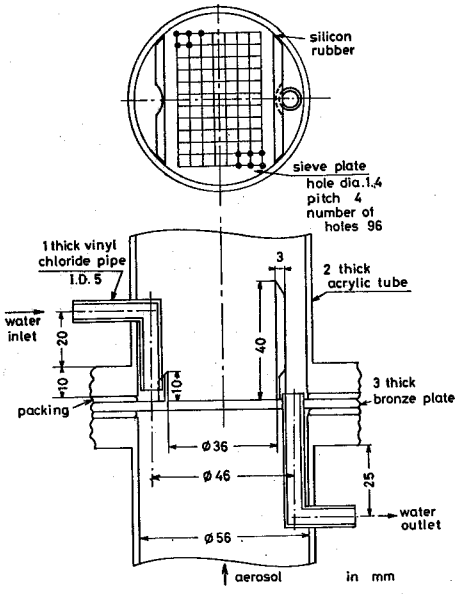

Figure 18 Sieve plate scrubber

Condensation——Adiabatic Expansion Method——

It is difficult to observe the particle size after growth at the venturi throat and then the dust

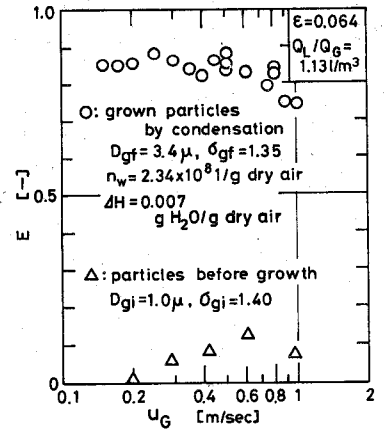

Figure 19(a) Experimental collection efficiency of sieve plate scrubber

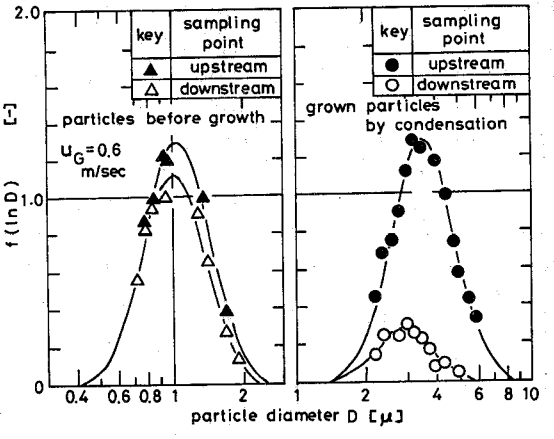

Figure 19(b) Particle size distribution before and after scrubber

collection efficiency was observed. Figure 20 shows the experimental method. As pointed out on Figure 14, the particle growth in this case depends upon the degree of saturation before adaibatic expansion, or at venturi inlet. Thus the experiment was made under different degrees of saturation at venturi inlet keeping all other operating conditions to be the same. The dust collection efficiency obtained under the inlet gas condition of 100% relative humidity is expected to be higher than that under the low humidity where no particle growth is expected.

Table 1 shows the experimental results. The collection efficiencies were observed by the ultramicroscopic method and were observed on number basis. The collection efficiencies, when inlet gas is saturated, seems to be improved. There are, however, some problems in these experiments: venturi was too small to make sufficient adiabatic expansion, particles were hygroscopic and initial particle size was too large. Further experiments will be necessary to confirm the condensation effect at the venturi throat.

Coagulation

Two kinds of experiments were made: one for turbulent coagulation in a stirred tank and the other for that in a pipe flow. The detail of the results of the former experiment appeared in our previous paper[2]. Figure 21 shows the stirred tank used in the experiment. The aerosols used in the experiment were tobacco smoke. Figure 22 shows the experimental results, which were also evaluated by Eqs.(11) to (13). It takes a long time to decrease number

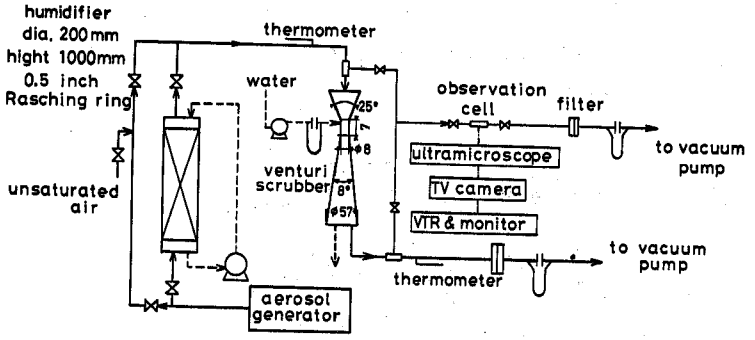

Figure 20 Schematic diagram of experimental apparatus

L [1/m^3]	inlet gas:100%R.H. n_w [1/g dry air]	D_{vi} [μ]	E [%]	inlet gas:70%R.H. n_w [1/g dry air]	D_{vi} [μ]	E [%]	ΔP [mmH$_2$O]
0.2	3.1×10^9	0.74	57.6	2.8×10^9	0.66	49.4	345
	3.9×10^9	0.62	71.3	3.8×10^9	0.61	62.5	370
0.3	4.2×10^9	0.68	69.5	4.0×10^9	0.66	64.9	420
	2.4×10^9	0.58	77.6	3.1×10^9	0.58	71.6	470
0.5	3.1×10^9	0.66	72.3	3.0×10^9	0.62	66.4	530

Table 1 Comparison of experimental collection efficiencies

concentration when particle concentrations and revolutions of the stirrer are low. Figure 23 shows the other experimental device where a long pipe is used to promote coagulation. The pipe length was changed from 20 to 100 meter. The plots in Figure 6 are the experimental results. The experimental conditions and properties of aerosols is shown in Table 2. As the average value of the energy dissipation rate, the relation of $\varepsilon_0=fu^3/D$ was used, where f is the Fanning's friction factor, D is pipe diameter and u is average velocity.

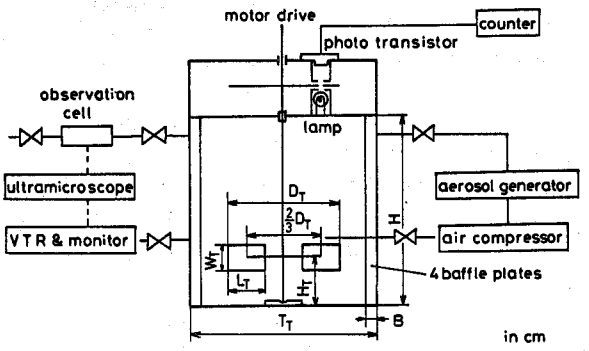

	H	T_T	D_T	H_T	W_T	L_T	B
stirred tankI	10.0	10.0	5.2	$T_T/3$	1.0	2.0	$T_T/10$
stirred tankII	20.5	19.0	8.9	$0.17T_T$	1.8	2.2	$T_T/10$

Figure 21 Experimental apparatus

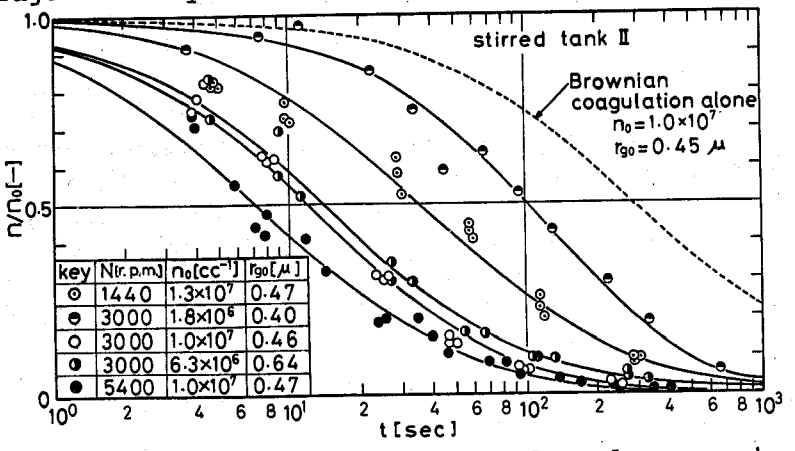

Figure 22 Effect of stirrer speed on decrease in particle number concentration of aerosol

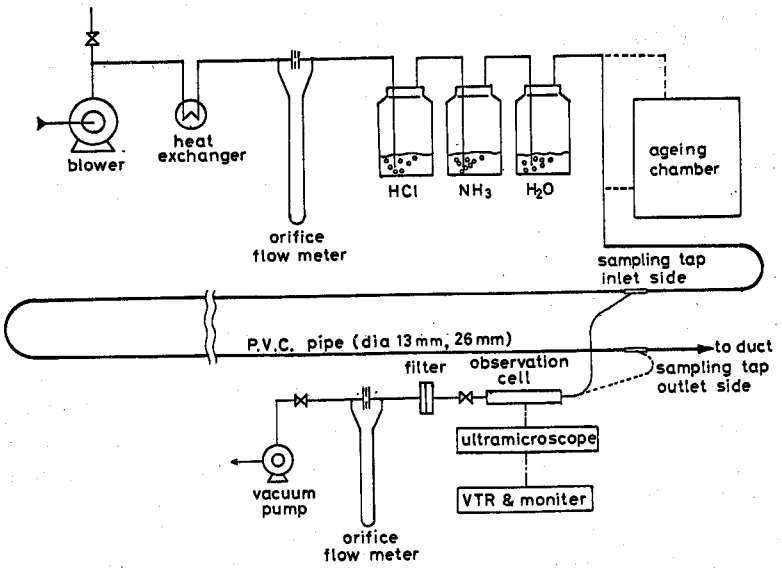

Figure 23 Experimental apparatus

Table 2 Experimental conditions and properties of aerosol

key	Re [-]	ε_0 [cm^2/sec^3]	n_0 [particles/cm^3]	r_{g0} [μ]	σ_{g0} [-]	K_D [-]	$r_{g0}\sqrt[3]{\varepsilon_0}$ [$cm^4/sec^{3/2}$]
Pipe diameter D = 13 mm							
◐	5000	1.35×10^6	$3.66\sim6.06 \times 10^7$	0.27~0.32	1.20~1.31	2.11	$2.29\sim3.81 \times 10^{-11}$
◐	"	"	$2.61\sim3.07 \times 10^6$	0.34~0.43	1.24~1.60	3.56	$4.57\sim9.24 \times 10^{-11}$
◐	"	"	$3.98\sim4.64 \times 10^7$	0.35~0.43	1.21~1.30	"	$4.98\sim9.24 \times 10^{-11}$
○	8000	4.93×10^6	$5.69\sim6.63 \times 10^7$	0.25~0.27	1.22~1.31	2.33	$3.47\sim4.37 \times 10^{-11}$
○	"	"	6.71×10^6	0.36~0.38	1.25~1.32	5.14	$1.04\sim1.22 \times 10^{-10}$
○	"	"	$2.54\sim3.98 \times 10^7$	0.32~0.41	1.30~1.40	"	$0.73\sim1.53 \times 10^{-10}$
●	7400	3.98×10^6	$1.01\sim2.37 \times 10^7$	0.37~0.41	1.21~1.38	5.39	$1.01\sim1.37 \times 10^{-10}$
⊗	10000	9.11×10^6	$1.10\sim3.17 \times 10^7$	0.30~0.48	1.23~1.27	7.64	$0.82\sim3.34 \times 10^{-10}$
⊖	13000	1.98×10^7	$1.85\sim2.09 \times 10^6$	0.31~0.34	1.32~1.48	6.60	$1.29\sim1.70 \times 10^{-10}$
⊖	22400	8.38×10^7	3.62×10^7	0.30	1.18	9.74	2.47×10^{-10}
Pipe diameter D = 26 mm							
◨	5000	8.47×10^4	$1.22\sim4.45 \times 10^7$	0.46~0.48	1.25~1.38	2.16	$2.83\sim3.22 \times 10^{-11}$
◨	"	"	$0.46\sim4.71 \times 10^6$	0.30~0.44	1.25~1.38	1.54	$0.79\sim2.48 \times 10^{-11}$
■	10000	5.69×10^5	$1.49\sim5.18 \times 10^7$	0.32~0.45	1.25~1.38	2.66	$2.47\sim6.87 \times 10^{-11}$
■	"	"	$0.77\sim3.74 \times 10^6$	0.35~0.40	1.25~1.38	2.54	$3.23\sim4.83 \times 10^{-11}$
△	"	"	$1.18\sim4.16 \times 10^6$	0.55~0.80	1.36~1.58	10.6	$1.26\sim3.86 \times 10^{-10}$
◆	15000	1.74×10^6	$4.60\sim9.94 \times 10^5$	0.63~0.83	1.37~1.67	21.8	$3.30\sim7.54 \times 10^{-10}$
▲	"	"	$1.31\sim2.19 \times 10^6$	0.55~0.90	1.35~1.51	21.8	$2.19\sim9.62 \times 10^{-10}$

CONCLUSION

Particle growth by condensation was found to be applicable to dust collection of the industrial exhaust gas which contains submicron particles in low number concentrations. Three industrially applicable methods, mixing, steam injection and adiabatic expansion methods, were proposed and the mean volume diameter after particle growth in these methods was evaluated. For the facility of the industrial application of these methods, some possible processes were illustrated according to the typical exhaust gas conditions.

Turbulent coagulation, on the other hand, is found to be effective to promote particle growth when particle number concentration is very high and when violent turbulence is applied to the aerosol. The effect of turbulent coagulation was evaluated. Industrial application of turbulent coagulation to dust collection, however, seems to be less favorable than that of condensation, since it takes a fairly long time to promote coagulation of aerosol particles contained in industrial exhaust gases.

NOMENCLATURE

$C_m(r)$ = Cunningham's correction facrot of r [-]

D, D_g = diameter and geometric mean diameter [μ] [cm]

D_{vi}, D_{vf} = volume mean diameter before and after growth respectively [μ] [cm]

E	= particle collection efficiency	[-]
E_C	= constant(=5121.9)	[-]
H	= absolute humidity	[g H_2O/g dry air]
ΔH	= condensable water vapor	[g H_2O/g dry air]
i	= enthalpy	[cal/g dry air] [cal/g steam]
L_s	= latent heat	[cal/g]
m	= (throat diameter/inlet diameter)^2	[-]
n	= particle number concentration	[particles/cm^3]
n_0	= particle number concentration	[particles/g dry air]
n_w	= particle number concentration	[particles/cm^3]
$n(r,t)$	= particle number concentration of r at t	[particles/cm^3]
p	= pressure	[mm Hg]
Q_G, Q_L	= flow rate of gas and liquid	[m^3/min] [l/min]
Q_{st}	= quantity of steam injection	[g steam/g dry air]
r	= radius of particle	[μ] [cm]
r_{g0}	= geometric mean radius at t=0	[μ] [cm]
R_h	= mixing ratio, g dry air of high temperature saturated air/g total dry air	[-]
S	= degree of saturation	[-]
T	= temperature	[°C] [°K]
t	= time	[sec]
$\bar{t}$	= dimensionless time shown in Figure 6	[-]
u_E	= gas velocity	[cm/sec]
u	= superficial velocity	[cm/sec]
u_G	= speccific volume	[kg/m^3]
v	= dryness	[-]
x		

Greek Letters

ε	= porosity of sieve plate	[-]
ε_0	= average energy dissipation rate	[cm^2/sec^3]
κ	= rstio of specific heats	[-]
ν	= kinematic viscosity	[cm^2/sec]
ρ	= radius of particle	[ ] [cm]
ρ_s	= density of condensed liquid	[g/cm^3]
σ_g	= geometric standard deviation	[-]

Subscripts

e	= equilibrium state of air
f	= final state shown in Figure 1
g	= initial state of air
i	= initial state
0	= venturi inlet
s	= saturated
sf	= saturated air in final state
sh	= high temperature saturated air
sl	= low temperature saturated air
st	= steam
T	= throat
wf	= water in final state

Superscripts

'	= wet
"	= dry

REFERENCES

1) Yoshida, T., Y. Kousaka and K. Okuyama. Growth of Aerosol Particles by Condensation. Ind. Eng. Chem., Fundam., 15, 37(1976)
2) Okuyama, K., Y. Kousaka, Y. Kida and T. Yoshida. Turbulent Coagulation of Aerosols in a Stirred Tank. J. Chem. Eng. Japan. 10, 142(1977)
3) Amelin, A. G. Theory of Fog Condensation. Israel Program for Scientific Translation 1967
4) Calvert, S., J. Goldshmid, D. Leith and N. Jhaveri. Feasibility of Flux Force/Condensation Scrubbing for Fine Particle Collection. Environment Protection Agency. PB 227 307, October 1973
5) Yoshida, T., Y. Kousaka and K. Okuyama. A New Technique of Particle Size Analysis of Aerosols and Fine Powders Using an Ultramicroscope. Ind. Eng. Chem., Fundam., 14, 47(1975)

TRANSIENT CHEMISORPTION OF A SOLID PARTICLE IN A REACTIVE ATMOSPHERE OF RECEDING GAS CONCENTRATION

Roa-Ling Wang, Ph. D.; P. E.
Montreal Engineering Company, Limited
Thermal Division
St. Catharines, Ontario L2R 7J9 Canada

ABSTRACT

Study has been conducted on a transient phenomenon of chemisorption of a solid absorbent particle in a gaseous enclosure where the mass of a reacting gas is conserved. The penetration of gas species into the solid reactant due to the chemisorption process leads to decrease reacting gas concentration in the enclosure. In the case of powder absorbents in flue gas desulfurization and pulverized coal combustion, the chemical reaction rate of these gas-solid interactions is, usually, much faster than the diffusion rate of their two-phase mass transport processes. Thus, the concentration of reacting gas in the gas-solid mixture system becomes one of the major factor in controlling the chemisorption rates. Other factors such as particle size, surface volume ratio of particles, particle density in the mixture system and material property of participating species are also important to the process of controlling chemisorption. The paper presents a method of computation to determine the rate of chemisorption under the transient case of various gas concentration depletions. The method has been extended to a particular condition of a large volume ratio between gas enclosure and a solid particle, so that the result of the transient solution can be compared with that of a steady state solution.

INTRODUCTION

The use of fossil fuels for electric power generation, industrial processes, house heating, etc. has suffered from sulfur dioxide emission in the combustion products. Many ways have been attempted by various investigations to combat the problem of sulfur dioxide removal. Three dry removal methods have been studied in the U.S. Bureau of Mines[1], the

Canadian Fuel Research Center[2] and the Japan Mitsubishi heavy Industry[3]. The method developed by the Bureau of Mines is of an absorption process, making use of passing flue gases through a fluidized bed reactor of solid particles. The Fuel Research Center demonstrated the application of solid additives to fuel oils, and, hence, during combustion absorbent particles suspend in flue gases and remove sulfur dioxide from the gases. In reference 3, efforts have been made on the injection of limestone powder into a boiler furnace for reducing sulfur dioxide emission level in a stack gas stream. As compared with any wet desulfurization, the dry methods have a great advantage to the natural draft force of a stack system due to no sensible heat loss in flue gases. For the dry methods, there is a common phenomenon that the desulfurization results from the chemisorption of reactant solids and that in all cases the gas reactant is always depleted of its concentration as the desulfurization takes place continuously.

Another similar physico-chemical phenomenon occurs in the combustion of pulverized coal and coal-oil mixture systems. In the fossil fuel burning systems, a conserved amount of oxygen encloses each particle which absorbs oxygen by gas-solid phase diffusion processes and subsequently produces carbon dioxed, water vapor and some minor compositions of combustion products diffusing through a solid product shell of ash into the surrounding gas layer. The actual phenomenon is further complicated by poly-phase multi-component diffusion processes associated with thermo-chemical kinetics and heterogeneous turbulent mixing. The existing theories can hardly deal with such interdisciplinary problems without any drastic simplication of conditions to be analyzed.

ANALYTICAL MODEL

In order to attempt at the fundamental understanding of transient diffusion in gas-solid interphase associated with a chemical reaction, a mathematical model presented in the paper is subject to the constraints as discussed below.

The whole gas-solid system of the present study is of a two-phase homogeneous mixture having a unique diameter of spherical solid particles. The whole system moves in a constant cross-section duct at a given velocity. Particle size and gas velocity have negligible effect on the momentum transfer between the two-phase interaction. In the result, particle density distribution along the flow path becomes an independent variable of time and locations within the system. Consequently, each particle may be assumed to be enclosed by a gaseous atmosphere of the same diameter. Within the atmosphere it con-

tains a gas species capable of reacting with the solid particles. Due to out-of-proportionality between the flow path length of the gas-solid system and the diameter of a gaseous atmosphere, the inter-boundary diffusion rate of the reactive gas in the two neighbouring atmospheres may be accounted to be negligibly small as compared with the diffusion rate at the gas-solid interface. Thus, within each enclosed system, the total mass of the reactive species will be conserved in a steady flow system. However, as soon as an irreversible chemical reaction starts up at the solid outer surface, the concentration of the reactive species in the gaseous atmosphere decreases accordingly. The product of the chemical reaction, for the present model, is assumed to form a layer of porous solid on the outer surface of the solid particle. The chemical product permits the reactive gas passing through its porous layer and producing a chemical reaction on the new contacting surface of the solid reactant underneath the product layer. This physico-chemical interaction theoretically yields the chemisorption process taking palce continuously until one of the two reactants completely consumed.

Generally, the gas-to-gas diffusion rate could be several orders of magnitude higher than the rate for gas-to-solid diffusion. In consequence, it is permissible to consider the enclosing gas system as a homogeneous mixture of inert and reactive gases. But in the mixture a reactive gas concentration decreases homogeneously and continuously as the chemisorption keeps going on.

Finally, it is also permissible to assume that the volumetric change in the product layer may be insignificant, if the particle diameter is reasonably smaller than the gaseous atmosphere diameter. Accordingly, the solid particle within a gaseous enclosure should maintain a constant shape and size during the chemisorption process.

Fig. 1 shows the configuration of the model. The model has fixed boundaries for gas and solid phases with radii R_g and R respectively. The radius R also designates the outer radius of the product layer once gas-solid chemical reaction taking place. The interface radius of the solid reactant and product is expressed by r_c. As a result of continuous chemisorption process occurring within the model, the reactant gas concentration C_s in the gas region is controlled by the following two-phase rective system,

$$N_1A_1 + N_2A_2 \longrightarrow N_3A_3 \qquad (1)$$

Where A_1, A_2 and A_3 are symbols of gas reactant, solid rectant and solid product respectively. N_1, N_2 and N_3 are the

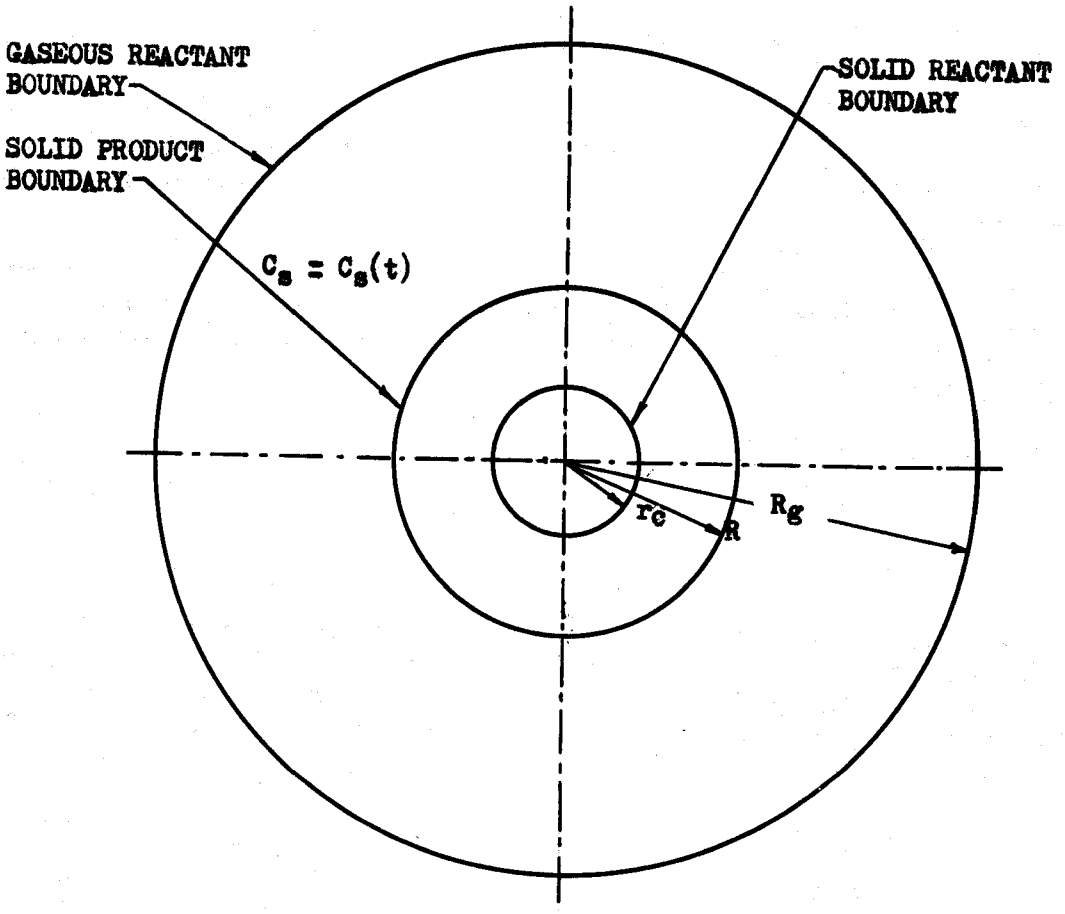

Fig. 1 Configuration of a solid-gas reaction in a receding reactive gas concentration atmosphere.

coefficients of the participating chemical species. For an irreversible reaction as presented in Eq.(1), the rate of the boundary movement dr_c/dt can be determined from mass conservation law applied to the stoichiometric reaction of Eq.(1),

$$\frac{dr_c}{dt} = -\frac{N_2 D M_2}{N_1 d_2}\left[\frac{\partial C(r_c,t)}{\partial r}\right]_{r=r_c} = -Y_1 D\left[\frac{\partial C(r_c,t)}{\partial r}\right]_{r=r_c} \qquad (2)$$

where D, M_2 and d_2 stand for material constants of gas-solid diffusivity, molecular weight of the solid reactant and density of the solid rectant respectively. Y_1 designates a group constant of N_2M_2/N_1d_2.

Since the mass transport process of the gas-solid system is restricted to a unilateral diffusion of gas into the solid body, the gas diffusion equation in the product layer becomes rather simple,

$$\frac{\partial^2 C}{\partial r^2} + \frac{2}{r}\frac{\partial C}{\partial r} = \frac{1}{D}\frac{\partial C}{\partial t} \qquad (3)$$

where C represents the reactive gas concentration in the product layer at a radial distance r from the solid sphere center. In order to satisfy the initial and boundary conditions of the chemisorption process, Eq.(3) must be subject to the following constraints:

$$C = C_o \quad \text{at} \quad r = R \qquad (4)$$

and when $t=0$

$$C = 0 \quad \text{at} \quad r < R \qquad (5)$$

where C_o = initial concentration of the reactive gas in the gas atmosphere
After the chemisorption taking place, i.e. $t > 0$

$$C = C_s(t), \quad \text{at } r = R \qquad (6)$$

and

$$C = 0, \quad \text{at } r = r_c \qquad (7)$$

The molar concentration of the reacting gas, A_1, in the gas region confined by radii R_g and R can be deduced from the chemical relationship of Eq.(1) and expressed in a rigorous form,

$$C_s(r_c,t) = C_o + \frac{1}{V_g}\int_R^{r_c} 4\pi r_c^2 \frac{N_1 d_2}{N_2 M_2}\left(\frac{dr_c}{dt}\right) dt$$

$$= C_o + Y_2(r_c^3 - R^3)/3 \qquad (8)$$

where Vg is the valume of the gas atmosphere and expressed as

$$V_g = \frac{4\pi}{3}(R_g^3 - R^3) \qquad (9)$$

and Y_2 is another material group constant which is in a form of

$$Y_2 = \frac{4\pi N_1 d_2}{V_g N_2 M_2} \qquad (10)$$

Equation (2), along with its non-linear boundary conditions presents formidable mathematical diffculties for obtaining a true solution. Some alternative methods for solving boundary-layer and heat transfer problems by Karman[4] and Vujannovic[5] are available to attempt at a closed form solution of equation (3). The technique employed in the paper is a type of Karman's integral method. Followed by this technique, one can formulate a non-linear boundary value problem into an ordinary initial value type of equation of which the solution can frequently be expressed in a closed analytical form. Goodman[6] has shown successfully the application of this method to a heat conduction problem involving a phase change phenomenon.

The principle of the integral method employed in the paper implies the overall mass-transfer-balance of the reactive gas in the gas atmosphere and product layer. Integrating with respect to r from R to r_c, Eq.(3) leads to a integro-differential form,

$$r^2 \frac{\partial C}{\partial r}\Big]_R^{r_c} = \frac{1}{D}\frac{dx}{dt} \qquad (11)$$

where

$$x = \int_R^{r_c} r^2 C \, dr$$

Since r_c is a function of t, i.e. $r_c = r_c(t)$, the total derivative of Eq. (7) with respect to t is,

$$\frac{d}{dt} C(r_c, t) = \frac{\partial}{\partial r_c} C(r_c, t)\frac{dr_c}{dt} + \frac{\partial}{\partial t} C(r_c, t)$$

$$= 0 \qquad (12)$$

Combining Eqs. (2) and (12) yields

$$\left[\frac{\partial C(r_c, t)}{\partial r}\right]^2_{r = r_c} = \frac{1}{Y_1 D}\frac{\partial C(r_c, t)}{\partial t}$$

Substituting Eq. (3) for the above $\frac{\partial C}{\partial t}$ leads to

$$\left[\frac{\partial C(r_c, t)}{\partial r}\right]^2_{r = r_c} = \frac{1}{Y_1 r^2}\frac{\partial}{\partial r} r^2 \frac{\partial}{\partial r} C(r_c, t)\Big]_{r = r_c} \qquad (13)$$

Equations (6) and (7) represent two boundary conditions of the shell of product layer; thus, the attempted solution for reacting gas concentration distribution in the layer can be expressed by a second order closed form,

$$C = B_1(r - r_c) + B_2(r - r_c)^2 \qquad (14)$$

where B_1 and B_2 are coefficients of the equation. The coefficients can be determined from Eqs.(6) and (7) and have explicit forms as,

$$B_1 = \frac{1}{Y_1}\left[\frac{R - 2r_c}{r_c(R-r_c)}\right]\left[1 - \sqrt{1 + 2Y_1 \frac{C_s\, r_c^2}{(R - 2r_c)^2}}\right] \qquad (15)$$

$$B_2 = \frac{C_s - B_1(R - r_c)}{(R - r_c)^2} \qquad (16)$$

Since C_s and r_c are dependent variables of time t, the coefficients are automatically the parameters of t. Then Eq.(14) can be expressed as

$$C = B_1(t)\left[r - r_c(t)\right] + B_2(t)\left[r - r_c(t)\right]^2 \qquad (17)$$

Substituting C into Eq.(11), one obtains

$$x = \frac{-1}{60}\left\{B_1\left[15R^4 - 20R^3r_c - 5r_c^4\right] + B_2\left[12R^5 - 30R^4r_c + 20R^3r_c^2 - 2r_c^5\right]\right\} \qquad (18)$$

Combining Eqs.(2) and (11), one has

$$\frac{r_c^2}{Y_1 D}\frac{dr_c}{dt} + \left[r^2 \frac{\partial C(r, t)}{\partial r}\right]_{r=R} = \frac{1}{D}\frac{dx}{dt} \qquad (19)$$

From Eqs.(18) and (19), the diffusion balance equation (19) may be further expressed in an ordinary differential form:

$$\frac{dr_c}{dt} = -\frac{R^2\left[B_1 + 2B_2(R - r_c)\right]}{r_c^2/Y_1 D + Z(t)/D} \qquad (20)$$

where

$$Z(r_c) = \frac{1}{60}\Big\{10B_2 r_c^4 + 20B_1 r_c^3 - 40B_2 R^3 r_c + 20B_1 R^3 + 30B_2 R^4 + \left[5r_c^4 + 20R^3 r_c - 15R^4\right]\frac{dB_1}{dt} + \left[2r_c^5 - 20R^3 r_c^2 + 30R^4 r_c - 12R^5\right]\frac{dB_2}{dt}\Big\} \qquad (21)$$

Since no exact solution exists for the problem of a solid absorbent surrounded by the transient concentration of a reacting gas, direct comparison between the closed-form solution and exact one is not possible. However, Weisz and Goodwin[7] studied the combustion of carbonaceous matter in the pores of solid granules for diffusion investigation. Following their experiments, it reveals that, during the regeneration of a conventional sillica-alumina cracking catalyst processed at a combustion temperature of 700°C, the phenomenon of moving boundary r_c is controlled apparently by the diffusion of oxygen into the solid. A semi-analytical equation for a constant concentration of a reactive gas atmosphere was formulated as

$$U = Y_1 D C_o t/R^2 \qquad (22)$$

where

$$U = \frac{1}{2}\left[1 - (r_c/R)^2\right] - \frac{1}{3}\left[1 - (r_c/R)^3\right] \quad (23)$$

Equation (23) has been verified by experimental data at least in the outer region of a solid body (approximately $(r_c/R)^3 = 0.5$). In the subsequent section comparison will be made on the numerical data resulting from the transient and steady state concentration models, when the radius ratio of R/R_g becomes significantly smaller for the transient model, so that the reactive gas concentration in the gas region becomes practically invariable during the first few minutes of a chemisorption process.

RESULTS AND DISCUSSION

The analytical results presented in the paper deal mainly with the parametric effects (D, Y_1, C_s and R_g) on the absorption of a reacting gas and on the growth rate of the solid product layer. For practical application of dry absorbents in flue gas desulfurization, particle size of solid absorbent is anticipated around the order of a few microns. Particle size in a submicron region may cause serious problems on the dust collecting process. The molecular weight of flue gas mixture should be in the vicinity of the average molecular weight of air owing to nitrogen constituting a major part of the mixture. Considering a flue gas state at 1 atmosphere and 400 K, the anticipated concentration is about 3×10^{-5} mole/c.c. On account of high pollutant gas (e.g. SO_2) generated from fuel combustion, the initial pollutant level, Co, used in the calculation is chosen along the order of magnitude of 10^{-6} mole/c.c. The corresponding molar fraction of the pollutant is about 0.3 percent. Material property parameters, Y_1 and D are considered to be in the range of 50 to 100 c.c./mole for the former and 10^{-5} to 10^{-4} sq. cm/sec for the latter. Particle concentration is related to the various assumed values of R/R_g ratio. These ratios employed in the study vary from 0.01 to 0.1, and hence, their equivalent volumetric ratios should be ranged from 10^{-6} to 10^{-3} c.c./c.c. In flue gas desulfurization, the upper limit of volumetric ratio for the solid-gas mixture is determined by the maximum dust load cacacity of the fly ash collecting equipment, whereas the lower limit is determined by the absorbability of the reactant solids. Calculated results based upon the above varieties of physical conditions are presented in Figs. 2 through 5.

Fig. 2 shows the development of moving boundary r_c/R under various conbinations of R and R/R_g. Curves (1) through (4) have the same R_g amounted to 0.1 cm, while for curves (5) through (7) the R_g value is 0.05 cm and 0.5 cm R_g for curves (8) to (10). Curves (1) and (5) have the same R, but different R_g. Curves (1), (2) and (5) show that during the first 3 minutes, the gas penetration into a solid is substantiallly fast, then it moves inward very slowly during the subsequent period of chemisorption. The phenomena can be reasoned by three factors:

1. The particle volumetric ratios of these three curves are considerably low, ranging from 10^{-6} to 8×10^{-6} c.c./c.c., and hence, the entire change in chemical state of a solid absorbent does not produce any significant effect on the reactant concentration in the gaseous enclosure. Then the whole reactive system resembles a condition of a solid absorbent under a reactive gas atmosphere of a fixed concentration. This gives a favorable condition for the reactant gas penetrating into the solid, especially, if a model is assumed to be controlled by diffusion process.

2. The chance for gas molecules to get into a solid depends essentially on the surface/volume ratio of the particle. This gives smaller particles to perform better chemisorption action than the larger ones. Comparing the characteristics of curves (1) and (5) against these of curve (2) reveals very clearly the importance of surface/volume ratio.

3. The diffusion equation (3) shows that when r_c reaches the inner region of a solid, the second term on the left-hand side of the equation becomes a dominant factor in governing the mass transport phenomena. Physically in this inner region neither $\partial^2 C/\partial r^2$ nor $\partial C/\partial t$ becomes infinite, so it is quite logical that as r_c approaches zero, $\partial C/\partial r$ tends gradually to zero. This leads to develop an asymptotic value of a moving boundary curve of r_c/R vs. t, as shown in Fig. 2.

A general trend has also demonstrated in Fig. 2 that increasing the R/R_g ratio increases the value of r_c/R at the end of 12-min. intervals. This shows the importance of solid-gas volumetric ratio to the depth of gas penetration. Moreover, increasing R/R_g increases the amount of the gaseous reactant to be removed. This situation enhances the higher R/R_g value curves to become flat early in the process of chemisorption.

Fig. 3 presents the relationship between the receding reacting gas concentration in the surrounding atmosphere and the depth of the moving boundary for a 12-min. of chemisorption. The significance of this presentation is that the trend of each curve is governed by the particle relative radius, R/R_g. Taking an example of the curve AIJK, it can be seen that curve AK(R=0.001 cm, $R/R_g = 0.05$) coincides with the others, AJ(R =

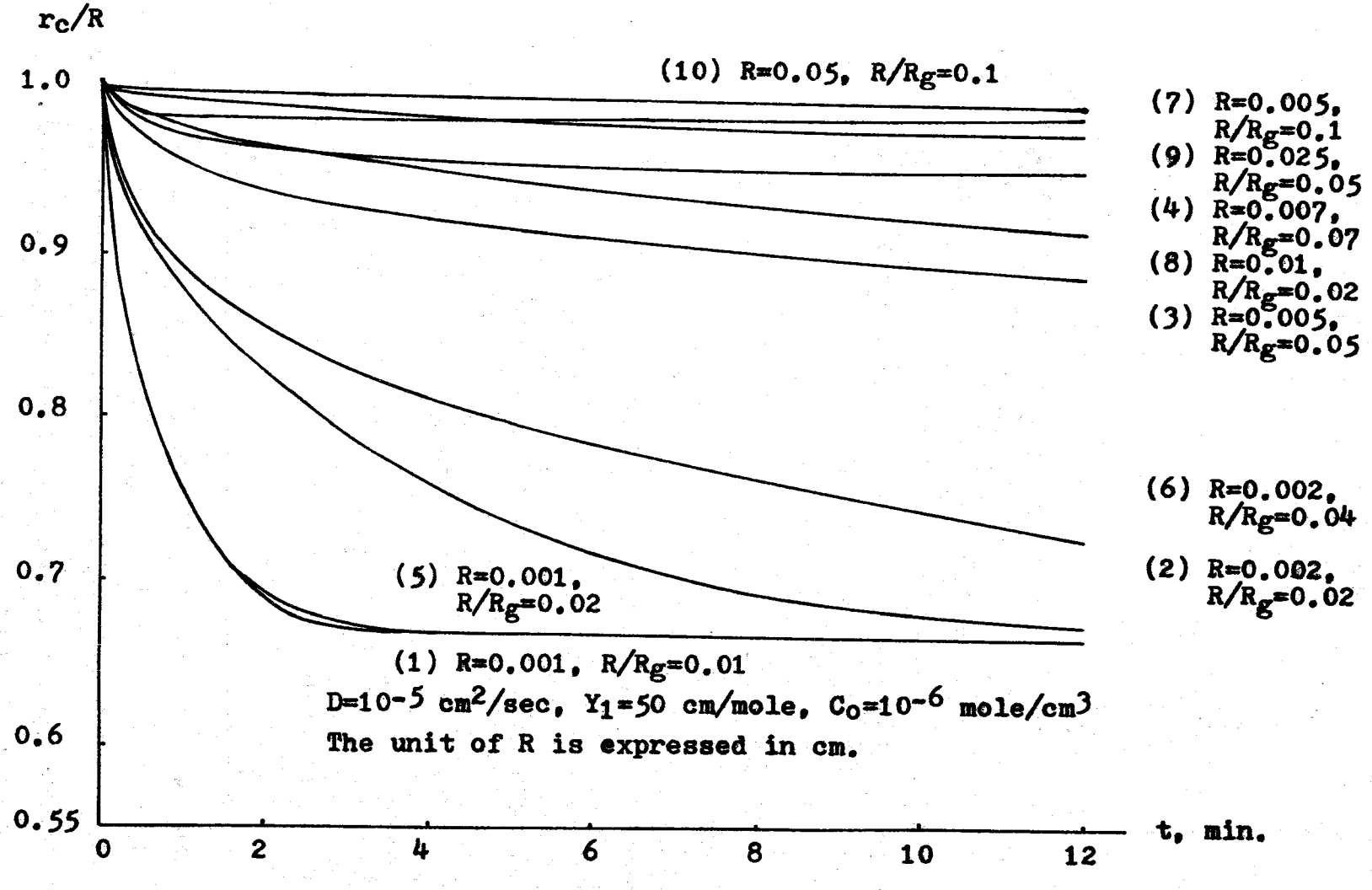

Fig. 2 The development of moving boundary

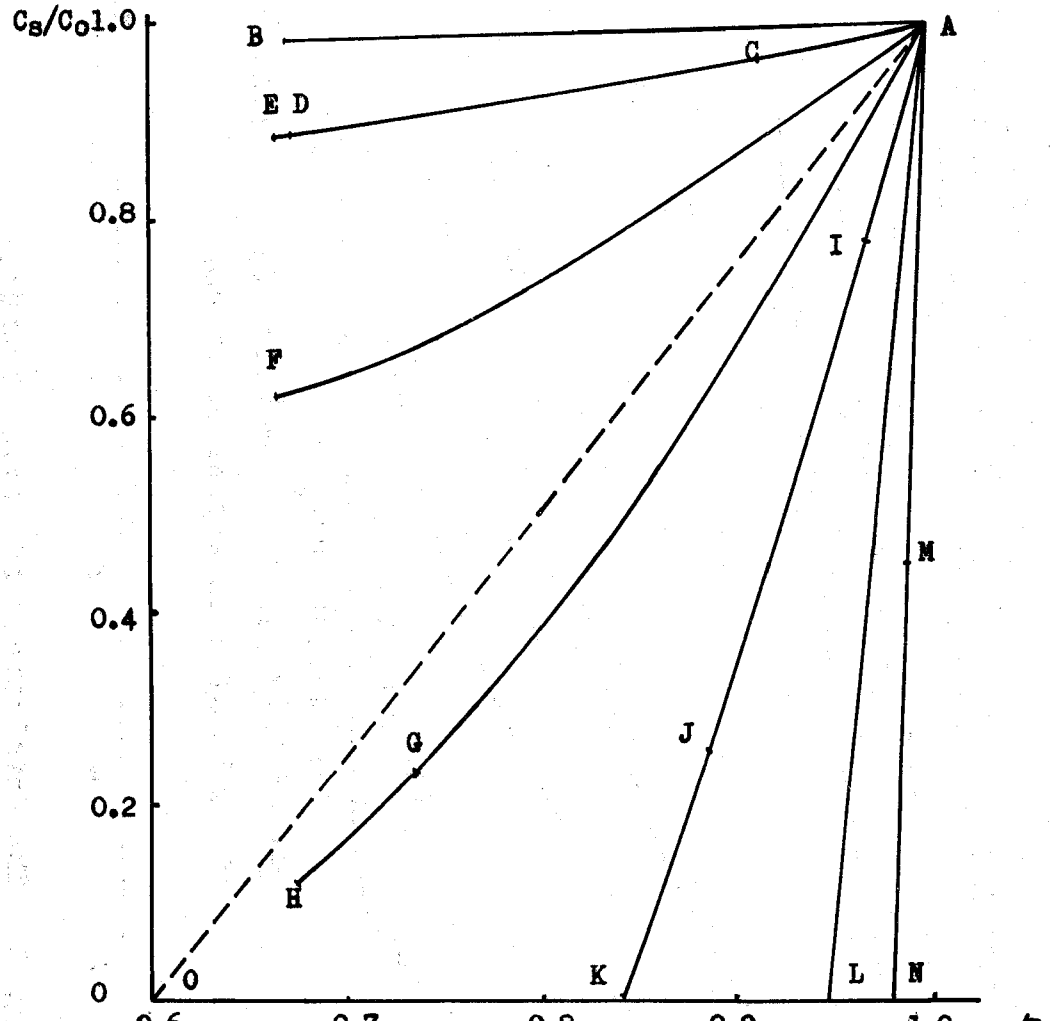

Curve	AB	AC	AD	AE	AF	AG	AH	AI	AJ	AK	AL	AM	AN
R, μ	1	10	2	1	1	2	1	25	5	1	7	50	5
R/R_g	0.01	0.02	0.02	0.02	0.03	0.04	0.04	0.05	0.05	0.05	0.07	0.10	0.10

Fig. 3 Relationship between reduction of surrounding gas concentration and depth of moving boundary.

0.005 cm, R/R_g = 0.05) and AI(R = 0.025 cm, R/R_g = 0.05). The only discrepancy among these three curves is the final values of C_s/C_o and r_c/R_g at the end of 12-min. of penetration. Thus, the curve AIJK reveals that the smaller the dimeter of a particle, the deeper the penetration occurs in a solid body within a given interval of time (i.e. 12-min. for the present study). The Fig. further demonstrates that increasing R/R_g ratio increases the slop of a curve. Consequently, optimum curves should lie in the vicinity of the line AO, because around the point O an absorbent is fully utilized and, at the same time, the reactant gas concentration in the surrounding gas region reduces to a considerably low level. Curves located in the upper left corner of the line AO present no significant removal of the reactant gas from the gas region because of lower particle concentration. On the other hand, curves located in the lower right corner of the line indicate poor utilization of solid absorbents because the formation of product layer is too thin. Furthermore, curves near the optimum line AO reveal markedly sensitive to the changes of R/R_g. This indication is essentially important to choosing a proper particle size in order to achieve an economical use of a solid absorbent. In Fig. 3, the global trend demonstrates that using fine particles can achieve higher absorption efficiency. However, fine particles of waste-absorbent may cause difficulties in dust collecting system. The optimization of using fine particles is beyond the scope of the present study.

Fig. 4 shows parametric effects of D, Y_1 and Co on the gas penetration process under an optimum condition such as curve AG in Fig. 3. The diffusivity D of curve AC in Fig. 4 is greater than that of curve AB by a factor of 10. By comparing these two curves, we can readily see that parameter D does not alter substantially the grobal characteristics of the two curves (e.g., their slopes, curvatures, etc.). If comparison is made on curves AB' and AC', it demonstrates that, in the early stage of chemisorption (when t = 2 min.), the gas penetration process is influenced markedly by increasing diffusivity. But the situation fades away exponentially as the penetration process approaches the asymptotic region. This can explain why the concentration C_s/Co difference between points B and C is so little. For curve AD the value of Y_1 is greater than the corresponding parameter for curve AB by a factor of 2. At the end of 12 min., the value of C_s/Co for curve AB is lower than that for curve AD by 33 percent. The penetration at point D gains 8 percent deeper than that at point B. This situation can be attributed to a fact that a higher value of Y_1 requires a large amount of solid absorbent to react with each mole of the reactive gas. For the calculated results of curve AD, the moving boundary r_c at the end of 12-min. penetration is quite close to its asymptotic value.

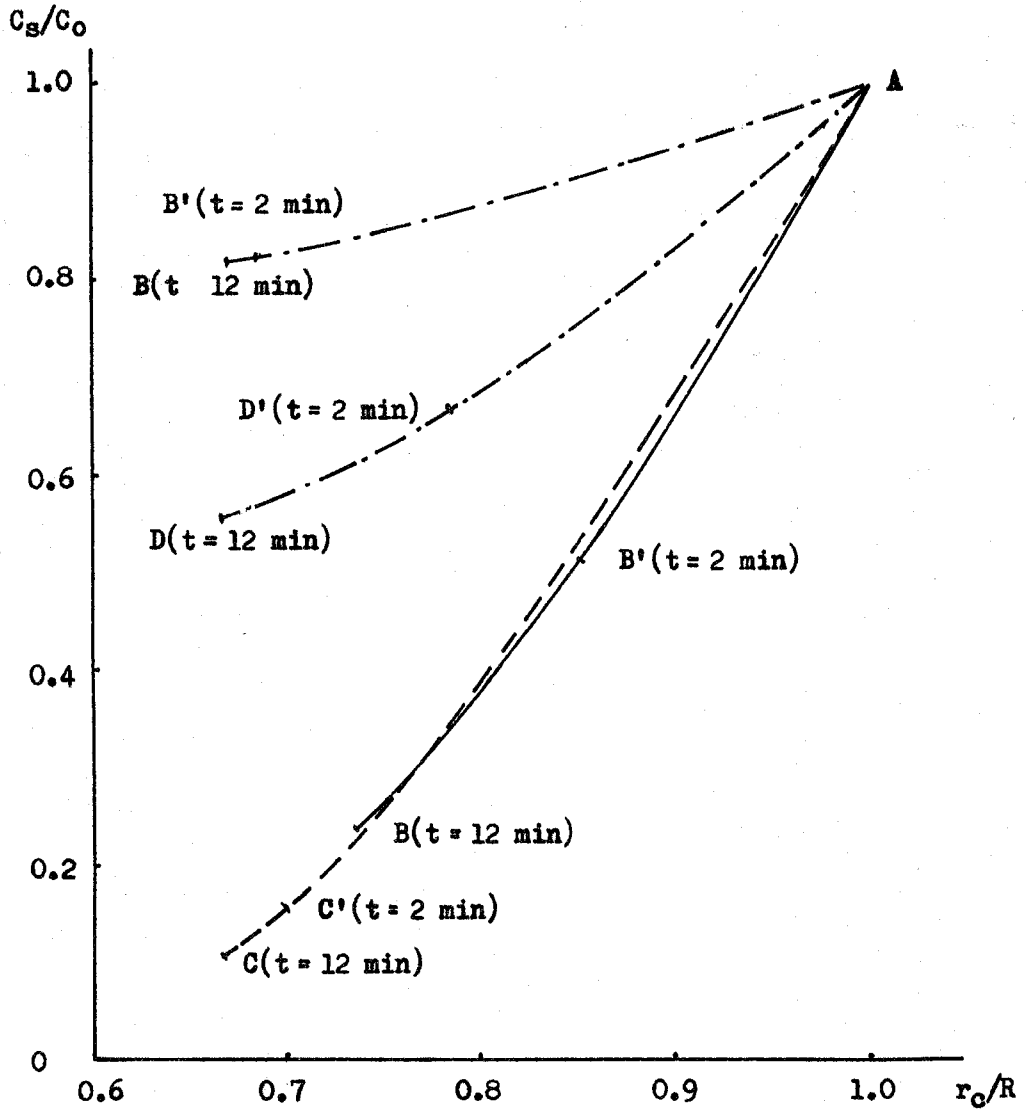

	R, μ	R/R_g	D, cm^2/sec	Y_1, cc/mole	C_o, mole/cc
AB	2	0.04	10^{-5}	50	10^{-6}
AC	2	0.04	10^{-5}	50	10^{-6}
AD	2	0.04	10^{-5}	100	10^{-6}
AE	2	0.04	10^{-5}	50	5×10^{-6}

Fig. 4 Parametric effects of D, Y_1 and C_o on the reduction of surrounding gas concentration.

Therefore, the increment of penetration appearing on curve AD is relatively small as compared with curve AB. Curve AE shows the effect of increasing concentration Co on the gas penetration process. The Co value of curve AE is higher than that of AB by a factor of 5. Since at the end of 12-min penetration, the moving boundary of curve AE reaches the neighborhood of its asymptotic value, increasing the initial gas concentration does not increase significantly the penetration demonstrating on curve AE as expected. Because of higher initial concentration Co and the asymptotic value of a moving boundary, the nondimensional reacting gas concentration C_s/Co at point E becomes much higher than that at point B by 75 percent. As compared with points B', C', D' and E' in Fig. 4, it can be seen that in the early stage of gas penetration (e.g. t = 2 min.), the characteristic curves of C_s/Co vs r_c/R of an absorbent is very sensitive to the parameters of Y_1, Co and D.

Fig. 5 shows the comparison of calculated data based on the closed form equation (17) and the semi-analytical equation (22). Eq. (22) is derived from the assumption of a constant reactive gas concentration bounded within a region between R_g and R. In order to make the comparison of these two equations on the same basis, a large value of R_g was used in the calculation so that the value of $C_s(t)$ will be approximately a constant when $r_c < R$. In the figure, a value of $L[= 1- (r_c/R)^3]$, which can be converted from the parameter U, represents a volumetric consumption of an absorbent in a dimensionless form. The line AB stands for the half consumption of the absorbent. The comparison of accuracy between equations (17) and (22) will be made on the basis of half consumption level. Two reasons can be explained for the choice of the half consumption basis: (a) the validity of equation (22) has been proved to be reasonably accurate in the outer region of the solid; and (b) due to the existence of an asymtote for each moving boundary curve (i.e., r_c/R vs. t), it seems that the region of interest for practical uses of a solid absorbent may be in the outer portion of the particle. Particular points C, D, E and F on the curves of equation (22) have the same amount of penetration time t required for their counterpart points G, H, I and J on curves resulted from equation (17). It can be seen that discrepancies for the values of L resulted from these equations at the half consumption level are about 3 percent. But it also reveals that discrepancy increases with increasing the values of L or U. Finally, it can be verified at least that the closed form solution of equation (17) for a diffusion control model has reasonable accuracy in the outer region of a solid absorbent.

CONCLUSION

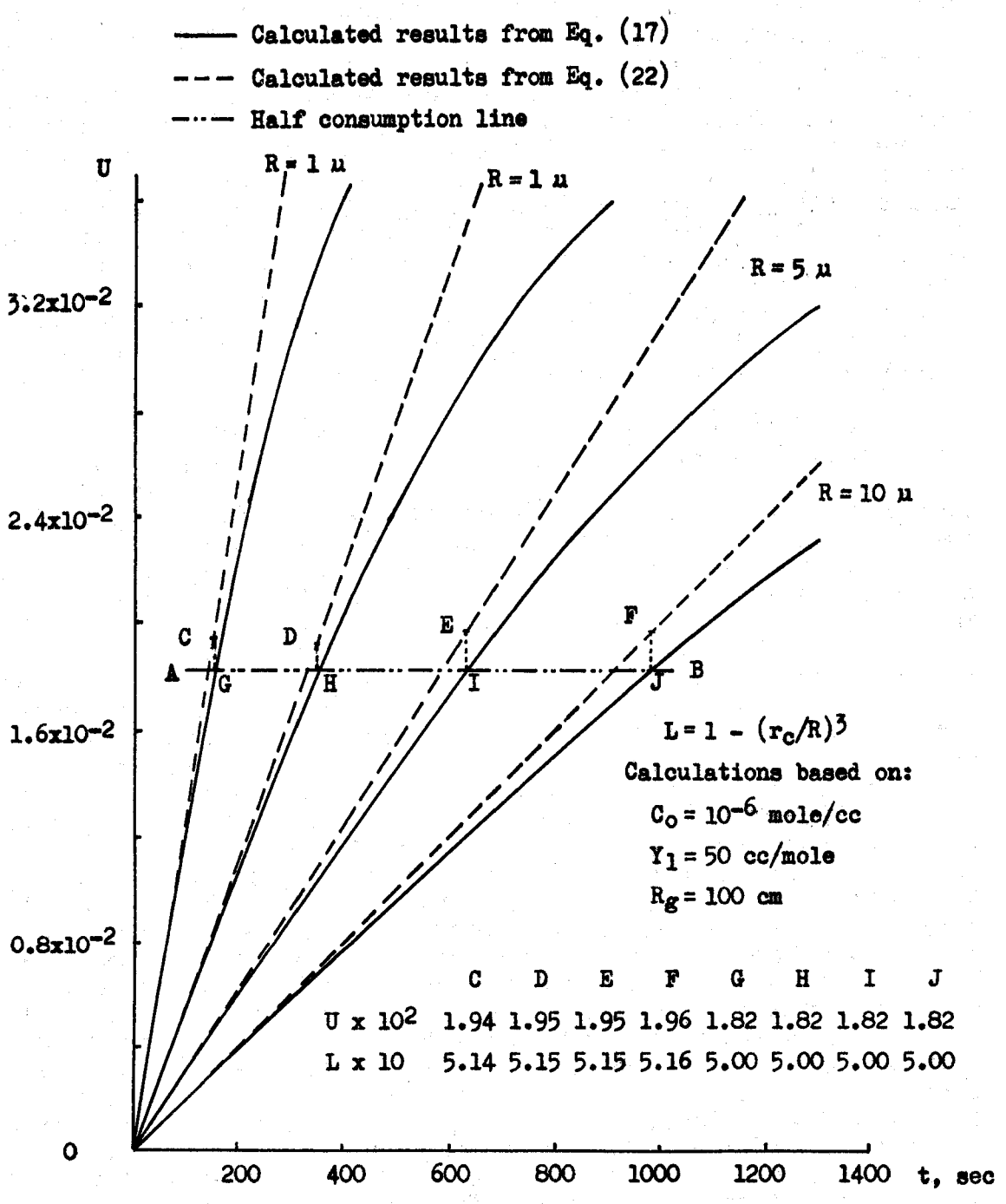

Fig. 5 Comparison of calculated results based on equations (17) and (22).

A diffusion control model of gas-solid reaction in an unsteady state of gas concentration atmosphere has been studied for the simulation of a solid absorbent in a SO_2 contaminated flue gas system. Parameters effects on the removal of pollutant concentration in a gas phase and the depth of gas penetration into a solid absorbent are discussed in general cases of various particle sizes and densities. Upon the analysis of calculated results, some conclusion can be drawn as follows:

1. The time rate of the moving boundary is very sensitive to the surface/volume ratio of a solid particle.
2. An asymptotic value of r_c appears near the center of the solid sphere.
3. The characteristics of curves C_s/Co vs r_c/R depend strongly upon the parameter R/R_g. Curves with the same R/R_g, but different R, occur on the same line.
4. Near the optimum region, the removal of the reactive gas concentration is very sensitive to the relative radius R/R_g of the particle and atmosphere.
5. Near the optimum region, the removal of reacting gas from the enclosed gaseous system is influenced strongly by the parameters, Co, D and Y_1, if the chemisorption time is reasonably short, for example, at the order of 2-min. or less.
6. In comparison with the published data, the present model is considerably accurate within the outer region of a solid absorbent.

REFERENCES

1. Mecrea, D. H., Mayers, J. G., and Forney, A. J., " Evaluation of Solid Absorbents for Sulfur Oxides Removal from Stack Gases," Paper No. EN-35A, Proceedings, Second International Clean Air Congress, Washington, D. C., Dec. 6-11, 1971.
2. Lee, G. K., "Control of Oil Ash Deposits and Pollution Abatement by an Additive, " The University of Sheffield, Fuel Society Journal, Vol. 20, 1969, pp. 8-176.
3. Ishibashi, Y., and Morita, M., "Study on Mechanism of Reaction with Sulfur Dioxide of Lime-stone Powder Blown into Combustion Gas," Paper No. 3413, The Japan Chemical Society, 24th Annual Meeting, Tokyo, March 1971.
4. Karman, Th. Von, "Uber Laminare und Turbulente Reibung," Z. angew. Math. Mech., Vol. 1, 1921, p. 237.
5. Vugjannovic, B., "An Approach to Linear and Nonlinear Heat -Transfer Problem Using a Lagrangian," AIAA Journal, Vol. 9, 1971, pp. 131-134.
6. Goodman, T. R., "The Heat-Balance Integral and Its Application to Problems Involving a Change of Phase," Transactions of the ASME, Vol. 80, 1958, pp. 335-342.
7. Weisz, P. B., and Goodwin, R. D., "Combustion of Carbonaceous Deposits Within Porous Catalyst Particles, I. Diffusion-Controlled Kinetics," Journal of Catalysis, Vol. 2, 1963, pp. 397-401.

STABILITY OF FINE WATER DROPLET CLOUDS

Y. Kousaka, K. Okuyama, K. Sumi and T. Yoshida
Chemical Engineering Department
University of Osaka Prefecture
Sakai, Japan 591

ABSTRACT

It will be important to evaluate the instability of fine water droplets which are contained in an industrial exhaust gas and are required to be collected from the gas. The rate of evaporation of monodisperse water droplet clouds was numerically calculated assuming the cellular model, and was discussed comparing with that of a single isolated water droplet which can be analytically obtained. The critical conditions where the droplet cloud can be stable were evaluated as the function of droplet number concentrations, droplet sizes and initial conditions of the surrounding air. The equilibrated system, where a droplet cloud is steadily mixed with an unsaturated air such as leaking air into a collector system, was also analyzed, and some of the analyses were verified by experiment.

INTRODUCTION

It is well known that under a certain supersaturation of water vapor excess water vapor condenses upon aerosol particles as the condensation nuclei to generate small water droplets. Such water droplet clouds are usually found when a combustion gas is cooled, a highly humid gas at a high temperature is mixed with one of a low temperature, and steam is injected into a gas. These droplets often have diameters less than ten microns and they are thought to be unstable because of their high vapor pressure at the surface. When these droplets being contained in an industrial exhaust gas are required to be collected from the gas, it will be necessary to evaluate the effect of instability of droplets or the decrease in droplet sizes and number concentrations in a collector system

under various operating conditions. The stability of droplet clouds is also important in measuring droplet size distribution and in evaluating the behavior of atmospheric aerosols.

Prior to discuss the stability of water droplet clouds, evaporation of a single isolated water droplet is briefly reviewed and discussed. Then the rate of evaporation of monodisperse pure water droplet clouds, which are led uniformly into a closed vessel initially containing air having certain humidity and temperature, is discussed using a cellular model[1,2], and comparing with that of a single isolated water droplet. The main purpose in this discussion is to evaluate the lifetime or the time required to be equilibrated of water droplets in terms of various initial air conditions, initial sizes and number concentrations of droplets. For the equilibrium state of droplet clouds, the system where a droplet cloud is steadily mixed with unsaturated fresh air is also discussed from enthalpy and material balance of the system for various conditions.

As the experimental technique, the ultramicroscopic size analysis previously developed by the authors[3] was applied. Because of the difficulty in measuring the unsteady size change during rapid evaporation, most of the experiment were limited to verify the analysis of the equilibrium state of droplet clouds.

RATE OF EVAPORATION OF A SINGLE ISOLATED WATER DROPLET

To clarify the difference between the life time of an isolated droplet and that of a droplet cloud, some typical and simplified analyses on evaporation of an isolated droplet are reviewed and discussed in this section.

Case 1 to 3 in Tables 1 and 2 show the typical analyses for the evaporation of an isolated droplet.

The surrounding temperature, T_∞, and the surrounding saturation, S, are usually assumed to be constant during evaporation of an isolated droplet, that is, $T_\infty=T_{\infty 0}$ and $S=S_0$.

Case 1 in Table 1 is the well known relationship[1], but it can not be applied to rapid evaporation of a small and volatile droplet, such as small water droplet, since the effect of evaporative cooling of the droplet is not taken into account. In Case 2, on the other hand, the effect of evaporative cooling is considered but the Kelvin effect is neglected, and thus this case can be applied to a large water droplet evaporation[4]. In Case 3, both the evaporative cooling and the Kelvin effect are taken into account, making the following approximations in temperature and vapor pressure in order to obtain an analytical solution.

1) $S_0<1$ (Table 1): The change in the absolute value of temperature fall, $(T_\infty-T_0)/T_\infty$, with the proceeding of evaporation is large, but the

Table 1 Typical analyses for evaporation of a single isolated droplet ($S_0<1$)

	CASE 1	CASE 2	CASE 3
investigator	Fuchs	Davies	ours
basic equation	$\frac{dr'}{dt'} = -\frac{DM}{r'\rho_S R}\left\{\frac{P_0(T_0,r')}{T_0} - \frac{S P_S(T_\infty)}{T_\infty}\right\}$		
T_∞ , S	constant ($T_\infty = T_{\infty 0}$, $S = S_0$)		
P_0	$P_0 = P_S(T_\infty)\left(1+\frac{2M}{\rho_S R T_\infty r'}\right)$	$P_0 = P_S(T_0)$	$P_0 = P_S(T_0)\left(1+\frac{2M}{\rho_S R T_0 r'}\right)$
T_0	$T_0 = T_\infty$	$T_0 = T_\infty - \frac{LDM}{KR}\left\{\frac{P_0}{T_0} - \frac{SP_S}{T_\infty}\right\}$	$T_0 = T_\infty - \frac{LDM}{KR}\left\{\frac{P_0}{T_0} - \frac{SP_S}{T_\infty}\right\}$
temp. and conc. field around the droplet	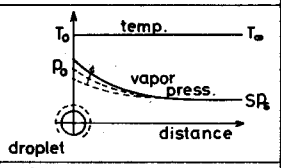	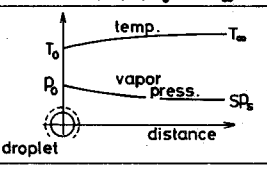	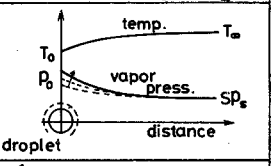
time dependent change in radius	$\frac{1}{2}(r_0'^2 - r'^2) - c_1(r_0' - r') + c_1^2 \ln\frac{r_0'+c_1}{r'+c_1} = c_2 t'$	$r_0'^2 - r'^2 = \frac{2DM}{\rho_S R}\left\{\frac{P_0(T_0)}{T_0} - \frac{SP_S(T_\infty)}{T_\infty}\right\} t'$	$\frac{1}{2}(r_0'^2 - r'^2) - c_3(r_0' - r') + c_3^2 \ln\frac{r_0'+c_3}{r'+c_3} = c_4 t'$
life time	$t'_{lK} = \frac{1}{c_2}\left\{\frac{1}{2} r_0'^2 - c_1 r_0' + c_1^2 \cdot \ln\frac{r_0'+c_1}{c_1}\right\}$	$t'_l = \frac{\rho_S R r_0'^2}{2DM} \times \frac{T_\infty T_0}{T_\infty P_0(T_0) - T_0 S P_S(T_\infty)}$	$t'_l = \frac{1}{c_4}\left\{\frac{1}{2} r_0'^2 - c_3 r_0' + c_3^2 \cdot \ln\frac{r_0'+c_3}{c_3}\right\}$

Table 2 Typical analyses for evaporation of a single isolated droplet ($S_0=1$)

	CASE 1	CASE 2	CASE 3
P_0	$P_0 = P_S(T_\infty)\left(1+\frac{2M\sigma}{\rho_S R T_\infty r'}\right)$	$P_0 = P_S(T_0)$	$P_0 = P_S(T_0)\left(1+\frac{2M\sigma}{\rho_S R T_0 r'}\right)$ $\fallingdotseq (a_0 + a_1 T_0)\left(1+\frac{2M\sigma}{\rho_S R T_0 r'}\right)$
T_0	$T_0 = T_\infty$	$T_0 = T_\infty$	$T_0 = T_\infty - \frac{LDM}{KR}\left\{\frac{P_0}{T_0} - \frac{SP_S}{T_\infty}\right\}$ $\fallingdotseq \frac{(c_7 - c_8/r') + \sqrt{(c_7 - c_8/r')^2 - 4c_5 c_6/r'}}{2c_5}$
temp. and conc. field around the droplet	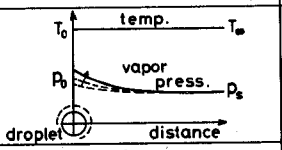	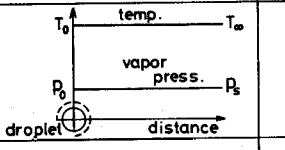	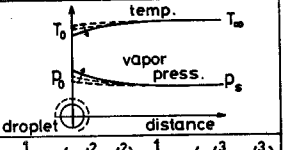
time dependent change in radius	$r_0'^3 - r'^3 = 6D\sigma P_S(T_\infty)\left(\frac{M}{\rho_S R T_\infty}\right)^2 t'$	$r' = r_0'$	$\frac{1}{2}c_6(r_0'^2 - r'^2) + \frac{1}{3}c_7(r_0'^3 - r'^3) + \{F(r_0') - F(r')\} = c_8 t'$
life time	$t'_{lK} = \frac{r_0'}{6D\sigma P_S(T_\infty)}\left(\frac{\rho_S R T_\infty}{M}\right)^2$	$t'_l = \infty$	$t'_l = \frac{1}{c_8}\left\{\frac{1}{2}c_6 r_0'^2 + \frac{1}{3}c_7 r'^3 + F(r_0') - F(0)\right\}$
note	$F(r') = \frac{X^{1.5}}{3c_9} - c_{12}(2c_9 r' + c_{10})X^{0.5} - c_{14}\ln\left\{\frac{2c_9 r' + c_{10}}{\sqrt{c_{13}}} - \sqrt{\frac{(2c_9 r' + c_{10})^2 + 1}{c_{13}}}\right\}$, $X = c_9 r'^2 + c_{10} r' + c_{11}$		

dependence of the value on the droplet size is very small in this case. Thus the droplet temperature, T_0, was approximated as the sixth row in Table 1, where the vapor pressure at the droplet surface, p_0, was substituted by the value of the fifth row putting initial droplet radius r'_0 into r'.
2) S_0=1 (Table 2) : The change in the absolute value of temperature fall, $(T_\infty - T_0)/T_\infty$, is small, but the dependence of the value on droplet size is not negligible in this case, as shown in Figure 1.Because of the small change in droplet temperature, $p_s(T_0)=a_0+a_1T_0$ was assumed and then p_0 was approximated as the second row in Table 2 leaving r' to be variable. These approximation gives the analytical solution of T_0 as shown in the lower equation of the third row in Table 2.

Figure 1 shows the droplet size change for Cases 1, 2 and 3. The abscissa is the diemnsionless time normalized by the life time of Case 1, t'_{1k}. The curves of Case 3 almost agree with those of Case 2 except the case of S_0=1. The difference at S_0=1 is reasonable because the Kelvin effect is neglected in the analysis of Case 2. It is seen that the analysis of Case 1 can not be applied to evaporation of water droplet because the temperature fall is neglected in this case.

In the above analyses, the evaporation coefficienct was assumed to be unity.

RATE OF EVAPORATION OF A WATER DROPLET CLOUD

In this section, the rate of evaporation of a water droplet cloud is discussed using the cellular model[1,2]. In the cellular model, a droplet cloud, where the droplets are distributed equidistantly each other, is assumed, and the cloud is divided into a number of identical

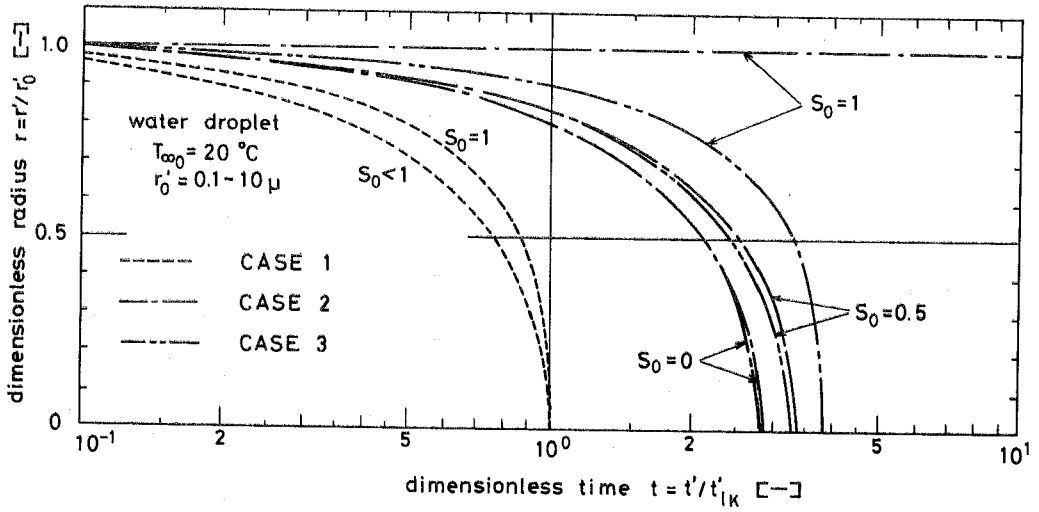

Figure 2 Time dependent change in radius of a single isolated water droplet for Cases 1, 2 and 3

cubic cells each of which is supposed to contain a single droplet in the center. The length of the edge of such a cube is then given as:

$$b = \sqrt[3]{1/n_0'} \tag{1}$$

No heat and mass transfer is assumed across the boundary of each cell, and the change in temperature and humidity of the surrounding of the droplet, which is caused by droplet evaporation, is assumed to be evaluated within each independent cell. Then the rate of change in droplet radius r' in the cell can be given as the following equation assuming evaporation coefficient to be unity[1,5].

$$\frac{dr'}{dt'} = -\frac{DM}{r'\rho_s R}\left\{\frac{p_0(T_0,r')}{T_0} - \frac{Sp_s(T_\infty)}{T_\infty}\right\}\left\{1 + \frac{p_0(T_0,r')+Sp_s(T_\infty)}{2p_t}\right\} \times \left\{\frac{Kn+1}{1.333Kn^2+1.71Kn+1}\right\} \tag{2}$$

S in the equation represents the degree of saturation, and $p_0(T_0,r')$ represents the vapor pressure at the surface of a droplet, which is given by the Kelvin's equation:

$$p_0(T_0,r') = p_s(T_0)\exp\left(\frac{2M\sigma}{\rho_s RT_0 r'}\right) \tag{3}$$

The fall in temperature of an evaporating droplet is given by the following equation taking account of Stefan flow.

$$T_0 = T_\infty - \frac{LDM}{KR}\left\{\frac{p_0(T_0,r')}{T_0} - \frac{Sp_s(T_\infty)}{T_\infty}\right\}\left\{1+\frac{p_0(T_0,r')+p_\infty(T_\infty)}{2p_t}\right\} \tag{4}$$

The rate of evaporation of a single droplet in a cell will be determined by the above equations, if the change in temperature T_∞ and vapor pressure $p_\infty(T_\infty)$ at the periphery of the cell are evaluated as follows.

While the change of the system is unsteady, the unsteady fields of temperature and pressure are established around each evaporating droplet. It is difficult, however, to calculate the change in particle radius strictly taking account of the unsteady fields. Then a quasi-stationary analysis, where temperature and pressure fields were considered to be constant during each step of time, was made. In calculation, the change in droplet radius was first evaluated by numerically giving the initial conditions.

When the radius of a spherical droplet, r_1', decreases to r_2' during a small time step according to Eq.(2), the quantity of evaporated water vapor, or water vapor diffusing to the medium, per unit mass of dry air

can be given as follows,

$$\Delta H_e = 4\pi(r_1'^3 - r_2'^3) n_w \rho_s / 3 \quad (5)$$

where, $n_w = n_0' \cdot v_H$ (6)

In consequence of evaporation of a droplet, there are an increase in humidity and a simultaneous fall in temperature of air. These changes are indicated by the slope of the adiabatic change in the humidity chart as shown in Figure 2. And relation among the temperature, the humidity and the degree of saturation during the successive evaporation will be given by the following expressions.

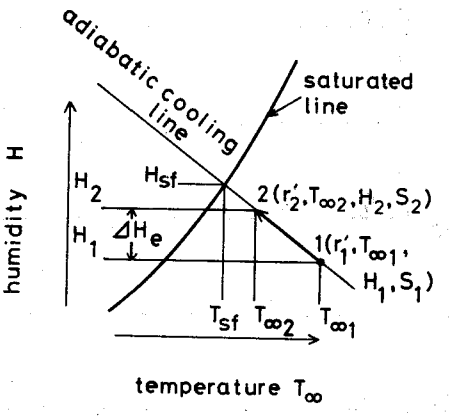

Figure 2 Change in humidity and temperature due to evaporation

$$T_{\infty 2} = T_{\infty 1} - \Delta H_e L/(0.24 + 0.45 H_2) \quad (7)$$

$$H_2 = H_1 + \Delta H_e \quad (8)$$

$$S_2 = p_\infty(T_{\infty 2})/p_s(T_{\infty 2}) = H_2(0.621+H_s)/\{H_s(0.621+H_2)\} \quad (9)$$

The subscripts 2 denotes the value after short time step. In deriving Eq.(7), the quantity of heat transferred to the droplet from the media was assumed to be equal the amount lost in evaporation. The denominator of the second term of Eq.(7) is the specific heat of air. This assumption implies that the effect of heat accumulation in the droplet on the temperature fall of the surrounding air is negligible and that T_∞ almost equals to the mean bulk temperature of surrounding air, because of the flat temperature profile excluding the very vicinity of the droplet. The humidity of the surrounding after slight evaporation of the droplet is then given by Eq.(8), and Eq.(9) is obvious from the definition.

The values obtained by Eqs.(7), (8) and (9) are substituted into Eq.(4) to obtain the droplet temperature for the successive time step. In the calculation at the second time step, these values obtained above were used as the same way as that at the first step, and this step was repeated until the driving force of evaporation became zero. The initial value of T_0, or T_0 at the first time step was assumed to be $T_{\infty 0}$. The temperature dependence of the physical properties appearing in the above equations was taken into consideration in the computation.

Some of the results thus calculated are shown in Figures 3 and 4. Figure 3 shows the time dependent change in radius of evaporating droplets under various particle number concentrations n_0' in initially saturated air (S_0=1). It can be seen that the fine droplets of micron order and having low number concentration tend to evaporate even in

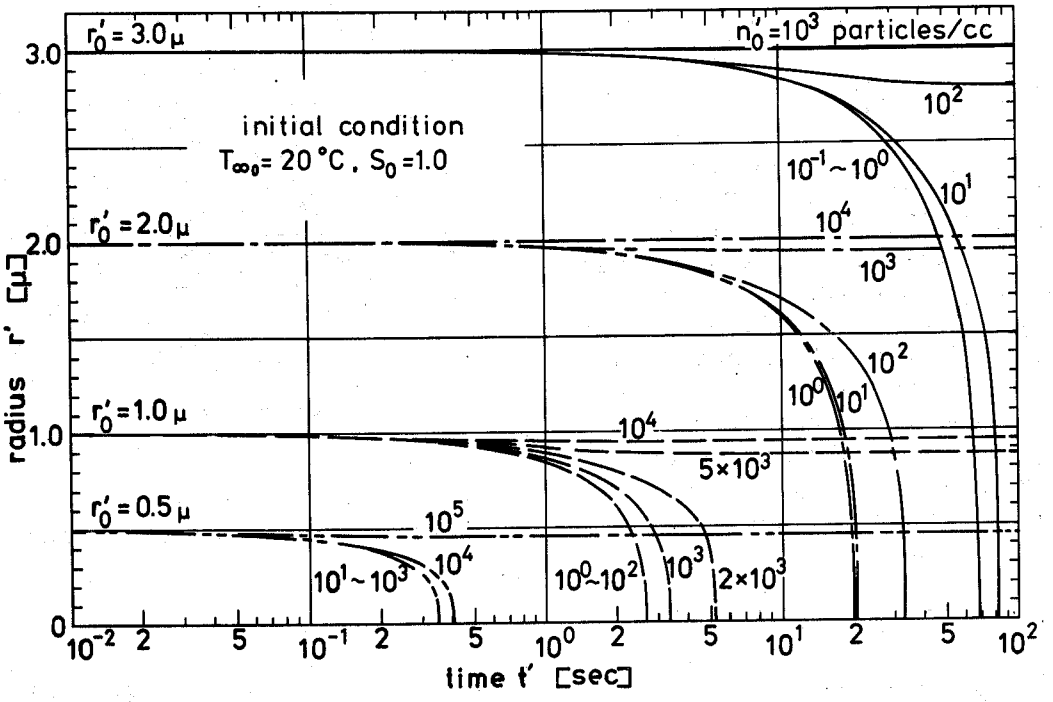

Figure 3 Evaporation of fine water droplet clouds in saturated air

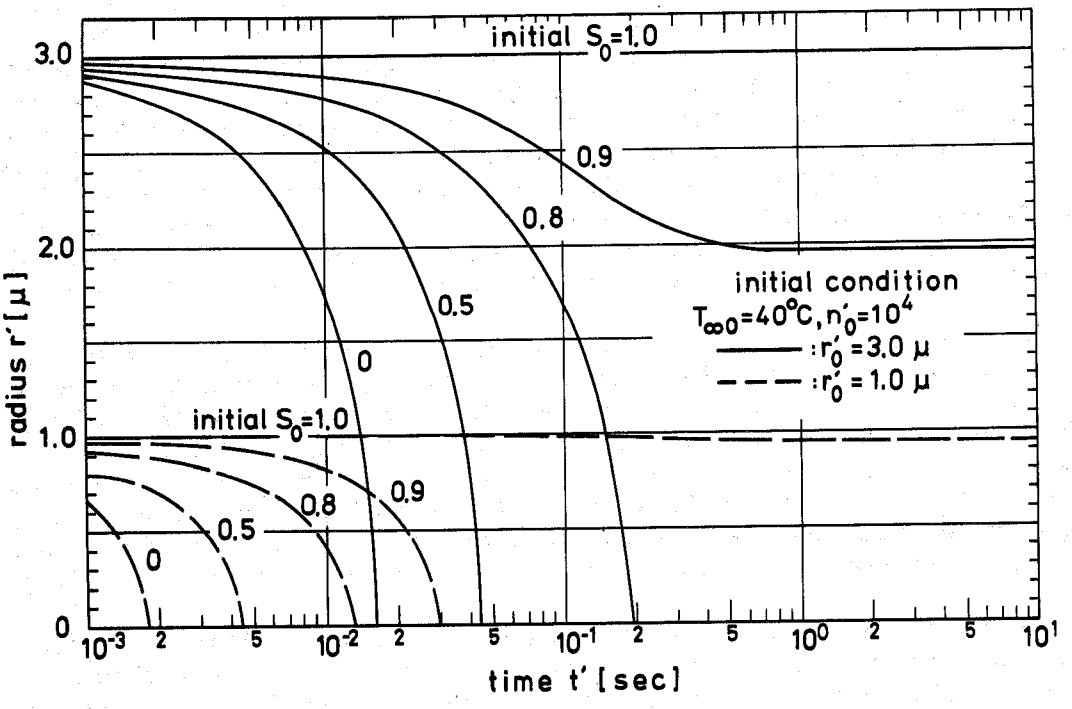

Figure 4 Evaporation of fine water droplet clouds in air having various degree of saturation

saturated air because of the Kelvin effect. With the increase of number concentration n_0', the decreasing rate in droplet radius becomes slow, and at n_0' larger than about 10^5 particles/cm^3 the droplets of 0.5 μ in radius seem to be almost stable because of the humidity rise and the simultaneous temperature fall. Figure 4 shows the dependence of evaporation rate of droplets on the degree of saturation under various conditions. As seen from Figures 3 and 4, the stability of water droplet clouds depends greatly upon the initial degree of saturation S_0 and number concentration n_0'. Under the low values of S_0 and n_0', the quantity of water vapor produced by evaporation of droplets is not enough to saturate the surrounding air and therefore droplets disappear completely. On the other hand, under the high values of S_0 and n_0', droplets continue to evaporate until the equilibrium vapor pressure as given by Eq.(3) is attained and because of the sufficient amount of water vapor to be evaporated in this case, the droplets are stable after a slight change in size.

Figure 5 shows the quantitative illustration of the above description. The solid line in the figure shows the vapor pressure rise dut to Kelvin effect, and the other curves show the rise in supersaturation of the surrounding air due to droplet evaporation taking account of temperature fall in adiabatic change of the system. If the curves of supersaturation are below solid line, evaporation proceeds. If the curves of supersaturation intersect the solid line, evaporation stops at the corresponding droplet sizes because of no driving force to evaporate. If there is no intersection in the figure, such droplet clouds will completely evaporate.

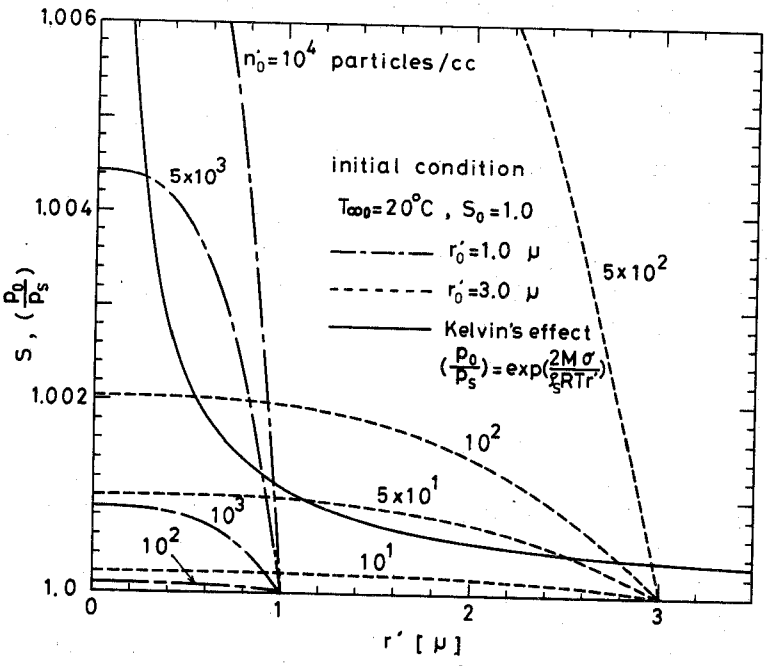

Figure 5 Relation between the vapor pressure rise due to Kelvin effect and the rise in supersaturation of the surrounding air due to droplet evaporation

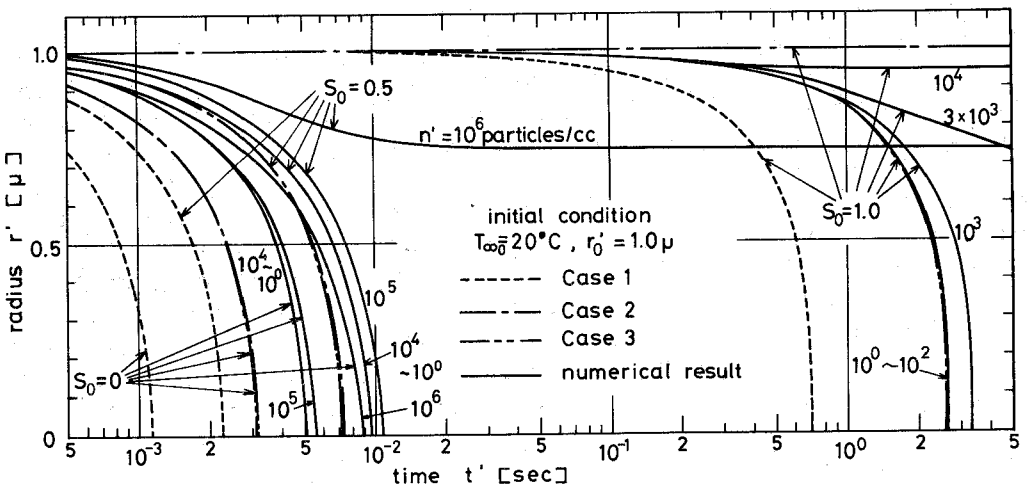

Figure 6 Comparison of time dependent change in radius of a single droplet with those of water droplet clouds at low number concentrations

The curves at low number concentration in Figures 3 and 4 will correspond to the single droplet evaporation. Figure 6 shows the comparison of such curves with those of the single droplet evaporation shown in Tables 1 and 2. Good agreement is found between curves of Case 3 in Tables 1 and 2 and those obtained by numerical calculation for the droplet cloud at low number concentrations. This agreement, on the other hand, suggests the validity of the numerical calculation. Figure 7 shows the similar comparison of life time among the above four cases. Again it is found that the curves for Case 3 agree well with those of the droplet cloud at sufficiently low number concentrations.

Figure 8 shows the critical conditions where the droplet clouds completely evaporate. The upper regions of each curves indicate that the droplet clouds can not evaporate completely. It is seen that submicron droplet clouds are unstable unless droplet number concentrations are sufficiently high.

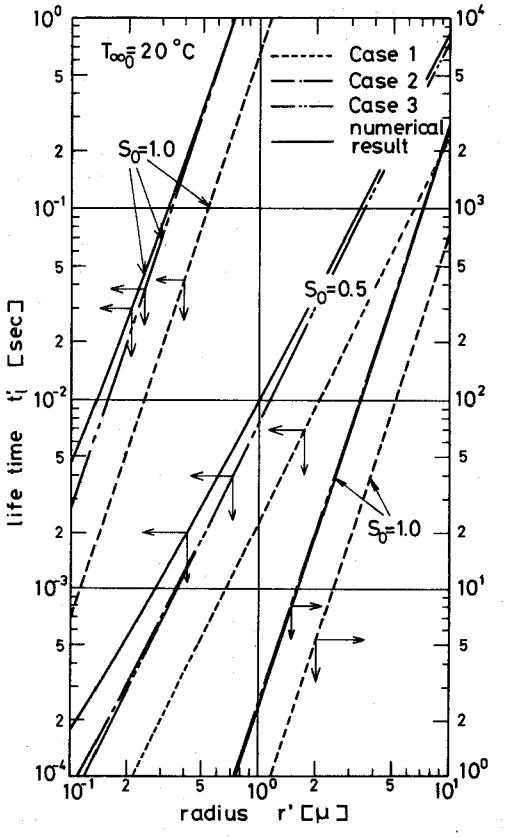

Figure 7 Comparison of the life time of a single droplet with that of a water droplet cloud at sufficiently low number concentrations

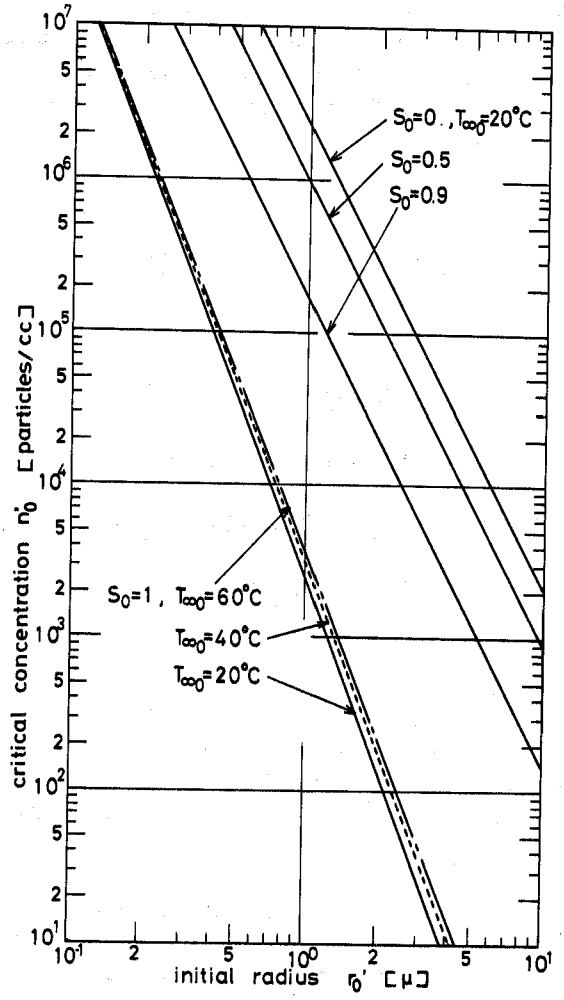

Figure 8 Critical conditions where the droplet clouds completely evaporate

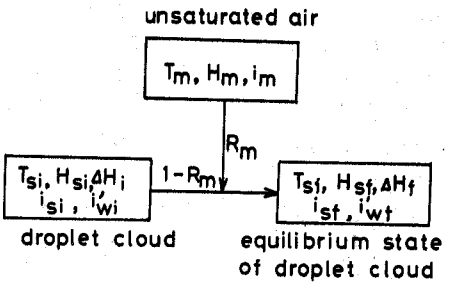

Figure 9 Schematic diagram of the system to be analysed

EVALUATION OF THE CHANGE IN DROPLET SIZE UNDER EQUILIBRIUM STATE BY MIXING OF DROPLET CLOUD WITH UNSATURATED AIR

Since the change in radius of a droplet by evaporation proceeds in a short time, as calculated in the former section, the droplet cloud which we can actually observe will be in the equilibrium state. Therefore there is an importance to analyse the equilibrium state of a droplet cloud for various situations.

Figure 9 shows a schematic diagram to be analysed in this section. Such a system, for instance, may be interpreted by that where an exhaust gas containing a certain amount of small water droplets encounters unsaturated air resulted from some leakage in a dust collector system.

As shown in Figure 9, when air containing droplets is mixed with

unsaturated fresh air at a certain mass ratio, the amount of water droplet containing in the resultant air is expected to be decreased. In such a system the following enthalpy and material balance equations are derived under the assumption of the existence of droplets in the equilibrium state after mixing of air, that is, $\Delta H_f \geq 0$:

(material balance of water)

$$R_m H_m + (1-R_m)H_{si} + (1-R_m)\Delta H_i = H_{sf} + \Delta H_f \qquad (10)$$

(enthalpy balance of the system)

$$R_m i_m + (1-R_m)i_{si} + (1-R_m)\Delta H_i i'_{wi} = i_{sf} + \Delta H_f i'_{wf} \qquad (11)$$

Another expression of Eq.(11) may also be written as follows:

$$R_m\{0.24T_m+(597.1+0.45T_m)H_m\}+(1-R_m)\{0.24T_{si}+(597.1+0.45T_{si})H_{si}\}$$
$$+(1-R_m)\Delta H_i T_{si} = 0.24T_{sf}+(597.1+0.45T_{sf})H_{sf} + \Delta H_f T_{sf} \qquad (11')$$

where, $H_{sf} = f(T_{sf})$ (12)

ΔH in the equations represents the mass of water droplets suspending in air per unit mass of dry air, and R_m the mixing ratio of unsaturated air to resultant air on mass basis of dry air. Since the Kelvin effect is small enough in the case of droplets larger than 0.1 μ in diameter, it was neglected in the following analysis.

In the case of $\Delta H_f=0$ The quantity of water droplets after mixing of unsaturated air, ΔH_f, in Eqs.(10) and (11) decreases with the increase of the mixing ratio of unsaturated air, R_m, and finally ΔH_f becomes zero, that is, all droplets disappear by evaporation. The relation among each variables appears in the above equations at such a critical condition can be calculated by putting $\Delta H_f=0$ in the equations. If the conditions before mixing are known, the values of R_m, H_{sf} and T_{sf} are obtainable from Eqs.(10), (11) and (12). One of the calculated results are shown in Figure 10.

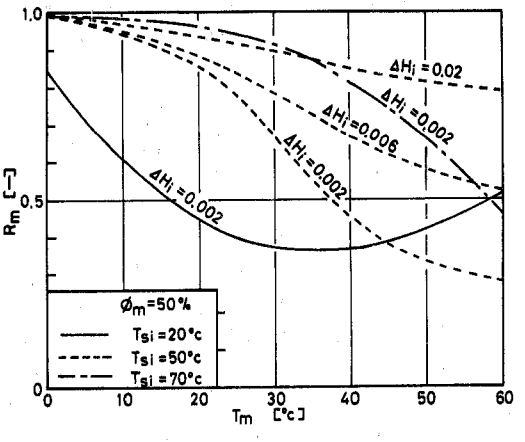

Figure 10 Correlation among mixing ratio R_m, mixing air temperature T_m, droplet quantity contained in air before mixing ΔH_i and temperature of the same air T_{si} ($\Delta H_f=0$)

In the case of $\Delta H_f>0$ The containable quantity of water droplets after mixing of air, ΔH_f kg water per kg dry air, can be essentially evaluated by Eqs.(10), (11) and (12). The relation among the variables in

the equations, however, is more complicated in this case. One of the calculated results are shown in Figure 11.

Evaluation of ΔH_f and D_{vf}— If the initial conditions of a droplet cloud and the state of unsaturated mixing air are given, the quantity of water droplets after mixing of air, ΔH_f, can be evaluated as described above. The volume mean diameter of the droplets after mixing of unsaturated air is then evaluated knowing the number concentration of the droplets, n_w, as follows.

$$D_{vf} = \left(\frac{\Delta H_f}{(\pi/6) n_w \rho_s} \right)^{1/3} \qquad (13)$$

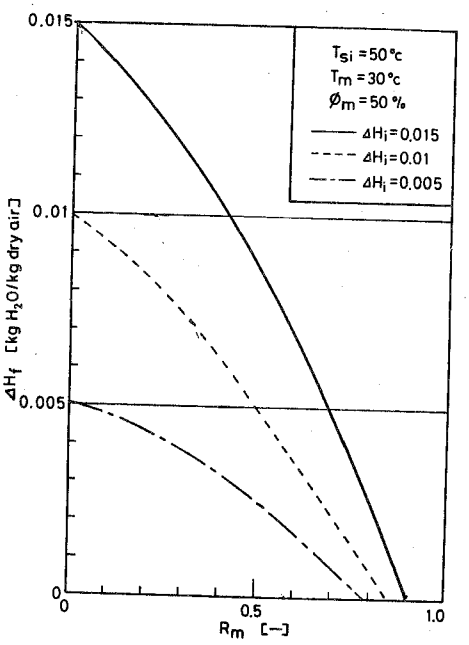

Figure 11 Effects of the quantity of initial droplets on those after mixing of unsaturated air

EXPERIMENTAL APPARATUS AND METHOD

Figure 12 shows the schematic diagram of the experimental apparatus

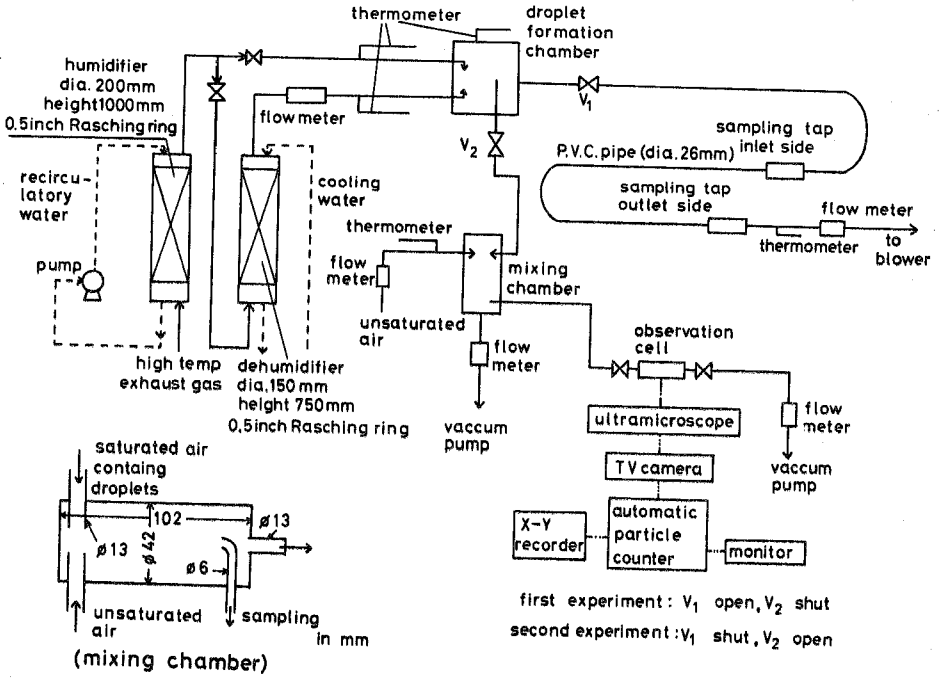

Figure 12 Schematic diagram of the experimental apparatus

to examine the analysis. The water droplet cloud was steadily generated by mixing hot saturated air with cold saturated air in the first experiment to see the rate of evaporation of water droplet cloud. The hot saturated air contains small dust particles having diameters around 0.05 μ which are generated in burning fuel gas. The gas is mixed with cold saturated air to produce supersaturation which causes droplet formation on the dust particles as condensation nuclei. Thus obtained saturated air containing a certain amount of small water droplets was continuously led into a vinyl chloride pipe with diameter of 26 mm to make a turbulent flow. The length of the pipe was 10 m, and at inlet and outlet of the pipe the aerosols were sampled with isokinetic condition. The second experiment to observe the analysis of droplet size change under mixing of unsaturated air was made by introducing the saturated air containing water droplets into a mixing chamber instead of the pipe, where unsaturated air was mixed. Then a part of the mixture was drawn out to observe size distribution and concentration of droplets by the ultramicroscopic method[3].

EXPERIMENTAL RESULTS AND DISCUSSION

Figure 13 indicates the comparison of the particle size distribution at inlet with that at outlet of the pipe. The residence time of droplets in the pipe is about 4 seconds in this case. If the evaporation theory of an isolated droplet is applied to this case the droplets smaller than about 1.6 μ disappear by evaporation. As seen from the graph, however, no appreciable change in the droplet size distribution occurs. This fact will be resonable because a droplet cloud having high number concentration, 10^6 particles/cm^3 in this experiment, is expected to be stable from the analysis shown in Figure 3.

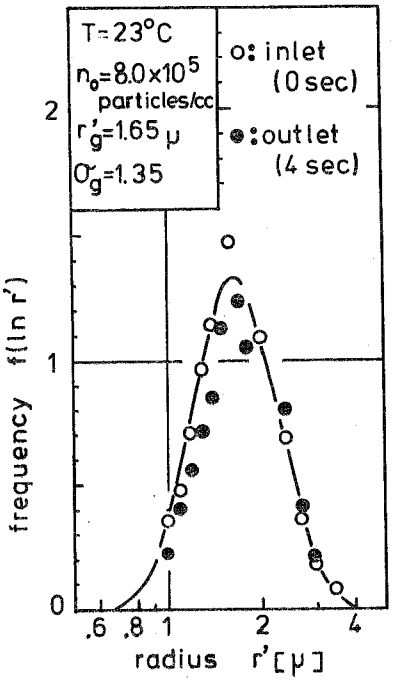

Figure 13 Comparison of the particle size distribution at inlet with that at outlet of the pipe

Figure 14 shows some examples of droplet size distributions obtained by the second experiment where the droplet cloud is mixed with unsaturated air in a mixing chamber. Figure 14(a) is the size distribution of droplets before mixing of unsaturated air, and Figures 14 (b) and (c) are those after mixing of unsaturated air. Slight difference is found among these three distributions, whereas fair difference in particle number concentration is found among them. All of the other experimental results showed the same tendency as those illustrated in these figures. Loss of water droplets due to mixing of unsaturated air shown in Figures 14 (b) and (c)

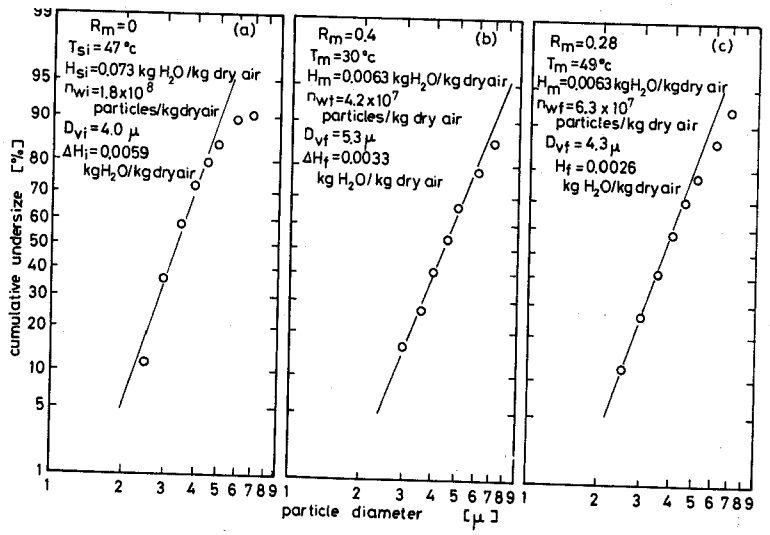

Figure 14 Change in size and number concentration of droplets before and after mixing of unsaturated air

will be caused by evaporation of some of the droplets.

Since the vapor pressure of small droplets is higher than that of larger ones as expected by the Kelvin's equation, the droplets once decreased their sizes for a certain reason, for instance local lack of uniformity of humidity, can easily evaporate. The smaller the droplets become, the quicker progresses their evaporation, and in consequence smaller droplets may not exist. It is an interesting phenomena that droplet sizes do not decrease uniformly but number concentration only decreases by mixing of unsaturated air, preserving the initial droplet size distribution itself. This phenomena will not be undesirable for dust collection, because some of the droplets produced by condensation upon small dust particles decrease their sizes to those of the orginal small dust particles which are difficult to collect.

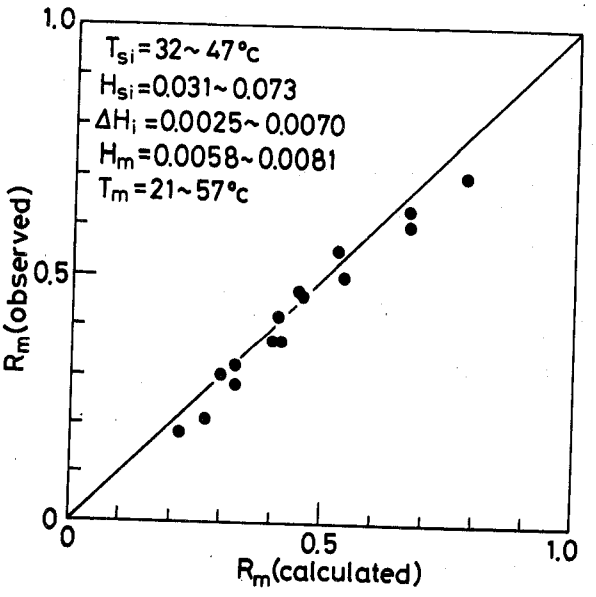

Figure 15 Comparison of mixing ratios, R_m, calculated and observed in the case of $\Delta H_f=0$

Figure 15 shows the comparison of the mixing ratio, R_m, calculated

from Eqs.(10), (11) and (12) with that observed, when droplets just disappear by evaporation, that is, $\Delta H_f=0$. Good correlation is found between them.

Some examples of the experimental results for $\Delta H_f>0$ are shown in Figures 16 and 17. Figure 16 shows the effect of the mixing ratio R_m and the temperature of mixing air T_m on the quantity of droplets remaining in air, ΔH_f, which was determined by Eq.(13). This figure suggests that loss of droplets is significant when leakage of fresh air having high temperature into a droplet cloud exists. The deviation of the experimental results from the calculated curves may be caused by the experimental error of D_{vf} which effects on ΔH_f at third power as seen in Eq.(13). Figure 17 shows the relation between the temperature after mixing of unsaturated air, T_{sf}, and the mixing ratio R_m. It is obvious that T_{sf} decreases with R_m because the droplet evaporation requires latent heat.

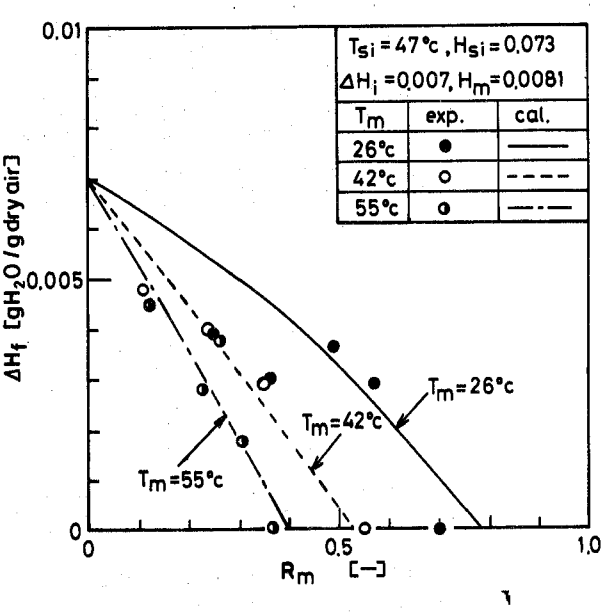

Figure 16 Effect of mixing ratio R_m and temperature of mixing air T_m on remaining droplet quantity ΔH_f

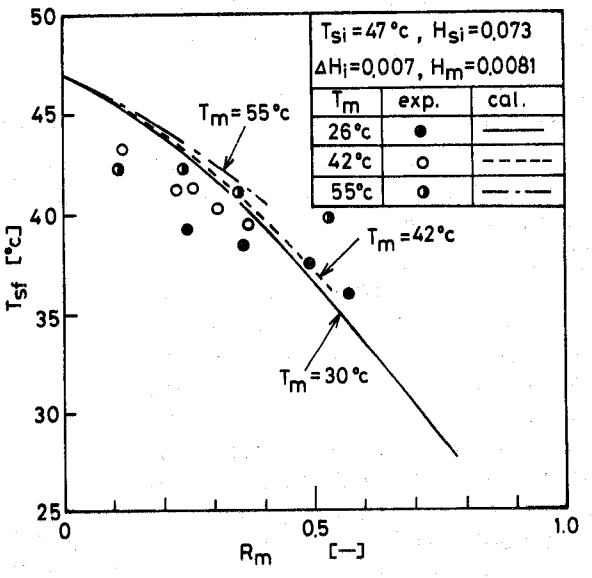

Figure 17 Effect of mixing ratio R_m and temperature of mixing air T_m on air temperature after mixing of unsaturated air, T_{sf}

CONCLUSION

The rate of evaporation of monodisperse pure water droplets was evaluated by numerically solving the modified Maxwell's equation, assuming the cellular model for a droplet cloud and considering the change in the surrounding air conditions caused by droplet evaporation. When the number concentrations of droplet clouds are sufficiently low, the results of the numerical calculation for

droplet clouds agree well with those of the analytically derived equation for a single isolated water droplet. When the number concentration of droplet clouds are sufficiently high, the droplet clouds becomes stable. The critical conditions where the droplet clouds can be stable were evaluated as the function of number concentration, droplet size and initial conditions of the surrounding air.

The equilibrated system, where a water droplet cloud is steadily mixed with unsaturated air, was also analysed on the basis of enthalpy and material balance of the system to evaluate the quantitative change of the total volume of the droplet. And the analysis was verified by experiments using the ultramicroscopic technique. As to the manner of the decrease in total volume of droplets, the unexpected decrease in droplet number concentration was observed instead of droplet size change.

NOMENCLATURE

a_0, a_1 = constant values [-]

b = length of the edge of a cubic cell [cm]

c_1 c_{15} = constant in Tables 1 and 2

$c_1=2M\sigma/\{\rho_s RT_{\infty 0}(1-S_0)\}$ $c_2=DMp_s(T_{\infty 0})\cdot(1-S_0)/\rho_s RT_{\infty 0}$

$c_3=2M\sigma p_s(T_0,r_0')\cdot T_{\infty 0}/\rho_s RT_0(r_0')[T_{\infty 0}p_s(T_0,r_0')-T_0(r_0')S_0p_s(T_{\infty 0})]$

$c_4=DM[T_{\infty 0}p_s(T_0,r_0')-T_0(r_0')S_0p_s(T_{\infty 0})]/\{\rho_s RT_{\infty 0}T_0(r_0')\}$

$c_5=a_1+KRT_{\infty 0}/LDM$, $c_6=2a_1M\sigma/\rho_s R$

$c_7=T_{\infty 0}(a_1+KRT_{\infty 0}/LDM)$, $c_8=4M\sigma K\cdot(a_0+a_1T_{\infty 0})\rho_s^2RL$

$c_9=T_{\infty 0}^2(a_1+KRT_{\infty 0}/LDM)^2$ $(=c_7^2)$

$c_{10}=-4M\sigma(a_1+KRT_{\infty 0}/LDM)(T_{\infty 0}+2a_0)/\rho_s R$

$c_{11}=(2a_1M\sigma/\rho_s R)^2$, $c_{12}=c_{10}/8c_9^2$

$c_{13}=4c_9c_{11}-c_{10}^2$, $c_{14}=c_{10}c_{13}/16c_9^{2.5}$

$c_{15}=2a_0M\sigma/\rho_s R$

D = diffusion coefficient of vapor [cm^2/sec]

D_v = volume mean diameter of the droplets [μ] [cm]

H = absolute humidity [kg H_2O/kg dry air]

ΔH_e = quantity of evaporated water vapor [kg H_2O/kg dry air]

i = quantity of water droplets [kcal/kg dry air]

Kn = Knudsen number ($=\lambda/r'$) [-]

K = heat conductivity [kcal/m sec °C]

L = latent heat of vaporization [kcal/kg]

M = molecular weight of evaporating substance [kg/kmole]

n_0' = droplet number concentration [particles/cm^3]

n_w = droplet number concentration on mass basis [particles/kg dry air]

p_0 = vapor pressure at the droplet surface [mmHg]

p_∞ = vapor pressure of surrounding air far away from droplet [mmHg]

p_t = total pressure [mmHg]

R = gas constant [m^3 mmHg/kgmole °C]

R_m = mixing ratio (=kg unsaturated air on dry air basis/kg total dry air) [-]

r' = droplet radius [μ] [cm]

r_g' = geometric mean radius [μ] [cm]

r	= dimensionless radius ($=r'/r'_0$)	[-]
S	= degree of saturation	[-]
T_0	= temperature at the dro!let surface	[°C] [°K]
T_∞	= temperature of surrounding air far away from droplet	[°C] [°K]
t'	= time	[sec]
t'_l	= life time	[sec]
t'_{lk}	= life time of Case 1	[sec]
t	= dimensionless time ($=t'/t'_{lk}$)	[-]
v_H	= humid volume	[m^3/kg dry air]

Greek letters

λ	= mean free path	[cm]
ρ_s	= density of droplet	[kg/m^3]
σ	= surface tension	[dyne/cm]
σ_g	= geometric standard deviation	[-]
ϕ	= percentage humidity	[%]

Subscripts

f	= final state of air mixing
i	= initial state of air before mixing which contains water droplets
m	= unsaturated mixing air
s	= saturated
w	= water
0	= initial state of air before evaporation

Superscripts

'	= for water

REFERENCES

1) Fuchs, N. A. "Evaporation and Droplet Growth in Gaseous Media", Pergamon Press. (1959)
2) Zung, J. T. Evaporation Rate and Lifetime of Clouds and Sprays in Air —The Cellular Model. J. Chem Phys., 46, 2064 (1967)
3) Yoshida, T., Y. Kousaka and K. Okuyama. A New Technique of Particle Size Analysis of Aerosols and Fine Powders Using an Ultramicroscope. Ind. Eng. Chem., Fundam., 14, 47 (1975)
4) Davies, C. N. "Evaporation of Airborne Droplets", Chapter 3, to be published from Wiley.
5) Davies, C. N. Evaporation of Fine Atmospheric Particles. Faraday Simp. of Chem. Soc., No.7 34 (1973)
6) Yoshida, T., Y. Kousaka and K. Okuyama. Growth of Aerosol Particles by Condensation. Ind. Eng. Chem. Fundam., 15, 37 (1976)

PARTICLE SIZE ANALYSIS OF AEROSOLS INCLUDING DROPLET CLOUDS BY SEDIMENTATION METHOD

Y. Kousaka, K. Okuyama and T. Yoshida
Chemical Engineering Drpartment
University of Osaka Prefecture
Sakai, Japan 591

ABSTRACT

The principle of the particle size analysis is somewhat similar to the existing Andreasen pipet method. The distinctive features are: (1) sedimentation is made in air; (2) sedimentation length is extremely shallow, say, around 1 millimeter; (3) particle concentration at a given depth in a sedimentation cell is detected by an ultramicroscope on the number basis. The lower limit of the measurable particle size is a few tenths of a micron in diameter and the upper several microns in most cases. The particle number concentrations required for measurement are more than 10^5 particles per cubic centimeter. Very quick measurement due to the short sedimentation length and the measurement of the particles as they are suspending are the major advantages. Automatic device of the technique is also feasible.

INTRODUCTION

Among many techniques of particle size analysis, the sedimentation method using an ultramicroscope has been thought to be very troublesome because the settling velocities of hundreds of individual particles must be observed by a microscope. The different technique has been developed to improve the existing ultramicroscopic method by combining a TV system and the principle of the Andreasen pipet method which is widely applied to water sedimentation.

Some of the distinctive features of this technique will be listed as follows: (1) quick size analysis can be made even for submicron particles because of the extremely short sedimentation length.

(2) particles suspending in water as well as in air can be analyzed. (3) particles themselves can be monitored by naked eyes on TV. (4) particle number concentration can be also measured. (5) volatile particles such as fine water droplets can be observed if the temperature control device is applied to the sedimentation cell. (6) high number concentrations of particles more than 10^5 particles per cubic centimeter are advantageous. (7) automatic device of the technique is also feasible.

The principle and the applications of the method are introduced in the following sections.

PRINCIPLE

Figure 1 shows the principle and the procedure of data reduction of this method. At first an aerosol is led into the cell as shown in Figure 1 and then the flow of the aerosol is stopped by closing the valves to the cell. At this time particles are uniformly dispersed throughout the cell and we define that this time equals to zero, say, t=0. At that time the distribution of various sizes of particles in the cell may be illustrated as that of t=0 and $N=N_0$ in Figure 1. After t_1 second the particles sedimentate with different velocities by gravity, and as the result the distribution of particles in the cell will change to the second illustration of $t=t_1$ and $N=N_1$. After t_2 second it may change to the third illustration of $t=t_2$ and $N=N_2$.

When the focus of the ultramicroscope is preliminarily set at the depth, h, as shown in Figure 1, the aerosol particles existing in the volume in focus, v_m, can be recognized because of their light scattering though they are as yet unknown in sizes. Thus the particle numbers at the depth h, N_0, N_1, $N_2 \cdots N_n$ corresponding to t_0, t_1, $t_2 \cdots t_n$ can be observed. Such particle numbers at the depth h will decrease with time as illustrated.

The settling velocity of the largest particles in the illustration which have the diameter of d_{p1}, is given by h/t_1. The settling velocity by gravity, on the other hand, is given by the Stokes-Cunningham equation as follows:

$$u_t = \frac{d_p^2 g(\rho_p - \rho_f)C_m}{18\mu} \quad (=h/t) \qquad (1)$$

The particle diameter, d_{p1}, is then given by the following equation, which is shown in the fourth column in the lower table in Figure 1.

$$d_{p1} = \sqrt{\frac{h}{t_1} \cdot \frac{18\mu}{g(\rho_p - \rho_f)C_m}} \qquad (2)$$

The larger particles than this size d_{p1} can not be observed at the depth h at the time t_1 because they have already sedimentated below the depth h.

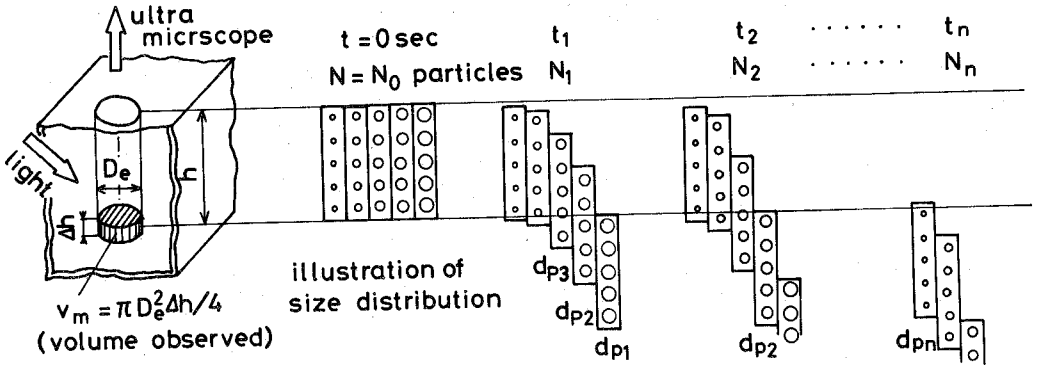

particle number concentration $n_0 = N_0 / v_m$

lapse of time t	particle number observed N	settling velocity u_t	particle diameter d_p	cumulative undersize F
0	N_0	—	—	1
t_1	N_1	$h/t_1 = d_{p1}^2 g(\rho_p - \rho_f) C_{m1} / 18\mu$	$\sqrt{18\mu h / t_1 g(\rho_p - \rho_f) C_{m1}}$	N_1/N_0
t_2	N_2	$h/t_2 = d_{p2}^2 g(\rho_p - \rho_f) C_{m2} / 18\mu$	$\sqrt{18\mu h / t_2 g(\rho_p - \rho_f) C_{m2}}$	N_2/N_0
⋮	⋮	⋮	⋮	⋮
t_n	N_n	$h/t_n = d_{pn}^2 g(\rho_p - \rho_f) C_{mn} / 18\mu$	$\sqrt{18\mu h / t_n g(\rho_p - \rho_f) C_{mn}}$	N_n/N_0

Figure 1 Illustration of the principle and procedure of data reduction

Accordingly the particles observed at the time t_1 and at the depth h are those having the undersizes of d_{p1}. Suppose that the particle number observed at $t=t_1$ is N_1 and the number at $t=0$ is N_0, then N_1/N_0 gives the cumulative undersize of the particles having the diameter of d_{p1} which is already determined in the above;

$$F_1 = N_1/N_0 = \int_0^{d_{p1}} f(d_p)\, dd_p \qquad (3)$$

After t_2 second the critical diameter of d_{p2} can be calculated by the same way as d_{p1} is calculated, and the cumulative undersize of d_{p2} is given by N_2/N_0. Successive measurement of the particle numbers N at various time t gives the size d_p and the corresponding cumulative undersize $F(=N/N_0)$. The lower table in Figure 1 shows the procedure above described. The particle number concentration, n_0 particles per cubic centimeter, can be determined by N_0/v_m, if volume v_m shown in Figure 1 is preliminarily measured.

Another method may also be true in principle. If the sedimentation depth h is varied instantaneously at the certain lapse of time, the particle size distribution can be determined by almost the same procedure

described above.

The principle described above is the same as that of the existing sedimentation method which is widely used for size analysis. The existing sedimentation methods, however, are usually observed in water and not in air, and they have long sedimentation length such as a few centimeters or much longer. Further, the particle concentration is usually detected on the weight or the projection area basis in the existing sedimentation methods. This method, on the other hand, can be applied to both water and airy sedimentation, and the sedimentation length, h, in Figure 1 is extremely short, say, around 1 millimeter. And the particle concentration is detected by an ultramicroscope in number basis monitoring the particles on TV.

Figure 2 is for the quick evaluation of d_p at a given value of h/t in the table of Figure 1, by which one may also understand the time required for measurement in this method.

In the principle above described, Brownian coagulation and Brownian deposition on the cell walls are neglected. When the particle number concentrations exceed about 10^7 particles per cubic centimeter, the effect of the Brownian coagulation will not be negligible[1], and when the particle sizes become less than about 0.2 micron, the effect of particle deposition on the walls caused by Brownian diffusion becomes significant[1]. The lower limit of particle size to which this technique can be applied

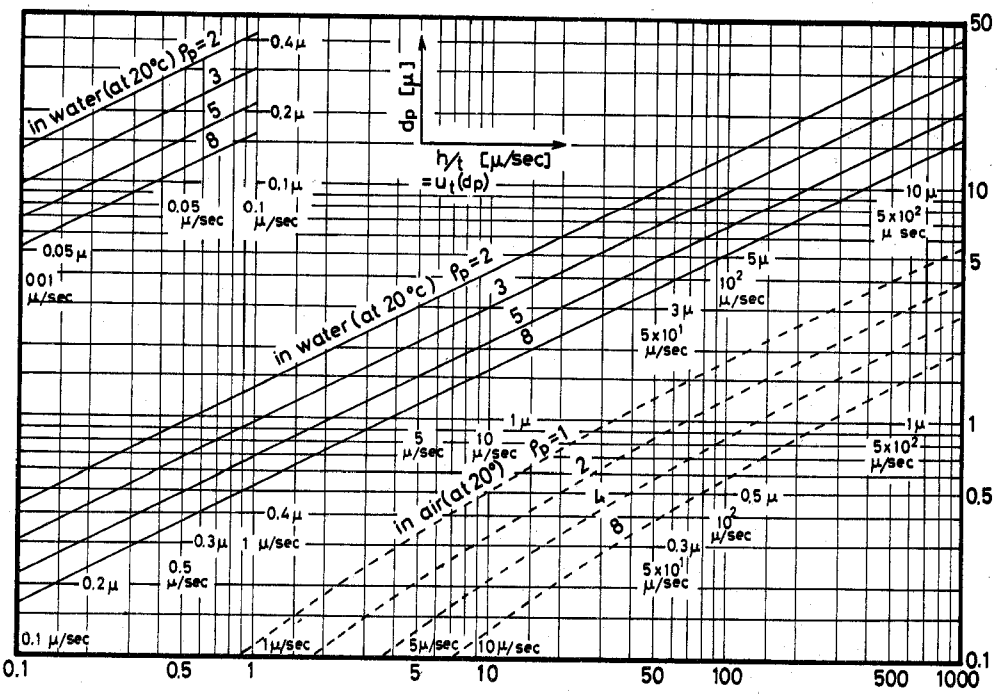

Figure 2 Relation of the gravitational settling velocity vs. particle diameter

is about 0.2 micron for aerosol in this reason. In water sedimentation, however, the lower limit may fall to 0.01 micron by applying centrifugal sedimentation. The lower limit of particle number concentration will be 10^5 particles per cubic centimeter, which is determined from the particle number N_0 statistically required.

APPARATUS

Figure 3 shows three typical arrangement. In the manual operation, the change in particle number with time is once recorded by a VTR. Then reproducing the tape, the particle number, N, at every lapse of time, t, is counted by naked eyes observing the still picture on TV monitor. In the semi-automatic system, an automatic counter is equipped and the output of the counter is connected to a recorder to obtain t-N curve, or sedimentation curve. In the full automatic system, a microprocessor and a digital printer are connected after the automatic particle counter to directly print out the size distribution.

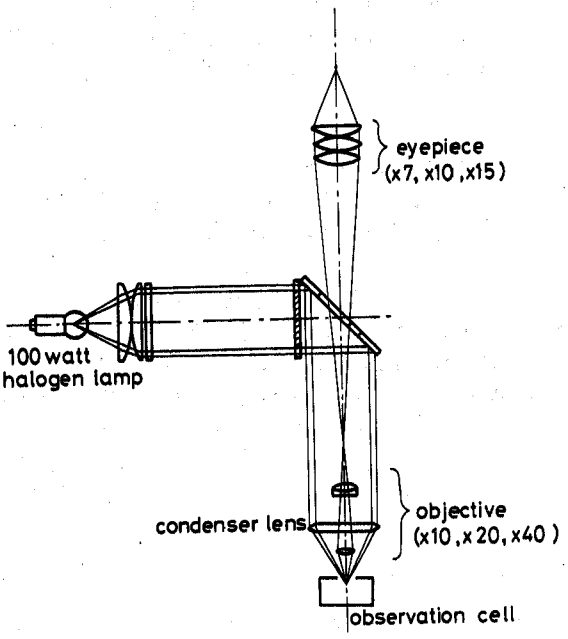

Figure 4 Optical system of ultramicroscope

Figure 4 shows the optical system of the ultramicrscope used

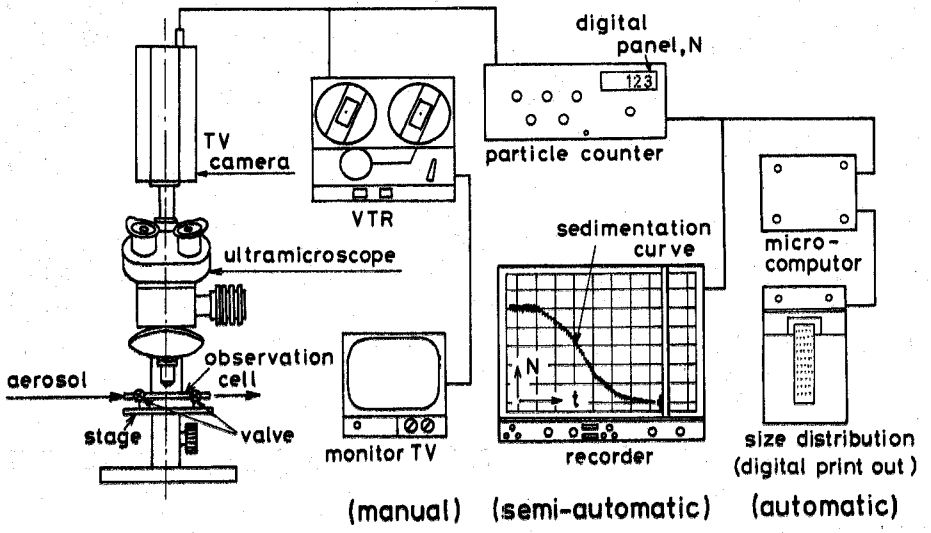

Figure 3 Three typical arrangement

Table 1 Characteristics of the ultramicroscope used

Eye-piece x objective	Max. value of h,μ	Δh,μ	v_m,cm^3	Visible particle diam.,μ	n_0[particles/cm^3] equiv. to over 20 particles in volume,v_m
10 x 10	5000	125	1.9×10^{-4}	>0.1	$>1.0\times10^{5}$
10 x 20	1800	40	1.4×10^{-5}	>0.05	$>1.4\times10^{6}$
10 x 40	400	15	1.2×10^{-6}	>0.01	$>1.4\times10^{7}$

in our study. The characteristics regarding the ultramicroscpe used are shown in Table 1.

The observation cells for various purposes are shown in Figure 5. Figure 5(a) is the cell for the usual particle size analysis for aerosols as well as particles suspending in water. The sectional area of the cell is very small to prevent convective flow. Figure 5(b) is the cell for the analysis of volatile particles such as fine water droplets which vary their size by evaporation or condensation with change in temperature. The outer cell is provided for temperature control of the aerosol to be observed in the inner cell. The cell shown in Figure 5(c) is for centrifugal sedimentation in water. Because of the low gravitational sedimentation velocity of submicron particles in water as shown in Figure 2, centrifugal sedimentation is useful to shorten the measuring time, and at the same time to minimize the effect of Brownian deposition to the cell walls.

PROCEDURE

In evaluation of volume v_m in Figure 1, it is necessary to know the diameter D_e and the height Δh of the small cylinder to be observed. The diameter D_e is easily determined by observing the microscale. The determination of Δh can be made as follows. Small numbers of particles to be analysed are firstly deposited on a glass by some way. Then the glass is mounted on the stage of the ultramicroscope and the deposited particles are observed while shifting the stage up and down. Then Δh is given as the total displacement of the stage over which the images of the particles are in sight with a certain clearness. Since the value Δh depends upon particle size, it should be checked when the particles to be measured are considerably changed in size. The sedimentation length h can be set as follows. The ultramicroscope is focused to the lower surface of the glass wall of the observation cell, and then the stage of the ultramicroscope is shifted upward to set at the certain depth h watching the micrometer equipped which indicates the displacement of the stage. The length h can not be large because of the short working distance of the microscope when magnification of the objective becomes large. The maximum lengths are shown in Table 1.

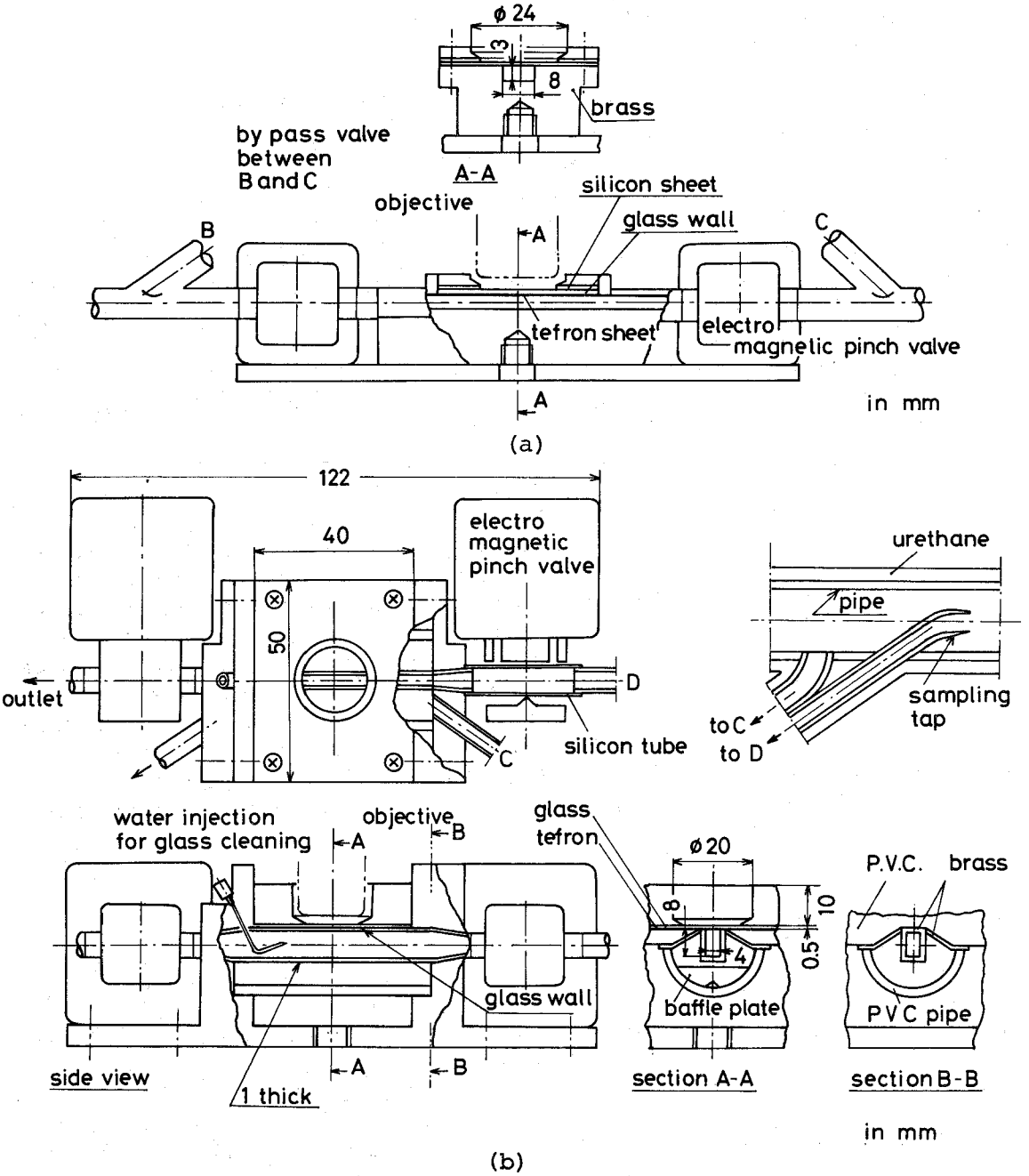

Figure 5 Observation cell

In water sedimentation the depth h must be multiplied by the factor of 1.33 which corresponds to the index of refraction of water.

Different kinds of images of particles appear on the TV monitor, such as particles in focus and out of focus, when the electro-magnetic valves installed at the inlet and the outlet of the cell are closed after an aerosol being led into the cell. In counting particle numbers by naked eyes, it is necessary to standardize the particles to be counted according to the degree in focus. Such standard may be fixed to all particles including out of focus which can be recognized or to the particles only clearly in focus. Since the particle number N at any lapse of time t are normalized by initial particle number N_0, that is N/N_0, and since it gives the cumulative undersize, it is necessary to count the particle numbers under the fixed standard through a series of measurement.

RESULTS OF SIZE ANALYSIS

Some of the results obtained by this technique are shown in Figures 6 to 10.

Figure 6 shows the result of the size analysis for stearic acid aerosols obtained by changing the sedimentation length h. Table 2 is an example of the data. No difference is found among the size distributions obtained under various depths in Figure 6. This means that the aerosol introduced into the cell is homogeneously dispersed, and also indicates no effect of particle diffusion to the walls and no effect of thermophoresis, which probably appear at the vicinities of the upper or the lower wall of the cell because of the larger gradient of concentration and temperature. The agreement also means that the Brownian coagulation, which must progress with the lapse of time or with the depth of sedimentation, has no effect in size analysis under such a number concentration. Further, no convective flow seems to occur in the cell.

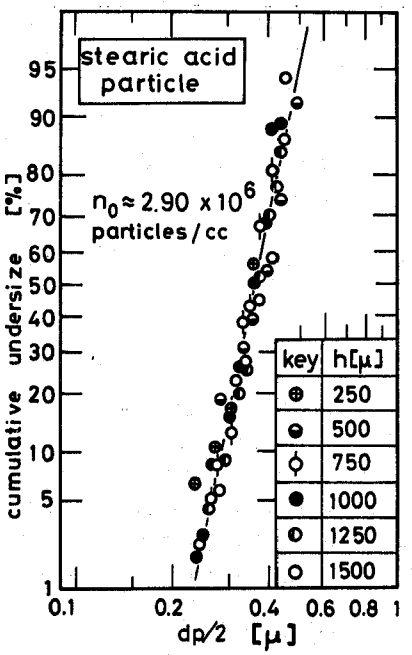

Figure 6 Particle size distribution of stearic acid aerosol for various sedimentation depths

Table 2 Example of experimental data(stearic acid aerosol; h=1000μ, eyepiece x10, objective x20, ρ_p=0.84 g/cm^3)

t, sec	N	d_p,μ	F= N/N_0
0	47		
20	46	1.31	0.98
40	42	0.90	0.89
50	32	0.80	0.68
60	24	0.73	0.51
70	12	0.67	0.26
80	7	0.62	0.15
90	8	0.58	0.17
100	4	0.55	0.085
110	1	0.51	0.021
120	1	0.48	0.021

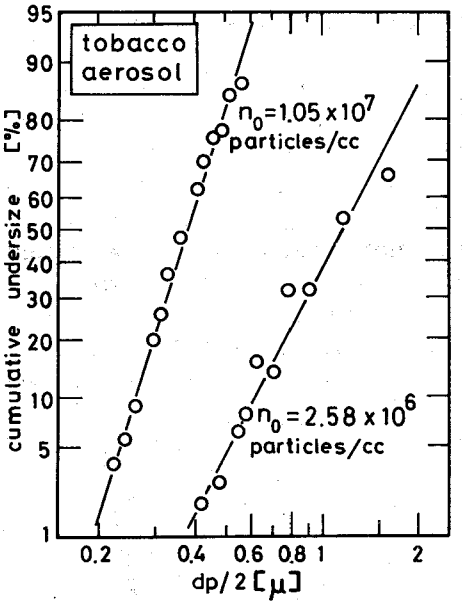

Figure 7 Particle size distribution of tobacco aerosol

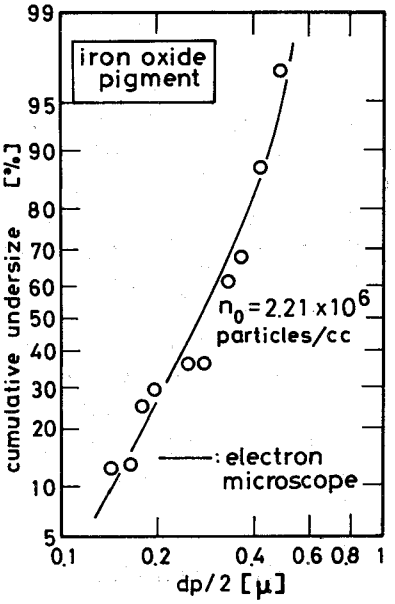

Figure 8 Particle size distribution of iron oxide pigment

Figure 7 shows two kinds of size distributions of tobacco aerosols: one is that measured after sufficient aging time to promote Brownian coagulation and the other is that measured after short aging time. The sizes of tobacco aerosols reported by other investigators[2,3,4] are smaller than those in Figure 7. Such difference is thought to be caused by the existence of water which is expected to adhere to the particle surface.

Figure 8 shows the result of size analysis of fine powders which were dispersed into air by means of a rotating blade type disperser. The result of size analysis by an electron microscope for the same powder is also shown in the figure.

Figure 9 shows the size distributions of a water droplet clouds[5] which has been thought to be difficult to analyze. The data were obtained by using such a cell as shown in Figure 5(b) and by using the semi-automatic apparatus as shown in Figure 3.

Figure 10 is the size distribution obtained under water sedimentation. The type of the cell used in this measurement was that shown in Figure 5(c). The centrifugal sedimentation was applied in this case so that the settling velocity was quickened by the factor of z, the ratio of centrifugal acceleration to acceleration of gravity, compared with the gravitational settling velocity.

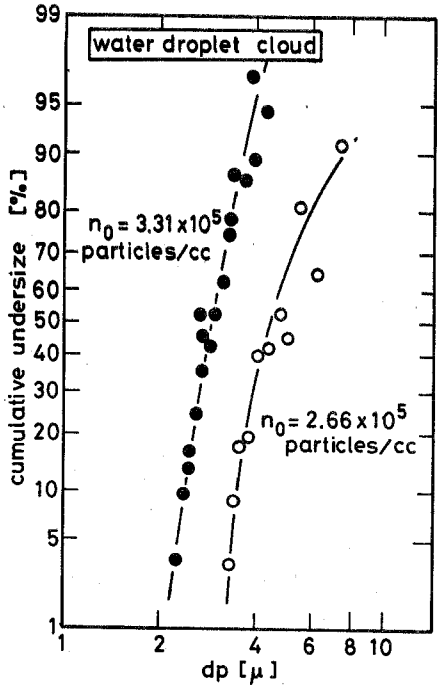

Figure 9 Particle size distribution of water droplet cloud

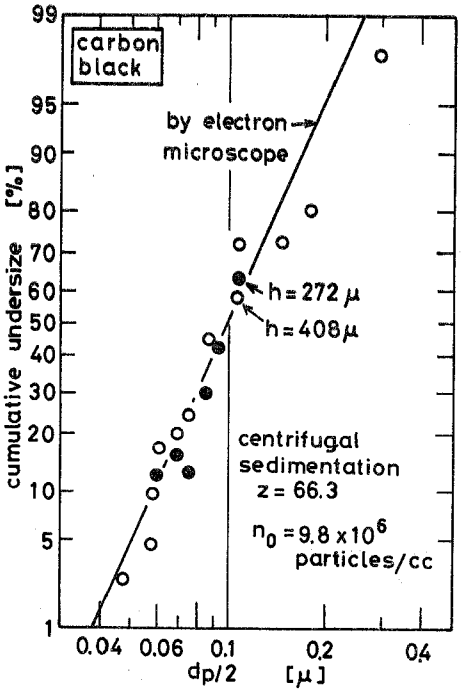

Figure 10 Particle size distribution of carbon black particles

CONCLUSION

The technique introduced herein has the advantage of the sedimentation method in which particles are observed while they are suspended. The usual disadvantage of the sedimentation method, that much time is needed for the fall of small particles, was overcome by an extremely short sedimentation length in this technique. The particle number concentration required in this technique, however, must be rather high, and this is both an advantage and a disadvantage of the method.

The usual lower limit of the particle size which can be measured in this technique is around 0.2 micron. The limit could be decreased by one tenth by applying centrifugal force in the case of water sedimentation. For the aerosol particles, the development of a method to decrease the lower limit by applying electric settling is being in progress.

NOMENCLATURE

C_m	= Cunningham's correction factor	[-]
F	= cumulative fraction undersize	[-]
D_e	= effective diameter of microscopic sight shown in Figure 1	[cm]
d_p	= particle diameter	[μ] [cm]

f(dp)	= particle distribution function	[-]
h, Δh	= values shown in Figure 1	[μ] [cm]
N	= particle number observed by ultramicroscope at t sec after the start of sedimentation	[particles]
n_0	= particle number concentration	[particles/cm^3]
t	= time elapsed	[sec]
u_t	= terminal settling velocity	[cm/sec]
v_m	= volume shown in Figure 1	[cm^3]

Greek Letters

μ	= viscosity	[g/cmsec]
ρ_p	= density of particle	[g/cm^3]
ρ_f	= density of fluid	[g/cm^3]

REFERENCES

1) Okuyama, K., Y. Kousaka, T. Miyazaki and T. Yoshida. Effects of Brownian Coagulation and Brownian Diffusion on Fine Particle Size Analysis by Sedimentation Method. J. Chem. Eng. Japan. 10, 46(1977)
2) Keith, C. H. and J. C. Derrick. Measurement of the Particle Size Distribution of Cigarette Smoke by the "Conifuge".J. Colloid Sci., 15, 340(1960)
3) Mukaibo, T., S. Suzuki and K. Adachi. Studies on Design of a Photographic Ultramicroscope. Sogo Shikensho Nempo, 20,No 2(1962)
4) Porstendorter, J. and J. Schraub. Staub, 32, 33(1972)
5) Yoshida, T., Y. Kousaka and K. Okuyama. Growth of Aerosol Particles by Condensation. Ind. Eng. Chem., Fundam., 15, 37(1976)

PARTICLE MASS DISTRIBUTION AND VISIBILITY CONSIDERATIONS FOR LARGE POWER PLANTS

Thomas L. Montgomery, Sc.D., and
J. Clement Burdick III, Ph.D., P.E.
Tennessee Valley Authority
Chattanooga, Tennessee 37401

ABSTRACT

The Clean Air Act Amendments of 1977 require the States and the Environmental Protection Agency to protect and improve visibility in mandatory Class I Federal areas. This may in turn require the retrofitting of additional air pollution control equipment on large stationary sources such as power plants. Measured and calculated mass distributions for power plant primary particulate emissions, power plant plume particulates, and ambient particulate samples collected near power plants are reported. Significant amounts of particulates emitted from a power plant that has efficient particulate control are fine particulates. These particulate data and relationships among experimental plume dispersion, plume pollutant conversion rates, and visibility reduction relationships were used to estimate the worst-case visibility reduction potential of power plant primary particulate emissions, secondary sulfates, and secondary nitrates. Results indicate that secondary sulfates are the principal pollutant causing visibility impairment for a power plant burning medium-sulfur coal without SO_2 emission control. However, if 90 percent of the SO_2 emissions are reduced by either installing scrubbers or by burning low-sulfur coal, the resulting visibility impacts of primary particulates, secondary sulfates, and secondary nitrates are about equal. The sensitivity of the calculation technique is also discussed, and the need for more detailed analysis to assess site-specific visibility relationships is demonstrated.

INTRODUCTION

The Clean Air Act requires the Environmental Protection Agency to promulgate visibility regulations for mandatory Class I Federal areas by August 1979. The States will then be required to revise their State Implementation Plans to attain visibility protection goals within a five-year period. These revisions may be directed toward controlling sources of pollutants that raise the concentration of fine particulates in the atmosphere because fine particulates, primarily in the range of 0.1 to 1.0 μm in diameter, are known to scatter visible light and reduce visibility.[1] Research has been reported which relates the visual range in the atmosphere to the mass concentration of fine particles for given particle size ranges.[1,2] Visual range is the maximum distance at which an average individual can distinguish an object from the horizon in a polluted atmosphere. Although other environmental factors also affect the visual range, preliminary estimates can be made of the potential impact of given sources on visibility in a specified area if their contribution to the mass concentration of atmospheric aerosols in specific size ranges can be estimated.

To better understand the potential impact of emissions from power plants on visibility, the Tennessee Valley Authority (TVA) has conducted studies to determine the characteristics of aerosols that occur near TVA's large, coal-burning power plants. Distributions of particle size and mass have been determined for power plant emissions and nearby ambient air samples. These results are used to relate the impact of emissions from typical, large power plants on atmospheric visibility.

Power Plant Particle Mass and Size Distributions

TVA has collected data for particle mass and size distributions at three types of locations: (1) at the outlet of an electrostatic precipitator; (2) in the plume downwind of a plant; and (3) at ground level in the vicinity of twelve different power plants. The mass distribution of particulate emissions at the electrostatic precipitator outlet was measured at a TVA power plant unit by using an Andersen Mark III sampler. Seven different samples were taken on five different days. The front wall-fired unit was operating at about 180 MW, which was about 90 percent of full load. During the tests, the coal burned had the following average characteristics: ash content, 16 percent; sulfur content, 4 percent; moisture content, 6 percent; and heat content, 12,000 Btu/lb. The combined efficiency of the mechanical collectors and electrostatic precipitators serving the unit was sufficient during the tests to meet a particulate emission level of 0.33 lb/10^6 Btu. Results of these tests were averaged to obtain an approximate particle mass distribution that is probably representative of a typical power plant unit (Table 1). This average mass distribution indicates that about 20 percent of the weight of the emissions was composed of particles that were less than

Table 1. MASS DISTRIBUTION OF

COAL-FIRED POWER PLANT PARTICULATE EMISSIONS

Particle size range (μm)	Average mass distribution (%)	Range of mass distribution for 7 samples (%)
<0.3	2.2	0.2 - 7.2
0.3 - 0.5	6.6	4.6 - 8.5
0.5 - 0.8	10.3	8.0 - 12.6
0.8 - 1.5	12.8	10.5 - 14.8
1.5 - 2.4	12.8	12.3 - 13.3
2.4 - 3.6	12.5	12.1 - 12.7
3.6 - 5.2	14.0	13.2 - 15.6
5.2 - 8.4	14.2	12.5 - 15.8
>8.4	14.6	13.1 - 17.1
Total	100.0	

1 μm in diameter and that more than 50 percent of the weight was composed of particles less than 4 μm in diameter. Therefore, the tested power plant particulate emissions did include a significant amount of fine particulates.

At a different power plant TVA conducted tests to determine the size distribution of the particles within the plume downwind from the plant.[3] Three different samples were taken in the relatively stable plume of this TVA power plant, which was operating with an efficient electrostatic precipitator. Particle size distributions were measured for these plume samples by an electron microscope technique.[4,5] These particle measurements were for particle count in each size range only. However, the mass distribution can be calculated with the assumption that the particles have spherical shapes and similar densities, which is a reasonable assumption for power plant plume particles. Table 2 shows the estimated plume particle mass distribution based on this data. This distribution shows that about 70 percent of the mass of plume particles ranged in size from 0.6 to 1.4 μm. The plume had relatively greater amounts of small particulates than the plant emissions shown in Table 1. This could be due to operating differences of the plants, atmospheric settling of larger particles, or the formation of additional small particulates by the reaction of plume constituents.

The size distribution of particles collected from the filters of high-volume samplers near TVA power plants was determined by a light microscope technique. For this technique, the particle number distributions were determined by sizing particles that were removed from the high-volume filter with the light microscope. Twelve samples, one for each of the twelve TVA power plant areas, were evaluated for this purpose at a time when particulate levels were relatively high. The results were converted to mass distribution by using the assumptions described for the plume particulates above. A typical size distribution, composed of composited samples from the twelve TVA power plants, is presented in Table 3. These ambient results indicate particle sizes that are larger than those found in samples from power plant emissions or plumes. Less than about 4 percent of the particle weight was in the size range smaller than 3 μm. The larger size is explained by the fact that the high-volume filters are run for 24-hour periods, resulting in samples that represent plume and other ambient particulates as well.

Potential Power Plant Impact on Atmospheric Visual Range

To place in perspective the potential visibility impact of atmospheric emissions from a large power plant, visual range was calculated for two different 1,000-MW power plants. Assumptions for worst-case primary pollutant concentrations were adopted for these calculations to identify the maximum potential. However, a range of conversion rates from primary to secondary pollutants and a range of light-scattering efficiencies were used because these parameters are not well understood. Some discussion of the effect of these assumptions is also provided.

Table 2. CALCULATED MASS DISTRIBUTION OF COAL-FIRED POWER PLANT PLUME PARTICULATES

Particle size range (μm)	Average mass distribution (%)	Range of mass distribution for 3 samples (%)
0.2 - 0.4	1.5	1.1 - 1.8
0.4 - 0.6	5.8	5.5 - 6.2
0.6 - 0.8	15.0	10.3 - 18.0
0.8 - 1.0	22.0	21.8 - 22.2
1.0 - 1.2	22.6	15.9 - 27.6
1.2 - 1.4	11.4	9.7 - 12.7
1.4 - 1.6	10.8	8.2 - 13.5
1.6 - 1.8	10.9	7.2 - 15.7
Total	100.0	

Table 3. CALCULATED MASS DISTRIBUTION OF PARTICULATE SAMPLES COLLECTED NEAR TVA POWER PLANTS

Particle size range (μm)	Average mass distribution (%)	Range of mass distribution for 12 samples (%)
<1.0	<0.1	<0.1
1.0 - 3.0	0.7	0.1 - 3.5
3.0 - 10.0	9.0	2.5 - 17.8
10.0 - 12.0	14.0	2.9 - 43.3
12.0 - 16.8	18.9	7.9 - 38.6
>16.8	57.3	10.6 - 80.1
Total	100.0	

The first plant was assumed to burn 2.35-percent-sulfur coal with no SO_2 removal. The second plant was also assumed to burn the same 2.35-percent-sulfur coal, but SO_2 emissions were assumed to be reduced by 90 percent. Visual range calculations were made for three different atmospheric pollutant components emitted by a large power plant: (1) primary emitted particulates, (2) secondary sulfates, and (3) secondary nitrates. Primary emitted sulfates are not included in this analysis, nor has their significance been evaluated.

Several assumptions and techniques were used for these calculations:

1. The primary particulate emissions were assumed to agree with the mass distribution given in Table 1 and to have a density of 2.26 g/cm^3, which on the basis of TVA experience is believed to be a reasonable value for power plant particulate emissions.

2. The equation, $V=2.9/B_{scat}$, for which V= visual range in meters and B_{scat} = light-scattering coefficient in $meters^{-1}$, was used to calculate visual range.[6] This equation, the Koschmieder formula, is based on a threshold brightness level of 0.055 for the human eye.[6]

3. Power plant primary particulate emissions were assumed to reduce visibility by their mass and size in accordance with the relationships presented by White and Roberts[1] for the best-estimate calculations. Extreme relationships reported by several authors[1,6,7] were used to calculate the expected range of visibility relationships. Here it was assumed that B_{scat} for particulates other than sulfates and nitrates ranged from 0.004 to 0.015 x 10^{-4} $m^{-1}/(\mu g/m^3)$.

4. Various authors[1,2,6,7] have related sulfate and nitrate concentrations to visual range. An average value of B_{scat} = 0.06 x 10^{-4} $m^{-1}/(\mu g/m^3)$ was assumed for this study for the best-estimate calculations for both nitrates and sulfates. To calculate expected ranges of visibilities, the sulfate B_{scat} was assumed to range from 0.03 to 0.10 x 10^{-4} $m^{-1}/(\mu g/m^3)$, and the nitrate B_{scat} was assumed to range from 0.03 to 0.13 x 10^{-4} $m^{-1}/(\mu g/m^3)$, as reported by these authors.[1,2,6,7]

5. The sulfate mass formed in the atmosphere was assumed to equal 1.95 x emitted SO_2 mass, and the nitrate mass was assumed to equal to 1.75 x emitted NO_x mass, expressed as NO_2;[1] this assumption is based on the sulfate and nitrate compounds that are most likely to be formed in the atmosphere. The rate at which SO_2 is converted to sulfates was assumed to be 1 percent per hour[8] for the best-estimate calculations. For the range of expected visibility relationships, the sulfate conversion rate was assumed to range from 0.5 to 10 percent per hour.[8] The rate of NO_x conversion to nitrates was assumed to be equal to the SO_2 values in the absence of available experimental measurements.

6. Visual range was calculated under the assumptions: (a) That the power plant emissions were dispersed in clean air, and (b) that pollutant light scattering was in addition to a B_{scat} value of 0.15×10^{-4} m^{-1} for blue sky scattering of visible light.[6] Additional visibility reduction calculations were performed under the assumption that the power plant emissions were dispersed in air having a visibility of only 24 km ($B_{scat} = 1.202 \times 10^{-4}$ m^{-1}) in order to determine the added visibility impact for this case.

7. Visual range reduction was calculated for clean air, where a B_{scat} value of 0.15×10^{-4} m^{-1} indicates a visibility of about 193 km, by subtracting the visual range resulting from the power plant pollutants from the visual range of clean air (193 km). Calculations were made similarly for the case in which the pollutants were assumed to be dispersed in air having a visibility of 24 km.

8. The primary pollutant (SO_2, NO_2, and particulates) concentrations were calculated under the assumptions that the critical atmospheric dispersion condition was trapping or limited layer mixing[9,10] and that the wind speed and direction persisted until steady-state conditions were achieved. Average maximum concentrations were estimated for a distance of 3 to 50 km from the plant, assuming that an observer was looking through the centerline of the ground-level plume away from or back toward the plant. The wind speed was assumed to be 3 m/sec. Therefore, the plume age or travel time would range from 0.3 to 4.6 hours for the distances of 3 to 50 km from the source. Concentrations would be much lower (maybe 10 percent of the value shown) if the observer were looking across the plume.

9. Detailed plant operating conditions and other assumptions for the two plants are presented in Table 4.

Results of the calculations are given in Tables 5 and 6. The calculations indicate that secondary sulfates are the principal pollutants contributing to visibility reduction for the plant without SO_2 emission control (Table 5). A wide range of expected visual ranges resulted from the wide range of input assumptions. For example, the visual range in clean air for the first plant with no SO_2 control ranged from 1 to 42 km for all three pollutants combined. However, when SO_2 emissions are reduced by 90 percent, particulates, secondary sulfates, and secondary nitrates contribute almost equally to visibility reduction (Table 6). These results are based on the assumptions described in this paper and the results of other cited research. Important inputs into these visibility calculations are (1) the ambient concentrations of the primary emissions of particulates, SO_2, and NO_x; (2) the conversion rates of SO_2 and NO_x to sulfates and nitrates; and (3) the light-scattering efficiency of the particulates, sulfates, and nitrates.

Table 4. OPERATING CONDITIONS AND CHARACTERISTICS FOR TWO 1000-MW POWER PLANTS

Condition	Units	Plant without SO_2 control	Plant with 90% SO_2 control
Plant size	MW	1000	1000
Stack exit velocity	m/s	21	21
Radius of stack	m	4.3	4.3
Wind speed	m/s	3	3
Temperature of stack gases	^oK	389	352
Air temperature	^oK	289	289
Stack height	m	244	244
Coal quality	Btu/lb	11,140	11,140
Max. plant heat input	10^6 Btu/h	8705	9227
Max. coal consumption	10^3 tons/year	3423	3628
Sulfur content of coal	%	2.35	2.35
SO_2 emission	lb/10^6 Btu	4.0	0.4
NO_x emission	lb NO_2/10^6 Btu	0.7	0.7
Particulate emission	lb/10^6 Btu	0.1	0.1
Plant efficiency	Btu/kWh	8705	9227

Table 5. ESTIMATED EMISSIONS, POLLUTANT CONCENTRATIONS, AND LIGHT-SCATTERING CHARACTERISTICS FOR FIRST 1000-MW POWER PLANT[a]

Pollutant	Emission rate ($lb/10^6$ Btu)	Ambient 1-h max. concentration[b] ($\mu g/m^3$)		B_{scat} (10^{-4} m^{-1})		Visual range in clean air (km)		Visual range reduction for clean air (km)		Visual range in 24-km-visibility air (km)		Visual range reduction for 24-km-visibility air (km)	
		Range	Best estimate	Range	Best estimate	Range	Best estimate	Range	Best estimate	Range	Best estimate	Range	Best estimate
SO_2	4.0	645-550	638										
NO_x as NO_2	0.7	113-96	112										
Particulates	0.1		16	0.064-0.240	0.187	136-74	86	57-119	107	23-20	21	1-4	3
Secondary sulfates		14-200	27	0.420-20.0	1.620	51-1	16	142-192	177	18-1	10	6-23	14
Secondary nitrates		2-31	4	0.060-4.03	0.240	138-7	74	55-186	119	23-6	20	1-18	4
Total				0.544-24.27	2.047	42-1	13	151-192	180	17-1	9	7-23	15

[a]Plant burns 2.35% sulfur coal and has no SO_2 removal.

[b]Averaged over 3 to 50 km from source.

Table 6. ESTIMATED EMISSIONS, POLLUTANT CONCENTRATIONS, AND LIGHT-SCATTERING CHARACTERISTICS FOR SECOND 1000-MW POWER PLANT[a]

Pollutant	Emission rate ($lb/10^6$ Btu)	Ambient 1-h max. concentration[b] ($\mu g/m^3$)		B_{scat} (10^{-4} m^{-1})		Visual range in clean air (km)		Visual range reduction for clean air (km)		Visual range in 24-km-visibility air (km)		Visual range reduction for 24-km-visibility air (km)	
		Range	Best estimate	Range	Best estimate	Range	Best estimate	Range	Best estimate	Range	Best estimate	Range	Best estimate
SO_2	0.4	69-59	68										
NO_x	0.7	120-102	119										
Particulates	0.1		18	0.072-.27	0.210	131-69	81	62-124	112	23-20	21	1-4	3
Secondary sulfates		1-21	3	0.030-2.1	0.180	161-13	88	32-180	105	24-9	21	0-15	3
Secondary nitrates		2-33	4	0.060-4.29	0.240	138-7	74	55-186	119	23-5	20	1-19	4
Total				0.162-6.66	0.630	93-4	37	100-189	156	21-4	16	3-21	8

[a] Plant burns 2.35%-sulfur coal, and 90% of the SO_2 emissions are removed.

[b] Averaged over 3 to 50 km from source.

In most cases, worst-case assumptions were made for these visual range calculations; other assumptions could produce drastically different results. For example, if (1) the ambient concentrations of particulates, SO_2, and NO_x were reduced by 50 percent, (2) the conversion of SO_2 and NO_x to sulfates and nitrates was assumed to proceed at only the rate of 0.1 percent per hour, and (3) the light-scattering efficiency of the sulfates and nitrates was assumed to be equal to the best estimate for primary emitted particulates (about 0.01×10^{-4} $m^{-1}/(\mu g/m^3)$) considerably different results, involving visual ranges greater than 110 km, would result for all the clean air cases presented in Tables 5 and 6. Furthermore, all the foregoing calculations assume that the plume conditions are persistent for several hours and that the observer is looking directly along the plume center line. To use the calculation technique details of the specific site and meteorological conditions must be provided.

Comparison of visual ranges for these different sets of assumptions indicates that the degree of potential visibility impairment depends greatly on the specific input assumptions used. This type of calculation technique, coupled with a sensitivity analysis of the input parameter, can be used to assess the potential impact of power plant emissions on regional visibility. TVA is planning further site-specific studies to examine actual relationships for some of its power plants. Studies of this type will provide some of the input to the overall evaluation of the visibility problem.

SUMMARY AND CONCLUSIONS

Measured and calculated mass distributions of power plant particulate emissions, power plant plume particulates, and ambient particulates near TVA power plants have been compared. These data show that a significant amount of the particulates emitted from a power plant with an efficient particulate control system are fine particles, less than 4 μm in diameter. These fine particulates are also observed in the power plant plume, 8 km from the plant. Measurements of ambient particulates include both the fine and larger particulates.

These particulate data have been combined with theoretical assumptions about the light-scattering potential of secondary power plant plume sulfates and nitrates to calculate the worst-case visibility for a plant burning medium-sulfur coal without SO_2 removal. Sulfates are the principal pollutant impacting visibility for this plant without SO_2 removal. However, when 90 percent of the SO_2 emissions are reduced by either installing scrubbers or by burning low-sulfur coal, primary particulates, secondary sulfates, and secondary nitrates contribute about equally to visibility reduction. However, these calculations are sensitive to the specific assumptions used and further investigation is planned to develop site-specific evaluations for some plants in the TVA system.

REFERENCES

1. White, W. H., and P. T. Roberts, 1977. On the Nature and Origins of Visibility-Reducing Aerosols in the Los Angeles Air Basin. Atmos. Environ. 11: 803.

2. Waggoner, A. P., et al. 1976. Sulfate-Light Scattering Ratio as an Index of the Role of Sulfur in Tropospheric Optics. Nature 261 (5556): 120.

3. Huang, C. M., et al. 1974. Investigation of Atmospheric Chemical Interactions in Coal-Fired Power Plant Plumes. Tennessee Valley Authority, Report Number E-AQ-74-1, Muscle Shoals, Ala.

4. Billings, C. E., and L. Silberman, 1962. Aerosol Sampling for Electron Microscopy. J. Air Pollut. Control Assoc. 12 (12): 586.

5. Morrow, P. E., and T. T. Mercer, 1964. A Point-to-Plane Electrostatic Precipitator for Particle Size Sampling. Am. Ind. Hyg. Assoc. J. 25 (1): 8.

6. Trijonis, J., and K. Yuan, 1978. Visibility in the Southwest: An Exploration of the Historical Data Base. Prepared by Technology Service Corporation for the Environmental Protection Agency, EPA-600/3-78-039.

7. Ursenbach, W. O., et al. 1976. Atmospheric Particulate Sulfate in the Western United States. Air Pollution Control Association Annual Meeting Paper No. 76-7.5.

8. Levy, A., et al. 1976. SO_2 Oxidation in Plumes: A Review and Assessment of Relevant Mechanistic and Rate Studies. Prepared by Battelle Pacific Northwest Laboratories for the Environmental Protection Agency, EPA-450/3-76-022.

9. Carpenter, S. B., et al. 1977. Principal Plume Dispersion Models: TVA Power Plants. J. Air Pollut. Control Assoc. 21 (8): 491.

10. Montgomery, T. L., et al. 1973. A simplified Technique Used to Evaluate Atmospheric Dispersion of Emissions from Large Power Plants. J. Air Pollut. Control Assoc. 23 (5): 388.

AN OPTICAL INSTRUMENT FOR DILUTE PARTICLE FIELD MEASUREMENTS

William D. Bachalo
Spectron Development Laboratories, Inc.
3303 Harbor Boulevard, Suite G-3
Costa Mesa, California 92626

ABSTRACT

Real time on-line measurement of particle field size and velocity distributions is possible with the light scatter detection instrument described in this paper. The instrument has been developed primarily for monitoring dilute particle flows. Two techniques have been incorporated into this device to satisfy the requirement of measuring particle size over approximately two decades (0.5 μm to 25 μm) in diameter and of measuring the particle velocity simultaneously.

By measuring the ratio of the light scattered from individual particles at two or more finite angles, the size of the particles can be determined. The technique has been proven practical in making *in situ* measurements of particle diameters in the range of 0.5 μm to 3 μm in diameter. Particle sizing interferometry is used to measure the particle size and velocity in the size range of 3 μm to 25 μm in diameter, and has been well characterized both analytically and experimentally in recent work.

Technology has been developed to extend the instrument's dynamic range (especially to smaller sizes). Work is currently in progress to implement this extended capability.

INTRODUCTION

Because of the potential threat to our environment, particle measurement instrumentation has become a key development area related to the utilization of coal and low grade fuels. A broad range of applications

exist in which particle monitoring is necessary both for process evaluation and the control of emissions. In facility research, the development and evaluation of particulate removal techniques necessitate the reliable measurement of the inlet and outlet size distributions. The ability to measure the particle size and velocity simultaneously would be especially useful in evaluating particle motility in electrostatic precipitators. Also, measurements of size and velocity would provide valuable information leading to an evaluation of the effectiveness of the various impaction clean-up systems. These data would be used in designing impactors, granular bed filters, and cyclone separators. Subsequent use of such particle detection instruments would be required to monitor the collection system while it is in operation. The instrument would act to continuously monitor the efflux size distribution and warn of excessive loadings.

Sizing techniques that are available fall into categories based on sampling and optical methods. Sampling requires the extraction of a sample from the flow which is then analyzed externally with instrumentation including microscopy, scanning electron microscopy, weighing, or a combination of these methods. Besides being tedious, the sampling process inherently disturbs the flow field and hence, the particle distribution, even when the sample is withdrawn isokinetically. Furthermore, agglomeration, redispersion, impaction, and deposition occur in the sampling processes. Combustion related particulates are often in a state of dynamic equilibrium and as such, should be measured *in situ* if a reliable size determination is to be obtained.

There are several advantages to applying optical methods. With optical methods, *in situ* particle size and velocity measurements in real time are possible. Laser light scatter detection sizing techniques that measure single particles at a time offer high information content, good spatial resolution, and signal-to-noise characteristics. Sophisticated electronics circuitry is available for use with these techniques to handle large quantities of data efficiently while the measurements are made non-intrusively in environments wherein material sampling probes would be rendered inoperable. Two optical techniques that perform size measurements independent of the absolute scattering intensity, particle sizing interferometry and scattering intensity ratioing, have been incorporated into the particle diagnostics system described in this paper. This system can measure particles in the size range of 0.5 μm to 25 μm in diameter as well as the particle velocity, thus allowing the determination of particle concentration. Relevant features of these systems produced by Spectron are discussed.

PARTICLE SIZING INTERFEROMETRY

Several laser light scatter detection techniques are available for particle sizing. However, the techniques that are based on the measurement of the absolute scattering intensity are subject to systematic errors when the facility windows become contaminated. Such contamination

is not uncommon in combustion processes. In addition, a numerical inversion scheme based on empirical calibrations is required to unfold the signal amplitude dependence on the unknown particle trajectory through the Gaussian intensity distribution[1]. These techniques are also dependent, to a degree, on the particle index of refraction, especially on the absorption of the particle.

The concepts used in the present instrument are independent of the absolute scattering intensity (except as it affects the signal-to-noise ratio) and hence are not drastically affected by the accumulation of contaminants on the windows. Instead, the well-defined shape of the forward-scattered lobes are measured and reduced to particle size analytically. Calibration is only required to verify the calculations.

The first technique, particle sizing interferometry, makes use of the relative amplitude modulation or visibility of a laser Doppler velocimeter signal. Visibility is defined as the ratio of the light scattered when the particle is centered over a bright interference fringe to when it is centered over a dark fringe and is given by

$$V = \frac{I_{max} - I_{min}}{I_{max} + I_{min}} \tag{1}$$

where I is the photocathode current of the photomultiplier tube.

A schematic drawing of a typical optical arrangement for particle sizing interferometry is shown in Figure 1a. An argon-ion laser (blue, $\lambda = 0.488$ μm) provides the necessary coherent light source for this technique. The laser beam is split into two equal intensity beams and focused with a lens to a crossover point. Careful optical design is required to ensure that the beam crossover and the foci coincide. At the crossover, the beams interfere to form a stationary set of fringes (Figure 1b). The spacing of these fringes can be determined very accurately either by direct measure or from the optical geometry and the following expression:

$$d_f = \frac{\lambda}{2 \sin \theta/2} \tag{2}$$

where λ is the wavelength of the incident beam and θ is the beam intersection angle.

Particles moving with the flow and passing through the focal volume scatter light in proportion to the spatially varying light intensity of the fringe pattern. Typical signals detected by the photomultiplier are shown in Figure 2. The Gaussian shaped envelope of the signals is indicative of the laser beam intensity distribution. The modulation of the signal occurs as a result of the particle's passing through the fringes. Variation in the depth of the modulation is a function of the particle size relative to the fringe spacing (i.e., a function of d/d_f, where d

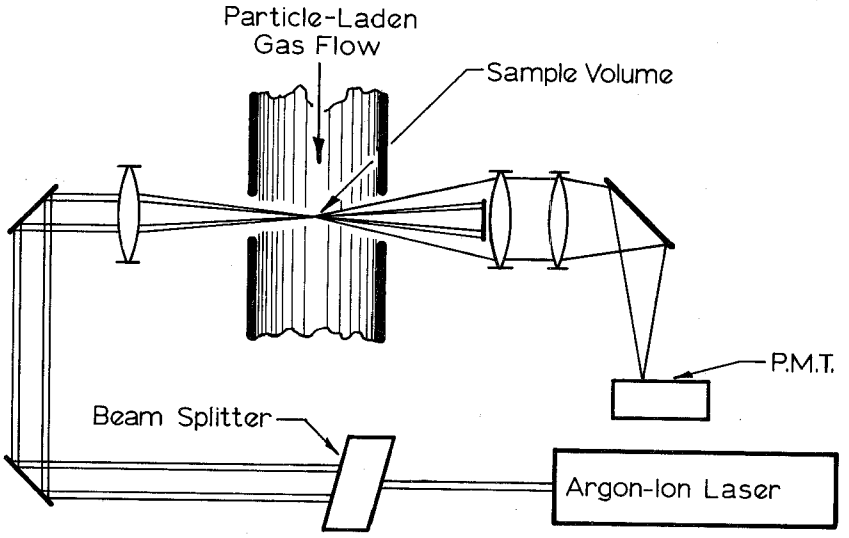

Figure 1a. Schematical diagram of the particle sizing interferometer optics.

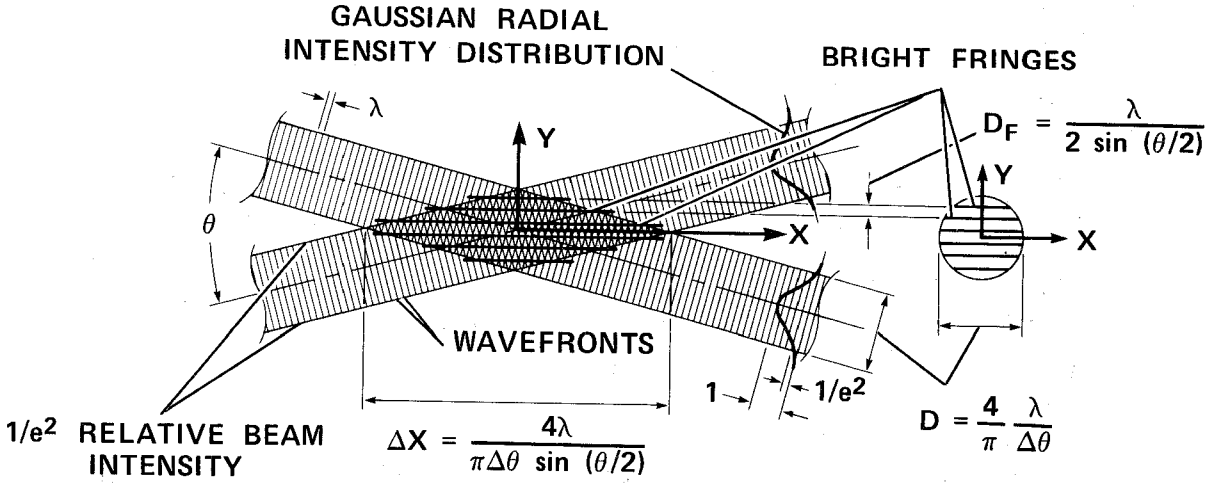

Figure 1b. Enlarged view of the probe region.

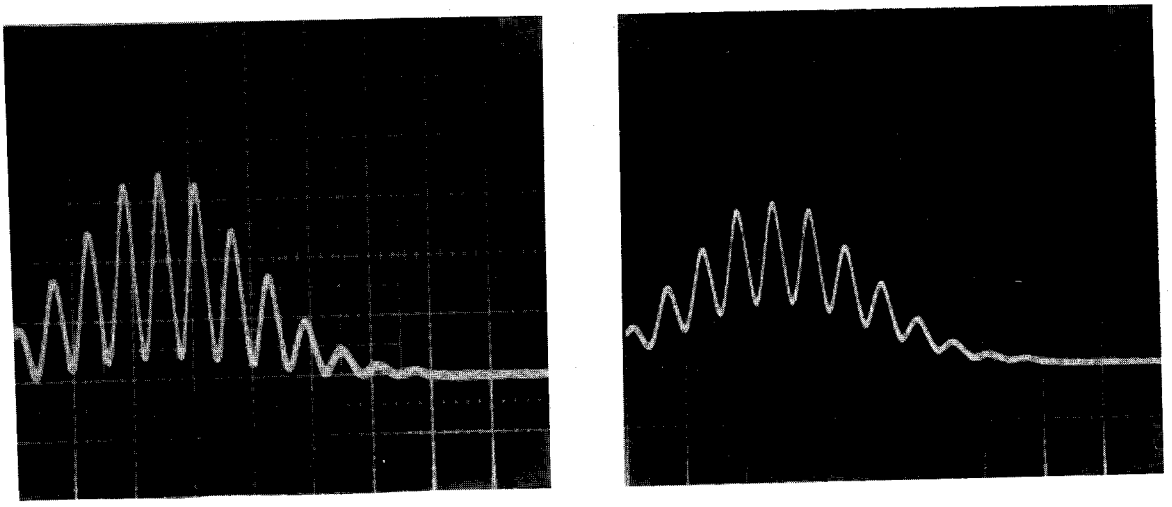

(a) $V = \frac{V_{max} - V_{min}}{V_{max} + V_{min}} = 0.84$ (b) $V = 0.47$

Figure 2. Oscilloscope traces of signals from the particle sizing interferometer for two different particle sizes.

is the particle diameter). A heuristic explanation of why the visibility varies with particle size is as follows. Particles much smaller than the fringe spacing crossing the probe volume will scatter light to trace out the sinusoidal fringe intensity distribution incident upon it. Increasing the particle size with respect to the fringe spacing will result in the particle scattering light from the fringe it is entering as well as the one it is leaving.

The theory behind the phenomena is essential in understanding and predicting the parametric behavior of the scattering and in evaluating the optics system. Fortunately, considerable research has been devoted to analyzing the multiple beam scattering to define the functional behavior relating visibility to particle size. One of the first analysis attempts was Farmer's[2] derivation which was based on the hypothesis that the scattered light intensity was proportional to the integral of the illuminating fringe pattern intensity distribution over the particle taken as a disk of equal projected area. With this approach and the assumption of small beam intersection angles, it was concluded that visibility, V, is given by

$$V = \left| \frac{2 J_1 (\pi d/d_f)}{\pi d/d_f} \right| \qquad (3)$$

where J_1 is the Bessel's function of the first kind. In addition, it was concluded that in the case of paraxial light collection, the

visibility is independent of the Mie scattering amplitudes, the particle shape, and index of refraction. The relationship is shown in Figure 3.

Subsequently, Robinson and Chu[3] derived the functional relationship using a more rigorous approach based on scalar diffraction theory. Diffraction theory does not include index of refraction effects and is valid only for scattering centers that are several diameters greater than the wavelength of light. The analysis concluded that the visibility is a function of the light collection aperture as well as the particle diameter. With paraxial forward scatter observations the theory was in good agreement with Farmer's results. More important is the fact that their experimental data and Farmer's agreed very well with the theory using the above assumptions. The theory was also able to predict experimental results for particle sizes down to only a few microns in diameter.

Evaluation of the possible effects of refractive index were made in a more recent paper by Chu and Robinson[4] using a detailed analysis of scattering from particles in two crossed coherent light beams. In this study the exact solutions of Maxwell's equations (Mie theory) were employed. For optics configurations wherein the scalar diffraction theory applied, the analysis was in agreement with Equation 3. The analysis showed reasonable agreement with the diffraction theory for scatterers that are absorptive. The scalar theory did, however, give consistently higher values of visibility than did the Mie calculations. For transparent spheres having little or no absorption, significant oscillations of the visibility function occurs for fringe spacings less

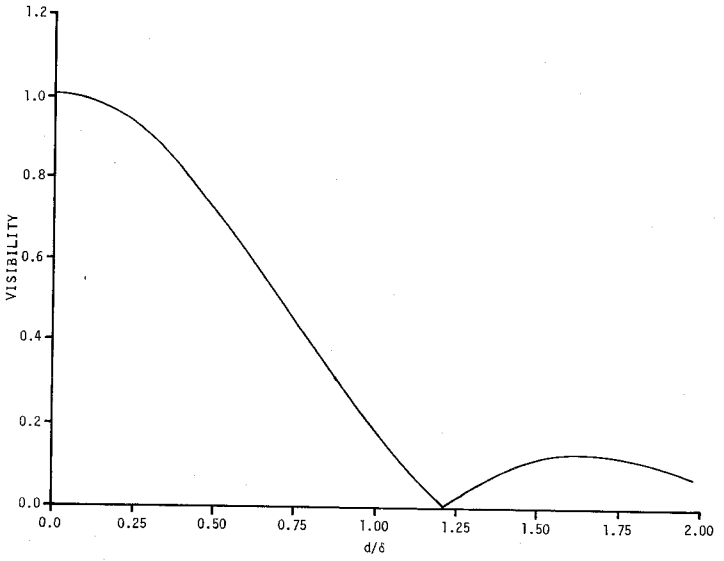

Figure 3. Simplified visibility relationship for particle sizing.

than 10 μm. This is due to interference of the refractive scattering of light passing through the sphere with the diffractive scattering. For comparison, Figure 4 shows the Mie scattering diagrams for a particle with and without absorption. For larger particles, the diffractive scatter is dominant about the near forward direction and the main forward scatter lobe is several orders of magnitude greater than the off-axis secondary lobes. Thus, in the dual beam scattering the interference between the forward lobe and the secondary lobes is diminished.

Roberds[5] examined some further aspects of the design of the optical geometry. In particular, the size of the collection aperture and beam stop, with respect to the beam spacing at the collection lens, were shown to affect the visibility. This result is not surprising in that the entire forward scattered lobes should be collected if the result is to agree with the analysis. The dependence was shown to be minimized with an adequately large collection F/number. His data also showed excellent agreement with the theory.

The effect of irregular shaped particles on the measurements requires some analysis. With this technique, measurements of size are one dimensional, producing a measure of the mean particle length in the direction normal to the interference fringes. For isometric particles, the measurement approaches that of a sphere of equivalent projected cross-sectional area. Particles that are elongated will tend to be measured as larger or smaller in projected area than the assumed equivalent sphere, depending upon their orientation to the fringe normal. However, such particles will probably be randomly orientated and so the size distribution, taken over several thousand samples, will approach the correct value.

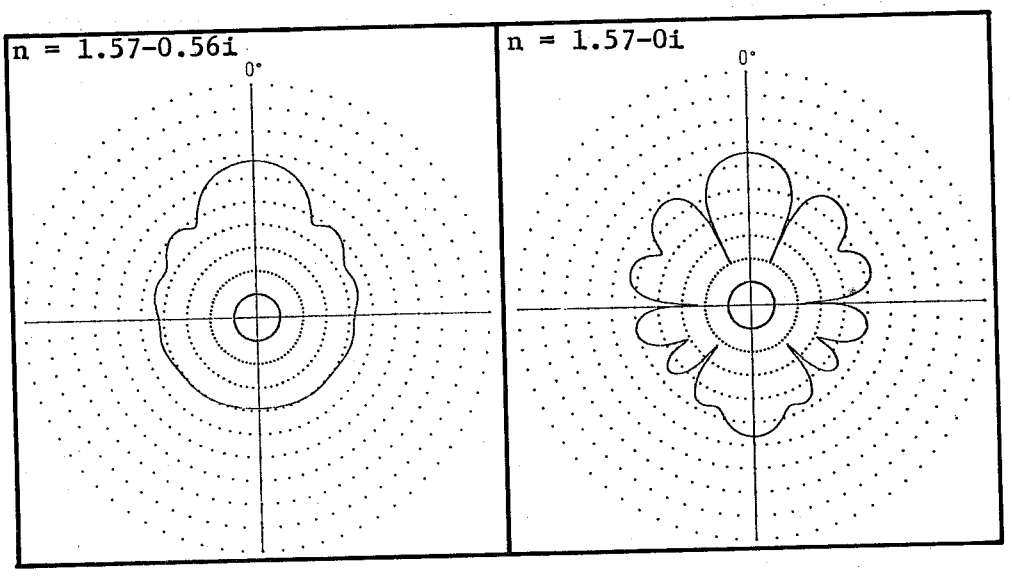

Figure 4. Comparison of Mie scattering diagrams with and without absorption.

SCATTERING INTENSITY RATIOING

This technique, based on the collection of scattered light at two angles in the near-forward direction (Figure 5), also makes use of a highly focused light source allowing for very high spatial resolution. The absolute scattering intensity does not enter into the size determination and because of the near-forward light collection, there is sufficient independence of particle shape and index of refraction (for absorbing particles).

Figure 6 is a schematic diagram of the optical geometry required for this system. An argon-ion laser is used to provide light of wavelength 0.5145 μm. To obtain the desired probe volume, beam expansion is used before the beam is focused by the transmitting lens to a spot of approximately 80 μm in diameter. The scattered light is detected by the collection lens and separated by a pair of annular masks into two angles of scatter; 2.5° and 8.5° in this case. Ratios of the signals from the photomultiplier tubes are taken in the electronics processor for conversion to particle size.

Reduction of the measured ratios requires the use of the polar scattering intensity distributions computed from the Mie theory. It is important to note that the ratios of radiant flux, F, scattered by a particle of diameter d is independent of the incident intensity. That is, the ratio

$$\frac{F(\theta_1)}{F(\theta_2)} = \frac{[i_1(\theta_1,\alpha,n) + i_2(\theta_1,\alpha,n)] \sin \theta_1 \Delta \theta_1}{[i_1(\theta_2,\alpha,n) + i_2(\theta_2,\alpha,n)] \sin \theta_2 \Delta \theta_2} \qquad (4)$$

for two finite collection angles θ_1 and θ_2 has I_o canceled from the expression. This is the desired result since the incident intensity on the particle is unknown as a result of intensity variation with trajectory through the focal volume and beam attenuation. The plot of the normalized scattering intensity ratio versus particle diameter is shown in Figure 7. A complex index of refraction given as $n = 1.57 - i0.56$ typical of soot was used in the calculation of this curve. The collection angle pair selected determines the sensitivity to size range. Using near-forward scattered light, the upper size limit of this technique is approximately 10 μm.

Because the particulates measured cannot be expected to be spherical, consideration of the instrument response to non-spherical particles must be made. Hodkinson[6] has shown that the forward scatter for a polydisperse system of irregular particles was similar to that of spherical particles of equivalent projected cross-sectional area. If the Fraunhofer diffraction theory is considered, it can be seen that the extent of the angular scatter by an irregularly-shaped particle depends on its dimensions in the respective directions (e.g., consider the scatter of a rectangle). When the scatter is detected with a circular aperture centered in the forward direction, the scatter from individual

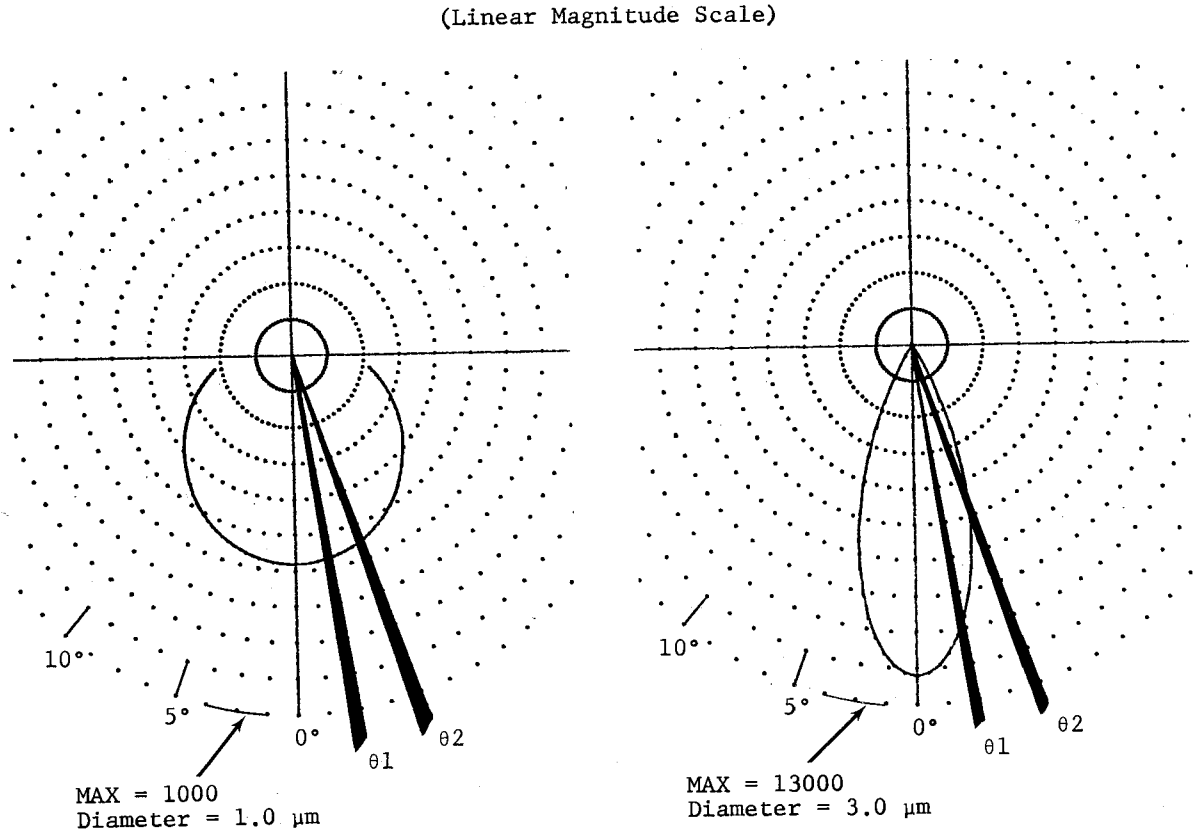

Figure 5. Expanded forward scatter lobes showing collection angles for intensity ratioing.

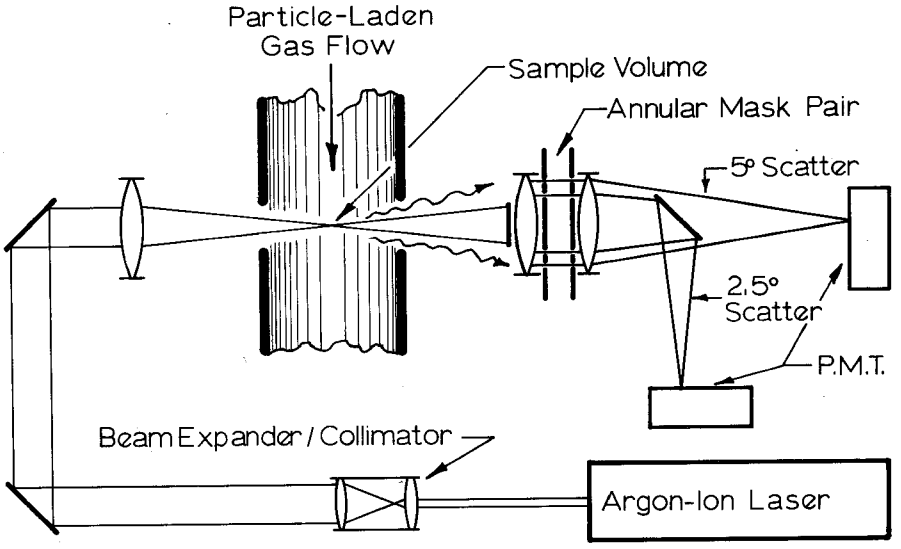

Figure 6. Schematic diagram of the ratioing optics system.

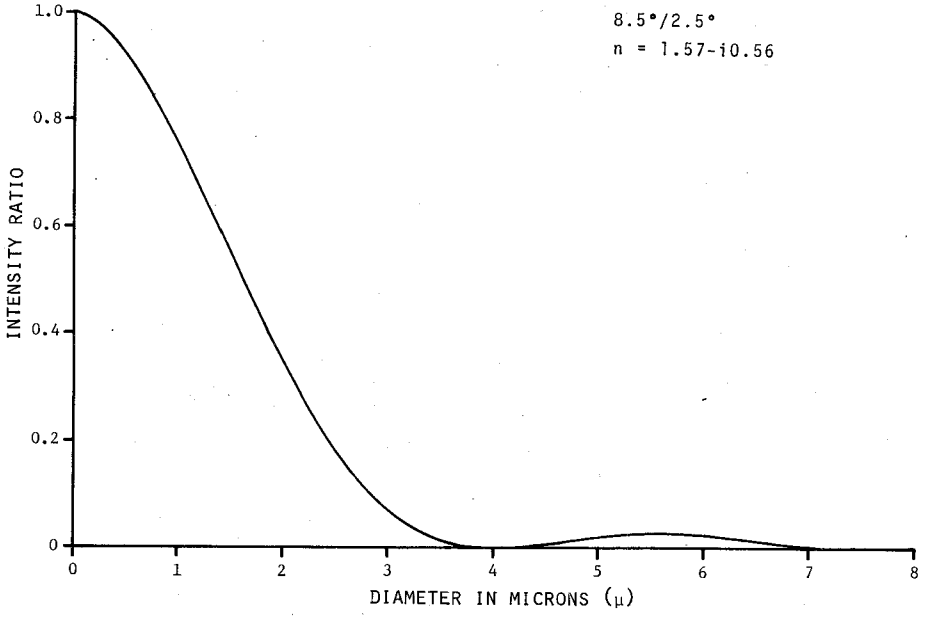

Figure 7. Scattering intensity ratio versus particle size.

particles is averaged over the aperture and produces a measurement approaching that of an equivalent sphere. Hirleman[7] investigated the scatter from irregularly-shaped particles (i.e., agglomerated polystyrene spheres) and found that the scattering patterns had forward lobes that appeared similar to that of spheres of equivalent diameter.

Since this technique measures a single particle at a time, an upper limit on the particle concentration is set by the requirement of having a low probability of having more than one particle in the probe volume at a time. Assuming that the particles are Poisson distributed, the probability of having n particles in the probe volume, V, at one time is given by:

$$P(n) = \frac{\exp(-\bar{N})\,\bar{N}^n}{n!} \qquad (5)$$

where $\bar{N}$ is the average number of particles in the probe volume at any time. For a practical probe volume of 2×10^{-6} cm^3, a concentration of 10^5 particles/cm^3 would produce multiple particle signals only 1.7 percent of the time. Ho, et al[8], showed that if more than one particle was in the probe volume at one time but the peaks were separable, the two pulses could be processed independently using peak detection. With this method of signal processing and a possible probe volume as small as 2×10^{-7} cm^3, the possibility of making measurements at concentration as high as 10^7 particles/cm^3 was stated.

INTEGRATED PARTICLE SIZING SYSTEM

Most realistic applications of particle sizing instrumentation require that they operate over a size range greater than one decade without manipulations of the optics. The present instrument was required to measure particles over an estimated size range of 0.5 μm to 25 μm in diameter. For this reason the two techniques, particle sizing interferometry and scattering intensity ratioing were combined into a single measurement system.

An argon-ion laser was used to produce both a blue (0.4880 μm) and a green (0.5145 μm) wavelength simultaneously. Figure 8 is a schematic drawing of the optics system. The wavelengths are separated with a dispersion prism and directed through the respective optical elements. Since the ratioing technique must be sensitive to the smaller size range in which the particles are, in general, more plentiful, the beam is expanded to achieve a focused spot diameter of approximately 80 μm to e^{-2} of the peak intensity level. The blue beam is split into two equal intensity beams and focused to a crossover of approximately 250 μm in diameter. Particles passing through the focal volume scatter light at both wavelengths. A dichroic mirror separates the signal by wavelength and directs the light to the appropriate photomultiplier tubes. The ratioing signal is passed through an annular mask to separate the scatter at the two set angles.

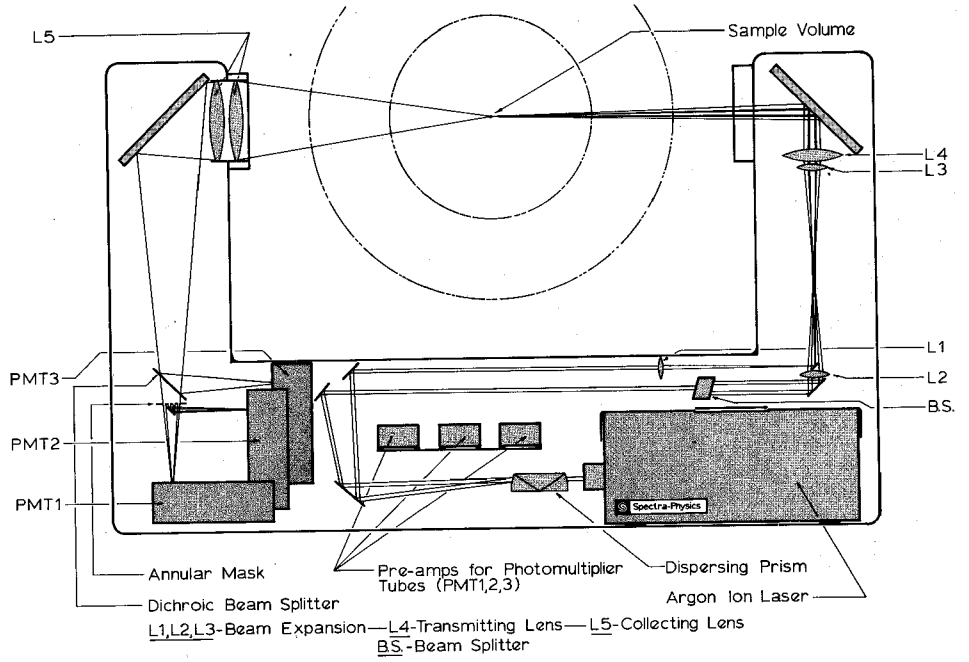

Figure 8. Integrated particle sizing system combining particle sizing interferometry and scattering intensity ratioing.

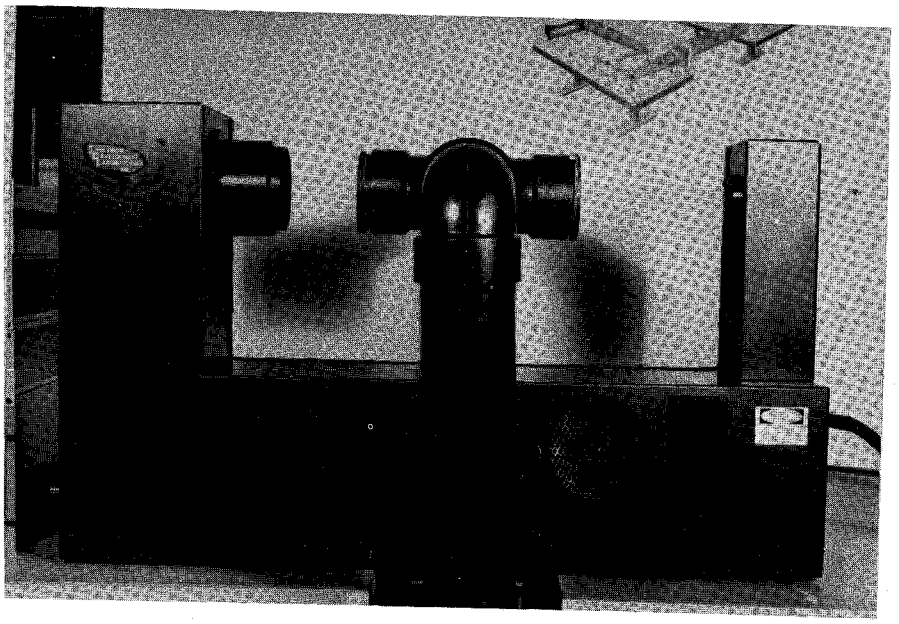

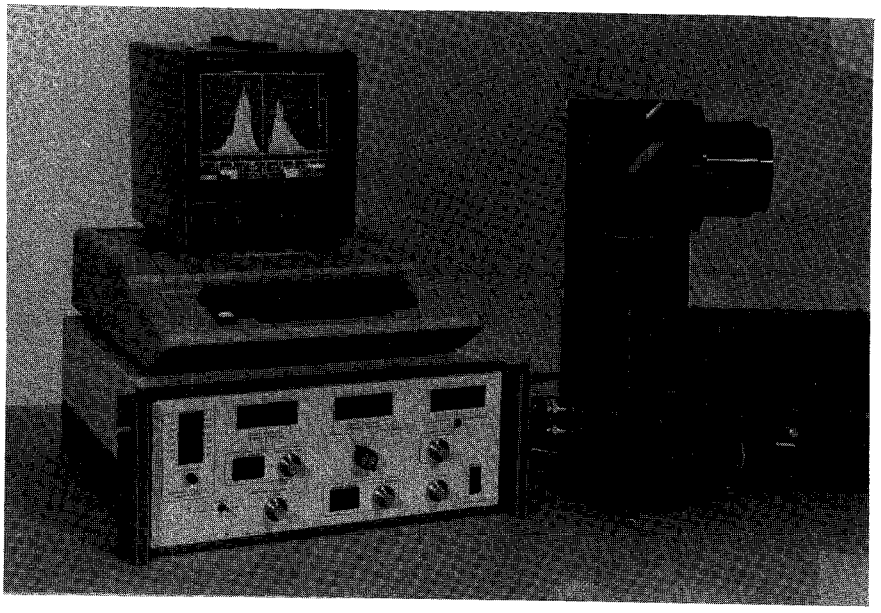

Figure 9. Particle sizing instrument shown with the test facility.

In the electronics, the signals are low pass filtered before being processed. The scattering intensity ratioing signals are integrated over the burst to eliminate the effects of any remaining noise on the signal. Ratios of the integrated values are taken and a 10-bit binary number proportional to the ratio is output. Particle sizing interferometry is more sensitive to noise on the signal so more sophisticated electronics processing is required. The usual 5/8 (or other count ratio) periodicity check is used primarily to reject multiple particle signal occurrences. To discriminate against noise, the multiple level signal test developed by Macrodyne was used. This technique has been proven to be exceptionally effective in the rejection of noise and can decrease the number of signals otherwise rejected by the periodicity check. Signals that pass the test are separated into high frequency (Doppler) and the low frequency (pedestal) components, integrated, and the ratio is taken. The output is a 10-bit binary number proportional to the visibility.

A microprocessor-based histogram generator that can store two histograms simultaneously (one from each technique) is used to manage the data. Samples are plotted on the video monitor as they are accumulated. When a preset number of samples have been accumulated, the histograms are plotted and the data is reduced to particle size and tabulated on hard copy. The system can operate at data rates as high as 10^4/sec. Photographs of the system are shown in Figure 9.

CONCLUSIONS

A particle monitoring system that determines the size distribution and concentration has been described. This system has incorporated two proven sizing techniques based on the detection of scattered laser light. Both techniques are made independent of the absolute scattered intensity which is important in view of the high probability of contamination of the facility access windows. The instrument has been designed to be sufficiently rugged in order to withstand the harsh working environments. Data acquisition has been simplified with the use of a microprocessor-based histogram generator. The microprocessor has the capability of reducing the data to whatever format is desired by the user. Graphics capability is also provided for data display and analysis.

Field-ready instruments have been produced and are currently undergoing testing at the Solids/Gas Test Facility, Argonne National Laboratories and on the Small Gas Turbine Pilot Fluidized Bed at Curtiss Wright.

REFERENCES

1. Holve, Don and Self, Sidney A. An Optical Particle-Sizing Counter for In-Situ Measurements. Project SQUID Technical Report SU-2-PU.

2. Farmer, W. M. The Interferometric Observation of Dynamic Particle Size, Velocity, and Number Density. Ph.D. Thesis, University of Tennessee. 1973.

3. Robinson, D. M. and Chu, W. P. Diffraction Analysis of Doppler Signal Characteristics for a Cross-Beam Laser Doppler Velocimeter. Applied Optics. 14:2177-2183, September 1975.

4. Chu, W. P. and Robinson, D. M. Scattering from a Moving Spherical Particle by Two Crossed Coherent Plane Waves. Applied Optics. 16:619-626, March 1977.

5. Roberds, D. W. Particle Sizing Using Laser Interferometry. Applied Optics. 16:1861-1868, July 1977.

6. Hodkinson, J. R. Light Scattering and Extinction by Irregular Particles Larger than the Wavelength. In: Proceedings of Interdisciplinary Conference on Electromagnetic Scattering. Permagon Press, Oxford 1963. p. 87-100.

7. Hirleman, E. D. Optical Technique for Particulate Characterization in Combustion Environments: The Multiple Ratio Single Particle Counter. Ph.D. Thesis, Purdue University. 1977.

8. Ho, C. W., Tveten, P. W., Chan, P. W., and She, C. Y. Particle Size Measuring Device in Real Time for Dense Particulate Systems. Applied Optics. 17:631-634, February 1978.

IMPACT OF SULFURIC ACID EMISSIONS ON PLUME OPACITY

John S. Nader and William D. Conner
Environmental Sciences Research Laboratory
U.S. Environmental Protection Agency
Research Triangle Park, North Carolina

INTRODUCTION

Emission standards for opacity and for mass concentration of particulate matter have been established for new sources and are applicable to fossil-fired combustion sources[1]. Continuous monitors for opacity (transmissometers) are required to be installed on these sources to verify the maintenance and satisfactory operation of control systems used to meet the emission standards[2]. Reference method 9 is the observer method of measuring the opacity of the plume which forms as the particulate matter exits the stack[1]. The Lidar (light detection and ranging) technique is an electro-optical instrumental technique to remotely measure the opacity of the plume[3,4]. The transmissometers are installed in the stack or in ducts leading to the stack. These monitors measure the opacity of the gas stream in the stack or duct prior to its exiting the stack.

The Stationary Source Emissions Research Branch (SSERB) of the Environmental Sciences Research Laboratory has had in its program during the past three years tasks to generate a data base of concurrent measurements of in-stack gas opacity (O_S) and plume opacity (O_P) for emissions from various industries. The purpose of these measurements was to identify those industries wherein the plume and in-stack opacities do not agree. Measurements conducted to date on combustion sources burning coal with sulfur $\leq$2% show that O_S and O_P are comparable[5,6]. These results would imply that no significant (observable effect on opacity) physical or chemical transformation was occurring in the contents of the gas stream as it was transported through the stack.

Similar opacity measurements were made on a power plant burning oil with 2.4% S (sulfur) and 200-600 ppm V (vanadium). In contrast with opacity measurements made at sources burning coal or oil of lower sulfur content the plume opacity was found to be significantly higher than the in-stack opacity. At this oil-fired power plant a concurrent study was being conducted on sulfuric acid emissions. The results of this acid study support the conclusion that a physical transformation occurs as the gas stream exits the stack and enters the atmosphere. The following phenomenon is indicated: The sulfuric acid is above its dew point at stack temperatures in excess of 150°C and does not affect the in-stack opacity. When the gaseous sulfuric acid leaves the stack and is cooled to ambient air temperatures which are below its dew point, it condenses and the sulfuric acid droplets increase the plume opacity. Additional studies have been conducted and are on-going to obtain more data and understanding of the effect of sulfuric acid emissions on plume opacity for various operating conditions, fuel composition, and control systems for a number of fossil-fuel-fired utilities. This paper presents and discusses the results of the above work that SSERB has conducted thus far.

The sulfur oxides potentially present in the stack gas stream at temperatures above the sulfuric acid dewpoint are as shown in Figure 1. The free H_2SO_4 and SO_2 are not sensed in the measurements of the opacity of the stack gas stream. In the plume with the temperature of the gas stream dropping below the acid dewpoint and approaching ambient air temperature, the free H_2SO_4 condenses to form acid droplets. The condensed acid droplets and the acid adsorbed on the fly ash add to the opacity of the plume. In our studies O_s was measured by transmissometers and O_p was measured by human observers or by a Lidar system; in some instances, O_p measurements were made by both of these methods.

COMBUSTION SOURCE FEATURES

Plume opacity measurements were conducted in conjunction with emissions characterization studies at 2 oil-fired and 3 coal-fired power plants. Table 1 summarizes the physical and operating features of the plants.

There is a marked difference in composition of the fuel utilized in the oil-fired sources in contrast to the coal-fired sources. The ash content of oil was two orders of magnitude less than the ash content of coal. The sulfur content of the coal was from 2 to 4 times the sulfur content of the oil. In addition, very high vanadium concentration (590 ppm) was found in the Venezuelan oil. Excess boiler oxygen was typically in the 3 to 5% range except for Plant A which operated at very low oxygen levels at about 0.2%. Oil-fired sources had no emission controls; however, fuel additives were used to minimize corrosion problems and did provide some reduction in sulfate emissions[7]. Coal-fired sources had either particulate emission controls (electrostatic precipitators, ESP) or both particulate and gaseous emissions controls (two-stage wet scrubbers).

SAMPLING LOCATIONS

Sampling locations for all in-stack measurements were at a common location between the emission controls and the stack except for Plants M and LC. At Plant M all in-stack measurements were at a common location in the stack proper. At Plant LC in-stack opacities were monitored in breechings leading into the stack and all other in-stack measurements were at the output of one of eight scrubber modules that operated in parallel for the total boiler output of 820 MW. Each module in effect handled about 100 MW of power output. Except as noted, plume opacities were measured within one stack diameter of the stack exit.

RESULTS

Emission data were obtained on particulate concentration, SO_2, and sulfates under various operating conditions of the boiler (excess O_2) and of the control systems (cutting back on electric fields of ESP). Opacity data, however, were obtained concurrently for a limited number of operating conditions. The Lidar system was inoperative and undergoing repairs during the studies on the coal-fired sources. Plume opacity data in these instances were limited to Method 9. Poor weather conditions (fog) also restricted plume observations during the study at Plant LC.

Data from the various plant studies on emission concentrations of gross particulate matter, SO_2, total water soluble sulfates ($SO_4^{=}$), plume opacity, and in-stack opacity were reviewed. As much as possible, data were selected for those periods of time when these measurements were made concurrently. Tables 2, 3, and 4 are a consolidation of these data. Table 2 summarizes the emission data for oil-fired power plants without any emission control systems, Table 3, for coal-fired power plants with ESP controls, and Table 4, for a coal-fired power plant with 2-stage wet scrubbers (particulate control plus flue gas desulfurization, FGD). Various constraints such as number of available sampling ports in a given location did not permit the desired measurements to be executed concurrently at Plant LC and this is reflected in the data in Table 4. These data represent sampling visits to this source on three different dates.

Figure 2 graphically portrays the data of Table 2 showing the comparison of the plume opacity data with the in-stack opacity data at the oil-fired power plants. Figure 2 also provides data on the effect of additional condensation on plume opacity with cooling of the plume downstream of the stack exit location.

DISCUSSION

At the oil-fired power plants M and A (Table 2) the most distinguishing features are the vanadium content of the fuel oil, levels of excess O_2, and their impact on plume opacity. Plant M was burning domestic fuel oil with about 15 ppm V and 1.2% S compared to Plant A which was burning Venezuelan fuel oil with 590 ppm V and 2.4% S. Both plants utilized fuel additives. A significant difference between plume and stack opacity existed for both fuels and for different levels of excess O_2.

The plume opacity at Plant A at normal operation was 31% at the stack exit and above the opacity emission standard of 20%. The opacity increased markedly to 43% further downstream as more condensation of sulfuric acid occurred with cooling of the plume. The observers tended to read higher opacity values than the Lidar.

Both solid particulate matter and condensed sulfuric acid (liquid droplets) affect opacity. Unfortunately, concurrent data are not complete in Table 2, but qualitative data from acid emission measurements in other studies[8,9,10] reinforce some observations which can be made from Table 2. The concentration of solid particulate matter increased as excess O_2 for combustion was decreased to reduce acid formation. We attribute this to unburned carbon soot particles which have been observed in a related study[11]. The increase of in-stack opacity with decrease in excess O_2 demonstrates this. Since the acid is in the gas phase in the stack, a decrease in acid with a decrease in excess O_2 does not affect the in-stack opacity data or the above interpretation of the data. As a matter of fact, the possibility of reduced sulfate salts exists with the decreased acid and this would tend to counteract the effect of the unburned carbon. This would imply a greater impact of acid on stack opacity than was actually observed.

In the plume, the acid (at temperatures below its dewpoint) appears as liquid droplets after condensation. With increased excess O_2, the increased acid and sulfate salts tend to increase the plume opacity but a counteracting effect is the concurrent reduction in unburned carbon resulting from more complete combustion of the oil. Since the condensation of the acid is a function of the plume temperature, one can infer

on a semi-quantitative basis the contribution of the condensed acid in the plume opacity relative to that of the solid particulate (both unburned carbon and sulfate salts) by a comparison of the plume opacity at the exit to that downstream of the exit. At 0.2% O_2 the plume opacity increase was from 31 to 43%. At 0.6% O_2 the increase was from 23 to 54%, indicating the presence of more acid at higher excess O_2 levels. The impact of the acid may actually be more than indicated because dilution of the plume downstream can reduce the opacity and counteract the effect of the increase in condensed acid.

It is of interest to note that there appears to be an increase (56%) in particulate loading as determined by Method 5 with an increase in excess O_2 (Table 2, Plant A). One might expect a decrease because of a reduction in unburned carbon with more complete combustion. There is the possibility of an increase in measured particulate loading due to the collection of the gaseous acid and sulfate salts by Method 5. Related studies in our laboratory have shown the glass fiber filter to be a good collector of the gaseous acid[12]. One can postulate that two overlapping functions (one an increase in sulfate salts and acid and another a decrease in unburned carbon with increasing excess O_2) contribute to the particulate loading. The former will be a curve with a positive slope, the latter a curve with a negative slope. The resulting curve on particulate loading as a function of excess O_2 would have a positive or negative slope depending upon which function has the steeper slope. The resulting curve would approach a straight line (zero slope) as the two functions tend to exactly counteract each other. Consequently, depending upon the amount of excess O_2, the particulate loading may be on either the rising or declining slope of the curve or it may be more or less constant.

The emission characterization data for high sulfur (>2% S) coal-fired power plants with ESP controls show no significant difference between plume and in-stack opacity under normal ESP operation or with reduced electric fields in the ESP's. It is possible that the high ash content of the coal and resulting high particulate loading in the emission have a predominant effect on the in-stack and plume opacity. In-stack opacity at normal operation of the ESP was close to the opacity emission standard for new sources and higher than that for the oil-fired power plants. The ratio of $SO_4^=$ to particulate matter for the coal-fired emissions is <1 and for the oil-fired emissions, >1.

The stack gas environment for the coal-fired power plant (LC) with particulate and gas controls (two-stage wet-scrubber) was unlike that for plants with ESP controls. The stack gas temperatures were below the sulfuric acid dewpoint and the water vapor content from the wet scrubbers was high. The result was that sulfuric acid will appear in the gas stream as condensed acid droplets and these directly affect the in-stack opacity.

Concurrent emission data could not be obtained for Plant LC (Table 4) in the same manner that it was for Plants P and MC (Table 3)

because the required number of sampling ports was not available. Nonetheless, the data obtained from the three visits to Plant LC do permit some qualitative observations. The emission data on the particulate loading appear to fall within a narrow range of values indicating consistent plant operation. The plume and in-stack opacity data show no significant difference but the very high opacity values are not consistent with the particulate loading, size, and composition normally associated with fly ash emissions. Optical transmittance measurements conducted at different wavelengths during the study gave data that varied with wavelength in the visible portion of the spectrum[13]. This variation with wavelengths is indicative of submicron size distribution. The submicron size was also substantiated with in-stack impactor measurements[14]. The acid composition of the gas stream was substantiated by the controlled condensation measurement data[7]. In this case, we attribute the high in-stack opacity levels to fine particle concentration with a mass mean diameter in the submicron size range and with a significant percentage of the composition consisting of condensed sulfuric acid.

There are a number of important questions raised by the data obtained thus far. More studies are needed to adequately address these questions and to determine the variation of these pollutant emissions with operating parameters. The questions can be briefly stated as follows:

- What is the quantitative distribution of H_2SO_4 in the gas stream between free acid and acid adsorbed on particulate matter?
- What is the distribution of the sulfate ion ($SO_4^=$) between acid and salts?
- What is the size distribution of acid and salts?

There is need for more data on the physical properties of H_2SO_4 in both the stack and plume environments to support proper interpretation of optical data.

SUMMARY

Emissions from oil-fired power plants without emission controls and coal-fired power plants with ESP's and with FGD systems were characterized for plume and in-stack opacity, SO_2, $SO_4^=$, and mass concentration. Sulfuric acid content of the emissions from the oil-fired power plant had a significant effect on the plume opacity but no effect on the in-stack opacity. In the case of the coal-fired power plants with ESP's the in-stack and plume opacities were essentially the same. This led to the conclusion that the concentration of acid was low relative to the non-acid particulate such that the acid did not contribute to any significant degree to the opacity of the plume beyond that normally associated with the fly ash. The in-stack and plume opacities of the emissions for the high sulfur coal-fired power plant with the two-stage wet scrubber system were comparable but significantly high (70 to 90%). The high opacity was attributed mainly to the sulfuric acid content of the emissions and to submicron size of the particulate matter.

REFERENCES

1. U.S. Environmental Protection Agency, Standards of Performance for New Sources. Fed Regist. 36, 24876-24895, 1971.

2. U.S. Environmental Protection Agency, Standards of Performance for New Sources. Fed Regist. 40, 43850-43854, 1975.

3. Cook, C. S., G. W. Bethke, and W. D. Conner. Remote Measurement of Smoke Plume Transmittance Using Lidar. Appl Opt. 11, 1742-1748, 1972.

4. Johnson, W. B., R. J. Allen, and W. E. Evans. Lidar Studies of Stack Plume in Rural and Urban Environments. U.S. Environmental Protection Agency, Research Triangle Park, N. C. Publication Number EPA 650/4-73-002. 1973. 112 p.

5. Peterson, C. M., and M. Tomaides. In-Stack Transmissometer Techniques for Measuring Opacities of Particulate Emissions from Stationary Sources. NTIS. Publication Number PB-212-741.

6. Herget, W. F., and W. D. Conner. Instrumental Sensing of Stationary Source Emissions. Environ Sci and Technol. 11, 962-967, 1977.

7. Homolya, J. B. Unpublished data. U.S. Environmental Protection Agency, Research Triangle Park, N. C. 1978.

8. Homolya, J. B., and J. L. Cheney. An Assessment of Sulfuric Acid and Sulfate Emissions from the Combustion of Fossil Fuels. In: Proceedings of Workshop on Measurement Technology and Characterization of Primary Sulfate Emissions from Combustion Sources. Southern Pines, N. C. April 24-26, 1978. J. S. Nader, Ed. EPA document in press.

9. Dietz, R. N., and R. F. Wieser. Operating Parameters Affecting Sulfate Emissions from an Oil-Fired Power Unit. In: Proceedings of Workshop on Measurement Technology and Characterization of Primary Sulfate Emissions from Combustion Sources, Southern Pines, N. C. April 24-26, 1978. J. S. Nader, Ed. EPA document in press.

10. Cheney, J. L., and J. B. Homolya. Characterization of Combustion Source Sulfate Emissions with a Selective Condensation Sampling System. In: Proceedings of Workshop on Measurement Technology and Characterization of Primary Sulfate Emissions from Combustion Sources, Southern Pines, N. C. April 24-26, 1978. J. S. Nader, Ed. EPA document in press.

11. Bennett, R. L., and K. T. Knapp. Chemical Characterization of Particulate Emissions from Oil-Fired Power Plants. In: Energy and the Environment, Proceedings of the Fourth National Conference, Cincinnati, Ohio. October 3-7, 1976. P. 501-506. AICHE, Dayton, Ohio, 1976. 594 p.

12. Cheney, J. L. Unpublished data. U.S. Environmental Protection Agency, Research Triangle Park, N. C. 1978.

13. Conner, W. D. Unpublished data. U.S. Environmental Protection Agency, Research Triangle Park, N. C. 1978.

14. Knapp, K. T. Unpublished data. U.S. Environmental Protection Agency, Research Triangle Park, N. C. 1978.

Table 1. SUMMARY OF PHYSICAL AND NORMAL OPERATING FEATURES OF POWER PLANTS STUDIED

Plant	Fuel Burned	Stack			Fuel Content			Excess[a] Boiler O_2 (%)	Emission Controls	Power Output (MW)
		Height (m)	Diameter (m)	Temperature (°C)	Ash (%)	S (%)	V (ppm)			
A	Oil	150	6.8	160	0.17	2.4	590	0.2	only fuel additives	525
M	Oil	60	3.	127	0.07	1.2	15	3	only fuel additives	190
P	Coal	88	4.1	154	8.	3.3	99	5.	ESP	100
MC	Coal	178	4.7	166	14.	3.9	35	4.	ESP	330
LC	Coal	213	7.	77	30.	5.4	50	3.8	2-stage wet scrubber (particulate plus FGD)	820

[a]As measured at economizer outlet

Table 2. EMISSION CHARACTERIZATION DATA FOR OIL-FIRED POWER PLANTS WITHOUT ESP

PLANT M

Date	Time	Part. (mg/Nm^3)	SO_2 (mg/m^3)	$SO_4^=$ (mg/m^3)	$SO_4^=/SO_x$ (%)	Plume Opac. (%) Lidar	Plume Opac. (%) Obs.	In-Stack[a] Opac. (%)	Remarks
8/10/76	1115-1215	27	1,600	68	4.1	10±2	6±1	2-3	15 ppm V; 4% O_2
				PLANT A					
8/19/76	1125-1145					31±4	30±1	18-22	590 ppm V; 0.2% O_2
8/19/76	1145-1200					43±3[b]	52±2[b]	18-22	590 ppm V; 0.2% O_2
8/17/76	1145-1205	250	3,800	340	8.2	23±3	42±1	11-15	590 ppm V; 0.4% O_2
8/19/76	0945-1000	390				23±2	37±2	11-15	590 ppm V; 0.6% O_2
8/19/76	1000-1015	390				54±3[b]	61±2[b]	11-15	590 ppm V; 0.6% O_2

[a]Transmissometer measurements.

[b]Measurements about 3 stack diameters (15 meters) downstream of stack exit.

Table 3. EMISSIONS CHARACTERIZATION DATA FOR COAL-FIRED POWER PLANTS WITH ESP's

Date	Time	Part. (mg/Nm^3)	SO_2 (mg/m^3)	$SO_4^=$ (mg/m^3)	$SO_4^=/SO_x$ (%)	Plume[c] Opacity (%)	In-Stack[d] Opacity (%)	Remarks
PLANT P[a]								
7/19/77	1551-1636	840	7,200	250	3/4	27	21	2 fields off
7/20/77	1020-1120	1,100	6,000	330	5.2	23	28	2 fields off
7/22/77	0939-1039	360	7,300	180	2.4	32	31	2 fields off
PLANT MC[b]								
7/26/77	1430-1545	330	5,900	210	3.4	18	21	1 field off
7/27/77	0915-1015	2,800	5,900	190	3.1	86	81	3 fields off
7/28/77	0900-1000	2,100	6,500	240	3.6	80	72	3 fields off
7/28/77	1110-1210	450	6,500	240	3.6	20	17	Normal operation

[a] 8% Ash, 3.3% S, 99 ppm V, 100 MW

[b] 14% Ash, 3.9% S, 35 ppm V, 330 MW

[c] Observer measurements

[d] Transmissometer measurements

Table 4. EMISSIONS CHARACTERIZATION DATA FOR COAL-FIRED POWER PLANT LC WITH FGD[a]

Date	Time	Part.[b] (mg/Nm^3)	SO_2[b] (mg/m^3)	$SO_4^=$[b] (mg/m^3)	$SO_4^=/SO_x$[b] (%)	Plume[c] Opacity (%)	In-Stack[d] Opacity (%)
9/19/77	1014-1121		2,000	190	8.7		
9/19/77	1201-1309		3,100	260	7.7		
9/19/77	1390-1500		4,200	170	3.9		
9/19/77	1528-1635		5,500	170	3.0		
11/2/77	1529-1629	240					59-67
11/3/77	1345-1445					75.	62-71
11/3/77	1530-1630	270					62-71
4/3/78	1245-1345	350				>90	>90
4/3/78	1515-1615	320				>90	>90
4/4/78	1145-1245	220				>90	>90
4/4/78	1345-1445	280				>90	>90
4/5/78	0930-1030	260				>90	>90
4/5/78	1130-1230	280				>90	>90

[a] 30% Ash, 5.4% S, 50-ppm V, 820 MW

[b] Measurements made on one of 8 parallel FGD modules.

[c] Observer Measurements

[d] Transmissometer measurements at stack breeching.

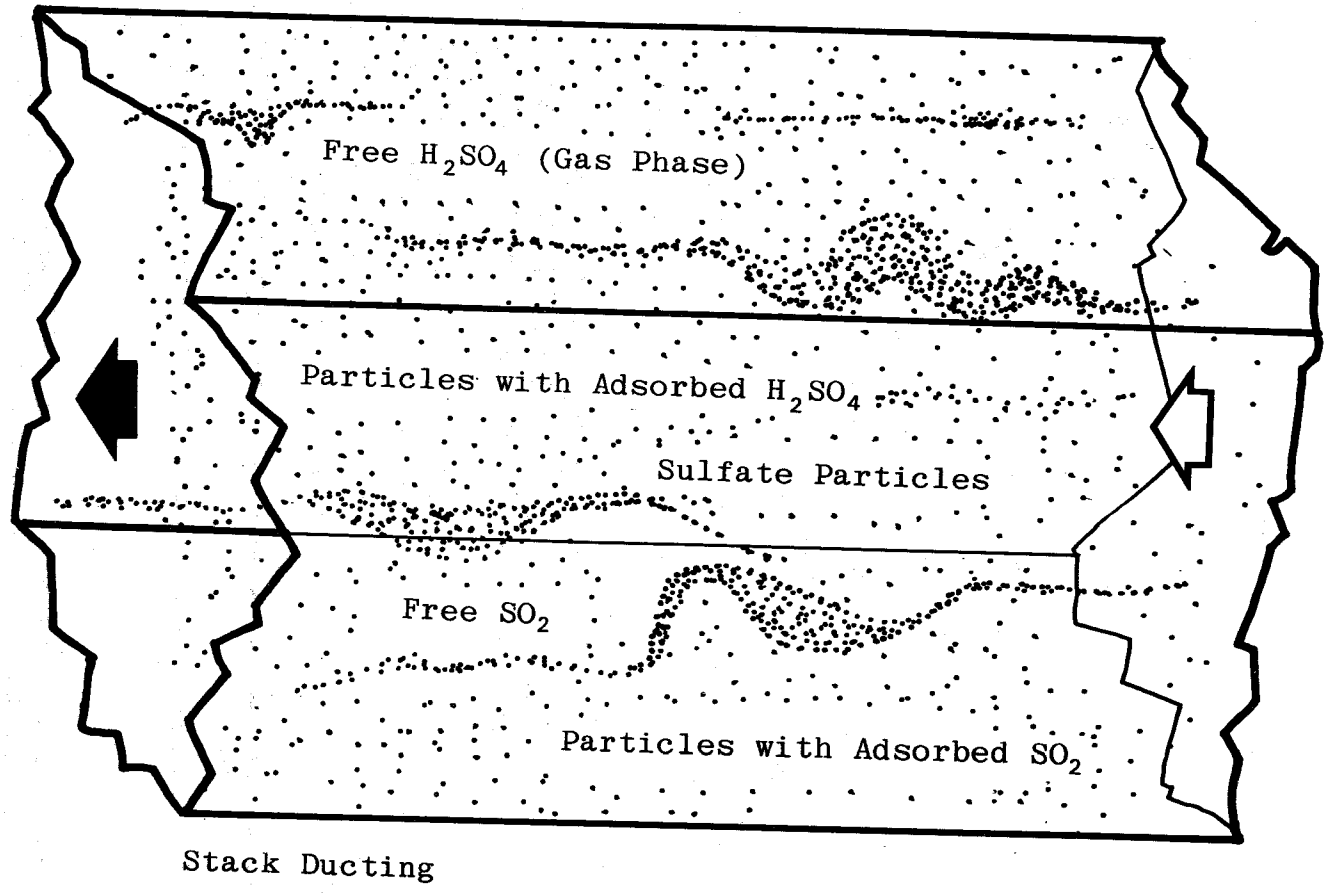

Figure 1. Sulfur Oxides Present in the Stack Gas Stream

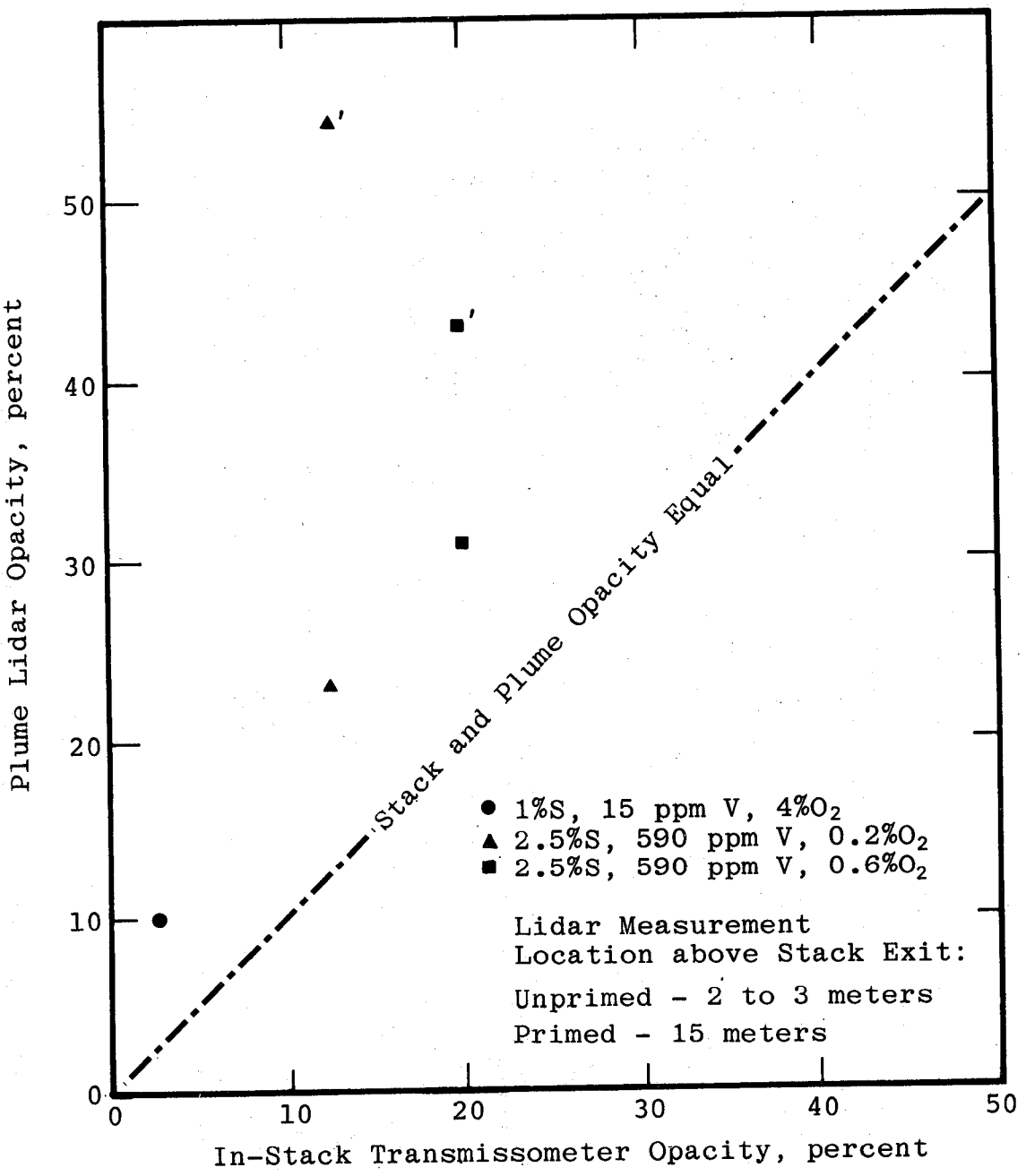

Figure 2. Concurrent Plume and In-Stack Opacity Data for Emissions from Oil-Fired Power Plants

PARTICLE CHARGE EFFECTS ON CASCADE IMPACTOR MEASUREMENTS

R. Patterson and P. Riersgard
Air Pollution Technology, Inc.
San Diego, California

D. Harmon
U.S. Environmental Protection Agency
Industrial Environmental Research Laboratory
Research Triangle Park, North Carolina

INTRODUCTION

In the past few years considerable emphasis has been placed on determining the performance characteristics of particulate control devices. These investigations seek to establish collection efficiency as a function of particle size. To do this requires accurate determination of the size distribution of particles at the inlet and the outlet of the control device. Cascade impactors are routinely used in these investigations for establishing the size distribution of particles greater than 0.5 μm diameter.

The particles which penetrate a particulate control device employing electrostatic forces for collection can have a higher level of charge than when they entered. Other investigators, Smith, et al.[1] and Brink, et al.[2], have found that the collection characteristics of cascade impactors can be altered when sampling charged particles.

This investigation was undertaken to evaluate the effect of charged particles on cascade impactor calibrations. The effect of particle charge on collection efficiency can be expected to be a function of the charge level on the particle. Therefore, a charge level was chosen for this study that is equivalent to that encountered on particles in electrostatic precipitators.

METHOD AND EXPERIMENTAL APPARATUS

The impactor was calibrated with charged and uncharged aerosols. The method for performing the calibration was adapted from the "Cascade Impactor Calibration Guidelines," Calvert et al.[3]. Figure 1 is a schematic of the impactor calibration system used.

The procedure involved generating the test aerosol and determining collection efficiency as a function of the flow rate through the cascade impactor. The average charge level on the test aerosol was determined for the charged particle runs. Charge neutralization was used to assure that the uncharged particles were electrically neutral.

Aerosol Generation

Monodisperse aerosols were produced using suspensions of polystyrene latex (PSL) microspheres. Particles of 0.5, 1.1, and 2.0 μm diameter were used for these calibrations. This is also the size range of most importance in fine particulate control device evaluation.

Useful suspensions of PSL were made by diluting small quantities of the original suspension with deionized water. The PSL was diluted to a concentration sufficient to minimize the occurrence of agglomeration. Dilutions of the 10% stock solutions of PSL can be estimated from a paper by Raabe[4], however, the amount of dilution necessary depends on the specific atomizer used. Concentrations of 0.01 to 0.2 weight % for particles of 0.5 to 2.0 μm diameter were found to be compatible with the atomizer used.

Drops containing PSL particles were produced from suspensions with a Collison atomizer. The atomizer has one hole and operates at 260 kPa. Number concentrations and PSL size distributions were constant throughout a run.

The aerosol was dried by passing it through a 1.8 m section of a 3.6 cm diameter glass tube. The tube was mounted horizontally with a layer of silica gel (~1.5 cm deep) spread evenly along the bottom.

Submicron aerosols less than approximately 0.1 μm diameter were removed by passing the dried aerosol through a diffusion battery. Aerosol leaving the diffusion battery was mixed with ionized air (approximately 45 ℓ/min). The air was ionized with a 20 mCi, Po^{210} alpha emitter to reduce the excess charge on the aerosol to the Boltzman equilibrium level. The mixture passed through 6 m of 1.3 cm diameter glass tubing to provide adequate residence time for charge neutralization of the aerosol and decomposition of the ions.

Charger

The effect of particle charge on the collection characteristics of cascade impactors was determined with particles having different levels

of charge. For the purposes of this experiment the different charge levels were produced by charging three different size aerosols to their saturation charge level by ion bombardment in a corona discharge. The charge levels are comparable to those obtained in conventional ESPs.

For a dielectric particle, such as PSL, field charging theory predicts the following saturation charge level, White[5].

$$n_s = \left[1 + 2\left(\frac{k-1}{k+2}\right)\right] \frac{E_o\, d_p^{\,2}}{(1200)e} \times 10^{-8} \qquad (1)$$

$$n_s = 2.9 \times 10^{-2}\, E_o\, d_p^{\,2} \quad \text{(for PSL)} \qquad (2)$$

The saturation charge level is seen to be proportional to the applied field strength, E_o, and surface area of the particle $\sim d_p^{\,2}$. Figure 2 gives the saturation charge level for field charging of particles in the size range of interest in this study.

The field charger used is a modified version of the design cited by Langer et al.[6]. The device shown in Figure 3 consists of a small Plexiglas box with two inlets and one outlet. The aerosol enters the charging region through the lower glass tube. The outlet is a brass tube cut at a 45 degree angle to the centerline of the pipe. The source of the ion flux is a small loop of platinum wire bent slightly and positioned so as to be equidistant from the outer edge of the tube. A DC power supply operating in the range of 0 to 12 kV was used for establishing the corona.

Cascade Impactor

A University of Washington Mark III source test cascade impactor was chosen for these tests. The impactor was calibrated with only one jet stage installed at a time according to the method of Calvert et al.[3] In this manner, the difference in collection efficiency between charged and uncharged particles could be studied.

The inertial impaction parameter, K_p, is used to characterize the collection efficiency for a given impaction stage. The inertial impaction paramerer is defined by:

$$K_p = \frac{d_p^2\, C'\, \rho_p\, u_j}{9\, \mu_G\, d_j} \times 10^{-8} = \frac{d_{pa}^{\,2}\, u_j}{9\, \mu_G\, d_j} \times 10^{-8} \qquad (3)$$

Aerodynamic diameter is defined as:

$$d_{pa} = d_p\, (C'\, \rho_p)^{\frac{1}{2}}, \ \mu mA \qquad (4)$$

For the case where the stage is 50% efficient (i.e., the cut point) equation (4) becomes:

$$K_{p50} = \frac{d_{p50}^2 \, C' \, \rho_p \, u_j}{9 \, \mu_G \, d_j} \times 10^{-8} = \frac{d_{pc}^2 \, u_j}{9 \, \mu_G \, d_j} \times 10^{-8} \qquad (5)$$

Choosing the proper jet stage depends on the particle size being studied and knowledge of the volumetric flow rate usually encountered in the field. For field operations this impactor is normally operated in the range of 1.4×10^{-2} to 2.8×10^{-2} m^3/min. With limits set on the desired volumetric flow rate, the following jet stages were chosen for the particle sizes used in this study:

Stage	Particle Dia. (μm)	Hole Dia (cm)	Number of Holes
4	2.0	0.079	90
5	1.0	0.051	110
6	0.5	0.034	110

A number of impaction substrates are used for determining size distributions in the field. The following substrates were chosen for study to give a representative sample of the conditions encountered:

1. Glass fiber filter on a metal impaction plate.
2. Greased metal impaction plate.
3. Ungreased metal impaction plate.
4. Greased aluminum foil on metal impaction plate.
5. Ungreased aluminum foil on metal impaction plate.
6. Teflon film on metal impaction plate.
7. Mylar film on metal impaction plate.

Optical Particle Counter

The number concentration of particles entering the leaving the cascade impactor was determined with a Climet CI-205 particle analyzer. The Climet device has the capability of counting all particles with diameters greater than a preset value (0.3, 0.5, 1.0, 3.0, 5.0, or 10.0 μm). Further discrimination is achieved by using a potentiometer to provide a continuous particle size selection over the range of 0.3 to 10.0 μm diameter.

The particle counter is used within a selected band of particle diameters, centered about the known PSL diameter. This reduces the effect of spurious counts resulting from fine impurities and agglomerates. The particle count for the larger diameter setting may be subtracted from that for the smaller diameter setting to determine the number concentration of particles within a desired size interval.

Charge Analyzer

A model 3030 electrical aerosol analyzer manufactured by Thermo Systems, Inc. was modified for measuring the charge level of the particles. The Faraday cup was remounted on the face of the instrument. The charged particles were collected in the Faraday cup and particle losses in the remainder of the instrument were thus avoided.

RESULTS

The collection efficiency was determined as a function of the impaction parameter for both charged and uncharged aerosols. Collection of charged particles in the impactor without the impaction plate in place was found to be negligible with each of the three jet stages used.

The electrical field strength in the charger shown in Figure 3 was 7,000 V/cm. Actual charge levels on the particles were somewhat less than the saturation charge because of the short residence time in the charging section. For the PSL particles used in this study the average charge level was:

Particle Diameter (μm)	Average Charge Level (No. of elementary units)
2.0	322
1.0	201
0.5	53

Single Stage Results

Figures 4 through 9 are the results obtained with the 0.5 μm PSL particles and the various substrates. These are similar to the results obtained with the other particle sizes. In all cases collection efficiencies were found to be greater for the charged particles than the uncharged particles.

Impaction of charged particles on the greased substrates was only slightly more efficient for a given value of the impaction parameter, K_p, than with uncharged particles. The effect was more dramatic for other substrates, with the efficiency being as much as 20% greater for the charged particles at a given K_p value.

The impaction efficiency was less than 100% for the PSL particles with all of the substrates tested because of particle bounce. This result is similar to that found by Rao[7]. The maximum obtainable impaction efficiency was increased by as much as 20% for substrates other than the greased impaction substrates.

Tables 1 through 3 give the value of K_{p50} and the maximum impaction efficiency for the three particle sizes tested.

TABLE 1. IMPACTION CHARACTERISTICS FOR VARIOUS SUBSTRATES (0.5 μm DIA.PSL)

	K_{p50}		Maximum Collection Efficiency %	
Substrate	Charged	Uncharged	Charged	Uncharged
Greased Plate	0.19	0.20	74	74
Greased Foil	0.19	0.20	80	80
Glass Fiber Filter	0.18	0.21	70	58
Ungreased Plate	0.19	0.22	60	42
Ungreased Foil	0.20	0.22	53	30
Mylar Film	0.21	0.22	48	27

TABLE 2. IMPACTION CHARACTERISTICS FOR VARIOUS SUBSTRATES (1.1 μm DIA.PSL)

	K_{p50}		Maximum Collection Efficiency %	
Substrate	Charged	Uncharged	Charged	Uncharged
Greased Plate	0.25	0.27	(a)	(a)
Greased Foil	0.22	0.24	(a)	(a)
Glass Fiber Filter	0.21	0.22	63	(a)
Ungreased Plate	0.21	0.24	70	55
Ungreased Foil	0.23	0.24	47	35

(a) Data did not include an inflection point, representing a maximum collection efficiency.

TABLE 3. IMPACTION CHARACTERISTICS FOR VARIOUS SUBSTRATES (2.02 μm DIA.PSL)

	K_{p50}		Maximum Collection Efficiency %	
Subs rate	Charged	Uncharged	Charged	Uncharged
Greased Plate	0.20	0.22	90	90
Greased Foil	0.19	0.22	90	90
Glass Fiber Filter	0.18	0.20	78	66
Ungreased Plate	0.19	0.21	72	61
Ungreased Foil	0.20	0.21	68	51
Mylar Film	0.20	0.22	68	56

The change in the impaction parameter, K_{p50}, amounted to approximately 10% for most substrates. The effect of particle charge level was insignificant as the change in K_{p50} was similar for each of the PSL particle sizes tested.

Multiple Stage Collection

Collection efficiencies were determined as a function of the impaction parameter for both charged and uncharged aerosols. Stages 1 through 6 were installed in the cascade impactor for these tests. The electrical field strength in the charger shown in Figure 3 was 7,000 V/cm.

Figure 10 shows the results with a greased Mylar substrate. This figure is similar to Figures 4 and 5 which are for collection on various greased substrates with only one impaction stage. The collection efficiency for a given flow rate is somewhat greater in Figure 10 than is shown in the other figures. This increased collection efficiency may be attributed to particle collection on the upper stages of the cascade impactor.

The collection characteristics for glass fiber filters is shown in Figure 11. This figure is similar to Figure 6 which was obtained with a single stage. This indicates that collection of charged particles with glass fiber filters is minimal on the upper stages.

An ungreased plate was used as the collection substrate for the data shown in Figure 12. The curves for charged and uncharged particles are quite similar to the ones found in Figures 7, 8, and 9 for other ungreased substrates. Again this indicates that the collection of the charged particles on the upper stages of the cascade impactor is minimal.

CONCLUSIONS

Impaction collection efficiency was shown to be as much as 20% greater for charged particles than uncharged particles with certain substrates for a given value of the impaction parameter, K_p. Single stage collection on greased substrates remained relatively unchanged, whereas multiple stage collection on greased substrates showed charged particle losses, presumably to the upper stages. Multiple stage collection with other impaction substrates gave results similar to the single stage results.

The effect that charged particles will have on the particle size distribution measured with the cascade impactor may be determined from equation (5). This equation shows that the stage cut diameter, d_{pc}, is related to K_{p50} in the following way:

$$d_{pc}\ \text{charged} \simeq d_{pc}\ \text{uncharged} \left[\frac{K_{p50}\ \text{charged}}{K_{p50}\ \text{uncharged}} \right]^{\frac{1}{2}} \qquad (6)$$

The results of this investigation show that the impaction parameter, K_{p50}, increases by 5 to 17% when collecting charged particles. The actual amount depends on the particle size and collection substrate used. For a 17% change in the impaction parameter, K_{p50}, the change in the stage cut diameter, d_{pc}, is 8%.

REFERENCES

1. Smith, W. B., K. M. Cushing, G. E. Lacey, and J. D. McCain. Particulate Sizing Techniques for Control Device Evaluation. EPA 650/2-74-102a, NTIS No. PB 245-184/AS. August 1975.

2. Brink, J. A., E.D. Kennedy, and H. S. Yu. Particle Size Measurements with Cascade Impactors. 65th Annual AIChE Meeting. New York, NY. 1972.

3. Calvert, S., C. Lake, and R. Parker, Cascade Impactor Calibration Guidelines. EPA-600/2-76-118, NTIS No. PB 252-656/AS. April 1976.

4. Raabe, O. G. Generation and Characterization of Aerosols. From: Inhalation Carcinogenesis, Proc. of the Biology Division, Oak Ridge Nat. Laboratory Conf. Gatlinburg, TN. October 8-11, 1969.

5. White, H. Industrial Electrostatic Precipitation. Addison-Wesley. Reading, MA. 1963.

6. Langer, G., J. Pierrard, and G. Yamate. Further Development of an Electrostatic Classifier for Submicron Airborne Particles. Intern. J. Air Water Poll. 8:167-176, 1964.

7. Rao, A. An Experimental Study of Inertial Impactors. Particle Technology Laboratory, University of Minn. Publication Number 269. 1975.

NOMENCLATURE

C' = Cunningham slip correction factor =

$$1 + \frac{2\lambda}{d_p} \left[1.257 + 0.40 \exp\left(-1.10\, d_p/2\lambda\right)\right]$$

d_j = jet diameter, cm

d_p = particle physical diameter, μm

d_{pa} = aerodynamic particle diameter, μmA

d_{pc} = aerodynamic cut diameter, μmA

$d_{p_{50}}$ = cut diameter or diameter at which stage is 50% efficient, μm

e = electronic charge value, 4.8×10^{-10} esu

E_o = applied electric field strength, kV/cm

k = dielectric constant for particle

K_p = inertial impaction parameter, dimensionless

$K_{p_{50}}$ = inertial impaction cut parameter, K_p, at 50% efficiency

n_p = particle charge level, elementary units

n_s = saturation charge level, elementary units

ρ_p = particle density, g/cm^3

μ_G = gas viscosity, poise, g/cm-s

μmA = μm $(g/cm^3)^{\frac{1}{2}}$

u_j = gas (particle) velocity through jet, cm/s

λ = mean free path of gas molecules, μm

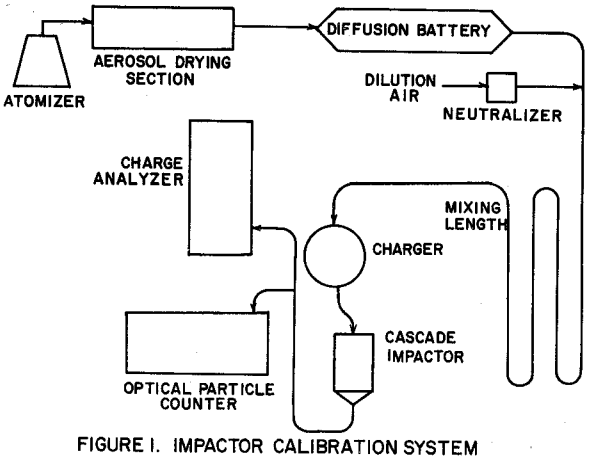

FIGURE I. IMPACTOR CALIBRATION SYSTEM

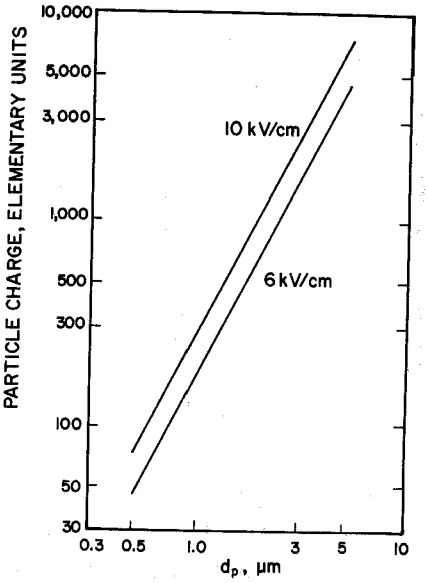

FIGURE 2. SATURATION CHARGE LEVEL ON PSL AEROSOL (DIELECTRIC CONSTANT, k= 2.55)

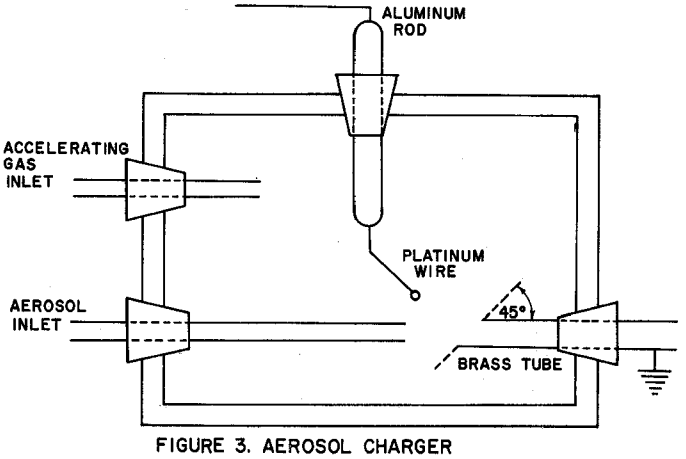

FIGURE 3. AEROSOL CHARGER

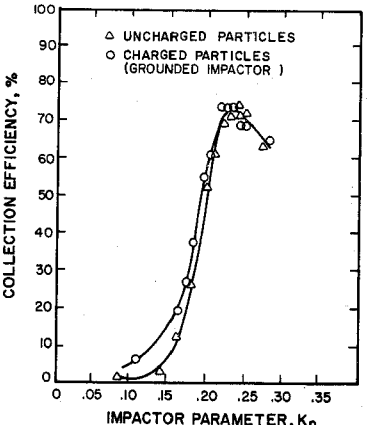

FIGURE 4. IMPACTION CHARACTERISTICS WITH GREASED PLATE (0.5 μm DIA. PSL)

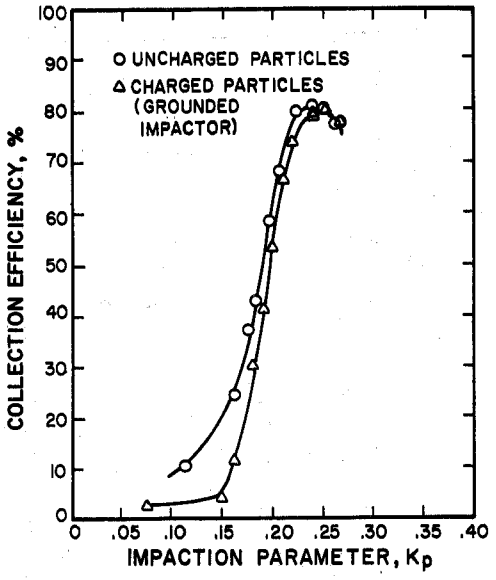

FIGURE 5. IMPACTION CHARACTERISTICS WITH GREASED FOIL (0.5 μm DIA. PSL).

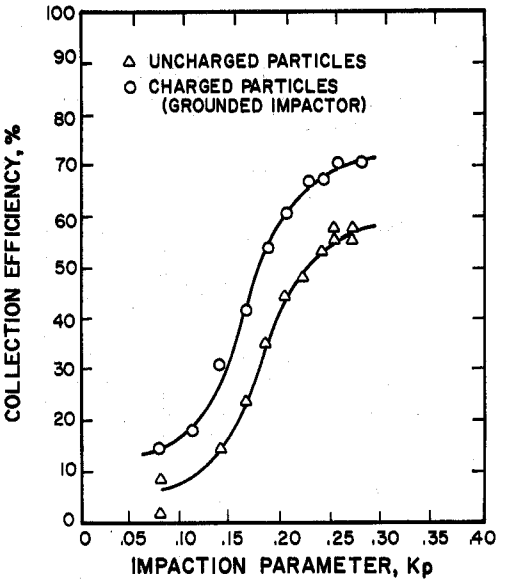

FIGURE 6. IMPACTION CHARACTERISTICS WITH GLASS FIBER FILTER (0.5 μm DIAMETER PSL).

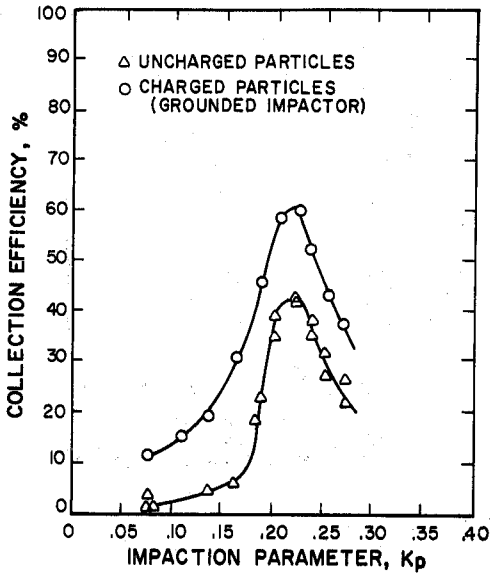

FIGURE 7. IMPACTION CHARACTERISTICS WITH UNGREASED PLATE (0.5 μm DIA. PSL)

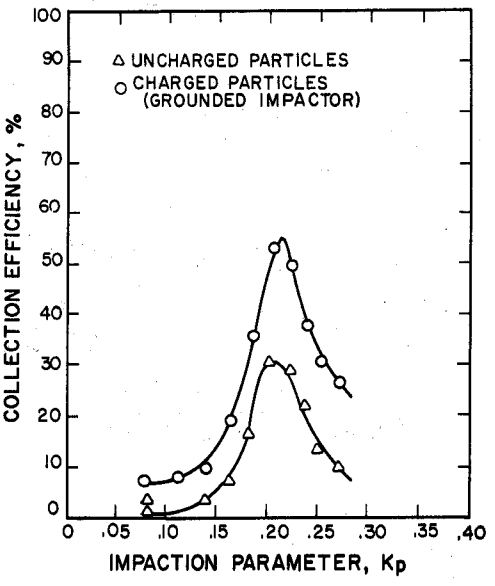

FIGURE 8. IMPACTION CHARACTERISTICS WITH UNGREASED FOIL (0.5 μm DIA. PSL)

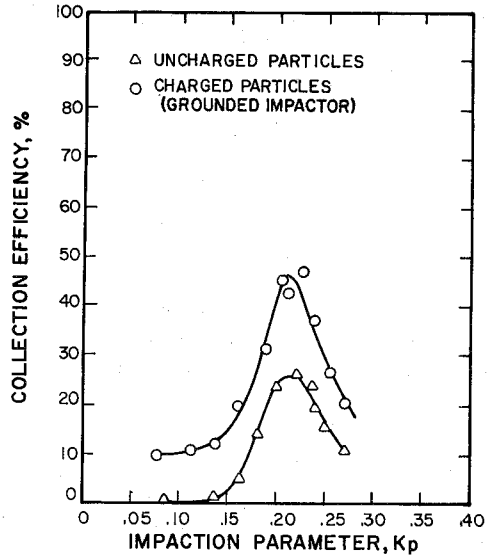

FIGURE 9. IMPACTION CHARACTERISTICS WITH MYLAR SUBSTRATE (0.5 μm DIA. PSL)

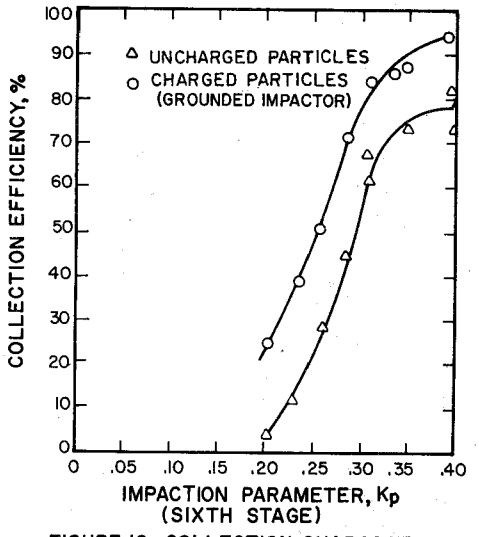

FIGURE 10 COLLECTION CHARACTERISTICS OF GREASED MYLAR SUBSTRATES WITH STAGES 1 THROUGH 6 INSTALLED (0.76 μm DIA. PSL)

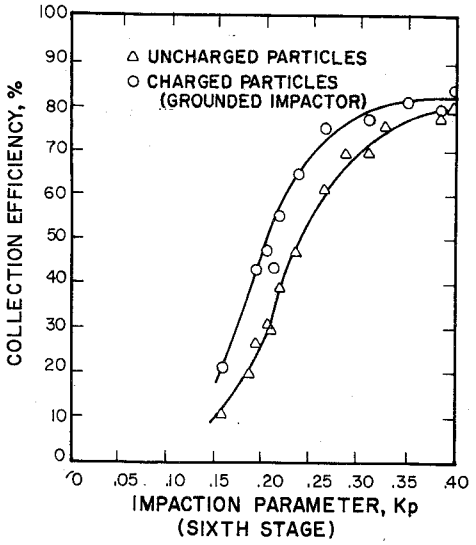

FIGURE 11. COLLECTION CHARACTERISTICS OF GLASS FIBER FILTER SUBSTRATES WITH STAGE 1 THROUGH 6 INSTALLED (0.76 μm DIA. PSL)

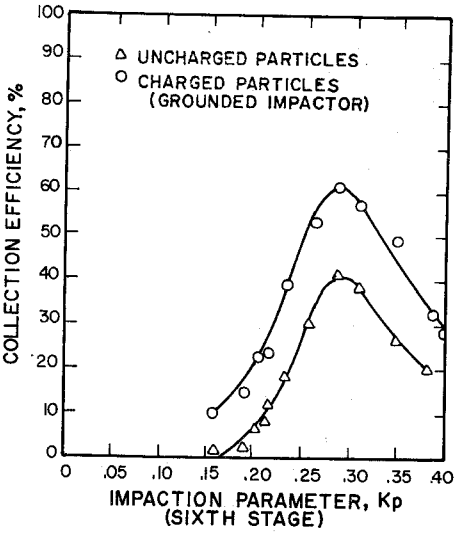

FIGURE 12. COLLECTION CHARACTERISTICS FOR AN UNGREASED PLATE WITH STAGES 1 THROUGH 6 INSTALLED (0.76μm DIA. PSL)

A HIGH-TEMPERATURE HIGH-PRESSURE ISOKINETIC/ISOTHERMAL SAMPLING SYSTEM FOR FOSSIL FUEL COMBUSTION APPLICATIONS

J.C.F. Wang*, R.R. Boericke, and R.A. Fuller
General Electric Company
Schenectady, New York

ABSTRACT

A high-temperature high-pressure (HTHP) isokinetic/isothermal sampling system has been developed for coal combustion efflux measurements, particularly those of a pressurized fluidized bed combustor at 1750°F and 80 psia. This HTHP system consists of a unique sampling nozzle, automatic self-cleaning isokinetic sensors and sampling controller, a five-stage cyclone train with positive filter, a vapor condenser and an environmental control vessel for the cyclone train. Determination of particulate loading and size distribution in the efflux stream can be accomplished along with a characterization of the vapor phase alkali metal content.

Measurements using this HTHP sampling system in an operating PFB environment have been performed at the Coal Utilization Research Laboratory, Leatherhead, England. Preliminary results of the probe operation and performance are presented.

INTRODUCTION

The major technology issues in the development of pressurized fluidized bed (PFB) combined cycle power plants are associated with the combustor/gas turbine interface.[1] The hot combustion gas contains

*Present Affiliation: Sandia Laboratories, Division 8353, Livermore, California 94550.

significant amounts of fine dust composed of coal ash and attrited sorbent bed material. This dust, impacting on the turbine blades at high velocity, can rapidly erode the metal and cause premature failure. In addition both the coal ash and the sorbent typically contain appreciable trace quantities of potassium and sodium.[2] These alkali metals can react with residual SO_2 in the gas stream to form sulfate-base condensates which cause rapid hot corrosion of conventional gas turbine alloys. An accurate definition of this hostile environment is needed to guide the development of hot gas cleanup equipment and improved high-temperature alloys and coatings. In particular, measurement of the alkali metal concentration and chemical form, are needed, together with the dust load and its size distribution and chemical composition.

The unique sampling system described in this paper was developed to meet specific needs associated with the development of PFB combustion of coal for electric power generation. Determination of particulate loading and size distribution is accomplished by an isokinetic and isothermal sampling process at the temperature and pressure of the PFB combustor exhaust. Aerodynamic diameters of the particulate are obtained directly through the use of a multistage cyclone collector, thereby eliminating uncertainties inherent in redispersal of the collected dust. Measurement of the alkali vapor content is achieved by maintaining the entire sampling train at the PFB exhaust temperature and pressure, and then condensing the vapor after the removal of essentially all particulates.

A demonstration test of this high-temperature, high-pressure (HTHP) isokinetic/isothermal sampling system was performed at the PFB facility at British National Coal Board's Coal Utilization Research Laboratory (NCB/CURL), Leatherhead, England in June of 1978. The operating experience and preliminary (unconfirmed) results obtained at this demonstration test are described in this paper in conjunction with a brief summary description of the sampling system.

BACKGROUND-ALKALI METAL CHARACTERIZATION

As noted previously, both the coal and the sorbent material contain alkali metals. In the coal ash, these alkalis exist primarily as silicates or aluminosilicates, which, because of their low volatility and chemical inertness, remain bound in the dust particles and do not contribute to corrosion. However, some of the alkali in the ash, and most of that in the sorbant, exists as sulfate,chloride and carbonate, which volatilizes during combustion. This vapor phase alkali can form sulfate-base condensates in the gas turbine due to the temperature drop through the turbine and due to contact with the air-cooled turbine blades, as noted in Figure 1.

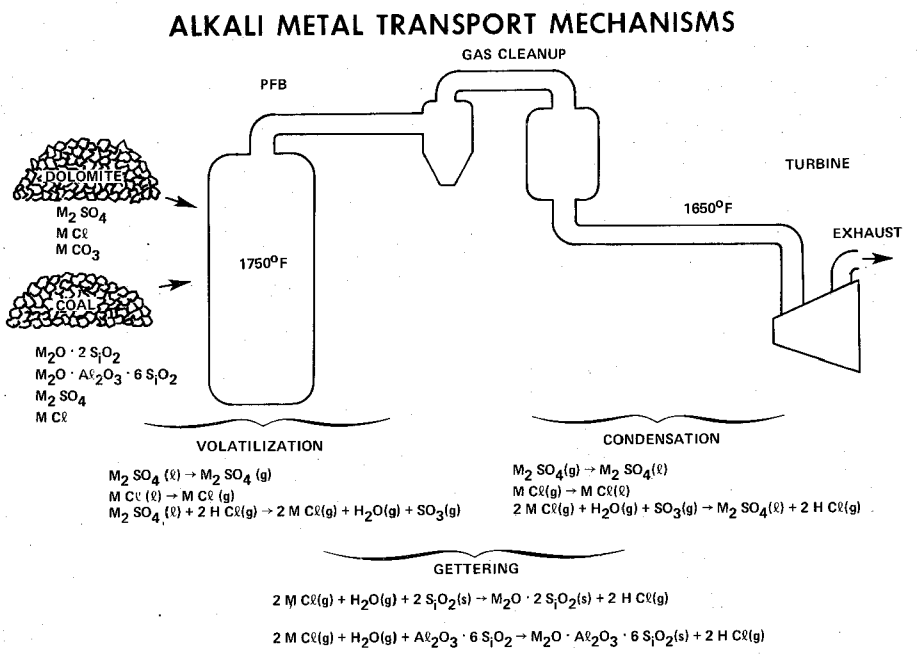

Figure 1 - Alkali metal transport mechanisms

Chemical thermodynamic calculations at General Electric have indicated that alkali vapor levels will range from one to two orders of magnitude larger than permitted by current gas turbine fuel specifications (.02 ppm Na + K in combustion gas, or 1 ppm in fuel). The actual vapor content depends on the initial alkali content of the feed stock, the chlorine content of the coal, the combustor bed temperature and the degree of equilibration with the low volatility aluminosilicates according to the "gettering" reactions shown in Figure 1. However, even with the most optimistic assumptions, the calculations indicate that sufficient alkali sulfate will condense on the turbine hot parts to pose a significant corrosion problem, even if complete particulate removal could be achieved in the gas cleanup system.

Preliminary measurements of alkali content at NCB/CURL have ranged from 0.5 to 7.9 ppm Na + K [4], and thus support the predicted, high, alkali levels in the combustion gases. The measurement technique [5] (flame photometry) responds only to the potentially corrosive chloride and sulfate forms. However, the measurements do not distinguish completely between the vapor and particulate-borne alkali. The alkali measurements were made on the cooled combustion gas after passing through a small cyclone with a (theoretical) 2μm cut size. [5] Consequently, the alkali vapor is condensed, probably onto dust particles in the gas, and a portion of the condensate has been removed in the

cyclone. The measurement therefore includes most of the original vapor content (as aerosol), plus an unknown contribution from initially condensed phases carried by the particles small than 2μm. These small particles constitute about 5% of the total dust load.[2] Thus although the measurements agree with the theoretical vapor levels, they are not conclusive.

The present apparatus has been designed to obtain an unambiguous measurement of the alkali vapor content, in order to validate the theoretical calculations. This is achieved by removing essentially all particulates from the sampled gas while maintaining the entire sampling train at the combustion gas temperature to avoid alkali condensation.

ISOKINETIC/ISOTHERMAL SAMPLING SYSTEM

A schematic of the high-temperature, high-pressure (HTHP) isokinetic/isothermal sampling system is shown in Figure 2. It consists of three major components.

1. Isokinetic sampling probe and controller
2. Isothermal environment controller
3. Particulate and vapor sampler.

Description of these components was reported in detail in Reference 6.

The sampling probe and sensors are backflushed with nitrogen to prevent them from being plugged in a high dust environment. The sampling nozzle is backflushed when no sample is taken, while the pressure-sensing ports are backflushed continuously.

The differential pressure between two static pressure sensors is related to the difference in gas velocity between the free stream and at the sampling nozzle inlet. A differential pressure of zero corresponds to isokinetic flow in the sampling nozzle, and is maintained automatically by an electronic controller. The controller is also designed to be operated manually via the control valve driver to match the computed isokinetic mass flow. This manual operation provides an independent backup system for the isokinetic controller.

To keep the sampled gas at the temperature of the PFB exhaust, the entire sampling system is insulated: from the sampling tube downstream from the nozzle to the entrance to the vapor condenser. A small electrical furnace (2 kw) is used around the high temperature shutoff valve and a large electrical furnace (16 kw) is used to maintain the temperature of the multistaged cyclone collector at the PFB efflux temperature. Temperature variation at 1750°F on these furnaces was demonstrated to be less than 15°F.

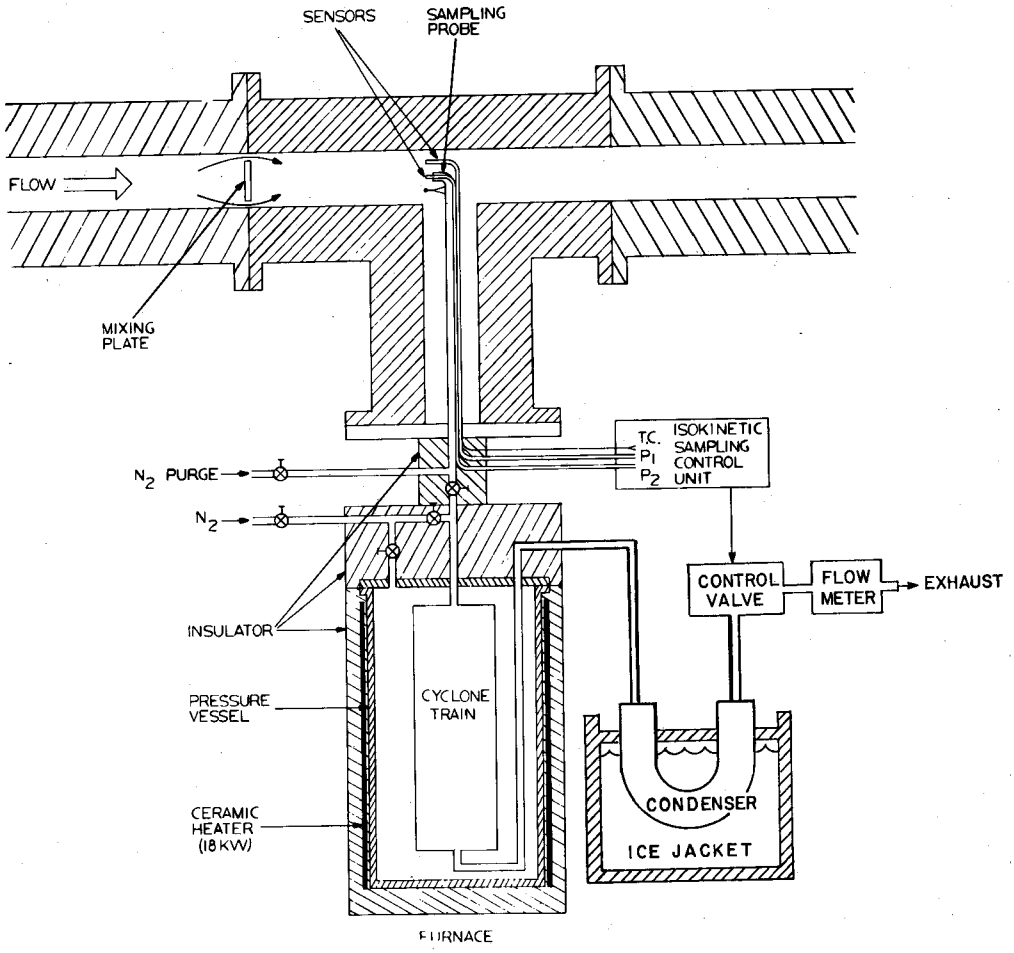

Figure 2 - Schematic of the HTHP isokinetic/isothermal sampling system

A multi-stage cyclone train designed and built by Southern Research Institute (SRI) for the Environmental Protection Agency, is used as the particulate sampler and collector. This cyclone train has five stages, each with a different cut-size ranging from 0.3μm to 7μm (for particle density of unity) at very low dust loading. Beyond the fifth stage, a 0.4 inch thick Astroquartz mat acts as a positive filter element to collect particulates of less than 0.3μm diameter. Results of SRI performance testing of these five cyclones at room temperature is shown in Figure 3.[7]

After the cyclone train and filter assembly, the sampled gas is passed through a vapor condenser which is made of two 24-inch long, 2-inch diameter U-shaped tubes surrounded by ice and water. Each U-tube is filled with 1/4 inch diameter stainless steel balls to increase the cooling surface area.

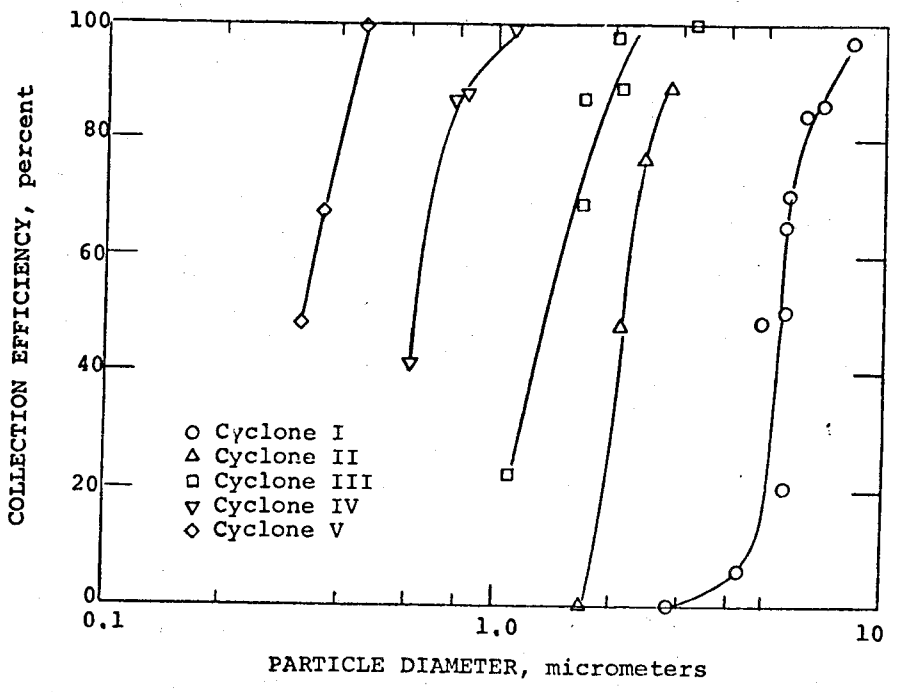

Figure 3 - Five stage cyclone train room temperature calibration data (courtesy of SRI)

The outputs from the sampling system consist of five dust samples collected in the five-stage cyclone train, one dust sample on the Astroquartz filter and one vapor condensate sample from the condenser. The dust loading is obtained by weighing the collected dust samples and dividing the total weight by the total flow sample. The aerodynamic size distribution of the particulate is obtained from the weight distribution of the dust samples from the individual cyclone collectors. Detailed size distributions can also be obtained from Coulter Counter analysis. Chemical analysis of the condensate and of the particulates in each size fraction can be obtained via atomic absorption and/or X-ray fluorescence analyzers.

DEMONSTRATION TEST AT NCB/CURL

Figure 4 shows a schematic of the test arrangement at NCB/CURL. Two HTHP isokinetic/isothermal sampling systems described above were installed in the secondary flow duct, upstream and downstream of the Aerodyne cyclone.

Both sampling systems were mounted on a cart which slid in and out horizontally with respect to the cover flange of a tee on the secondary duct. This arrangement allows quick disconnect and disassembly of the pressure vessel during the sampling tests. Once the pressure

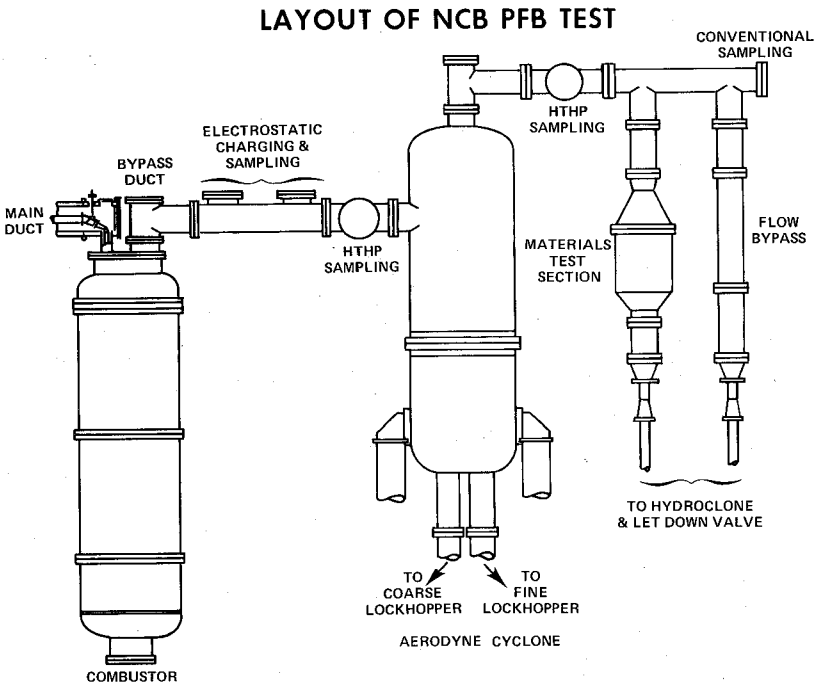

Figure 4 - Schematic of NCB/CURL PFB test

vessel and furnace assembly is disconnected from the cover flange, the multi-stage cyclone collector can be exposed to air and cooled down very rapidly. Figure 5 shows a picture of the assembled sampling system at the inlet of the Aerodyne cyclone.

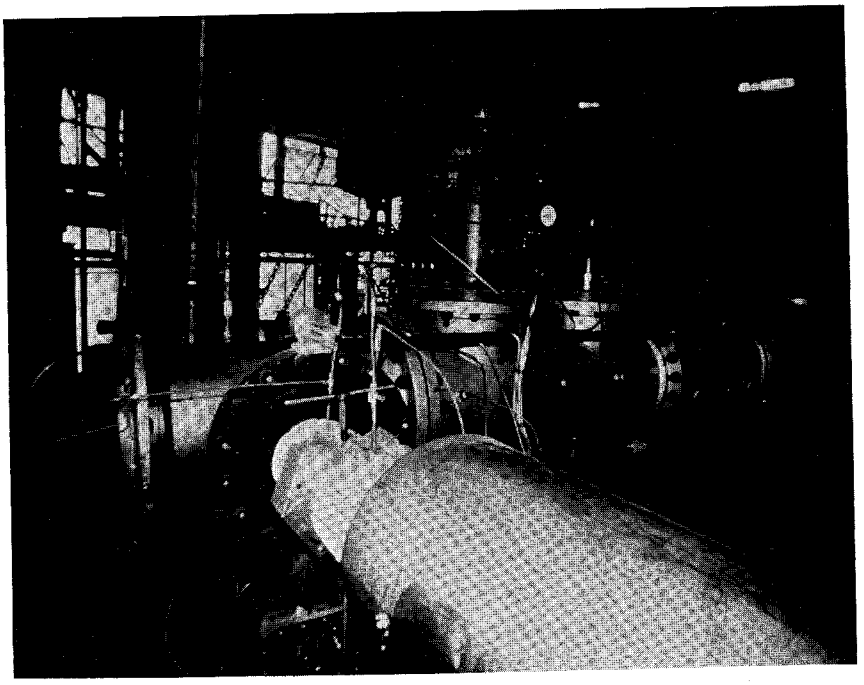

Figure 5 - Photograph of assembled sampling system

Operating procedures were established for the sampling system after some experimentation during the demonstration test. The nitrogen purge was an all the time for the isokinetic sampling sensors and the sampling nozzle. The pressure vessel which housed the multi-stage cyclone collector was filled with argon at a pressure slightly higher than that of the PFB exhaust at the sampling station. It took about 1 to 1-1/2 hours to heat the sampling system to a stable preset temperature after the two furnaces were turned on. Just before sampling, the nitrogen purge to the sampling nozzle was turned off and a bypass valve opened to bleed gas through the sampling nozzle and the tube upstream from the Kaymr shutoff valve. This bypass bleeding allowed us to heat the sampling line to the desired temperature before any sample was taken. Then, the bypass valve was closed and the Kaymr valve opened to begin sampling. During sampling, a 1/8 inch tube connecting the pressure vessel and the sampling tee section was also opened to automatically maintain the pressure inside the vessel close to that inside the PFB exhaust duct.

When the sampling process stopped, the Kaymr valve was closed and the nitrogen purge was turned on to back flush the sampling nozzle. The argon in the pressure vessel was exhausted through the multi-stage cyclone collector and the sampling system control valve. This allowed the last sampled gas inside the sampling system to be flushed through the cyclone collector and the condenser.

PRELIMINARY TEST RESULTS

Sampling System Performance

The sampling nozzle did not plug throughout the test. However, many of the static taps on the free stream and the sampled flow sensors were plugged. Figure 6 shows the heavy buildup of deposit on the nozzle and sensor assembly after the test. The plugging of the static taps was detected during the test and was attributed to inadvertant interruption of backflush nitrogen supply to the sensors. Once the static taps were plugged, some high pressure pulsed backflushes were employed without success to unplug them. It appears that the backflush for the sensors is necessary and should be on without interruption during the test. The manual sampling control worked as designed and was used after the sensor became plugged.

One of the two Kaymr high temperature shutoff valves failed during the first sampling tests. Because of this failure, the back-flush nitrogen to the sampling nozzle leaked through this Kaymr valve into the pressure vessel and the multi-stage cyclone collector. The titanium nuts and bolts used on the cyclone collector, normally protected by the argon atmosphere, were nitrided by the leaked nitrogen and caused corrosion of the Hastelloy-X cyclone collector body. This cyclone collector was severely damaged and was unusable for the remainder

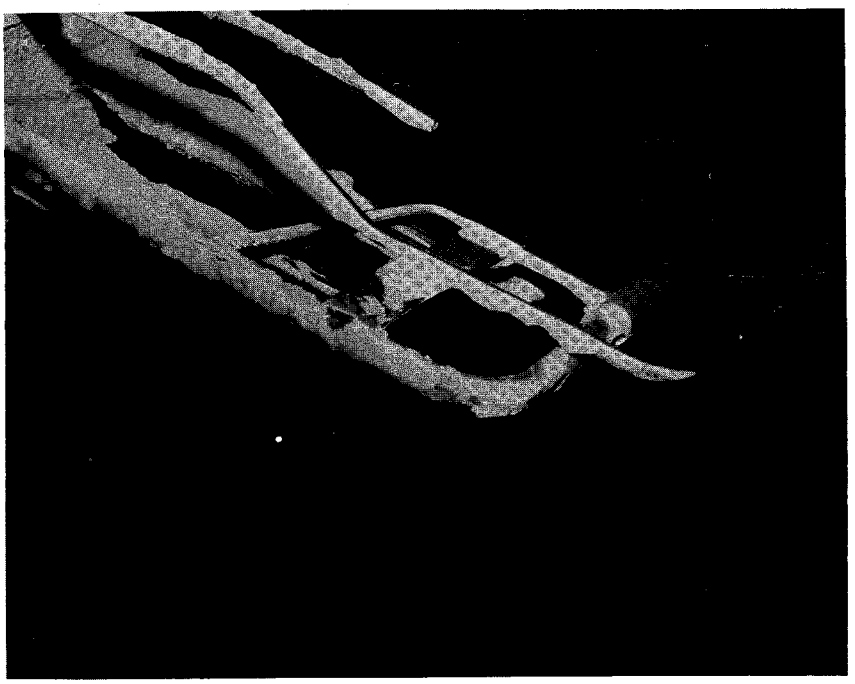

Figure 6 - Photograph of sampling probe after operation

of the test series. Stainless steel nuts and bolts were used on the remaining cyclone collector after this incident. Post-test inspection revealed that the failure of the Kaymr valve was due to damage in the Grafoil gasket. It worked properly after the gasket was replaced with a new one. The other Kaymr valve at the inlet of the Aerodyne cyclone worked properly throughout the test.

During the initial operation of the sampling system, difficulties were encountered with the furnace temperature control, causing the furnace to overheat to 1900°F, or 250° above the planned operating temperature of 1650°F. Post test inspection and checkout showed that the overheating was due to a poor choice of thermocouple location within the furnace. Meanwhile, operation of the sampling system, with manual temperature control, was without incident at 1400°F. Operation up to 1700°F should be possible without any difficulty either manually or with the relocated control thermocouple.

The sampling procedure described in the preceeding section was tested successfully. About an hour was required to reach operating temperature. The sampling period ranged from 10 minutes to one hour, followed by a half-hour cooldown. Disassembly of the cyclone system and sample preparation required about an hour, and an additional half-hour was required for reassembly. Total time between samples was thus approximately four hours. A full-time sampling technician with a half-time assistant were necessary to operate the two sampling systems simultaneously.

PFB Efflux Measurements

The efflux from the NCB/CURL's PFB combustor was sampled by the HTHP sampling system at the inlet to the Aerodyne Cyclone. Two samples were taken at each of three flow rates: 1.0, 1.6 and 2.4 lb/sec. The outlet flow from the Aerodyne Cyclone at 1.0 lb/sec and 2.4 lb/sec was also sampled by relocating the upstream probe to the downstream location. Due to the sensor probe plugging, samples were obtained by manual control at the calculated isokinetic flow rates.

Figure 7 shows the measured dust loading in the secondary duct at various flow rates. A clear trend of increasing dust load with increasing flow rate is apparent. Since the PFB combustor operating conditions were the same throughout the test series, the variation of dust load with flow is attributable to flow splitting between the original and the secondary exhaust ducts. This is supported by preliminary analysis of samples obtained by NCB/CURL in the main exhaust duct.

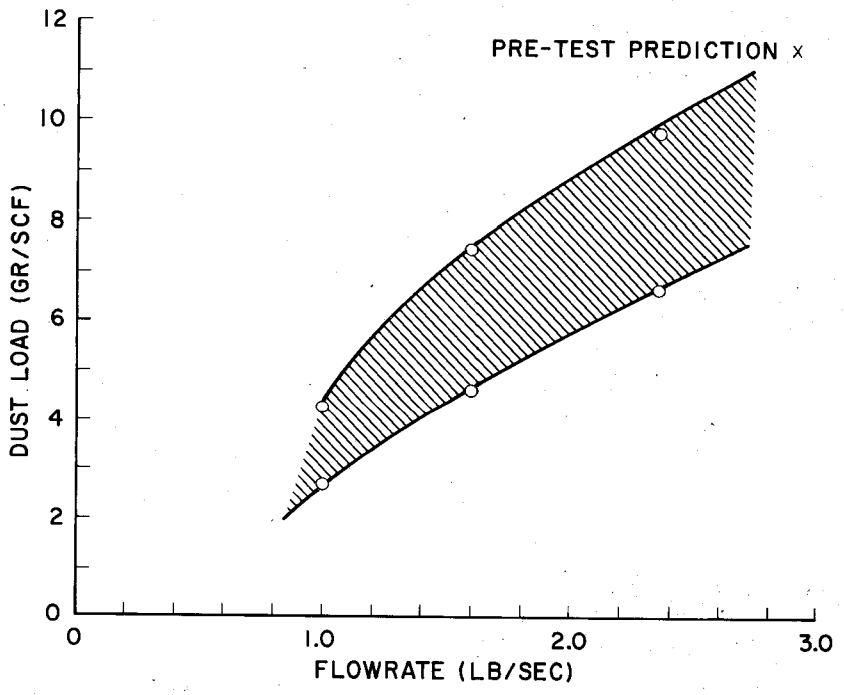

Figure 7 - Dust loading as a function of flowrate

Considerable scatter is apparent in the data shown in Figure 7. Some of this scatter is probably caused by departures from isokinetic sampling. However, the scatter may also have been caused by real variations in the dust load caused by transients in combustor operation due to dolomite addition, cyclone dumping, etc. This point will be explored further by comparisons with NCB/CURL sampling data.

The three data points forming the upper line in Figure 7 were all obtained under nearly isokinetic conditions, and are thus believed to be more representative of the true dust load. The upper line also agrees well with a pre-test prediction of the dust load at this PFB operating conditions, based on prior efflux characterization studies.[2]

The dust collected in the individual SRI cyclones has been analyzed by Coulter Counter to give typical results shown in Figures 8a through 8d. Data for cyclone #1 are shown only in Figure 8d corresponding to the downstream sample. Samples taken upstream of the Aerodyne contain more coarse particulates, requiring sieving before Coulter analysis, and were consequently not available to meet the publication deadline.

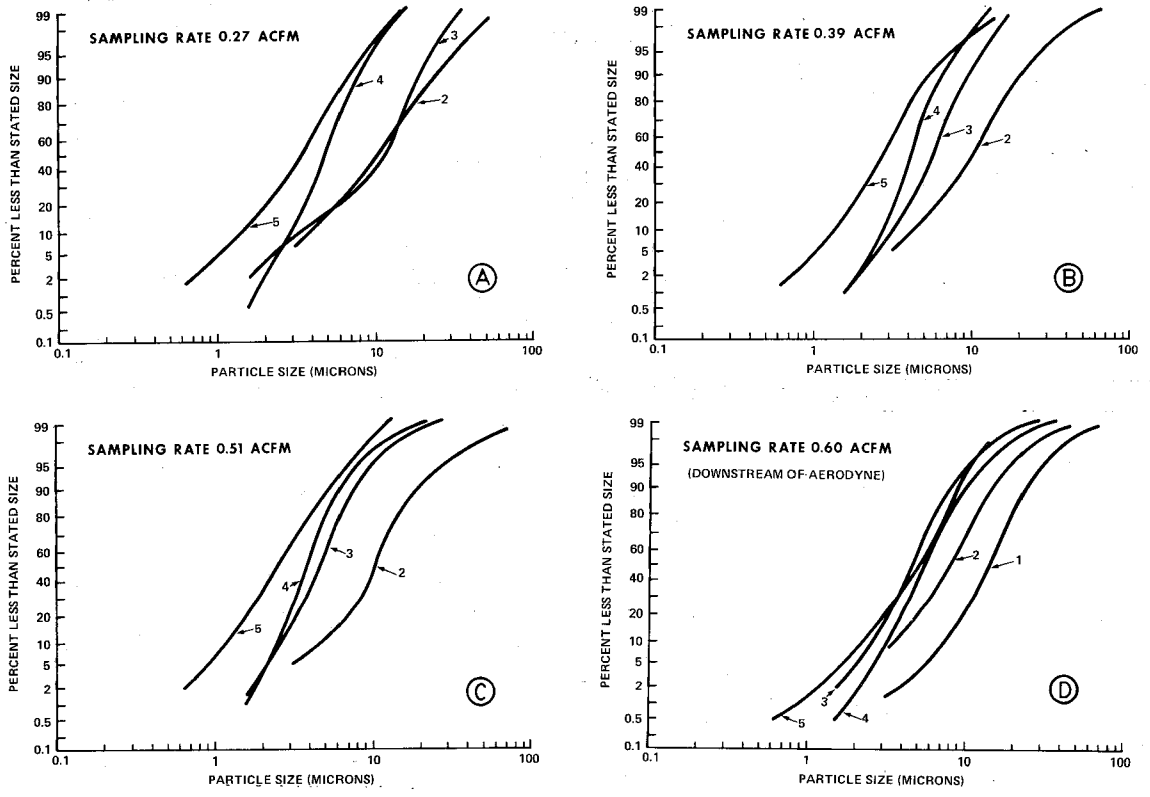

Figure 8 - Size distributions for individual cyclone catches at various sampling rates

In Figures 8a through 8d, the measured dust distributions are substantially different than the calibration curves of Figure 3. In particular, the size discrimination of each cyclone collector is not nearly as sharp, and, as a consequence, there is considerable overlap in the size fractions collected by the individual cyclones. This

degradation in cyclone performance is probably related to operation at sub-rated flow, as necessitated by the combination of duct size and system flow rate. The actual sampling flows range from 0.27 to 0.60 scfm in Figures 8a through 8d, compared to a design flow of about one scfm. However, within this range of sampling rates, there is no clear-cut correlation apparent between the sharpness of the size discrimination and the sampling flow rate.

The relatively poor size discrimination observed in Figures 8a through 8d limits the accuracy obtainable in deducing the particle size distribution directly from the weight captured in each cyclone. However, useful approximations are possible, and more accurate size distributions can be constructed from Coulter Counter analyses of the individual cyclone captures. Hopefully, operation of the cyclones closer to their design flow rate will sharpen the size discrimination and improve the accuracy of this measurement technique.

The cut size (50% efficiency) of the individual cyclones depends upon the operating temperature and sampling flow rate. Although theoretical estimates of the effect of flow rate and temperature are possible, experimental calibration is necessary to confirm these estimates and improve the accuracy of the technique. Figure 9 is a preliminary calibration deduced from the dust size distributions, samples of which are shown in Figures 8a through 8d.

In Figure 9, the separation in cut sizes between the various cyclones is evident from the trend line drawn through the data. However, considerable experimental scatter is also apparent, and some data points seem clearly out of line. The Coulter analyses of these samples will be repeated to test for possible procedural errors.

The lines through the data in Figure 9 are drawn at a slope corresponding to a cut size variation with flowrate of $d_c \sim Q^{-\frac{1}{2}}$, as predicted by inertial separator theory. It is apparent that within the limits of the data scatter, the inertial theory matches the data quite well. However, the resulting extrapolation of the dust sizes to the rated flow of one cfm falls far short of the performance shown in the calibration curves of Figure 3, even after allowing for an expected 60% increase in cut size caused by high temperature operation.

One of the highest priority measurements was the alkali vapor content. Three such measurements were obtained. The first measurement was the vapor trap sample accumulated during 58 minutes of sampling with the downstream probe before it failed. During this period the furnace was maintained at a temperature of 1900°F as discussed previously. The second alkali trap sample was a composite of 106.5 minutes of sampling under various flow conditions with the upstream probe. The third measurement was a composite of 135.7 minutes operation with the upstream probe relocated to the downstream sampling station. During collection of both the second and third samples above, the furnace temperature was maintained at 1450°F.

The calculated gas phase concentrations for each of the three vapor samples is shown in Table I. The actual alkali concentration in the 1650° combustion gases should be bracketed by the results in Table I, i.e., the true alkali vapor concentration lies between 0.6 and 3.4 ppmw. During Sample Series 6, the 1900°F furnace temperature may have caused additional volatilization of alkali from the particulates so that the measured concentration of 3.4 ppm is probably too high. On the other hand, during the subsequent tests, when the furnace was maintained at 1450°F, some condensation of alkali vapor onto particulates probably occurred. The two measured concentrations values of 0.6 ppmw are therefore probably too low.

Table I

Measured Alkali Vapor Concentrations

Sample Description	PPMW As Vapor Na	K	(Na+K)
A. Downstream Probe, Sample Series 6 (1900°F) (58 minutes)	1.52	1.87	3.39
B. Upstream Probe, Sample Series 6-11 Composite (106.5 minutes) (1450°F)	0.28	0.26	0.55
C. Downstream Probe, Sample Series 12-13 Composite (135.7 minutes) (1450°F)	0.16	0.47	0.63

The measured values appear to be consistent with current thermochemical calculations, and are somewhat lower than the NCB/CURL measured values which include some contribution from particulates smaller than 2μm.

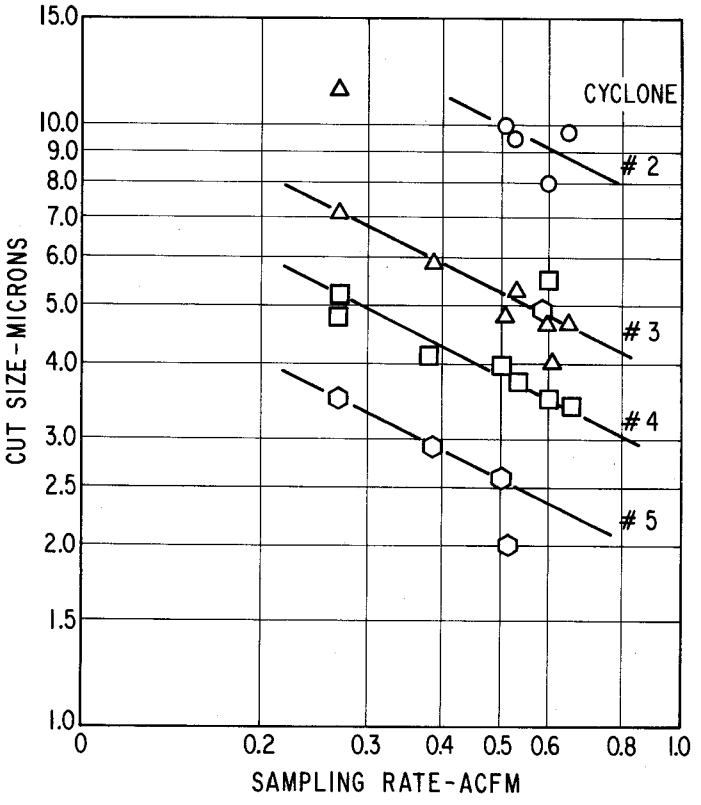

Figure 9 - Cyclone cut size versus sampling rate

CONCLUSIONS AND RECOMMENDATIONS

Sampling System Development

The performance of the high-temperature high-pressure sampling system has been demonstrated to be satisfactory. Minor improvements are desirable to cope with operational problems uncovered during the demonstration test:

- Improved multi-stage cyclone design to provide quick disconnect/disassembly and higher operation temperature.
- Sensor backflush control to prevent unexpected interruption during test which can cause plugging in the static taps.
- Automation of the sampling procedure to simplify operation and improve turn-around time.
- Replaceable sampling nozzle or smaller duct size to raise sampling rate to the rated capacity of the multi-stage cyclone thereby improving the size discrimination.

Dust Sampling

A total of eight sets of dust samples were obtained during the demonstration test. Analysis of the total dust capture and the individual cyclone captures has led to the following advances in PFB efflux characterization:

- Definition of the dust load as a function of flow split between primary and secondary ducts has been achieved. Despite some data scatter, the projected dust load confirms earlier estimates based on analysis and conventional sampling equipment results.

- The possibility of transient fluctuation in dust loading due to dolomite addition, cyclone dumping, etc., has been identified as a potentially important issue.

- Although the size discrimination of the multi-stage cyclone collector was not as sharp as anticipated, good definition of the particle size distribution was obtained by performing Coulter analyses on the individual cyclone captures. The Coulter analysis is considerably simplified by the relatively narrow size range within each sample.

- The individual cyclone cut sizes were shown to vary with sampling flowrate according to inertial separator theory.

Alkali Vapor Sampling

Three alkali vapor samples were obtained during the demonstration test, under various sampling conditions. Analysis of these samples gave results which bracket the alkali vapor content of the combustion gases between 0.6 and 3.4 ppmw (NA + K as vapor, predominately chlorides and sulfates), in substantial agreement with pre-test predictions based on thermochemical modeling studies.

The confirmation of high alkali vapor levels in the combustion gases has important implications for the PFB system design. The PFB combustion gases contain one to two orders of magnitude more corrosive vapor than the .02 ppmw maximum allowable specified for conventional industrial gas turbines, thus posing a significant corrosion threat. This corrosion potential cannot be eliminated by improving the particulate removal efficiency in the hot gas cleanup system.

ACKNOWLEDGEMENT

The authors wish to thank C. M. Thoennes of GE for his consistent support of this work; P. Dietz of GE for his help during the demonstration tests; A. Roberts, W. Gearling, A. Lindsay and V. Wood of NCB/CURL and G. Reed of NCB/Stoke Orchard for their cooperation and hard work to make this demonstration test successful; V. Siminski, R. Hoke, M. Ernst and J. Bond of Exxon Research and Engineering for sharing their experience on the multi-stage cyclone collector operation; N. Marotta at GE for speedy Coulter analysis.

One of the authors (J.C.F. Wang) wishes to thank D. Hartley and D. Hardesty of Sandia Laboratories for allowing him to participate in the demonstration test and for providing him with partial financial support.

The work reported here was sponsored by the New York State Energy Research and Development Authority and by the United States Department of Energy under contract No. EX-76-C-01-2357.

REFERENCES

1. Brooks, R.D., and Peterson, J.R., "Combined Cycle General Electric Pressurized Fluidized Bed Power Generation Power Plant for Electric Power", paper presented at Fifth International Conference on Fluidized Bed Combustion, Washington, D.C., Dec. 1, 1977.

2. "Hot Gas Clean-up Efflux Characterization for Commercial Plant (Task 4.1.1)", General Electric Co., Energy Systems Programs Department, Report Number FE-2357-36, Sept. 1977, Contract EX-76-C-01-2357.
Also:
Bekofske, K., Giles, W., and Thoennes, C., "Characterization of Efflux from a Pressurized Fluidized Bed Combustor", paper presented at Fifth International Conference on Fluidized Bed Combustion, Washington, D.C., Dec. 1977.

3. "Combustion Chemistry Modification Evaluation", General Electric Co., Energy Systems Programs Department, Report Number FE-2357-40, to be issued, Contract EX-76-C-01-2357.

4. "Pressurized Fluidized Bed Combustion" NCB Coal Utilization Research Laboratory, Technical Progress Reports Nos. FE-1511-36 through FE-1511-40, Contract No. EX-76-C-01-1511.

5. Ounsted, D., "A Flame Photometer for Measuring Sodium Aerosol Concentrations in Furnace Gases", J. Inst. of Fuel, Nov. 1958, pp. 474-479.

6. Wang, J.C.F., Ringwall, C.G., and Thoennes, C.M., "A High-Temperature High-Pressure Isokinetic/Isothermal Sampling System for Pressurized Fluidized Bed Application", paper presented at Fifth International Conference on Fluidized Bed Combustion, Washington, D.C., Dec. 1977.

7. McCain, J.D., "Impactors: Theory, Practical Operating Problems, and Interferences", Proceedings of the Workshop on Sampling, Analysis, and Monitoring of Stack Emission, PFB-252748, April 1976.

A PROTOTYPE OPTICAL SCATTERING INSTRUMENT FOR PARTICULATE SIZING IN STACKS

A. L. Wertheimer, W. H. Hart, M. N. Trainer
Leeds & Northrup Company
North Wales, PA 19454

ABSTRACT

A new optical instrument has been built for in-situ measurements of particle size in stacks. Optical light scattering is used to measure volumetric loading of particulate in five size channels over the 0.1 to 10.0 micron diameter range. A unique aspect of this unit is the combination of a new technique using 90° scattering for measurement of submicron fractions, and low angle forward scattering for the larger size fractions. The device has been built to perform measurements of material while withstanding the high temperatures and corrosive atmospheres commonly encountered in stacks. Descriptions of the design and performance characteristics are provided.

INTRODUCTION

Light scattering is ideally suited for measurements of particulates in real time situations. The characteristics of the materials are not disturbed during the course of the measurements, measured sizes can be correlated well with standard optical microscopy, and the technique is rapid and, in general, real time. Frequently it is of interest to measure the mass or volume of particulates within a given size interval, and recent developments have produced low angle forward light scattering industrial process instruments capable of real time measurements of particle size and volume in either liquid or gases in the 2 to 200 micron diameter range.[1,2] These instruments are also unique for their ability to simultaneously accomodate multiple sizes of particles in the sensing region, so the loading level is considerably higher than is normally possible with single particle counters.

Performance of many particulate control devices depends on the size distribution of the particulate matter. Sufficient detail about the size distribution can explain unexpected operational characteristics and apparent poor performance.[3] In addition, plume opacity is highly influenced by particles in the 0.1 to 10 micron size range, and proper measurement of size fractions within this range is important to the control of opacity.

This paper discusses a new application of optical scattering, combining low angle forward scattering, for larger particle size analysis, with right angle scattering, which is more responsive to the smaller particle sizes. This combination of techniques has been incorporated in a prototype instrument, intended for use on a stack for rapid determination of particle size and loading.

PRINCIPLES OF OPERATION

Light scattering analysis is frequently based on the assumption of spherical material. Alternately, for non-spherical but randomly oriented material, an excellent approximation to the scattered signal can be obtained by modelling the particles with spheres of equivalent size. In any case, recent studies of the morphology of fly ash have shown the majority of material to be spherical in shape.[4] Accordingly, rigorous scattering theory for spheres of all diameters, first discussed by Gustav Mie[5] in 1908, has been used here for design and analysis of the instrument. Some simplifications, namely scalar diffraction theory, for particles much larger than the wavelength of light, and Rayleigh scattering theory, for particles much smaller than the wavelength, have commonly been used to analyze light scattering. However, since the size range of particle diameters for this work is comparable to the wavelength of light in the visible, the full theoretical treatment must be applied. A more complete description of the light scattering theory used to develop this instrument appears in Reference 6, so this paper provides only a summary of the physical principles.

For particles greater than about one micron in diameter, using visible light, the scale of angular distribution of the scattered flux pattern is inversely proportional to the diameter. Smaller particles scatter flux over a wider area, generally into the forward direction (within a few degrees of the direction of the optical probe beam). By measuring the flux at discrete angles in the forward direction, one may combine the readings, algebraically, into signals proportional to the volume of particulates within specific size ranges. An example of this is discussed in Reference 2.

For particles smaller than one micron in diameter, the variations of angular distribution in the forward lobe are negligible, and low angle forward scattering is not capable of determining size or mass fractions. However, at 90° to the probe beam, there is a significant variation in scattered light as a function of polarization, and by taking

the difference in intensities of two scattered, orthogonally polarized beams, one may obtain a volume response which peaks sharply for particles whose diameter is approximately one half the wavelength of the illuminating beam. For two wavelengths, 0.45 and 0.9 microns, two size fractions peaked at approximately 0.21 and 0.43 microns can be obtained. When combined with forward scattering for the larger particle range, volumetric responses peaked at 1.0, 3.5, and 7.0 microns in diameter can be produced. The five volumetric responses are shown in Figure 1, and they cover a range of approximately 0.1 to 10.0 microns.

The curves in Figure 1 are for non-absorbing material of relative refractive index of 1.5. Changes in refractive index will change the curves somewhat, but the effects are not very great. In particular, the size discrimination offered by the intensity difference approach for the small particle channels (1 and 2) is considerably less sensitive to refractive index than other light scattering techniques for that size range.

A significant distinction between this approach and other light scattering instrumentation is that volumetric fractions can be determined directly when many particles of different sizes are present in the beam. Analysis of the composite scattered light pattern is done through the instrument's microprocessor. Thus, single particle counting is not necessary.

DESCRIPTION OF THE INSTRUMENT

A prototype was built to incorporate these principles of light scattering in a unit designed for the unique structural and environmental requirements of real time stack measurements. In order to withstand the high stack temperatures, special fiber optic cables were employed capable of sustained operation up to 260°C. The probe was constructed out of stainless steel to resist the hot acid atmosphere. To maintain clear optical windows for collection of the scattered light, an air purge system was incorporated into the probe. The insertable portion of the unit was kept to a diameter of 9 cm (3 1/2 inches) to provide some clearance for a standard 4 inch access port.

A photograph of the entire system is shown in Figure 2. The insertable probe is the 1.5 meter long tubular section on the transceiver unit. In the transceiver housing are the light source and optical focusing system. The fiber optics terminate in the transceiver housing, and detectors convert the optical signals to electrical signals. The other components housed separately are the lamp power supply, the electronic control console, a digital printer for recording measurements, and the air purge system. Only the transceiver need be right at the stack port. The other components have connector cables which allow them to be up to 25 feet away.

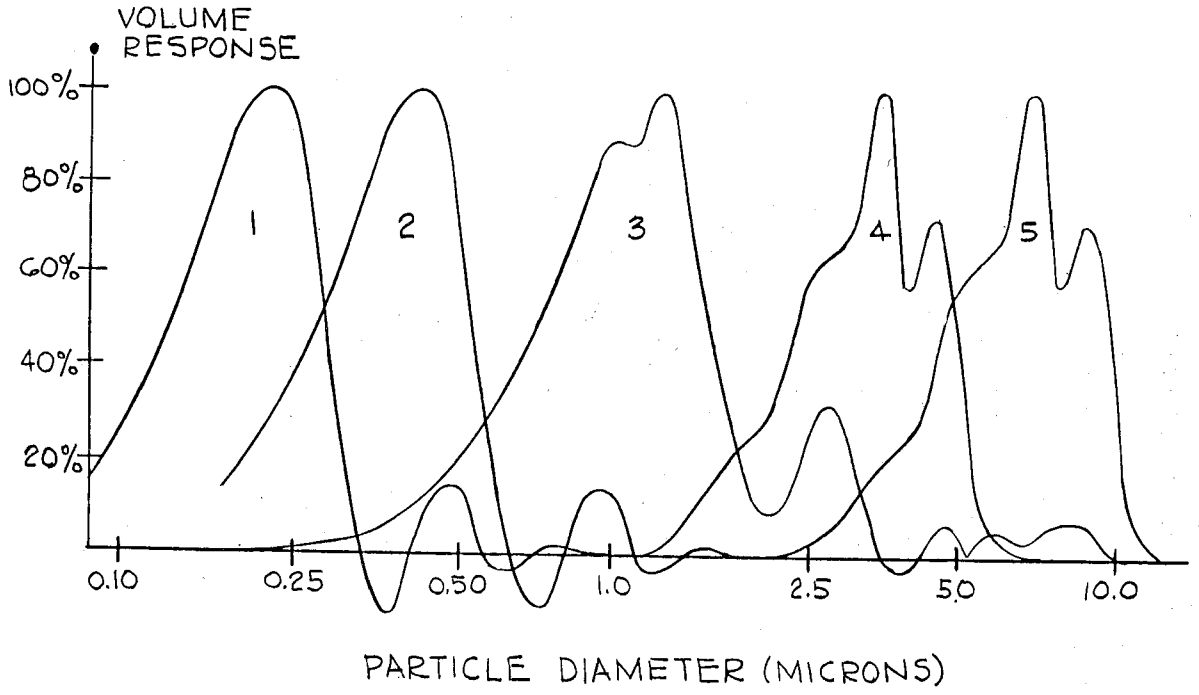

Figure 1. Volume response as a function of particle diameter for each measurement region. Curves 1 and 2 are obtained with 90° scattering, while curves 3, 4, and 5 are from forward scattering.

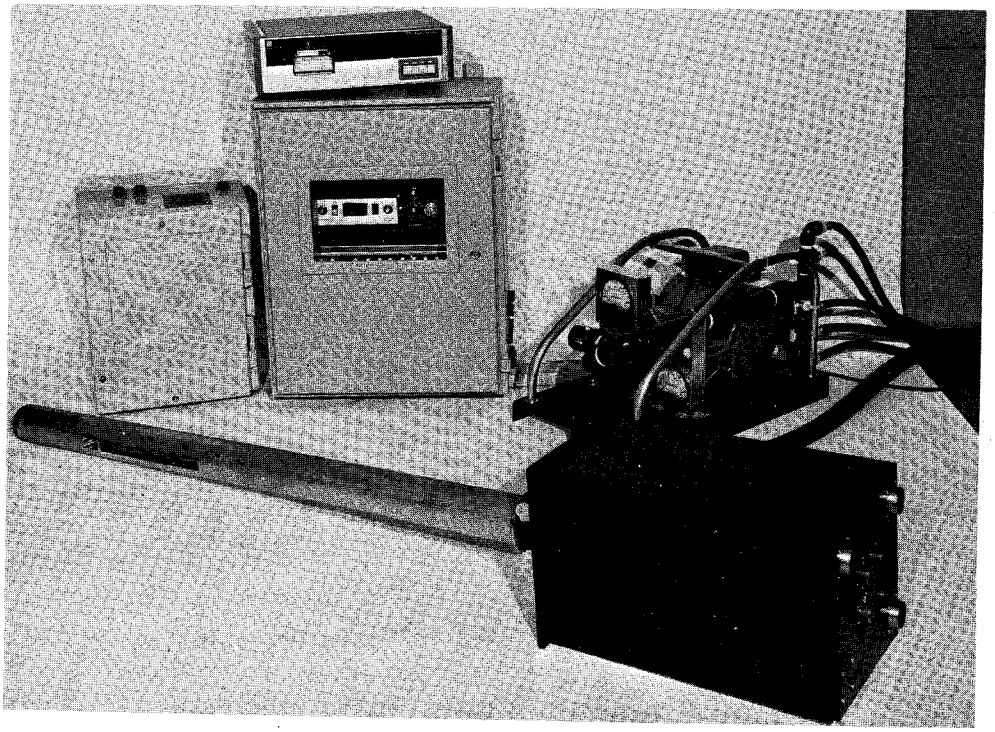

Figure 2. Prototype stack particulate monitor system, showing (l to r), lamp power supply, digital printer (top), electronics package, air blower, and probe.

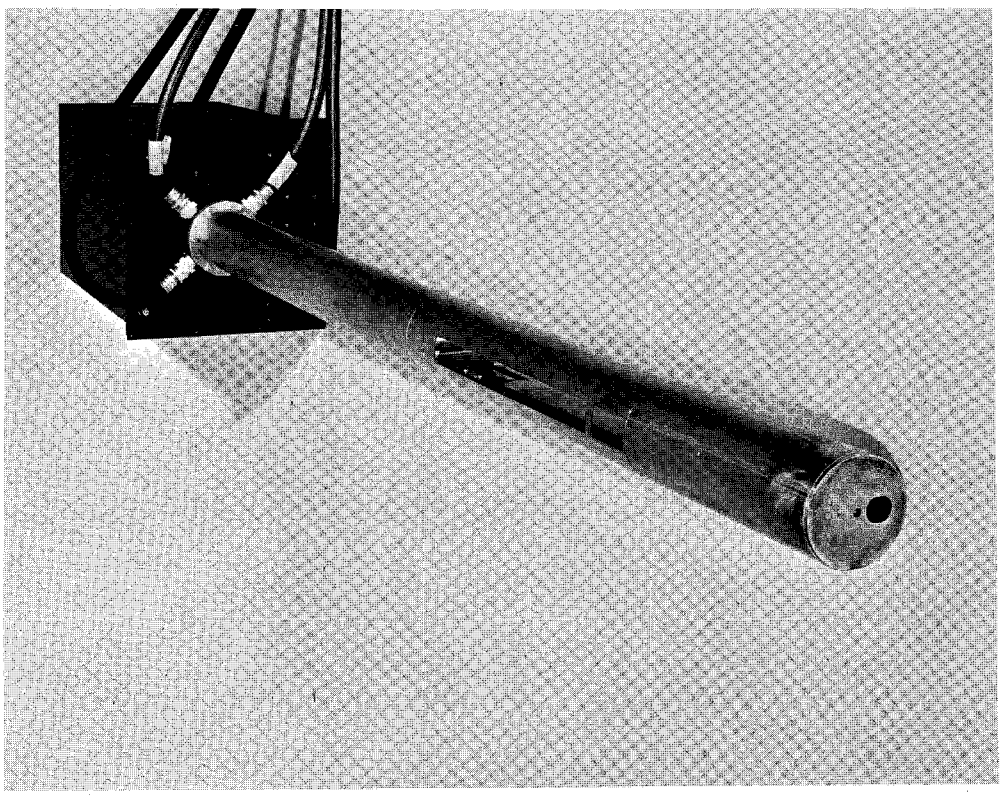

Figure 3. The transceiver, showing the 3½ inch diameter stainless steel probe section. Stack gases flow through the sample slot, which is 36 cm long by 3 cm wide. The lamp and detectors are enclosed at the end of the probe. The hoses for the air purge system attach to fittings at the collar.

Optical Design

The light source for the prototype is a xenon arc, spectrally filtered to produce polarized light at two wavelengths, 0.45 and 0.9 microns. These two wavelengths are alternately projected down the center of the probe. Due to the high temperatures, it is not possible to place detectors in the probe. High temperature flexible fiber optic cables are used to collect the light at five discrete locations, and bring the signals out to the transceiver housing. Each fiber cable terminates at its own detector, and a sixth detector is employed to monitor the strength of the illuminating beam.

The probe beam provides a 1.3 cm diameter circle of light at the end of the probe. At that end there is a 36 cm long by 3 cm wide opening for the stack gases to pass through, and the optical beam illuminates the material passing through this region. The probe portion is shown in greater detail in Figure 3.

Each of the fiber cables is directed at a slightly different portion of the illuminated volume, with significant overlap of some of the viewing angles, but it is assumed that the material is uniformly distributed, on the average, within this region. The air purge system for the optical windows was designed to provide laminar flow across the optical surfaces so as to cause minimal disruption to the flow of particulate material.

Prototype Mechanical Design

The insertable portion of the probe is made from stainless steel, while the rest of the transceiver unit is made of light-weight metal to minimize the total weight. The other components, as shown in Figure 2, are separate for ease of transportation. They are interconnected at the site with coded electronic cables.

The air purge system requires a blower for cooling the lamp and providing the air curtains to shield the optical components from the particulate material. The purge rate is set to full flow during insertion and removal of the probe, and then reduced to the appropriate level depending on the flow rate of the stack gases. The purge system is designed to protect the optics over a total range of stack flow velocities from 10 to 60 feet per second. Prior to the stack measurements, the flow rate is measured so that the proper settings can be made.

Electronics Design

The prototype employs digital electronics to measure and process the electrical signals generated by the six detectors. The gain of the system is set to accomodate loadings in the range of 4 to 400 parts per billion by volume (assuming a specific gravity of 2.5 for stack particulates). A sophisticated microprocessor program accumulates the data

during a measurement cycle, set by the user for an integration range from 4 to 256 seconds. A total of twelve separate signals are measured, five scattering signals from each of the two wavelengths of light, and one reference signal for each wavelength. These signals are first combined to produce the volumetric curves, as shown in Figure 1, and then a matrix decoupling removes most of the effects of the response curve overlaps. A normalized five channel histogram of the volume distribution is displayed on a digital printer. Additionally, the volume mean diameter, which is an indication of the mean size of the material, is computed from the histogram. Finally, a number is displayed proportional to the total volume of particulates in the beam in the size range from 0.1 to 10 microns. This loading signal, in combination with the duct air flow rate, can be used to calculate the mass or volume of material within this size range flowing through the stack during the measurement time.

Operational Characteristics

Initial set-up involves interconnection of the air hoses for the purge system and electronic cables between the power supply, transceiver, and control console. An on-site alignment of the lamp is necessary, and can be accomplished through two access holes located in the transceiver cover. A reading outside the stack is taken to set the electronic and optical zero for the unit. A single run, with the probe tip wrapped in black, light excluding material is taken, and the microprocessor then stores the background readings for subsequent subtraction from the measurements in the stack.

After the probe is inserted, the instrument can be set to run either continuously or for single step readings. The entire measurement process can be completed and analyzed in as short a time as 4 seconds. At this speed, the response time can be on the order of a transmissometer, but with as much detail about size distributions as obtained only after significant time delay when conventional impactors are used.

SUMMARY

This paper has described some of the design and operational characteristics of a new prototype instrument for use in measuring the size of particulates in stationary sources. A summary of the instrument is provided in Table 1. This unit has been developed for the Environmental Protection Agency, and will be delivered to them for further testing and evaluation. Initial field testing of the unit has begun, but results are incomplete at this time.

The advantages of this approach are in the rapid and real time analysis capabilities for in-stack analysis of particle size without the need for dilution or extraction of material. The measurement is on a

Table 1. CHARACTERISTICS OF PROTOTYPE LIGHT SCATTERING INSTRUMENT

Size Range (Particle Diameter)	0.1 to 10.0 microns
Size Measurement	Five volume fractions with centers at 0.2, 0.4, 1.0, 3.5, and 7.0 microns
Anticipated Loading Range	0.01 to 0.1 grams of material/meter^3 or 4 to 40 parts/billion by volume (with s.g. of 2.5)
Operational Range	4 to 400 parts/billion
Mode of Operation	Low angle forward scattering and 90° polarization dependent scattering
Power Requirements	115 volts, 60 hertz, 45 amps
Operational Temperature	Probe portion in stack: up to 260°C (500°F)
	Transceiver portion and other electronics outside stack: 0° to 43°C (32° to 110°F)
Speed of Measurement Sequence (Acquisition of Data)	Integration time selectable from 4 to 256 seconds

volumetric basis, and the histogram of sizes covers the respirable particle range. Accordingly this device provides a unique and valuable measurement capability for monitoring of particulate matter in source emissions.

ACKNOWLEDGEMENTS

The development, design, and construction of the prototype was funded by the U.S. Environmental Protection Agency, under EPA contract #68-02-2447, "Instrumentation to Measure Particle Size in Source Emissions."

REFERENCES

1. Wertheimer, A. L. and Wilcock, W. L. Light Scattering Measurements of Particle Distributions. Applied Optics. 15:1616-1620, June 1976.

2. Wertheimer, A. L., et. al. Light Scattering Instrumentation for Particulate Measurements in Processes. In: SPIE Vol. 129 - Effective Utilization of Optics in Quality Assurance. Bellingham, WA, SPIE, 1977. p. 49-58.

3. Sparks, L. Importance of Particulate Size Distribution. In: EPA Symposium on Transfer & Utilization of Particulate Control Technology, July 1978.

4. Fisher, G. L., et. al. Physical and Morphological Studies of Size-Classified Coal Fly Ash. Environmental Science and Technology. 12:447-451, April 1978.

5. Mie, G. Annalen der Physik. 24:377-445, No. 3. 1908.

6. Wertheimer, A. L., Trainer, M. N., and Hart, W. H. Optical Measurements of Particulate Size in Stationary Source Emissions. In: EPA Symposium on Advances in Particle Sampling and Measurement, May 1978. (Proceedings in Press.)

UTILIZATION OF THE OMEGA-I LIDAR IN EPA ENFORCEMENT ACTIVITIES

Arthur W. Dybdahl and Michael J. Cunningham
Remote Sensing Section
National Enforcement Investigations Center
Office of Enforcement
U.S. Environmental Protection Agency
Denver, Colorado 80225

ABSTRACT

The EPA-NEIC Omega-1 Lidar, purchased in May 1977, has been thrust into the EPA enforcement program for monitoring particulate emissions from stationary sources. This lidar mounted in a van can be placed in a desired testing position and in full operation within 5 to 10 minutes. It is capable of collecting plume opacity data at a measurement rate of 1 measurement/second for hours if required. The lidar contains a 3.1 joule/pulse ruby laser, a 20.3 cm reflective telescope, a photo multiplier detector of special design and the asociated analog/digital electronics in addition to a computer which also records the lidar return signals on magnetic tape for permanent record. The principle and modes of operation of the Omega-1 Lidar are discussed. The variables of the day and night modes of operation are presented. The field and laboratory calibration techniques as required by EPA enforcement procedures are discussed. Data processing and the resultant data presentations or records are discussed.

INTRODUCTION

The EPA-NEIC is now using a mobile lidar (laser radar) for the quantitative monitoring of the opacity of particulate emissions from stationary sources. The lidar is equally capable of making opacity measurements during either day or night time lighting conditions with significantly greater accuracy and consistency than any other remote measurement method or subjective observations employed to date. The lidar has the inherent capability of measuring plume opacity with consistent accuracy under a variety of background contrast conditions. These are a major advantage when used in the EPA Air Enforcement Program over the restricted daylight viewing hours imposed upon the present opacity monitoring method.

PRINCIPLE AND MODES OF OPERATION

The Omega-1 lidar consists of an optical transmitter, optical receiver and associated signal processing electronics [Figure 1]. A ruby [wavelength of 6943°A (red light)] laser is used to generate the pulses of light. The laser normally produces these light pulses, having a peak

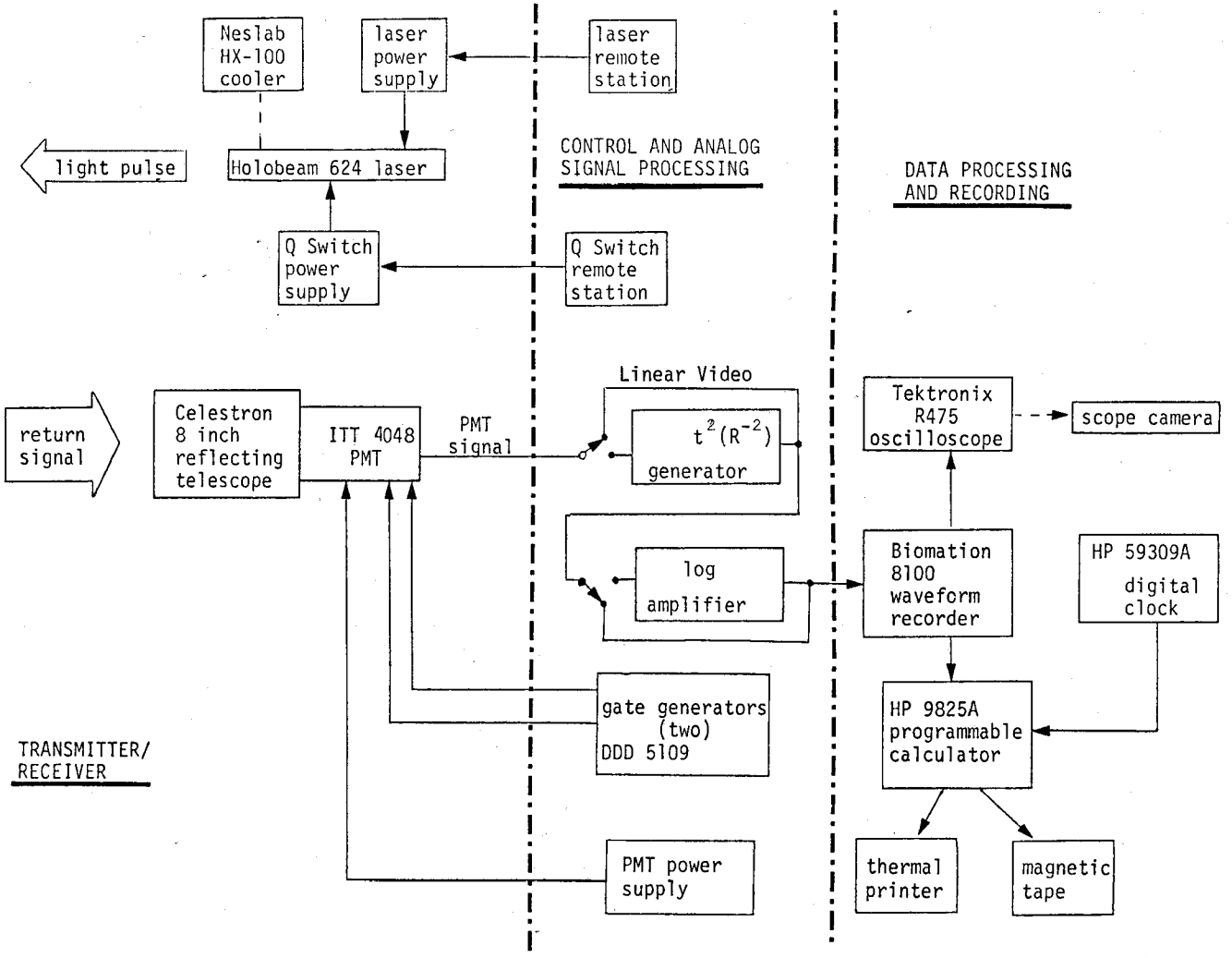

Figure 1. Schematic diagram of the Omega-1 lidar system

optical power of 30 to 220 megawatts with a pulse duration of 30 to 10 nanoseconds (10^{-9} sec). The light pulses are transmitted toward a target such as a smoke plume in a highly collimated (pencil) beam through the intervening atmosphere, and is backscattered along this path toward the lidar's receiver. The red light, backscattered by the atmospheric path of propagation and the smoke plume, is collected by the receiver, a 20.3 reflective telescope, and detected by a special photomultiplier tube (PMT). The PMT converts the optical signal into an electronic signal which is in turn displayed on an oscilloscope for viewing by the lidar operator. The scope's presentation to the operator is usually in the form of backscatter signal amplitude as a function of range along the lidar's line-of-sight [Figure 2].

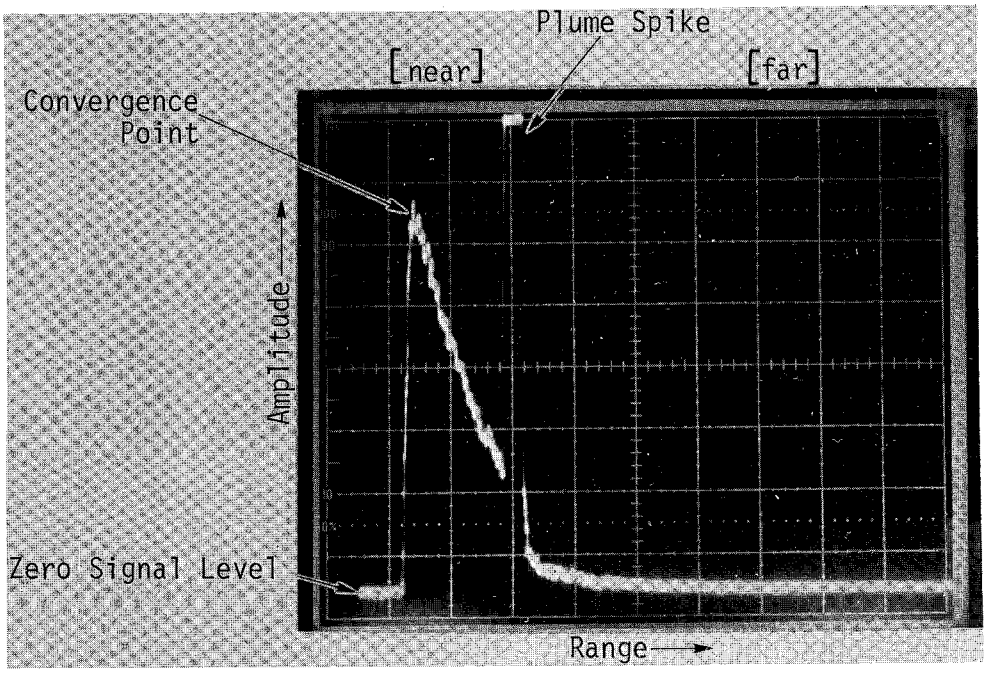

Figure 2 Linear Channel Video Signal, 40% Opacity (Uncorrected for $1/R^2$)

The scope "trace" increased quite rapidly from the zero signal level at the left, to a peak which corresponds to the spatial point where the field-of-view (FOV) of the receiver converges with the "pencil" beam of the laser. (The receiver is blind to the laser pulse until it has entered its FOV).

The signal then decreases in amplitude as the inverse-range squared (R^{-2}) in accordance with the general lidar equation, Collis[1], Dybdahl[2]. The spike in the trace is representative of the backscatter signal from a smoke plume. Its amplitude is much greater than that of the atmospheric return because the particulate density is far greater in the plume than in the surrounding air.

The electronic signal that is displayed on the scope is also sent through a digitizer to the lidar's computer where it is written on magnetic tape and subjected to analysis. First, the signal is systematically corrected for the inverse-range-square fall-off giving rise to a modification of Figure 2, as shown in Figure 3.

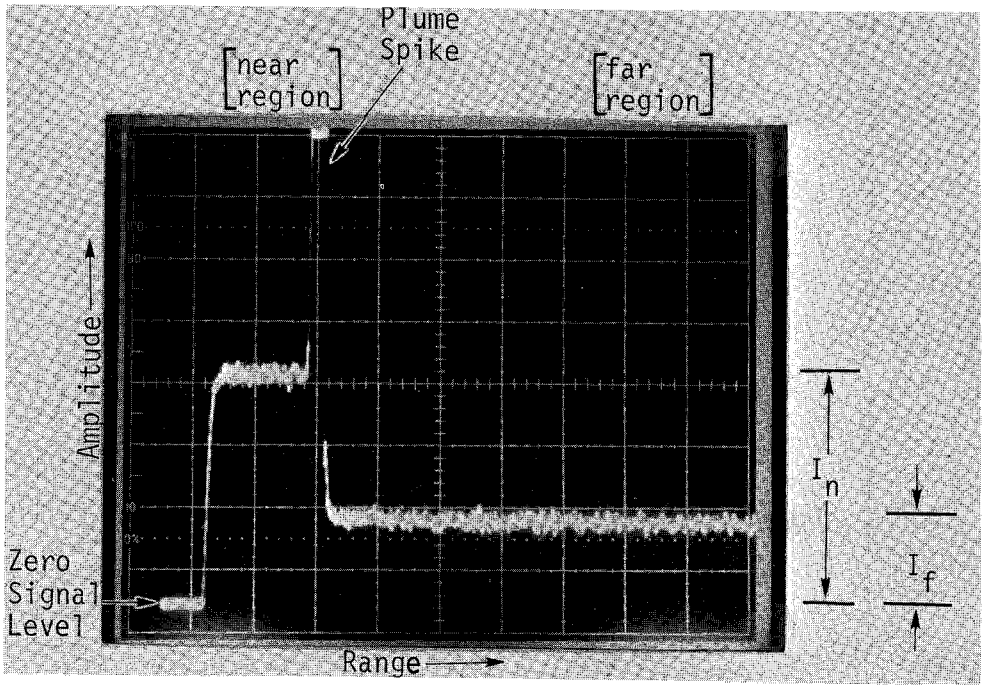

Figure 3 Linear Channel Video Signal, 40% Opacity (Corrected for $1/R^2$)

Smoke plume opacity (O) is determined by measuring the plume transmittance (T) with the lidar. Opacity is defined as:

$$O = 1 - T \qquad (1)$$

where:

O is the plume optical opacity at 6943°A.
T is the plume optical transmittance at 6943°A.

The value of T is calculated within the lidar computer from the signals I_n and I_f depicted in Figure 3. I_n, I_f are the atmospheric backscatter signals from ahead and behind the plume, respectively. The opacity value is printed out on the computer's thermal printer.

The Omega-1 lidar has two data processing (video) channels located ahead, electronically speaking, of the digitizer/computer system [Figure 1]. The first is a linear channel the output of which is given in Figure 2. The lidar return signal from along its atmospheric path is amplified by a constant factor before being presented to data analysis. The second is a logarithmic channel that deamplifies (gain <1) large amplitude return signals while amplifying small amplitude signals to a much greater level. The major utility of this channel is in the measurement of high opacities (<50%) especially in an urban area where the ambient pollutant levels are quite high.

Figure 4 shows a logarithmic channel video signal resulting from a laser pulse propagating through a plume of 80% opacity.

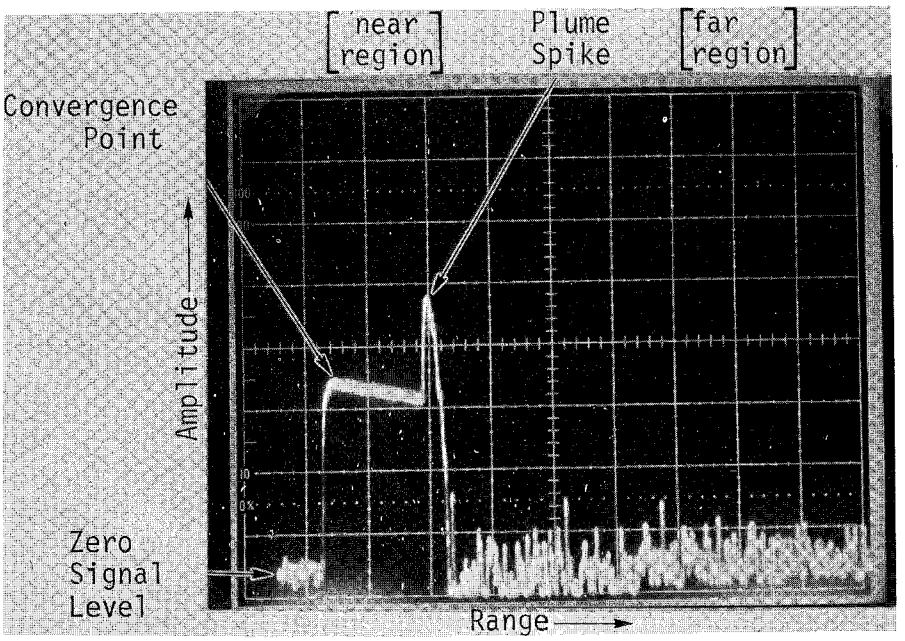

Figure 4 Logarithmic Channel Video Signal, 80% Opacity (Uncorrected for $1/R^2$)

Notice that the signal level at the convergence point is much less than, nearly half, the same respective point in Figure 2, the linear channel data. The signal level beyond the plume spike (in range) would be near zero in the linear channel. In the logarithmic channel the signal is much greater in amplitude. The inverse-range-squared signal, derived from Figure 4 is shown in Figure 5.

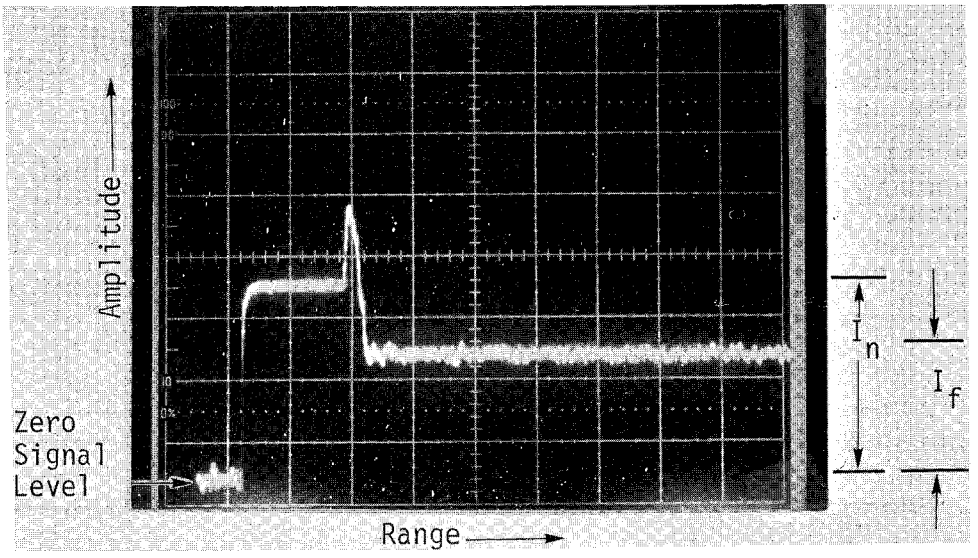

Figure 5 Logarithmic Channel Video Signal, 80% Opacity (Corrected for $1/R^2$)

The signal amplitudes I_n and I_f are then used to calculate the plume opacity. For this opacity the I_f signal level is far above the zero level, where in the linear channel this is not the case. The resultant accuracy in the opacity calculation for plumes over 50% is greater in the logarithmic channel than in the linear channel.

With the data processing capability inherent in the Omega-I Lidar, accurate opacity measurements are effectually made over a range of 0% to 100% with a rate as great as 1 measurement per second that can continue for hours.

In addition to the remote monitoring of plume opacity, lidar is used for the monitoring of particulates spatially and temporally in the following modes:

a) plume drift and dispersion characteristics
b) plume behavior such as fumigation, coning, etc.
c) location and movement of the combining of plumes
d) plume density variations
e) vertical burden and inversion layers.

These modes in addition to the remote measurement of plume opacity can be conducted during either day or nighttime hours. The lidar receiver is solar-blind; however, it cannot be aimed directly into the sun.

LIDAR CALIBRATION TECHNIQUE

The Omega-1 Lidar has a built-in calibration mechanism that tests the entire receiver, electronics and data processing systems. This is accomplished by using a highly-controlled small solid-state laser and light-emitting diodes to inject an optical signal, which simulates an actual lidar return signal from a given atmospheric path through a plume, or in clear air, into the receiver ahead of the PMT detector. This device, called an optical generator, simulates real optical signals representing clear air or 0% opacity, 10%, 20%, 40%, 60% and 80% opacities.

This calibration test is carried out periodically in the field while the lidar is in use requiring about 3 to 4 minutes to perform. Each of the above mentioned optical signals is fed into the lidar receiver and the resultant opacity is calculated in just the same manner as the real data collected in the field, and each value is recorded on magnetic tape, paper printout and in a permanent log book.

If the lidar-measured opacity value is not within $\pm$3% (absolute based or full scale or 100% opacity) of the actual value of the optical generator input, then the lidar is considered out of calibration and remedial action is taken.

The optical generator itself is periodically subjected to an exacting calibration in which all signal levels are held to within a fraction of a percent of the required value.

The extensive calibration is carried out to support the field data gathered for use as evidentiary material in enforcement proceedings.

DATA PROCESSING AND PRESENTATIONS

The backscatter data from each lidar shot is recorded on magnetic tape immediately after it is collected in the receiver and processed through the selected electronics. The lidar operator initially inspects the quality and integrity of the signal and makes any further adjustments to the system before proceeding with further measurements. He has to give a command to the computer which defines the locations or regions in the "near backscatter" and "far backscatter" signals (I_n and I_f in Figure 5) where the data shall be extracted, called pick points. The regions of the pick points, which are before the plume and after the plume, are about 15 meters in length. The backscatter data over each of the regions are averaged and the associated statistics calculated prior to the actual opacity calculation. From these signal levels, the opacity of the plume-under-test is calculated along with the resultant statistics.

The output of the computer on the paper thermal printer is the following:

a) time of the lidar shot to the nearest second
b) location of the digital file on magnetic tape
c) the location of the "near" pick point along with its average value and (statistical) standard deviation
d) the location of the "far" pick point along with its average value and standard deviation
e) the calculated opacity value and its overall standard deviation.

The data analysis is usually carried out in the field at the time the data is collected and again performed at NEIC as a double check of its quality and integrity.

The opacity data is documented in an enforcement report usually in the form of tables and two-dimensional plots. An actual example of a plot is shown in Figure 6. Each opacity value is plotted with respect to time along with its standard deviation bars. Each plot also contains the upper limit of the applicable state or local opacity regulation. The opacity data are also further processed so that they can be directly applied to the state or local regulation being enforced, such as 5- or 6-minute averages.

OMEGA-1 LIDAR ACCURACY

The entire Omega-1 Lidar system has been carefully evaluated over the past year. The optical generator test revealed that the lidar consistently computes opacity to within approximately 1% of the calibrated value (actual values: mean of 0.2% with a standard deviation 0.6% based on over 3,000 data shots).

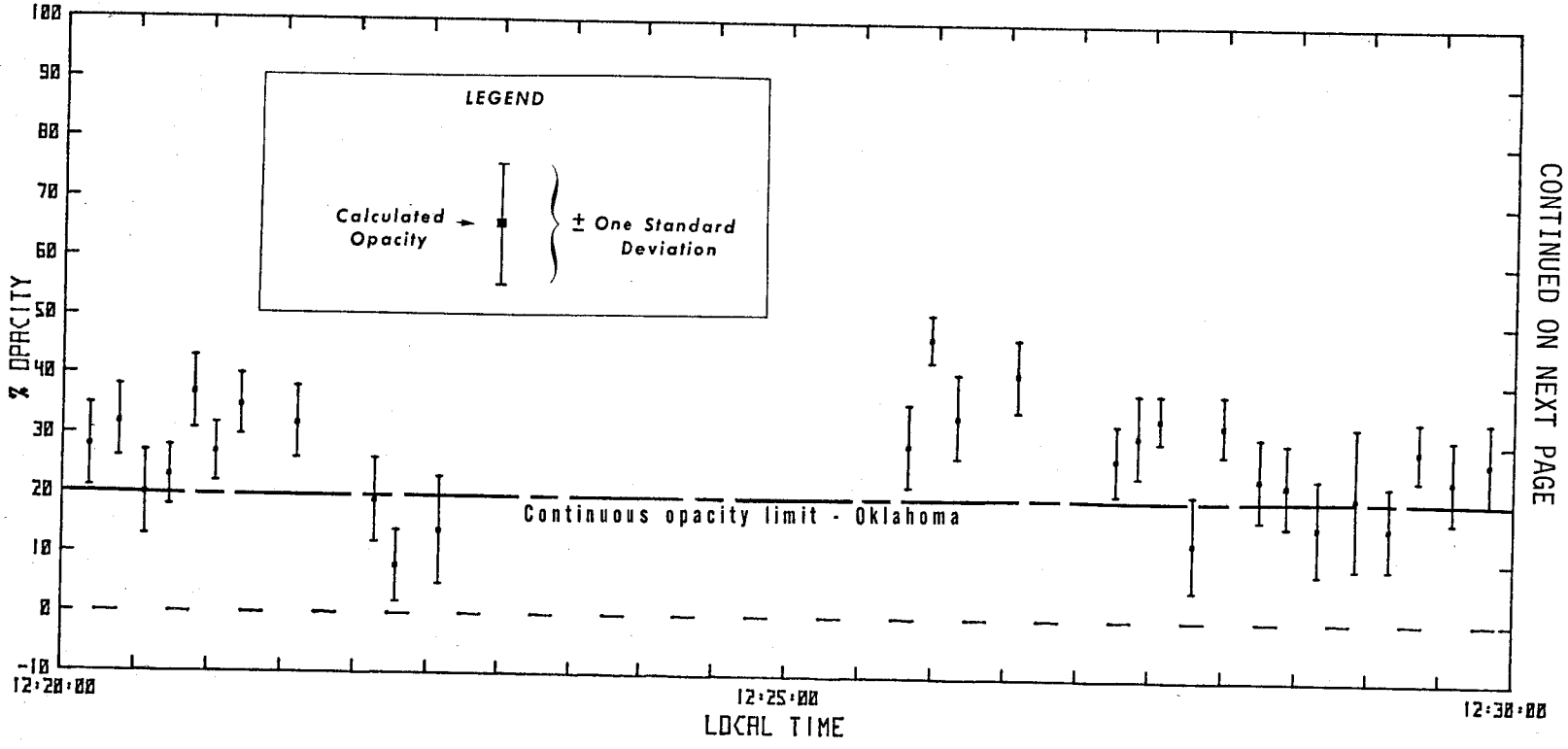

Figure 16

LIDAR OPACITY MEASUREMENTS - CO BOILER STACK

Figure 6 Two-Dimensional Plot of Omega-1 Lidar Opacity Data

With the laser pulse propagating through the atmosphere the absolute accuracy of the lidar-measured opacity is less than ±6% full scale (100% opacity), with a nominal value of ±3% full scale during both day and night operations. Ambient particulates along the lidar's line-of-sight in a heavily burdened environment such as fumigating emissions from a nearby source add noise and consequently error to the accuracy of an opacity measurement. This is the reason for quoting the two values above.

REFERENCES

1. R.T.H. Collis, Applied Optics 9, 1782 (1970)
2. A.W. Dybdahl, The Use of Lidar For Emissions Source Opacity Determination, U.S. Environmental Protection Agency-NEIC Technical Report, In Publication.

THE MONITORING OF PARTICULATES USING A BALLOON-BORNE SAMPLER*

James A. Armstrong and Phillip A. Russell
Denver Research Institute
University of Denver
Denver, Colorado 80208

ABSTRACT

A lightweight remote controlled sampler which is carried aloft by a tethered balloon has been developed to collect particulates from the plumes of point source emitters at various downwind distances. The sampling system is discussed as well as the field programs in which the system was employed to monitor emissions from fossil fuel power plants and the analysis of the collected samples. In the future the sampling system will be used to investigate the impact of conditioning treatments on power plant emissions. In situ plume sampling should lead to a better understanding of how plant operations, e.g., addition of SO_3, H_2SO_4, lime, etc., can alter particulate emissions. The sampling system can also be used to monitor other point and non-point source emitters where sampling from the ground, from towers, or by aircraft is impractical.

INTRODUCTION

The traditional methods of monitoring airborne particulates from point source emitters, such as fossil fuel power plants, have been to use ground based samplers, tower based samplers and/or samplers carried by aircraft. When monitoring a specific, well-defined source, a number of ground based samplers are usually positioned at considerable distances from the source. Dispersion modeling is normally required to analyze the distribution of particulates collected by the samplers in order to calculate the source strength. Considerable error is incurred when using this technique because of the simplicity of atmospheric dispersion models. In addition, there is considerable uncertainty that fine

* This work was supported under Grant No. 80492010 by the Industrial Environmental Research Laboratory, U.S. Environmental Protection Agency, Research Triangle Park, NC.

particulates will be representatively sampled. The use of towers allows for better vertical resolution in terms of sampling source emissions, but they are limited by the practical height they can sample and by their obvious lack of mobility. Monitoring of source emissions using aircraft is not feasible at low flying altitudes and in the proximity to the source because of the poor time and spatial resolution, due to the necessary speed of aircraft, and for safety reasons. While all of the above techniques are useful for monitoring source emissions under certain conditions, an additional sampling system is needed which has vertical and horizontal mobility and is capable of relatively long sampling times.

With this need in mind, the Denver Research Institute (DRI) of the University of Denver has developed and field tested a lightweight, remote controlled particulate sampler which is carried aloft by a tethered balloon. This sampling system has been specifically developed to investigate particulate emissions from fossil fuel power plants which use flue gas conditioning treatments. The sampling system can also be used to monitor other point and non-point emitters, especially where the areas to be sampled have difficult accessibility.

BALLOON-BORNE PARTICULATE SAMPLING SYSTEM

Design Criteria

General design goals for the tethered balloon particulate sampling system were to develop a system that is readily transportable in the field, thus having horizontal mobility, and that is capable of operating to reasonably high selected altitudes, thus giving the system vertical mobility. Specific design goals for the balloon-borne sampling package included that it be capable of long sampling times, that it be controllable from the ground, that it be simple to operate, that it be versatile in terms of being able to collect time resolved "streak" samples or a number of discrete samples and also be able to collect samples on various types of filter media. Finally, the sampling system should be relatively inexpensive.

The major design constraint involved developing a sampling package which has the above features but is still light enough in weight so that it can be carried aloft by a tethered balloon having a buoyant gas capacity no greater than 3.25 cubic meters. Tethered balloons up to this size do not require Federal Aviation Administration waivers to Federal Aviation Regulations, Part 101 in order to be flown.

Balloon System

Based upon the above criteria, an aerodynamic (blimp shaped) 3.25m^3 balloon and battery powered winch were purchased for this program from the A.I.R. Company of Boulder, Colorado. The balloon has a static lift

at sea level of 1.9 kilograms when inflated with helium. The balloon is constructed of plastic and for observation and safety reasons is bright red in color. The portable winch, which weighs 27 kilograms, contains a 12 volt battery to power a forward-reverse, variable speed motor which drives the tetherline spool. The extremely lightweight tetherline has a breaking strength of 535 newtons (120 pounds) and a mass per length ratio of 0.4 kilograms per kilometer. This balloon system is capable of lifting a package weighing 1,200 grams to altitudes of 800-1000 meters in winds up to 10 meters per second and to survive winds of 20 meters per second.

In addition to the balloon and winch, a battery powered transmitting meteorological package, designed to be carried by the above balloon, and a battery powered receiving ground station were also purchased from the A.I.R. Co. This entire system was obtained so that atmospheric soundings could also be made through plumes of power plants being sampled for particulate emissions. The meteorological package measures dry and wet bulb temperatures, pressure, wind velocity, and direction. The weight of this package is 1175 grams.

Particulate Sampling Package

The balloon-borne particulate sampler has all of the above design goals incorporated into it. The total weight of the sampling package has been held to 1170 grams so that it is possible to fly and operate the package to heights of one kilometer using the above balloon system.

Basically, the sampler, which is battery powered, consists of a movable sampling head connected via flexible tubing to a piston type suction pump and a flow adjust needle valve loop followed by a flow meter. A nozzle attached to the sampling head translates along a filter strip which is used to collect airborne particulates when air is sucked through it. The sampling head is translated by means of a guide mechanism consisting of a guide rod and a motor driven leadscrew. The sampler contains a radio receiver-servo system used to selectively control, from the ground, the suction pump and the motor of a translate mechanism as well as a flight termination system which deflates the balloon in case of a tetherline failure. The sampler also contains a radio transmitter system used to verify that the sampler is operating correctly.

A sketch showing the front perspective view of the particulate sampling package is presented in Figure 1. The overall dimensions of the package are 43 x 11.4 x 8.9 centimeters. The sampler housing consists of a rectangular box which has been fabricated using thin aluminum sheeting. Aluminum, plastic, and nylon have been used extensively throughout the package in order to minimize its weight. The means of suspending the package to the balloon is also shown in the figure. The two lines that attach to the balloon do so on opposite sides of the balloon body. This method of attachment allows the package to be orientated so that the filter collecting the particulates is either pointing into or away from the wind and, thus, the emitting source.

The exploded portion of Figure 1 shows a rectangular aperture in the front wall of the housing. Into this aperture fits a thin slotted aluminum plate onto which a linear filter strip has been mounted by means of an adhesive to its back surface. A framing plate attached to the inside of the housing wall holds the filter plate flush to the housing surface. To date, a 0.4 micrometer nuclepore substrate has been used as the filter. The nozzle that comes in contact with this filter has a sampling area of 0.7 square centimeters through which the suction pump of the package is capable of drawing air at a maximum rate of 1.5 liters/minute. Other filter media, such as millipore or glass fiber, are also compatible with the sampler.

A filter cover plate having a port in registry with the nozzle of the movable sampling head is employed to insure that only the portion of the filter on which particulates are being collected is exposed so that the remainder of the filter strip is protected from the outside atmosphere.

The internal mechanical and electronic components of the sampler are shown in Figure 2 which is a top plane view of the package with the top of the housing removed.

Figure 3 is an electronic block diagram of the radio operated, remote control system. The package contains a radio receiver for receiving command signals from a ground operated transmitter operating at 72.4MHz. This receiver is electronically connected to a flight termination servo circuit, a translate servo circuit and a pump servo circuit.

The flight termination servo circuit connects, via wire leads, to a flashbulb assembly attached to the skin of the balloon. In case of an accidental release of the balloon from the tetherline, the ground operator commands this circuit to supply power from the sampler battery pack to the bulbs. Once the bulbs ignite, a hole is melted through the balloon skin. This allows helium to escape and causes the balloon to descend, thus averting the loss of the sampler.

The translate servo circuit is connected to the leadscrew motor and controls the actuation of the motor. With the leadscrew motor actuated, once the sampling head reaches a new filter location, which corresponds to one of the detents or notches on the index track shown in Figure 2, the microswitch mounted on the sampling head enters the detent. This causes the microswitch to deactuate the leadscrew motor and to key a verify and battery alarm circuit. This circuit generates a signal to a 27 MHz transmitter, located within the housing of the sampler, which broadcasts a signal down to a verify receiver located with the ground operator. By this means the operator is informed that the sampling head has in fact been translated to a new sampling position.

The index track has ten detents which correspond to a start location, eight discrete sampling locations, and an end location. When the sampling head is either in the start or end location, the entire filter strip is covered by the cover plate shown in Figure 1.

The pump servo circuit is connected to the sampling pump which in turn is connected to the verify and battery alarm circuit. When the pump servo circuit actuates the pump in response to servo control signals received from the radio receiver, the verify and battery alarm circuit senses that the pump has been actuated, and transmits a pump actuation verification signal to the package transmitter. The transmitter in turn broadcasts a signal down to the verify receiver in order to alert the ground operator that the pump is on.

The verify and alarm circuit also constantly senses the power output of the battery pack and, when appropriate, generates a "weak battery" signal to the operator via the package transmitter. This indicating that the battery pack power is inadequate for further sampler operations.

The battery pack used to supply power to the electronics, translate motor, and pump motor of the airborne sampler is a system of three silver cells. The battery pack is a large capacity source that is compact, lightweight, and has a high current drain capability. The battery pack weight is 156 grams. This will operate the system for eight hours.

The balloon-borne particulate sampler can also be operated in a time-resolved "continuous streak" sample mode. When this is desired, the ground operator first actuates the sampling pump and then continuously holds the translate control lever of the radio transmitter to the command position. This causes the sampling head to continuously translate across the filter strip as the nozzle draws air. This allows for a single sample streak to be taken across a portion of the filter strip.

FIELD PROGRAMS

Arapahoe Field Tests

The first power plant checkout flights of the balloon-borne particulate sampling system were made on July 6 and 12, 1977, at the Arapahoe Steam Electric Generating Station of the Public Service Company of Colorado. They were conducted during the early morning hours when surface radiational inversions commonly are observed. The flights were conducted to determine the operating characteristics of the sampling system, effective sampling times, and to establish sampling procedures and positioning of the balloon in power plant plumes. Highlights of the flight operations and the analysis of the collected particulates for the July 6 tests are presented. Complete details of the Arapahoe field tests have been reported elsewhere.[1]

Flight Operations-

On July 6, the east stack plume of the Arapahoe Station was sampled between 0630 and 0800 hours-MDT, while the west stack plume was sampled between 0830 and 1000 hours. The east stack is fed by the steam generators of Unit #1 (full load capacity of 46 megawatts) and Unit #2 (47 megawatts). The west stack is fed by the steam generators of Unit #3 (47 megawatts) and Unit #4 (113 megawatts). All of the steam generators are equipped with electrostatic precipitators preceded by conditioning systems which inject SO_3 into the flue gas. In addition, Unit #4 is equipped with a wet scrubber, which was not operational during these tests. Properties of the low sulfur coal burned at the Arapahoe Station as well as operating loads of the four units during the test days are reported in Reference 1.

The launch locations for these tests were the coal piles just north of the plant. The balloon winch was positioned directly below the plume to be sampled. Vertical positioning of the balloon in a plume was accomplished by watching the balloon behavior from the launch position. During ascents, the horizontal motion of the balloon was minimal until the balloon entered the plume. Once there, the horizontal tracking motion of the balloon matched the visible smoke motion of the plume passing by the balloon. Also, when the balloon was in the plume, a portion of the plume smoke could be seen below the balloon. In addition to observations made from the Arapahoe launch site, the location of the balloon relative to the plant stacks was established by an observer stationed on the fourth floor of a Denver University building located slightly over three miles due east of the Arapahoe station. The observer, using a 35mm camera equipped with a 400mm telephoto lens, took slides of the flight operations. Since the wind on the morning of July 6, 1977, was from the south, reasonably accurate measurements of the horizontal and vertical distances of the balloon downwind from the top of the stacks have been determined from the photographic slides. During the July 6 tests, the horizontal distance varied between 92 and 99 meters while the vertical distance above the 76.2 meter high stacks varied between 47 and 52 meters. Sample times for collecting material from the east and west plumes were purposely varied and ranged from 10 seconds to 15 minutes.

Particulate Analysis-

Particulates collected during the Arapahoe checkout flights were examined with the DRI AMR 900 scanning electron microscope which includes a KEVEX energy dispersive X-ray analyzer. This was a cursory examination to ascertain "typical" particle size, concentration and composition. Sections of nuclepore substrates containing material collected by the balloon sampler during the July 6 tests were attached to aluminum SEM stubs which had previously been coated with parlodion. The samples were then vacuum coated with approximately 100 Å of carbon and examined by scanning electron microscopy/energy dispersive X-ray spectrometry. The

samples prepared by the above technique are also suitable for bulk sample X-ray analysis using X-ray excitation. For the present investigation, this analysis was not conducted.

For the "stacks to balloon" separation distances reported above, 30 second samples proved to be adequate for SEM work and 15 minute samples are believed to be adequate for X-ray excitation analysis. The 15 minute samples from the east stack and the west stack were examined in some detail using scanning electron microscopy.

East stack samples--SEM photographs showing typical particle size and concentration and X-ray traces showing the composition of selected areas of material from the east stack plume are presented in Figures 4, 5, and 6 (X-ray traces were taken at the arrow locations). Most of the flyash was mainly composed of silicon and aluminum with small amounts of iron (Figure 4). The next most predominant species in terms of number were relatively rich in calcium. A number of large particle agglomerates rich in sulfur were observed in the east stack sample (Figure 5). In addition, a number of small particles with relatively high sulfur concentrations were observed adhering to the surface of relatively large flyash particles (Figure 6). A few particles rich in phosphorous were also noted in the east stack sample (an X-ray trace of this is not shown).

West stack samples--The basic flyash from the west plume was generally the same in terms of size, concentration and composition as that from the east plume. Carbon particles, however, were obvious in material collected from the west plume (Figure 7) while carbon was almost totally absent in the east plume samples. The carbon material generally contained trace amounts of sulfur (Figure 7) or phosphorous (Figure 8).

Hayden Field Tests

The first field measurements of particulates from the plume of a rural fossil fuel power plant were made at the Hayden Station of the Colorado-Ute Electrical Association, Inc. The tests were conducted from November 29 to December 1, 1977. The location of this plant allows for the plume sampling to be conducted at various distances downwind from the stacks until the definitive shapes of the plumes are lost. The objectives of this field program were to establish effective sampling times for various downwind distances and to verify that the sampling system is capable of being operated in a cold ambient environment. Highlights of this test program are presented. Complete details of the test program can again be found in Reference 1.

The Hayden Station consists of two coal-fired steam electric generating units: Unit #1 having a full load capacity of 190 megawatts and Unit #2 having a full load capacity of 282 megawatts. The flue gas of Unit #1 is fed to a 72.6 meter (250 foot) stack while that of Unit #2 is fed to a 122 meter (399 foot) stack. The station normally operates with both

units at full load capacity using low sulfur coal from the nearby Hayden Plant Reserves.

Both generating units utilize electrostatic hot-side precipitators to collect flyash particulates from the gas streams before they enter the stacks. In order to comply with state and federal regulations concerning particulate emissions, Colorado-Ute has found it necessary to inject the Apollo Chemical Company conditioning agent LPA-40 into the flue gas of Unit #2 upstream of the electrostatic precipitator.[2] This agent is normally injected at a rate of 12 to 15 gallons per hour. Only the plume of Unit #2 was sampled during the three day field program.

Flight Operations-

The local weather during the flight operations of the tethered balloon sampling system was less than ideal in terms of the cloud cover and atmospheric stability. In the absence of weather fronts, morning temperature inversions normally occur at the Hayden site during this time of year in which the wind is from the east (downslope conditions). Only on the first test day, November 29, was there a weak morning inversion with the wind from the east to northeast. On this day the plume from the 122 meter stack was sampled from 0845 to 1023 hours-MST for various sampling times ranging from 2 to 15 minutes. The horizontal sampling distance was estimated to be 150 meters from the stack.

The ambient temperature, measured by a meteorological station which is permanently located on the plant property, varied from -13°C (8°F) at 0800 hours to -9°C (15°F) at 1000 hours on November 29.

On the second and third test days, November 30 and December 1, the wind was from the west so that upslope conditions persisted. Fortunately on these days, the winds in the mornings and early afternoons were of sufficiently low velocity so that plume sampling could be safely conducted. The weather during this period was dominated by fast moving fronts in the evenings with snow showers occurring nightly.

Due to the plant layout it was not possible to sample in close to the plant with the wind coming from the west. On the second and third test days, the balloon was launched from a north-south service road located approximately 675 meters due east of the 122 meter stack. On November 30 the plume from this stack was sampled from 0918 to 1253 hours for sampling periods ranging from 5 minutes to 45 minutes. On December 1 the same plume was sampled from 0950 to 1410 hours for sampling periods ranging from 20 minutes to 120 minutes. The downwind distances of the balloon-borne sampler from the stack during flight operations on the second and third test days have been estimated to be between 900 and 1000 meters which are distances of seven to eight times greater than the maximum sampling distance of the Arapahoe tests. Attempts to monitor the plume at greater "stack to balloon" distances were not made on these days because the atmospheric instability caused the plume to become somewhat undefined at further distances.

Particulate Analysis-

All sections of the substrates on which particles were collected were examined using scanning electron microscopy/energy dispersive X-ray spectrometry to determine the collection effectiveness of various sampling times for the "source to balloon" separation distances reported above. In addition, the samples were examined to determine the particle size range, particle morphology and selected particle elemental composition. Sample preparation involved mounting portions of the exposed sections of the substrates onto standard glass slides using double sided adhesive tape. The mounted samples were vacuum coated with approximately 100Å of carbon and then analyzed.

For the November 29 test, the 5 minute sample was adequate for SEM work and the 15 minute sample is believed to be adequate for X-ray excitation analysis. The samples from the November 30 and December 1 tests revealed that a 20 minute sampling time is reasonable for SEM analysis. As far as the suitability for X-ray induced X-ray analysis, most samples were too lightly loaded to permit sensitivities to assess trace elements; the longest sample (120 minutes) is believed, however, to contain an adequate coverage to permit trace elemental analysis using X-ray excitation.

Particle size--The most predominant species observed was typically single spheres with a radius of 1.0 - 2.0μm in diameter. Single spheres up to 9μm in diameter were also observed. Single spheres < 1.0μm were rare. Agglomerates of particulates were also prevalent and ranged up to 55μm in effective diameter (Figure 9). These agglomerates often contained a relatively large number of particulates 0.5 - 1.0μm in diameter as well as larger particles. In general, the Hayden Station, during the time observed, was producing larger particulates than observed at the Arapahoe Station and more agglomerates as well.

Particle composition--Individual and agglomerated flyash spheres were usually composed of silicon and aluminum with some calcium, potassium, and iron, although flyash composed mainly of silicon and calcium were also observed. Sulfur rich material was usually observed with agglomerates (Figure 9) and larger spheres of flyash (Figure 10). The sulfur rich material associated with flyash agglomerates usually appeared to form the matrix binding material. Whether it is from the coal itself or is a byproduct of the LPA-40 conditioning agent, which is known to be an aqueous solution containing a large fraction of ammonium sulfate[2,3], cannot be determined from this brief test program. In order to address this question it is hoped that in the future a more controlled test program of the Hayden Unit #2 plume can be conducted in which plume samples will be collected while the unit is operating both with and without the conditioning treatment.

CONCLUSIONS

The results of this program have demonstrated that the basic concept of *in situ* sampling of particulates from the plumes of point sources (in this case, fossil fuel power plants) is feasible using a remote controlled balloon-borne sampler. In particular, it has been shown that:

1. A versatile and inexpensive airborne particulate sampler can be designed and fabricated, which is controllable from the ground via a telemetry link and yet is light enough to be carried by a tethered balloon designed to operate without FAA waivers to FAR, Part 101.

2. It is definitely possible to position the sampling system in the visible plume of a fossil fuel power plant at desired downwind distances from the stack.

3. With the sampling system properly placed in a visible plume, adequate filter loading for energy dispersive X-ray fluorescence, scanning electron microscopy and transmission electron microscopy are readily attainable.

4. The sampling system is capable of operating at ambient temperatures down to at least -13^{o} Celsius.

ACKNOWLEDGMENT

We wish to thank Dr. Leslie E. Sparks of the EPA Industrial Environmental Research Laboratory for his suggestions, support and encouragement concerning the development of the balloon-borne particulate sampling system.

REFERENCES

1. Armstrong, J. A., P. A. Russell, and R. E. Williams. Balloon-Borne Particulate Sampling for Monitoring Power Plant Emissions. EPA Report to be published.

2. Bryant, R. W., L. Michael, and J. R. McNamara. In: Prepared Testimony Before the Air Pollution Control Commission of the State of Colorado. Colorado-Ute Electrical Association, Inc. November 14-15, 1977.

3. Pressey, R. E., et al. Four Corners Unit 4 Gas Conditioning. Denver Research Institute Report No. 5584. September, 1977.

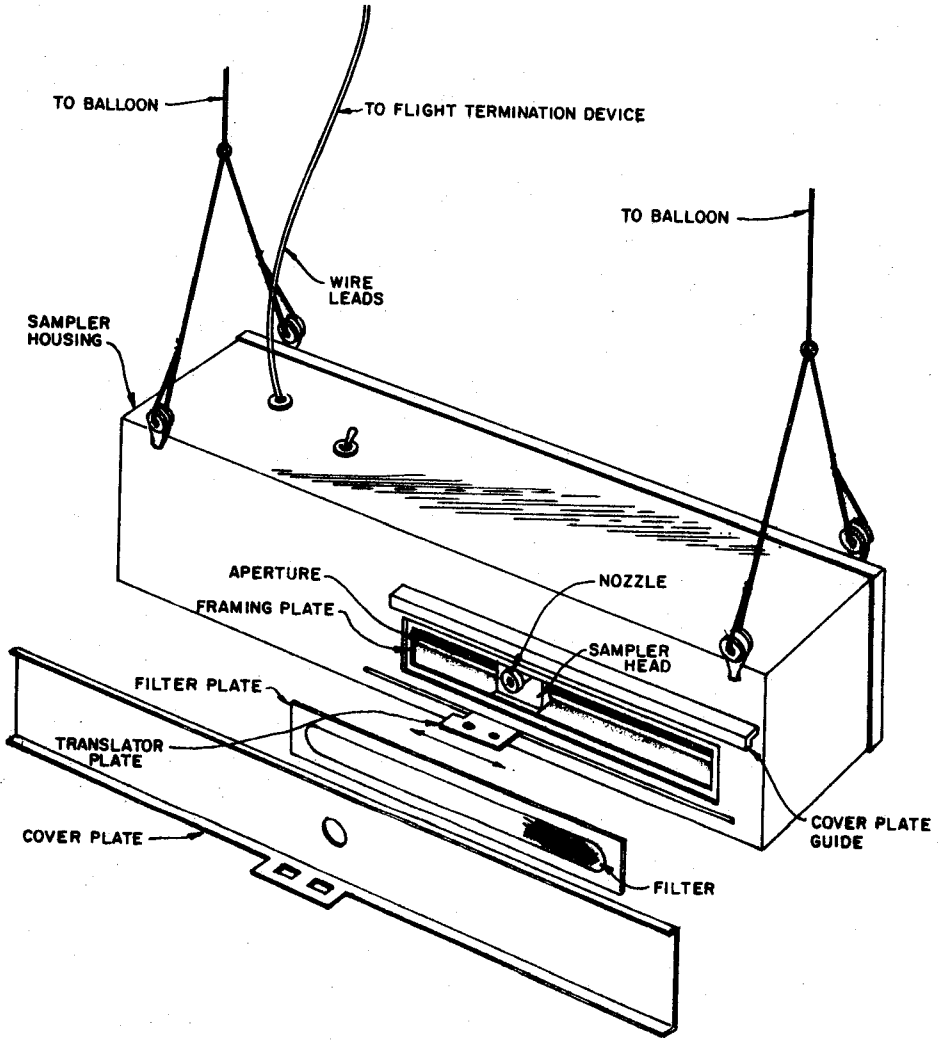

Figure 1. Front perspective view of particulate sampler.

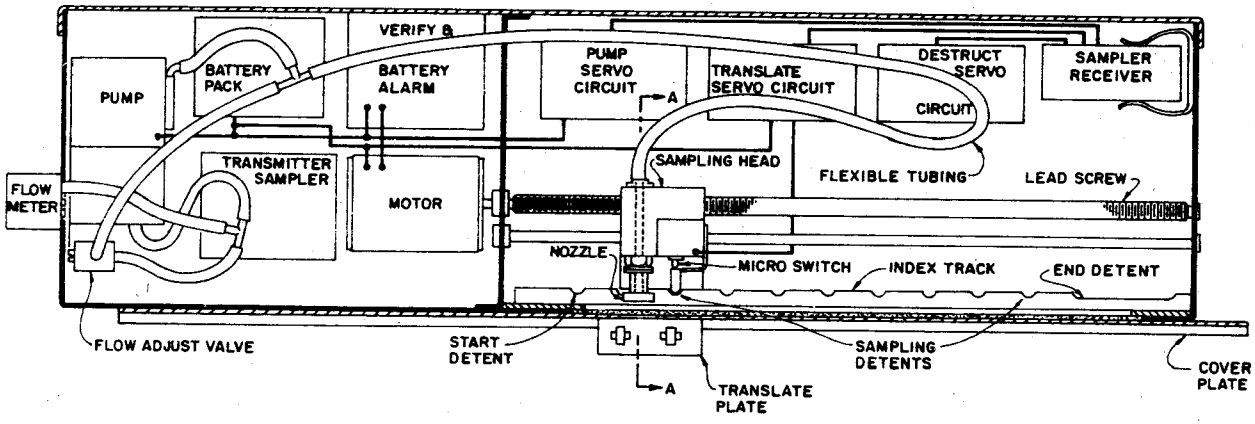

Figure 2. Top plane view of particulate sampler.

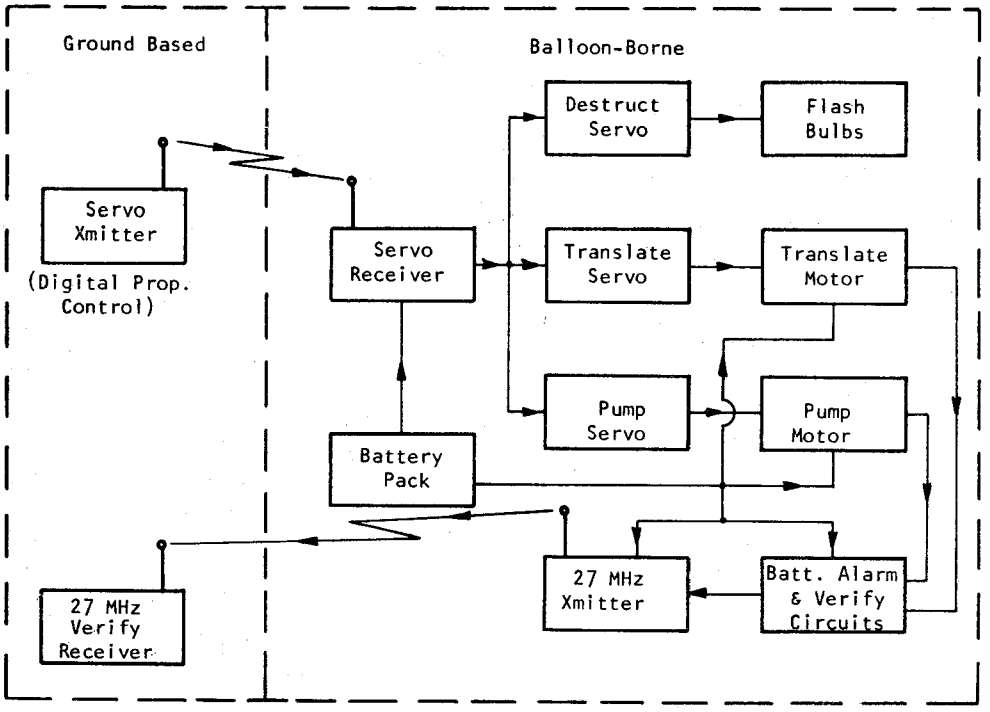

Figure 3. Electronic system block diagram.

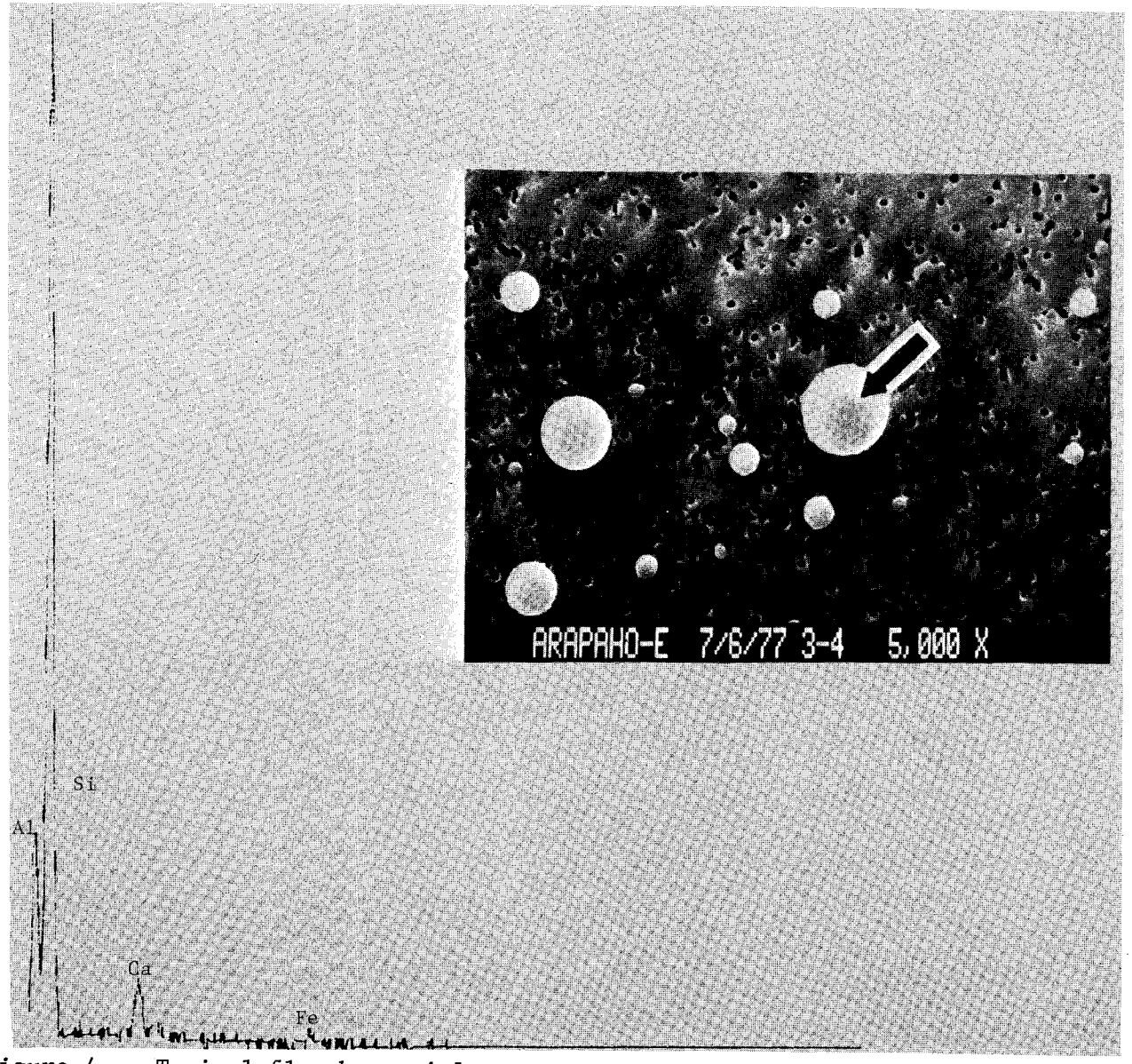

Figure 4. Typical flyash particles - east plume, Arapahoe Station.

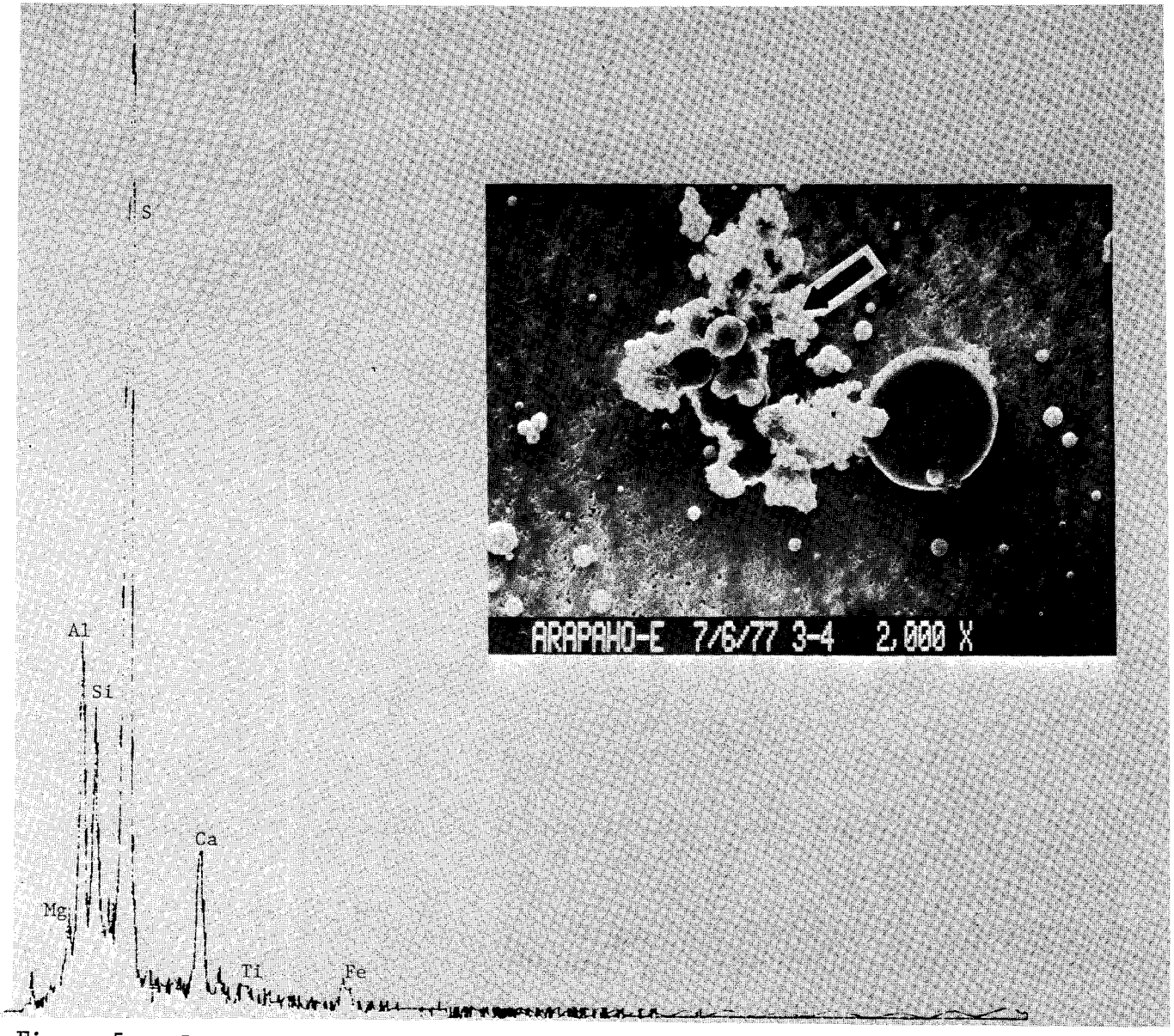

Figure 5. Large Particle agglomerate rich in sulfur - east plume, Arapahoe Station.

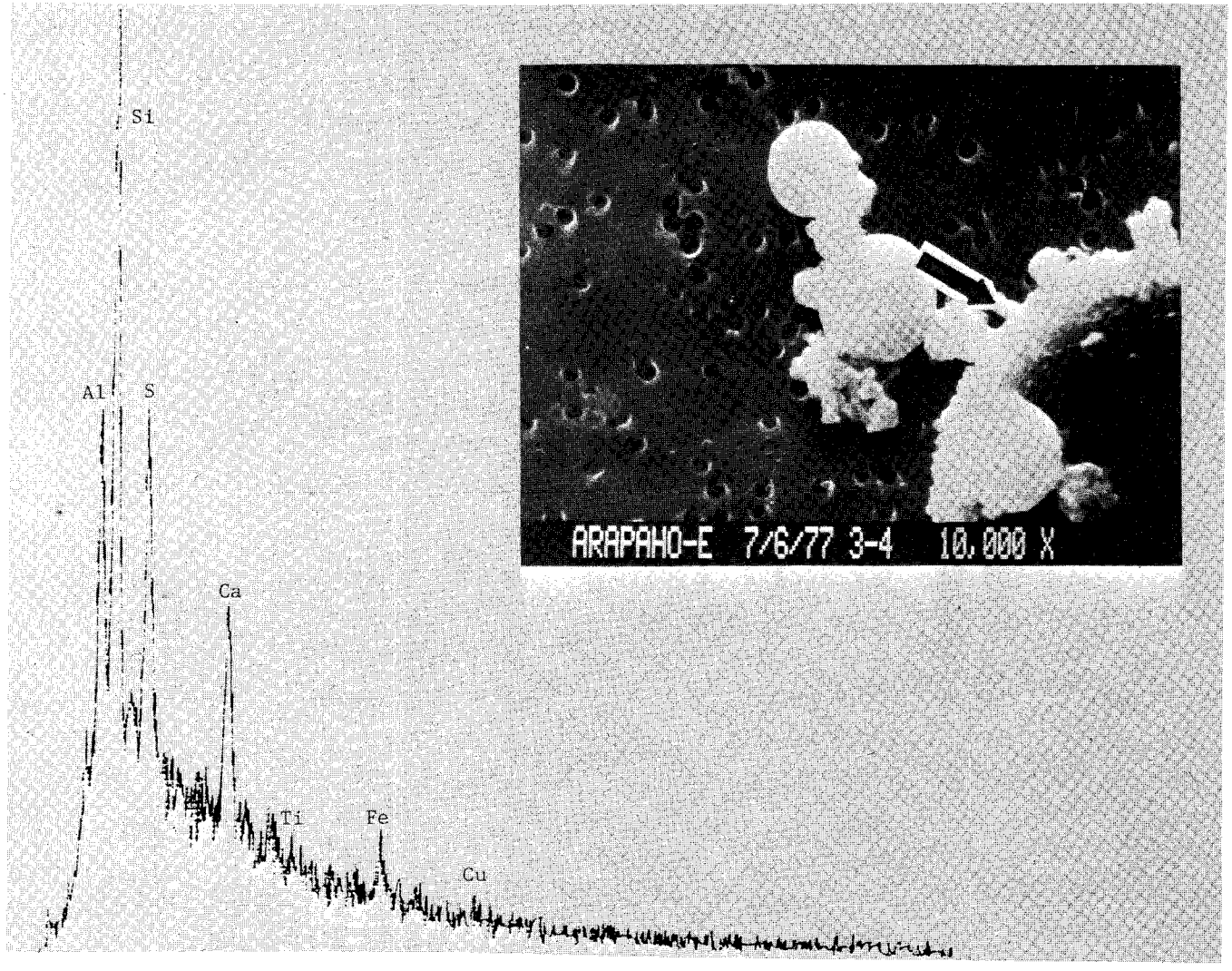

Figure 6. Small particles rich in sulfur attached to large flyash particle - east plume, Arapahoe Station.

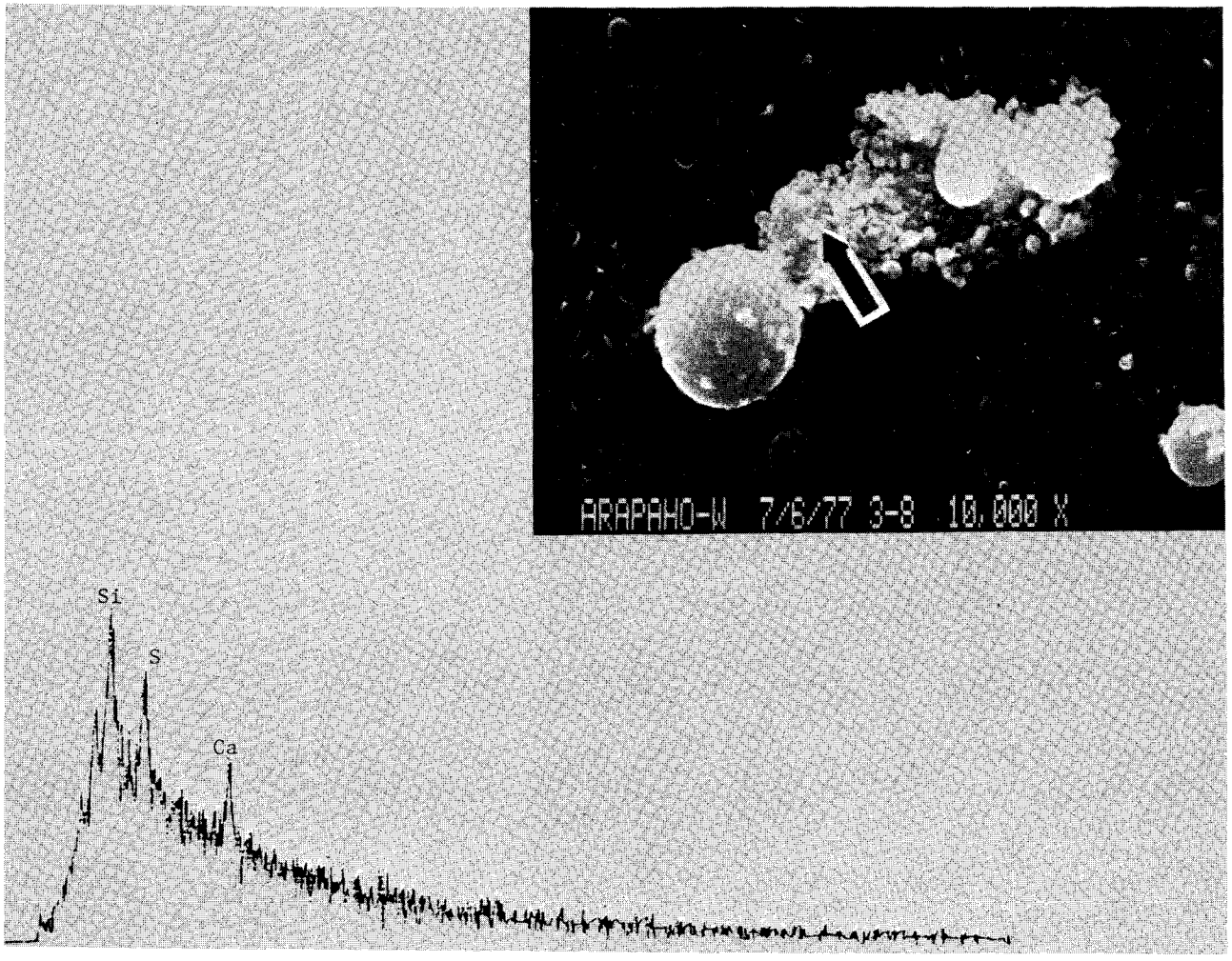

Figure 7. Carbonaceous particle agglomerate - west plume, Arapahoe Station.

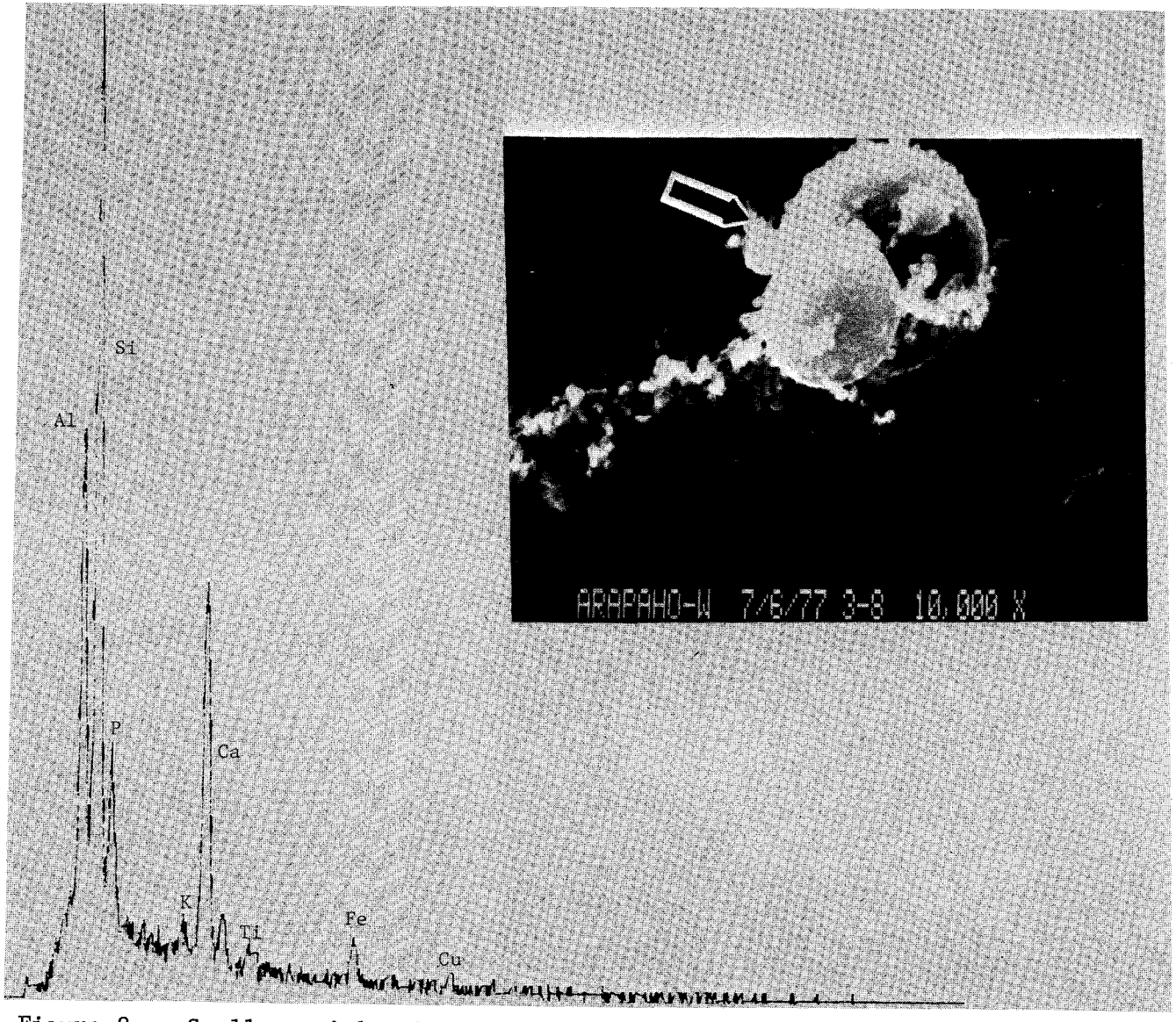

Figure 8. Small particle rich in phosphorous attached to flyash - west plume, Arapahoe Station.

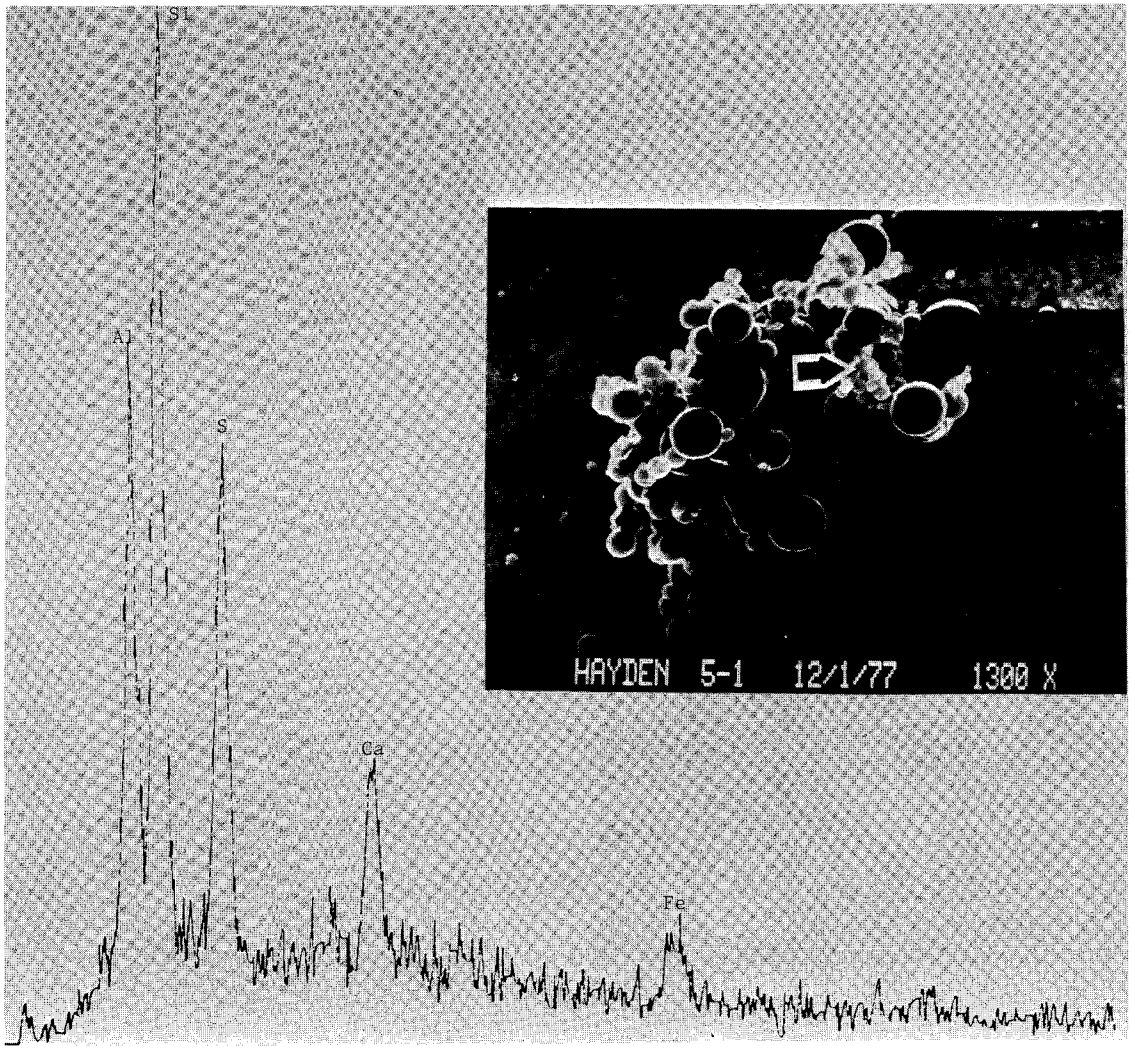

Figure 9. Large flyash agglomerate - Unit #2 plume, Hayden Station.

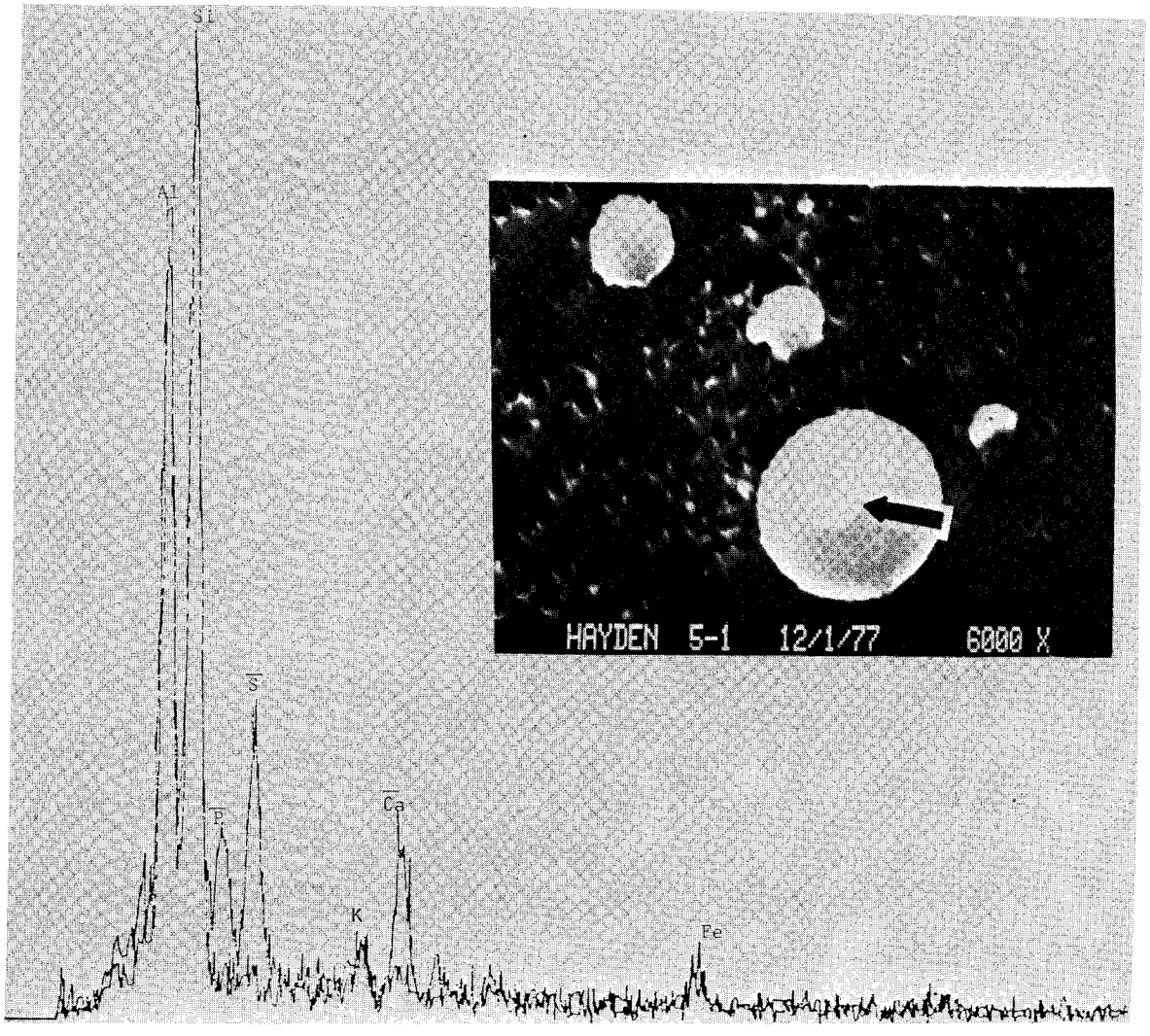

Figure 10. Sulfur rich particle associated with flyash (arrow). Spectrum shows increased concentrations of sulfur, phosphorous, and calcium - Unit #2 plume, Hayden Station.

A STUDY OF PHILADELPHIA PARTICULATES USING MODELING AND MEASUREMENT TECHNIQUES

Frank A. Record
Robert M. Bradway
GCA Corporation
GCA/Technology Division
Bedford, Massachusetts

and

William E. Belanger
U.S. Environmental Protection Agency Region III

ABSTRACT

This paper summarizes the results of a program to apportion the measured particulate loading at 13 monitoring sites within the City of Philadelphia to six major source categories, and to acquire background information on the respirable-nonrespirable fractions of the suspended particulates and the elemental composition of each fraction. Diffusion modeling was used to calculate the contributions of five of the source categories. Historical data, site visits and a field program to investigate the contribution of vehicle related fugitive dust to nearby monitors provided the necessary additional information.

Measurements were made with conventional hi-vols at four heights near an intersection and at rooftop level on either side of the main street. Special instrumentation included the EPA Dichotomous Sampler and GCA Ambient Particulate Monitor. A test was conducted to measure the effectiveness of a 3-day period of intensive street flushing in reducing ambient particulate levels.

INTRODUCTION

This paper is based on the results of a program designed to increase understanding of the principal sources of particulates within the City of Philadelphia prior to the development of implementation plans for the achievement of the ambient standards. The approach was twofold, involving field experiments to measure the influence of specific sources through the deployment of hi-vols and other sampling

equipment, and diffusion modeling to calculate the contributions of major emission categories to particulate loadings at the various monitoring sites. In the course of the program, a number of different measurement techniques were used and considerable insight into the physical and chemical composition of the airborne particulates was gained as a result. The principal thrust of the paper, however, is to present the results obtained by the straightforward application of the Air Quality Display Model (AQDM), tempered by the results of observations and modeling at a downtown intersection.

More details of the study are contained in the final report submitted under the contract.[1]

NATURE OF THE PHILADELPHIA PARTICULATE PROBLEM

Citywide average TSP concentrations in Philadelphia dropped abruptly from about 240 $\mu g/m^3$ in 1956 to about 165 $\mu g/m^3$ in 1958. This rapid decrease was followed by a gradual downward trend, accelerated between 1966 and 1968, through 1972. For the last 5 years, the citywide average concentration has exhibited only minor year-to-year variations and appears to have leveled off just slightly above the primary annual standard of 75 $\mu g/m^3$. However, this standard is still being exceeded at eight of the 13 monitoring stations, and annual concentrations less than the secondary standard of 60 $\mu g/m^3$ are found at only three monitoring stations. These three stations are located in the western and northeastern parts of the city and are removed from the centers of urban activity. Furthermore, the highest annual concentrations are found at sites that are located in close proximity to busy streets (i.e., sources of vehicular emissions and reentrained dust), although high annual concentrations and rather frequent violations of the 24-hour secondary standard also occur at sites subject to more general sources of fugitive dust or specific industrial or commercial sources.

It is apparent that the particulate problem of the early 1950's has been greatly alleviated by the control of emissions from major industrial, fuel combustion, and solid waste disposal sources. However, because the most feasible and effective emission reductions from these sources have already been achieved, it is now necessary to investigate possible reductions from other source categories. A first step in the development of appropriate additional control plans is, therefore, to estimate the relative contribution of each major source category to the particulate burden of the city.

PRELIMINARY RESULTS FROM THE AIR QUALITY DISPLAY MODEL

When applying AQDM to the Metropolitan Philadelphia Interstate AQCR under a separate contract,[2] GCA found that the use of standard emission factors for reentrained dust led to excessively large contributions from paved roadways. By omitting fugitive dust emissions and

accepting a high "background" concentration, however, satisfactory agreement between calculated and observed values could be obtained. Figure 1 shows the results for 1974 that were obtained for the New Castle and Philadelphia monitors by this procedure. The CAMP station (FRI) was assumed to be greatly influenced by a local parking lot and traffic sources and was omitted from the regression analysis. A realistic handling of roadway emissions offered the promise of reducing the background estimate while maintaining the good correlation between observed and calculated values.

FIELD MEASUREMENTS

Design of Measurement Program

Because of this recognized need for a better understanding of vehicle-related emissions, including the resuspension of street dust, a comprehensive measurement program was undertaken to define the three-dimensional particulate field near a heavily traveled street in downtown Philadelphia. The site selected for these measurements included an intersection at the corner of South Broad and Spruce Streets, where a 12.2-meter tower was erected next to the city's monitoring trailer, and the rooftops of two buildings located approximately 275 meters to the south on either side of Broad Street. Building heights ranged from about 5 to 82 meters near the intersection to a more uniform two- to three-story height to the south.

Hi-vols were mounted in pairs on the roof of the trailer and at three levels on the tower. This made 24-hour observations possible at each of the four levels without requiring the presence of an operator at midnight to change filters. In addition, an EPA Dichotomous Sampler and a GCA Ambient Particulate Monitor were operated to provide particle size information and short-term concentration data. Traffic counts were automatically recorded at four locations on Broad and Spruce Streets.

At 500 South Broad Street, the existing hi-vol on the roof of the Health Building was supplemented by hi-vols on the front and back edges of the roof. Windspeed and direction sensors were positioned on an elevated portion of the roof near the back of the building. Directly across the street from 500 South Broad, on the roof of the Philadelphia Center for Older People, two additional hi-vol sites were established. This resulted in a horizontal array of five hi-vols at nearly the same elevation (11 meters) above Broad Street. The three on the roof of the Health Building were on the west side of Broad Street at distances of approximately 9, 30, and 58 meters from the street. The hi-vols on the east side of Broad Street were approximately 9 and 34 meters from the street.

The hi-vol network was operated from 4 February to 20 February 1977 and from 7 June to 20 June 1977. These observations were supplemented

with APM and dichotomous sampler data from the trailer-top roof during the 2-week sampling period in February; at the end of this period, the dichotomous sampler was moved to the rooftop at 500 South Broad Street and operated for an additional 2-week period. Intensive street washing was carried out by the City of Philadelphia in the vicinity of the monitors on the 15th, 16th, and 17th of June 1977. At the end of the third day of street washing, the hi-vols at Broad and Spruce were operated on a 4-hour schedule. This 4-hour schedule continued until 2000 e.d.t. on the 19th.

Spatial Distribution of Particulates

At the Broad and Spruce Streets intersection, street-level emissions usually were quite uniformly mixed with height because of locally induced turbulence from buildings, exhaust heat and passing vehicles. Concentrations measured at a height of 11 meters on the tower averaged about 88 percent of those measured at the top of the trailer in February, and about 96 percent of those at the trailer in June. At an equivalent height on the roof of the building at 500 South Broad Street, concentrations averaged about 72 percent of those at the trailer during the February experiments.

Rooftop concentrations 9 meters downwind from Broad Street averaged about 15 percent higher than upwind concentrations during the February experiments. Any increase at the downwind distance of 34 meters fell within the measurement precision of the hi-vol. Variations in rooftop concentrations during the June experiments appeared to be dominated by nontraffic-related local sources, and the effect of reentrained street dust and vehicular emissions could not be isolated at either distance.

SELECTION OF AN EMISSION FACTOR FOR REENTRAINED DUST

Emission rates of particulates from roadways are typically expressed in mass per vehicle (or axle) per unit length of roadway. Although estimates of emission rates, based on limited observations, are available for a number of situations, emission rates and the size distribution of the emitted particles vary widely within any urban roadway network as a result of differences in a number of factors. Among the more important of these factors are: (1) amount, distribution, and physical properties of the roadway dust and dirt; (2) geometry and exposure of the roadway configuration; (3) vehicle mix and speed; and (4) meteorological conditions. However, the necessary quantitative relationships between emission rates and these factors were judged to be insufficiently well established to justify the major effort that would be required to prepare a detailed spatial emission inventory of roadway dust. Consequently, an average emission factor was employed. This average factor was selected on the basis of current estimates and test calculations in which calculated concentrations were compared

with the experimental measurements at Broad and Spruce Streets and with annual average concentrations allocated by source category at other sites within the monitoring network.

Some idea of the tremendous range in street dust emission rates can be gained from a Final Report Draft prepared by Midwest Research Institute.[3] In this report, the following relationship is proposed for the calculation of emission factors, and values of the independent variables judged to be appropriate for a number of roadway conditons are given:

$$e = KLs \qquad (1)$$

where e = emission factor (kg/veh/km)

K = proportionality constant (vehicle^{-1})

L = surface loading (kg/km)

s = silt content of the surface material (fraction)

To obtain an emission factor for use in our exploratory calculations, the following assumptions were made:

1. The particulates of concern have diameters $\leq$ 5 μm.

2. $K = 3.00 \times 10^{-5}$. This number was obtained by averaging the values for the 37th Street and Fairfax Trafficway sites given in Table 18 of the MRI Draft Report.

3. L = 165 kg/km. This is the weighted average found for commercial areas. (Table 1 of the MRI Draft Report.) Table 1 indicates that this loading should be increased by a factor of 4.1 for residential areas, and by a factor of 9.7 for industrial areas.

4. S = 0.085. Reported values of the silt content of surface dust from paved streets typically range from 5 to 15 percent.

Entering Equation (1) with the above values results in an emission factor (e) of 0.42 g/veh/km.

From the start of the program, it had been recognized that the Broad Street test site deviates greatly from the "ideal" site originally used in the development and validation of line source models. Further complications in modeling street-level particulate emissions in downtown areas arise from the difficulty of either measuring or reliably estimating background concentrations, and in assigning appropriate emission factors. For these reasons, it is not at all obvious that conventional modeling procedures can be of much use in evaluating street contributions and control strategies at this, or similar locations.

Such locations are, however, quite typical of downtown traffic-oriented sites which experience violations of the particulate standards.

To get some quantitative feel for the appropriateness of an emission factor of 0.42 g/veh/km near the test site, a number of exploratory calculations were carried out. The approach taken was to assume that the street contribution to concentrations measured at the tower is simply the difference between the tower concentrations and the rooftop concentration measured at 500 South Broad Street. It was further assumed that the street contribution came from both Broad and Spruce Streets and that emissions were directly proportional to traffic volume. Current information was judged to be insufficient to warrant making adjustments in the emission rates of either reentrained street dust or tailpipe particulate emissions according to vehicle speed or operating mode. The exploratory calculations at the Broad and Spruce Street intersection included the application of a Gaussian line source model and a box model first for a 24-hour period, and then for a 1-year period. The "cut-section" submodel of HIWAY was used to calculate the average annual impact of reentrained dust at rooftop level at 500 South Broad Street and at the Philadelphia Center for Older People. One example calculation is provided here; details of the remaining trial calculations are given in the final report.[1]

February 8, 1977, a day with westerly winds and the requisite hourly traffic and meteorological data, was chosen for the 24-hour exploratory calculations. The emission rate of 0.42 g/veh/km was used for reentrained dust and AP-42 emission factors of 0.21 and 0.12 g/veh/km were used respectively for tailpipe exhaust and tire wear. It was assumed that the source height of these emissions was 1.0 meters above street level and that σ_z was equal to 1.5 meters at the source. An adaptation of the HIWAY model (Intersection-Midblock model) was run for each hour of the day for four receptor heights on the tower and the results averaged over the 24-hour period. The solid curve in Figure 2 is the result. The rapid decrease in concentration with height is to be expected in view of the assumed vertical dimension at the source and the fact that no adjustment in stability class was made to account for additional turbulence induced by the building structures. Using Figure 2, a comparison can be made between the calculated amount of traffic-related particulates and the observed amount as indicated by the difference in concentration between the tower and the rooftop at 500 South Broad Street. This concentration difference, estimated to be 18 $\mu g/m^3$ over the height of the tower, is indicated in the figure by the dashed vertical line. An approximate agreement between calculated and observed flux of particulates by the tower is suggested by the close equivalence of the two shaded areas. However, the fact that concentrations at the top of the tower were substantially higher than those at the equivalent rooftop height indicate that the street contribution extended to even greater heights. This suggests that the true vehicle-related emission factor was somewhat greater than the assumed 0.75 g/veh/km (0.42 + 0.21 + 0.12).

It was concluded from the various calculations that 0.42 g/veh/km was an acceptable approximation for calculating rooftop concentrations in the commercial area, but that for trailer-top locations near major streets, this emission factor should probably be increased by a factor of 2 or 3. The next step was to introduce the emission factor of 0.42 g/veh/km for reentrained dust from paved roads into the Air Quality Display Model and calculate the contribution of major source categories to the annual mean concentration at each of the 13 monitoring sites. For this model run, the 1974 emission inventory was used with 1976 meteorological data.

MODEL ESTIMATES OF SOURCE CONTRIBUTIONS

In the more residential areas of the city free from local influences of major significance, the modeled sources accounted for 36 $\mu g/m^3$ of an annual arithmetic average of 62 $\mu g/m^3$, with 9 $\mu g/m^3$ coming from reentrained dust. The balance of 26 $\mu g/m^3$ was thus left to be attributed to background and uninventoried sources, a value which appears to be quite reasonable. On the other hand, if the emission factor for reentrained roadway dust were increased by a factor of 4, more in line with current estimates for residential areas, all of the observed concentration would be accounted for and nothing could be assigned to background and uninventoried sources.

Next, the model contributions to the arithmetic annual means were scaled to approximate geometric mean values at the various monitoring sites and used to prepare Figures 3 and 4. At 500 South Broad Street, as shown in Figure 3, the four modeled source categories contribute 45 $\mu g/m^3$ out of the observed 74 $\mu g/m^3$, leaving 29 $\mu g/m^3$ to be attributed to background and uninventoried sources. This is only slightly greater than the value estimated for the western edge of the city. The excess 43 $\mu g/m^3$ measured at Broad and Spruce is attributed to local low-level sources, principally reentrained street dust and other vehicular emissions.

In Figure 4, the model estimates of the four contributing source categories have been plotted cumulatively on top of an assumed background of 29 $\mu g/m^3$ at all 13 monitoring sites. The top of each calculated bar (dashed line) can be compared with the observed concentration (solid line), and the difference attributed to the local impact from reentrained dust, other vehicle-related emissions, and perhaps very local uninventoried sources. At Allegheny, the 82 $\mu g/m^3$ contribution calculated by the model from a grain loading facility approximately 300 meters from the monitor and with an estimated emission rate of 100 tons per year has been omitted from the point source estimate.

Figure 4 shows quite acceptable agreement between calculated concentrations and observed concentrations at ROX, BEL, N/E, 500, LAB, FRI DEF. The first three of these sites are exterior to the main urban area and uninfluenced by major street-level emissions. The next three sites

are centrally located, but the monitors are at rooftop level; and the last of the seven sites, DEF, is within the enclosed area at the Defense Supply Depot. Thus, the sites where large contributions appear to have been made from local traffic or other uninventoried sources are S/E, INT, AFS, NBR, ALL, and SBR. The magnitude of these contributions are given in Table 1.

Table 1. ESTIMATED IMPACT OF LOCAL TRAFFIC AND UNINVENTORIED SOURCES

Site	Concentration ($\mu g/m^3$)	Height above ground (m)	Nearby traffic		
			Street	Traffic count[a] (veh/day)	Distance from monitor (m)
S/E	17	1		Not applicable	
INT	35	4	Island Ave.	6,000 (1972)	11
			(No data since beginning of I-95 construction)		
AFS	16	9	Aramingo Ave.	18,500 (1976)	19
			Huntington Ave.	2,100 (1974)	10
NBR	32	4	North Broad St.	6,000 (1975)	7
			Butler St.	2,200 (1975)	6
			Germantown Ave.	6,400 (1975)	16
ALL	26	4	Allegheny Ave.	5,200 (1976)	18
SBR	43	4	South Broad St.	23,500 (1977)	9
			Spruce St.	7,400 (1977)	6

[a]Average daily traffic at INT; average weekday traffic at other locations.

The highest concentration listed in Table 1, 43 $\mu g/m^3$, was observed at SBR, the site with the greatest amount of local traffic. The second highest concentration, 35 $\mu g/m^3$, was observed at INT where the volume of traffic increased an unknown but substantial amount with the construction of I-95, and which is located in a part of the city characterized by numerous fugitive dust sources, including earth moving. The third highest concentration was at NBR, where most of the 32 $\mu g/m^3$ observed at this site can be attributed to street sources. The 26 $\mu g/m^3$ at ALL can be attributed to a combination of traffic on Allegheny Avenue, emissions from the nearby grain elevator and other fugitive dust emissions. Local traffic is insignificant at the S/E site and probably has a relatively small impact at AFS because of the height of the monitor. The 17 $\mu g/m^3$ and 16 $\mu g/m^3$ values at these two sites may well be a result of general fugitive and fugitive dust emissions in the area which have not been adequately taken into account in the emission inventory. It is quite likely that street loadings and

resulting fugitive dust emissions in the industrial and less developed areas of the city are substantially greater than those in the CBD and residential areas.

Figure 4 is an attempt to place in perspective the contributions of the major classes of particulates to the annual concentrations measured throughout the city. At downtown rooftop monitors outside of the principal industrial areas and at trailer-top monitors in outlying residential areas, observed concentrations are adequately explained by contributions from inventoried point and nonvehicle-related area sources, tailpipe and tire wear, and reentrained street dust emitted at a rate of 0.42 g/veh/km, plus a background concentration of 29 $\mu g/m^3$. Relatively small reductions in any or all of these sources could result in the achievement of the primary standard at these sites. On the other hand, at trailer-top monitors within either commercial or industrial areas, or at rooftop level in industrial areas, substantial additional reductions in emissions will be required to meet the primary standard. At several sites, these reductions must clearly come from vehicle-related sources. This is particularly true at the two Broad Street trailer sites where the estimated concentrations remaining after the elimination of all contributions from point and nonvehicle-related area sources are still in excess of the standard. It may also be true at the Allegheny and International Airport sites as well, but at these locations the impact of other fugitive dust and fugitive emissions needs further clarification.

In summary, an emission factor of 0.42 g/veh/km for reentrained dust from paved roadways was judged to be an appropriate average value for commercial and residential areas of Philadelphia. With this value, the Air Quality Display Model was used in conjunction with an emission inventory of traditional sources to estimate the contributions of various source categories to the particulate loading at rooftop monitors and at monitors removed from obvious local influences. Major deviations from these "rooftop" model estimates were attributed to local sources. In heavily industrialized areas, the emission rate from paved roadways should probably have been increased by a factor of 2 or 3. Emissions of the larger particles which affect trailer-top concentrations near major streets are not included in these emission factor estimates.

PARTICLE SIZES

The hi-vol and dichotomous sampler data obtained during this program makes possible a rough separation of collected mass into three particle size categories. The fine fraction of particles captured by the dichotomous sampler has an aerodynamic 50 percent cutoff of 3.5 μm, and is considered respirable, and the coarse fraction captured by the dichotomous sampler is composed of particles roughly 3.5 to 20 μm in diameter. The difference in mass between the total collected by the dichotomous sampler and the hi-vol can, therefore, be considered greater

than 20 μm. Table 2 presents a composite picture of the spatial distribution measured during February and March. Dichotomous sampler data at the two sites were acquired with one instrument, operated on an approximate every-other-day schedule for about 2 weeks on the roof of the trailer, and for a similar period on the roof at 500 South Broad Street.

Table 2. COMPARISON OF DICHOTOMOUS SAMPLER AND HI-VOL RESULTS

Location	Height (m)	Concentration ($\mu g/m^3$)			
		Dichotomous Sampler			
		Fine	Coarse	Total	Hi-Vol
Top of tower	11				130
Rooftop	11	30	13	43	95
Trailer top	4	34	23	57	149

At the rooftop (500 SB) the respirable fraction comprises 70 percent of the total measured by the dichotomous sampler; at the trailer top the respirable fraction is 60 percent of that total. Perhaps of greater interest, however, is a comparison of the concentration of respirable particulates with the concentration determined by the hi-vol. In this case, the respirable fraction represents 32 percent of the mass measured by the hi-vol at rooftop level and only 23 percent of that measured by the hi-vol at trailer top. Also, assuming a cut-off of 20 μm by the dichotomous sampler, approximately 55 percent of the particulate mass collected by the hi-vol at rooftop level was composed of particles of aerodynamic diameter greater than 20 μm. At the trailer-top location, this percentage increased to approximately 62 percent.

ELEMENTAL COMPOSITION OF PARTICULATES

Table 3 lists in decreasing order the six elements found to have the highest concentrations in the dichotomous samples, and the most probable major source of each. Tabulated concentrations are based on the totals found in the two size fractions. The bottom line was obtained from the total mass of particulates collected by the dichotomous sampler.

Of these six elements, sulfur had the highest concentration and, when expressed as SO_4, made up 19 and 25 percent, respectively, of the mass at the Broad and Spruce, and 500 South Broad locations. Eighty-seven percent of the sulfur was found in the fine fraction. There was

a reduction in sulfur concentration of only 2 percent with height, indicating thorough mixing and transport from nonlocal sources.

Table 3. AVERAGE CONCENTRATIONS OF SIX MOST COMMON ELEMENTS

Element	Major source	Concentration ($\mu g/m^3$)		Average percent fine	Percent reduction with height
		Broad and Spruce	500 South Broad		
Sulfur	Fuel combustion	3.65	3.58	87	2
Silicon	Crustal material	2.71	1.50	12	45
Calcium	Crustal material	1.15	1.08	14	6
Lead	Motor vehicles	1.36	0.86	85	37
Iron	Crustal material	1.22	0.63	24	48
Aluminum	Crustal material	0.87	0.56	8	36
TSP		56.4	42.8	64	24

Of the remaining five elements, all but lead are presumed to be primarily of mineral origin and are most abundant in the coarser fraction, with the percent fine ranging from 8 to 14 percent. Also, with the exception of calcium, their concentrations decrease substantially with height (from 36 to 48 percent), indicating strong contributions from local fugitive dust sources. The third most common element at Broad and Spruce, and the fourth most common at 500 South Broad Street, is lead. Lead, like sulfur, is found predominantly in the fine particulates, but unlike sulfur, shows a rapid decrease in concentration with height (37 percent), in agreement with the hypothesis that motor vehicles are its principal source.

EFFECT OF STREET FLUSHING ON AMBIENT PARTICULATE LEVELS

Over 100,000 gallons of water per day were applied on 3 consecutive days between the hours of 0700 and 1830 e.d.t. to streets in the vicinity of the Broad and Spruce Street monitoring site. This intensive street flushing not only failed to reduce 24-hour concentrations but appeared to increase concentrations dramatically immediately following the flushing operation. Concentrations at the monitoring site rose to levels which were roughly 100 $\mu g/m^3$ higher than would have been expected from observations at other locations within the city.

TSP concentrations preceding, during, and following the flushing experiment have been plotted in Figure 5. The Broad and Spruce curve shows the average concentration for the trailer and tower hi-vols; x's

indicate average 4-hour concentrations at this location. The 500 South Broad Street curve shows the average concentration measured at this nearby rooftop location. The third curve shows the average concentration measured at the two other sites in the city with approximate daily sampling.

The increase in local particulate concentrations following the street flushing may be explained by assuming that the vigorous, forced flushing, plus splashing by motor vehicles, redistributed particulates that had previously become concentrated adjacent to the curbs, and that many of these redistributed particulates became airborne as soon as the street became dry. This hypothesis is supported by a strong relationship between traffic volume and TSP concentrations during this period.

ACKNOWLEDGMENTS

We wish to express our appreciation to Mr. Robert K. Stevens of the Environmental Services Research Laboratory, U.S. EPA, Research Triangle Park, North Carolina for providing the dichotomous samplers and arranging for the analysis of the exposed filters. We also wish to thank members of the Philadelphia Air Management Services Laboratory and Sanitation Department for their cooperation during the program. Finally, we wish to express our thanks to all members of the GCA/Technology Division who worked on the program; especially to Mr. Victor Corbin, who carried out the computer modeling described in this paper.

This project has been funded at least in part with Federal funds from the Environmental Protection Agency under contract number 68-02-2345. The contents of this publication does not necessarily reflect the views or policies of the U.S. Environmental Protection Agency, nor does mention of trade names, commercial products, or organizations imply endorsement by the U.S. Government.

REFERENCES

1. Record, F. A. and R. M. Bradway. Philadelphia Particulate Study. GCA/Technology Division, Bedford, Mass. Final Report, EPA Contract No. 68-02-2345. June 1978. EPA-903/9-78-003. 135 pp. plus appendices.

2. GCA/Technology Division, Bedford, Mass. Emission Inventory and Sulfur Dioxide Alternatives for the Metropolitan Philadelphia Region. Final Report, EPA Contract No. 68-02-1376, Task Order No. 24. August 1977. EPA 903/9-77-030. 217 pp.

3. Midwest Research Institute. Quantification of Dust Entrainment from Paved Roadways. Draft Final Report, EPA Contract No. 68-02-1403, Task Order No. 25. March 4, 1977.

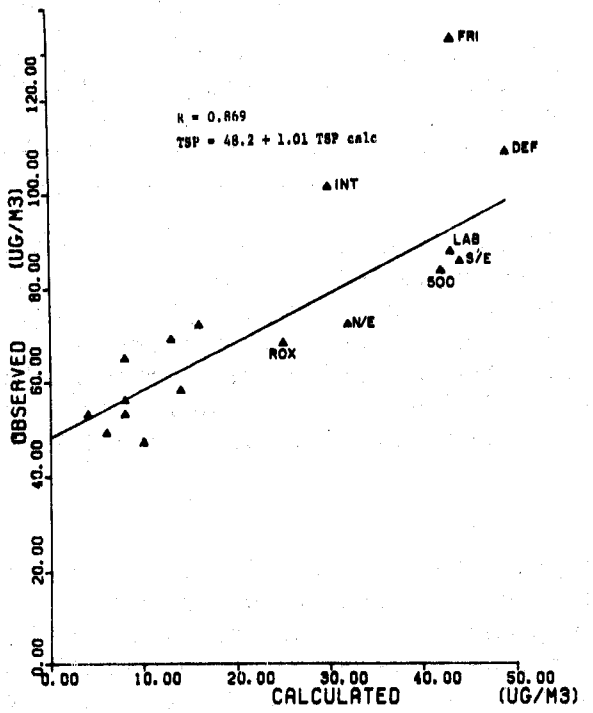

Figure 1. TSP calibration for the New Castle and Philadelphia monitors. Philadelphia monitors are indicated by their usual identifiers.

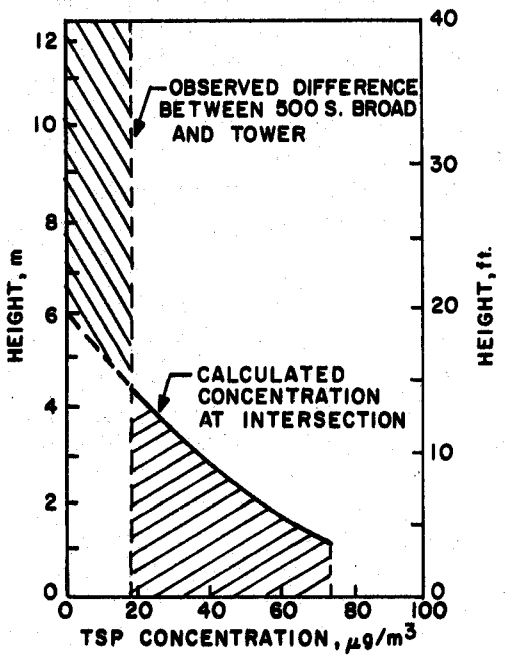

Figure 2. Comparison of calculated and observed vertical TSP profiles on 8 February 1977

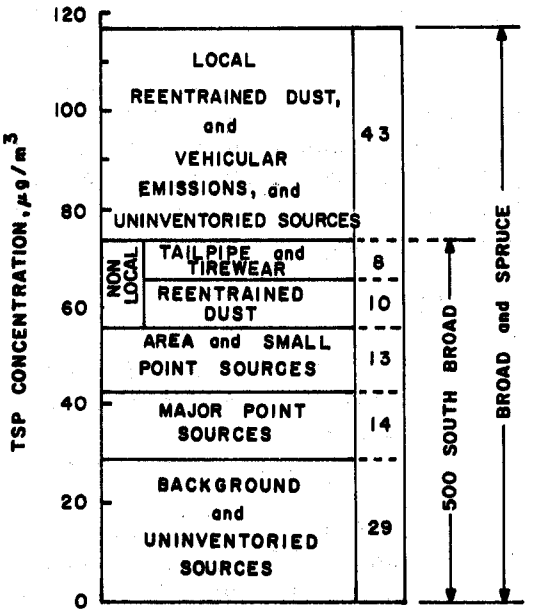

Figure 3. Source contributions to annual geometric means at the 500 South Broad, and Broad and Spruce Street sites in 1976

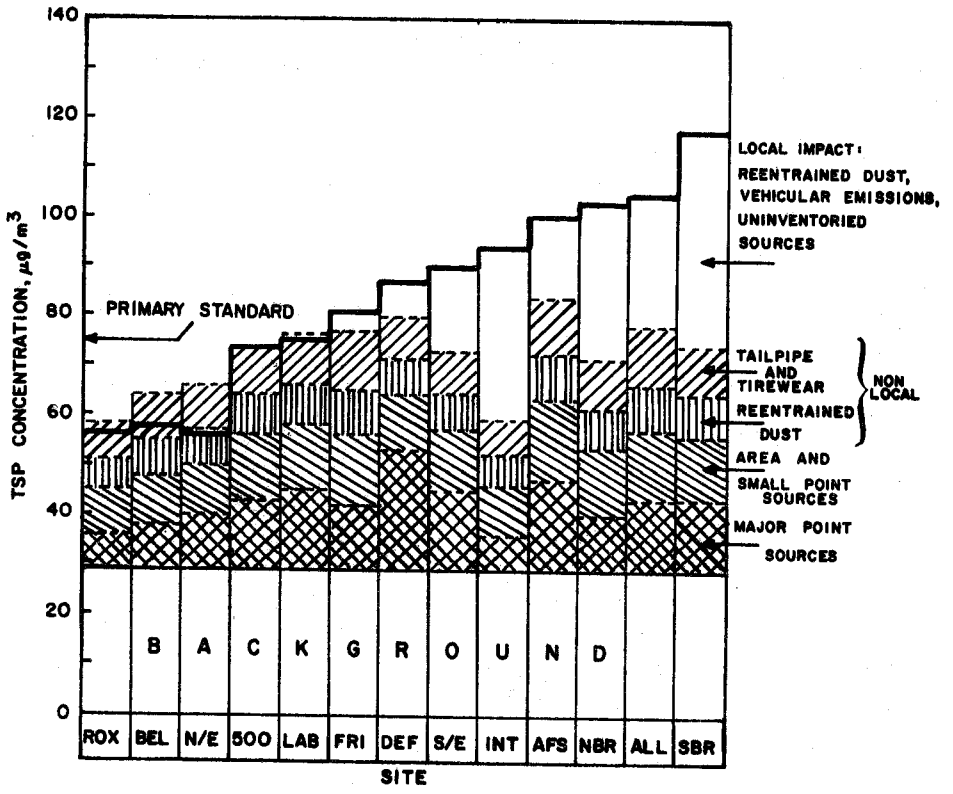

Figure 4. Allocation of TSP concentrations to source categories at 13 Philadelphia monitoring sites

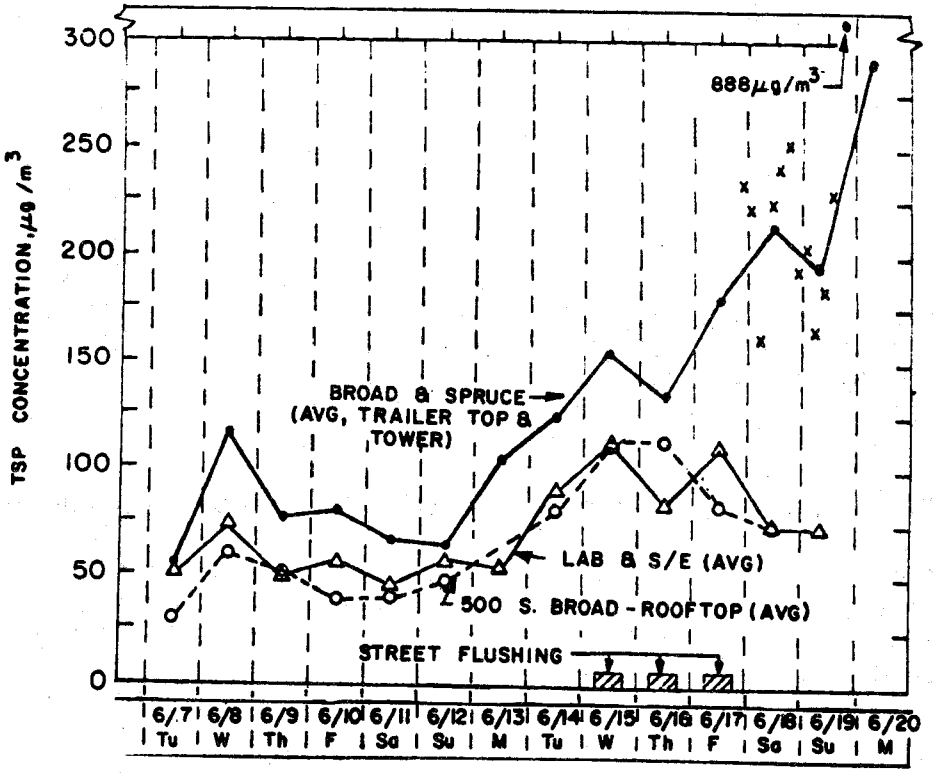

Figure 5. TSP concentrations for 7 June to 20 June field program.

DECISION-TREE ANALYSIS OF THE RELATIONSHIP BETWEEN TSP CONCENTRATIONS AND METEOROLOGY

John Trijonis
Technology Service Corporation
Route 3, Box 124-K
Santa Fe, New Mexico 87501

and

Yuji Horie
Technology Service Corporation
2811 Wilshire Boulevard
Santa Monica, California 90403

ABSTRACT

Decision-tree analysis, based on the AID computer program, is used to investigate the relationship between TSP concentrations and meteorology. The logic of AID is outlined and its application to TSP and meteorological data in EPA Region VI is described. The application uses 3 years of data for TSP and 18 meteorological variables at 25 locations in Arkansas, New Mexico, Oklahoma, and Texas.

The TSP-meteorology relationships determined by AID are discussed and are compared to results of multiple regression analyses. It is demonstrated that the AID results can be used to gain insight as to the types of sources that cause high ambient TSP levels at various locations. The use of AID results in normalizing historical TSP trends for meteorology is also discussed.

INTRODUCTION

This paper describes the results of a study, recently completed at

Technology Service Corporation, which involved statistical analyses of ambient total suspended particulate data and meteorological data in EPA Region VI[1]. The entire study included several types of analyses:

- Data quality checks (using three methods to identify potential outliers in the TSP data and three methods to validate those outliers)
- Analyses of cumulative frequency distributions of TSP data (using the exponential and lognormal distribution functions)
- Computation of summary statistics for TSP data (such as means, standard deviations, expected maximal values, etc.)
- Analyses of the TSP/meteorology relationship (using the AID decision tree program[2], regression methods, and nomogram techniques)
- Interpretation of the TSP/meteorology relationship (to identify source types causing high TSP concentrations)
- Time series analyses (involving both regression studies and normalization based on meteorological classes)

Because of space limitations, this paper will not discuss all aspects of the study. Rather, we will focus on the most novel and interesting parts of the project -- the application of decision-tree methods to analyze the relationship between TSP and meteorology, and use of the decision-tree results to identify sources causing high TSP levels and to normalize time series data for meteorology. Specifically, the remainder of this paper will be organized as follows:

1. General description of decision-tree analysis and the computer program AID (Automated Interactive Decision).
2. Application of the AID program to analyze the relationship between TSP and meteorology in EPA Region VI.
3. Use of the meteorological classes defined by AID to identify sources of high TSP levels.
4. Use of meteorological classes to normalize TSP time series for meteorology.

THE "AID" DECISION-TREE PROGRAM

In order to conduct a decision-tree analysis of the relationship between TSP and meteorology, we have chosen to use the AID computer program developed at the University of Michigan Institute for Social Research[2]. The AID program simulates the procedures of a good researcher

in searching for predictors that best account for the variations of a dependent variable. AID sequentially splits the data among prestated ranges in the independent variables, at each stage choosing the split that maximizes the variance explained in the dependent variable. The result is a decision-tree that accounts for the variance in the dependent variable (TSP) according to groups (meteorological classes) defined by ranges in the independent variables.

The data base for AID consists of a set of "n" measurements:

$A_1, \ldots, A_n$ for the dependent variable, and

$x_1, \ldots, x_n$; $y_1, \ldots, y_n$; $z_1, \ldots, z_n$; etc. for the independent variables.

Each of the independent variables is represented by discrete numbers, e.g. x might assume values of 1, 2, 3, or 4; y might assume values of 1, 2, 3, 4, 5, 6, or 7; z might assume values of 1, 2, 3, 4, or 5; etc. To achieve discreteness, the raw data for the independent variables are usually divided in ranges. For example, if the variable z represents wind speed (WS), one might define z = 1 if $0 \leq WS < 3$ mph; z = 2 if $3 \leq WS < 7$ mph; z = 3 if $7 \leq WS < 15$ mph; z = 4 if $15 \leq WS < 25$ mph; and z = 5 if 25 mph $\leq$ WS.

The first step of AID determines the independent variable that can be split into two groups (say z = 1 and 4 versus z = 2, 3, and 5) which maximize the residual sum of squares (RSS) explained in the dependent variable. If the two groups (G1 and G2) have group means $\overline{A1}$ and $\overline{A2}$, then the RSS explained by splitting the data is

$$\Delta RSS = RSS_0 - RSS_1 - RSS_2 , \tag{1}$$

where

$$RSS_0 = \sum_{j=1}^{n} (A_j - \overline{A})^2 = \text{RSS for entire data set} , \tag{2}$$

$$RSS_1 = \sum_{G1} (A_j - \overline{A1})^2 = \text{RSS for } G_1 , \tag{3}$$

and

$$RSS_2 = \sum_{G2} (A_j - \overline{A2})^2 = \text{RSS for } G_2 . \tag{4}$$

The program considers all possible partitions of the data among all the independent variables and selects the specific independent variable and specific partition that maximizes ΔRSS.

The partitioning process is repeated on each of the groups G_1 and G_2 to yield subgroups. These and all further subgroups are divided until either (1) no subgroup can be split to achieve a ΔRSS above a preset lower bound, (2) further division will produce a subgroup with number of elements less than a preset bound, or (3) the number of terminal sub-

groups reaches a prespecified limit. The specific termination criteria that we used in our applications were as follows: each step had to explain at least 1% of the original variance in the dependent variable; no groups were allowed with less than 3 elements; and no more than 10 terminal nodes were permitted.

APPLICATION OF "AID" TO TSP AND METEOROLOGICAL DATA

The AID program was applied to TSP and meteorological data for 25 locations in EPA Region VI. The study locations were chosen based on three criteria:

1. Each was a nonattainment site for the 24-hour and/or annual mean national standards for TSP.

2. Each site had fairly complete air quality data ($\sim$ 100-200 data points) for the three study years, 1973-1975.

3. The sites represented a variety of site characteristics (climate, geography, local site environment, etc.).

The 25 TSP study sites (Hi-Vol sampler locations) are illustrated as open dots in Figure 1.

For each study location, meteorological data were obtained from nearby weather stations. Figure 1 shows the location of the 10 surface weather sites (solid dots) and 6 upper-air weather sites (open triangles) that were used. The meteorological data were acquired from three types of tape provided by the National Climatic Center; surface data were from Surface Weather Tapes and Climatic Summary Tapes, while upper-air data were from Mixing Height Tapes.

Table 1 lists the 18 meteorological variables included in the analysis. Those marked with a double asterisk are significant variables in the decision-trees at many of the 25 study locations. Those with a single asterisk are significant at a few locations.

Figure 2 presents an example of a completed decision-tree for Forrest City, Arkansas. Each box in Figure 2 represents a group of data with "N" specifying the number of data points and "$\bar{Y}$" specifying the average TSP concentration in $\mu g/m^3$. The ten terminal nodes of the decision-tree are numbered in decreasing order of average TSP concentrations.

Averaged over the 25 study locations, the AID decision-trees explain 51% of the variance in TSP concentrations; this is equivalent to a correlation coefficient 0.71. AID decision-trees with a relaxed set of program termination criteria (allowing approximately 15 terminal nodes) explain 59% of the variance, averaged over the 25 sites. The

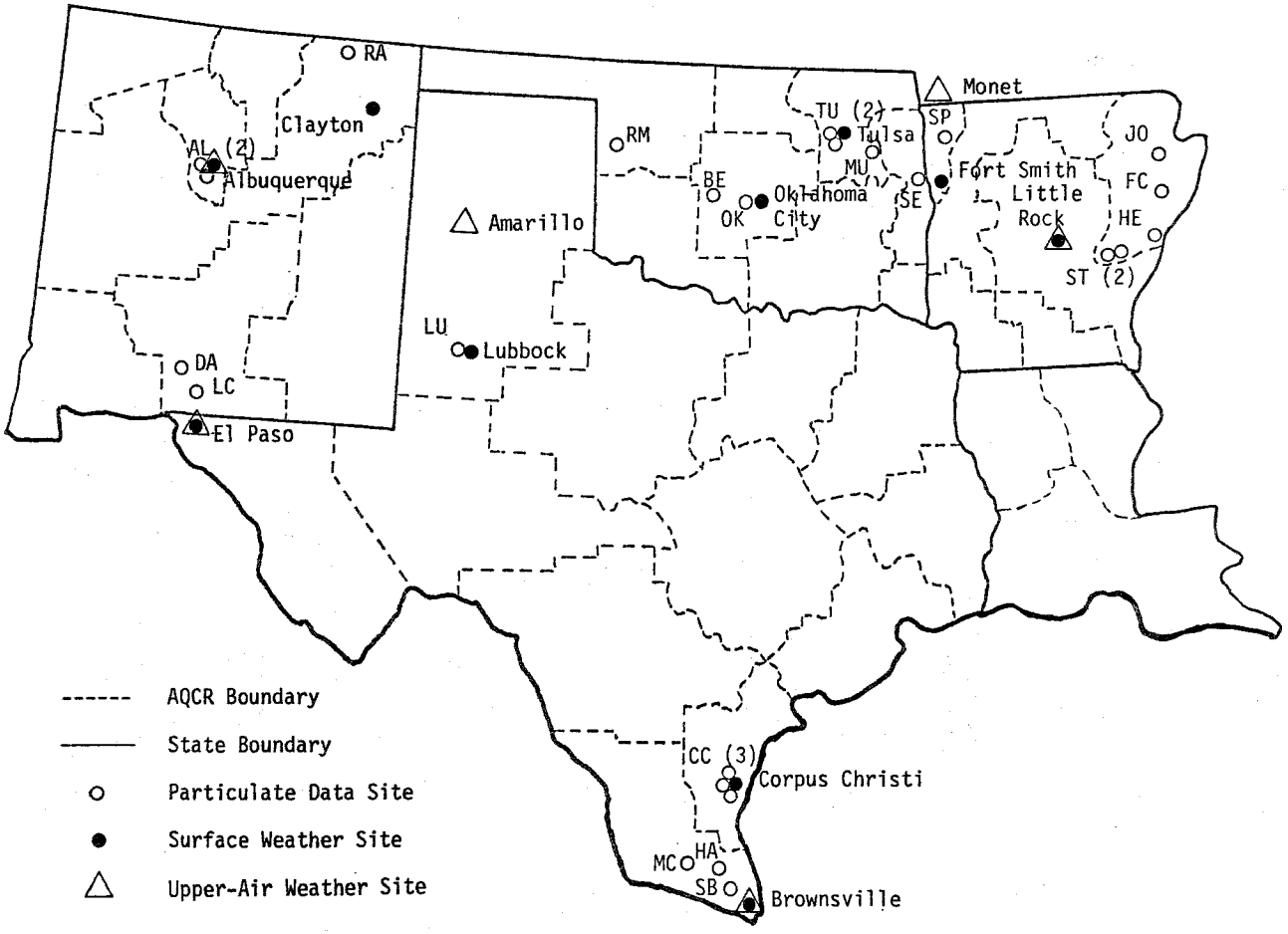

Figure 1. Map of study locations and weather data sites.

Table 1. EIGHTEEN METEOROLOGICAL VARIABLES USED IN THE REGION VI STUDY

WIND SPEED

AVWS - Average Daily Wind Speed**
WSMAX - Maximum Daily Wind Speed**
PMWLY - Afternoon Vertically Averaged Wind Speed**
AMWLY - Morning Vertically Averaged Wind Speed*

MIXING HEIGHTS

PMMH - Afternoon Mixing Height**
AMMH - Morning Mixing Height**

WIND DIRECTION

AVWD - Average Daily Wind Direction**
WV - Wind Variability**

PRECIPITATION

ND - Number of Days Since Last Precipitation**
PREC3 - 3-Day Total Precipitation**
PREC1 - 1-Day Total Precipitation*
NPREC - 1-Day Number of Precipitation Observations

TEMPERATURES

MXTMP - Maximum Temperature**
MNTMP - Minimum Temperature**

OTHERS

MON - Month of Year**
AVRH - Average Daily Relative Humidity**
AVVIS - Average Daytime Visibility*
NBLO - Number of Blowing Dust Observations

** Significant variable in decision-trees for many locations.

* Significant variable in decision-trees for a few locations.

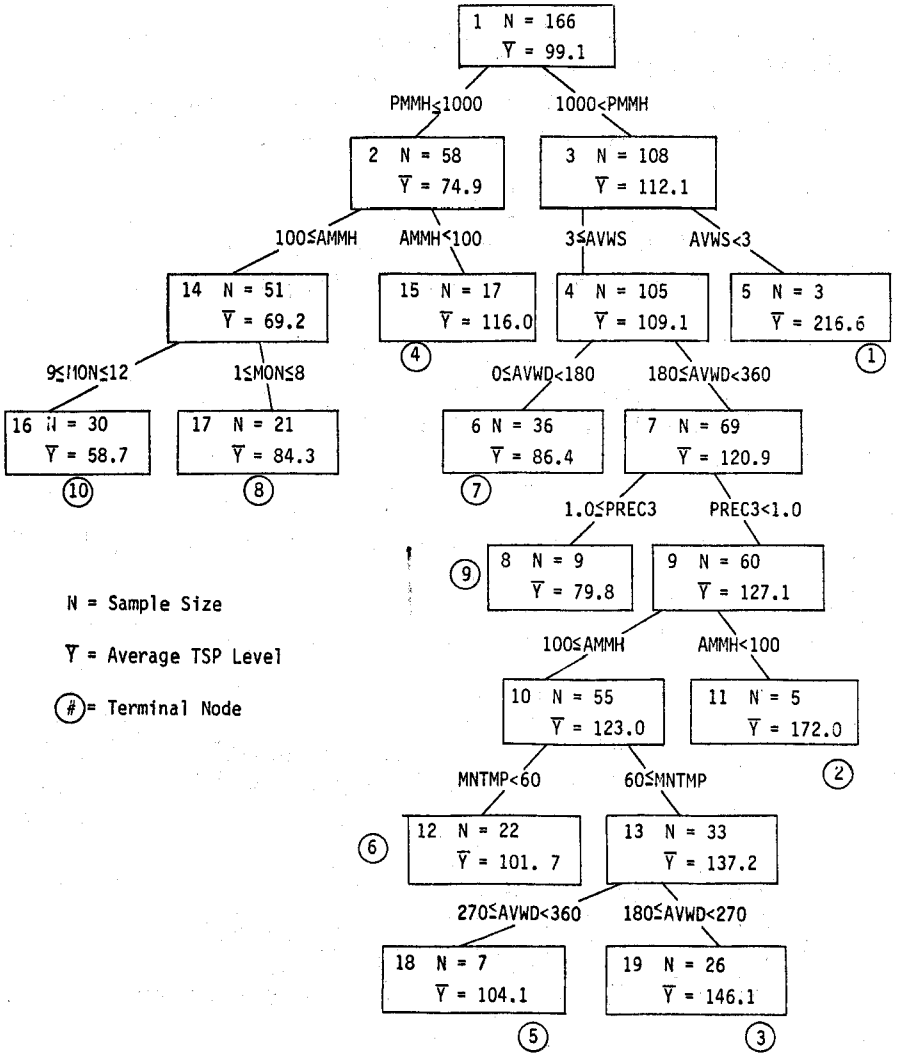

Figure 2. AID decision-tree for Forrest City, AR.

performance of AID is significantly better than multiple regression; multiple-linear and multiple-log-linear regressions (using all 18 meteorological variables) account for only 36% and 39% of the variance in TSP, respectively. The AID decision-trees also display several other advantages over regression, such as the following:

- The decision-tree method is based on a very general form of the least-squares principle which does not involve restrictive assumptions such as additivity and linearity.
- The meteorological classes defined by AID can be interpreted on physical grounds more easily than regression coefficients relating TSP to meteorology.
- The meteorological classes defined by AID are ideal for meteorological normalization of TSP trends (see later discussion).

IDENTIFICATION OF SOURCES CAUSING HIGH TSP LEVELS

One of the uses made of the AID decision-trees was to identify the types of sources causing high TSP concentrations. By interpreting the decision-trees, we attempted to identify three general types of sources: 1. wind blown dust (e.g. dust storms), 2. man-made dust sources*(e.g. dust from unpaved roads), and 3. conventional man-made sources (e.g. industrial stack emissions). The decision-trees were interpreted by searching for certain types of meteorology that were associated with high and low TSP concentrations. For example, wind-blown dust would be implicated if high TSP were associated with very high wind speeds, high mixing heights, and dry ground, and if low TSP were associated with the opposite conditions. An extensive discussion of how all 18 meteorological variables can be used to identify source types is contained in Reference 1.

By interpreting the decision-trees, we arrived at qualitative descriptions of the types of sources affecting each of the 25 locations. In almost all cases, the predominate sources appeared to be dust related -- usually man-made dust, but sometimes wind-blown dust.

In order to check this method of identifying source types, we were fortunate to obtain results from a very comprehensive study performed by the Texas Air Control Board (TACB).[3] The TACB study used several types of analysis to arrive at a detailed characterization of the sources affecting each of the 7 Texas locations included in our study. By comparing our results with the TACB report, we found that the accuracy of our qualitative descriptions of sources was generally fair to good.

*Actually, the distinction between "wind-blown" dust and "man-made" dust involves a misnomer becuase some of the wind-blown dust (such as that from agricultural fields, construction sites, and storage piles) is related to human activities.

Despite the reasonable level of success obtained (in the sense that the decision-tree method characterized the TSP/meteorology relationship well, that we were able to interpret the decision-trees as to types of sources affecting the sites, and that the results checked fairly well against the TACB study), we concluded that our method should not be used alone to classify TSP sites as to cause of nonattainment for the purpose of regulatory planning. The reasons for this negative recommendation are as follows:

- The results of interpreting the AID decision-trees (i.e. the TSP/meteorology relationship) are very qualitative. In some cases, the results are somewhat ambiguous in the sense that contributions from both wind-blown dust and man-made sources are apparent but there is little indication as to which predominates. There does not appear to be a reliable and accurate way of translating the results into quantitative statements concerning which sites would or would not exceed the TSP standards if wind-blown dust were discounted.

- Although the results of our study agree fairly well with the results of the comprehensive TACB study, the concurrence is by no means perfect. Greater reliability would be wanted if the results were to be used to support regulatory policy.

- The method used here is essentially directed at distinguishing wind-blown dust from man-made sources. A finer resolution of these source types could be desirable for planning purposes. In particular, it would be desirable to know what part of wind-blown dust represents regional dust storms (which can reasonably be considered uncontrollable) and what part represents more localized wind-blown dust from agricultural fields, storage piles, construction sites, etc. (which may be amenable to some control).

Although the above method is not adequate to support a detailed classification of sites for the purpose of regulatory decisions, we found that our results could support a simple 3-class categorization of sites with respect to contributions from wind-blown dust. This 3-class categorization of the sites is illustrated in Figure 3. Figure 3 demonstrates that there is a distinct geographical pattern in Region VI with respect to contributions from wind-blown dust. At Region VI locations in the Texas Panhandle or within approximately 150 miles of the Texas Panhandle, wind-blown dust tends to be a significant contributor, and often the dominant contributor, to high TSP concentrations. In Arkansas (and, based on climatology, probably Louisiana), wind-blown dust tends to be a minor, often insignificant, contributor to high TSP concentrations. At other Region VI locations, wind-blown dust may or may not be a significant source of high TSP levels.

The conclusions with respect to the geographical distribution of wind-blown dust contributions confirm the results of other investigators.

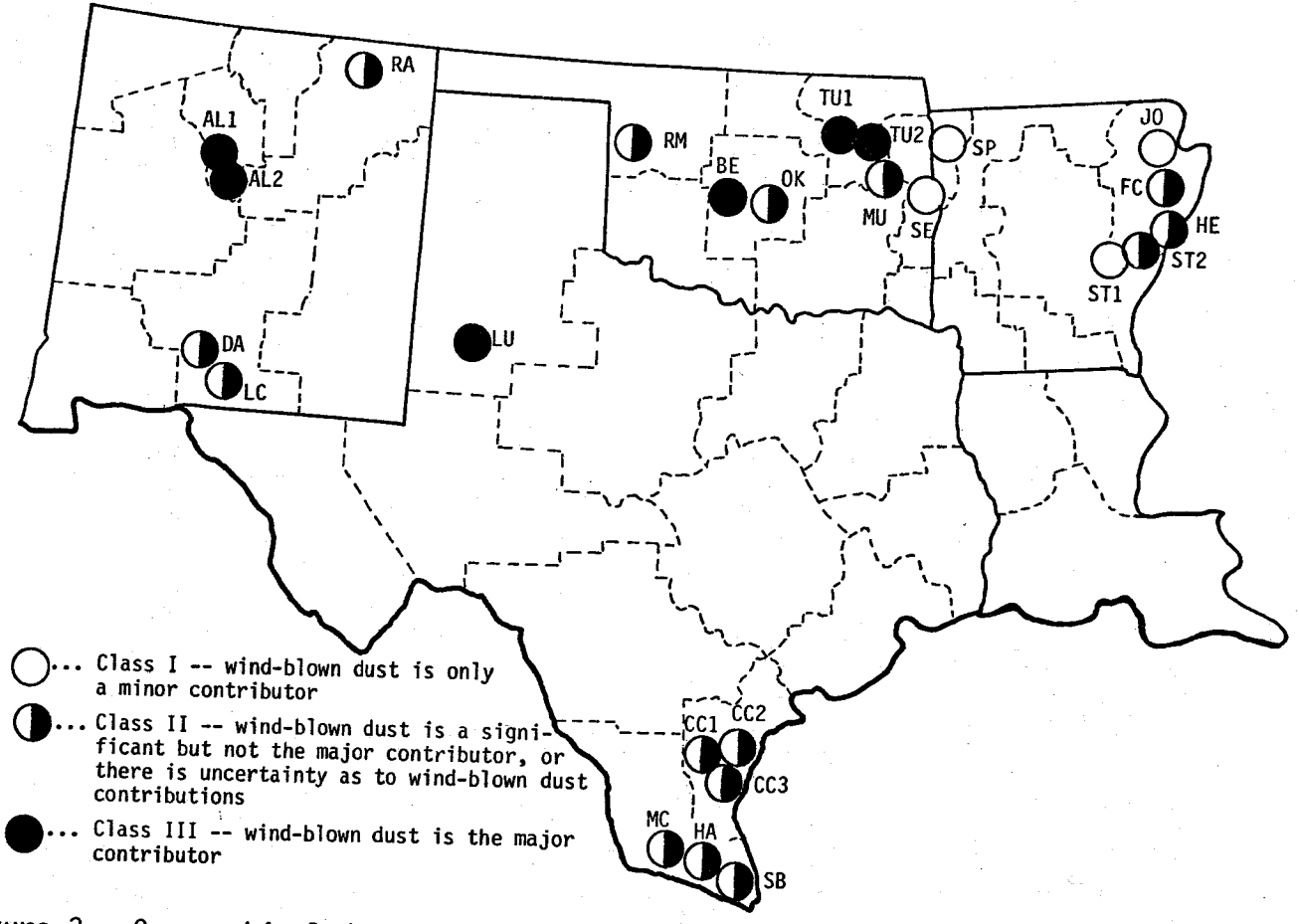

Figure 3. Geographical distribution of sites classified according to causes of high TSP levels.

By using airport observations of wind-blown dust, other investigators[4,5] have found that the Texas panhandle is the "hot-spot" for wind-blown dust in Region VI, while wind-blown dust is relatively rare in Arkansas and Louisiana.

METEOROLOGICAL ADJUSTMENT OF TSP TIME SERIES

Another use made of the decision-tree results was meteorological adjustment of TSP time series data. At each location, the 10 terminal groups in the decision-trees were combined to form meteorological classes (usually 5 classes, indexed by i = 1, ..., 5). The number of groups was reduced from 10 to 5 in order to increase the number of data points in each class.

Two methods were used to adjust the TSP time series for meteorology. The first was simply to stratify the data for meteorology, plotting the data separately for each class. The second involved computation of meteorologically normalized annual statistics using the method recommended by Zeldin and Meisel[6] in a recent guideline document prepared for EPA. For example, meteorologically normalized annual means were computed according to the following formula:

$$\overline{Y}_{NORM} = \sum_{i=1}^{5} \overline{Y}_i \, P_i, \qquad (5)$$

where $\overline{Y}_{NORM}$ = meteorologically adjusted annual mean for a given year,

Y_i = average value for TSP in meteorological class "i" during that year,

and P_i = frequency of occurrence of meteorological class "i" during <u>all</u> years.

Essentially, Equation (5) allows one to adjust the data each year so that all years have the same distribution of meteorology (i.e. the same distribution of days among meteorological classes).

Trial applications of the meteorological normalization procedure, i.e. Equation (5), to the study locations revealed that the method was not reliable using just 3 years of TSP data. The basic problem is that there are too few data points in just 3 years of data for an intermittently sampled pollutant such as TSP; becuase of the sparsity of data, biases (which affect the normalization procedure) can be introduced in determining the meteorological classes. We recommend that at least 5 years of TSP data be available before meteorological normalization of TSP time series is attempted.

CONCLUSIONS

Decision-tree analysis has proven to be a useful tool for investi-

gating the relationship between TSP concentrations and meteorology. Decision-tree analysis involves less restrictive assumptions and explains more variance in the data than conventional regression methods; the decision-trees are fairly easy to interpret as to physical meaning; and the decision-tree classes are well suited for meteorological adjustment of TSP data. The decision-tree method should be useful for other types of application as well -- in particular, it should be very useful for initial data exploration in cases (such as we faced) where there is a rather large number of independent variables and a relatively small number of data points.

ACKNOWLEDGEMENTS

The work described in this paper was supported by Contract No. 68-02-2828 from the Environmental Protection Agency. The authors gratefully acknowledge the many helpful comments received from Miguel Flores (Project Officer) and Frank Hall (Region VI Meteorologist) during the course of the project.

REFERENCES

1. Trijonis, J., Y. Horie, and D. Bicker. Statistical Analysis of TSP and Meteorological Data in EPA Region VI. Environmental Protection Agency, Region VI, Dallas, Texas. Prepared under Contract No. 68-02-2828. May 1978.

2. Sonquist, J.A., E.L. Bakerm and J.N. Morgan. Searching for Structure. Institute for Social Research. University of Michigan. 1973.

3. Price, J.H., J.P. Gise, H.E. Sievers, S.E. Ehlers, and B.K. Knape. Attainment Analysis, Volume I, Causes of Nonattainment. Texas Air Control Board. Austin, Texas. January 1977.

4. Orgill, M.M. and G.A. Sehmel. Frequency and Diurnal Variation of Dust Storms in the Contiguous U.S.A. Atmospheric Environment. 10: 88, 1976.

5. Hagen, L.J. and N.P. Woodruff. Air Pollution from Dust Storms in the Great Plains. Atmospheric Environment. 7:323, 1973.

6. Zeldin, M.D. and W.S. Meisel. Guideline Document on Use of Meteorological Data in Air Quality Trend Analysis. EPA Office of Air Quality Planning and Standards. Prepared under Contract No. 68-02-2318. November 1977.

DESIGNING A SYSTEMATIC REGIONAL PARTICULATE ANALYSIS

James A. Throgmorton and Kenneth Axetell, Jr.
PEDCo ENVIRONMENTAL, INC.
Kansas City, Missouri 64108
and
Thompson G. Pace
U.S. Environmental Protection Agency
Research Triangle Park, North Carolina 27711

ABSTRACT

A wide variety of techniques have been used to analyze and evaluate particulate air quality data. These techniques--generally classifiable as ones analyzing temporal patterns, analyzing spatial patterns, assessing the effect of meteorological variables, inventorying emissions and predicting concentrations, interpreting chemical and elemental data, and interpreting particle sizing data--can provide a higher degree of enlightment if they are synthesized into a systematic approach to the study of a particulate problem. This paper suggests a means of producing such a synthesis. A preliminary process of screening out ineffective or resource-excessive techniques is described, a sequence of applying the remaining techniques and resolving any conflicts that emerge is suggested, and a hypothetical example of how these processes would be applied is presented. The synthesis is designed to lead the research analyst to an identification of the major sources or source categories impacting upon NAAQS-violating sampling sites.

INTRODUCTION

As a part of a recent research effort, a large number of particulate data analysis techniques have been reviewed and compiled into digest format.[1] In that digest each technique is discussed in terms of its general applicability, resource requirements, and interrelationships with other techniques. That information is necessary in

order to permit the analyst to decide whether or not a certain technique applies to the problem he faces and whether or not he can afford to use it. However, more information is necessary for the analyst to integrate these techniques and synthesize the various findings that emerge. In this article, the analyst will be presented some guidance as to how to select, apply, and interpret the results of these techniques in light of the specific problem he faces.

SELECTING TECHNIQUES

Three general questions confront the analyst preparing to study a total suspended particulate (TSP) problem:

- What is the general nature of the particulate problem that needs to be investigated?
- What techniques can be used to define this problem better and then to resolve it?
- How much effort can be expended?

The general nature of the problem at hand can vary considerably. The analyst might be interested in learning how the chemical composition of the aerosol changes over space and time. He might want to define the lead emission rate from automobile exhaust in terms of g/VMT. He might want to develop a regional control strategy which will ensure the attainment and maintenance of TSP National Ambient Air Quality Standards (NAAQS) throughout a metropolitan area. Or he might want to investigate a host of other problems.

For the purposes of this paper, it will be assumed that the analyst is primarily interested in developing a regional TSP control strategy. This is not meant to denigrate the importance of the other types of problems he faces. Rather, it is simply to focus attention upon the type of problem which will probably be uppermost in the mind of the typical user of this article.

Once he has generally identified his problem, the analyst will need to define that problem as well as possible and to select those techniques which are most likely to help solve it. This initial decision as to which techniques to use can be aided by the early application of a simple screening procedure. This screening procedure consists of assessing the applicability and task-effectiveness of the various techniques, and then assessing their utility in terms of resource requirements and the sponsoring organization's resources.

The general applicability of each technique, as well as resource-related information which will be explained in the next few paragraphs, is summarized in Table 1. Each technique is ranked on a scale of 1 through 5 (where 5 indicates the greatest potential) for each of the

Table 1. SUMMARY OF TECHNIQUES

Technique (Section)	Task rankings: Characterize aerosol	Identify source categor.	Quantify specific src.imp.	Resource requirements: Manpower	Skill	Computer	Data	Cost-effectiveness: Characterize aerosol	Identify source categor.	Quantify specific src.imp.
Long term trends (2.1)	2	1	1	2	1	2	1	.3	.2	.2
Seasonal patterns (2.2)	2	1	1	2	1	2	1	.3	.2	.2
Daily patterns (2.3)	2	1	1	2	1	2	1	.3	.2	.2
Diurnal variation (2.4)	2	2	1	4	1	1	2	.3	.3	.1
Emission patterns (2.5)	1	2	2	4	1	1	2	.1	.3	.3
Site classification (3.1)	3	2	1	4	1	2	1	.4	.3	.1
Inter-site correlation (3.2)	4	1	1	2	2	2	1	.6	.1	.1
Pollution rose (3.3)	2	2	2	2	1	2	2	.3	.3	.3
Upwind/downwind (3.4)	2	1	3	2	1	2	2	.3	.2	.4
Correlation and regression (4.1)	1	2	1	6	3	3	2	.1	.1	.1
Decision-tree (4.2)	1	2	1	6	3	3	2	.1	.1	.1
Precipitation (4.3)	1	2	1	2	1	2	2	.1	.3	.1
Wind speed (4.4)	1	2	1	2	1	2	2	.1	.3	.1
Trajectory analysis (4.5)	2	2	1	6	3	3	2	.1	.1	.1
Emission inventory (5.1)	1	3	1	10	2	2	1	.1	.2	.1
Microinventory (5.2)	1	4	1	6	2	1	1	.1	.4	.1
Diffusion modeling (5.3)	4	4	5	4	4	3	1	.3	.3	.4
Temporal, spatial, and meteorological (6.1)	4	2	2	2	2	2	5	.4	.2	.2
Enrichment factor (6.2)	3	2	1	2	2	1	5	.3	.2	.1
Chemical element balance (6.3)	2	4	1	4	5	3	5	.1	.2	.1
Interspecies correlations (6.4)	4	2	1	4	3	2	5	.3	.1	.1
Pattern recognition (6.5)	4	3	1	4	4	3	5	.3	.2	.1
Factor analysis (6.6)	4	3	1	6	5	3	5	.2	.2	.1
Microscopy (6.7)	4	3	2	8	5	2	2	.2	.2	.1
Frequency distribution (7.1)	3 (4)	2	1 (3)	2 (4)	2 (3)	1 (3)	4	.3	.2 (.1)	.1 (.2)
Species-specific (7.2)	5	4	1	4	2	2	5	.4	.3	.1

general problem areas most pertinent to TSP control strategy development. As that table and Table 2 below indicate, different techniques are more effective at different tasks and none of the techniques is effective at all of the tasks.

Table 2. EFFECTIVENESS RANKINGS

Aerosol characterization	Source category identification	Specific source impact quantification
Species-specific size distribution	Diffusion modeling	Diffusion modeling
Inter-site correlation	Microinventorying	Upwind/downwind
Diffusion modeling	Chemical element balance	Emission patterns
Temporal, spatial, and meteorological variations of chemicals	Species-specific size distributions	Temporal, spatial and meteorological variations of chemicals
Interspecies correlations	Emission inventorying	Pollution rose
Pattern recognition	Factor analysis	Microscopy
Factor analysis	Pattern recognition	
Microscopy		

It should be noted that these rankings are necessarily somewhat subjective due to the fact that there are no absolute measures of the relative accuracy of these techniques. However, one can assess the accuracy of each technique in its own terms. For example, the true correlation among TSP measurements at different sites can be assigned confidence limits which are dependent upon the sample correlation and the number of samples. Likewise, the accuracy of microscopy results can be assessed by analyzing replicate samples. But there is no accepted way of comparing the results of one technique with those of another.

Once he has conducted this initial screening, the analyst will want to know whether or not he can afford to implement those techniques which he considers most promising. To answer this question he can use the information presented in Table 1.

Table 1 summarizes resource requirements in terms of skill,

computer, and data needs. It would be best to present these data in common units (e.g., dollars) so that the overall resource needs could be calculated in a direct manner. Unfortunately, there can be so much variation in the cost of applying any one technique that this is not really possible. A diffusion model run may, for example, cost anywhere from $20 to 1,000+ depending on the complexity of the model and the situation to which it is being applied. As a surrogate for dollar cost, skill, computer, and data requirements are rated at 1 through 5 (5 being most resource intensive). Due to the greater cost that is normally associated with manpower activities, that resource is given twice the weight of the other three and is rated at 1 through 10. It has been assumed that the cumulative resources required to apply a given technique are represented by the sum of four individual resource areas (e.g., the combined resource requirement for the chemical element balance technique is 17).

The analyst must inventory his organization's resources to determine whether or not they are sufficient to apply the set of analytical techniques which he previously identified as being most promising. Those techniques which exceed his agency's resources must be excluded, unless the analyst is able to obtain financial or in-kind assistance from another organization.

In addition to excluding resource-excessive techniques, the analyst must also exclude techniques which are dependent upon those excluded techniques. Diffusion modeling is, for example, dependent upon emission inventorying. If an organization cannot afford to conduct an inventory, then it will not be able to apply a diffusion model.

The analyst will also be concerned about getting the most for his money. Thus, he will be concerned about cost-effectiveness as well as cost or effectiveness alone. By dividing individual task rankings by combined resource requirements, a general assessment of each technique's cost-effectiveness can be derived. The chemical element balance technique, for example, has been assigned task rankings of 2, 4, and 1 for aerosol characterization, source category identification, and source impact quantification, respectively, and a combined resource requirement of 17. This results in cost-effectiveness ratings of 0.1, 0.2, and 0.1. As shown in Table 1, the techniques listed in Table 3 below are assessed as being most cost-effective:

Table 3. COST-EFFECTIVENESS RANKINGS

Aerosol characterization	Source category identification	Specific source impact quantification
Inter-site correlation	Microinventory	Upwind/downwind
Species-specific size distributions	Species-specific size distributions	Diffusion modeling
Site classification	Precipitation	Pollution rose
	Wind speed	Emission patterns
	Pollution rose	
	Emission patterns	

At this point, the analyst will be left with a general set of cost-effective techniques that can provide answers to his specific questions without imposing excessive strain on his organization's resources. He will now want to apply those techniques to the specific problem at hand.

APPLYING TECHNIQUES AND INTERPRETING RESULTS

Two more specific questions confront the analyst at this point:

- In what sequence should the available techniques be applied?
- How should conflicting results be handled?

In line with the reasoning previously presented, it is recommended that the available techniques first be used to define the existing problem as explicitly as possible. The resulting definition should be in terms of the regional/local, short-term/long term, improving/worsening/no change nature of the problem and should be discussed in terms of statistical significance.

Whether or not the problem is long-term and/or short-term should be assessed for each site and described in terms of probability. Hence, the analyst should calculate the probability that the primary annual NAAQS (75 ug/m^3) is exceeded for the entire year and the number of days that the secondary 24-h standard (150 ug/m^3) would be expected to be exceeded during the entire year.

The analyst should then assess whether or not the problem is region-wide or local. This can be accomplished by plotting the

measured concentrations geographically, by determining inter-site correlations, by applying a diffusion model, by classifying sites by type of environment, and/or by applying other less cost-effective techniques listed in Table 1. Correlations should be qualified by also determining their true confidence limits.

Thirdly, the trend of past data should be determined. The analyst should determine whether or not there has been a statistically significant trend in annual averages.

At this point, the analyst should have a pretty good definition of the specific problem he faces. For example, he should be able to say that there is a region-wide primary annual NAAQS problem which is worsening or a local short-term secondary 24-h NAAQS problem which is remaining generally stable. And he should be able to attach statistical significance to his definition. However, it may well be that there are not enough sampling sites in the region or number of samples at each site to do so. In this case, the analyst would conclude that he cannot define his problem clearly. If this occurs, he must weigh the consequences of developing a TSP control strategy with an inadequate problem definition vs the consequences of delaying major control strategy implementation while he conducts a special study which has been designed to fill the gaps in available data.

Once he has defined the problem to his satisfaction, the analyst should determine whether that problem is primarily caused by a clearly identifiable source. To do so, he can compare the temporal patterns of the TSP data with the activity patterns of a suspected source, perform upwind/downwind analyses, apply a diffusion model, calculate a pollution rose, or--if agency resources are sufficient--calculate interspecies correlations, analyze filters microscopically, perform factor and cluster analyses, apply the chemical element balance technique, and/or evaluate the source contributions indicated by the previously applied diffusion model. If there is a major source significantly responsible for measured concentrations, each of these techniques should point out that source.

In some cases, however, results will conflict. When this occurs, the analyst should evaluate the techniques in terms of the statistical significance of their results. Of the techniques identified above, only the microscopy and chemical element balance technique cannot be assessed in terms of confidence limits about the mean. If, for example, the pollution rose fails to indicate a source identified by all of the other techniques, a statistical analysis may reveal that the shape of the rose may not identify that source simply because of the small number of samples upon which each directional mean is based. If the results of the various techniques are each statistically significant but still conflict, then the analyst should see if a clear majority of the techniques indicate one source. If that is the case, he should accept the results as sufficient evidence of that source's role.

If there is no clear majority, he should attach more weight to the techniques ranked highest in task effectiveness (see Table 1).

If no single source can be clearly identified, the analyst should attempt to identify the source categories which have the greatest effect upon TSP concentrations. Where the first stage of the study indicated a localized problem, a microinventory should be performed in the vicinity of the violating sampler. Where the problem was regional in nature or where additional evidence in support of the microinventory is desired, it is suggested that species-specific size distributions (if available), the effects of precipitation and wind speed, and the results of pollution rose and emission pattern calculations should be analyzed. Where resources are sufficient, other techniques can be applied as well.

If no source category is shown to be the primary cause of violations, then a special study which takes the techniques listed in Table 1 and the resources of the agency into consideration should be initiated.

The analyst may also consider applying some of the other meteorology-related techniques listed in Table 1. Specifically, stepwise multiple linear regression or the AID decision-tree technique can be used to determine the percent of variance in TSP concentrations that can be explained by meteorological variables. These techniques can be especially useful when the problem has been defined as being short-term.

In some cases, the analyst will conclude that he has not defined the problem clearly, found a culpable source or source category, or found that meteorological conditions are having an effect. In these cases, he whould determine the reasons for this inability and initiate their correction if at all possible.

EXAMPLE APPLICATION: LARGE CITY/COMPLEX AEROSOL

This example is a Southeastern United States bistate metropolitan area of approximately 700,000 people located along a major river valley characterized by gently rolling hills. The climate is rather moist with an annual average rainfall of 43 inches. Most roads in the city are paved, but there is a large aggregation of chemical and power generation industrial facilities in the area. Overall, there are more than 100 point sources which emit 25 ton/year or more in the area. Growth in population is expected to average around 2 percent per year, and a large industrial park is planned for an area to the southwest of the city.

There are three governmental agencies responsible for air pollution control activities in the metropolitan area: a 37-man local agency, a 91-man state agency with heavy responsibilities in other portions of its state, and a 104-man state agency. Given their sizes,

these agencies are staffed with a broad range of skills and expertise. All three agencies have ready access to computers required for sophisticated analyses. The data base for the area consists primarily of the following:

- Eighteen high volume sampler sites, most of which have more than five years of standard TSP data
- Meteorological data for at least three sites
- An emission inventory which has been updated annually
- Particle sizing data from a number of sites covering periods of six weeks each; monthly composites for sulfates, nitrates, and 13 metals at most sites, available from 1971 on; microscopy capabilities are also readily available

The three agencies seek to define their TSP problem clearly, to identify major contributing source categories, and to quantify the impact of specific sources. Hence, it is assumed that they would be generally interested in applying all the techniques discussed in this article. As indicated previously, though,these agencies do not have sufficient resources to apply every available technique without access to outside resources. For the purpose of this discussion, it will be assumed that manpower resources are not exceeded due to the relatively large staff sizes of the three agencies. It will also be assumed that data resources are exceeded by those techniques rated 4 or higher unless it has been explicitly noted that the agency has the resources necessary to implement that specific technique. Techniques which are cost-ineffective may also be excluded if the analyst so desires. For illustration purposes, it is assumed that cost-ineffective techniques are defined as those which are rated no higher than 0.2 for any one task area (see Table 1) and which are rated at less than 0.2 for the other two areas.

These reasonably available techniques resulting from this screening process are identified in Figure 1. Twenty-two techniques survived this screening process. Table 4 suggests how these techniques could be applied to the example city and suggests some qualifications that would probably be applicable to the specific situation described for this example city.

Creating a hypothetical situation, let it be assumed that the following conditions are found after applying the techniques identified in Table 4:

- TSP concentrations from the 18 available sites are analyzed. Five of them are found to exceed the primary annual and secondary 24-h NAAQS. For two of these sites, there is a reasonably good probability that the annual standard is

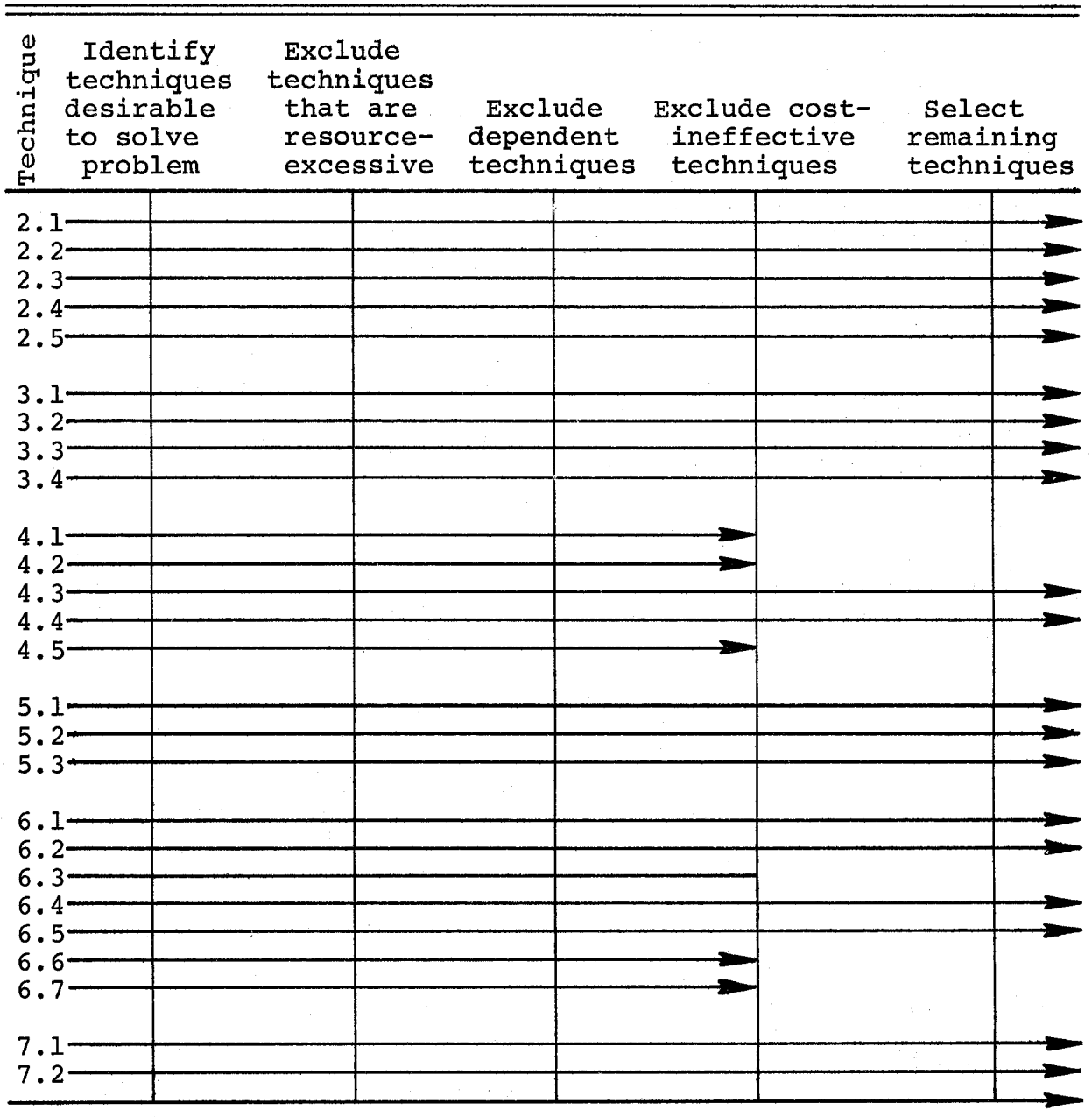

Figure 1. Screening techniques for example city.

Table 4. APPLYING TECHNIQUES TO EXAMPLE CITY

Task	Applicable technique	Comments
Assess regionality	3.1	May be useful due to river valley conditions
	3.2	None
	5.3	Relatively large number of sampling sites will permit tight calibration assessment
Determine direction of past data	2.1	Large time period will permit good assessment
Determine whether a specific source is clearly culpable	2.5	Dependent upon analysis of temporal TSP patterns and some measure of emission patterns
	3.3	Wind direction data may not be representative
	3.4	Wind direction data may not be representative
	5.3	As above
	6.4	Limited number of samples increase confidence limits
	6.5	Broad confidence limits; monthly composite data may create difficulties
	6.6	Same as for 6.5 above
	7.2	Limited number of samples increase confidence limits
Determine whether a source category is culpable	2.5	Same as above
	3.3	Same as above
	4.3	None
	4.4	None
	5.2	None
Investigate meteorological effects	4.3	Same as above
	4.4	Same as above

not really being exceeded. Two violating sites are in the industrialized western side of the metropolitan area, one is in the central business district, one is in a suburban commercial/residential area, and the fifth is in a newly suburbanizing area near a large cement factory.

- Classifying sites by environment does not produce meaningful results.

- Of the five sites which are exceeding the primary annual NAAQS, two in the industrial area correlate very well together (based upon >50 samples). Correlations among the other sites are $\leq$+0.50.

- An AQDM run for the current year predicts TSP concentrations well and correlates with observed concentrations at +0.72, based upon 18 sites. This implies a true r of +0.35 to +0.87 and is considered to be good. NAAQS violations are predicted at all violating sites except for the suburban commercial/residential one.

- All violating sites showed a steady long-term trend toward improved TSP levels until 1976 when a slight increase was noted.

- Another of the violating sites, located downtown, shows a strong TSP vs daily traffic correlation (+0.87). No other significant emission vs air quality patterns are revealed.

- Pollution roses for the two industrial area sites point in the general direction of those industrial facilities, but no other significant relationships are seen.

- One of the violating sites, in a semiurban, largely unpaved area, shows higher concentrations than surrounding upwind sites. Other relationships are not significant.

- Diffusion modeling indicates that area sources are the largest contributor to violating sites, but that point source impact is greatest in the western industrial area.

- Certain species are shown to covary strongly with TSP at various violating sites but there is a strong probability that the correlation is still zero due to the small number of samples. The downtown site varies with lead, the industrial sites with vanadium, and a fourth site (located near a cement factory) varies strongly with calcium. No other sites show high correlations.

- Limited particle size/chemical data reveal no meaningful relationships.

- Concentrations at the downtown and suburban site vary strongly with days since rainfall, but not with wind speed. The relationship is much weaker at the site near the cement factory.

- Microinventories of those three sites show that there are large amounts of fugitive dust emitted near the downtown and suburban sites, but no such results are shown for the cement plant site.

Based upon these data, the analyst arrives at the following conclusions.

- Identifiable industrial sources are the primary causes of NAAQS violations at the two western sites. Evidence: Good correlation between those two sites; The Air Quality Display Model (AQDM) predicts violations and identifies those industrial facilities as major contributors; pollution roses for those two sites point toward the industrial facilities; TSP concentrations at those two sites apparently vary most strongly with vanadium.

- Fugitive dust sources (primarily unpaved areas and reentrained dust from paved roads) are the most probable causes of violations at the downtown and suburban commercial/residential sites. Supporting Evidence: AQDM predicts violations at the downtown site; the downtown site varies strongly with daily traffic; TSP concentrations at the suburban site are relatively high when compared with surrounding upwind sites; AQDM identifies reentrained dust and unpaved roads as the major contributing source categories to those two respective sites; the downtown site varies most strongly with lead; TSP levels at these two sites vary strongly with days since precipitation; and microinventories of the two sites reveal large emissions from fugitive dust sources. Conflicting Evidence: AQDM does not predict violations at the suburban site. This conflicting evidence is outweighed by the evidence produced by the other techniques.

- The cement factory may be the primary cause of violations at the newly suburbanizing site but the results are certainly not conclusive. Evidence: AQDM predicts NAAQS violations; TSP concentrations vary strongly with calcium. The analyst concludes that the data are insufficient and that a special study is warranted.

ACKNOWLEDGEMENTS

Many of the ideas expressed in this article are a direct outgrowth of the authors' participation in a research effort and workshop sponsored by U.S. Environmental Protection Agency.

REFERENCES

Digest of Ambient Particulate Analysis and Assessment Methods (Draft). PEDCo Environmental, Inc. Prepared for U.S. Environmental Protection Agency, Research Triangle Park, North Carolina. July 1978.

IMPORTANCE OF PARTICLE SIZE DISTRIBUTION

L. E. Sparks
Particulate Technology Branch
Industrial Environmental Research Laboratory
U. S. Environmental Protection Agency
Research Triangle Park, N. C.

ABSTRACT

The need to consider the particle size distribution in all phases of particulate control technology development is discussed. Errors caused by characterizing an aerosol by the mass mean diameter (or any other mean diameter) are discussed. Theoretical calculations are used to show the effect of changes in size distribution parameters on particulate control equipment and plume opacity. Similar calculations show that much, if not all, of the so-called non-ideal data for particle collection is caused by failure to consider the particle size distribution.

INTRODUCTION

Most people recognize the importance of particle size in aerosol studies. In fact for many air pollution related studies the particle diameter is the most important physical property of a single particle. The particle's light scattering properties, its collectibility in particulate control equipment, some of its health effects, and even the method used to measure its diameter all depend on the particle diameter. As a result there is a large body of literature which describes the behavior of a single particle in many situations as a function of its diameter.

If real life aerosols were composed of monodisperse particles, theories, data, and general experience based on single particle concepts could easily be applied. And, in fact, many attempts have been made to apply monodisperse concepts to real aerosol problems; generally without success.

The fact is real aerosols are composed of polydisperse particles. And the distribution of particle diameters or the particle size distribution is the most important physical property of a real aerosol--whether it be a laboratory aerosol or an air pollution particulate emission. The light scattering properties, collectibility in particulate control equipment, etc. of an aerosol all are strong functions of the particle size distribution.

Failure to properly account for the particle size distribution, or to think in terms of a polydisperse aerosol, has resulted in considerable confusion in many areas of aerosol research as will be discussed later. Attempts to account for the effects of the size distribution by using an average particle diameter (usually the mass mean diameter) are inadequate and add to the confusion. There are an infinite number of particle size distributions with the same mass mean diameter. But that's all they have in common. As will be shown in this paper, use of an average diameter to predict the behavior of a polydisperse aerosol will result in large errors.

The purpose of this paper is to demonstrate the importance of particle size distribution by looking at examples from three areas important to air pollution control: effects of particle size distribution on plume opacity, effects of particle size distribution on electrostatic precipitators, and effects of particle size distribution on scrubbers.

OPACITY

It has long been known that the opacity of a plume is somehow related to the particulate matter contained in the plume. Air pollution control regulations often contain limitations on both mass emission and plume opacity. The assumption is often made that if a given plant in a specific industry can meet both the mass emission and plume opacity limitations, all similar plants can also comply with both limitations. Unfortunately, this may not be the case because of differences in particle size distribution emitted by various plants.

Ensor[1] has shown that the opacity of an aerosol can be estimated by

$$O = \exp [- WL/K\rho) \qquad (1)$$

where O = opacity, fraction
W = mass concentration of particulate, g/m^3
L = optical path length, μm
K = light scattering parameter, cm^3/m^2
ρ = particle density, g/cm^3

The parameter K is given by

$$K = \frac{4/3 \int_0^\infty r^3 \, (f)dr}{\int_0^\infty r^2 \, Q_{ext} \, (\alpha,m) \, f(r) \, dr} \qquad (2)$$

where
- r = the particle radius
- $Q_{ext}(\alpha,m)$ = light extinction efficiency factor
- α = size parameter = $2 \ r/$
- λ = wavelength of light
- m = refractive index of particle relative to air
- $f(r)$ = particle fractional frequency distribution $[\int_0^\infty f(r)dr = 1]$

Equations (1) and (2) have been solved for the case of a log-normal size distribution for the following conditions

- $W = 0.02$ g/m^3
- $L = 10$ m
- $\rho = 2.4$ g/cm^3
- $m = 1.33$
- $\lambda = 550$ nm
- d_g (geometric mass mean diameter) = 0.8 μm
- σ_g (geometric standard deviation) = 1.0 to 5.0

The results of this calculation are shown in Figure 1. Note the strong dependence of opacity on the geometric standard deviation.

The results shown in Figure 1 offer a qualitative explanation for the observation that the plume opacity for a given mass loading, particle density, and optical path length can vary from plant to plant depending on the particle size distribution of the emissions.

The strong influence of the geometric standard deviation on the behavior of a polydisperse system will be demonstrated for electrostatic precipitators and scrubbers.

ELECTROSTATIC PRECIPITATION

The penetration of a monodisperse aerosol through an electrostatic precipitator (ESP) is given by the Deutch-Anderson equation

$$Pt(d) = \exp - [\, w(d) \, Ap/V] \text{ or} \qquad (3)$$
$$Pt(d) = \exp - [\, w(d) \, Ap/(A_c \, v_g)]$$

where $Pt(d)$ = penetration of particles with diameter d
$w(d)$ = electrical migration velocity of particles with diameter d

EFFECT OF GEOMETRIC STANDARD DEVIATION ON OPACITY FOR CONSTANT MASS CONCENTRATION AND MASS MEAN DIAMETER

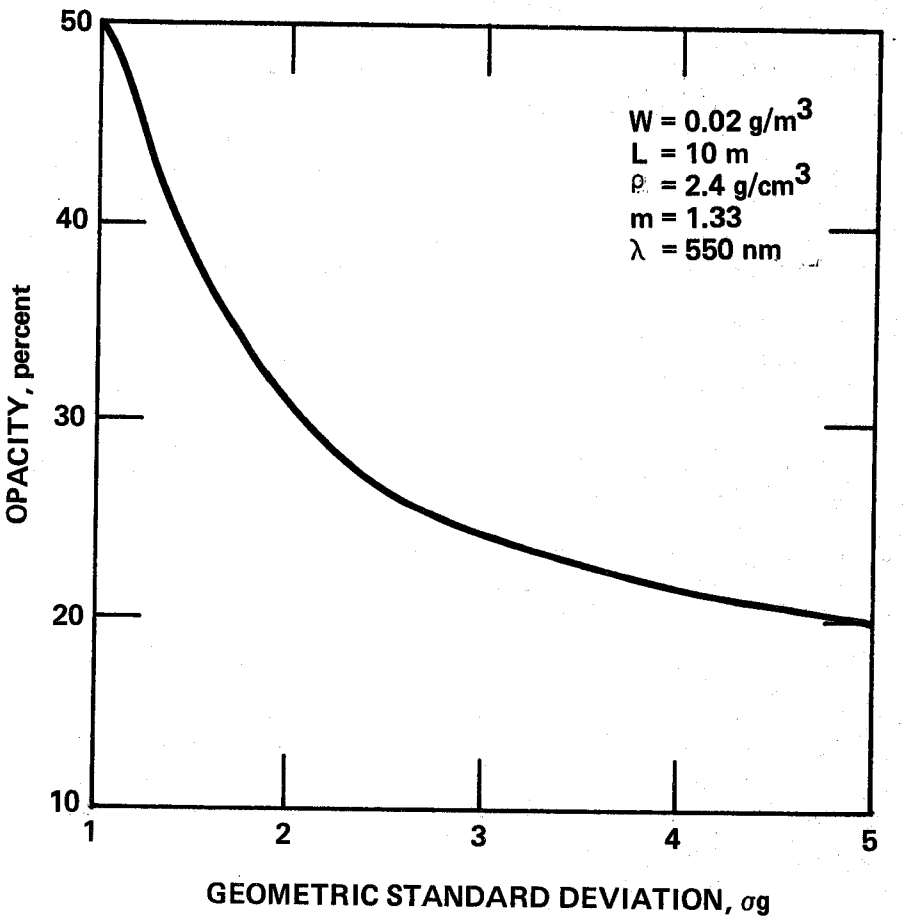

Figure 1. Effect of geometric standard deviation on opacity for constant mass concentration and mass mean diameter.

Ap = collector plate area
V = volumetric gas flow rate = A_c v_g
v_g = gas velocity
A_c = cross sectional area

(The ratio AV is called the specific collector area (SCA).

The Deutsch-Anderson equation as originally derived describes the behavior of a monodisperse aerosol in an electrostatic precipitator. For this condition, the parameter w(d) is the terminal velocity of a charged dust particle under the influence of an electric field where this motion is opposed by the viscous drag force of the gas stream.

The Deutsch-Anderson equation is commonly used to describe the penetration of a polydisperse aerosol through an ESP. In this case

$$Pt_o = esp - [w A/V] \quad (4)$$

where Pt_o = overall penetration
w = precipitation rate parameter

Note that $w \neq w(d) \neq w(d_{average})$

Several investigators have observed that for an ESP collecting a polydisperse aerosol the change in penetration with gas velocity or A/V was less than would be predicted from the Deutsch-Anderson equation. Mathematically, this would appear as though the precipitation rate parameter, w_p, increased with increasing gas velocity or decreasing AN (see Figure 2). Since w is defined by Deutsch in terms of particle charge and electric field, it appeared that w should be constant and that the change in w with gas velocity of SCA constituted non-Deutschian behavior of an ESP.

Several investigators have addressed the apparent failure of the Deutch equation to fit ESP data.

Cooperman[2] attributed this phenomenon to a diffusional transport mechanism in the direction of the gas flow.

Robinson[3] related this velocity dependent precipitation rate parameter (w) to an assumption that the inlet dust contains a non-precipitable reentraining fraction. Heinrich[4] suggested that the increased turbulence transports a larger percentage of the dust particles near the corona wire in a higher field region where a larger charge is applied. Williams and Jackson[5] considered diffusion transport augmented by electrostatic particle convection as the mechanism for this behavior.

Nichols and Gooch[6] conducted a theoretical and experimental study under EPA sponsorship to determine the reasons for the apparent failure

PRECIPITATION RATE PARAMETER (ω), cm/sec

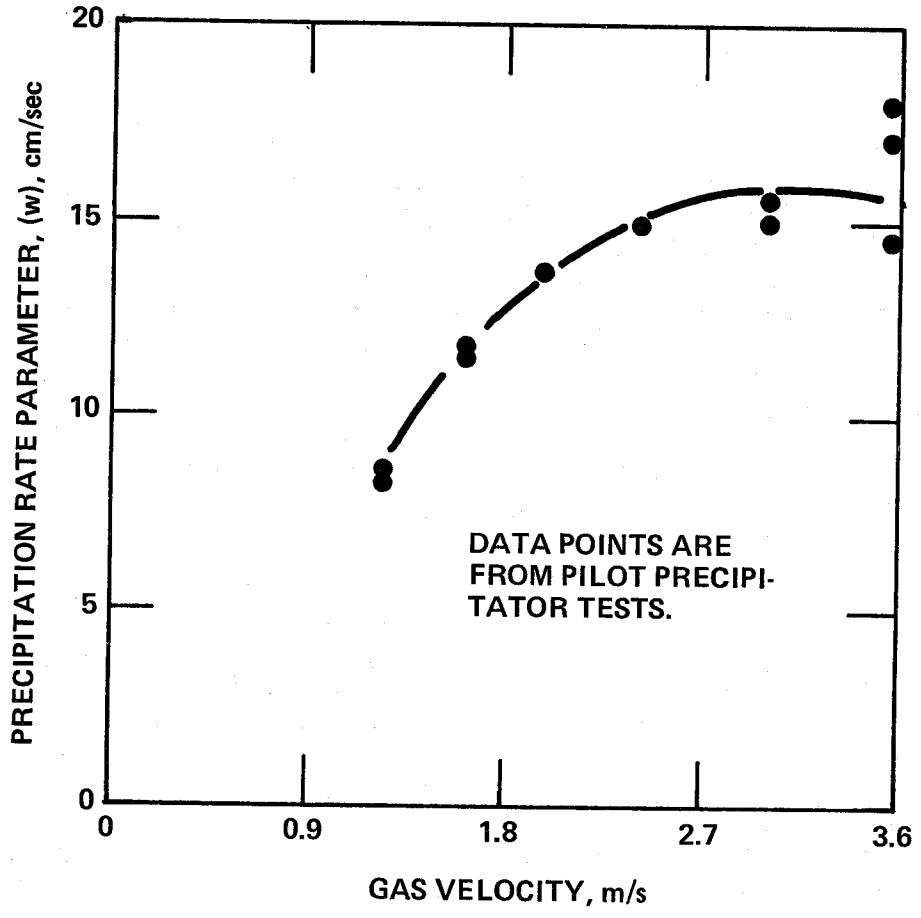

Figure 2. Precipitation rate parameter vs. gas velocity. From reference 6.

of the Deutsch-Anderson equation. They calculated the overall penetration for a polydisperse aerosol from

$$Pt_o = \int_0^\infty f(d) \exp - [\, w(d)\ A/V]\ dd \qquad (5)$$

where f(d) is the diameter frequency function. They then calculated the precipitation rate parameter from

$$w = - \ln Pt_o/A/V \qquad (6)$$

The calculated results are given in Figure 3 and show that w increased as gas velocity increased.

Thus, we see a variation in precipitation rate parameter with gas velocity based on purely theoretical considerations for polydisperse dusts, while the collection efficiency for each size interval is based on the Deutsch-Anderson equation with a fixed migration velocity and an area-to-volume ratio depending upon the gas velocity.

"...Thus, the increase in migration velocity with gas velocity is not an anomalous behavior based on diffusion phenomena or electric wind, but rather is predictable from purely theoretical considerations due to the large variation in migration velocity for a wide range of particle sizes. The primary misunderstanding comes from a misuse of the Deutsch-Anderson equation in a manner that violates the initial assumptions.(page 27)[6]

Attempts to account for variation in particle size distribution by using mass mean diameter are hopeless--especially for high efficiency ESP. The SCA required for a given penetration or the penetration for a given SCA are strong functions of the particle size distribution. Gooch et al.[7] have used a mathematical model of ESP to study the effects of changing particle size distribution on ESP performance. The results of their calculations for constant geometric mass mean diameter of 10 μm and varying geometric standard deviation are shown in Figure 4. Note that, as was the case for plume opacity, changes in geometric standard deviation have a large effect.

WET SCRUBBERS

Semrau and Witham[8] and Semrau et al.[9] published results of extensive experimental studies of particle collection in wet scrubbers. The experiments were conducted under controlled conditions using fine slightly polydisperse aerosols. The experimental results were plotted as number of transfer units, N_t, [$N_t = \ln (1/Pt_o)$] versus effective friction loss. Typical results are shown in Figure 5. Note the change in slope in the curve. This two-branched curve, typical of all their results, was unexpected.

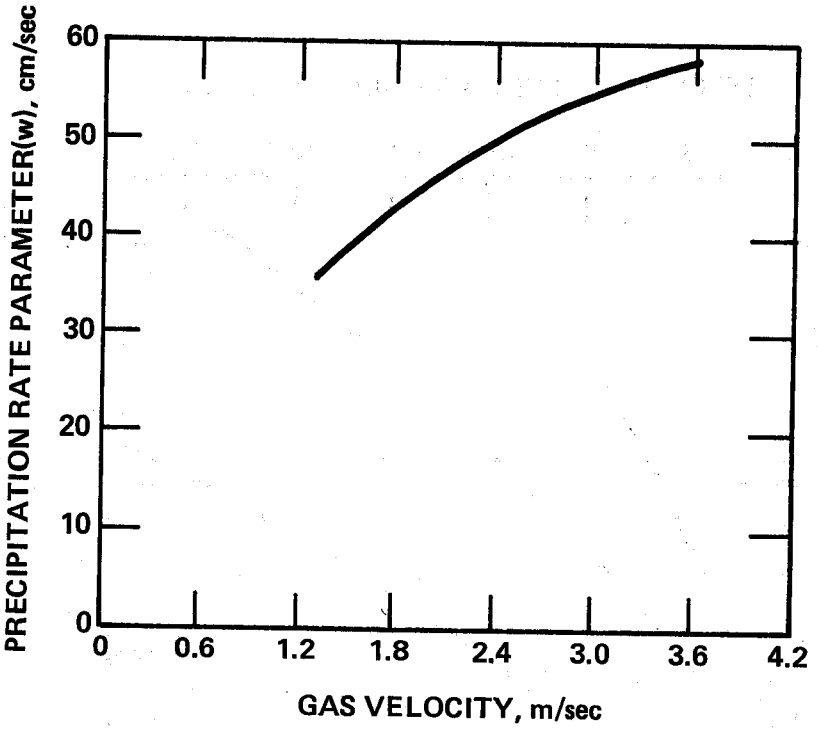

Figure 3. Graph of computed precipitation rate parameter showing increase in w with increasing gas velocity.

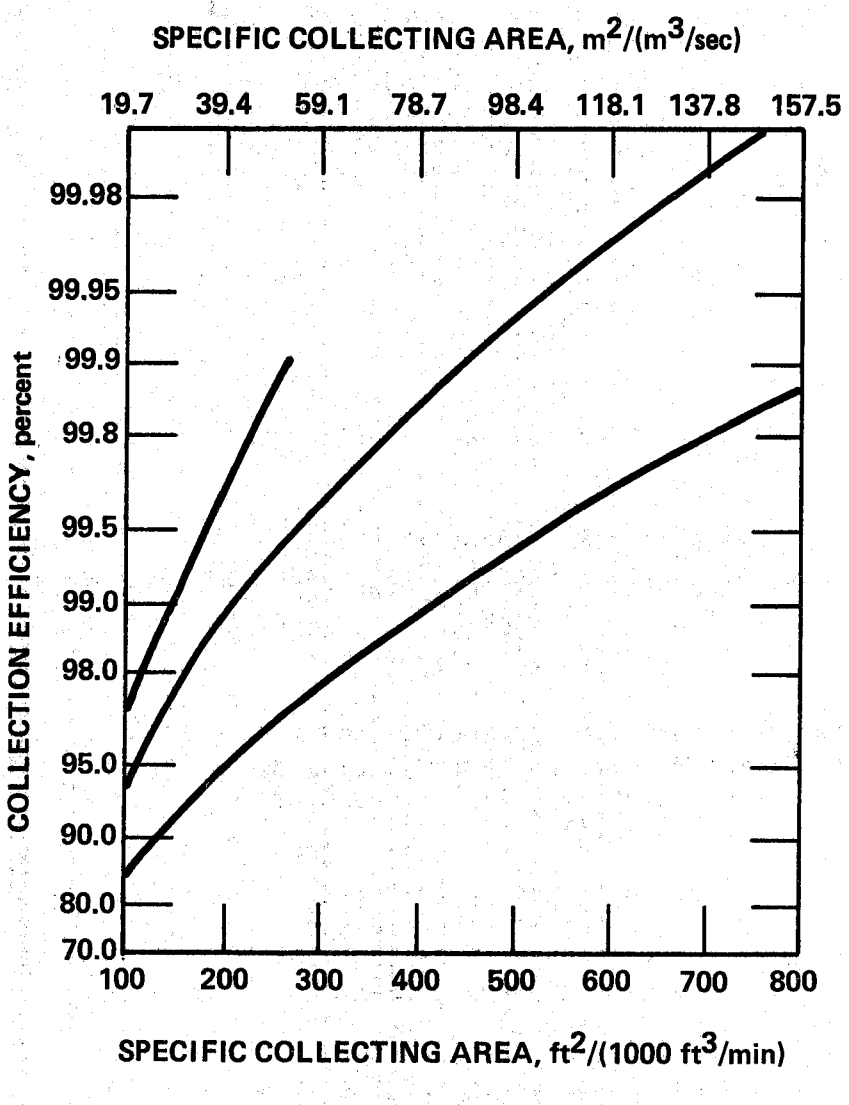

Figure 4. Effect of particle size distribution standard deviation on computed performance. From reference 7.

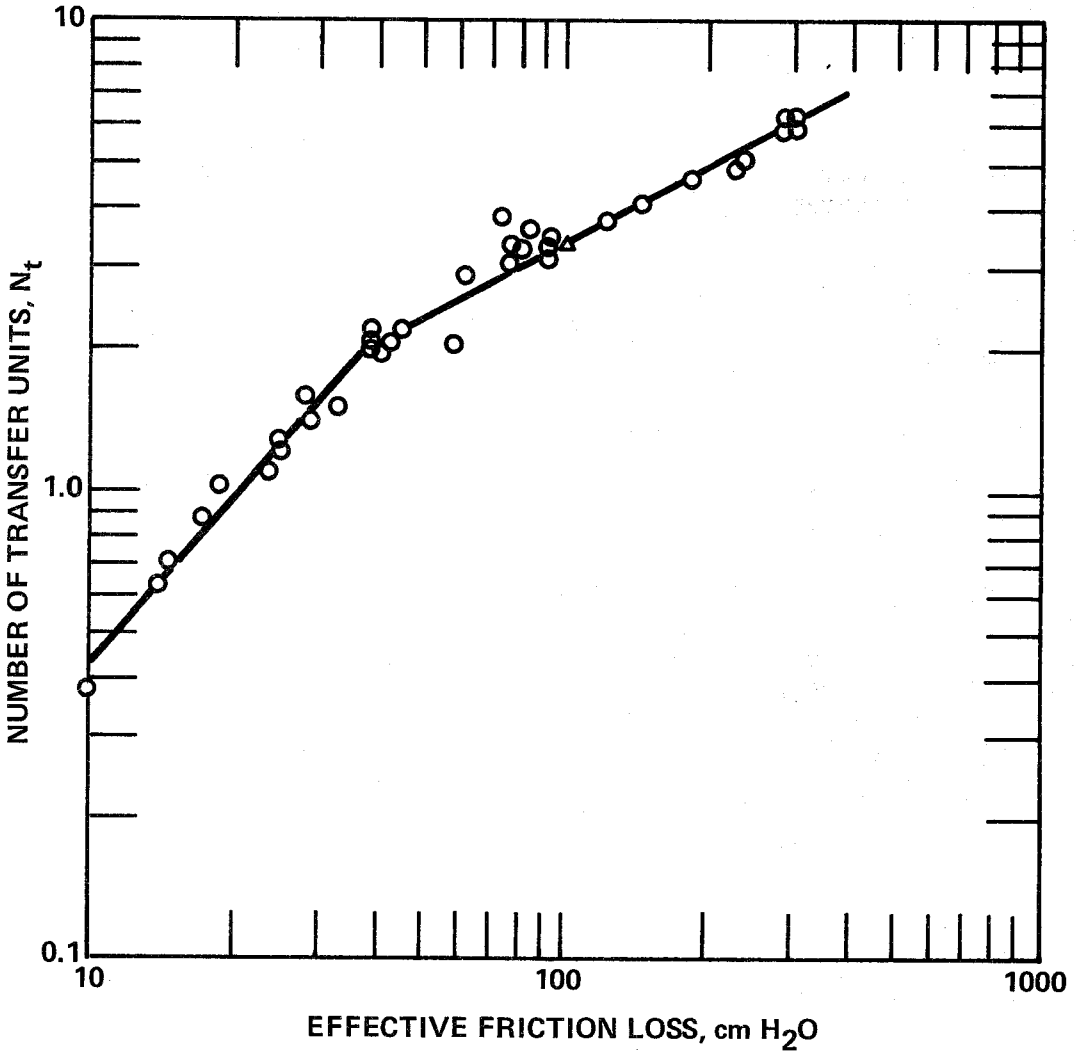

Figure 5. Orifice scrubber performance curve for aerosol D. From reference 9.

Semrau et al. offered the following explanation for the curves:

"A performance curve slope greater than 1.0 indicates that the aerosol becomes more readily collectable as higher collection efficiencies are attained with increasing contacting power. It is difficult to visualize any single collection mechanism that would give such behavior. Inertia gives preferential collection of larger particles and diffusion preferential collection of finer particles Either mechanism operating alone should presumably give a performance curve with a slope less than 1.0, since operation at higher contacting powers and efficiencies would result in preferential depletion of the more readily collectable fraction of the aerosol. Possibly the steep lower branch of the performance curve represents a region in which both diffusion and inertia were operative but neither was strongly dominant. The lower branch did represent a region of relatively low overall efficiency. On aerosols of the sizes under study, the inertial collection efficiency was low in this contacting power range, and presumably collection by diffusion was low in any case. However, if both mechanisms were increasing in effectiveness in this region of operation, it seems that some such behavior as was observed might result. This would certainly depend on how the efficiency of each mechanism was varying with contacting power and how these efficiencies were varying with respect to each other.

"The 'knee' in the performance curve, or transition from the lower branch to the upper branch, possibly represents the point (or narrow region) at which inertial deposition reached such effectiveness that it clearly dominated the overall collection efficiency.

"The foregoing speculations are probably still too crude to be termed a hypothesis. Nevertheless, projecting some such combination of mechanisms seems necessary to permit visualizing a physical process that could yield the observed phenomena." (page 93)[9]

A theoretical analysis of the system used by Semrau et al.[10], using a venturi scrubber model developed by Calvert[10] and programmed by Sparks,[11] was undertaken to see if the effect observed by Semrau et al. could be explained by particle size distribution effects. The model assumes that inertial impaction is the only mechanism for particle collection.

The number of transfer units for a polydisperse aerosol is given by

$$N_t = \ln [1/Pt_o] = \ln [1/\int_0^\infty f(d)Pt(d)dd] \qquad (7)$$

The particle size distribution used in the theoretical analysis was log-normal with geometric mass mean diameter of 1.1 μm and geometric standard deviation of 1.57. This size distribution approximates aerosol D used by Semrau et al..

The results of the theoretical calculations are shown in Figure 6. The agreement between the theoretical calculations and the experimental data is very good, especially for pressure drops greater than 30 cm H_2O. The model tends to slightly overpredict the number of transfer units for low pressure drops.

The calculations were repeated for several other log-normal size distributions with the same result. The N_t versus Δp curve has two straight line branches.

As was the case with ESP, it is possible to explain apparent anomolous experimental results by correctly accounting for the fact that the test aerosols were polydisperse.

As was the case with ESP and opacity it is necessary to fully specify the particle size distribution and not depend on an average diameter. The effects of changes in geometric standard deviation on scrubber pressure drop required to give a penetration of 0.05 for a log-normal size distribution with geometric mass mean diameter, d_g, equal to 1.1 μm are shown in Figure 7. Note that, as in the two previous cases, changes in geometric standard deviation have a major impact.

CONCLUSION

The results presented in this paper establish that the particle size distribution must be considered in all aerosol research. Disregard of or failure to consider the importance of the size distribution has resulted in considerable confusion in the literature. Data have been misinterpreted, reasonable theories have been rejected, unnecessarily complex theories have been proposed, and particulate pollution control has been improperly designed. All because of failure to recognize the importance of the polydisperse particle size distribution.

The effects of the particle size distribution can be accounted for by integration over the particle size distribution. However, they cannot, in general, be accounted for by calculations based on some "average" particle diameter.

In the future, when an aerosol experiment gives a strange result, examine the data for effects of the particle size distribution before seeking explanations in new mechanisms or inadequate theories.

REFERENCES

1. Ensor, D. S., "Smoke Plume Opacity Related to the Properties of Air Pollutant Aerosols" Ph.D. Dissertation, University of Washington, 1972.

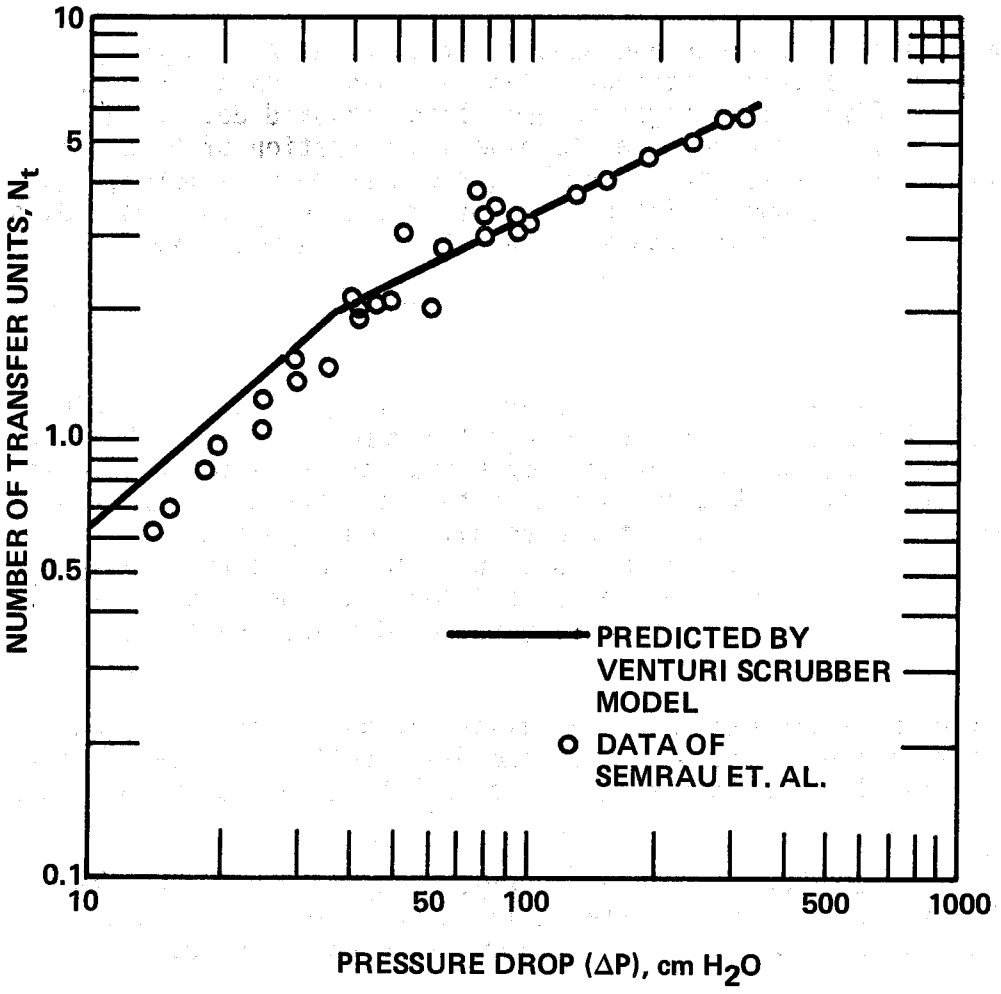

Figure 6. Comparison of number of transfer units versus pressure drop predicted by venturi scrubber model with data of Semrau, et. al.

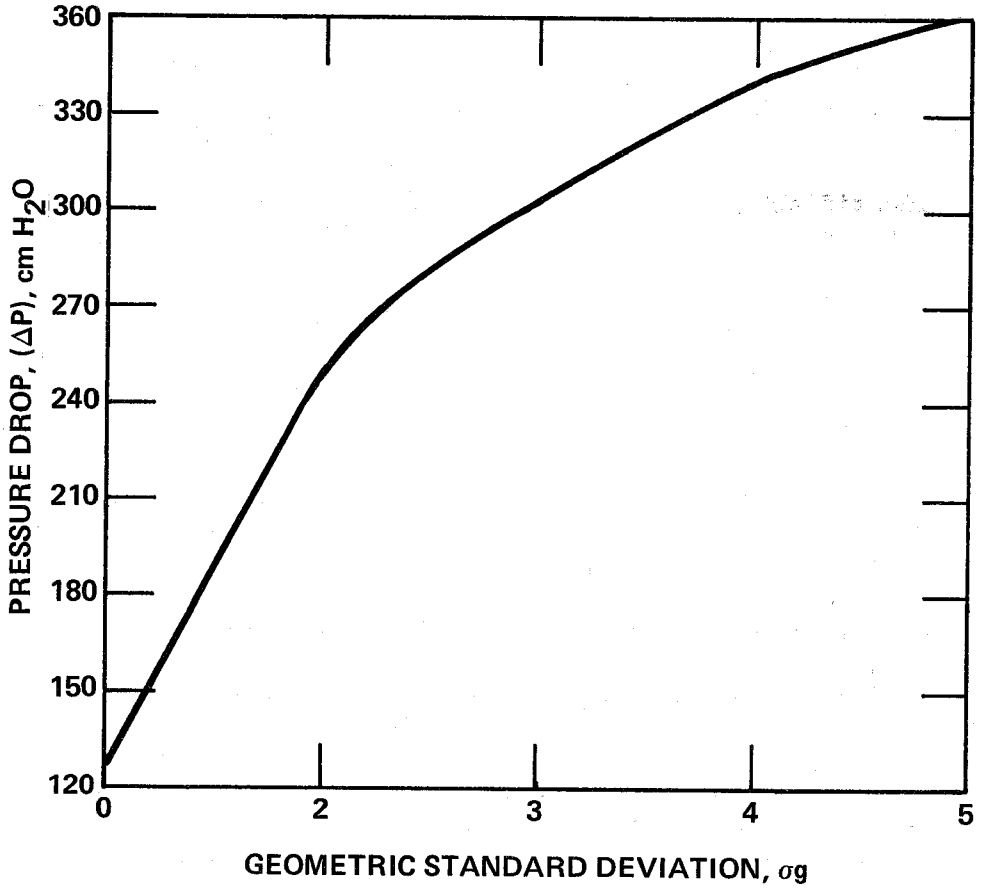

Figure 7. Effect of geometric standard deviation on pressure drop required for Pt = 0.05 with geometric mass mean diameter $\leqslant$ 1.1 μm.

2. Cooperman, P., "A New Theory of Precipitator Efficiency" APCA Paper 69-4, 1969.

3. Robinson, M., Atmos. Environ. 1, 193, 1967.

4. Heinrich, D. O., Staub 23, 83, 1963.

5. Williams, J. C. and Jackson, R., Proc. Symp. Interaction Fluids Particle, Inst. Chem. Engrs. (London) 282. Discussion 291-293, 297-298, 1962.

6. Nichols, G. B. and Gooch, J. P., "An Electrostatic Precipitator Performance Model" EPA-650/2-74-132 (NTIS PB 238-923/AS), July 1972.

7. Gooch, J. P., McDonald, J. R., and Oglesby, S., Jr., "A Mathematical Model of Electrostatic Precipitation" EPA-650/2-75-037 (NTIS PB 246-188/AS), April 1975.

8. Semrau, K. T., and Witham, C. L. "Wet Scrubber Liquid Utilization" EPA-650/2-74-108 (NTIS PB 237-749/AS), October 1974.

9. Semrau, K. T., Witham, C. L., and Kerlin, W. W., "Energy Utilization by Wet Scrubbers" EPA-600/2-77-234 (NTIS PB 276-435/AS), November 1977.

10. Calvert S., "Source Control by Wet Scrubbing" Chapter 46 in Air Pollution, A. Stern ed., Academic Press, 1968.

11. Sparks, L. E., "SR-52 Programmable Calculator Programs for Venturi Scrubbers and Electrostatic Precipitators" EPA-600/7-78-026 (NTIS PB 277-672/AS), March 1978.

THE MORPHOGENESIS OF COAL FLY ASH

Gerald L. Fisher
Radiobiology Laboratory
University of California
Davis, California 95616

ABSTRACT

Coal fly ash is demonstrated to contain a variety of morphological particle types. A morphogenesis scheme is described relating the particle types to the probable mechanism of formation, including discussion of significant physical and chemical factors. Studies describing the morphogenesis of coal fly ash are briefly reviewed.

INTRODUCTION

With the increasing national dependence on coal as a major energy source, a greater concern for the production and fate of coal combustion products has recently been manifested. Fly ash, the primary particulate emission from coal combustion, is presently considered to be one of the most abundant solid waste products in the United States. This report briefly reviews physical and chemical factors related to the morphogenesis of coal fly ash.

FLY ASH MORPHOLOGY

In a study of the physical and morphological properties of size-classified, stack-collected fly ash, Fisher et al.,[1] related the shape of fly ash particles to exposure history in the combustion zone of a coal-fired electric power plant. A morphogenesis scheme was proposed relating opacity to probable chemical composition and shape to particle formation. Eleven morphological classes were distinguished and the relative abundance of each quantitated by light microscopy. Photomicrographs

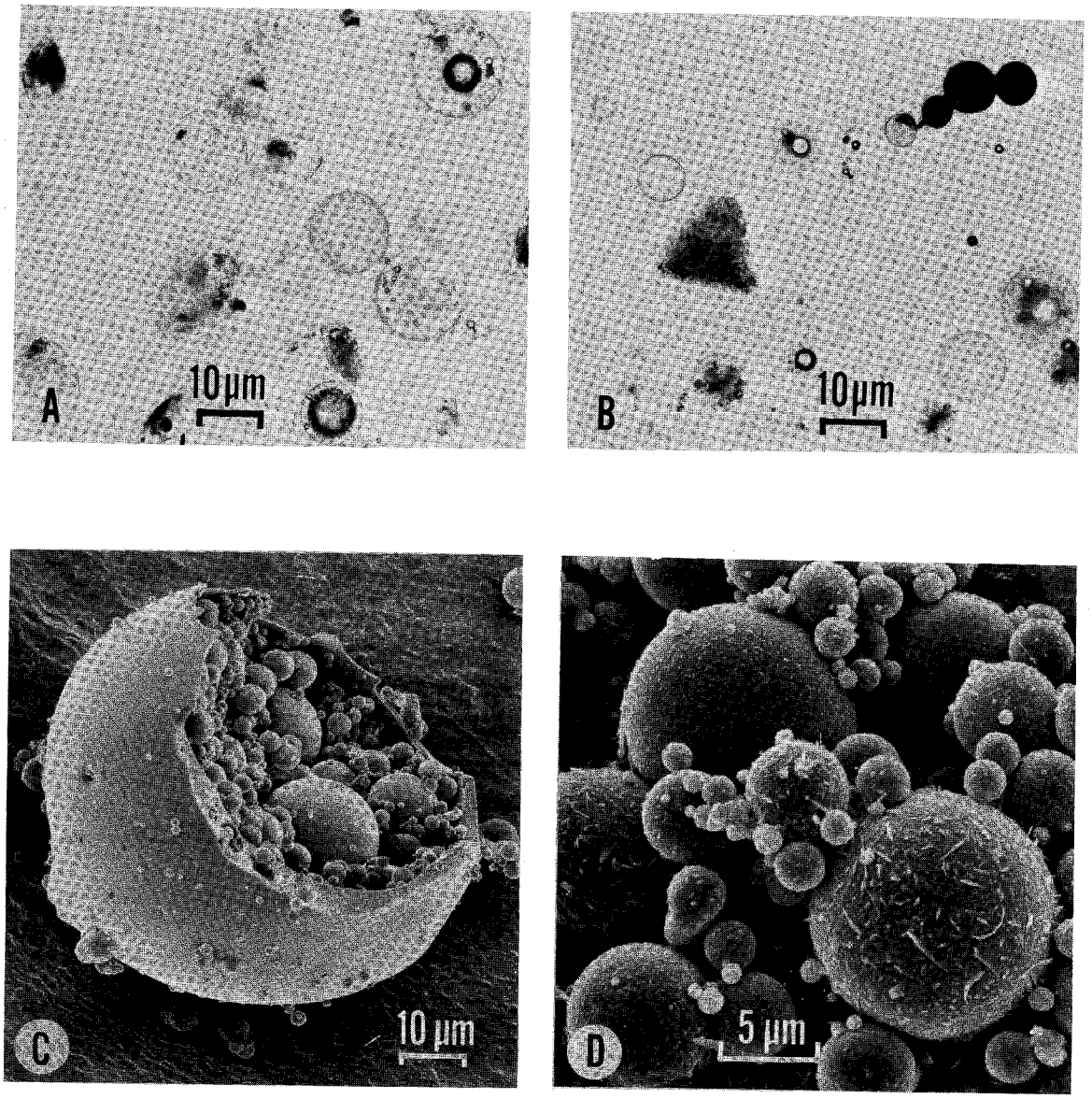

Figure 1. Light micrographs (A, B) and scanning electron micrographs (C, D) illustrating a variety of morphological types of fly ash particles, including: (A) cenospheres, crystalline spheres and amorphous particles, (B) opaque and nonopaque solid spheres, and vesicular particles, (C) a plerosphere, and (D) microcrystals on the surface of spherical particles.

representing most of the morphological classes are presented in Figures 1A - 1D. Specifically, the eleven classes include: (a) amorphous, nonopaque particles, (b) amorphous, opaque particles, (c) amorphous, mixed opaque and nonopaque particles, (d) rounded, vesicular, nonopaque particles, (e) rounded, vesicular, mixed opaque and nonopaque particles, (f) angular, lacy, opaque particles, (g) cenospheres or hollow spheres, (h) plerospheres or encapsulating spheres, (i) nonopaque, solid spheres (j) opaque spheres, and (k) spheres with either surface or internal crystals. Opaque amorphous particles and angular, lacy opaque particles were tentatively classified as unoxidized carbonaceous material or iron oxides.[1] Subsequent SEM-X-ray analysis indicated that these opaque particles were composed of low atomic number matrices.[2] Furthermore, calculation of the effective atomic number of class b particles based upon Bremstrahlung production indicated that this class is predominantly composed of elemental carbon.[3] The opaque spheres (class j) appear to be predominantly magnetite and may be identified by (1) magnetic separation or passing a magnet near a liquid mount of the sample under a microscope and (2) by observation of small clusters of these particles. The amorphous and rounded vesicular, nonopaque particles (classes a and d) appear to be aluminosilicate particles. Rounding and vesicularity reflect increased exposure to boiler conditions. Further heating of these particles will give rise to nonopaque spheres which are either solid, hollow, or packed with other particles. Similarly, the mixed opaque, nonopaque, amorphous or rounded classes will give rise to spherical particles upon increased exposure to combustion conditions in the boiler. Sphere formation, including cenospheres and plerospheres, is discussed in detail later in this manuscript. The nonopaque, solid spheres ranged in color from water white to yellow to orange and deep red. Analysis of single particles in this class by SEM-X-ray techniques indicated that the variation in color was associated with iron content.[3] Crystal formation within glassy spheres (as determined by light microscopy) is probably the result of heterogeneous nucleation at the surface of the molten silicate droplet.

SURFACE CRYSTAL FORMATION

Surface crystals (Figure 1D) identified by scanning electron microscopy (SEM) have been explained as reaction of sulfuric acid with metal oxides. This crystal formation process is relatively slow compared to the time required for particle formation. Fisher, et al.,[4] have hypothesized that surface crystal formation results from SO_2 hydration and subsequent oxidation on fly ash surfaces to form H_2SO_4 which then reacts with metal oxides, predominantly CaO, or with ambient NH_3 to form either $CaSO_4$ or $(NH_4)_2SO_4$. Such a mechanism could also result in formation of relatively more soluble compounds from insoluble oxides, e.g., conversion of PbO to $PbSO_4$. Fine particulate matter has also been observed by SEM on fly ash surfaces by a number of investigators.[5-8] Small[8] has identified four surface morphologies based on SEM analysis. Spheres with smooth surfaces comprised the most commonly encountered particle morphology. Spheres with small surface particles

and relatively large surface-associated droplets were also observed. Elemental analysis of these two particle classes indicated the surface was predominantly Si and Al and the underlying particle was mainly Fe. A fourth class of spherical particles with high Fe concentrations was found to display an unusual pattern of coarse surfaces. Sarofim et al.[7] reported the presence of submicron silica particles on laboratory-generated fly ash. As an extension of the vaporization-condensation mechanism of Davison et al.[9] for trace elements, Sarofim, et al.,[7] suggest that silica deposition resulted from formation of fine silica particles which agglomerate on fly ash surfaces. The formation of submicron silica particles was thought to be due to nucleation of SiO resulting from reaction of SiO_2 with carbon.

CENOSPHERE FORMATION

The mechanism of formation of cenospheres, i.e., hollow spheres, has been the subject of a number of reports. Raask[10] demonstrated that sphere formation may result from melting of mineral inclusions in coal on a nonwetting surface, namely carbon. He also demonstrated that gas generation inside the molten droplet resulted in cenosphere formation. He reported two stages of gas evolution. In the first stage, directly after melting coal-ash slag, SO_2 and N_2 were released. The SO_2 was thought to result from sulfate decomposition and N_2 from air trapped in the melt. Further heating resulted in CO evolution which was catalyzed by addition of iron or iron oxide to the melt. In a subsequent report, however, Raask[11] described the physical and chemical properties of cenospheres in pulverized fuel ash collected by the electrostatic precipitators. Analysis of the gas content of the cenospheres after breaking the particles indicated the presence of approximately 0.2 atm (20°C) of gas composed of CO_2 and N_2. No detectable CO or O_2 was present. Raask suggested that the source of the CO_2 was the oxidation of carbon by iron oxide. In contrast to this view, Bauer and Natusch[12] have suggested that cenosphere formation results from the injection of coal-derived CO_2 into molten mineral.

It is also possible that the observed CO_2 in cenospheres is due to carbonate mineral decomposition. Assuming a diameter of average volume of 100 micron, a density of 0.5 g/cm^3 and 0.5% CaO, only 20% of the calcium need be associated with carbonate mineral to provide sufficient CO_2. In this regard, Fisher et al.[4] have postulated that the CO_2 detected after crushing fly ash under vacuum (after thorough degassing) was the result of carbonate mineral decomposition. In those studies, CO_2 and H_2O were the only gases released. The H_2O was thought to be due to clay mineral decomposition. In particular, based on the stoichiometry of major elements, Fisher et al.[4] suggested that the major clay mineral in the parent coal (western U. S.) was kaolinite. In a detailed study of the transformation of mineral matter in pulverized coal, Sarofim et al.[7] demonstrated that the three major components in a bituminous coal were 50% kaolinite, 40% pyrite and 10% calcium sulfate and carbonate and in a lignite were 50% kaolinite, 10% pyrite and 40%

calcium sulfate and carbonate. The mass median diameter of the mineral matter was 2 microns for both coals. The optimal temperature for cenosphere formation based on ash density was demonstrated to be 1500°K. This optimum was rationalized by calculating the time for sphere formation. At higher temperatures gas evolution is too rapid and gas will escape from the molten ash, while at lower temperatures sphere formation is too slow relative to the duration of molten state within the furnace. Padia et al.[13] have summarized the principal reactions that take place in mineral matter during coal combustion. These include (1) kaolinite decomposition resulting in loss of lattice water, (2) carbonate mineral decomposition resulting in CO_2 generation, (3) sulfate decomposition, and (4) pyrite oxidation. Thus, it appears reasonable to assume that the driving force for cenosphere formation is gas production resulting from carbonate and clay mineral decomposition.

PLEROSPHERE FORMATION

Light and electron microscopic studies (Figure 1C) have identified a morphological class of spherical particles containing encapsulated smaller spheres.[4,5,6] These encapsulating spheres[6] or plerospheres[4] are similar to cenospheres in that they are composed of an aluminosilicate shell which is filled with individual particles rather than gas. Matthews and Kemp[5] and Natusch et al.[6] have established that plerosphere formation is truly the result of encapsulation during particle formation rather than filling of a ruptured cenosphere. For these studies, either the electron beam of a scanning electron microscope[5] or an argon ion milling machine[6] were used to etch through the individual particle surfaces. Subsequent examination of the etched particles indicated the presence of numerous smaller particles within the plerosphere, thus confirming that encapsulation occurred during particle formation. Fisher et al.[4] have hypothesized a mechanism of plerosphere formation.

Plerosphere formation is hypothesized to result from a process similar to cenosphere formation.[4] As the aluminosilicate particle is progressively heated, a molten surface layer develops around the solid core. Mineral decomposition with evolution of CO_2 and H_2O then results in formation of a bubble around the core, which remains attached to the molten shell. Further heating will lead to additional gas formation causing the core to boil away from the shell. This process may result in concomitant formation of fine particles. The process can be repeated until the plerosphere is full of other plerospheres or solid particles or until the particle freezes. Similarly, Bauer and Natusch[12] have proposed that fine aluminosilicate particles result from "explosion" of molten clay mineral. In their model, intimate contact of molten mineral with combusting coal results in fine particle formation due to coal-evolved CO_2, which provides energy for fragmentation of the mineral.

OTHER GLASSY MICROSPHERES

Although the mechanism of formation of fly ash particles is not well understood, it is interesting to note the natural (nonanthropogenic) occurrence of glassy spheres with morphological appearance similar to fly ash. Glassy spherules have been reported to be present on shatter cone surfaces.[14] These spherules were presumed to be the result of meteorite impact. Similarly, glassy spheres have been identified in lunar dust samples. Nagy et al.[15] reported the presence of fine glass beads which were either spherical, nearly spherical, or dumbbell shaped in Apollo II lunar samples. Some broken glass beads were hollow and vesicular similar to cenospheres; particle surfaces generally were coated with fine particulate matter. CH_4, CO, and CO_2 were found to be entrapped in the glass beads. Carter and MacGregor[16] reported that glass spheres ranged in color from colorless through green, brown, wine-red, to opaque. The spheres are thought to form from splattered molten beads resulting from meteorite impact on moon's surface.

ACKNOWLEDGMENTS

This work was supported by the U. S. Department of Energy. The author gratefully acknowledges the technical assistance of Mr. B. Prentice.

REFERENCES

1. Fisher, G. L., B. A. Prentice, D. Silberman, J. M. Ondov, A. H. Biermann, R. C. Ragaini, and A. R. McFarland. Physical and Morphological Studies of Size-Classified Coal Fly Ash. Environ. Sci. & Technol. 12:447-451, April 1978.

2. Fisher, G. L., C. E. Chrisp, and T. L. Hayes. Carbonaceous Particles in Coal Fly Ash. In: Proceedings of the Conference on Carbonaceous Particles in the Atmosphere, T. Novakov (ed.). Berkeley, March 1978. (in press).

3. Hayes, T. L. and G. L. Fisher, unpublished data.

4. Fisher, G. L., D. P. Y. Chang, and M. Brummer. Fly Ash Collected from Electrostatic Precipitators: Microcrystalline Structures and the Mystery of the Spheres. Science. 192:553-555, 7 May 1976.

5. Matthews, B. J. and R. F. Kemp. Development of Laser Instrumentation for Particle Measurement. TRW, Systems Group, Redondo Beach, TRW report no. 14103-6003-RO-00, June 1971. 64 p.

6. Natusch, D. F. S., C. F. Bauer, H. Matusiewicz, C. A. Evans, J. Baker, A. Loh, R. W. Linton, and P. K. Hopke. Characterization of Trace Elements in Fly Ash. In: International Conference on Heavy

Metals in the Environment, Toronto, Ontario, Canada, October 27-31, 1975. p. 553-576.

7. Sarofim, A. F., J. B. Howard, and A. S. Padia. Physical Transformation of the Mineral Matter in Pulverized Coal Under Simulated Combustion Conditions. Combust. Sci. and Technol. 16:187-204, 1977.

8. Small, J. A. An Elemental and Morphological Characterization of the Emissions from the Dickerson and Chalk Point Coal-Fired Power Plants. Ph.D. thesis, Univ. of Maryland, April 1976. 360 p.

9. Davison, R. L., D. F. S. Natusch, J. R. Wallace, and C. A. Evans, Jr. Trace Elements in Fly Ash; Dependance of Concentration on Particle Size. Environ. Sci. & Technol. 8:1107-1113, December 1974.

10. Raask, E. Slag-Coal Interface Phenomena. Journal of Engineering for Power, Trans. ASME. 88:40-44, 13 December 1965.

11. Raask, E. Cenospheres in Pulverized-Fuel Ash. Journal of the Inst. of Fuel. 339-344, September 1968.

12. Bauer, C. F. and D. F. S. Natusch, personal communication.

13. Padia. A. S., A. F. Sarofim, and J. B. Howard. The Behavior of Ash in Pulverized Coal Under Simulated Combustion Conditions. In: Combustion Institute Central States Section Spring Mtg. April 5-6, 1976.

14. Gay, N. C. Spherules on Shatter Cone Surfaces from the Vredefort Structure, South Africa. Science. 194:724-725, 12 November 1976.

15. Nagy, B., W. M. Scott, V. Modzeleski, L. A. Nagy, C. M. Drew, W. S. McEwan, J. E. Thomas, P. B. Hamilton, and H. C. Urey. Carbon Compounds in Apollo II Lunar Samples. Nature. 225:1028-1032, 14 March 1970.

16. Carter, J. L. and I. D. MacGregor. Mineralogy, Petrology, and Surface Features of Lunar Samples 10062,35, 10067,9, 10069,30, and 10085,16. Science. 167:661-663, 30 January 1970.

THE EFFECT OF TEMPERATURE, PARTICLE SIZE AND TIME EXPOSURE ON COAL-ASH AGGLOMERATION

Keh C. Tsao, Jeffrey F. Bradley, Kuang T. Yung
The College of Engineering and Applied Science
The University of Wisconsin--Milwaukee 53201

ABSTRACT

The agglomeration effect on coal and fly ash particles was investigated to determine the rate of agglomeration as a function of temperature, time of exposure, mixture composition, and particle size. Procedural aspects include: the screening of coal and fly ash to determine mesh size, calibration of static furnace to establish temperature accuracy, temperature profile response of crucible and sample, determination of optimal compositional mixture of coal and fly ash for agglomeration, and the heating of samples at constant temperature for various time intervals.

Interpretation of the results included microscopic examination followed by screening analysis leading to a practical correlation expression by statistical methods. The correlation expression will be used for design considerations in the construction of a high temperature cyclone for particulate removal from fluidized bed combustion gas products and coal gasification processes.

INTRODUCTION

The removal of particulates from the high temperature, high pressure flue gases of fluidized bed combustion products by a multi-inlet, multi-pass cyclone, with insitu combustion, requires an understanding of the agglomeration rate of the coal-ash particles. The agglomeration of the coal-ash particles is based on the heating of the particles to their fusion temperature, inducing a pseudo-molten state which allows adhering of adjacent particles thus increasing their size [1-4]. The multiple jet cyclone will utilize this phenomena [5], in that when the

fusion temperature is reached, and the pseudo-molten state established, centrifugal forces will cause impactions, collisions, and subsequent adherance of the particles to increase removal efficiency. Therefore, as a design and operating criteria for the cyclone, the agglomeration rate must be known in conjunction with the probability of particle collisions. The agglomeration rate is a function of temperature, time of high temperature exposure and initial coal-ash size or composition. The value of the agglomeration rate at various operating conditions allows an efficient operation of the cyclone by maximizing the probability of collision, the subsequent agglomeration, and the removal efficiency. The goal of this paper attempts:

1. To experimentally determine the agglomeration rate of coal-ash particles as a function of temperature, time of exposure, and composition;
2. To formulate a correlation expression relating the agglomeration rate to temperature, time of exposure and composition.

Experimental Approach

A multiple 2^3 factorial experimental design was used to determine the agglomeration rate as a function of temperature, time of exposure, and composition. Preliminary experimental conditions require: 1.) the screening of the coal and flyash to predetermined mesh sizes. The coal and fly ash was screened to mesh size ranges as indicated in Table I. 2.) The calibration of the static furnace, to establish the accuracy of the furnace temperature controls and thermocouple readings. The procedure includes the placement of an additional calibrated Chromel-Alumel thermocouple inside the furnace, then by varying the furance temperature, the output reading was recorded. This allows a comparison of the furnace controls to the standard thermocouple. The results of the calibration are plotted as shown in Figure 1. The calibration indicates negligible temperature variations between the furnace temperature and the standard thermocouple in the temperature ranges of 1000 °F to 2000 °F. 3.) The determination of the temperature response of the crucible and sample to establish an initial warm-up time. The procedure involved imbedding a Cr-Al thermocouple in a 4.00 gram sample of -400 mesh flyash in a Al_2O_3 crucible. Then by introducing the sample to a designated furnace temperature, the thermal response of the flyash was determined by means of an output recorder connected to a calibrated thermocouple. For selected furnace temperatures, this temperature response is presented in Figure 2. From Figure 2, the initial warm-up time (I.W.T.) is defined as the time required for the sample center to reach 90% of the actual operating temperature. The initial warm-up time for the respective operating temperature in the range of 1600°F to 1900 °F is plotted in Figure 3. 4.) The establishment of optimal compositional mixtures of coal and flyash to best simulate actual fluidized bed combustion products. The presence of residual carbon in combustion product is closely approximated by the use of mixture ratios of unburned coal and flyash for the agglomeration rate determination. The coal ash mixture ratio is selected and based on the maximum observ-

able agglomeration in the sample while preventing the formation of a single piece of molten clinker. Initial laboratory observations indicate that the lower the coal percent in the sample, the less chance of caking after exposure. In order to have a measurable quantity of agglomerated sample within the exposure time limit, it was decided that a 5% coal and 95% ash will provide the needed accuracy in the sample weighing. Also this composition simulates closely a real sample in fluidized bed combustion products. 5.) Microscopic examination of a testing sample to physically establish the agglomeration phenomena. An initial sample of 5% coal and 95% ash was exposed to 1750°F for 3 minutes and examined microscopically. Figure 4 presents evidence of the agglomeration phenomena in the photographs before and after exposure.

Experimental Procedure

The agglomeration rate was determined by a multiple 2^3 factorial design, with the variables of temperature, time of exposure, and composition. The variables are summarized in Table II. Table III list the various combinations of the variables, along with the corresponding sample number for each trial.

The experimental procedure involves the heating of five 4.00 gram samples of coal-ash mixtures simultaneously for 30 to 60 seconds exposure time. A total of 20.0 grams sample of agglomerated coal-ash is obtained. The test were randomly performed. The exposed samples were then screened by sieve analysis to show the effect of agglomeration. The agglomerates were divided into five mesh sizes and are shown in Table IV.

Agglomeration Rate Determination

In parallel with the particulate size differentiation as commonly used in air pollution [6,7] analysis, the agglomeration rate for this study as defined in equation (1) is:

$$\overline{A.R.} = 1 - \frac{\Sigma\,(\%\text{ of screened sample after exposure})(\text{wt. fraction})(\text{size})}{(\%\text{ ash before exposure})(\text{wt. of ash})(\text{size}) + (\%\text{ coal before exposure})(\text{wt. coal})(\text{size})} \quad (1)$$

where the percent implies the ratio of screened sample after exposure to original 20.0 gram sample before exposure. This definition gives an average "size weighed" agglomeration rate ($\overline{A.R.}$). Values of the average agglomeration rate indicate the percent increase in overall size from one operating condition to another. Table V shows the experimental results of 54 sample runs. To insure data reproducibility and to determine the margin of variability, a triplicated testing scheme was employed. For every operating conditoin, three randomly selected experiments were performed. Columns 4, 5, and 6 of Table V present such data. The date are classified according to their corresponding operating condition. The mean "size weighed" agglomeration rate ($\overline{A.R.}$), represents

the average of the three trial runs, which is shown in the last column of Table V. Among the 18 operating conditions, the mean agglomeration rate indicates, for 95% ash of -400 mesh size and 5% coal of -230/+325 mesh size sample, an increase from 16.4% at 1520°F to 46.4% at 1805°F. And at 1663°F, the mean size weighed agglomeration rate increased from 39.9% to 61.7% when the mesh size of ash is varied from -325/+400 to -230/+325.

Figures 5 and 6 present the average agglomeration rate versus computed sample particle size before exposure. The sample particle size is calculated based on the equation:

$$\text{sample particle size} = (\%\ \text{ash before exposure})(\text{wt. ash})(\text{size}) + (\%\ \text{coal before exposure})(\text{wt. coal})(\text{size}) \quad (2)$$

The majority of test data falls within a range of ± 15% with two exceptions of ± 18.6% and ± 24%. The reproducibility of the data is considered to be good because all the tests were run randomly. In general, the $\overline{A.R.}$ increases with increasing temperature at approximately a constant rate. Also the $\overline{A.R.}$ increases with sample particle size. The exposure time exerts a greater effect in coal ash agglomeration at 1663°F and smaller particle size.

Agglomeration Rate Correlation

A plot of all experimental data points versus sample number is shown in Figure 7. A mathematical model equation is constructed through all the data points even though the operating conditions are different for various runs. In view of the preliminary nature of these data as presented, the correlation line appears in good agreement with the experimental data. The correlation equation as a function of temperature, exposure time, and sample particle size is:

$$\overline{\overline{A.R.}}_{\text{calculated}} = -4.695 + 0.00445\,(X) + 0.00394\,(\tau) + .00247\,(T) \quad (3)$$

where X is the computed sample particle size in microns, τ the exposure time in seconds and T is the temperature in °F. The equation is developed through multiple linear regression analysis. The multiple regression coefficient is 0.991 with F value of 138.87 which is considered to be a very good fit.

An attempt was made to further examine the correlation with respect to the effect of second order and interactions among the variables. Factorial analysis was employed to establish the importance of the single factor effects, two factor interaction and three factor interactions. Results indicated that the mean agglomeration rate is a function of the single variables, independently of each other. The multiple factor

interaction and second order interactions were negligible compared to the single factor effects.

Figure 8 is a comparison plot between the calculated mean agglomeration rate (equation 3) versus the observed mean agglomeration rate. It indicates the close correlation between the experimental and predicted values.

With the given statistical characteristics as derived from the prediction equation of mean agglomeration rate, it is concluded that the predicted values are acceptable with confidence.

ACKNOWLEDGEMENTS

This research was sponsored by the U.S. Energy Research and Development Administration under Starter Grants--University Projects in Coal Research. Use of computing facility through a grant from the Graduate School, the University of Wisconsin at Milwaukee is sincerely acknowledged.

REFERENCES

1. W.M. Goldberger, "Collection of Flyash in a Self-Agglomerating Fluidized Bed Coal Burner," ASME Publications, presented at the Winter Annual Meeting Energy Systems Expositoin in Pittsburgh, PA, November 12-17, 1967.

2. W.M. Goldberger, "Flyash Emission and Erosion by Flyash from Self-Agglomerating Fluidized-Bed Coal Burner," AIChE Symposium Series, Volume 70, Number 141, p. 88-96.

3. J. Yernshalmi, M. Nalodney, R.A. Graft, A.M. Squires, R.D. Harvey, "Agglomeration of Ash in Fluidized Beds Gasifying Coal: The Godel Phenomenon, Science, Vol. 187, Feb. 1975, p. 646-648.

4. K.P. Ananth, L.J. Shannon, "Evaluation of Thermal Agglomeration For Fine Particle Control, Environmental Protection Technology Series, EPA-600/2-76-067, March 1976.

5. K.C. Tsao, K.T. Yung, and J.F. Bradley, "Multiple Jet Particle Collection in a Cyclone by Reheating Fluidized-Bed Combustion Products," Fifth International Conference on Fluidized-Bed Combustion, paper No. 78, Washington, D.C., December, 1977.

6. A.C. Stern, Air Pollution, Academic Press, 1968, Volume I.

7. M. Crawford, Air Pollution Control Theory, McGraw-Hill Inc., 1976, pp. 129-140.

Table I. COAL AND FLYASH SCREENED MESH RANGES

Coal Designation	Mesh Range	Micron Range	Average Size for Range (M)
A	-230/+325	63 > P*> 45	54
B	-200/+230	75 $\geq$ P > 63	69

Fly Ash Designation	Mesh Range	Micron Range	Average Size for Range (M)
1	-400	38 $\geq$ P	38
2	-325/+400	45 $\geq$ P > 38	42
3	-230/+325	63 $\geq$ P > 45	54

*P denotes particle size

Table II. VARIABLES FOR DETERMINATION OF AGGLOMERATION RATE

Temperature, °F	Time of exposure (sec.)	Composition*
1520	30	1A
1663	60	2B
1805		3B

*Refer to Table I for coal and flyash mesh size.

Table III. COMBINATION OF VARIABLES AND THEIR CORRESPONDING SAMPLE NUMBERS

		1520°F Sample Number Trial			1663°F Sample Number Trial			1805 °F Sample Number Trial		
Composition	Time(sec)	I	II	III	I	II	III	I	II	III
1A	30	1	19	37	2	20	38	3	21	39
1A	60	4	22	40	5	23	41	6	24	42
2B	30	7	25	43	8	26	44	9	27	45
2B	60	10	28	46	11	29	47	12	30	48
3B	30	13	31	49	14	32	50	15	33	51
3B	60	16	34	52	17	35	53	18	36	54

Table IV. AGGLOMERATES MESH SIZES

Mesh Range	Micron Range	Average Size for Range
+200	P* > 75	75
-200/+230	75 $\geq$ P $\geq$ 63	69
-230/+325	63 $\geq$ P $\geq$ 45	54
-325/+400	45 $\geq$ P $\geq$ 38	42
-400	38 $\geq$ P	38

*P denotes particle size

Table V. AVERAGE "SIZE WEIGHED" AGGLOMERATION RATES $\overline{A.R.}$ AND MEAN "SIZE WEIGHED" AGGLOMERATION RATES $\overline{\overline{A.R.}}$ FOR THREE TRIALS

Sample Number			$\overline{A.R.}$			$\overline{\overline{A.R.}}$
I	II	III	I	II	III	
1	19	37	.165	.170	.157	.164
2	20	38	.226	.282	.330	.279
3	21	39	.539	.433	.419	.464
4	22	40	.200	.184	.159	.181
5	23	41	.392	.370	.369	.377
6	24	42	.435	.469	.546	.480
7	25	43	.276	.234	.241	.250
8	26	44	.403	.412	.381	.399
9	27	45	.630	.521	.554	.568
10	28	46	.358	.220	.277	.285
11	29	47	.549	.497	.428	.491
12	30	48	.656	.564	.581	.600
13	31	49	.598	.539	.658	.569
14	32	50	.583	.655	.612	.617
15	33	51	.744	.710	.714	.723
16	34	52	.567	.565	.620	.584
17	35	53	.675	.646	.609	.643
18	36	54	.751	.741	.734	.742

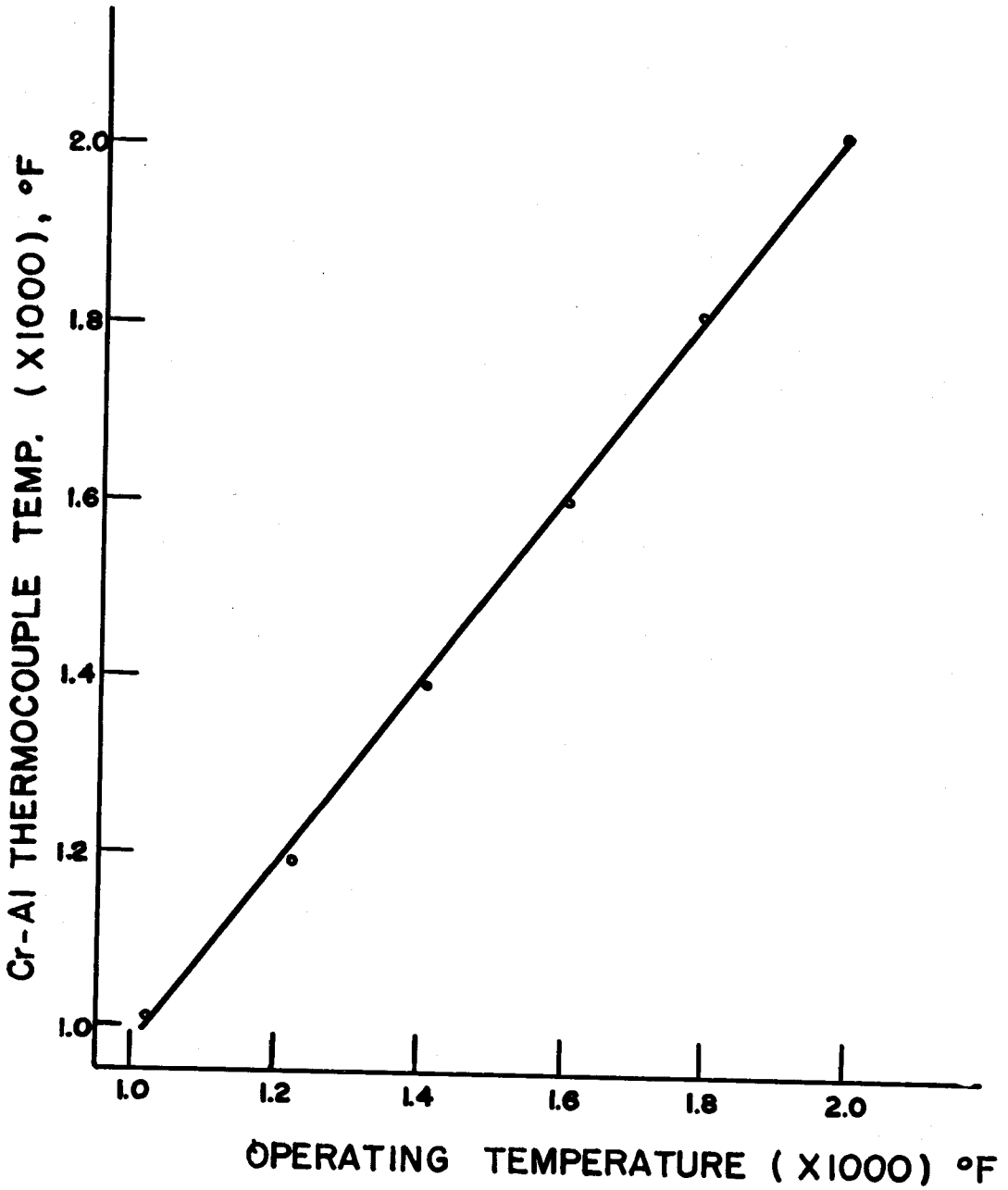

FIG. 1 Thermal calibration chart

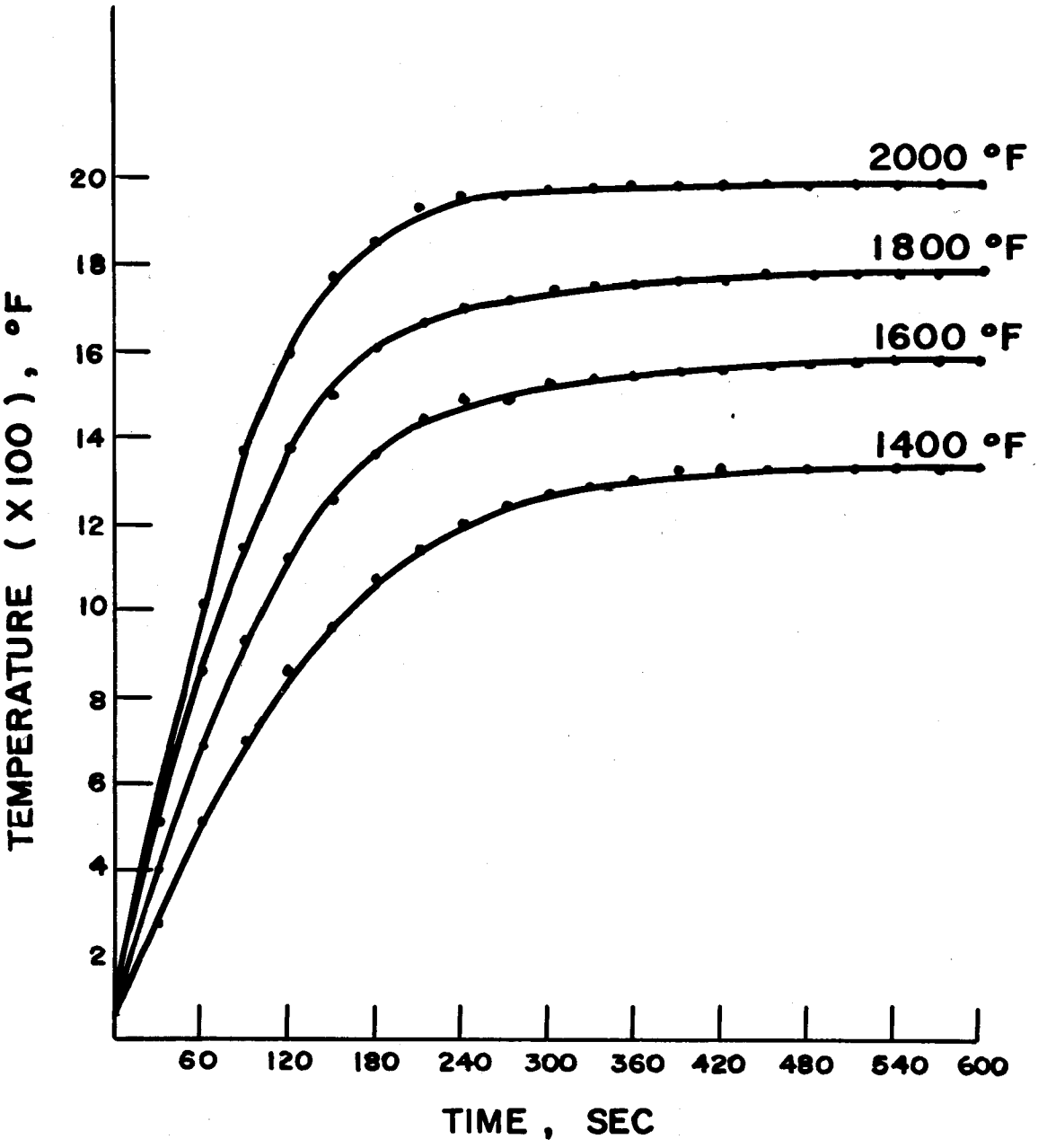

FIG. 2 Response for fly ash samples at initial operating temperature

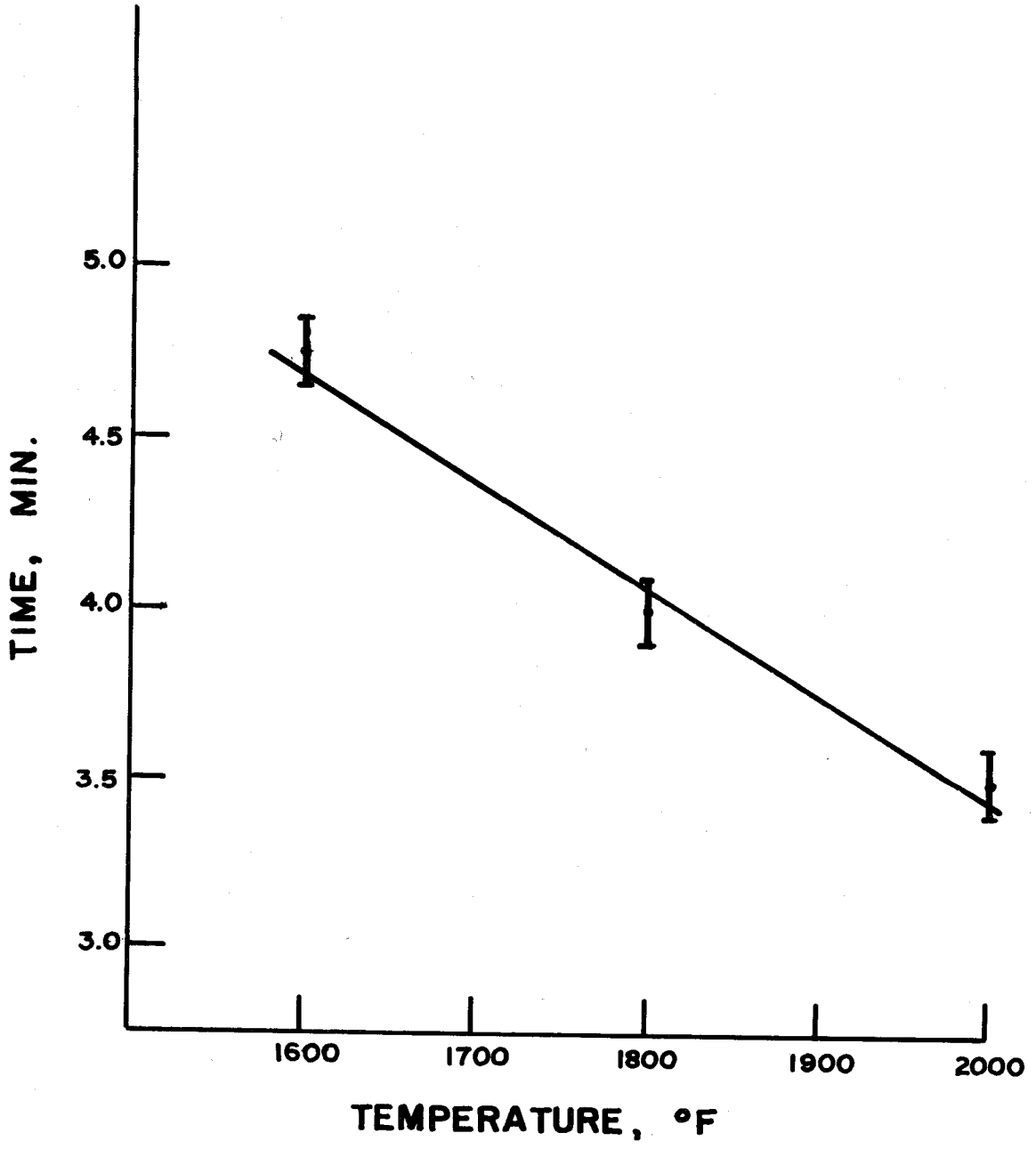

FIG. 3 Initial warmup time as a function of operating temperature

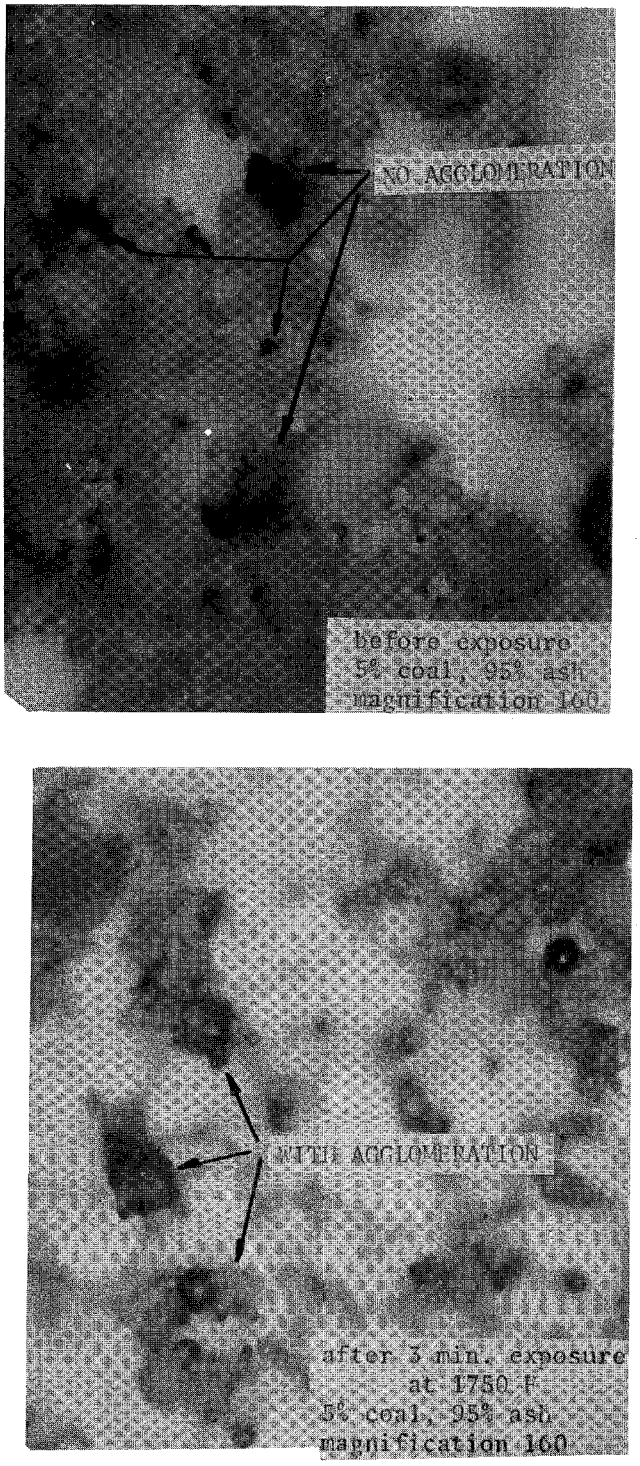

Figure 4. The agglomeration phenomena after exposure to 1750°F for three minutes. Magnification 160X (5% coal, 95% ash).

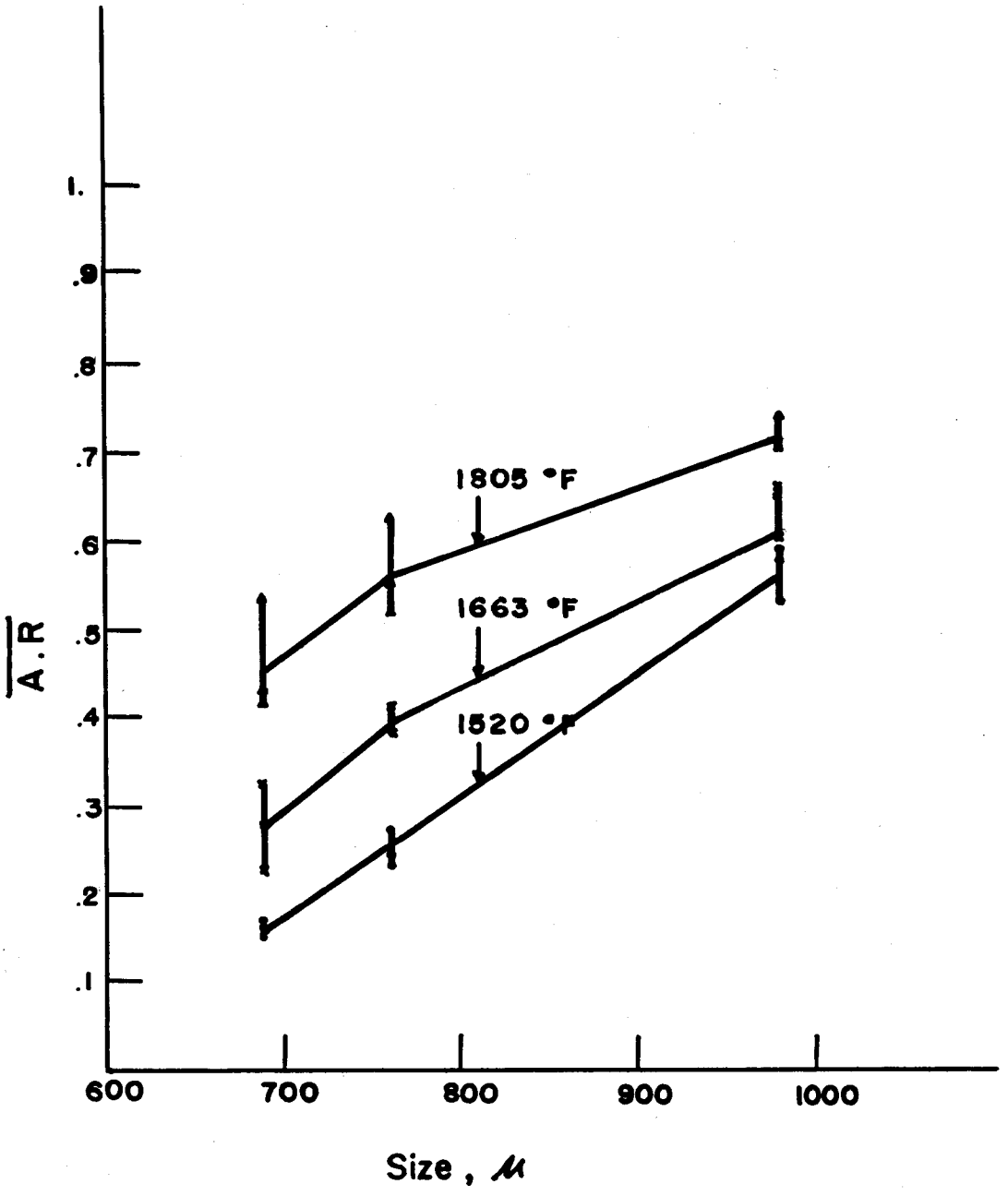

FIG. 5 Average "size weighed" agglomeration rate versus sample particle size for 30 second exposure time

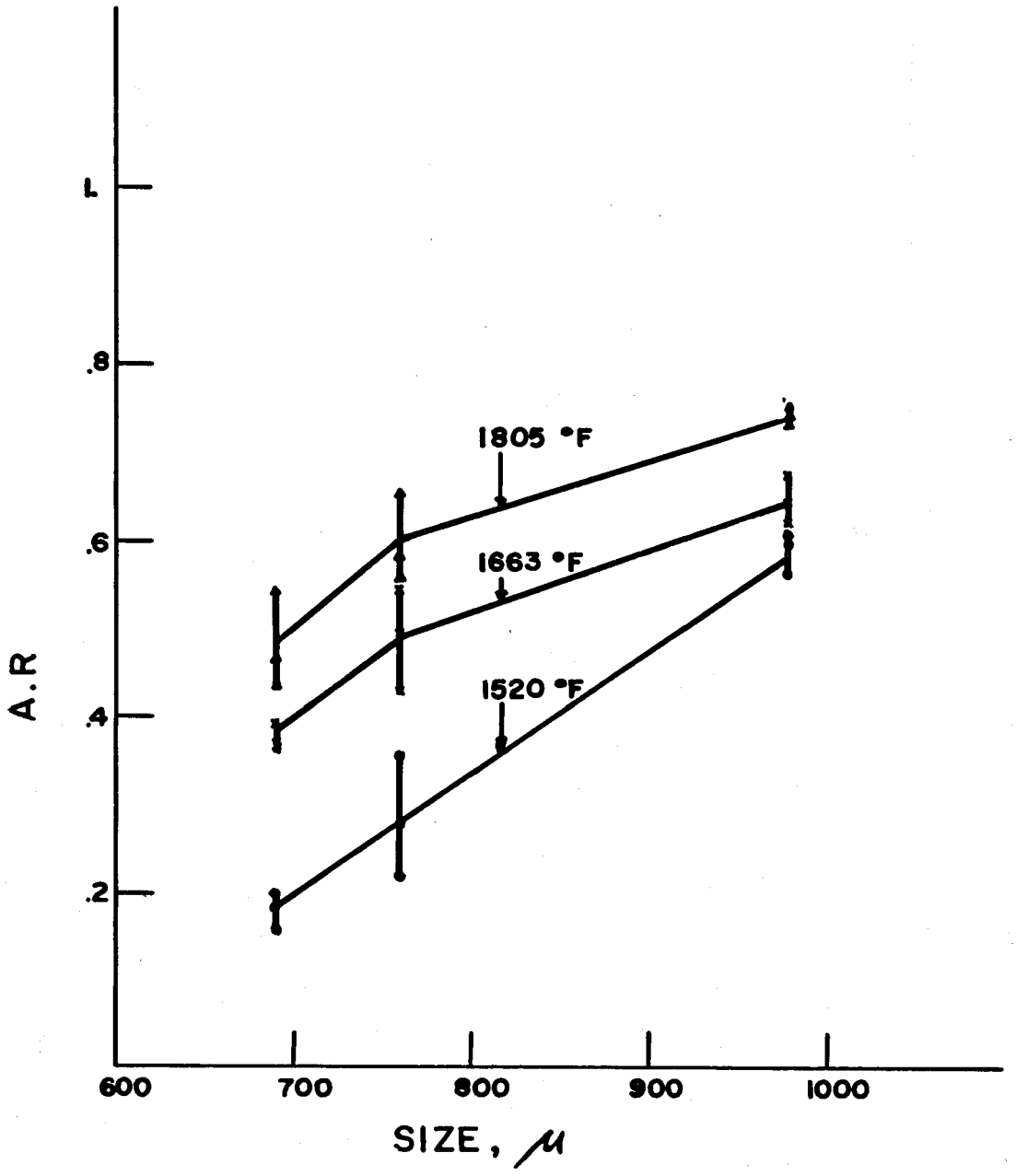

FIG. 6 Average " size weighed" agglomeration rate versus sample particle size for 60 second exposure time

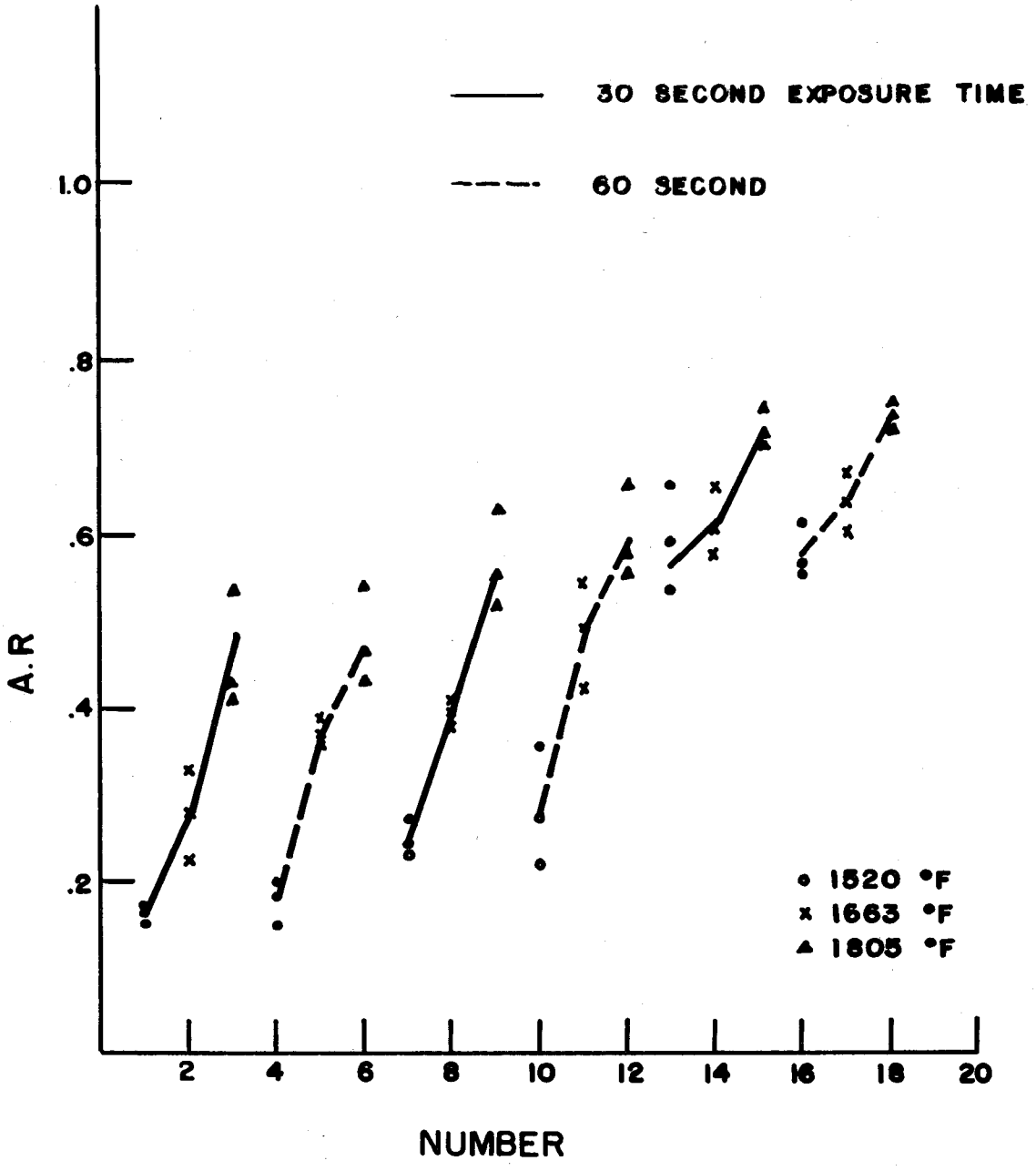

FIG. 7 Average size weighed agglomeration rate versus sample number

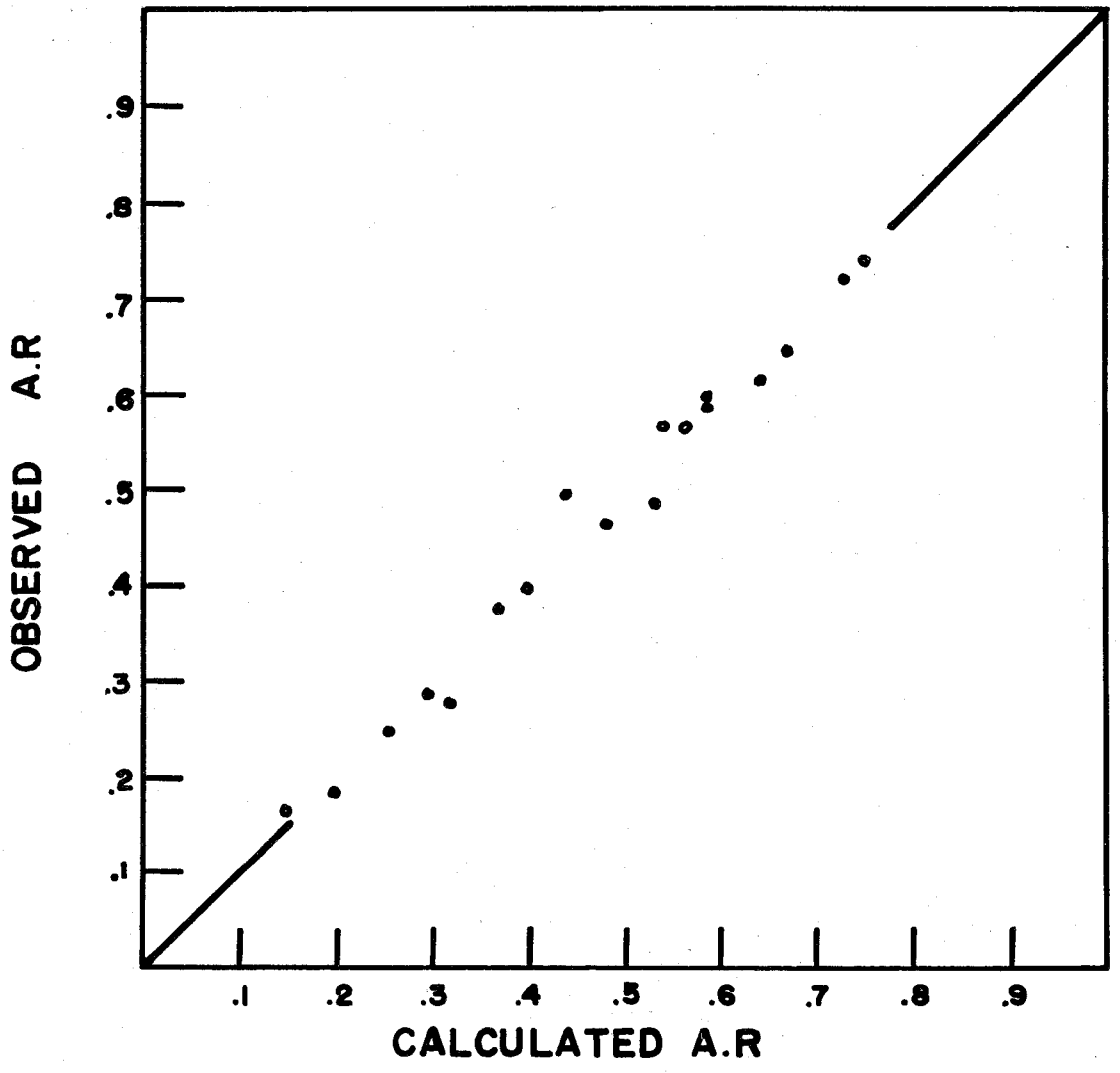

FIG. 8 Observed versus calculated mean "size weighed" agglomeration rate

TEST PROGRAM TO UPDATE EQUIPMENT SPECIFICATION AND DESIGN CRITERIA FOR STOKER FIRED BOILERS

Stratton C. Schaeffer, P.E.
Consulting Engineer
Suite 110
355 N. 21st. St.
Camp Hill, Pennsylvania 17011

Unfortunately, there has been a growing dependence since 1945 on two of our limited resources - oil and natural gas. This dependence was further ag ravated in 1970 by Clean Air Act Implementation plans. To a limited extent, state implimentation plans adversely affected energy management. In certain coal fired plants, maximum combustion efficiency had to be compromised by as much as 10% to keep the plant in compliance with particulate and opacity regulations. In other cases, pollution abatement devices such as mechanical collectors, bag houses, or electrostatic percipitators were added requiring the operation of relatively high horsepower motors with a negative impact on energy management and capital requirements.

Despite an increasing national effort since 1973 to shift our energy use from oil and natural gas to coal, boiler plants have been converted in the opposite direction. An illustration of this point is the Commonwealth of Pennsylvania that allegedly had a strong coal use policy. These state owned facilities contained boilers in the ten to fifty thousand pounds per hour class. All have been converted from coal to oil or gas since 1973(1).

- California State College of Pennsylvania
- Chyney State College
- Dixmont State Hospital
- Eastern Pennsylvania Psychiatric Institute
- Kutztown State College
- Mayview State Hospital
- Philadelphia State Hospital
- Pittsburgh Correctional Institution
- Scotland School
- South Mountain Restoration Center
- Woodville State Hospital

Most conversions were rationalized by using local, state or federal air quality regulations as the reason for the removal of the coal fired equipment. However, in 1976, I was retained by the Bureau of Research and Development, an agency of the Commonwealth of Pennsylvania, to first define the real constraints to coal utilization and then formulate a plan of action to overcome these constraints. To do this, I went into the field and examined the circumstances surrounding 30 boiler plants converted from coal since 1973. Three categories emerged as the true reasons for these conversions:

- Economics
- Alleged air quality violations
- Real air quality violations

Economics

First we'll concentrate on the economics of coal vs. oil or gas fired plants. For the past ten years it has been difficult, using a conventional engineering economic analysis to justify the renovation or new construction of a coal fired plant. It requires approximately $60.00 per pound of steam capacity to build a new coal fired plant today, while oil fired plants can be constructed for $15.00 per pound(2). This capital requirement of four-to-one also applied to plant renovation. Unfortunately, operating costs also worked against coal plants. Labor requirements for coal fired plants are more than double those for gas or oil(3). Therefore, the conclusion of these cost studies usually favored oil or gas rather than coal.

Today, the unavailability of natural gas and increased oil costs have changed the outcome of some engineering studies even though coal plants require more capital to construct or renovate. This is especially true of industrial processes where a good boiler plant load factor exists. However, no general rule-of-thumb is appropriate.

Misuse of AP-42

Now lets concentrate on the second major constraint to coal stoker utilization - alleged air regulation violations. Emission

factors for coal stokers are published by the United States Environmental Protection Agency in a publication called "Compilation of Air Pollutant Emission Factors", or more commonly known as AP-42.

The published formulas for particulate were derived from emperical test data and differentiate only spreader stokers from other coal stoker technology.

Table 1. AP-42 PARTICULATE EMISSION PREDICTION
(Expressed in lbs/ton of coal burned)

STOKER TYPE	FACTOR x % ASH BY WT.
Bituminous spreader stokers	13
Bituminous non-spreader stokers	5
Anthracite stokers	2

Factors such as stack gas velocity, breeching arrangements, stack height, and plant operating procedure are not considered in the formula. Compounding the prediction error is a lack of consideration of coal quality and stoker design. Size consist and ash fusion temperature are two aspects of coal quality that significantly affect particulate emissions.

Stoker design can also compound emission problems. Stoker types are listed below with a rating for limiting particulate emissions:

- Spreader (Poor)
- Vibra-Grate (Fair)
- Single Retort (Fair)
- Multiple Retort (Good)
- Traveling Grate (Excellent)

For the past five years, there was a growing evidence the particulate formulas were not accurate. Unfortunately, federal and state regulatory agencies used these formulas in the preliminary steps for issuing citations to existing plants or in predicting the loading of abatement hardware on new plant design. The well-intentioned enforcement procedures resulted in a number of unnecessary stack tests by boiler plant operators. Ironically, the cost of conducting stack tests is not the major expense. Miscellaneous safety precautions such as the erection of scaffolding to meet O.S.H.A. requirements usually cost far more than the actual gas test. The coal fired boiler plant located on the campus of Pennsylvania State University is an illustrated example of this point. The stack tests were conducted for less than ten thousand dollars. However, the Physical Plant Department at the university estimates scaffolding and other safety precautions cost in excess of thirty-five thousand dollars[4].

Table 2. EMISSION TESTS VS. AP-42 PREDICTIONS

Location	Stoker Type	Unit Size (M.B.H.)	Emission Test-Lb/ M.B.T.U.	AP-42 Prediction	% Error
Ebensburg Hospital (Bituminous)	Multiple Retort	21,000	0.36	2.6	700
	Multiple Retort	21,000	0.36*	2.6	700
	Multiple Retort	21,000	0.36*	2.6	700
Rockview Prison (Bituminous)	Single Retort	21,000	0.38	1.9	500
	Single Retort	21,000	0.38*	1.9	500
	Multiple Retort	38,000	0.89	1.9	210
Ashland Hospital (Anthracite)	Single Retort	13,000	0.22	0.9	400
	Single Retort	13,000	0.22	0.9	400
	Single Retort	13,000	0.22*	0.9	400
	Single Retort	13,000	0.22*	0.9	400

* Units identical to adjacent stokers tested.

1976 Pennsylvania Test Program

Recognizing AP-42 particulate formulas as being inaccurate, a series of tests were conducted in 1976 to measure emissions. The tests were arranged with the cooperation of Pennsylvania's Bureau of Research and Development. The tests involved ten coal fired boilers at three plants.

- Rockview State Prison
- Ebensburg State Hospital
- Ashland State Hospital

This work was supervised by the Pennsylvania State University Engineering Advisory Service with field crews from the Department of Environmental Resources conducting the stack gas tests. To avoid the major cost burden of stack scaffolding, test ports were located in main breechings in accordance with U.S. Environmental Protection Agency Method #5 criteria. Thirty-six points were sampled in the cross section of each breeching.

The test results are shown in Table 2, along with theoretical emission predicted by the AP-42 formulas. In Pennsylvania, these units are restricted to less than 0.4 pounds of particulate emissions per million B.T.U. of coal input to be in compliance with air quality regulations. AP-42 formulas predicted air quality violations for all units. However, the field tests show nine of the units within compliance. One test site, Ebensburg State Hospital, shows a prediction error of 700%. Fortunately, these boilers will not be converted to oil. However, at least ten other state or federally owned boiler plants in Central Pennsylvania were converted since 1971 because of alleged air quality violations predicted by the AP-42 formulas[5]. None of these projects had emission field tests conducted. A post conversion investigation of the coal characteristics and stoker technology used at these projects indicates most plants may have been in compliance. These projects are classic examples of coal to oil conversion based on alleged air quality violations.

Selecting Abatement Hardware

Unfortunately, a number of existing coal fired plants are in violation of particulate emission regulations and represent our third category, "Real Violations". If the violation has been factually determined, a decision must be made to bring the plant into compliance. New plants or plant addition also fall in this category. The decision becomes one of selecting the best control device for the project. To make the best selection, certain things should be factored into the study:

- Mechanical Collectors: Efficiencies of better than 80% can be expected if most of the particulate size is ten microns or

larger. However, efficiencies as low as 50% have been recorded when a large percentage of the particulate occurs below ten microns[6].

- Electrostatic Percipitators: Performance is adversely affected by high ash resistivity that accompanies low sulfur coals. If SO_2 air compliance regulations require coals with sulfur content below 1.5 percent, percipitator performance will suffer[7].

- Bag Houses: Operation and maintenance of these systems will be a problem if operating personnel are not given special training. Beware of turn-key costs vs. hardware costs. The ratio can exceed three-to-one[8].

Combination Firing

Another emission control technique is combination firing. It is possible to install an oil or gas burner in the side wall of boilers above 30,000 pounds, allowing the unit to be coal base loaded with sudden swing loads handled with oil. This combination firing method has been successfully applied to control SO_2 emissions at the Bellefield boiler plant located in a critical air basin at Pittsburgh. This plant contains five coal stokers with a combined rating of 435,000 pounds per hour fired in conjunction with natural gas burners. All units are discharged to a common stack. Coal still provides more than 50% of the energy requirements at the Bellefield plant.

Another successful application of combination firing to reduce particulate is the Central plant of Penn State University. A series of stack gas tests showed the plant violating particulate emission regulations under certain operating conditions despite the existance of a mechanical collector. Gas/oil burners were retrofitted into the side wall of two 100,000 pound per hour vibra-grate units to reduce particulate emissions and opacity while still utilizing coal for 80% of the annual energy requirements[4].

Combination firing for existing or new coal stoker plants has a number of possible advantages:

- Low installed cost
- Reduces emissions
- Quick response to load swings
- Reduces opacity problems with turbulence
- Utilizes coal for up to 90% of energy input

1977 ABMA Test Program

The American Boiler Manufacturers Association (ABMA) submitted an unsolicited proposal to the United States Department of Energy and the United States Environmental Protection Agency. The proposal, which was

funded in 1977, involved six field test sites throughout the United States. Each site contained a spreader stoker in the 125,000 to 200,000 pound range. The program involved multiple point testing at each site under a variety of operating conditions. Examples of operating variables are:

- Excess air
- Reinjection of fly ash
- Load swings

The test results would be analyzed for a variety of emissions. The emissions to be analyzed include:

- Sulfur dioxide
- Nitrogen oxide
- Particulates

By July 1978, the program had progressed to the third test site. Several detailed technical papers will be presented during the winter of 1978. One of these papers is scheduled for the winter meeting of the American Society of Mechanical Engineers. The program should be completed at all six field sites during 1979.

ABMA Small Boiler Program

A supplemental program was instigated by American Boiler Manufacturers Association (ABMA) with additional funds provided by the United States Department of Energy during 1977. This program would concentrate on smaller boilers. For the purpose of this program, the definition of a small boiler is five to seventy million Btu's per hour rating. This program consists of a two-pronged effort. First, the Penn State Engineering Advisory Service was retained to continue field testing small coal fired stoker units. Six tests will be completed during calendar year 1978. At each test site, particulate weight loadings will be taken at the inlet and outlet side of a mechanical collector. In addition, an analysis of particulate size distribution will be made.

A second effort in the small boiler program consists of a search for existing test data. My services were retained by the ABMA to accomplish this task. To date, I have collected test results from sixty coal fired plants located throughout the country. These test results include ten sites where particle size distribution was analyzed.

Summary

Recent stack gas test results indicate a need for refinement of the AP-42 emissions prediction factors for non-spreader stokers. The misuse of these prediction factors has acted as a major constraint to coal utilization during the past ten years. The past and on-going research activities coordinated by the ABMA will be a major contribution

towards updating equipment specifications and design criteria for stoker fired boilers. However, additional research is needed to more accurately assess emissions from coal fired stokers under a variety of operating conditions with various stoker technologies and United States Coals.

REFERENCES

1. Bureau of Research and Development, Commonwealth of Pennsylvania
   Gerald Bowman, P.E., Energy Management Chief

2. American Boiler Manufacturers Association, Arlington, Virginia
   William Axtman, Acting Executive Director

3. Pennsylvania State University Engineering Advisory Service
   Keith Owens, P.E., Mechanical Engineer

4. Pennsylvania State University, Physical Plant Department
   Charles Martin, Manager of Power Plants

5. "Constraints to the Utilization of Pennsylvania Coals", Prepared for the Bureau of Research and Development by
   Stratton C. Schaeffer, P.E., February 1976

6. Huntingdon Prison Stack Gas Test Results, conducted by Center for Air Environment Studies, Pennsylvania State University, June 1978

7. "Electrostatic Precipitator Performance in the U.S. Utility Industry", prepared by Stratton Schaeffer, P.E., June 1976

8. "Retrofitting Baghouses on Coal-Fired Boilers - A Case Study"
   J.M. Osborne, Environmental Engineer, 3M Company

TRACE ELEMENT EMISSIONS FROM COPPER SMELTERS

Richard L. Meek and Grady B. Nichols
Southern Research Institute
2000 Ninth Avenue, South
Birmingham, Alabama 35205

ABSTRACT

Field tests conducted on electrostatic precipitators used to control particulate emissions from reverberatory furnaces in two Western copper smelters have provided preliminary data on trace-metal emissions. These tests were sponsored by the Environmental Protection Agency, Cincinnati Industrial Environmental Research Laboratory.

Concentrations of trace-metal components in the feed to the reverberatory furnace were determined, and material balance estimates were made across the reverberatory furnace and the electrostatic precipitators with particular emphasis on analysis and control of volatile metals such as arsenic.

INTRODUCTION

Historically, nonferrous metals such as aluminum, copper, lead, tin, zinc, and nickel and the more exotic metals such as silver and gold have been extracted from metal-bearing ores by various hydrometallurgical and pyrometallurgical techniques primarily designed to recover the valuable base metal while rejecting extraneous by-products and wastes. At one extreme, panning for gold is probably the simplest hydrometallurgical process since the gold dust is easily washed free of siliceous gange, and the subsequent smelting and refining into ingots or bullion is relatively straightforward with minimal environmental consequences.

At the other extreme, the pyrometallurgical operations that are used for processing copper, lead, zinc, and many other nonferrous ores are very complex and present formidable problems in the recovery of the base metal, extraction of valuable by-products, rejection of unwanted wastes, and control of emissions and effluents from the processes. In the pyrometallurgical systems, the raw materials or benficiated ores are subjected to high-temperature processes which may involve selective oxidation, reduction, volatilization, melting, and slagging to separate the waste materials and by-products from the valuable nonferrous metals. In most of the high-temperature pyrometallurgical processes, large volumes of off-gases are evolved which contain large quantities of particulate matter, much of which is a metallic compound of the ore being processed. Generally, this particulate must be efficiently recovered and recycled to the process, and in the early operation of most smelters, the primary motivation for recovery of the particulate was purely economic. However, under today's circumstances, recovery of particulate evolved in nonferrous processing can be for either economic or environmental reasons, or both.

Since many of the nonferrous minerals occur in nature as sulfidic ores, the pyrometallurgical off-gases frequently contain SO_2, SO_3, and sulfuric acid mist in addition to the particulate matter. To further complicate the problem, some metals such as antimony, arsenic, cadmium, mercury, selenium, and zinc may be volatilized at the high temperatures involved and become part of the pyrometallurgical off-gases. Other materials such as fluorine, chlorine, phosphorus, and perhaps organics may also be converted to the gaseous state under pyrometallurgical conditions.

Until recent years, most nonferrous smelters were concerned only with recovery or removal of the valued particulate and highly noxious materials, and in most cases recovery of SO_2 was not practiced except in those rare situations where utilization of the SO_2 or elemental sulfur was technically and economically feasible. When sulfuric acid is produced as a by-product, extensive measures are taken to remove particulate matter and extraneous gases or vapors before processing the gas stream for by-product recovery. However, whether the gas stream is to be further processed or not, particulate matter is normally removed by electrostatic precipitators, fabric filters, and various types of scrubbers. The recovered particulate may be recycled to the process or disposed of as solid waste, depending on its composition and value.

One cannot safely generalize on the type of particulate control equipment that should be used in the various segments of the nonferrous industry, and indeed many combinations of scrubbers, fabric filters, and electrostatic precipitators are used. The choice of the type of control device obviously depends on numerous criteria, such as the specific ore or operating requirements, capital and operating costs, secondary pollution problems (such as scrubber purges creating wastewater problems), and the type of pollutant to be controlled.

Some typical applications of particulate control devices in the nonferrous metals industry may be cited as follows: wet electrostatic precipitators are widely used in the aluminum industry to control emissions from reduction cells; dry electrostatic precipitators are used in primary copper smelters on roasters, reverberatory and electric furnaces, and converters; fabric filters are used on primary lead updraft sinter machines and blast furnaces; and electrostatic precipitators are used on zinc roasters and downdraft sinter machines. There are numerous exceptions to all of these generalizations, however.

Since there are many unknowns regarding performance of control devices on metallurgical off-gases, EPA's Metals and Inorganic Chemicals Branch initiated a program to obtain the necessary information to evaluate performance of control devices such as electrostatic precipitators. Southern Research Institute has been involved in research on electrostatic precipitators for a number of years under EPA sponsorship, and one of our current programs for EPA's Cincinnati Industrial Environmental Research Laboratories is concerned with the evaluation and control of particulates from nonferrous smelting operations, with particular emphasis on ESP's.

Thus far, our results from tests on copper smelters indicate that, at the ESP's operating temperature of about 600°F, constituents contained in the process off-gases exist in both particulate and gaseous phases. Such readily volatile elements as arsenic and fluorine generally should not exist as particulate matter while passing through hot ESP's. However, after leaving the control device, some of these materials may condense as fine particulate and enter the environment as air pollutants unless secondary control devices are used. Therefore, even though ESP's and fabric filters may operate at high particulate matter collection efficiency, they are only efficient on the particulate matter that they actually "see" at the operating temperature of the control device.

POTENTIAL CONTROL DEVICES

The three primary control devices that could be used for particulate control are wet scrubbers, fabric filters, and electrostatic precipitators. The particulate characteristic that tends to limit the performance of each of these devices is the particle size distribution. In addition, the electrical resistivity of the particulate influences the operating characteristics of the electrostatic precipitator.

The major factors influencing the selection of a particulate control device, with the exception of economic considerations, include collection efficiency as a function of particle size, hostility of the constituents in the effluent stream, (corrosion, temperature limitations, etc.) and the particulate removal efficiency required.

The off-gases from nonferrous smelting operations often contain significant quantities of submicron particles, as well as material that may condense to form these fine particles. The scrubber is less efficient in collecting these very small particles than either the fabric filter or the electrostatic precipitator.

In principle, either the fabric filter or the electrostatic precipitator could be used in the control of emissions. In the absence of disturbing influences, both exhibit similar efficiencies as a function of particle size distribution.

The limitation in the use of fabric filters in the nonferrous metals industry is largely related to the availability of fabric filter materials able to survive the temperatures encountered in the effluent gas streams. Apart from these considerations, the fabric filter is an acceptable device for controlling emissions from these installations.

In the situation where the electrical resistivity of the particulate matter is unusually high, as produced by lead smelters, the fabric filter tends to compete favorably with the electrostatic precipitator for particulate collection. However, in most other nonferrous applications, the electrostatic precipitator is the most common particulate control device used in the United States.

COPPER SMELTER TESTS

In the primary copper-smelting industry, electrostatic precipitators are frequently used in association with roasters, reverberatory furnaces, electric furnaces, and converters. One facet of Southern Research Institute's program for EPA has been concerned with field testing and evaluation of electrostatic precipitators used for control of emissions from copper reverberatory furnaces. We have conducted tests on reverb ESP's in two major copper smelters, and while we recognize that every smelter has its own peculiar characteristics based on individual ores and smelter operating practices, we believe that some of our results are illustrative of ESP performance within the industry.

Initially, the tests provided an opportunity to evaluate particulate test methods that had been developed and used extensively on coal-fired utility applications. Since off-gases from a copper reverberatory furnace are substantially different from those of coal-fired utilities, we recognized that some test modifications would be required, primarily to allow testing under the more hostile environments encountered in copper smelters. In general, we found that the reverb particulates were "sticky" and that some test-equipment seals had to be replaced more frequently than usual; however, for the most part, no major problems were encountered with the test equipment.

A simplified flow diagram of a typical copper smelter is shown in Figure 1. The raw ore from the mine is beneficiated to obtain a concentrate which typically contains 20 to 25% copper with associated iron, sulfur, and minor elements. The concentrate is usually received at the smelter as a slurry or wet cake. In a typical process scheme, the concentrate may be partially roasted to eliminate some sulfur and to provide a dry calcine as feed to the reverberatory furnace. Autogenous roasting is usually carried out at about 1150-1200°F, and the off-gases usually contain enough SO_2 for efficient conversion to sulfuric acid. The reverberatory furnace requires an external fuel source, such as natural gas, fuel oil, or coal, and is operated at about 2200-2500°F. The primary functions of the reverb are to provide a balanced Cu-Fe-S matte for feed to the converter while removing extraneous Fe, SiO_2, etc. as slag. Normally, off-gases from the reverberatory furnace are low in SO_2 and are most frequently vented to the atmosphere after removal of particulate matter. The converters are also operated at about 2200-2500°F on a cyclic basis to obtain a product blister or anode copper and an iron slag which is normally recycled to the reverberatory furnace. Converter off-gases have highly cyclic flow patterns, but the SO_2 content is usually high enough for processing to acid.

Since off-gases from reverberatory furnaces are most often vented to the atmosphere while the gases from roasters and converters are more likely to be processed for recovery of SO_2 and conversion to sulfuric acid, we focused our initial test efforts on ESP's associated with reverbs. In one case, the feed to the reverb was a partially roasted calcine (essentially as shown in Figure 1); in the other case, a "green" concentrate was fed to the reverb. In the latter case, the feed was a dried but unroasted concentrate. Otherwise, operation of the two units was quite similar and is illustrated in Figure 2. Both units are equipped to use either natural gas or fuel oil, and both have waste-heat boilers preceding the ESP's.

Design parameters for one of the precipitators are shown in Table 1. This precipitator was operated at 600°F with a gas flow of about 160,000 acfm. Inlet particulate loading was 0.60 gr/scf and the outlet loading was 0.02 gr/scf. The SO_2 in the gas varied from about 0.4 to 1.7% depending on the operating cycle of the reverberatory furnace.

The mass tests across the ESP's were conducted with an ASME-type mass train inserted into the flue and maintained at near in-line temperatures. This is somewhat different from the EPA Method 5 test, in which the filter temperature is maintained at 250°F. The in-stack filter method was used to assure that the particulate captured in the mass train actually entered or passed through the precipitator as a particulate rather than a gas or condensate.

The particle-size distribution was measured at the inlet and outlet of the precipitators using cascade inertial impactors, five-stage cyclones, and two real-time measurement systems. The inertial systems

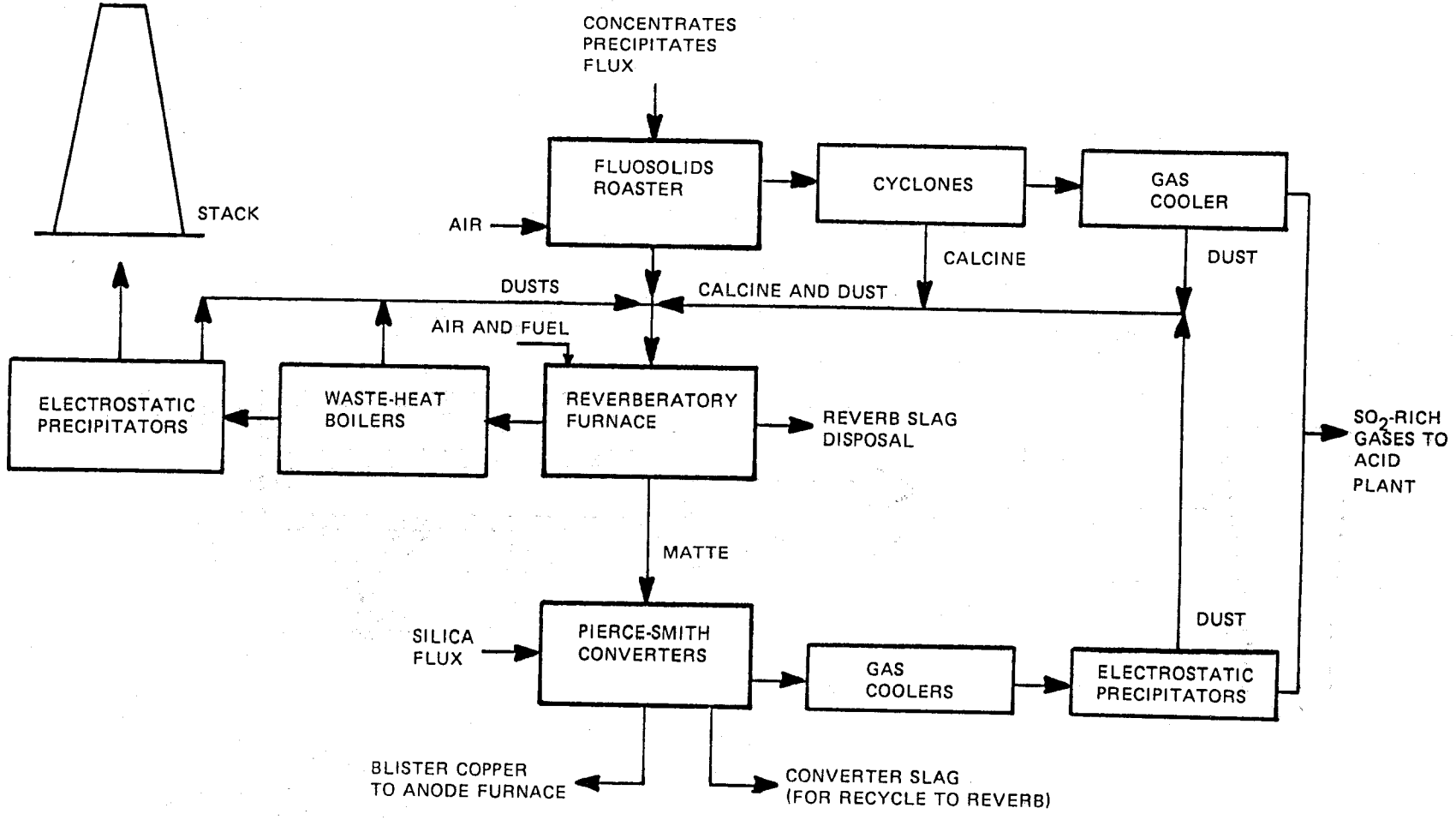

Figure 1. Simplified Flow Diagram of Copper Smelter.

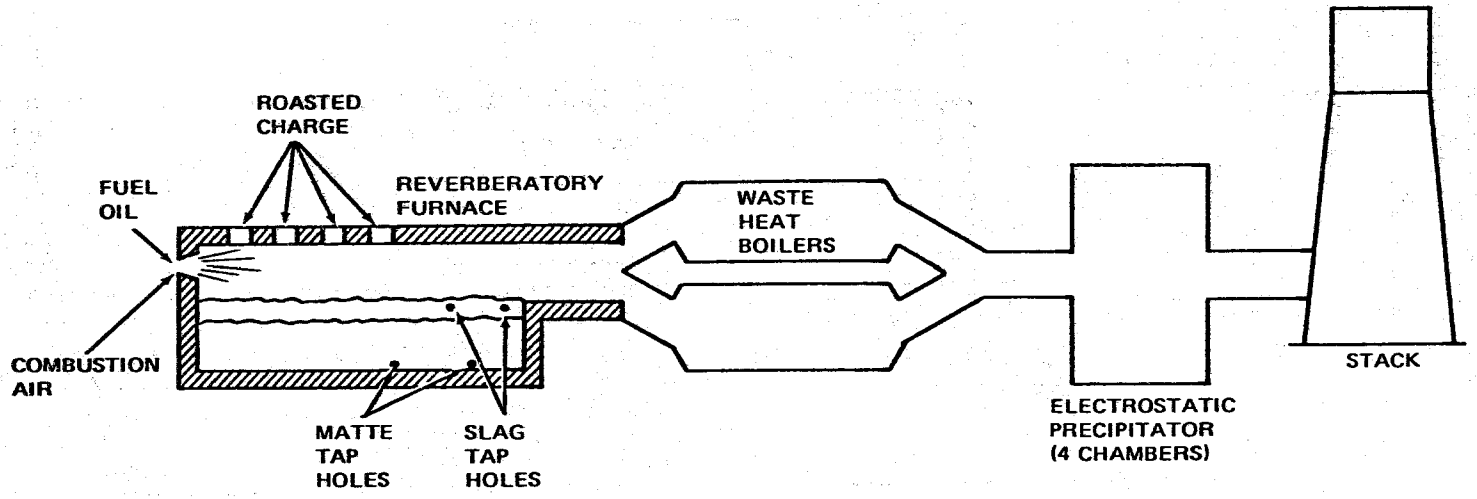

Figure 2. Reverberatory Furnace Schematic

Table 1. ELECTROSTATIC PRECIPITATOR DESCRIPTIVE PARAMETERS. REVERBERATORY FURNACE FOR PLANT A

Item	English	Metric
Collection electrode area (A)(total-2 ESP)	39,744 ft^2	3,692.4 m^2
Inlet set area (power set C)	19,872 ft^2	1,846.2 m^2
Outlet set area (power set A)	9,936 ft^2	923.0 m^2
Outlet set area (power set B)	9,936 ft^2	923.0 m^2
Collection electrode spacing	9 in.	0.229 m
Corona electrode diameter (round wire)	0.1055 in.	2.7 mm
Collection electrode dimension	9 ft x 24 ft	2.74 m x 7.32 m
Number of gas passages (total-2 ESP)	46	
Gas passage length (active)	18 ft	5.49 m
Volume flow rate design (V)	150,000 acfm	70.8 m^3/sec
Design temperature	600-700°F	315-371°C
Design efficiency	96.83%	
Design precipitation rate parameter (w)	0.21 ft/sec	6.5 cm/sec
Specific collection electrode area (A/V)	265 ft^2/1000 cfm	52 m^2/m^3 sec

provide time-integrated size distributions, while the real-time systems provide information on the variability of particle-size distributions with time. These test methods are described in a report prepared for the Industrial Environmental Research Laboratory entitled "Procedures Manual for Electrostatic Precipitator Evaluation".

One purpose of our test program was to evaluate the overall performance of the precipitator during "on-stream" operations. Results of the impactor and mass-train measurements showed an overall efficiency ranging from 96.4 to 96.8% which was identical to the design efficiency of 96.8%. During the test period, no major operating problems were encountered. Some variations in particulate and gas emissions from the ESP were observed but these were regarded as normal for the cyclic operation of reverberatory furnaces. A summary of the data is shown in Table 2 which reflects some of the cyclic variations. Mass loading - particle size data is shown in Figure 3.

Table 2.

MASS CONCENTRATIONS AND EFFICIENCY, PLANT A

Mass Concentration				Efficiency, %	
Inlet, mg/DSCM		Outlet, mg/DSCM			
Impactor	Mass Train	Impactor	Mass Train	Impactor	Mass Train
1146	1407	41	48	96.4	96.6
641	1304	21	41	96.7	96.8

SULFUR OXIDE CONCENTRATIONS, PLANT A

Sampling Rate, l/min	Furnace Charge Cycle	% By Volume	
		SO_2	SO_3
3.2	after	1.0	0.024
2.9	before	0.42	0.019
2.4	after	0.73	0.018
1.9	before	0.63	0.025
1.0	after	1.7	0.067

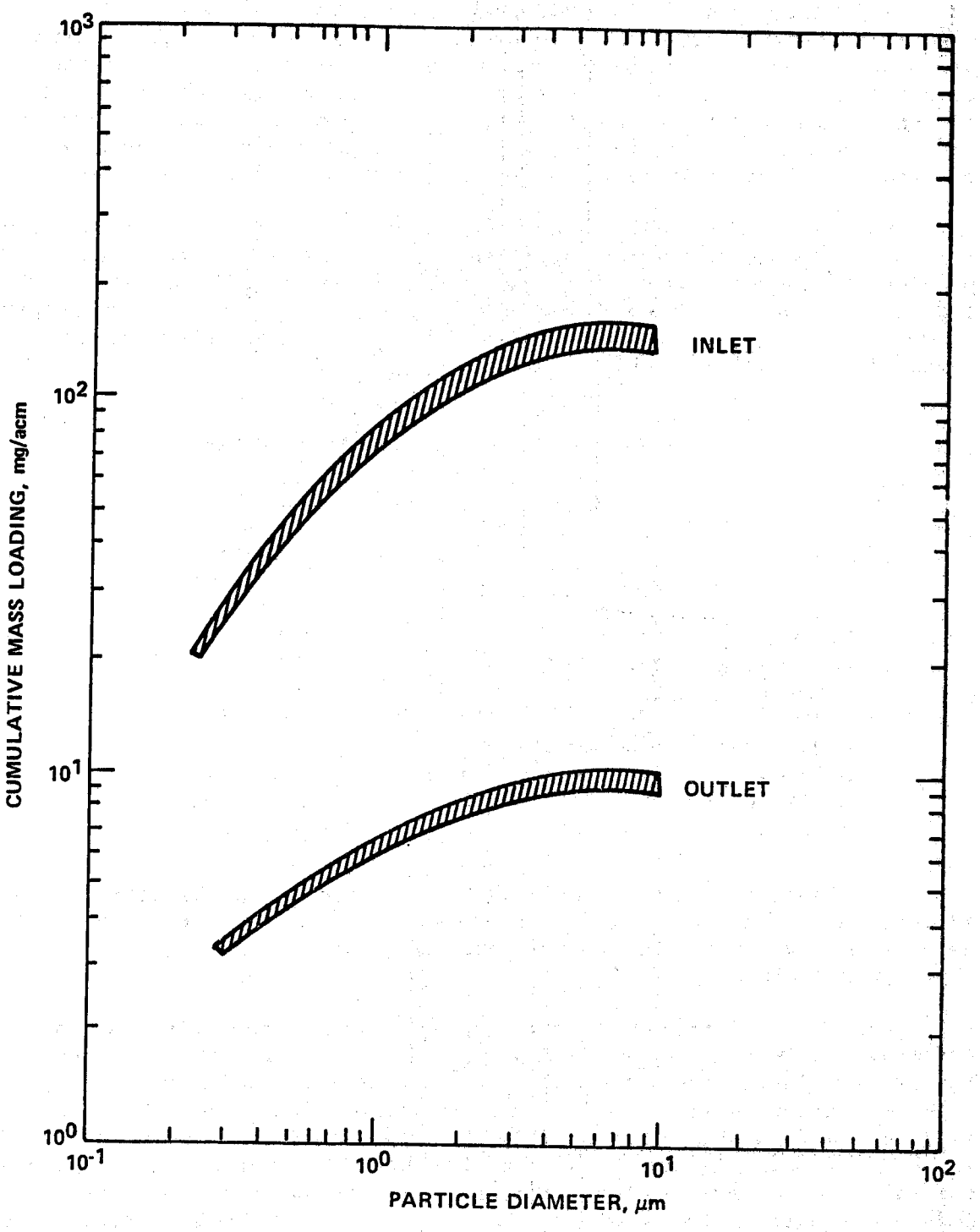

Figure 3. Average cumulative inlet and outlet mass loading vs. particle size, Plant A copper reverberatory furnace.

As a part of our study, we also investigated the fate of some of the minor elements of environmental concern. Samples were collected from the gas streams with a wet-electrostatic-precipitator train, a series of external impingers, cyclone separators, and glass-fiber thimbles. Most elemental analyses were made using a spark-source mass spectrometer and atomic absorption. Fluorine content was determined with an ion-selective electrode, and selenium was determined by a fluorometric procedure.

The feed to the reverberatory furnace was not a constant composition and the composition varied significantly depending on the amount of particulate recycled from the waste-heat boilers and ESP as well as the amount of converter slag recycled and some variation in the copper concentrate itself. Composite analyses of the minor elements in the reverb feed, slag, and matte are shown in Table 3.

Table 3. MINOR ELEMENTS IN REVERBERATORY FURNACE FEED, SLAG, AND MATTE

	Feed		Slag		Matte	
	ppm	#/hr	ppm	#/hr	ppm	#/hr
Arsenic	4000	200	1300	50	1100	50
Molybdenum	1600	80	2400	80+	200	10
Cadmium	1200	60	10	>1	900	40
Lead	1000	50	350	15	2000	80
Zinc	800	40	800	30	750	30
Selenium	200	10	150	5	5	>1
Antimony	100	5	90	3	100	5
Fluorine	70	3	50	2	Tr.	Tr.

These analyses are not rigorous by any means and the data are not adequate for a complete material balance; however, we can make some general observations from the data and the known operating conditions in the copper smelter.

Nearly all of the molybdenum and some of the lead, zinc, selenium, antimony, and arsenic are discharged to waste in the reverb slag. Most of the cadmium leaves the reverb in the matte as feed to the converter and does not return to the reverb in the converter slag. Some of the lead, zinc, antimony, and arsenic which leaves in the matte also is not returned in the converter slag and is probably caught in the converter particulate control system. Some of the selenium may leave the reverb as a vapor as does about half of the arsenic. Clearly, in this situation, arsenic is the predominant volatile metal evolved from the reverberatory furnace. The fluorine analysis in the slag may be suspect, and the fluorine probably leaves the reverb in some gaseous form such as SiF_4 and would not be caught by the ESP.

Some of the arsenic (primarily as arsenic trioxide) is caught by the electrostatic precipitator and is eventually returned to the reverb. Plant analyses show the ESP and waste-heat boiler dusts to contain up to 6.5% arsenic (typically 4-5%), but since these dusts are recycled to the reverb, the ultimate disposition of arsenic must be in either the ESP off-gas, the reverb slag, the converter off-gas, or the product copper or sulfuric acid.

Typical values for arsenic concentrations in this particular smelter are shown in Table 4. Since the matte, reverb ESP and converter dusts, and converter slag are not final products or wastes, the arsenic in these streams ultimately ends up in the product anode copper, the reverb slag, the acid plant purge water, or in the ESP outlet gas.

Table 4. ARSENIC CONCENTRATIONS IN SMELTER STREAMS

Copper Concentrate	0.26%
Matte	0.08
Reverb Slag*	0.06
Reverb ESP	4.4
Converter Dust	1.8
Converter Slag	0.015
Anode Copper*	0.03
Acid Plant Purge Water*	0.001

*Final product or waste.

An approximate arsenic balance over the entire smelter system is given in Table 5. In this smelter, about 5% of the arsenic remains in the copper product and will eventually be removed in the electrolytic refining of the copper. About half of the arsenic ends up in either the reverb slag or the acid plant purge water, about equally divided between the two. The remaining 40-45% is not caught as fine particulate by the hot ESP and is vented to the atmosphere.

Table 5. APPROXIMATE ARSENIC DISTRIBUTION

Reverb Slag	25 - 30%
Acid Plant Purge Water (Converter off-gases)	25 - 30%
Blister (or Anode) Copper	5%
Reverb ESP Outlet	40 - 45%

Since both the reverberatory furnace slag and the acid plant purge water are waste streams from the smelter, they could constitute potential environmental problems if the arsenic and other toxic metals are not bound in an innocuous form. Clearly, the volatilized minor elements such as arsenic and fluorine that are not caught by the electrostatic precipitator or other control devices would go up the stack and become a potential environmental problem if emitted in significant concentrations.

With reference back to the overall smelter schematic in Figure 1, we can make a few qualitative generalizations on some of the trace elements in a copper smelter. Very few of the minor elements in the copper concentrates would be evolved in the roaster at 1150-1200°F since the temperature is relatively low, the retention times in roasters are fairly short, and most copper roasters only partially roast the ores. Some arsenic, mercury or fluorine could be evolved from the roasters but probably not in significant amounts except when the roaster temperature is increased or the concentrate is dead-roasted.

By contrast, at the operating temperatures of reverberatory furnaces, electric furnaces, and converters (2200-2500°F), a number of metals or oxides can be volatilized including arsenic, antimony, barium, bismuth, cadmium, lead, mercury, molybdenum, rhenium, and selenium, in addition to fluorine and phosphorus, and of course sulfur. Some of the minor elements such as molybdenum may end up in the reverberatory furnace slag and some may remain (at least partially) in the product copper.

The volatilized metals may be partially or totally captured by control devices associated with the roasters, reverberatory furnaces, converters, and acid plants, but in many cases, arsenic, fluorine, phosphorus, and other minor elements will be exhausted from smelter stacks and could become an environmental problem.

We do not represent our limited findings as being typical of the nonferrous industry, and we recognize that minor-element emissions will vary widely from one smelter to another depending on the specific processing, control devices, and the ore being processed. However, we believe that additional research is needed to develop a better understanding of minor-element emissions from nonferrous smelters and to improve the control systems to avoid adverse environmental effects.

ACKNOWLEDGMENTS

We would like to acknowledge Radian Corporation for their collaboration with Southern Research Institute on these studies, especially Dr. Klaus Schwitzgebel and Mr. Robert V. Collins. We also appreciate the cooperation of the management and personnel at the copper smelters, and the support of EPA through Mr. George S. Thompson, Jr. and our project officers, Ms. Margaret Stasikowski and Mr. John O. Burckle.

TECHNICAL REPORT DATA (Please read Instructions on the reverse before completing)		
1. REPORT NO. EPA-600/7-79-044d	2.	3. RECIPIENT'S ACCESSION NO.
4. TITLE AND SUBTITLE Symposium on the Transfer and Utilization of Particulate Control Technology: Vol. 4. Fugitive Dusts and Sampling, Analysis and Characterization of Aerosols		5. REPORT DATE February 1979 6. PERFORMING ORGANIZATION CODE
7. AUTHOR(S) F. P. Venditti, J.A. Armstrong, and Michael Durham		8. PERFORMING ORGANIZATION REPORT NO.
9. PERFORMING ORGANIZATION NAME AND ADDRESS Denver Research Institute P.O. Box 10127 Denver, Colorado 80208		10. PROGRAM ELEMENT NO. EHE624 11. CONTRACT/GRANT NO. Grant R805725
12. SPONSORING AGENCY NAME AND ADDRESS EPA, Office of Research and Development Industrial Environmental Research Laboratory Research Triangle Park, NC 27711		13. TYPE OF REPORT AND PERIOD COVERED Proceedings: 10/77-10/78 14. SPONSORING AGENCY CODE EPA/600/13
15. SUPPLEMENTARY NOTES IERL-RTP project officer is Dennis C. Drehmel, Mail Drop 61, 919/541-2925.		

16. ABSTRACT Papers in the proceedings were presented at the Symposium on the Transfer and Utilization of Particulate Control Technology, in Denver, Colorado, July 24 through 28, 1978. The symposium was sponsored by the Particulate Technology Branch of EPA's Industrial Environmental Research Laboratory--Research Triangle Park, and was hosted by the University of Denver's Denver Research Institute. The symposium brought together researchers, manufacturers, users, government agencies, educators, and students to discuss new technology and to provide an effective means for the transfer of this technology out of the laboratories and into the hands of the users. The three major categories of control technologies--electrostatic precipitators, scrubbers, and fabric filters--were of major concern. These technologies were discussed from the perspectives of economics; new technical advances in science and engineering; and applications. Several papers dealt with combinations of devices and technologies, leading to a concept of using a systems approach to particulate control, rather than device control.

17. KEY WORDS AND DOCUMENT ANALYSIS			
a. DESCRIPTORS		b. IDENTIFIERS/OPEN ENDED TERMS	c. COSATI Field/Group
Pollution	Fabrics	Pollution Control	13B 11E
Dust	Economics	Stationary Sources	11G 05C
Aerosols	Sampling	Particulate	07D 14B
Electrostatic Precipitators		Fabric Filters	13I
Scrubbers		Fugitive Dust	07A
Filtration			

18. DISTRIBUTION STATEMENT	19. SECURITY CLASS (This Report)	21. NO. OF PAGES
Unlimited	Unclassified	506
	20. SECURITY CLASS (This page) Unclassified	22. PRICE

EPA Form 2220-1 (9-73)

☆U.S. GOVERNMENT PRINTING OFFICE: 1979-640-013/4205 REGION NO. 4